

Electronic and Steric Effects on C–H Activation at Ir and Rh Half-Sandwich Complexes

Thesis submitted for the degree of
Doctor of Philosophy
at the University of Leicester

by
Neringa Tamosiunaite
Department of Chemistry
University of Leicester

October 2019

Title: Electronic and Steric Effects on C–H Activation at Ir and Rh Half-Sandwich Complexes

Author: Neringa Tamosiunaite

Abstract

A range of cyclometallated phenylpyridine, phenylNHC and benzylnhc Ir(III) and Rh(III) half-sandwich complexes and their respective ligands have been synthesised. All new compounds were characterised by ^1H and ^{13}C NMR spectroscopy, mass spectrometry and several complexes have been structurally characterised by X-ray crystallography. DFT calculations (carried out by the group of Prof. S. A. Macgregor, Heriot-Watt University) are also discussed in Chapter three.

Chapter one introduces mechanisms of C–H activation particularly key mechanistic studies on carboxylate-assisted AMLA and CMD mechanisms with Pd(II), and Ir(III) and Rh(III) half-sandwich complexes. Chapters two, three and four describe studies of steric and electronic effects on cyclometallation via AMLA C–H activation at Ir(III) and Rh(III) and Chapter five summarises the overall conclusions. Intermolecular competition experiments with phenylpyridines showed that cyclometallation reactions were faster with electron-donating substituents (Chapter two). However, the thermodynamic selectivity favoured electron withdrawing substituents. Intramolecular competition experiments with phenylimidazolium salts (Chapter three) were difficult to interpret. Under most of the conditions studied, imidazolium C–H activation is rate limiting and phenyl C–H activation was not under kinetic control. DFT calculations suggest that HOAc/chloride exchange as well as the C–H activation step could be contributing to the selectivity. The use of benzyylimidazolium salts (Chapter four) which form six-membered metallacycles allowed observation of kinetic selectivity which showed very little electronic preference with no clear trend. For all ligands studied the thermodynamically more stable complexes are formed by cyclometallation on the ring substituted with the more electron-withdrawing group. The *meta*-substituted ligands are sensitive to steric effects with a thermodynamic preference for the *para*-isomers except for R = F. All of the experimental work and full characterisation of ligands and complexes are given in Chapter six.

Acknowledgements

First of all, I would like to thank my supervisor Prof. Dai L. Davies for his continuous support throughout my PhD, for his help, patience and immense knowledge. His guidance, insight and expertise helped me during my research as well as writing stages of this thesis. I could not have asked for a better supervisor for my PhD.

I would like to thank Dr G. A. Griffith for 2D NMR spectra and Dr V. Timmermann for the assistance with NMR. Mr M. Lee and Dr S. C. Mistry for the mass spectra and Mr K. Singh for the X-Ray structure determinations. I would also like to thank the group of Prof. S. A. Macgregor at Heriot-Watt University for the computational studies.

Many thanks go to my second supervisor Dr A. Stuart and the past members of the DLD group especially Raissa whose support at the beginning of my PhD was invaluable in helping me to settle into the new lab and department.

I would also like to thank members of labs 2.14 and 0.21 who welcomed me into the Department of Chemistry and were a pleasure to work with. I want to especially thank Vicki, Simran, Alisha, Natasha, Lucy and Martyna amongst many other of PhD friends, whose support and encouragement throughout my PhD, especially during difficult times, was crucial for me in completing my thesis.

Finally, I would like to thank my family and friends for their ongoing support and encouragement throughout my degree.

Table of Contents

Abstract	i
Acknowledgements	ii
Table of Contents	iv
Abbreviations	viii
Chapter One	1
1.1 General introduction.....	1
1.2 Methods to study C–H activation mechanisms	2
1.2a Kinetic isotope effect	2
1.2b H/D exchange	6
1.2c Electronic effects	7
1.2d Computational studies	9
1.3 Mechanisms of C–H activation up to 2005	10
1.3a Oxidative addition	10
1.3b σ -bond metathesis.....	13
1.3c 1,2-addition	15
1.3d Electrophilic activation.....	17
1.4 AMLA/CMD	20
1.4a AMLA/CMD at Pd/Ir	20
1.4b AMLA/CMD at Half-Sandwich Ir and Rh Complexes.....	30
1.5 Conclusions	47
1.6 Bibliography.....	49
Chapter Two	54
2.1 Introduction	54
2.2 Results and Discussion.....	60
2.2.a Synthesis of substituted phenylpyridines.....	60
2.2.b Cyclometallation of <i>para</i> -substituted phenylpyridines	61
2.2.c Cyclometallation of <i>meta</i> -substituted phenylpyridines	65
2.2.d Competition experiments with <i>para</i> -substituted phenylpyridines	72
2.2.e Phenylpyrazole to phenylpyridine exchange at Ir and Rh	77
2.3 Conclusions	78
2.4 Bibliography.....	81

Chapter Three	83
3.1 Introduction.....	83
3.2 Results and discussion.....	88
3.2a. Preparation of diphenylimidazolium salts	88
3.2bi Preparation of Ir and Rh half-sandwich NHC complexes by direct C-H activation	92
3.2bii Preparation of Ir and Rh half-sandwich NHC complexes by transmetallations.....	105
3.2c Influence of chloride concentration	112
3.2d Preliminary DFT studies with Ir.....	123
3.2e Synthesis of <i>meta</i> -substituted phenylimidazolium salts	127
3.2f Cyclometallations of <i>meta</i> -substituted phenylimidazolium salts with Ir and Rh.....	128
3.2g Conclusions	132
3.3 Bibliography.....	135
Chapter Four	137
4.1. Introduction.....	137
4.2 Results and discussion.....	140
4.2a Preparation of dibenzylimidazolium salts	141
4.2bi Complexation of dibenzylimidazolium salts.....	142
4.2bii Cyclometallation of dibenzylimidazolium salts	146
4.2c Preparation of <i>meta</i> -substituted monobenzylimidazolium salts	160
4.2di Complexation of <i>meta</i> -substituted monobenzylimidazolium salts	161
4.2dii Cyclometallation of <i>meta</i> -substituted monobenzylimidazolium salts	163
4.2e Conclusions.....	168
4.3 Bibliography.....	171
Chapter Five	172
5.1 Conclusions and Future Directions for Steric Effects on C–H Activation	172
5.2 Conclusions and Future Directions for Electronic Effects on C–H Activation ..	174
5.3 Overall Conclusions	177
5.4 Bibliography.....	178

Chapter Six	179
6.1 General information and materials.....	179
6.2 Experimental procedures for Chapter 2	180
6.2a Synthesis of <i>para</i> and <i>meta</i> -substituted phenylpyridines	180
6.2b Cyclometallation of <i>para</i> -substituted phenylpyridines L2.6-R with {IrCp*} and {RhCp*}	182
6.2c Cyclometallation of <i>meta</i> -substituted phenylpyridines L2.3-R with {IrCp*} and {RhCp*}	188
6.2d General procedure for measuring steric effects with <i>meta</i> -substituted phenylpyridines L2.3-R	192
6.2e General procedure for deuterium incorporation experiments.....	192
6.2f General procedure for competition experiments.....	193
6.2g Procedure for phenylpyrazole to phenylpyridine exchange	193
6.3 Experimental procedures for Chapter 3	194
6.3a Preparation of diphenylimidazolium salts L3.12-R₁,R₂ and their starting reagents 3.10-R₁, 3.11-R₂	194
6.3b Cyclometallation of diphenylimidazolium salts L3.12-R₁,R₂ with {IrCp*} and {RhCp*}	203
6.3c General procedure for D-incorporation experiments.....	220
6.3d Transmetallation from Ag and Cu-NHCs with {IrCp*} and {RhCp*}	220
6.3e Preparation and study of acetate complexes 3.12a/b-R,R(OAc)	225
6.3f Synthesis of <i>meta</i> -substituted phenylimidazolium salts L3.18-R and their precursors 3.17-R	227
6.3g Cyclometallation of <i>meta</i> -substituted phenylimidazolium salts L3.18-R with {IrCp*} and {RhCp*}	231
6.4 Experimental procedures for Chapter 4	237
6.4a Synthesis of dibenzylimidazolium salts L4.10-R₁,R₂ and their precursors 4.9-R₂	237
6.4b Complexation of dibenzylimidazolium salts L4.10-R₁,R₂ with {IrCp*} and {RhCp*}	241
6.4c Cyclometallation of 4.10a/b-R₁,R₂	245
6.4d Procedures for deuterium incorporation experiments	255
6.4e Synthesis of <i>meta</i> -substituted benzylimidazolium salts L4.13-R	255
6.4f Complexation of <i>meta</i> -substituted benzylimidazolium salts L4.13-R with {IrCp*} and {RhCp*}	257
6.4g Cyclometallation of 4.13a/b-R	260
6.4h General procedure for deuterium incorporation experiments with 4.13a/b-R	264

6.5 Bibliography.....	265
Appendix.....	266

Abbreviations

NMR

br.d	broad doublet
br.s	broad singlet
d	doublet
dd	doublet of doublets
ddd	doublet of doublets of doublets
dt	doublet of triplets
m	multiplet
q	quartet
t	triplet
td	triplet of doublets
s	singlet
COSY	correlation spectroscopy
HMBC	heteronuclear multiple bond correlation
HSQC	heteronuclear single quantum correlation
Hz	Hertz
NMR	nuclear magnetic spectroscopy
NOE	nuclear Overhauser effect
NOESY	nuclear Overhauser effect spectroscopy
TOCSY	total correlation spectroscopy
ppm	parts per million
δ	Delta (NMR chemical shift)

Other techniques

DFT	density functional theory
ESI-MS	electrospray mass spectrometry
HRMS	high resolution mass spectrometry

Others

Å	Angstroms
AMLA	ambiphilic metal ligand activation
BIES	base-assisted internal electrophilic substitutions
<i>ca.</i>	circa (around/about)
cal	calories
<i>c.f.</i>	confer (compare)
Calcd.	calculated
CMD	Concerted-metallation deprotonation
DG	directing group
EA	electrophilic activation
E_{dist}	distortion energy
E_{int}	interaction energy
eq.	equivalents
<i>et al.</i>	and others
ΔG	Gibbs free energy change
$\Delta\Delta H$	enthalpy of activation
<i>i.e.</i>	id est (that is)
IES	internal electrophilic substitution
KIE	kinetic isotope effect
kcal mol^{-1}	kilocalorie per mole
kJ mol^{-1}	kilojoules per mole
LFER	linear free energy relationship
N.D.	not detected
OA	oxidative addition
OATS	oxidatively added transition states
OHM	oxidative hydrogen migration
rds	rate-determining step
ris	rate-influencing step
RE	reductive elimination
SBM	sigma-bond metathesis
S_{EAr}	electrophilic aromatic substitution
$S_{\text{E}3}$	trimolecular electrophilic aromatic substitution

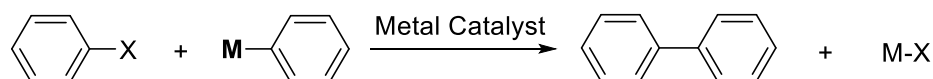
TS	transition state
Chemical	
acac	acetylacetonate
Cp	cyclopentadienyl anion
Cp*	1,2,3,4,5-pentamethylcyclopentadienyl anion
Cy	cyclohexyl
BArf	tetrakis[3,5-bis(trifluoromethyl)phenyl]borate]
DBU	1,8-Diazabicyclo[5.4.0]undec-7-ene
DCE	1,2-dichloroethane
DCM	dichloromethane
DDQ	2,3-dichloro-5,6-dicyano-1,4-benzoquinone
DMA	dimethylacetamide
DMBA	N,N-dimethylbenzylamine
DMF	dimethylformamide
DMSO	dimethyl sulfoxide
EtOAc	ethyl acetate
HOAc	acetic acid
mCPBA	<i>meta</i> -chloroperoxybenzoic acid
NHC	N-heterocyclic carbene
OAc	acetate
OTf	trifluoromethanesulfonate
PEPPSI	pyridine-enhanced precatalyst preparation stabilisation and initiation
PivOH	pivalic acid
<i>t</i> -AmOH	tertiary amyl alcohol
TFE	2,2,2-trifluoroethanol
THF	tetrahydrofuran
TMS	tetramethylsilane
Tp	tris(pyrazoyl)borate

Chapter One

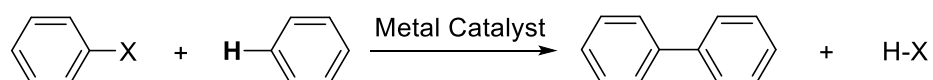
1.1 General introduction

The formation of C–Y (Y = C, O, N) bonds is a key part of the synthesis of new molecules and has seen huge advancement since the transition metal cross-coupling reactions (e.g. Suzuki, Stille, Negishi) were originally reported.¹⁻⁶ Cross-coupling reactions involve the coupling of an electrophile, such as an aryl halide, with an organometallic reagent, such as boronic acids, stannanes and others, by a transition metal catalyst, usually Pd(II) (**Scheme 1.1 i**). This approach requires pre-functionalisation of the substrates and produces MX waste that often can be toxic. An alternative is to use a C–H containing substrate which is coupled with one pre-functionalised coupling partner (**Scheme 1.1 ii**). Ideally two substrates with only C–H bonds are coupled (**Scheme 1.1 iii**) as this removes the need for substrate pre-functionalisation as well as reducing the quantity and toxicity of the waste produced. In addition, C–H functionalisation exploits relatively cheap substrates containing C–H bonds which are ubiquitous in nature.

i) Traditional cross - coupling



ii) C-H activation cross - coupling



iii) C-H activation



X = Cl, Br, I, OTf
M = B, Sn, Mg, Zn

Scheme 1.1: Comparison of cross-coupling reactions to C–H activation.

The challenges in C–H functionalisation are overcoming the inertness of the C–H bond and controlling the selectivity of C–H activation. The former can be solved by using transition metal catalysts, whilst selectivity control often requires employment of directing groups to functionalise a specific C–H bond, however, recently there has been

a lot of progress in overcoming this through non-directed C–H activation.⁷ Early examples of transition metal catalysed C–H activation were reported in the 1970s but the most significant developments in the area have happened in last 10 years.⁸ Various transition metal catalysts (Ru,⁹ Rh,¹⁰ Ir,¹¹ Pd,¹² and others^{13,14}) have been employed in catalytic C–H functionalisation reactions (e.g. arylations,¹² annulations,¹⁵ olefinations¹⁶, halogenations¹⁷). Nowadays, C–H functionalisation is a key part of synthetic chemistry with multiple applications in natural product and pharmaceutical synthesis.^{18-20,21-26} Overall, C–H functionalisation provides a greener approach than conventional cross-coupling reactions, and potentially enables the use of wide variety of substrates making these desirable reactions for synthetic chemistry. To further expand this area it is crucial to understand the mechanism(s) *via* which C–H activation takes place. The vast majority of papers in the area of C–H functionalisation focus on the practical applications of these reactions and will often include one or two mechanistic studies and a proposed mechanism. However, few papers are focussed specifically on the mechanism of C–H activation. The introduction of this thesis will focus on mechanisms of C–H activation and the experiments that can be done to distinguish different mechanisms.

1.2 Methods to study C–H activation mechanisms

The mechanism(s) of C–H bond activation have been investigated both experimentally and computationally.²⁷⁻³⁰ Some of the most common experimental methods to study C–H activation are (a) kinetic isotope effect (KIE), (b) deuterium incorporation to examine reversibility, and (c) competition experiments to examine electronic and steric influences, whilst (d) density functional theory (DFT) is the most popular computational method. Each of these is discussed briefly below.

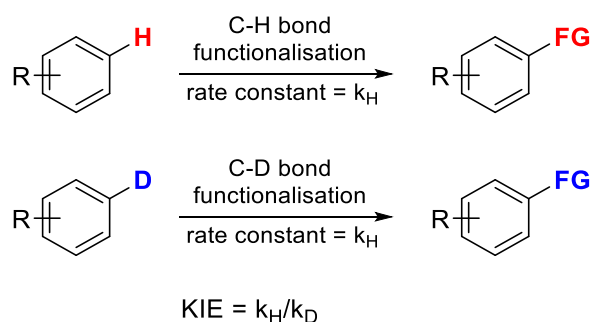
1.2a Kinetic isotope effect

A kinetic isotope effect is a result of different zero-point energies (the energy a molecule possesses in the ground vibrational state) when bonded to one isotope of an element compared to when bonded to another isotope of the same element.³¹ Kinetic isotope effects can provide insight on whether C–H activation is the rate-determining step (rds). H/D are the most common isotopes investigated in C–H activation reactions due to availability of deuterated substrates and relatively simple determination of KIE for H/D

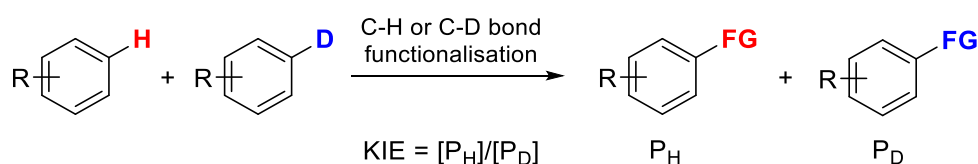
(DKIE). $^{12}\text{C}/^{13}\text{C}$ KIE can also be investigated but is rarely used due to the limited availability of ^{13}C enriched substrates and complicated measurement of $^{12}\text{C}/^{13}\text{C}$ KIE.^{32, 33}

In 2012 Hartwig summarised the three most popular DKIE experiments and discussed their interpretation. He pointed out that in principle the different types of experiment provide different information and that some data has been interpreted incorrectly in the literature.³⁴ The three different KIE experiments are (i) two pot two substrate reactions (parallel, **Scheme 1.2 type A**), (ii) one pot two substrate reactions (intermolecular competition, **Scheme 1.2 type B**) and (iii) one pot one substrate reaction (intramolecular competition, **Scheme 1.2 type C**).

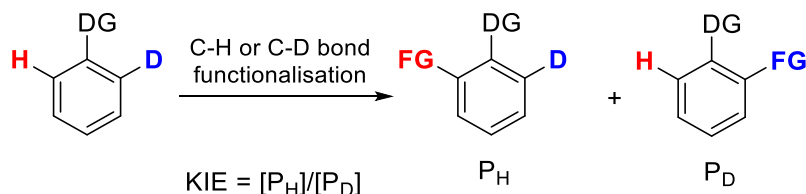
Type A: Comparing rates from two parallel reactions



Type B: Comparing yields from *intermolecular* competition



Type C: Comparing yields from *intramolecular* competition



Scheme 1.2: Three types of D kinetic isotope effect experiments.³⁴

Parallel reactions (**Scheme 1.2 type A**) have the substrate and deuterated substrate in different reaction vessels, so the reactions are performed separately. The rate constants for these experiments are determined independently and the ratio of the rate constants

(k_H/k_D) gives the DKIE value. The major limitation of this method is possible variability in reaction conditions and the precision of measurement of the individual rate constants. Additionally, this method is only meant to measure initial rates. In intermolecular competition experiments (**Scheme 1.2 type B**) protio and deuterio substrate are placed in the same reaction vessel and compete for reaction with limiting quantities of a substrate/reagent. The DKIE is usually determined by the ratios of the yields ($[P_H]/[P_D]$) of two formed products. This method ensures that each substrate is reacting under the same conditions. Additionally, only one measurement is required to determine the DKIE and yield ratios can be obtained at greater precision compared to parallel experiments. It will depend on the excess of other reagents whether the experiment is limited to determining only the initial rates. The third type of experiment is intramolecular competition between C–H and C–D (**Scheme 1.2 type C**). The DKIE is measured in same way as for intermolecular experiments by calculating the ratios of product formed ($[P_H]/[P_D]$). Intramolecular competition guarantees that competing reactions are under exactly same conditions and are relatively easy to perform with precise results.

Hartwig discusses several different reaction pathways to illustrate what information can be inferred from the different DKIE experiments. In the first example (**Figure 1.1 i**) C–H cleavage is a rate-determining and irreversible step. In this case a DKIE is expected to be observed for all three methods. In the second example the rds involves a substrate that does not undergo C–H activation. C–H cleavage in this example occurs after the rds step and is still irreversible (**Figure 1.1 ii**). As C–H activation is not the rds, the overall rate of reaction will not be affected by breaking of C–H or C–D bonds so no DKIE would be observed in parallel experiments. However, because the C–H activation step is irreversible the product yields ($[P_H]$ and $[P_D]$) are affected by the different rates of irreversible C–H/C–D activation, hence a DKIE will be observed with intermolecular and intramolecular competition experiments. In the third example the rds step involves the substrate that eventually will undergo C–H bond cleavage. C–H activation again occurs after the rds and is irreversible (**Figure 1.1 iii**). As C–H activation is not the rds a DKIE will not be observed with parallel experiments. No DKIE will be observed from an intermolecular experiment as the irreversible substrate binding step is now also the product-determining step. However, a DKIE will be observed from intramolecular experiment because H and D are on the same substrate and different rates of C–H and C–D cleavage will make irreversible C–H activation the product-determining step.

The last two examples both involve reversible C–H activation, in the fourth example C–H bond activation occurs before the rds step (**Figure 1.1 iv**). As C–H activation is reversible a large KIE will not be observed for any of the methods. A small DKIE could still be seen with all three methods in cases where the equilibrium concentration of species involved in the rds are strongly influenced by C–H/C–D elongation. Any DKIE observed then is due to an equilibrium isotope effect that depends on the rate of forward and backwards reactions.

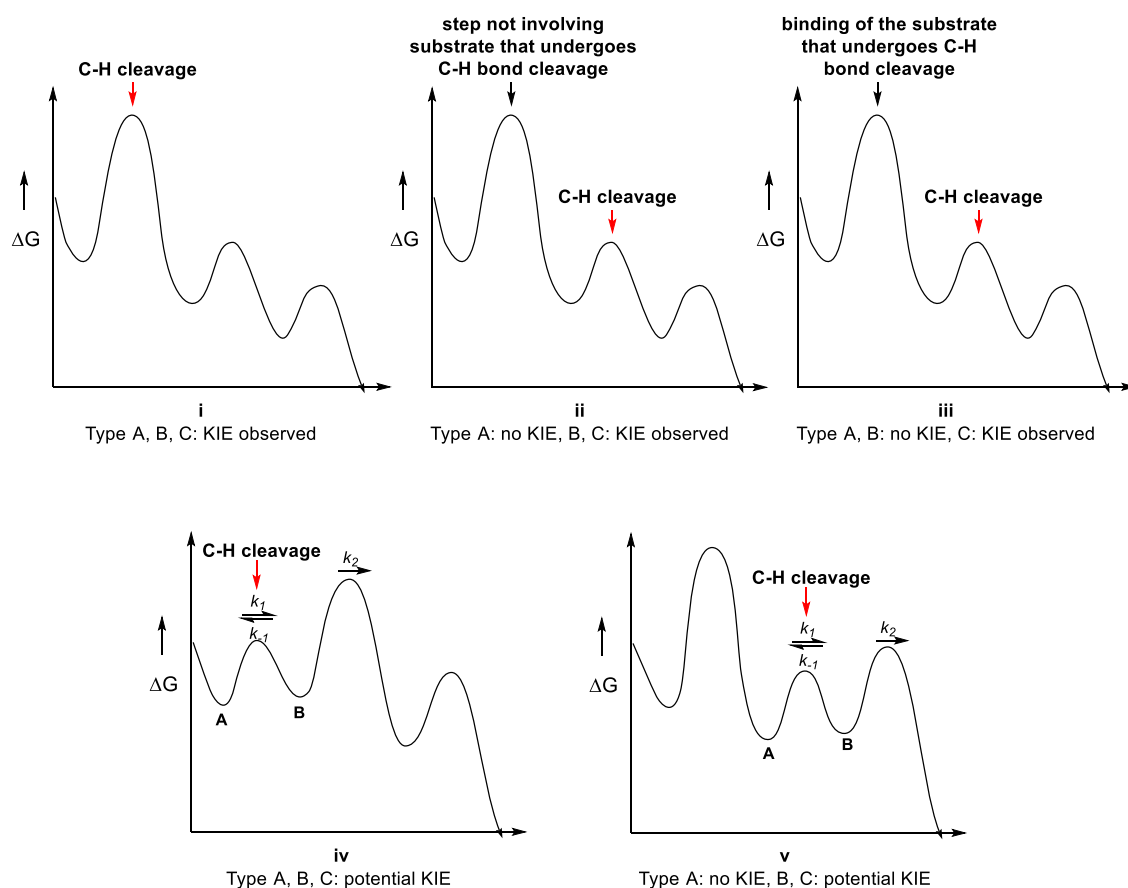


Figure 1.1: Different reaction pathways and DKIE observation for three types of experiments.³⁴

In the final example, the C–H activation step comes after the rds and is reversible (**Figure 1.1 v**), meaning that again no large DKIE will be observed from any of the experiments. As C–H activation occurs after the rds it does not affect the relative rate of reaction and no DKIE will be observed from a parallel experiment. However, replacement of a C–H bond with C–D bond could affect the equilibrium concentration and subsequent product formation step resulting in a small DKIE from intermolecular and intramolecular

experiments. To summarise parallel experiments are the only ones that can provide conclusive information on whether C–H bond activation is the rate-determining step.

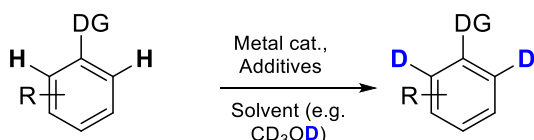
A DKIE for catalytic transformations can be determined but care has to be taken when interpreting results as catalytic reactions work “under steady-state conditions where the overall rate for each step is equal”. For this reason, a single step cannot be the rds.³⁵ In such cases the transition state with the highest barrier is referred to as turnover-limiting or turnover-determining transition state and the step associated with it is called the turnover-limiting step. An important point to note is that as a reaction progresses and the concentrations of reagents/intermediates/products are changing the turnover-limiting step can change during a reaction. Therefore, due to these complications intermolecular or intramolecular competition DKIE experiments should not be used to determine whether C–H activation is the turnover-limiting step. Even for parallel reactions whilst the presence of a DKIE means that C–H activation is the rate-determining step the converse *i.e.* no DKIE does not necessarily mean that C–H activation is not rate-determining. No DKIE would be observed even if C–H activation was the rds, if there was no significant elongation of C–H bond in the transition state. Additionally in a catalytic reaction more than one step may contribute to the overall rate leading to more complications when interpreting DKIEs.³⁴⁻³⁶ During this thesis, in cases where more than one step influences the overall rate such steps will be called rate-influencing steps (ris). Overall, an important distinction has to be made between rate-limiting step and product/selectivity-determining step, as whilst the product-determining step can be the rate-limiting step it does not have to be one.

1.2b H/D exchange

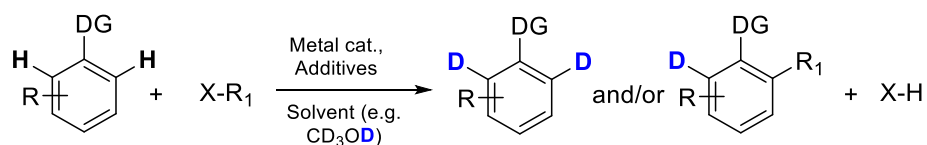
H/D exchange is another common method used to gain insight into the mechanism of C–H activation. It is used to determine whether the C–H activation step is reversible as well as the regioselectivity of the C–H activation step. One of the most common methods is performing the reaction in deuterated solvent without (**Scheme 1.3 i**) or with reagent (**Scheme 1.3 ii**) and analysing the product and unreacted starting material by ¹H (and ²H) NMR spectroscopy to assess the location and extent of any D-incorporation. Alternatively a deuterated substrate can be used and levels of H-incorporation can be measured.³⁷⁻³⁹ This works well if reactions are done in solvents that have readily available H or D to exchange such as alcohols and water, but for reactions done in solvents that do

not have readily available H/D (e.g. DCM, DCE, toluene) a lack of H/D exchange will not necessarily mean that C–H cleavage is not reversible. From reactions without substrate it can be concluded whether C–H activation is reversible, whilst reactions with substrate can additionally give information on rate of subsequent steps compared to the reverse of C–H activation.

i) Reaction without substrate



ii) Reaction with substrate



Scheme 1.3: Examples of deuterium incorporation/scrambling experiments.

1.2c Electronic effects

Investigation of electronic effects can provide important information on the mechanism of C–H activation. As above, electronic effects can only give information on steps that affect the overall rate, which may not be the C–H activation step. Any step involving the reactivity of the newly formed M–C bond would also be expected to be sensitive to the nature of any substituents. Hammett plots and the Hammett equation (1.1) have been established as a key means to interpret electronic effects.⁴⁰⁻⁴² Hammett equation represents a linear free-energy relationship relating reaction rate constants (k) or equilibrium reaction constants (K) with two parameters: a reaction constant and a substituent constant.

$$\log \frac{K_X}{K_H} = \rho\sigma \quad (1.1)$$

K_X = either a rate constant (k) or an equilibrium constant (K) for *meta* or *para* substituted arenes.

K_H = either a rate constant (k) or an equilibrium constant (K) for the corresponding unsubstituted arene.

ρ = the reaction constant, depends on the reaction and its conditions, slope (gradient) of Hammett plot is equivalent to the reaction constant.

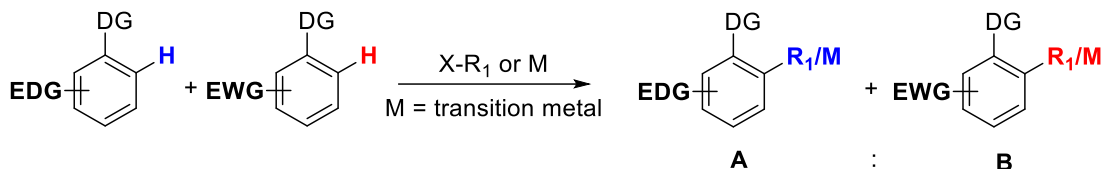
σ = the substituent constant for the corresponding position (*meta* or *para*), depends only on electronics of the substituent.

A Hammett plot is typically linear with either a positive or negative slope (ρ), the magnitude of which is an indicator of how sensitive a reaction is to the electronics of the substituents. A negative slope is a characteristic of development of positive charge at the reaction centre in the transition state of the rds, hence the rate of such reaction is enhanced by electron-donating substituents. A positive slope on the other hand is characteristic of development of negative charge and is enhanced by electron-withdrawing substituents. As will be mentioned later in the **section 1.4** and **Chapters 2-4** Hammett plots have been used in the mechanistic studies of the C–H activation reactions to aid the identification of the reaction mechanism.

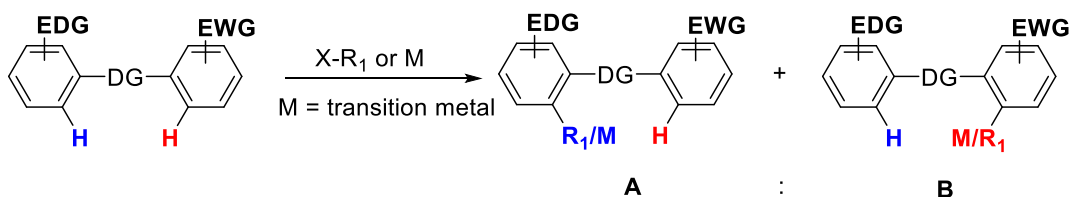
One of the most common methods used to look at electronic effects on C–H activation is intermolecular competition experiments between two substrates in the same pot (**Scheme 1.4 i**). During intermolecular competition two substrates with different electronic properties compete for a limited amount of another reactant. Ratios between the two products are then determined by NMR spectroscopy and reflect the relative reactivity of the two arenes. This type of competition experiment will be discussed in more detail in **Chapter 2**. The second type of competition experiment is an intramolecular one involving a substrate with two different R groups (**Scheme 1.4 ii**).⁴³ In an intramolecular competition if a ligand binding step is the first step it will be the same for both rings and so should not affect selectivity. This method ensures that the different substituents will affect the C–H activation step but the interpretation may be dependent on whether C–H activation is rate determining. Intramolecular competition reactions will be discussed in more detail in **Chapter 3**. Another possible intramolecular competition is between two hydrogens on the same arene ring with two different R groups at *meta* positions relative to the directing group (DG) (**Scheme 1.4 iii**). The main problem with this competition

experiment is that the difference in steric bulk of the substituents can have a larger effect than any electronic difference.

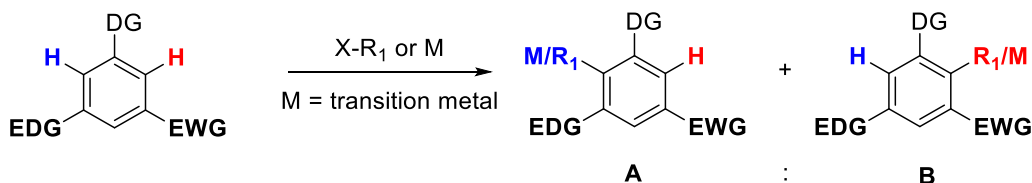
i) Intermolecular competition between two substrates



ii) Intramolecular competition between two arene rings



iii) Intramolecular competition between two H positions



Scheme 1.4: Different one-pot competition experiments to probe electronic selectivity.

1.2d Computational studies

Computational studies, especially use of DFT have proven to be an invaluable tool in studying the mechanisms of C–H activation.^{28, 44-46} Computational studies can provide information on transition states, intermediates and other species that are either short-lived or impossible to observe experimentally. The calculations can provide an energy profile for the reaction, though it should be borne in mind that concentration effects may also influence the overall experimental pathway.

DFT calculations are commonly used due to their ability to give reliable results in a reasonable time. In general calculating absolute energies is quite difficult with DFT and the use of different functionals gives different absolute energies, however different functionals usually give the same trends for related substrates. Calculating solvent effects is now routine though it should be noted that it usually involves modelling the dielectric of the solvent and not specific solvation. Modelling specific solvation is in principle

possible but is impractical in terms of the time required.^{45,47} Recently (in the last 5 years or so) consideration of dispersion effects has been shown to be important for accurate modelling of reaction profiles.^{28, 48}

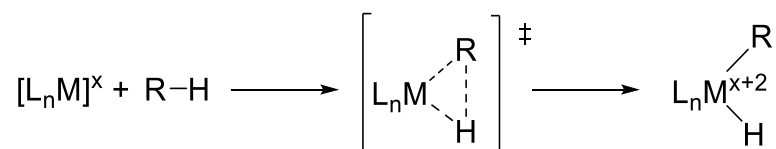
Davies, Macgregor and McMullin in their 2017 review discussed the challenges of modelling inorganic metal salts MX (often used as bases) in organic solvents.²⁸ Metal salts are often considered as a discrete molecular ion-pair MX, which is at best a simplification. In addition, it is rarely known experimentally how additives interact with the catalyst or substrate hence any calculations dealing with the effects of additives need to be treated with some caution.^{28, 49,50} Finally calculations require input of mechanistic hypotheses and so thoroughness of the calculations is dependent on the user input.⁴⁶ Therefore ideally DFT calculations would be paired with experimental studies so that the calculations can be benchmarked against real experimental data.²⁸

1.3 Mechanisms of C–H activation up to 2005

The mechanisms of metal catalysed C–H functionalisations have been investigated both computationally and experimentally. By 2005 the five most commonly proposed C–H activation mechanisms were: (i) oxidative addition, (ii) σ -bond metathesis, (iii) 1,2–addition, (iv) electrophilic activation including electrophilic aromatic substitution, and (v) radical mechanism. The main features of each mechanism, except radical which is not discussed further, are outlined below.

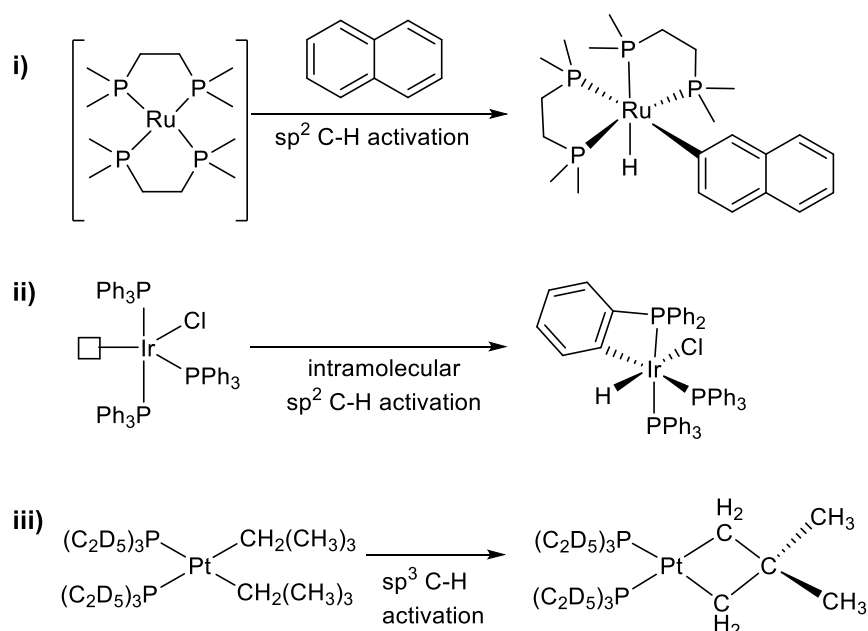
1.3a Oxidative addition

In oxidative addition (OA) C–H bond cleavage occurs *via* a three-membered transition state with formation of new M–C and M–H bonds (**Scheme 1.5**). This leads to an increase of the oxidation state and coordination number of the metal by two units. Therefore, the OA requires electron rich and low valent metal centres and is most commonly observed with late transition metals (e.g. Os(II), Rh(I), Ir(I), Pd(II)).⁵¹ During the reaction the elongation and then cleavage of the C–H bond is the rds step hence large DKIEs are usually observed. H transfer onto the metal is one of the defining features of OA.⁵¹⁻⁵³



Scheme 1.5: Mechanism of oxidative addition with three-membered transition state.

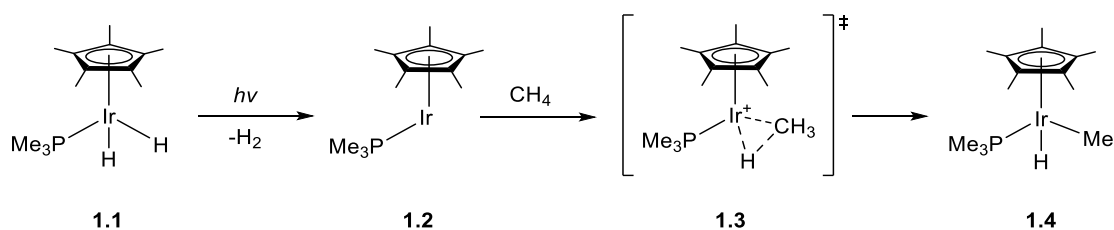
The first example of C–H activation *via* OA involved activation of a naphthalene C–H sp^2 bond with Ru(0) and was reported by Chatt and Davidson in 1965 (**Scheme 1.6 i**).⁵⁴ Later Bennett and Milner published intramolecular Ir(I) sp^2 C–H activation of a triphenylphosphine (**Scheme 1.6 ii**).⁵⁵ Whitesides and Foley reported Pt(II) intramolecular OA to an sp^3 C–H bond (**Scheme 1.6 iii**).⁵⁶



Scheme 1.6: i) First OA reported by Chatt and Davidson,⁵⁴ **ii)** intramolecular sp^2 OA with Ir,⁵⁵ **iii)** intramolecular sp^3 OA with Pt.⁵⁶

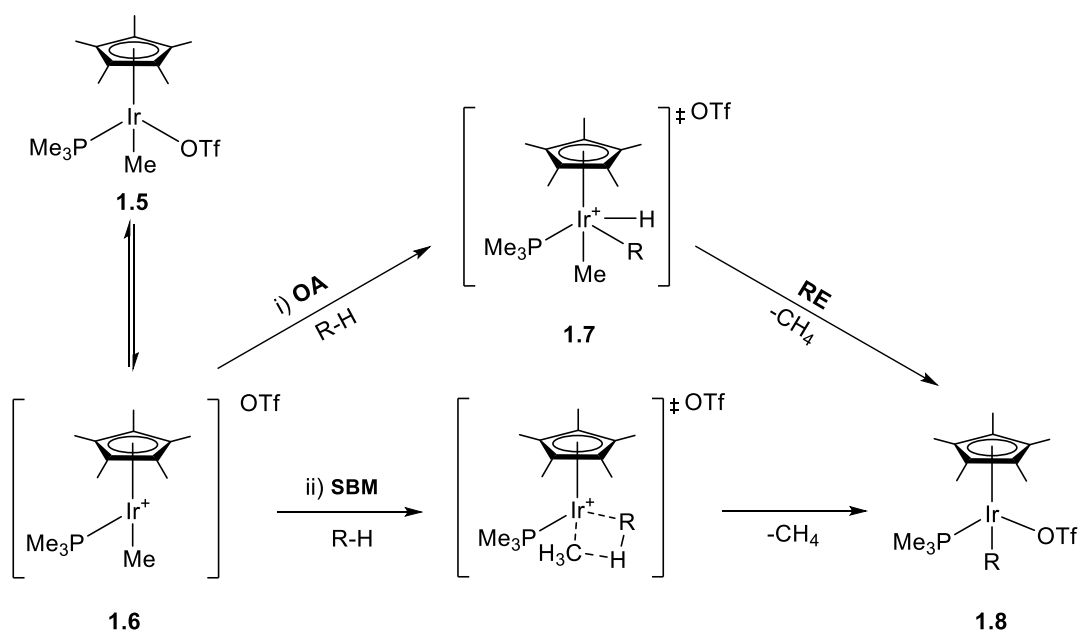
The early studies of intermolecular C–H activation by OA were carried out in the mid-1980s by the Bergman,⁵⁷ Graham⁵⁸ and Jones⁵⁹ groups using saturated 18-electron complexes $[MH_2LCp^*]$ ($M = Ir, Rh$; $L = CO, PMe_3, PPh_3$) or $[Ir(CO)_2Cp^*]$. Detailed studies showed that formation of reactive 16-electron species $[MLCp^*]$ ($M = Ir, Rh$; $L = CO, PMe_3, PPh_3$) was essential before C–H activation could take place.^{60–62} Thus, photolysis of $Ir(H_2)(Cp^*)(PMe_3)$ (**1.1**) gives **1.2** that can undergo OA of methane to give Ir(III) complex **1.4** *via* a transition state (TS) **1.3** (**Scheme 1.7**).^{57, 63} At the same time

Graham *et al.* demonstrated that the less electron-rich $\{\text{Ir}(\text{CO})\text{Cp}^*\}$ fragment can also undergo the OA with methane.⁵⁸



Scheme 1.7: Photolysis of $\text{Ir}(\text{H}_2)(\text{PMe}_3)(\text{Cp}^*)$ and subsequent OA with methane.⁶³

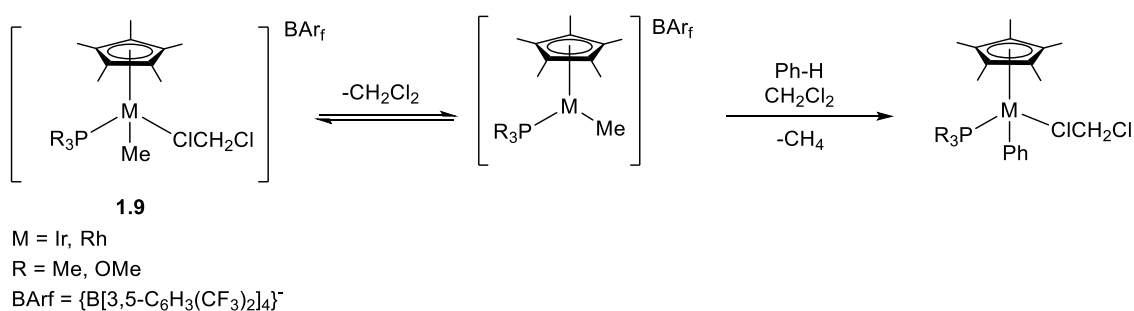
Bergman *et al.* demonstrated that even an Ir(III) complex $[\text{IrMe}(\text{OTf})(\text{PMe}_3)\text{Cp}^*]$ (**1.5**) can be used to activate C–H bonds of alkanes under mild conditions.⁶⁴ Two possible mechanisms were proposed: i) the OA of R–H to the cationic Ir(III) complex **1.6** to give Ir(V) species **1.7** that after reductive elimination (RE) of methane forms **1.8** or ii) concerted σ -bond metathesis (**Scheme 1.8**).⁶⁴



Scheme 1.8: C–H activation of alkanes with $\{\text{IrMe}(\text{PMe}_3)\text{Cp}^*\}$.⁶⁴

The rate of reaction was shown to depend on the ease of triflate dissociation and the formation of the 16-electron species **1.6**.⁶⁵ Hence, the related complex **1.9** ($\text{M} = \text{Ir}$) (**Scheme 1.9**) reacted faster than **1.5** due to easier dissociation of CH_2Cl_2 and less coordinating BARf $\{\text{B}[3,5\text{-C}_6\text{H}_3(\text{CF}_3)_2]_4\}$ compared to triflate. Additionally, in the case of the Ir complexes **1.9** ($\text{R} = \text{Me}, \text{OMe}$), reaction of the more electron donating PMe_3

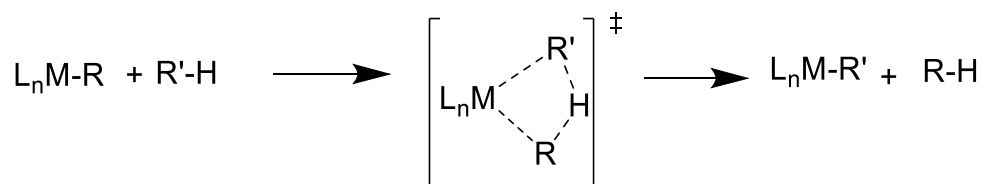
complex was 30 times faster than the P(OMe)₃ complex which was ascribed to easier dissociation of CH₂Cl₂ from more electron rich PMe₃ complex suggesting that this step is the rds rather than C–H activation.⁶⁶ For the analogous Rh complexes **1.9** (R = Me, OMe), the rate of reaction for the PMe₃ and P(OMe)₃ complexes were about the same suggesting that in this example faster dissociation in the PMe₃ complex is offset by faster C–H activation in P(OMe)₃ complex.⁶⁵ Computational studies by Hall and Niu showed that for the reaction of [IrMe(PMe₃)Cp]⁺ the σ-bond metathesis pathway is higher in energy compared to OA.⁶⁷



Scheme 1.9: OA of an Ir or Rh complex after CH₂Cl₂ dissociation.^{65, 66}

1.3b σ-bond metathesis

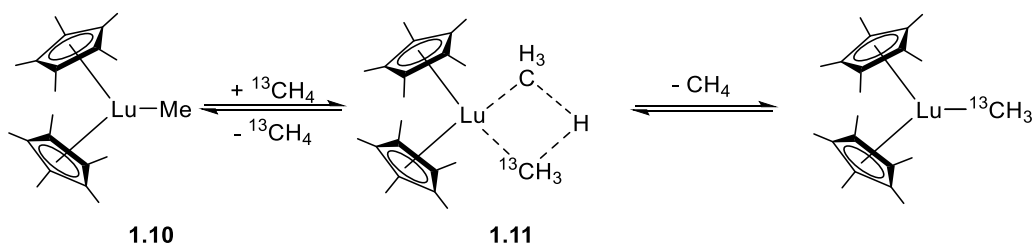
The σ-bond metathesis (SBM) mechanism proceeds *via* breaking of M–R and C–H σ-bonds and formation of M–C and R–H σ-bonds (also called [2σ + 2σ] cycloaddition) *via* a concerted 4-centre 4-electron transition state (**Scheme 1.10**). Complexes that undergo SBM usually consist of electron-poor high valent d⁰ transition metal or lanthanide complexes. These metals have no d-electrons so cannot react *via* OA. SBM often has a significant KIE indicating a high degree of C–H cleavage in the transition state.^{52, 68, 69}



Scheme 1.10: Mechanism of σ-bond metathesis.

Watson in 1983 reported one of the first well-studied examples of SBM of a C–H bond of methane by a lanthanide complex.⁷⁰ The authors proposed that exchange of a methyl group in [LuMe(Cp*)₂] **1.10** with ¹³CH₄ occurred *via* a four-membered transition state

1.11 (Scheme 1.11). Following this it was shown that organolanthanides can activate other sp^3 and sp^2 C–H bonds and this topic has been reviewed.⁷¹ Bercaw *et al.* demonstrated that $[\text{ScRCp}^*_2]$ (R = alkyl, aryl) complexes undergo similar reactions with a range of substrates containing sp , sp^2 , sp^3 C–H bonds.⁷² Initially it was proposed that the transition state for SBM reactions may be relatively non-polar⁷² but later computational studies by Eisenstein *et al.* found that bonding in the transition state is actually rather polarised ($\text{M}^{\delta+} - \text{C}^{\delta-}$).⁶⁹

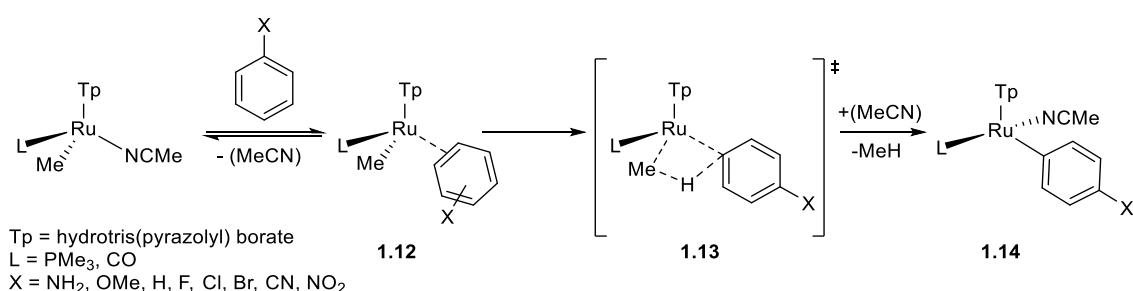


Scheme 1.11: SBM of $\text{LuMe}(\text{Cp}^*)_2$ with $^{13}\text{CH}_4$.⁷⁰

Lin, Eisenstein and co-workers carried out computational studies on methane activation with $[\text{TpM}(\text{Me})(\text{PH}_3)]$ (Tp = hydrotris(pyrazolyl)borate, M = Fe, Ru, Os) complexes.⁷³ ⁷⁴ Calculations demonstrated that barriers for the C–H activation follow the order $\text{Fe} > \text{Ru} > \text{Os}$. For Fe and Ru complexes the four-membered transition states were computed whilst for Os a three-membered OA transition state was found. In addition, for Fe complexes the C–H activation was found to proceed in one step with a short Fe–H distance (1.53 Å). This showed some Fe–H bonding which indicated oxidative character in the TS. Computed transition states demonstrated that late transition metals often show an M–H bond, therefore, Lin called these “oxidatively added transition states” (OATS) mechanism.⁷⁴

Goddard *et al.* published a computational study on the arylation of ethene with benzene catalysed by $[\text{IrPh}(\text{acac})_2(\text{pyridine})]$. The reaction was shown to proceed *via* a four-membered SBM-like transition state and not OA. However, a short Ir–H bond distance (1.58 Å) was observed suggesting oxidation at the metal centre so the authors termed this an “oxidative hydrogen migration” (OHM) mechanism.⁷⁵ Gunnoe *et al.* published experimental and computational studies on C–H activation with $[\text{TpRuMe}(\text{L})(\eta^2\text{-C}_6\text{H}_5\text{X})]$ **1.12** that produces methane and $[\text{TpRu}(p\text{-C}_6\text{H}_5\text{X})(\text{L})]$ **1.14** (L = CO, PMe_3 ; X =

NH₂, OMe, H, F, Cl, Br, CN, NO₂) (**Scheme 1.12**). The reaction was proposed to go by a SBM mechanism *via* transition state **1.13**.^{76, 77}

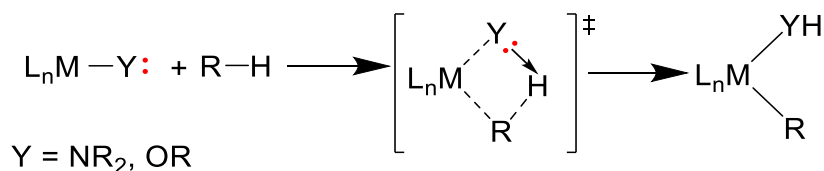


Scheme 1.12: C₆H₅X C–H activation by {TpRu}.^{76, 77}

Overall, OATS (proposed by Lin⁷⁴) and OHM (proposed by Goddard^{78, 79}) can be considered as a sub-classes of SBM that exhibit some oxidative character. Vastine and Hall studied mechanisms of SBM, OATS, OHM and OA/RE and proposed that the SBM and the OA/RE are two extremes of the continuum with the sub-classes being somewhere in the middle.⁸⁰

1.3c 1,2-addition

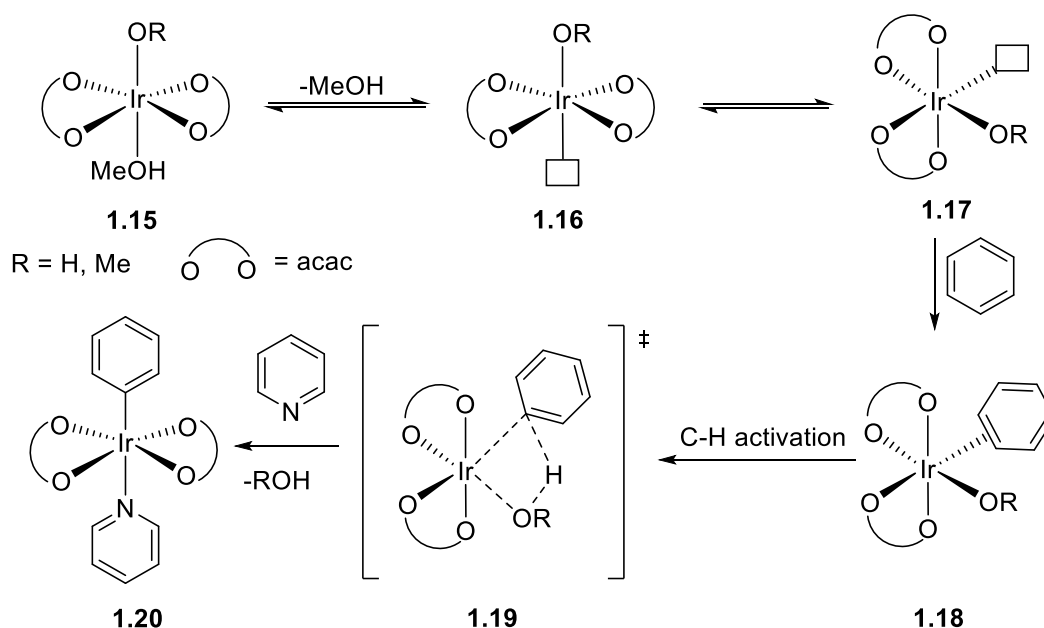
There are two types of 1,2-addition: i) addition of C–H to an M=X bond – usually favoured by early/middle transition metals⁸¹ and ii) addition of C–H to a late transition metal M–Y bond (Y is formally mono-anionic ligand such as amido or alkoxy that possess at least one lone pair) (**Scheme 1.13**).⁸¹ Only the latter will be discussed here. The 1,2-addition to an M–Y bond occurs *via* a four-centre transition state just like the SBM. However, unlike in SBM, in 1,2-addition the Y ligand's lone pair is involved making it overall a 4-centre 6-electron TS compared to the 4-centre 4-electron TS of SBM. In this case the Y ligand receives a proton and so acts as an intramolecular base.⁸¹



Scheme 1.13: Mechanism of 1,2-addition into a M–Y bond.

The first examples of the 1,2 addition to an M–Y bond were reported by Periana *et al.*⁸² and Gunnoe *et al.*⁸³ independently in the mid 2000s. Periana's group demonstrated that

Ir complex **1.15** (R = Me) can activate the C–H bonds of benzene to form **1.20** (Scheme 1.14). The proposed mechanism involved the loss of MeOH (**1.16**) followed by *trans* to *cis* isomerisation (**1.17**), then benzene coordination (**1.18**). Methoxide then acts as an intramolecular base to deprotonate benzene (**1.19**) and the replacement of MeOH with pyridine forms product **1.20**. When C₆D₆ was used instead of benzene CH₃OD formation was observed indicating that methoxide does abstract H/D from benzene.⁸²



Scheme 1.14: Proposed mechanism for Ir alkoxide activation of benzene.⁸²

Based on computational studies with **1.15** (R = H) it was tentatively suggested that the reaction goes *via* a four-membered SBM TS.⁸⁴ However, further studies by Periana's group concluded that the reaction proceeds *via* an electrophilic metal attack on benzene with deprotonation by alkoxide; they termed this Internal Electrophilic Substitution (IES).⁸⁵ No M–H bonding interaction is observed in the TS and M–Y (Y = O, N) bond cleavage and Y–H bond formation are not based on the same orbital, therefore, the process is intrinsically different from SBM.⁸⁵

Gunnoe's group reported [TpRu(Y)(PMe₃)₂] (Y = OH) (**Figure 1.2**) catalysed H/D exchange with benzene.⁸⁶ From kinetic studies they proposed that PMe₃ first dissociates to give a 5-coordinate Ru species which then undergoes 1,2-addition with benzene.^{76, 86} Subsequent studies of the same reaction with [TpRu(Y)(PMe₃)₂] (Y = OPh, NHPH, SH, Cl, OTf) demonstrated that H/D exchange was only plausible when Y = OH or NHPH.

Therefore, the authors concluded that the basicity of the ligand receiving the H affects the ease of the C–H activation step.^{86, 87} The mechanism resembled SBM, however, computational studies on benzene activation by 16-electron [TpRu(Y)(PMe₃)] (Y = Me, NH₂, OH) demonstrated that there is significant variation in transition states depending on the Y ligand (**Figure 1.2**).³³ When Y = NH₂, OH (heteroatoms with available lone pairs) the C–H activation barriers were lower with longer Ru–H distances, but when Y = Me the Ru–H bond was shorter suggesting oxidative character. Therefore, they concluded that when Y = Me the reaction goes *via* OHM, whilst when Y = NH₂ or OH it goes *via* 1,2-addition.⁸⁶

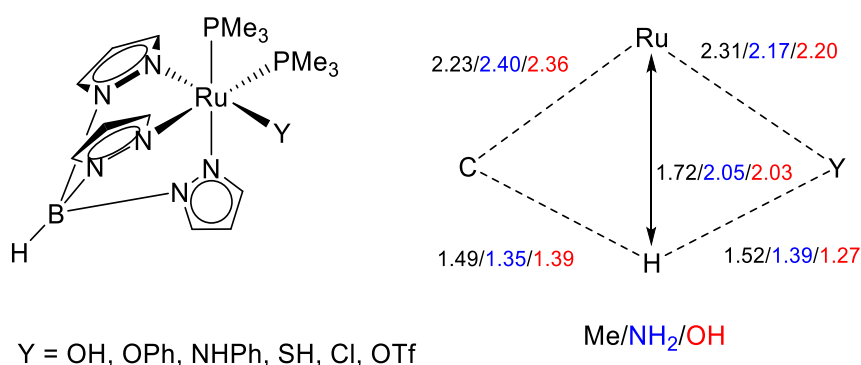


Figure 1.2: Bond distances for transition states for [TpRuY(PMe₃)₂] mediated C–H activation of benzene, Y = Me, NH₂, OH, distances in Å.⁸⁶

In conclusion, the 1,2-addition mechanism discussed in this section proceeds with late transition metal alkoxy/amide complexes. The transition state is four-membered and similar to a SBM transition state with the key difference being the involvement of heteroatom lone pairs in the 1,2-addition. The 1,2-addition mechanism (including IES) to M–Y can also be called AMLA-4 mechanism (discussed later in the chapter).

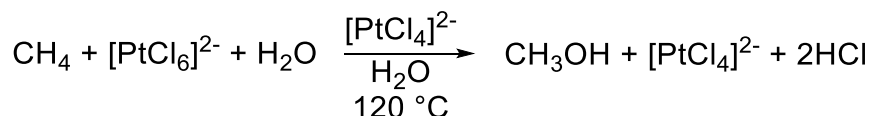
1.3d Electrophilic activation

In general electrophilic activation (EA) with metals proceeds *via* attack of an electron-poor late transition metal (Pd, Pt) on an electron-rich carbon atom with proton loss and generation of new metal-carbon bond (**Scheme 1.15**).^{51, 52}



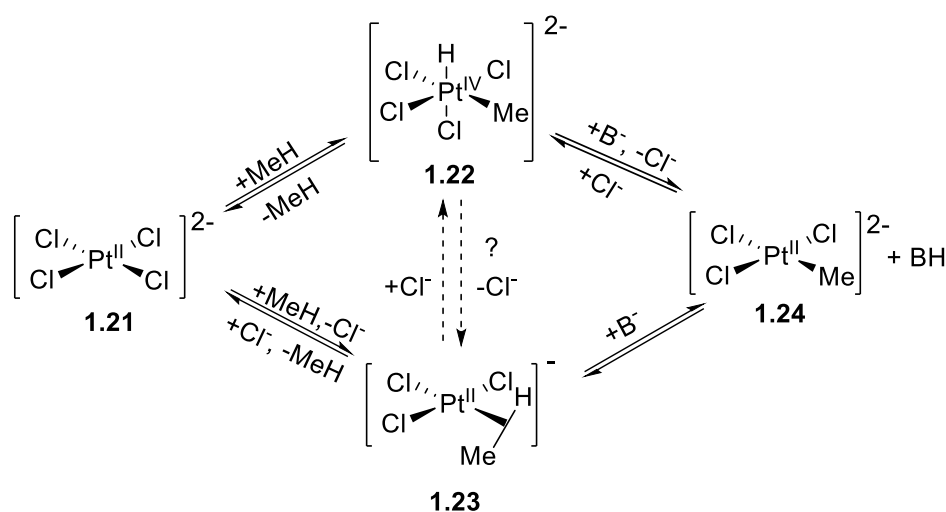
Scheme 1.15: Mechanism of electrophilic substitution.

One of the first examples of the methane C–H activation that was proposed to go *via* EA was published in 1969 by Shilov *et al.* and involved methane oxidation to methanol by a Pt^{II}–Pt^{IV} system (**Scheme 1.16**).⁸⁸ The reaction was catalytic in Pt^{II} but stoichiometric in Pt^{IV} due to it being an oxidant, making this method expensive. This Pt^{II}/Pt^{IV} system is now called the Shilov system.⁸⁸⁻⁹¹



Scheme 1.16: Shilov system used for oxidation of methane.⁸⁸

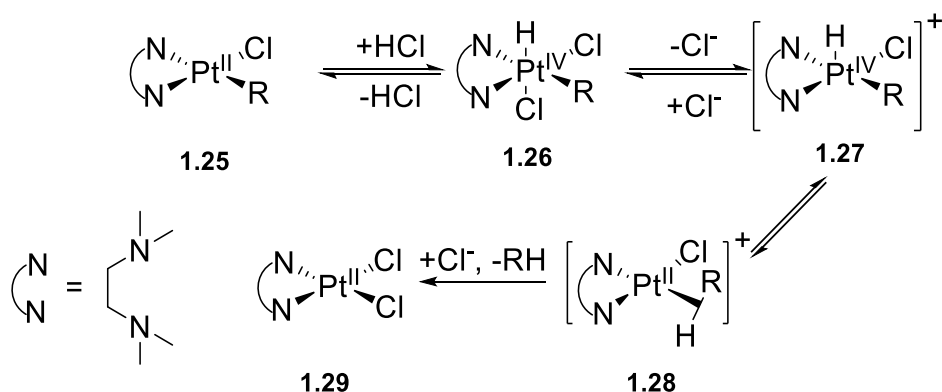
Two different mechanisms were proposed for the electrophilic activation of methane by Pt (**Scheme 1.17**). The first pathway involves oxidative addition of methane to Pt^{II} complex **1.21** to form Pt^{IV} complex **1.22** and then deprotonation to give Pt^{II} complex **1.24**. A second pathway involves deprotonation of Pt alkane – σ – adduct **1.23** to give complex **1.24**.



Scheme 1.17: Two proposed mechanisms for electrophilic C–H activation by Pt^{II}.^{88,92}

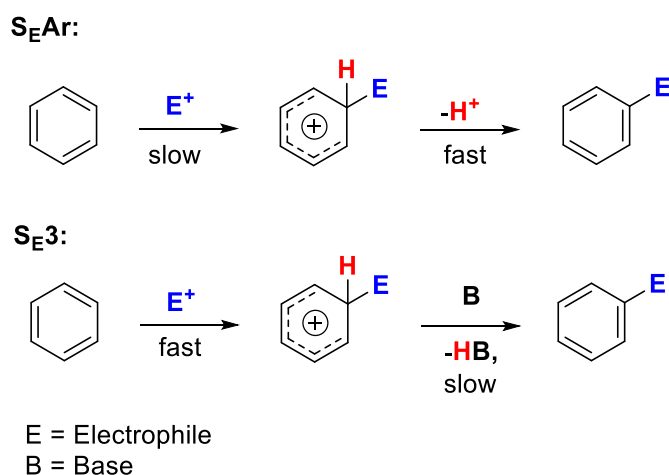
Mechanistic and computational studies supporting both routes have been published.^{92, 93} Experimental investigations of the Shilov system are difficult due to the harsh reaction conditions (120 °C). Therefore, mechanistic studies have concentrated on investigating the reverse reaction: i.e. protonolysis of Pt^{II} complexes **1.25** (**Scheme 1.18**). In this reaction HCl (or solvent) addition to Pt complex **1.25** generates Pt^{IV} species **1.26** that upon loss of chloride forms **1.27**. Reductive elimination then gives the σ -adduct **1.28** and

is followed by an irreversible alkane dissociation. In a deuterated solvent (DCI) H/D incorporation was observed into the alkyl position implying that equilibration between **1.27** and **1.28** has to occur before alkane elimination.^{94, 95} This suggests that both proposed Pt^{II} and Pt^{IV} complexes are intermediates,⁹¹ therefore, suggesting further that Pt catalysed methane oxidation might occur *via* OA rather than electrophilic activation.



Scheme 1.18: Proposed mechanism for alkylplatinum(II) complexes formation.⁹²

A subsection of electrophilic activation is electrophilic aromatic substitution (S_{EAr}), which as the name implies is only applicable to activation of aromatic compounds. For a long time it was also assumed to be the mechanism for late transition metal (e.g. Pd^(II)) based C–H functionalisation of aromatic substrates.⁸⁸ Traditionally, electrophilic aromatic substitution (**Scheme 1.19** S_{EAr}) is thought of as a two-step process, namely electrophilic attack on the arene to form a cationic arenium (Wheland) intermediate (also called a σ -complex), which is then followed by a proton abstraction to form the product. The formation of an arenium ion is the rds which happens without significant C–H elongation and so usually no DKIE is observed for the S_{EAr} .⁹⁶ In the Wheland intermediate the ring is de-aromatised and the positive charge is delocalised. As electron donating groups stabilise positive charge, S_{EAr} reactions work best with such substituents. In general, electron poor arenes (e.g. perfluorobenzenes) either require harsh conditions or do not react *via* S_{EAr} altogether.⁹⁷



Scheme 1.19: General mechanisms for electrophilic aromatic substitution reactions.

It has been noted that in some cases addition of base is necessary for electrophilic aromatic substitution reactions. These are called trimolecular electrophilic substitution (S_E3) reactions and they are often base catalysed.⁹⁸ During the S_E3, a C–E bond is formed relatively quickly with the subsequent deprotonation leading to product formation being the slow step (**Scheme 1.19 S_E3**). As deprotonation is the rds it leads to a significant elongation of the C–H bond, hence a DKIE is usually expected.⁹⁸ Generally in the past C–H activation reactions with Pd²⁺ were proposed to go *via* an electrophilic mechanism, however, if carbonate, carboxylate or phosphate additives are present then the reaction may go *via* a different mechanism (see below).

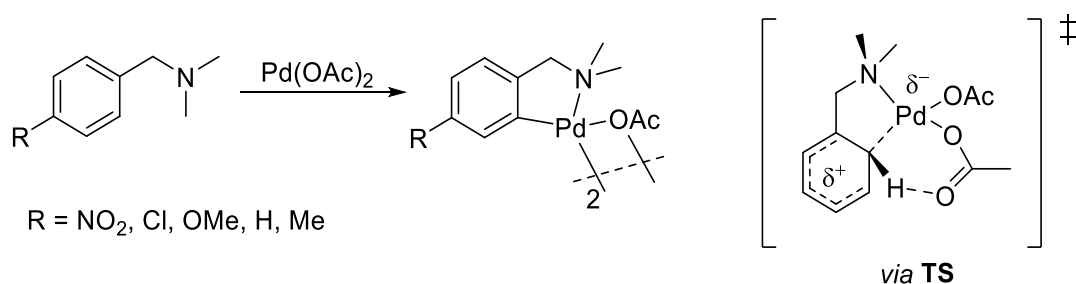
1.4 AMLA/CMD

One of the most recently proposed metal C–H activation mechanisms involves an electrophilic type activation but with the assistance of a coordinating base usually carboxylate. The mechanism was first proposed with Pd⁹⁹⁻¹⁰¹ and then later on with Ir¹⁰² and then Rh and Ru half-sandwich complexes.^{27, 103 104, 105} This section will outline some of the key studies and the historical development of this mechanism first with Pd and non-half sandwich Ir complexes then with Ir and Rh half-sandwich complexes.

1.4a AMLA/CMD at Pd/Ir

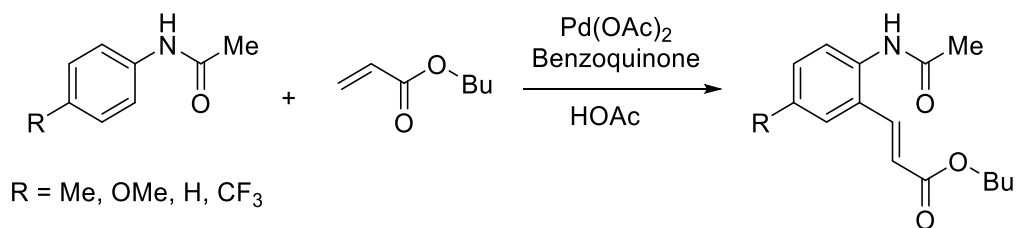
In 1985 Ryabov *et al.* published kinetic studies of cyclometallation of dimethylbenzylamines (DMBA) with Pd(OAc)₂ (**Scheme 1.20**).¹⁰⁶ In acetic acid a DKIE

of 1.1 was observed and substrates with electron-withdrawing substituents were favoured over those with electron-donating groups. Additionally, a good correlation was observed with σ_p but not with σ_m . This indicated that the electronic effects observed were not representing C–H activation (occurring at *meta* position to the substituent) but rather protonation of DMBA in acetic acid. In contrast, in chloroform a DKIE of 2.2 was observed indicating that C–H bond cleavage is involved in the rds. This illustrates that the step affecting product formation may vary depending on the reaction solvent. In addition, for reactions carried out in chloroform substrates with electron-donating substituents were now kinetically favoured with the Hammett plot having a slope of -1.6, which the authors ascribed to an S_EAr pathway. The relatively low DKIE was thought to indicate an intramolecular early-transition state in which the Pd–C bond is being formed whilst the C–H bond is just starting to elongate. The enthalpy and entropy of activation (11 kJ mol^{-1} and -254 kJ mol^{-1} respectively) were in support of a highly ordered six-membered Wheland transition state (**Scheme 1.20**).^{106, 107}



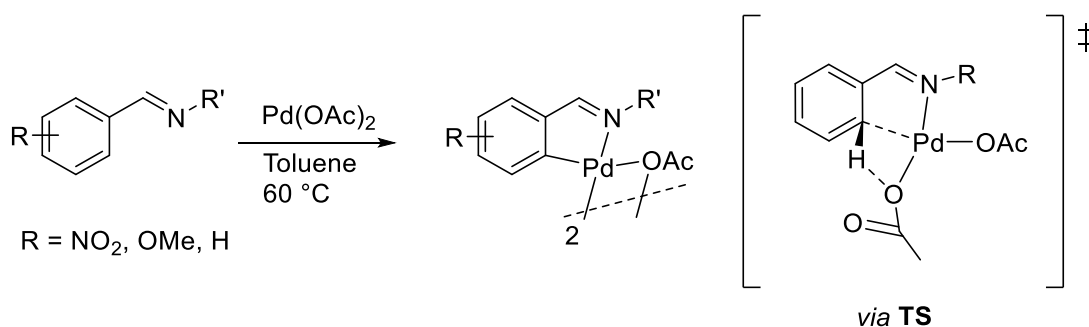
Scheme 1.20: Cyclometallation of Pd(OAc)₂ with substituted DMBA and Wheland transition state proposed by Ryabov *et al.*¹⁰⁶

One of the early catalytic reactions in the presence of carboxylates (reported in 2002) was the oxidative coupling of anilides with olefins catalysed by Pd(OAc)₂ (**Scheme 1.21**).¹⁰⁸ The presence of carboxylate at the Pd centre was shown to be crucial for the catalysis and the addition of chloride sources (NaCl, HCl) hampered the reaction. The authors concluded that this is caused by chloride coordinating to the Pd centre instead of acetate. The competition experiments showed that substrates with electron-donating substituents reacted faster with a Hammett plot slope of -2.2. A DKIE of 3.0 indicated that C–H activation is involved in the rds. Based on this the authors suggested that reaction proceeds *via* a Wheland transition state.



Scheme 1.21: Pd(OAc)₂ catalysed anilides coupling with olefins.¹⁰⁸

In 1997 Gomez, Martinez and co-workers published a mechanistic study of the reactions of Pd(OAc)₂ with various substituted imines to produce five-membered palladacycles (Scheme 1.22).¹⁰⁹ Unlike the two examples above, the reactions were relatively insensitive to electronic effects. The activation entropies (-100 to -180 kJ mol⁻¹) indicated a highly-ordered transition state and the authors proposed that the C–H activation proceeds *via* a four-membered TS with acetate acting as an internal base (Scheme 1.22).



Scheme 1.22: Cyclopalladation of imines and proposed transition state by Gomez, Martinez *et al.*¹⁰⁹

In 2000 Sakaki *et al.* published DFT studies of the intermolecular activation of benzene and methane by M(η^2 -O₂CH₂)₂ and M(PH₃)₂ (M = Pd, Pt).¹¹⁰ The calculations showed that with M(η^2 -O₂CH₂)₂ all of the reactions were exothermic whilst with M(PH₃)₂ (M = Pd, Pt), only the activation of benzene with Pt was slightly exothermic, whilst the other reactions were endothermic. The C–H activation of benzene and methane with M(η^2 -O₂CH₂)₂ each proceed through a concerted six-membered TS (Figure 1.3 TS shown for benzene) in which the Pd–C bond is forming whilst the C–H bond is breaking. The formate assists the deprotonation by hydrogen bonding to the C–H bond of benzene or methane. Formation of the TS for benzene activation with M(η^2 -O₂CH₂)₂ has a significantly lower activation energy (E_a = 16.1 and 21.2 kcal mol⁻¹ for M = Pd, Pt

respectively) than the C–H activation by $M(\text{PH}_3)_2$ ($E_a = 28.4$ and $17.1 \text{ kcal mol}^{-1}$ for $M = \text{Pd}, \text{Pt}$ respectively) which proceeds *via* oxidative addition.¹¹⁰

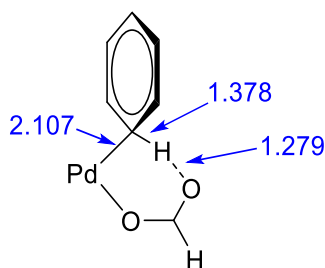


Figure 1.3: TS proposed for benzene activation by $\text{Pd}(\text{OAc})_2$.¹¹⁰ Bond distances in Å.

In 2005 Davies and Macgregor published a DFT study on the cyclopalladations of dimethylbenzylamines reported by Ryabov.⁹⁹ Three transition states were investigated: oxidative addition, a four-membered ring similar to that proposed by Martinez *et al.*¹⁰⁹ and a six-membered ring similar to that proposed by Ryabov (**Figure 1.4 1.30A-C** respectively). The latter was shown to be the most accessible out of the three (activation energy = 25.7 , 34.3 and 13 kcal mol^{-1} **1.30A** and **1.30B** and **1.30C** respectively).

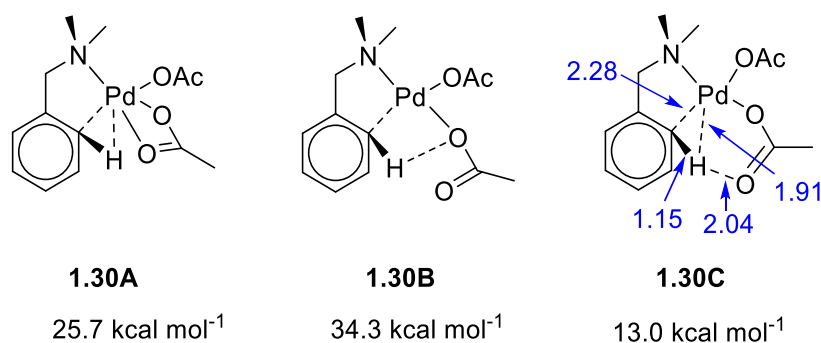
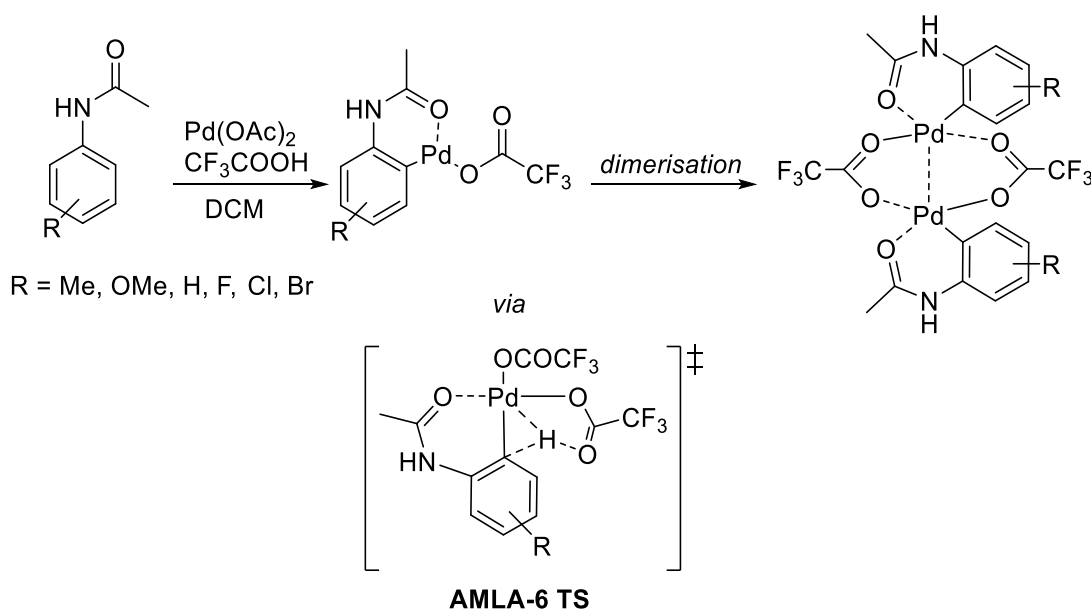


Figure 1.4: Computed transition states for cyclopalladation of DMBA–H.⁹⁹ Bond distances in Å.

For TS **1.30C** the calculations showed no evidence of an increase in positive charge on the benzene ring being activated, hence TS **1.30C** is not a Wheland transition state as originally proposed by Ryabov. A short Pd–H distance (1.91 Å) and a slightly elongated C–H bond (1.15 Å) implies formation of an agostic complex with the unbound oxygen of acetate hydrogen bonding to the H. The agostic Pd–C interaction polarises the C–H bond making the H more acidic and easier to transfer to acetate, simultaneously acetate hydrogen bonding creates a more electron rich C–H bond which facilitates the agostic interaction. Later this mechanism was termed ambiphilic metal ligand activation

(AMLA) emphasising the synergistic metal and ligand effect.²⁷ The TS **1.30C** corresponds to the rds and involves only a slight elongation of the C–H bond giving a calculated DKIE of 1.2 consistent with the small DKIE (2.2) observed experimentally. In addition, the activation energy of the C–H bond is lower with electron-donating substituents, therefore, some selectivity towards electron-donating groups is expected as evident by a negative slope in the experimental Hammett plot.²⁷

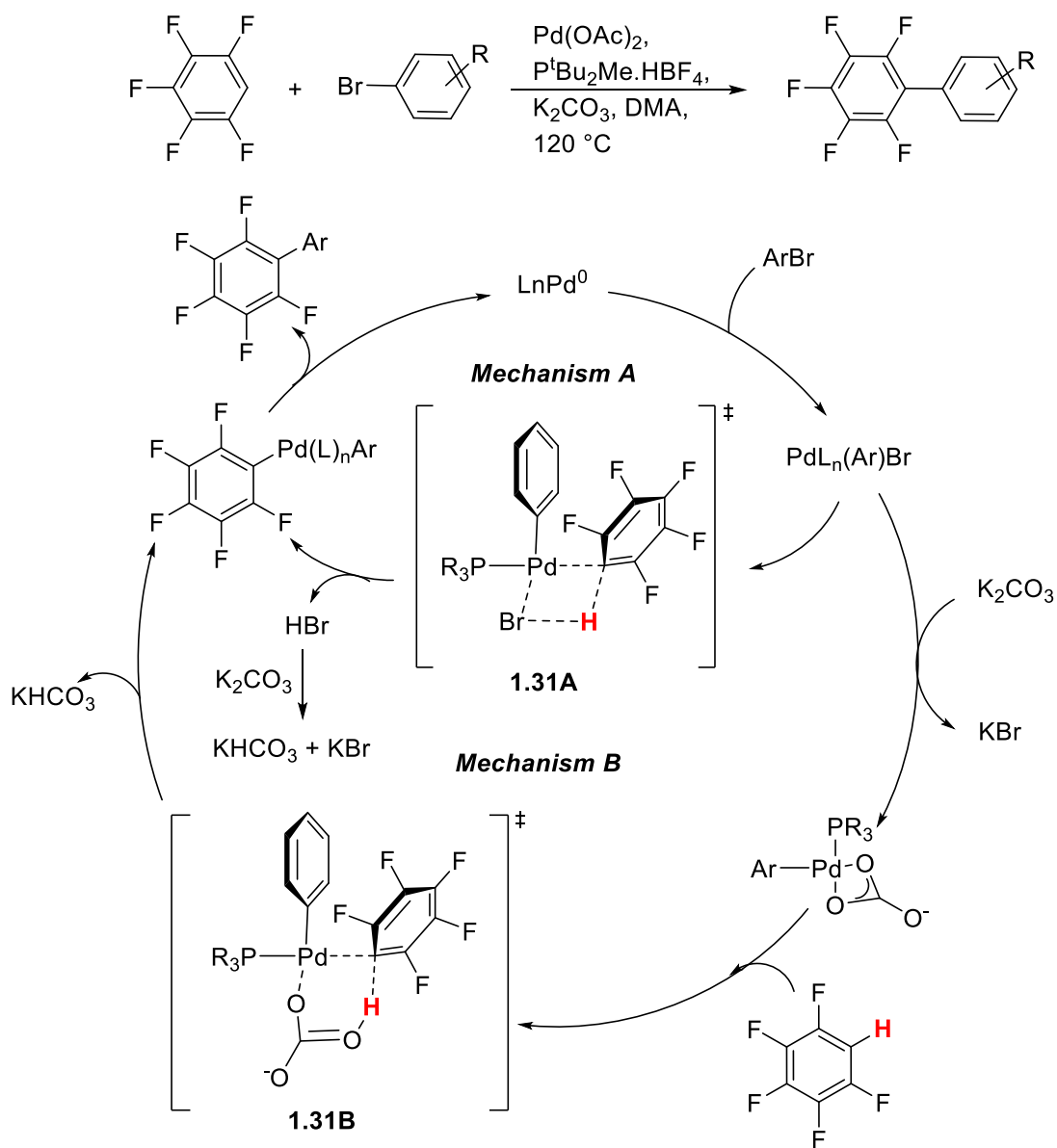
Very recently a computational and experimental study was reported for C–H activation of *meta*- and *para*-substituted acetanilides by Pd(OCOCF₃)₂ (**Scheme 1.23**).¹¹¹ The formation of organopalladium species in the reaction mixtures were monitored using ESI-MS and UV–vis spectroscopy and this data was used to produce a Hammett plot. Linear Hammett plots were obtained with slopes (ρ) of -1.5 for ESI-MS, -1.6 for UV–vis which were in agreement with the computed value of -1.7. The DFT calculations indicated that C–H activation is taking place *via* an agostic AMLA-6 TS and not a Wheland-type TS supporting that electron-donating groups can be favoured in an AMLA C–H activation.



Scheme 1.23: C–H activation of acetanilides by Pd(OCOCF₃)₂ and agostic TS.¹¹¹

The field of catalytic non-directed C–H activation was pioneered by Fagnou’s group. They reported the first Pd catalysed intermolecular arylation of perfluoroarenes (**Scheme 1.24**, top).¹⁰⁰ DFT calculations were performed but no pathway was located for OA or S_EAr. Instead, two possible pathways **A** and **B** (**Scheme 1.24**) were computed. The first mechanism involves formation of a four-membered TS **1.31A** with a coordinated

bromide accepting the proton. The second mechanism proceeds *via* formation of a six-membered concerted transition state with the carbonate hydrogen bonding to the C–H (**Scheme 1.24 1.31B**). The TS for mechanism **B** had a lower activation barrier compared to mechanism **A** (9.9 and 23.7 kcal mol⁻¹ respectively) and therefore this was the mechanism favoured by the authors.

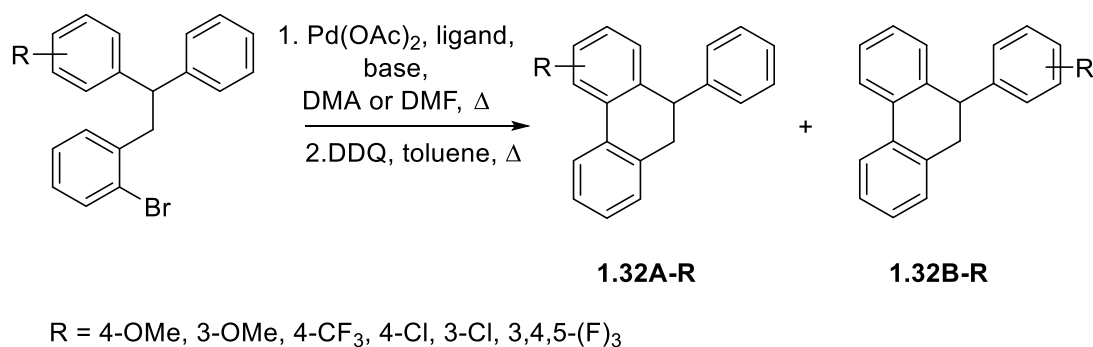


Scheme 1.24: Arylation of perfluorinated benzene and possible reaction mechanisms.¹⁰⁰

Another study by Fagnou's group showed that the addition of pivalic acid enhanced the reaction.¹¹² DFT calculations showed that the energy of the C–H activation TS with a pivalate anion was lower compared to a carbonate anion (24.9 cf. 26.2 kcal mol⁻¹). The

authors concluded that catalytic pivalate transfers a proton from arene to the stoichiometric carbonate.

At about the same time, Echavarren and co-workers reported several studies of Pd catalysed intramolecular arylation *via* a proton abstraction (**Scheme 1.25**). The substrates used had two potential C–H activation sites on the substituted ring to give products **1.32A-R** and on the unsubstituted ring to give products **1.32B-R**. In general, cyclisation on substituted rings was marginally favoured even with electron withdrawing groups (F, Cl, CF₃) which is incompatible with S_EAr.¹¹³ No reaction was observed in the presence of Et₃N or DBU (and later on NaH, Na₂HPO₄, NaH₂PO₄) as a base, but high conversions were achieved with K₂CO₃ (and later with KHCO₃, K₃PO₄).^{114, 115} In addition, large intramolecular DKIEs of 5-6.7 were observed indicating that C–H bond cleavage is involved in the rds.



Scheme 1.25: Selected substrates used in Pd catalysed intramolecular arylation.¹¹⁴

DFT calculations were used to investigate three possible mechanisms: i) with the coordinating bromide acting as a proton acceptor (**Figure 1.5 1.33A**), ii) intramolecular assistance by bicarbonate (**Figure 1.5 1.33B**) and iii) intermolecular assistance by bicarbonate (**Figure 1.5 1.33C**). In the first mechanism, the activation energy barrier (43.3 kcal mol⁻¹) for the TS is very high and is also inconsistent with the observation that the reaction only proceeds with certain bases. Whilst replacement of bromide with HCO₃⁻ gave a significantly lower activation barrier for the intramolecular assisted pathway **1.33B** (23.5 kcal mol⁻¹) and intermolecular pathway **1.33C** (17.4 kcal mol⁻¹) both of which were shown to be consistent with the experimentally observed preference for the electron-withdrawing substituents.^{113,114}

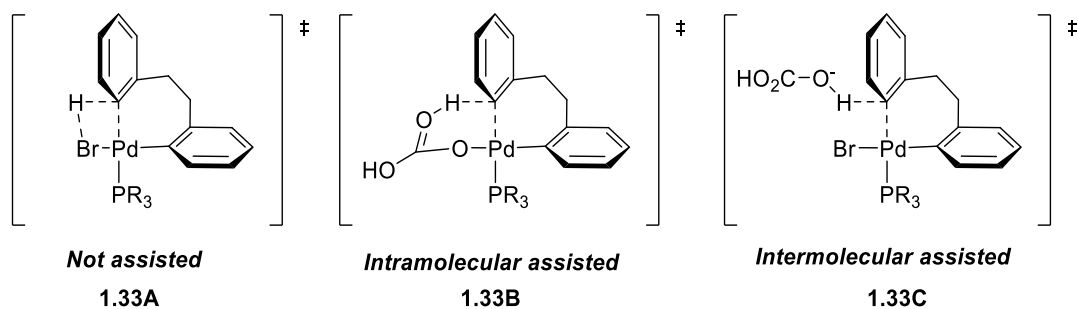


Figure 1.5: Investigated transition states for the Pd catalyzed intramolecular arylations.¹¹³

Similarly to Pd, the mechanism of intermolecular C–H activation of benzene at $[\text{Ir}(\text{acac})_2(\text{OAc})]$ was investigated and a DFT study was reported by Ess *et al.*¹⁰⁴ The reaction proceeds through an acetate-assisted activation and formation of either a four or six-membered TS (**Figure 1.6**). For the four-membered TS the C–O bond lengths are quite different (1.35 and 1.21 Å) whereas, in the six-membered TS they are quite similar (1.25 and 1.28 Å). The latter has a lower distortion energy (discussed below) resulting in a more favourable formation of a six-membered TS ($\Delta G^\ddagger = 25.4 \text{ kcal mol}^{-1}$) compared to the four-membered TS ($\Delta G^\ddagger = 44.7 \text{ kcal mol}^{-1}$). The authors called this mechanism an internal electrophilic substitution.¹⁰⁴ The four- and six-membered transition states are very similar to AMLA-4 and AMLA-6 transition states.

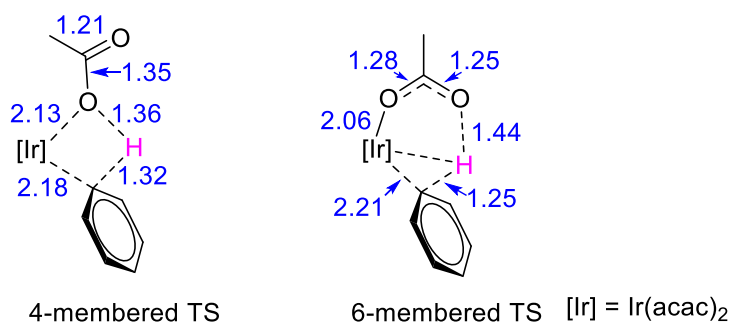
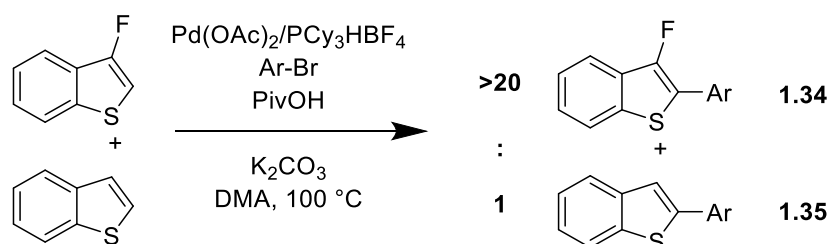


Figure 1.6: Computed TSs for acetate assisted benzene activation by $[\text{Ir}(\text{acac})_2(\text{OAc})]$. Bond distances in Å.¹⁰⁴

Fagnou's group also studied the arylation of thiophenes with Pd.¹⁰¹ A competition experiment between 3-fluorobenzothiophene and benzothiophene favoured formation of the more electron deficient **1.34** compared to the **1.35** (**Scheme 1.26**). Further investigation of other arenes also showed preference for more electron deficient arenes. To gain insight into the reaction mechanism the DFT calculations were carried out and

showed that there was almost no charge delocalised in the aromatic ring and aromaticity was retained for all the substrates investigated. This, and a preference for the reaction with electron deficient arenes indicated that the reaction does not go *via* an S_EAr mechanism. For all substrates DFT calculations predicted a six-membered concerted intramolecular TS and an example of it for benzene is shown in **Figure 1.7**. The authors termed this base assisted mechanism concerted-metallation deprotonation (CMD).



Scheme 1.26: Competition between benzothiophenes.¹⁰¹

The substrate reactivity in the CMD mechanism was analysed by Fagnou and Gorelsky *et al.* using an activation-strain analysis (**Figure 1.7**).¹⁰¹ Two key factors were found to be involved; distortion energy (E_{dist}) and interaction energy (E_{int}). E_{dist} is the energy cost resulting from distortion of the catalyst and arene geometry from the ground state (**Figure 1.7 I and II**) to the transition state (**Figure 1.7 III and IV**) whilst the electronic interaction energy E_{int} is the energy gain from the formation of TS **V** from **III** and **IV**. The analysis showed that π electron rich arenes benefit from a large and negative E_{int} but have large E_{dist} penalties. Electron poor arenes do not benefit from a large E_{int} but due to facile distortion have small E_{dist} penalties making the TS relatively accessible. This explains why fluorinated benzothiophene reacts faster than its unsubstituted counterpart. The presence of the fluorine has little effect on E_{int} but leads to decreased E_{dist} compared to benzothiophene resulting in lower activation energy and a faster reaction.¹⁰¹ Hence, the activation energy is a result of the trade-off between distortion energy (E_{dist}) and interaction energy (E_{int}) indicating that the preference of electron rich or poor substrates will depend on the energy offset. Therefore both electron rich and electron deficient substrates could be favoured by the CMD pathway.

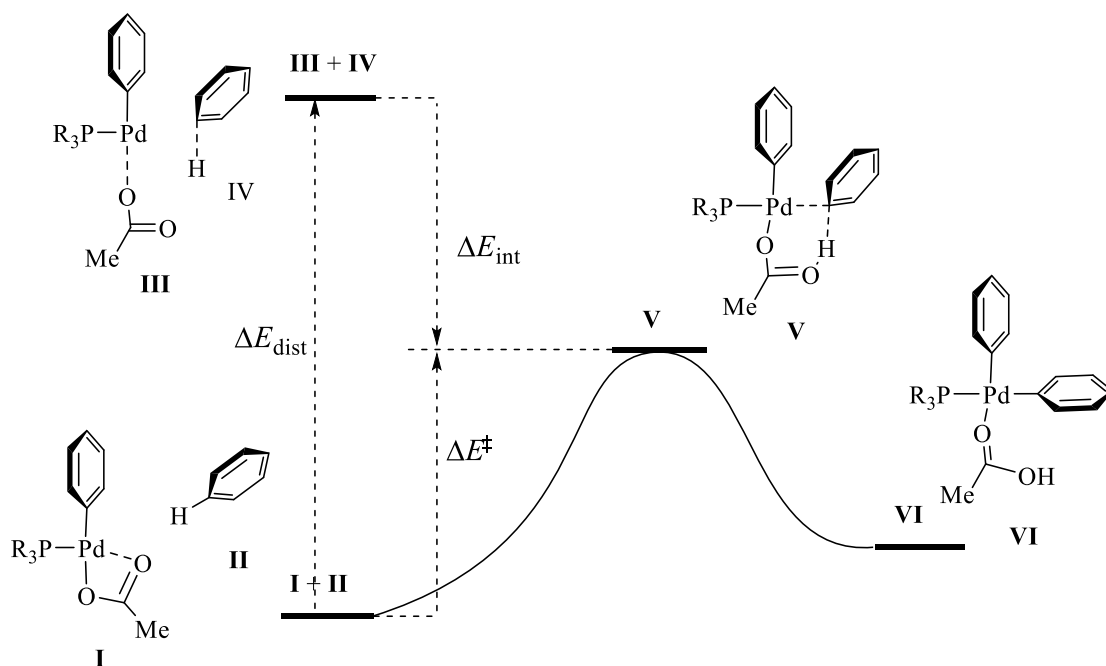


Figure 1.7: CMD pathway for benzene showing ΔE_{dist} , ΔE_{int} , and ΔE .¹⁰¹

Additional distortion-interaction analysis of a wide range of arenes concluded that arenes and heteroarenes can be classified into three categories (**Figure 1.8**).¹¹⁶ For class I arenes the regioselectivity is governed by the difference in the distortion energies ΔE_{dist} . For example, benzothiophene reacts at C2–H and not C3–H because of the lower distortion energy of arylation at C2–H compared to C3–H (37.5 and 39.8 kcal mol⁻¹ respectively). For Class II arenes ΔE_{int} controls regioselectivity. For example for arylation of furan the C2–H position is more reactive than the C3–H position because of a larger ΔE_{int} gain (-44.8 compared to -40.0 kcal mol⁻¹). For the third class of arenes the regioselectivity is controlled by both distortion and interaction energies. For example, thiophene C2–H is more reactive than C3–H because of lower E_{dist} (by 1.9 kcal mol⁻¹) and more negative E_{int} (by 3.6 kcal mol⁻¹).¹¹⁶

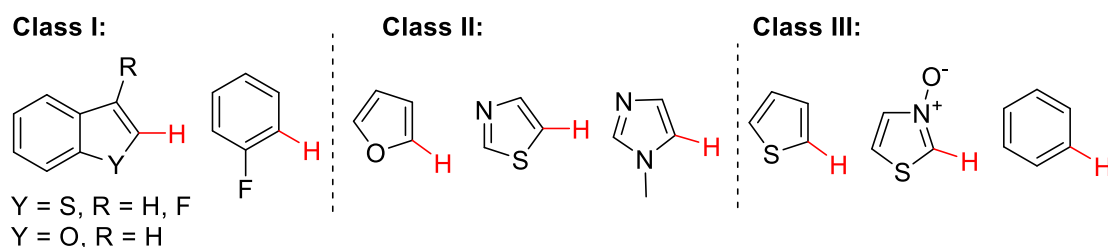


Figure 1.8: Examples of arenes from the three categories based on distortion-interaction analysis.¹¹⁶ Red bonds correspond to the site of arylation.

In 2012 Ess and co-workers published a DFT study on the regioselectivity of non-direct Pd C–H activation.¹¹⁷ Substrates from the three categories of arenes reported by Gorelsky *et al.* (**Figure 1.8**) were chosen and their respective (ArH)(PMe₃)Pd(OAc) complexes and their formation *via* a CMD TS **1.36** were modelled (**Figure 1.9**). In general, the calculations showed that the lowest energy TS corresponded to the most stable Pd-aryl intermediate (**Figure 1.9**). This also implies that the strongest C–H bond will be activated as it will lead to the most thermodynamically stable Pd–C bond.¹¹⁷

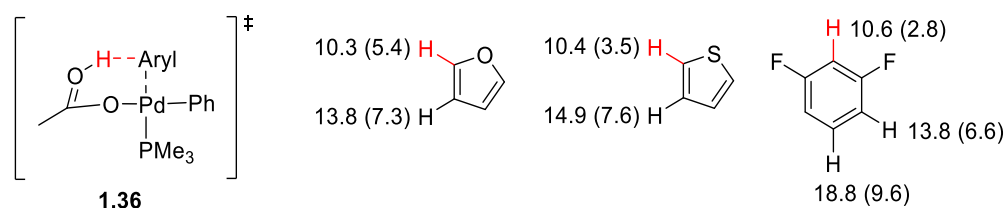


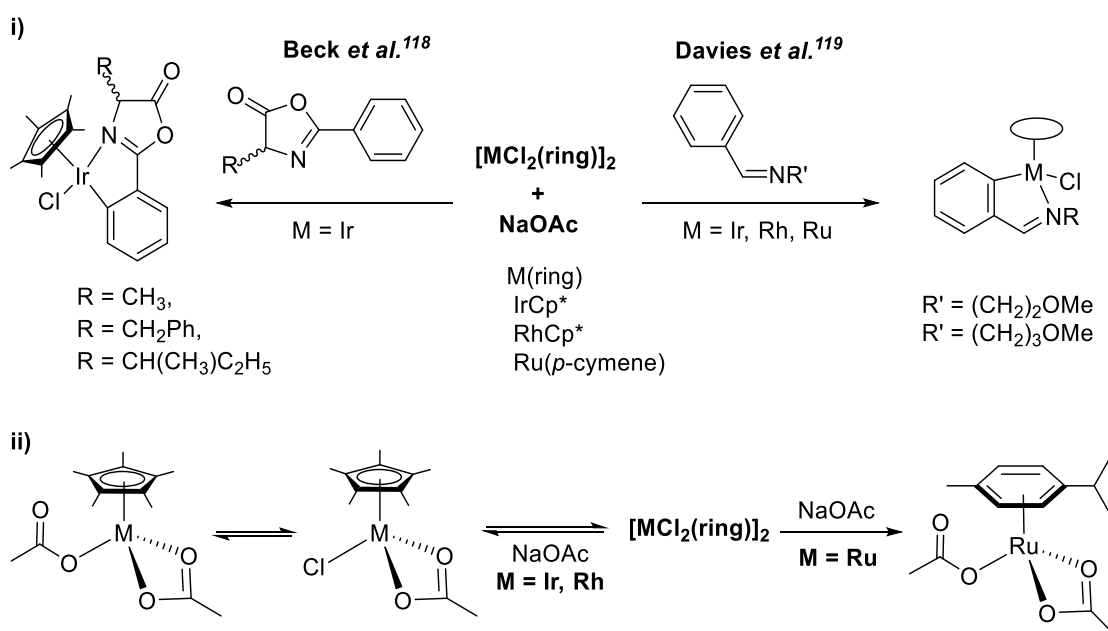
Figure 1.9: Computed Pd-Aryl TS and selected examples of arenes studied, their C–H bond activation energies and Pd aryl thermodynamics (in parentheses).¹¹⁷ Energy values given in kcal mol⁻¹. Red bonds correspond to the site of arylation.

1.4b AMLA/CMD at Half-Sandwich Ir and Rh Complexes

After AMLA/CMD was proposed for acetate-assisted C–H activation reactions with Pd⁹⁹⁻¹⁰¹ the mechanism was also investigated with half-sandwich complexes primarily of Ir, Rh and Ru.^{27, 103 104, 105} This section will focus on Ir and Rh and will outline some of the key mechanistic investigations first of stoichiometric and then catalytic reactions.

1.4bi Stoichiometric AMLA/CMD at Half-Sandwich Ir and Rh Complexes

In 1998 Beck *et al.* reported the first acetate assisted cyclometallation with $[\text{IrCl}_2\text{Cp}^*]_2$ (**Scheme 1.27 i**).¹¹⁸ In 2003 Davies *et al.* demonstrated similar reactions with Ir, Rh and Ru half-sandwich complexes with benzylamines and imines which occur at room temperature (**Scheme 1.27 i**).¹¹⁹ The reactions did not proceed in the absence of NaOAc even when Et_3N was added as a base. This indicates that acetate acts as more than just a base (Note, Et_3N and NaOAc are unable to deprotonate starting imines). All three metal dimers react with NaOAc in the absence of a substrate (**Scheme 1.27 ii**).¹¹⁹



Scheme 1.27: i) Early examples of cyclometallations of half-sandwich Ir, Rh, Ru in the presence of sodium acetate.^{118,119} ii) reaction of $[\text{MCl}_2(\text{ring})]_2$ with sodium acetate.

119

Davies, Macgregor and co-workers in 2006 investigated the DMBA cyclometallation with $[\text{IrCl}_2\text{Cp}^*]_2$ using DFT calculations.¹⁰² $[\text{Ir}(\text{DMBA})(\text{OAc})(\text{Cp})]^+$ species was computed to be the precursor to C–H activation. Three transition states were investigated: OA, 1,2-addition and an acetate-assisted electrophilic mechanism which the authors later called AMLA (**Figure 1.10**). The latter was calculated to have the lowest activation energy barrier and the computed TS showed a minimal agostic interaction (Ir–H 2.22 Å, Ir–C 2.66 Å) interaction and only a slight C–H (1.11 Å) elongation and so limited role of metal centre in the C–H activation TS. Overall the results showed that acetate assisted C–H bond activation is not exclusive to Pd complexes.

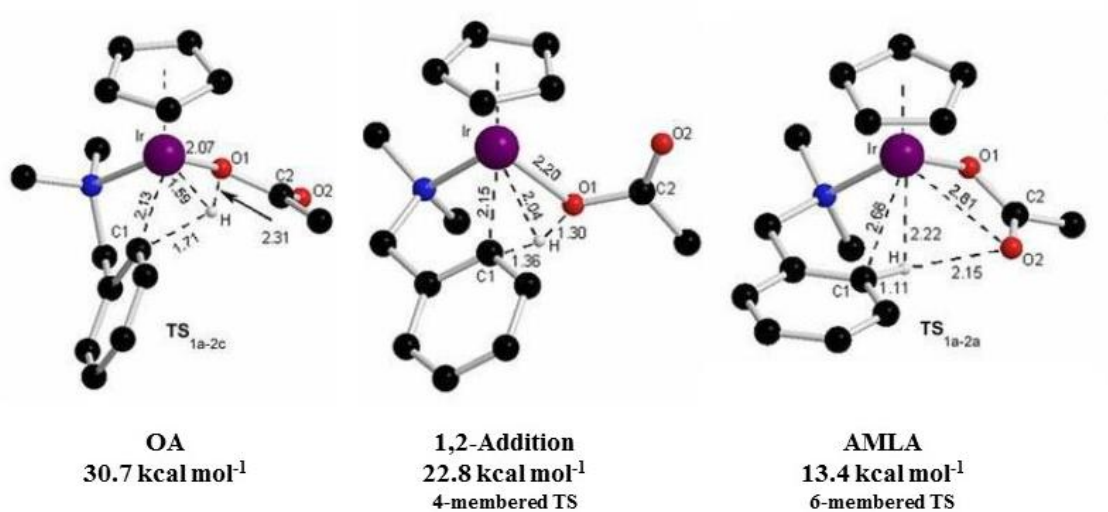


Figure 1.10: Computed transition states for DMBA cyclometallation with Ir.^{102, 120} Adapted from reference 102 and 120.

Later, DFT studies suggested the C–H activation process can be a two-step process (**Figure 1.11**).¹²⁰ Step 1 corresponds to κ^2 – κ^1 displacement of acetate leading to the formation of computational intermediate **1.37int** with a barrier of 13.4 kcal mol⁻¹. Cleavage of the C–H bond (step 2) then occurs *via* an AMLA-6 TS with a barrier of less than 1 kcal mol⁻¹ to form **1.37B** which after HOAc/Cl⁻ exchange gives the final product **1.37C**. Note in this example, the step during which the actual C–H bond elongation and cleavage is taking place is almost barrierless. Hence a low DKIE would be expected as highest energy transition state corresponds to κ^2 – κ^1 acetate displacement and not C–H bond cleavage. Therefore, the authors concluded that C–H activation may be a multi-step process “in which the establishing the correct framework i.e. making available an intramolecular base and allowing the substrate to approach the metal centre, may incur the major activation barrier”.¹²⁰

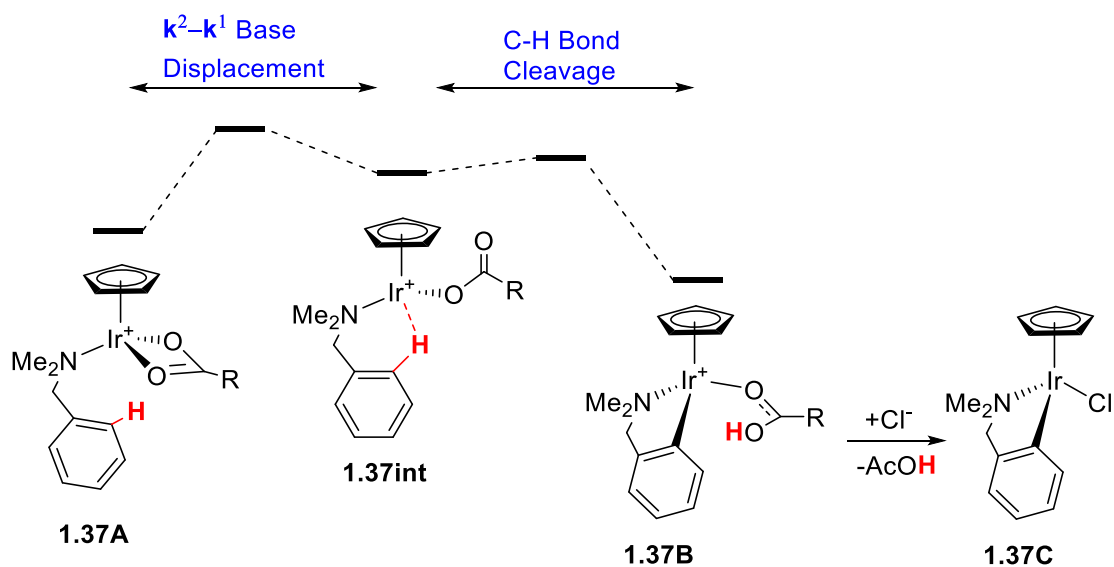
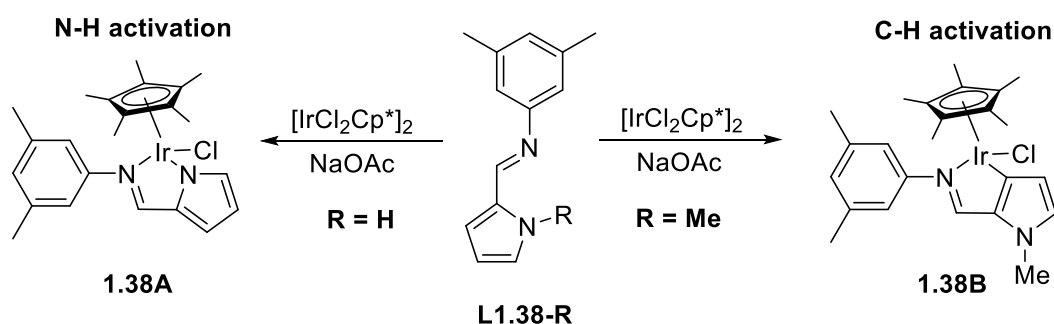


Figure 1.11: AMLA C–H activation of DMBA by {IrCp} profile.¹²⁰

The effect of the carboxylate on the AMLA process was examined computationally and experimentally using $[\text{Ir}(\text{DMBA})(\kappa^2\text{-RCO}_2)\text{Cp}]^+$ ($\text{R} = \text{Ph}, \text{CCl}_3, \text{CF}_3, \text{OH}$) or with OTf in place of RCO_2 (**Figure 1.11**).¹²⁰ The $\kappa^2\text{-}\kappa^1$ displacement of the chelating base was rate determining with the exception of OTf where C–H cleavage became rate determining. The stronger coordinating bases had higher activation barriers for the displacement due to a stronger M–O bond with activation barriers in the order $\text{OTf} < \text{R} = \text{CF}_3 \approx \text{CCl}_3 < \text{OH} < \text{CH}_3 < \text{Ph}$, but with the overall profiles being fairly similar. Experimental studies, showed that reaction is significantly more facile with NaOAc than NaOTf and also better with OAc than other carboxylates. DFT calculations of the whole reaction profile including breaking of the dimer and C–H activation steps demonstrated that with OAc the process is highly exothermic ($\Delta E = -34.0 \text{ kcal mol}^{-1}$) whilst with OTf the reaction was overall thermo-neutral ($\Delta E = -0.2 \text{ kcal mol}^{-1}$) which explains why reactions with acetate are more facile. Additional calculations with other carboxylates gave intermediate results. Overall, OAc is an optimal intramolecular base for these reactions as both more basic and more acidic bases lead to slower reactions; the former due to higher C–H activation barriers, and the latter leading to less exergonic, and hence more reversible, reactions.¹²⁰

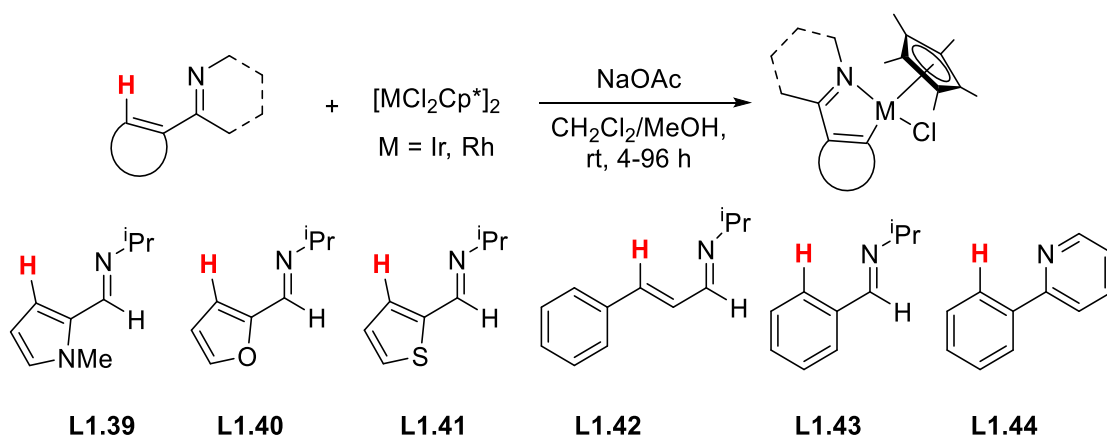
Cyclometallation of pyrrole imines (**L1.38** $\text{R} = \text{H}$) with Ir in the presence of NaOAc (**Scheme 1.28**)¹²¹ gave only the N–H activated product **1.38A**. Reaction of **1.38** $\text{R} = \text{Me}$ gave the C–H activated product **1.38B**. DFT calculations showed that for **1.38** $\text{R} = \text{H}$ NH

activation is a lower energy process than C–H activation, though formation of **1.38B** shows that C–H activation is energetically feasible.



Scheme 1.28: N-H vs C-H cycloiridation of pyrrole imines.¹²¹

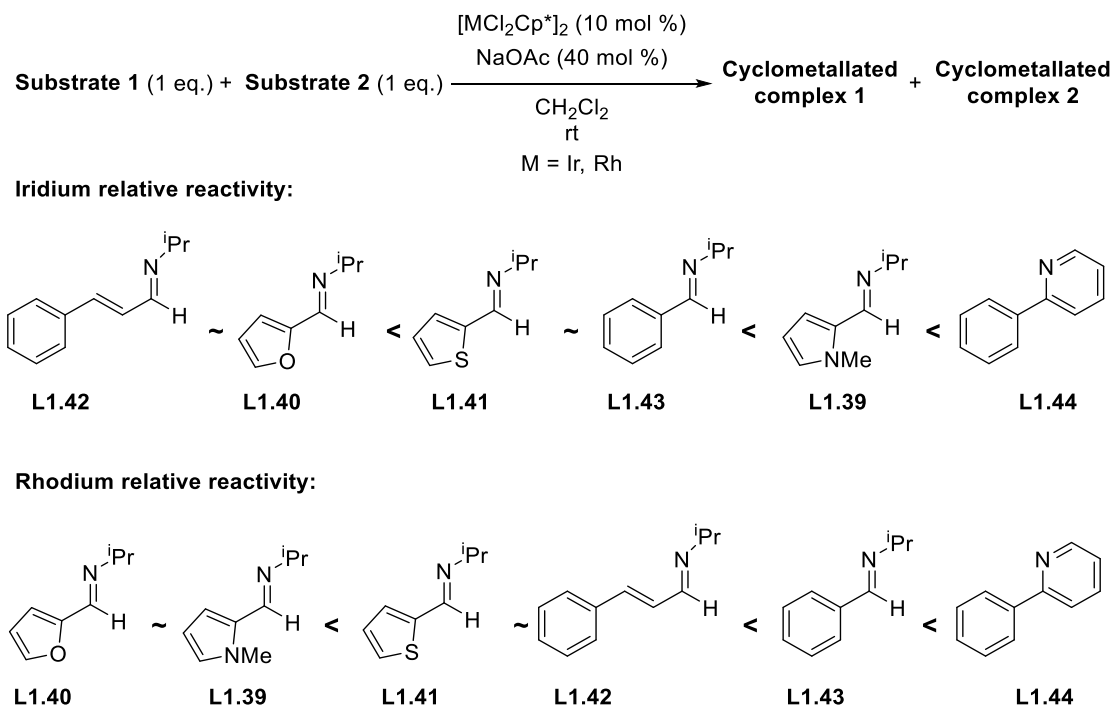
The reactivities of the different substrates (**L1.39-1.44**) via an AMLA C–H activation with Ir and Rh were assessed by Davies *et al* (**Scheme 1.29**).¹²² The reactions at Ir proceed smoothly in either MeOH or CH₂Cl₂ whilst those with Rh proved more difficult and some complexes were not isolated (Rh-**1.39**, Rh-**1.40**) due to low conversions. When H/D exchange experiments with Ir were carried out only **L1.39** showed some D incorporation, implying that under the standard conditions, reactions at Ir are irreversible and under kinetic control. However, with Rh H/D exchange was observed for all of the substrates indicating that reactions at Rh are reversible, consistent with the low conversions and that these reactions are under thermodynamic control.¹²²



Scheme 1.29: Substrates investigated for the C–H activation with Ir and Rh.¹²²

To gain a better insight into the selectivity of the AMLA mechanism a series of competition experiments were carried out where the relative reactivities of substrates

L1.39-1.44 with Ir and Rh were assessed (**Scheme 1.30**).¹²² Judging by the product ratios, with Ir, **L1.39** and **L1.44** were the most reactive whilst with Rh **L1.39** was one of the least reactive substrates.



Scheme 1.30: Relative substrate reactivities at Ir and Rh.¹²²

To understand the cause for the different order of reactivity at Ir and Rh, the reaction mechanism was modelled using DFT calculations with the substrate **L1.41** (**Figure 1.12**). The reactions of **L1.41** at Ir (MeOH) and Rh (MeOH) have similar overall reaction barriers ($\Delta G^\ddagger = 10.5$ and $11.8 \text{ kcal mol}^{-1}$ for Ir and Rh respectively), however, the C–H activation at Ir is substantially more exergonic ($\Delta G = -11.9 \text{ kcal mol}^{-1}$) compared to Rh ($\Delta G = -4.0 \text{ kcal mol}^{-1}$). This is in agreement with the experimental observation that the reactions at Ir are kinetically controlled whilst reactions at Rh are reversible and so exhibit thermodynamic control. Therefore, the observed order of reactivity of the substrates is different at Ir than at Rh.

The reaction solvent was demonstrated to have a significant effect on the C–H activation barrier. The formation of cationic species **IV**_{M-1.41} from substitution of Cl⁻ in **II**_M (or OAc⁻ in **III**_M) by neutral ligand **L1.41** is favoured in MeOH (**II**_M → **IV**_{M-1.41}) compared to DCM (**II** → **IV**). On the other hand, the HOAc/Cl⁻ substitution (**VI**_{M-1.41} → **VII**_{M-1.41}) is less favoured in MeOH compared to DCM. Hence, the overall thermodynamics are not

significantly influenced by the reaction solvent with Ir still being under kinetic whilst Rh under thermodynamic control.¹²²

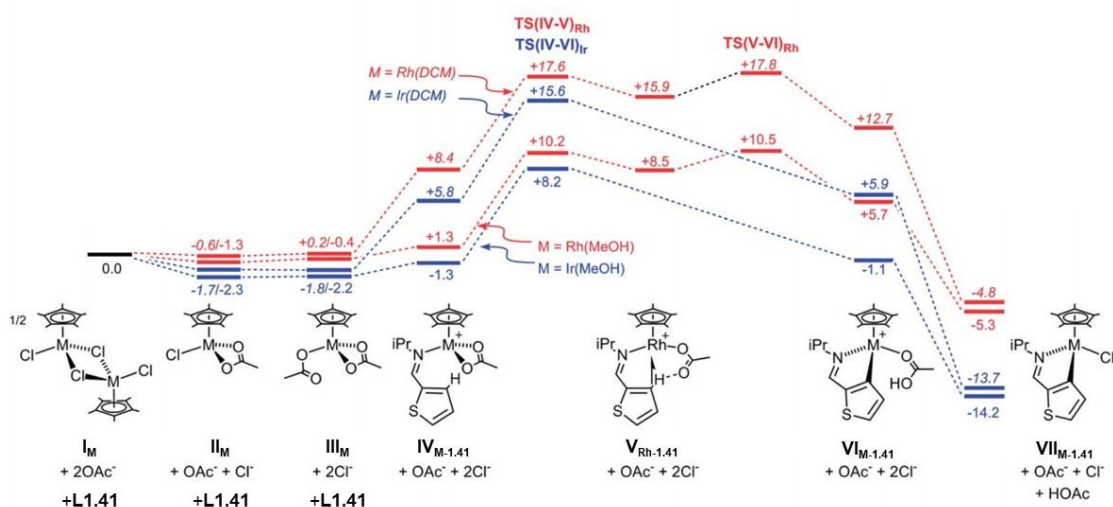
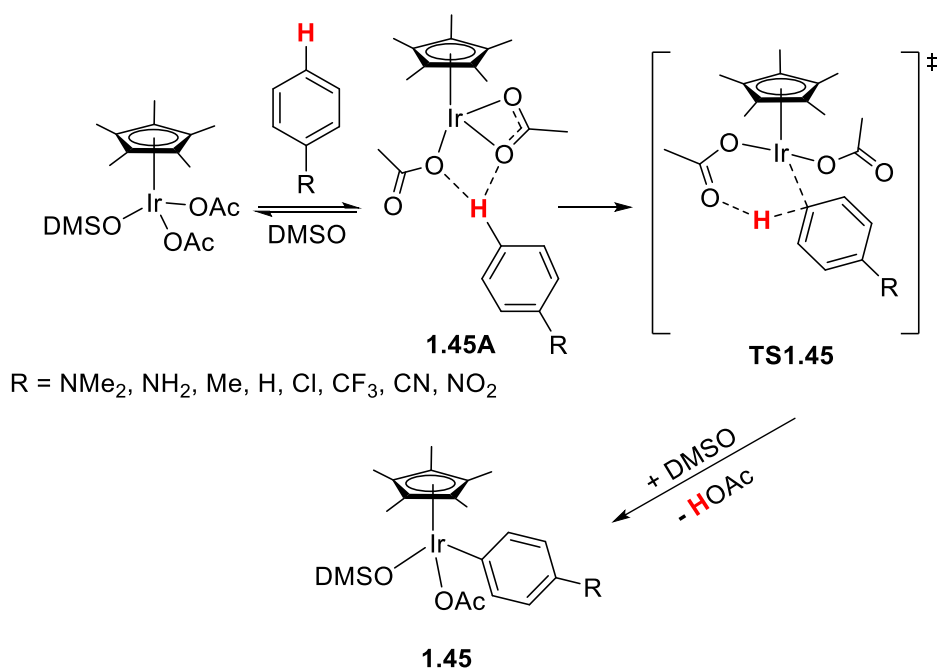


Figure 1.12: Computed reaction mechanism of **L1.41** with Ir or Rh with energies (kcal mol⁻¹) computed in MeOH and DCM.¹²² Adapted from reference 122.

Similar progress has been made in studying intermolecular C–H activation at Ir. Ison *et al.* reported experimental and computational studies on the non-directed stoichiometric C–H activation of arenes with [Ir(OAc)₂Cp*DMSO] (**Scheme 1.31**).¹²³ Three plausible pathways were computed for the reaction of benzene: 1,2-addition ($\Delta E^\ddagger = 51.9$ kcal mol⁻¹), OA ($\Delta E^\ddagger = 47.9$ kcal mol⁻¹) and AMLA-6/CMD ($\Delta E^\ddagger = 34.4$ kcal mol⁻¹) with the latter being the most favourable. The computed reaction mechanism indicated that loss of DMSO from [Ir(OAc)₂Cp*DMSO] and coordination of the arene leads to formation of **1.45A** which can then undergo C–H activation *via* an AMLA TS (**TS1.45**) with a barrier of 28.2 kcal mol⁻¹. The experimentally observed DKIE of 10 indicates that C–H bond cleavage is taking place in the rds. Subsequent HOAc/DMSO exchange leads to the formation of the product **1.45**.¹²³



Scheme 1.31: C–H activation of arene with Ir studied by Ison *et al.* Only a selected few examples are shown.¹²³

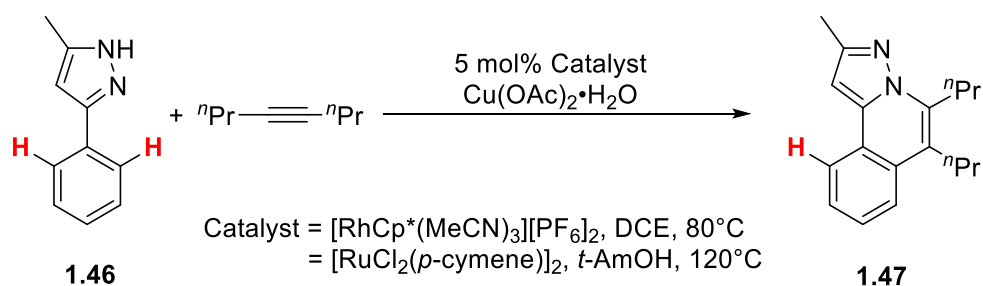
The electronic effects of the arene substituent were computed and presented in a Hammett plot of change in enthalpy of activation ($\Delta\Delta H^\ddagger$) versus σ^+ . Overall, the trend was non-linear with two regions: a linear region in which the $\Delta\Delta H$ increases with the decrease in the electron-donating ability of a substituent ($\rho = 1.67$, $\sigma^+ = ca. -2$ to 0 e.g. NMe₂ to Me) and the region above ($\sigma^+ = 0$) where there is no correlation between σ^+ and the $\Delta\Delta H^\ddagger$ (e.g. Cl, CF₃, CN, NO₂). Usually a non-linear Hammett plot indicates a change in the mechanism. In this case the computed reaction pathways for R = NH₂, H, and NO₂ indicate that electron-withdrawing and electron-donating substituents affect different steps of the reaction with electron-withdrawing groups promoting formation of **1.45A** rather than C–H cleavage step whilst the electron-donating groups facilitate the actual C–H bond cleavage step.¹²³

1.4bii Mechanistic Aspects of Catalytic C–H Functionalisation by AMLA/CMD with Half-Sandwich Complexes

The field of catalytic carboxylate assisted C–H functionalisation with half-sandwich complexes has grown substantially in the last decade. Many directed C–H functionalisation reactions have been reported e.g. heterocycle formation,^{15, 124} arylations,¹⁰ alkylations,^{11, 125} and others.¹²⁶ Understanding what factors control the

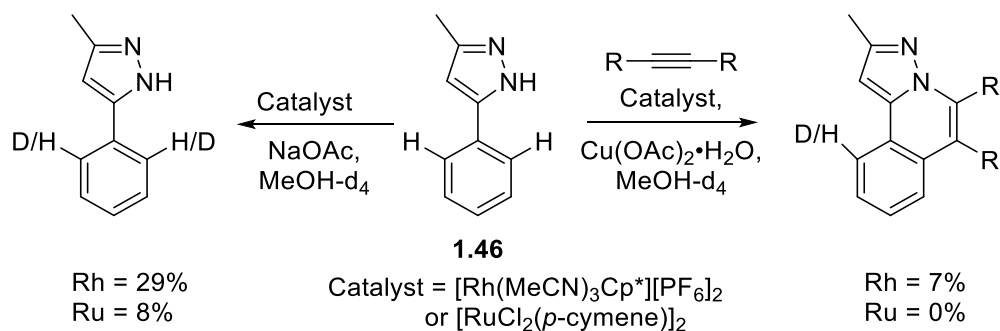
reaction outcomes would aid in improving the efficiency and the scope of these reactions. This section will discuss the mechanistic aspects of catalytic C–H functionalisations with half-sandwich complexes with emphasis on {RhCp*}.

Attempts have often been made to establish the rate-determining step. However, since catalytic reactions may involve several steps, it should be remembered that more than one step may affect the overall rate and the rate determining step may not be the product determining step. As discussed in section 1.2a DKIE and H/D exchange experiments can be used to get insight into whether C–H activation is involved in the rds, however, it may not always be straightforward as illustrated by the following example. Davies, Macgregor *et al.*¹²⁷ reported Rh and Ru catalysed annulation of 3-phenyl-5-methyl-pyrazole with 4-octyne (**Scheme 1.32**).



Scheme 1.32: Rh and Ru catalysed 3-phenyl-5-methylpyrazole annulation with 4-octyne.¹²⁷

H/D exchange studies with Rh showed that the C–H activation step is reversible in the absence of alkyne (**Scheme 1.33**). However, in the presence of 4-octyne, D incorporation was only observed when the reaction was allowed to go to completion, indicating that in the early stages of catalysis (high alkyne concentration) alkyne insertion is favoured over the reverse of the C–H activation reaction, however, as the reaction proceeds the alkyne concentration reduces and the reverse C–H activation is competitive in rate. In the case of Ru only 7% D incorporation was observed in the absence of alkyne and none in the presence of alkyne. This indicates that for Ru the insertion of alkyne is significantly easier compared to the reverse of C–H activation. A DKIE of 2.7 ± 0.5 was observed for the Rh reaction suggesting that C–H bond cleavage is potentially involved in the rds, whilst a DKIE value of 1.1 ± 0.2 was measured for Ru.



Scheme 1.33: D incorporation experiments of 3-phenyl-5-methylpyrazole with Rh or Ru catalyst in presence and absence of alkyne.¹²⁷

DFT calculations showed the reactions proceed through N–H then C–H bond activation, HOAc/alkyne exchange, migratory insertion, and then C–N reductive coupling. The computed reaction profile for Rh is shown in **Figure 1.13 (i)**. After N–H activation the formed neutral Rh complex **B** undergoes C–H activation. C–H activation consist of two steps: κ^2 - κ^1 displacement of acetate (**TS(B-C)1** at 13.2 kcal mol⁻¹) and the actual C–H bond cleavage (**TS(B-C)2** at 14.6 kcal mol⁻¹ respectively). The latter was the C–H activation high point and this **TS (Figure 1.14)** shows a significantly elongated C–H bond (1.31 Å) which is consistent with the observed DKIE. The C–H activation process (**B** → **C**₁) and migratory insertion (**D** → **E**) were calculated to have the highest energy transition states and they both have the same in energy ($G = +14.6$ kcal mol⁻¹) (**Figure 1.13**). This is in agreement with the reduced H/D exchange at the *ortho*-C–H position of **1.46** in the presence of alkyne. In addition, both of these steps will have a significant effect on the reaction rate, demonstrating that in catalysis more than one step can influence the overall rate.

However, for Ru (**Figure 1.13, ii**) the TS for migratory insertion **TS(D-E)** at 11.9 kcal mol⁻¹ is significantly lower in energy than the highest **TS(B-C)1_{Ru}** for the C–H activation process at 16.8 kcal mol⁻¹. In this instance **TS(B-C)1_{Ru}** (**Figure 1.14**) corresponds to the κ^2 - κ^1 acetate displacement whilst the actual C–H bond cleavage is barrierless. Since **TS(B-C)1_{Ru}** does not involve a significant elongation of the C–H bond (1.11 Å) no significant DKIE is expected in agreement with the observed value of 1.1 ± 0.2 . In conclusion, even when the C–H activation process is rate determining it can show a low DKIE (close to 1) if there is no significant elongation of the C–H bond in the highest TS. In addition, the choice of the catalyst can affect which step or steps are rate determining.

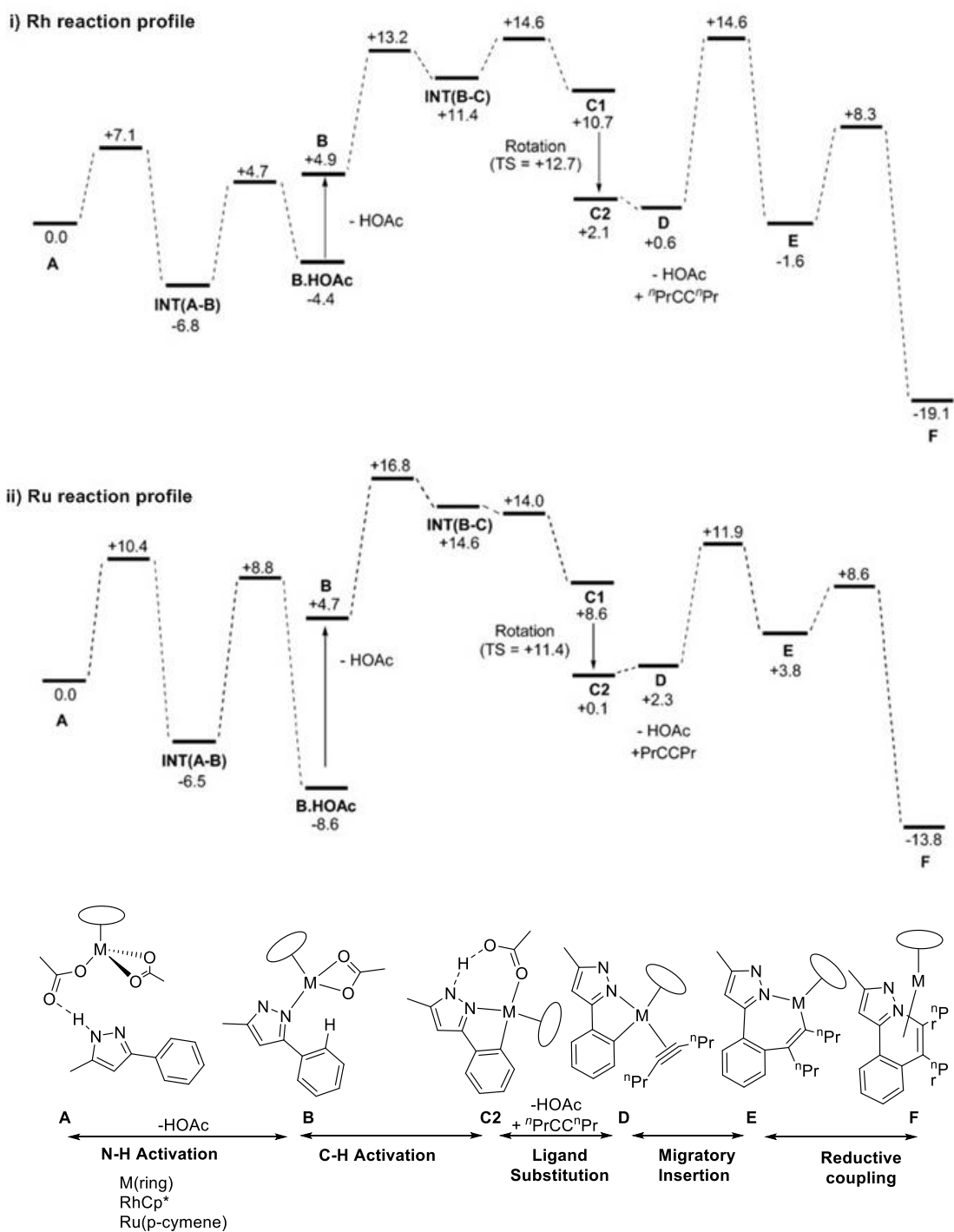


Figure 1.13: Reaction profiles for coupling of **1.46** with ⁿPrCCⁿPr at Rh(i) and Ru(ii). G in kcal mol⁻¹.¹²⁷ Adapted from reference 127.

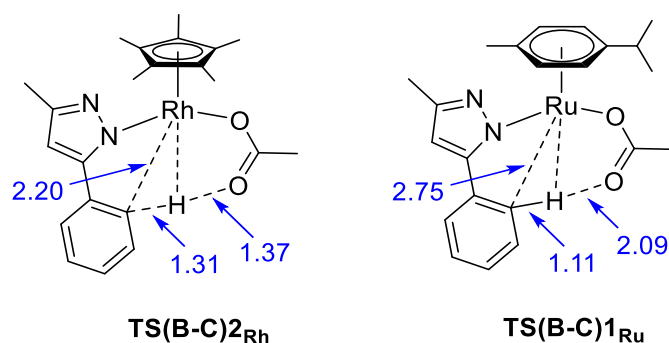
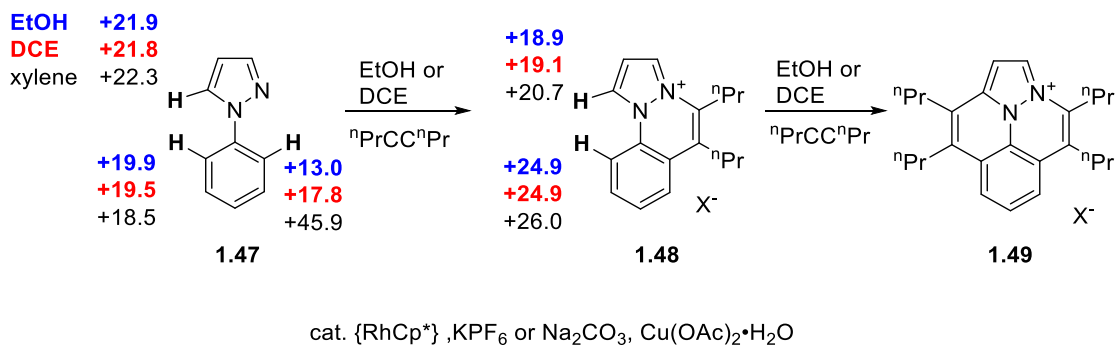


Figure 1.14: The structures of computed rds TS for C–H activation of **1.46** with Rh – **TS(B-C)2_{Rh}** and Ru **TS(B-C)1_{Ru}**.¹²⁷ Bond distances in Å.

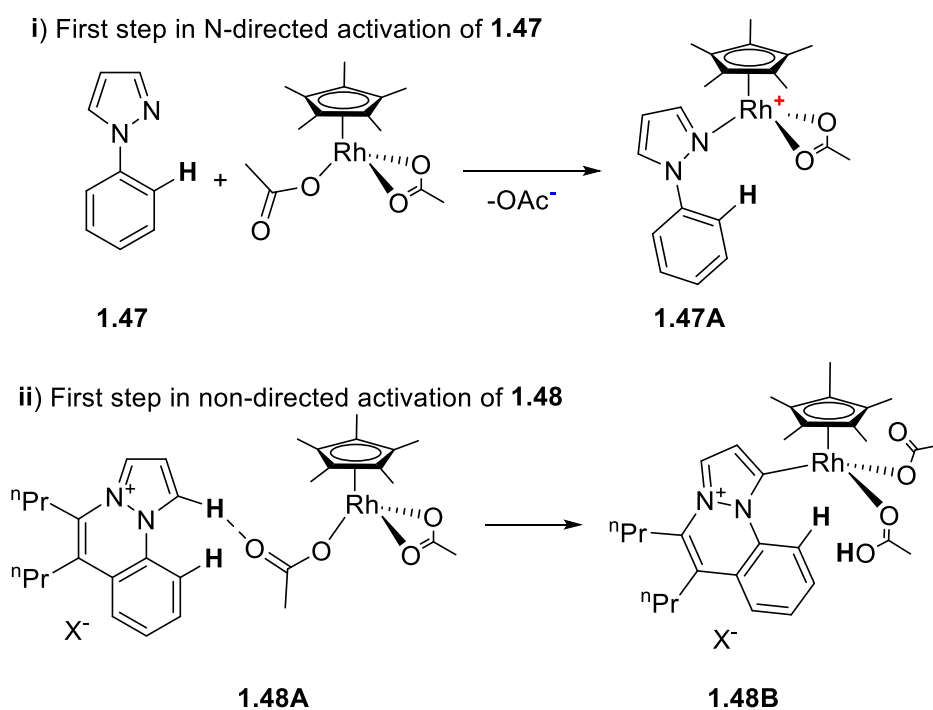
Davies *et al.* also reported {RhCp*} catalysed coupling of 1-phenylpyrazole with 4-octyne (**Scheme 1.34**).¹²⁸ When reactions were performed in EtOH at short reaction times (3h), mono-insertion product **1.48** was the major species whilst over time the double-insertion product **1.49** became the major species. This suggested that **1.48** is an intermediate in the formation of **1.49**. When the catalytic reaction was carried out in DCE the major species formed was **1.49** even at short reaction times with traces of **1.48**. This suggests that in DCE, formation of **1.49** is significantly faster than the conversion of **1.47** into **1.48**.



Scheme 1.34: Rh catalysed C–N and C–C coupling of 1-phenylpyrazole with alkyne in EtOH and DCE¹²⁸ and xylene¹²⁹ and the overall barriers for C–H activation at the indicated sites in kcal mol⁻¹, calculated in EtOH (blue), DCE (red), xylene (black).¹²⁸

Computed C–H activation barriers for the reaction of 1-phenylpyrazole in EtOH, DCE and xylene are shown in **Scheme 1.34**. The DFT calculations show that C–H activation of **1.47** proceeds *via* a cationic metal complex **1.47A** (**Scheme 1.35 i**) where formation is favoured by more polar solvents ($\Delta G^\ddagger = 13.0$ kcal mol⁻¹ in EtOH and 17.8 kcal mol⁻¹ in DCE). In contrast, C–H activation of **1.48** starts with a non-directed C–H activation

(**Scheme 1.35 ii**) at a neutral metal species **1.48A** hence it is not significantly affected by the solvent ($G_{\text{EtOH}} = 18.9 \text{ kcal mol}^{-1}$ cf. $G_{\text{DCE}} = 19.1 \text{ kcal mol}^{-1}$). In EtOH the C–H activation reaction of **1.47** ($\Delta G_{\text{EtOH}}^{\ddagger} = 13.0 \text{ kcal mol}^{-1}$) is kinetically favoured over the reaction of **1.48** ($\Delta G_{\text{EtOH}}^{\ddagger} = 18.9 \text{ kcal mol}^{-1}$), therefore, **1.48** builds up before conversion to **1.49**. However, in DCE the C–H activation reactions for the formation of **1.48** and **1.49** are competitive ($\Delta G_{\text{DCE}}^{\ddagger} = 17.8 \text{ kcal mol}^{-1}$, $\Delta G_{\text{DCE}}^{\ddagger} = 19.1 \text{ kcal mol}^{-1}$), therefore, **1.48** is used up quickly to form **1.49**. Whilst in an even less polar solvent xylene N-directed C–H activation reaction of **1.47** is inaccessible ($\Delta G^{\ddagger} = \text{ca. } 46 \text{ kcal mol}^{-1}$).¹²⁹ Overall, as the solvent become less polar the non-directed C–H activation becomes competitive with the directed C–H activation as the latter occurs *via* a cationic species which is stabilised in polar solvents like EtOH but is disfavoured in less polar solvents.

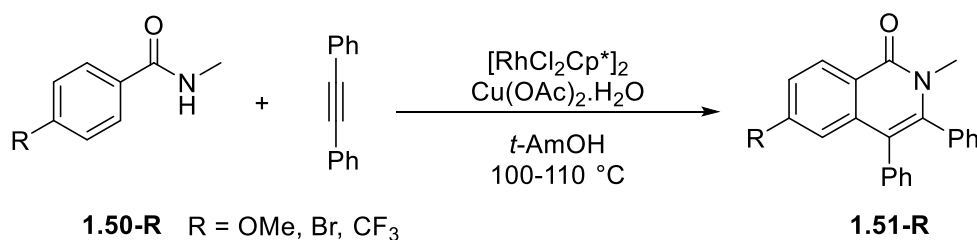


Scheme 1.35: First steps in **1.47** and **1.48** Rh catalysed coupling with 4-octyne.¹²⁸

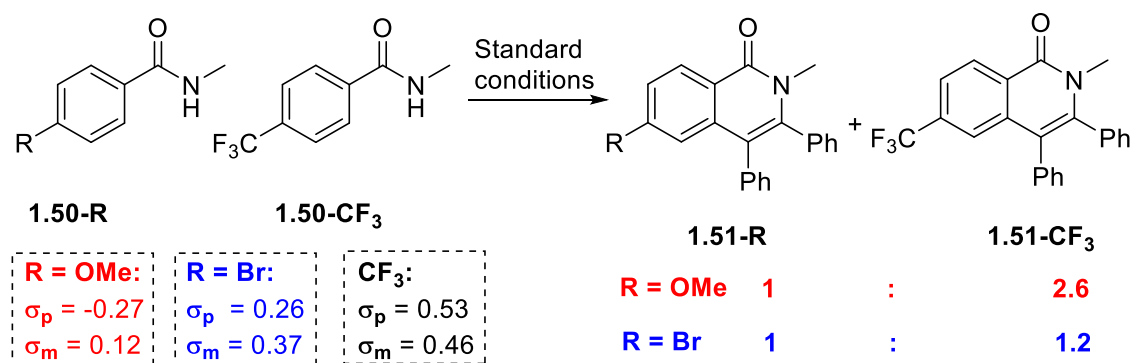
Substrate substituent steric and electronic effects can also affect the selectivity of the products and/or the rate of the reaction and they are often investigated by means of competition experiments as discussed in **section 1.2.c**. Important to note is that electronic effects reflect the selectivities of the product determining step, therefore, for conclusions on C–H activation to be made it has to be proven C–H activation is indeed the product determining step, for which DKIE is often employed.

Rovis and Hyster reported the Rh-catalysed cycloaddition of alkynes and benzamides (**Scheme 1.36 i**).¹³⁰ Competition experiments between **1.50-OMe** and **1.50-CF₃** under standard reaction conditions lead to the formation of **1.51-R** in favour of the more electron deficient **1.51-CF₃** (**Scheme 1.36 ii**). This selectivity could be due to either N–H or C–H activation being the turnover limiting step. To assess this, competition experiment between **1.50-Br** and **1.50-CF₃** was carried out. The **1.51-Br** and **1.51-CF₃** formed in very similar amounts (1:1.2 in favour of **1.51-CF₃**). The two *para* substituents have a significantly different σ_p ($\sigma_p(\text{Br}) = 0.26$ *cf.* $\sigma_p(\text{CF}_3) = 0.53$) but similar σ_m values ($\sigma_m(\text{Br}) = 0.37$ *cf.* $\sigma_m(\text{CF}_3) = 0.46$). Therefore, the authors concluded that this ratio is consistent with a small difference in the σ_m values and so with C–H activation (occurring *meta* to the substituent) being the first irreversible step. If N–H activation (occurring *para* to the substituent) was controlling the selectivity there would be a larger preference for **1.51-CF₃**.

i) Catalysis reaction



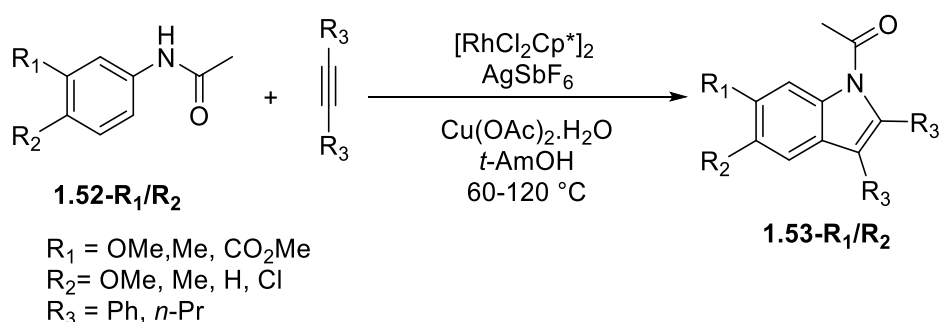
ii) Competition experiments



Scheme 1.36: i) Cycloaddition of alkynes and benzamides catalysed by Rh, ii) Competition experiments with benzamides.¹³⁰

Fagnou *et al.* reported the synthesis of indole derivatives **1.53-R₁/R₂** from various acetanilides **1.52-R₁/R₂** and alkynes (**Scheme 1.37**).^{131, 132} From parallel experiments a DKIE of 4.2 ± 0.9 was observed indicating that C–H bond cleavage is the rds. The reaction

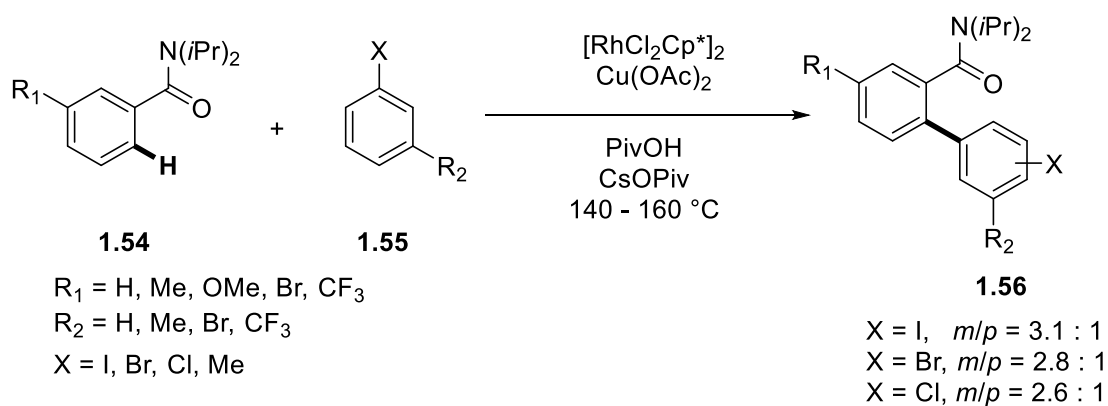
was shown to be sensitive to steric effects and the substrates **1.52-R₁** (R₁ = OMe, Me, CO₂Me) lead to C–H functionalisation at the least sterically hindered site. For substituents at the *para* position, **1.52-R₂** (R₂ = OMe, Me, H, Cl) substrates with electron-donating substituents reacted faster than ones with electron-withdrawing groups which is in contrast with Rovis' results. This is possibly because for reactions reported by Fagnou *et al.*²⁹ (Scheme 1.37) C–H activation is O-directed and takes place at cationic metal centre (equivalent to reaction in Scheme 1.35 i) and so is consistent with the reported preference for electron-donating groups. Whilst for reactions reported by Rovis *et al.*¹³⁰ (Scheme 1.36) C–H activation will take place after N–H activation at a neutral metal centre equivalent to reaction depicted in Figure 1.13 and Scheme 1.35 ii. Some other catalytic reactions with substrates containing directing groups have been shown to favour electron-donating over electron-withdrawing substituents such as {RhCp*}-catalysed alkynylation of benzoates¹³³ and {Ru(*p*-cymene)} catalysed alkynylation of phenylsulfonic acids.¹⁰⁵ Note, the latter example was proposed to go *via* a base-assisted internal electrophilic substitution (BIES)¹⁰⁵ which is essentially the same as IES. There are also examples of electron-withdrawing groups being preferred such as {Ru(*p*-cymene)} catalysed hydroarylation of 2-phenylpyridines with alkenes.¹³⁴ Therefore, electronic effects on the catalytic system will depend on the actual reaction and substrates used and even minor difference in substrates can affect the electronic selectivity.



Scheme 1.37: Rh catalysed synthesis of indole derivatives.¹³²

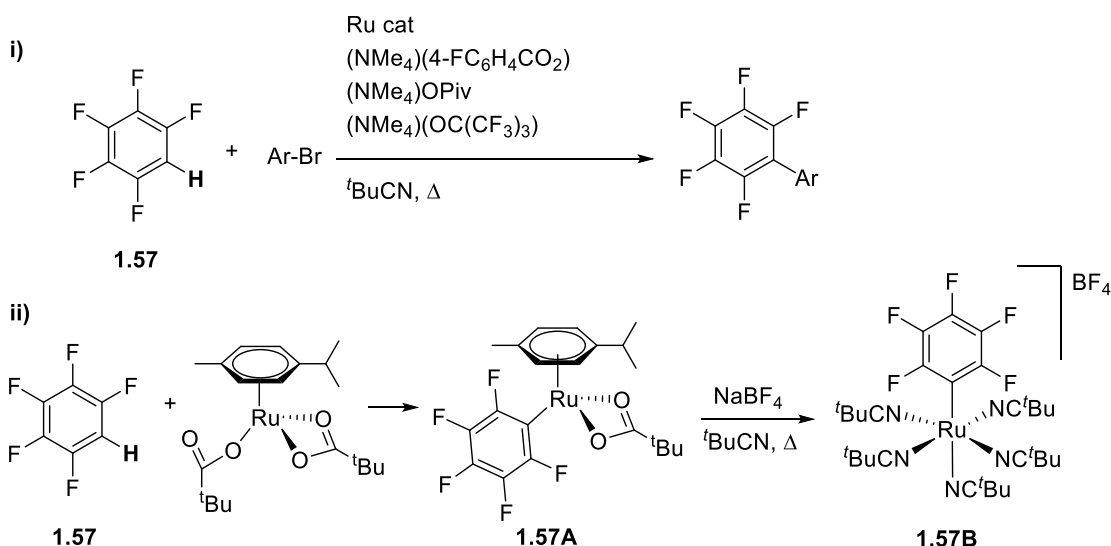
Non-directed C–H functionalisations catalysed by half-sandwich complexes have also been reported and were reviewed recently⁷ and some examples are discussed below. Glorius *et al.* reported the first example of Rh catalysed direct arylation (Scheme 1.38).¹³⁵ Two C–H activation events are taking place, directed *ortho* activation of benzamide **1.54** and non-directed C–H activation of the aryl halide **1.55** (X = I, Br, Cl, R₂ = H). The reaction scope was later expanded to the arene **1.55** (X = Me, R₂ = Me, Br, CF₃).¹³⁶ The

competition experiments between two substituted benzamides **1.54** ($R_1 = \text{OMe, Me, Cl}$) showed a preference for electron-donating groups. Whilst for arenes ($X = \text{Me, R}_2 = \text{Me, Br, CF}_3$) no clear preference for electron-donating or electron-withdrawing groups were observed. This might suggest that arene activation is influenced by an interaction-distortion energy trade-off discussed in Pd section.



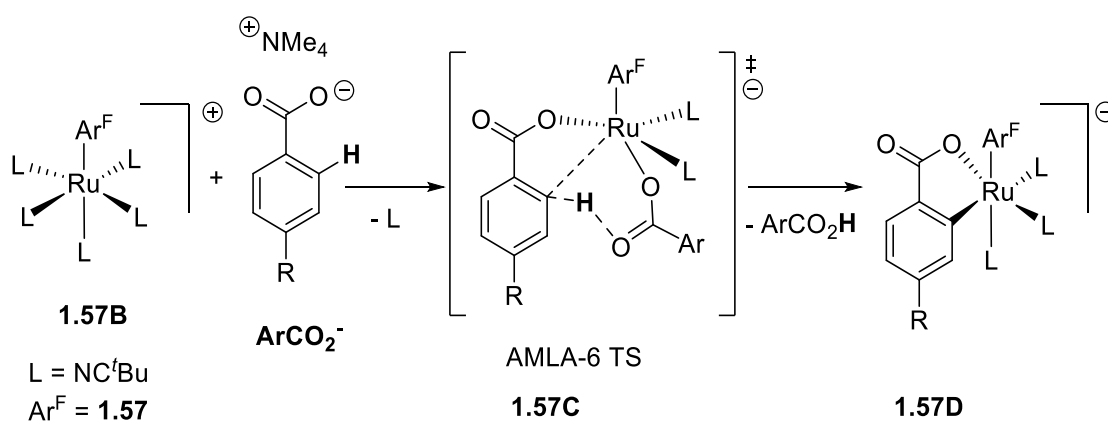
Scheme 1.38: Rh catalyzed dehydrogenative arylation of benzamides.¹³⁵

Larrosa *et al.* reported the first example of Ru catalyzed non-directed C–H arylation of arenes (**Scheme 1.39 i**).¹³⁷ It was shown that $[\text{RuCl}_2(p\text{-cymene})]_2$ forms $[\text{Ru}(\text{OPiv})_2(p\text{-cymene})]$ and subsequently **1.57A** (**Scheme 1.39 ii**). The dissociation of *p*-cymene from **1.57A** during the reaction was crucial to form redox active **1.57B** that can carry out bromoarene coupling to the fluoroarene, showing that at least in some cases the *p*-cymene ligand does not stay coordinated to the Ru. Thus, it can be difficult to determine the nature of the active catalyst, which is crucial for the accurate modelling of the reaction profile using computational calculations.



Scheme 1.39: i) Ru catalysed non-directed arylation of fluoroarenes and ii) synthesis of catalytic Ru species.¹³⁷

For the reaction above (**Scheme 1.39 i**) addition of benzoate ((NMe₄)₄-FC₆H₄CO₂) was found to be necessary for the bromoarene coupling step whilst addition of (NMe₄)OC(CF₃)₃ was found to facilitate the reaction.¹³⁸ Experimental and DFT studies indicated that complex **1.57B** with benzoate forms anionic cyclometallated complex **1.57D** via an AMLA C–H activation where the second benzoate acts as intramolecular base (**Scheme 1.40 1.57C**).¹³⁸



Scheme 1.40: Formation of the catalytic Ru species with benzoate via AMLA TS.¹³⁸

From parallel experiments a DKIE of 1.4 was observed for the *ortho* C–H activation of the benzoate which indicates that the cyclometallation of the benzoate is kinetically relevant. The electronic effects on the transformation (**1.57B** → **1.57D**) were assessed with variously substituted benzoates (ArCO₂⁻). Surprisingly both electron-withdrawing

and electron-donating groups were found to enhance the overall rate leading to a V shaped Hammett plot. Computational studies, demonstrated that the binding of benzoate is facilitated by electron donating groups in the *para* position, whilst the cyclometallation *via* C–H activation (**1.57C**) occurs *meta* to the R group and is facilitated by electron-withdrawing groups. Therefore, both *para* and *meta* effects are observed. This was corroborated by a Jaffé analysis (see **Chapter 3**). Additionally, it was found that the role of additive (NMe₄)OC(CF₃)₃ is to deprotonate the produced benzoic acid (ArCO₂H) in the catalytic cycle and push the C–H activation pre-equilibrium toward the anionic Ru **1.57D** species. The more acidic benzoates (substituted with electron-withdrawing groups) will be deprotonated more readily and further promote the reaction. This example demonstrates the challenging nature of studying catalytic reactions as electronic effects of additives/ligands can be interlinked and affect multiple steps of the catalytic cycle, benzoate binding, cyclometallation, and deprotonation of benzoate in this case.

1.5 Conclusions

In the last fifteen years the identification of carboxylate assisted C–H activation has led to a huge increase in the applications of catalytic C–H functionalisation in synthesis. However mechanistic investigations have not advanced so substantially and indeed there is evidence that some mechanistic conclusions in the literature may be wrong, as highlighted by Hartwig in the case of KIE studies.³⁴ In addition, mechanistic investigations of catalytic reactions are necessarily more complicated with the possibility that more than one step may be affected by any change and that this may alter the nature of the rds. A small number of studies of stoichiometric cyclometallation reactions have provided valuable information. In some cases, for both catalytic and stoichiometric investigations computational studies have provided corroborating evidence.

As discussed above initial investigations by Fagnou's and Echavarren's groups showed that direct arylation reactions take place *via* a proton abstraction (CMD) mechanism and favoured substrates with electron-withdrawing groups.^{101, 114} In contrast for the cyclopalladation of dimethylbenzylamines (**Scheme 1.20**)^{99, 106} C–H activation is faster with electron-donating groups and was later shown to go *via* an AMLA mechanism. Similar benzene and methane activation with [Ir(acac)₂(OAc)] was regarded as an intramolecular electrophilic substitution¹⁰⁴(IES later called BIES)¹⁰⁵ and as such would be expected to show increased reactivity with electron-donating groups. Computational

studies show that these reactions proceed *via* similar acetate-assisted transition states. Indeed, in a 2010 paper Fagnou clearly regarded them as at least related,²⁹ if not the same, whilst Davies and Macgregor regarded AMLA and CMD as the same in a 2017 review.²⁸ In addition, Fagnou showed that with an interaction-distortion analysis CMD was not limited to electron poor substrates and that electron rich substrates could also react *via* CMD.¹⁰¹ However, despite this, it is clear in the literature that for some reactions that are favoured by electron-donating groups the authors rule out the reactions being CMD preferring to assign them as BIES^{105, 139} implying that CMD and BIES are different. The aims of this work are to study electronic and steric effects on stoichiometric acetate-assisted C–H activation at Ir and Rh employing inter- and intramolecular competition reactions. It is hoped that this study will increase understanding of acetate-assisted C–H activation reactions and bring some clarity to the apparently opposing electronic effects observed in some catalytic reactions and assess whether CMD/AMLA and BIES are indeed essentially all the same mechanism. The work builds on a previous study in the Davies group on cyclometallation of substituted phenylpyrazoles which finished during the course of this work.¹⁴⁰ **Chapter 2** will report the cyclometallation of *para*- and *meta*-substituted phenylpyridines and electronic effects observed from their one-pot intermolecular competition reactions. **Chapter 3** will describe electronic and steric effects on intramolecular competition reactions for cyclometallation of diphenylimidazolium salts to give five-membered metallocycles whilst **Chapter 4** examines similar reactions with dibenzylimidazolium salts to give six-membered metallocycles. Some preliminary DFT calculations carried out by the group of Professor S. A. Macgregor (Heriott Watt University) are mentioned in **Chapter 3**. **Chapter 5** will contain conclusions and future work whilst **Chapter 6** will have all the experimental data.

1.6 Bibliography

1. N. Miyaura, T. Yanagi and A. Suzuki, *Synth. Commun.*, 1981, **11**, 513-519.
2. D. Milstein and J. K. Stille, *J. Am. Chem. Soc.*, 1979, **101**, 4992-4998.
3. E. Negishi, A. O. King and N. Okukado, *J. Org. Chem.*, 1977, **42**, 1821-1823.
4. R. F. Heck, *J. Am. Chem. Soc.*, 1968, **90**, 5518-5526.
5. J. P. Wolfe, S. Wagaw, J.-F. Marcoux and S. L. Buchwald, *Acc. Chem. Res.*, 1998, **31**, 805-818.
6. J. F. Hartwig, *Acc. Chem. Res.*, 1998, **31**, 852-860.
7. P. Wedi and M. van Gemmeren, *Angew. Chem. Int. Ed.*, 2018, **57**, 13016-13027.
8. R. H. Crabtree and A. Lei, *Chem. Rev.*, 2017, **117**, 8481-8482.
9. P. B. Arockiam, C. Bruneau and P. H. Dixneuf, *Chem. Rev.*, 2012, **112**, 5879-5918.
10. D. A. Colby, R. G. Bergman and J. A. Ellman, *Chem. Rev.*, 2010, **110**, 624-655.
11. S. Pan and T. Shibata, *ACS Catal.*, 2013, **3**, 704-712.
12. D. Alberico, M. E. Scott and M. Lautens, *Chem. Rev.*, 2007, **107**, 174-238.
13. O. Daugulis, H.-Q. Do and D. Shabashov, *Acc. Chem. Res.*, 2009, **42**, 1074-1086.
14. T. Gensch, M. N. Hopkinson, F. Glorius and J. Wencel-Delord, *Chem. Soc. Rev.*, 2016, **45**, 2900-2936.
15. A. Peneau, C. Guillou and L. Chabaud, *Eur. J. Org. Chem.*, 2018, **2018**, 5777-5794.
16. X. Chen, K. M. Engle, D.-H. Wang and J.-Q. Yu, *Angew. Chem., Int. Ed.*, 2009, **48**, 5094-5115.
17. Z.-J. Shi, *Homogeneous Catalysis for Unreactive Bond Activation*, Wiley, 2014.
18. K. Godula and D. Sames, *Science*, 2006, **312**, 67-72.
19. M. Wegmann, M. Henkel and T. Bach, *Org. Biomol. Chem.*, 2018, **16**, 5376-5385.
20. D. Basu, S. Kumar, S. S. V and R. Bandichhor, *J. Chem. Sci.*, 2018, **130**, 71.
21. J. R. Hummel, J. A. Boerth and J. A. Ellman, *Chem. Rev.*, 2017, **117**, 9163-9227.
22. L. Ping, D. S. Chung, J. Bouffard and S.-g. Lee, *Chem. Soc. Rev.*, 2017, **46**, 4299-4328.
23. A. F. M. Noisier and M. A. Brimble, *Chem. Rev.*, 2014, **114**, 8775-8806.
24. J. Yamaguchi, A. D. Yamaguchi and K. Itami, *Angew. Chem. Int. Ed.*, 2012, **51**, 8960-9009.
25. T. Cernak, K. D. Dykstra, S. Tyagarajan, P. Vachal and S. W. Krska, *Chem. Soc. Rev.*, 2016, **45**, 546-576.
26. F. Zhang and D. R. Spring, *Chem. Soc. Rev.*, 2014, **43**, 6906-6919.
27. Y. Boutadla, D. L. Davies, S. A. Macgregor and A. I. Poblador-Bahamonde, *Dalton Trans.*, 2009, 5820-5831.
28. D. L. Davies, S. A. Macgregor and C. L. McMullin, *Chem. Rev.*, 2017, **117**, 8649-8709.
29. D. Lapointe and K. Fagnou, *Chem. Lett.*, 2010, **39**, 1118-1126.
30. X. Qi, Y. Li, R. Bai and Y. Lan, *Acc. Chem. Res.*, 2017, **50**, 2799-2808.
31. K. B. Wiberg, *Chem. Rev.*, 1955, **55**, 713-743.
32. J. S. Hirschi, T. Takeya, C. Hang and D. A. Singleton, *J. Am. Chem. Soc.*, 2009, **131**, 2397-2403.
33. C. Colletto, D. Whitaker and I. Larrosa, *Top. Catal.*, 2017, **60**, 589-593.
34. E. M. Simmons and J. F. Hartwig, *Angew. Chem. Int. Ed.*, 2012, **51**, 3066-3072.

35. S. Kozuch and S. Shaik, *Acc. Chem. Res.*, 2011, **44**, 101-110.
36. M. Gómez-Gallego and M. A. Sierra, *Chem. Rev.*, 2011, **111**, 4857-4963.
37. C. M. Yung, M. B. Skaddan and R. G. Bergman, *J. Am. Chem. Soc.*, 2004, **126**, 13033-13043.
38. M. H. G. Precht, M. Hölscher, Y. Ben-David, N. Theysen, R. Loschen, D. Milstein and W. Leitner, *Angew. Chem. Int. Ed.*, 2007, **46**, 2269-2272.
39. J. Atzrodt, V. Derdau, T. Fey and J. Zimmermann, *Angew. Chem. Int. Ed.*, 2007, **46**, 7744-7765.
40. L. P. Hammett, *J. Am. Chem. Soc.*, 1937, **59**, 96-103.
41. C. Hansch, A. Leo and R. W. Taft, *Chem. Rev.*, 1991, **91**, 165-195.
42. L. P. Hammett, *Chem. Rev.*, 1935, **17**, 125-136.
43. B. J. Stokes, K. J. Richert and T. G. Driver, *J. Org. Chem.*, 2009, **74**, 6442-6451.
44. T. Sperger, I. A. Sanhueza, I. Kalvet and F. Schoenebeck, *Chem. Rev.*, 2015, **115**, 9532-9586.
45. T. Sperger, I. A. Sanhueza and F. Schoenebeck, *Acc. Chem. Res.*, 2016, **49**, 1311-1319.
46. A. S.-K. Tsang, I. A. Sanhueza and F. Schoenebeck, *Chem. Eur. J.*, 2014, **20**, 16432-16441.
47. E. Lyngvi and F. Schoenebeck, *Tetrahedron*, 2013, **69**, 5715-5718.
48. S. Grimme, *Wiley Interdisciplinary Reviews: Computational Molecular Science*, 2011, **1**, 211-228.
49. M. Anand, R. B. Sunoj and H. F. Schaefer, *J. Am. Chem. Soc.*, 2014, **136**, 5535-5538.
50. P. Vidossich, A. Lledós and G. Ujaque, *Acc. Chem. Res.*, 2016, **49**, 1271-1278.
51. M. Albrecht, *Chem. Rev.*, 2010, **110**, 576-623.
52. J. A. Labinger and J. E. Bercaw, *Nature*, 2002, **417**, 507-514.
53. T. G. P. Harper, P. J. Desrosiers and T. C. Flood, *Organometallics*, 1990, **9**, 2523-2528.
54. J. Chatt and J. M. Davidson, *J. Chem. Soc.*, 1965, 843-855.
55. M. A. Bennett and D. L. Milner, *Chem. Comm. (London)*, 1967, 581-582.
56. P. Foley and G. M. Whitesides, *J. Am. Chem. Soc.*, 1979, **101**, 2732-2733.
57. A. H. Janowicz and R. G. Bergman, *J. Am. Chem. Soc.*, 1982, **104**, 352-354.
58. J. K. Hoyano, A. D. McMaster and W. A. G. Graham, *J. Am. Chem. Soc.*, 1983, **105**, 7190-7191.
59. W. D. Jones and F. J. Feher, *J. Am. Chem. Soc.*, 1984, **106**, 1650-1663.
60. R. H. Crabtree, *Chem. Rev.*, 1995, **95**, 987-1007.
61. W. D. Jones and F. J. Feher, *Acc. Chem. Res.*, 1989, **22**, 91-100.
62. B. A. Arndtsen, R. G. Bergman, T. A. Mobley and T. H. Peterson, *Acc. Chem. Res.*, 1995, **28**, 154-162.
63. A. H. Janowicz and R. G. Bergman, *J. Am. Chem. Soc.*, 1983, **105**, 3929-3939.
64. P. Burger and R. G. Bergman, *J. Am. Chem. Soc.*, 1993, **115**, 10462-10463.
65. D. M. Tellers, C. M. Yung, B. A. Arndtsen, D. R. Adamson and R. G. Bergman, *J. Am. Chem. Soc.*, 2002, **124**, 1400-1410.
66. B. K. Corkey, F. L. Taw, R. G. Bergman and M. Brookhart, *Polyhedron*, 2004, **23**, 2943-2954.
67. S. Niu and M. B. Hall, *J. Am. Chem. Soc.*, 1998, **120**, 6169-6170.
68. R. Waterman, *Organometallics*, 2013, **32**, 7249-7263.
69. D. Balcells, E. Clot and O. Eisenstein, *Chem. Rev.*, 2010, **110**, 749-823.
70. P. L. Watson, *J. Am. Chem. Soc.*, 1983, **105**, 6491-6493.

71. P. L. Watson and G. W. Parshall, *Acc. Chem. Res.*, 1985, **18**, 51-56.
72. M. E. Thompson, S. M. Baxter, A. R. Bulls, B. J. Burger, M. C. Nolan, B. D. Santarsiero, W. P. Schaefer and J. E. Bercaw, *J. Am. Chem. Soc.*, 1987, **109**, 203-219.
73. W. H. Lam, G. Jia, Z. Lin, C. P. Lau and O. Eisenstein, *Chem. Eur. J.*, 2003, **9**, 2775-2782.
74. Z. Lin, *Coord. Chem. Rev.*, 2007, **251**, 2280-2291.
75. J. Oxgaard, R. P. Muller, W. A. Goddard and R. A. Periana, *J. Am. Chem. Soc.*, 2004, **126**, 352-363.
76. N. J. DeYonker, N. A. Foley, T. R. Cundari, T. B. Gunnoe and J. L. Petersen, *Organometallics*, 2007, **26**, 6604-6611.
77. N. A. Foley, T. B. Gunnoe, T. R. Cundari, P. D. Boyle and J. L. Petersen, *Angew. Chem. Int. Ed.*, 2008, **47**, 726-730.
78. J. Oxgaard, R. A. Periana and W. A. Goddard, *J. Am. Chem. Soc.*, 2004, **126**, 11658-11665.
79. R. N. Perutz and S. Sabo-Etienne, *Angew. Chem. Int. Ed.*, 2007, **46**, 2578-2592.
80. B. A. Vastine and M. B. Hall, *J. Am. Chem. Soc.*, 2007, **129**, 12068-12069.
81. J. R. Webb, S. A. Burgess, T. R. Cundari and T. B. Gunnoe, *Dalton Trans.*, 2013, **42**, 16646-16665.
82. W. J. Tenn, K. J. H. Young, G. Bhalla, J. Oxgaard, W. A. Goddard and R. A. Periana, *J. Am. Chem. Soc.*, 2005, **127**, 14172-14173.
83. Y. Feng, M. Lail, K. A. Barakat, T. R. Cundari, T. B. Gunnoe and J. L. Petersen, *J. Am. Chem. Soc.*, 2005, **127**, 14174-14175.
84. W. J. Tenn, K. J. H. Young, J. Oxgaard, R. J. Nielsen, W. A. Goddard and R. A. Periana, *Organometallics*, 2006, **25**, 5173-5175.
85. J. Oxgaard, W. J. Tenn, R. J. Nielsen, R. A. Periana and W. A. Goddard, *Organometallics*, 2007, **26**, 1565-1567.
86. T. R. Cundari, T. V. Grimes and T. B. Gunnoe, *J. Am. Chem. Soc.*, 2007, **129**, 13172-13182.
87. Y. Feng, M. Lail, N. A. Foley, T. B. Gunnoe, K. A. Barakat, T. R. Cundari and J. L. Petersen, *J. Am. Chem. Soc.*, 2006, **128**, 7982-7994.
88. A. E. Shilov and A. A. Shteinman, *Coord. Chem. Rev.*, 1977, **24**, 97-143.
89. E. S. Aleksandr, *Russ. Chem. Rev.*, 1987, **56**, 442-464.
90. J. A. Labinger and J. E. Bercaw, *J. Organomet. Chem.*, 2015, **793**, 47-53.
91. S. S. Stahl, J. A. Labinger and J. E. Bercaw, *Angew. Chem. Int. Ed.*, 1998, **37**, 2180-2192.
92. S. S. Stahl, J. A. Labinger and J. E. Bercaw, *J. Am. Chem. Soc.*, 1996, **118**, 5961-5976.
93. P. E. M. Siegbahn and R. H. Crabtree, *J. Am. Chem. Soc.*, 1996, **118**, 4442-4450.
94. S. S. Stahl, J. A. Labinger and J. E. Bercaw, *J. Am. Chem. Soc.*, 1995, **117**, 9371-9372.
95. H. A. Jenkins, G. P. A. Yap and R. J. Puddephatt, *Organometallics*, 1997, **16**, 1946-1955.
96. G. A. Olah, *Acc. Chem. Res.*, 1971, **4**, 240-248.
97. M. Jacques, *Arene Chemistry: Reaction Mechanisms and Methods for Aromatic Compounds*, United States: John Wiley & Sons Inc, 2015.
98. H. Zollinger, *Adv. Phys. Org. Chem.*, 1964, **2**, 163-200.
99. D. L. Davies, S. M. A. Donald and S. A. Macgregor, *J. Am. Chem. Soc.*, 2005, **127**, 13754-13755.

100. M. Lafrance, C. N. Rowley, T. K. Woo and K. Fagnou, *J. Am. Chem. Soc.*, 2006, **128**, 8754-8756.
101. S. I. Gorelsky, D. Lapointe and K. Fagnou, *J. Am. Chem. Soc.*, 2008, **130**, 10848-10849.
102. D. L. Davies, S. M. A. Donald, O. Al-Duaij, S. A. Macgregor and M. Pölleth, *J. Am. Chem. Soc.*, 2006, **128**, 4210-4211.
103. Y. Boutadla, O. Al-Duaij, D. L. Davies, G. A. Griffith and K. Singh, *Organometallics*, 2009, **28**, 433-440.
104. D. H. Ess, S. M. Bischof, J. Oxgaard, R. A. Periana and W. A. Goddard, *Organometallics*, 2008, **27**, 6440-6445.
105. W. Ma, R. Mei, G. Tenti and L. Ackermann, *Chem. Eur. J.*, 2014, **20**, 15248-15251.
106. A. D. Ryabov, I. K. Sakodinskaya and A. K. Yatsimirsky, *J. Chem. Soc., Dalton Trans.*, 1985, 2629-2638.
107. A. D. Ryabov, *Chem. Rev.*, 1990, **90**, 403-424.
108. M. D. K. Boele, G. P. F. van Strijdonck, A. H. M. de Vries, P. C. J. Kamer, J. G. de Vries and P. W. N. M. van Leeuwen, *J. Am. Chem. Soc.*, 2002, **124**, 1586-1587.
109. M. Gómez, J. Granell and M. Martinez, *Organometallics*, 1997, **16**, 2539-2546.
110. B. Biswas, M. Sugimoto and S. Sakaki, *Organometallics*, 2000, **19**, 3895-3908.
111. J. Váňa, T. Terencio, V. Petrović, O. Tischler, Z. Novák and J. Roithová, *Organometallics*, 2017, **36**, 2072-2080.
112. M. Lafrance and K. Fagnou, *J. Am. Chem. Soc.*, 2006, **128**, 16496-16497.
113. D. García-Cuadrado, P. de Mendoza, A. A. C. Braga, F. Maseras and A. M. Echavarren, *J. Am. Chem. Soc.*, 2007, **129**, 6880-6886.
114. D. García-Cuadrado, A. A. C. Braga, F. Maseras and A. M. Echavarren, *J. Am. Chem. Soc.*, 2006, **128**, 1066-1067.
115. S. Pascual, P. de Mendoza, A. A. C. Braga, F. Maseras and A. M. Echavarren, *Tetrahedron*, 2008, **64**, 6021-6029.
116. S. I. Gorelsky, D. Lapointe and K. Fagnou, *J. Org. Chem.*, 2012, **77**, 658-668.
117. A. Petit, J. Flygare, A. T. Miller, G. Winkel and D. H. Ess, *Org. Lett.*, 2012, **14**, 3680-3683.
118. W. Bauer, M. Prem, K. Polborn, K. Sünkel, W. Steglich and W. Beck, *Eur. J. Inorg. Chem.*, 1998, **1998**, 485-493.
119. D. L. Davies, O. Al-Duaij, J. Fawcett, M. Giardiello, S. T. Hilton and D. R. Russell, *Dalton Trans.*, 2003, 4132-4138.
120. Y. Boutadla, D. L. Davies, S. A. Macgregor and A. I. Poblador-Bahamonde, *Dalton Trans.*, 2009, 5887-5893.
121. D. L. Davies, S. M. A. Donald, O. Al-Duaij, J. Fawcett, C. Little and S. A. Macgregor, *Organometallics*, 2006, **25**, 5976-5978.
122. K. J. T. Carr, D. L. Davies, S. A. Macgregor, K. Singh and B. Villa-Marcos, *Chem. Sci.*, 2014, **5**, 2340-2346.
123. D. A. Frasco, S. Mukherjee, R. D. Sommer, C. M. Perry, N. S. Lambic, K. A. Abboud, E. Jakubikova and E. A. Ison, *Organometallics*, 2016, **35**, 2435-2445.
124. Y. Yamamoto, *Chem. Soc. Rev.*, 2014, **43**, 1575-1600.
125. G. Song, F. Wang and X. Li, *Chem. Soc. Rev.*, 2012, **41**, 3651-3678.
126. C. Wang and J. Xiao, *Chem. Commun.*, 2017, **53**, 3399-3411.
127. A. G. Algarra, W. B. Cross, D. L. Davies, Q. Khamker, S. A. Macgregor, C. L. McMullin and K. Singh, *J. Org. Chem.*, 2014, **79**, 1954-1970.

128. D. L. Davies, C. E. Ellul, S. A. Macgregor, C. L. McMullin and K. Singh, *J. Am. Chem. Soc.*, 2015, **137**, 9659-9669.
129. N. Umeda, K. Hirano, T. Satoh, N. Shibata, H. Sato and M. Miura, *J. Org. Chem.*, 2011, **76**, 13-24.
130. T. K. Hyster and T. Rovis, *J. Am. Chem. Soc.*, 2010, **132**, 10565-10569.
131. D. R. Stuart, M. Bertrand-Laperle, K. M. N. Burgess and K. Fagnou, *J. Am. Chem. Soc.*, 2008, **130**, 16474-16475.
132. D. R. Stuart, P. Alsabeh, M. Kuhn and K. Fagnou, *J. Am. Chem. Soc.*, 2010, **132**, 18326-18339.
133. E. Tan, O. Quinero, M. Elena de Orbe and A. M. Echavarren, *ACS Catal.*, 2018, **8**, 2166-2172.
134. M. Schinkel, I. Marek and L. Ackermann, *Angew. Chem. Int. Ed.*, 2013, **52**, 3977-3980.
135. J. Wencel-Delord, C. Nimphius, F. W. Patureau and F. Glorius, *Angew. Chem. Int. Ed.*, 2012, **51**, 2247-2251.
136. J. Wencel-Delord, C. Nimphius, H. Wang and F. Glorius, *Angew. Chem. Int. Ed.*, 2012, **51**, 13001-13005.
137. M. Simonetti, G. J. P. Perry, X. C. Cambeiro, F. Juliá-Hernández, J. N. Arokianathar and I. Larrosa, *J. Am. Chem. Soc.*, 2016, **138**, 3596-3606.
138. M. Simonetti, R. Kuniyil, S. A. Macgregor and I. Larrosa, *J. Am. Chem. Soc.*, 2018, **140**, 11836-11847.
139. Y.-F. Liang, L. Yang, T. Rogge and L. Ackermann, *Chem. Eur. J.*, 2018, **24**, 16548-16552.
140. R. A. Alharis, C. L. McMullin, D. L. Davies, K. Singh and S. A. Macgregor, *J. Am. Chem. Soc.*, 2019, **141**, 8896-8906.

Chapter Two

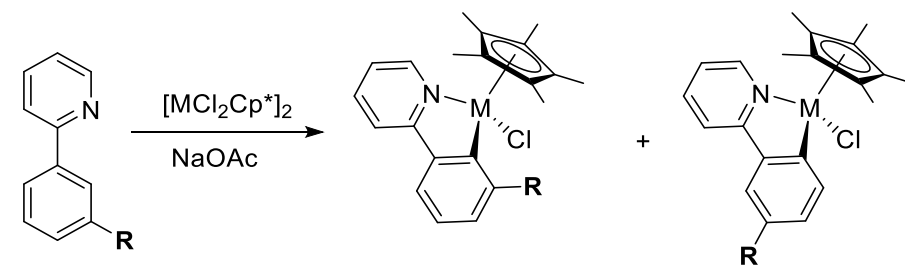
2.1 Introduction

The cyclometallation of ligands by transition metals is one of the most common organometallic reactions with the first example reported in the early 1960s¹ and the term “cyclometallation” introduced in the early 1970s.² Cyclometallated complexes have a vast range of applications in organic synthesis,³⁻⁵ catalysis,⁶⁻⁸ photochemistry,⁹⁻¹¹ organic-light emitting diodes (OLEDs),^{12, 13} sensors,¹⁴⁻¹⁶ biology¹⁷⁻¹⁹ and medicine.²⁰⁻²² Additionally, they are often intermediates in catalytic reactions, and are used in mechanistic investigations.²³⁻²⁵ Many cyclometallation reactions taking place via a C–H bond cleavage have been used to probe the mechanism and selectivities of the C–H activation. As mentioned in Chapter 1 Ryabov’s studies on cyclometallation of substituted dimethylbenzylamines with Pd(OAc)₂ (**Scheme 1.20**) showed preferential reactivity with electron-donating substituents and was proposed to take place through an S_EAr mechanism via an arenium ion.²⁶ However, later DFT calculations indicated an AMLA-6 transition state for this reaction which also favoured electron-donating substituents (**Figure 1.4**).²⁷ Cyclometallations of different *N*-alkylimines (**L1.39-1.44**) via an AMLA-6 mechanism with [IrCl₂Cp*]₂ (**Scheme 1.29**) were shown to favour activation of the more electron-rich pyrrole compared to furan, thiophene and phenyl.²⁸ Below, the most significant studies of steric and electronic effects on carboxylate assisted cyclometallation at half-sandwich complexes are described and their implications for understanding the mechanism(s) of C–H activation are discussed.

Jones *et al.* reported cyclometallation of *para*-(**L2.1-R**, R = OMe, CF₃) and *meta*-substituted phenylimines (**L2.2-R**, R = OMe, Me, F, COOH, CF₃, CN) (**Scheme 2.1**, **Table 2.1**) with [MCl₂Cp*]₂ (M = Ir, Rh) in the presence of NaOAc.²⁹ The reaction of **L2.1-R** (R = OMe) was faster than the strongly electron-withdrawing (R = CF₃) ligand (**Scheme 2.1**, **i**). Additionally, reactions with Ir were found to be 2-4 times faster than the respective ones with Rh. The authors argued that greater reaction rates with electron-donating groups and increased reactivity with Ir were indicators that these cyclometallations proceed via an S_EAr mechanism.

OMe and CN) two isomers were formed but the *para*-isomer was still preferred. However, for **L2.2-F** the *ortho*-isomer was favoured. The formation of *ortho*-fluorine compounds in C–H activation reactions has been observed before and is known as the “*ortho* effect”.³⁰⁻³² In the same publication, Jones *et al.* investigated cyclometallation of *meta*-substituted phenylpyridines **L2.3-R** (R = OMe, Me, CF₃) with [MCl₂Cp*]₂ (M = Ir, Rh) (**Table 2.2**).²⁹ The reactions showed similar selectivity with *para*-isomers favoured for more bulky substituents but the selectivity was less than with the imines. The authors suggested this is because the phenyl imines are more bulky than the corresponding pyridines. There was no discussion in the paper whether the electronic selectivity or the regioselectivity of these reactions is kinetic and/or thermodynamic in origin.

Table 2.2: Regioselectivities of cyclometallation of *meta*-substituted phenylpyridines **L2.3-R** with [MCl₂Cp*]₂ (M = Ir, Rh).²⁹



L2.3-R
R = OMe, Me, CF₃

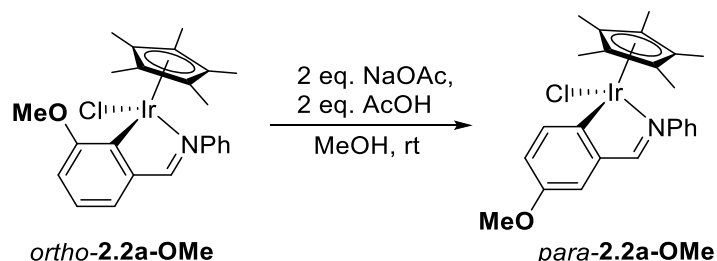
M = Ir, **a** *ortho*-2.3a-R
M = Rh, **b** *ortho*-2.3b-R

para-2.3a-R
para-2.3b-R

R	M = Ir, <i>o:p</i>	M = Rh, <i>o:p</i>
OMe	1:1.1	1:2.6
Me	<i>para</i> -only	1:50
CF ₃	1:6.4	1:8.4

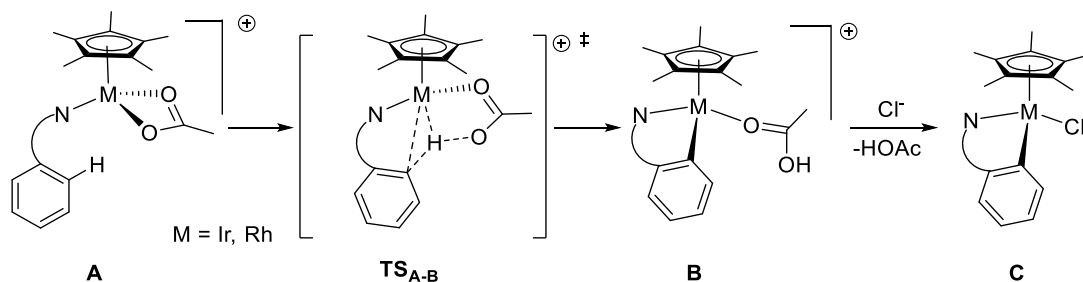
Solvent and temperature effects on the reactions were also investigated with ligand **L2.2-OMe** with Ir and Rh. The reactions with both metals were faster at higher temperatures (up to 85 °C) however with *ortho:para* isomer ratios remaining the same for Rh and slightly increasing in favour of *para*-isomer for Ir (from 1:1.3 in MeCN at rt to 1:1.7 in MeCN at 85 °C). Reactions for both metals were also faster in MeOH compared to DCM or MeCN. In addition, with Ir the *ortho:para* ratios showed a small variation with solvent (1:1.1 in MeOH, 1:1.3 in MeCN, 1:1.7 in DCM), whilst for Rh the isomer ratios did not change with solvent. In addition, heating isolated *ortho*-2.2a-OMe with AcOH in MeOH (**Scheme 2.2**) gave 5% conversion to the *para*-2.2a-OMe isomer indicating that the C–

H activation is reversible under these conditions. Using trifluoroacetic acid in MeOH an equilibrium ratio of 1:1.1 *ortho:para* **2.2a-OMe** was observed in 2 hours. Similar acid-promoted rearrangements have been observed previously with palladacycles.³³ The slow reversibility of the reaction with added AcOH suggests that the reactions with Ir are under kinetic rather than thermodynamic control.



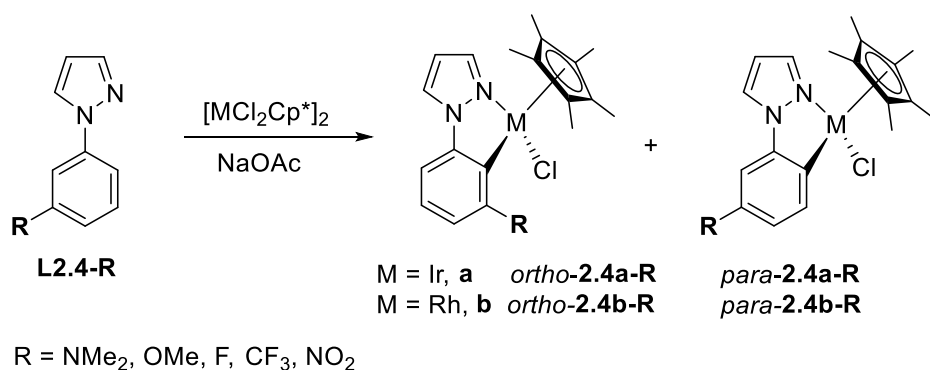
Scheme 2.2: Acid effect on C–H activation with **2.2a-OMe** complex.²⁹

Later computational studies by Zhang *et al.*³⁴ on the cyclometallations of phenylimines (**Scheme 2.1**) suggested that these reactions proceed through three steps (**Scheme 2.3**): (i) formation of a precursor for C–H activation **A** (this itself maybe two steps: ligand binding and anion dissociation) (ii) C–H activation via **TSA-B** and (iii) substitution of acetic acid by chloride to form **C**.³⁴ Overall this is very similar to the mechanism proposed by Davies and Macgregor (**Scheme 1.29, Figure 1.12**) for C–H activation of various *N*-alkylimines (**L1.39-1.44**).²⁸ In the study by Zhang *et al.*, the reaction of phenylimine was computed to be favoured kinetically and thermodynamically at Ir over Rh.³⁴ This agrees with the Ir reactions being faster experimentally but the higher activation energies for Rh are inconsistent with the reversibility of the reactions often seen at that metal. Indeed Davies *et al.* used H/D exchange experiments to demonstrate the reversible cyclometallation of *N*-phenylbenzaldimine at $[\text{RhCl}_2\text{Cp}^*]_2$ whereas no exchange was seen with $[\text{IrCl}_2\text{Cp}^*]_2$.²⁸ In that case computational studies showed similar activation barriers of around 18 kcal mol⁻¹ at both Rh and Ir, but that cyclometallation at Ir was significantly more exergonic.



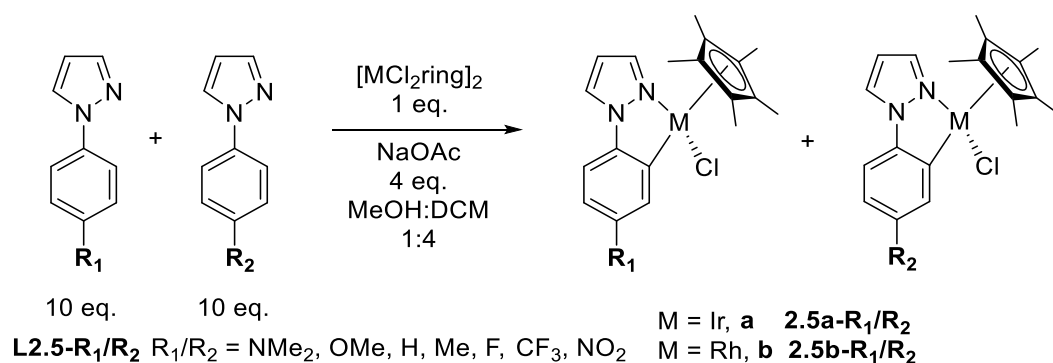
Scheme 2.3: C–H activation via an AMLA-6 TS activation of ligands containing *N*-directing groups with $[\text{MCl}_2\text{Cp}^*]_2$ ($\text{M} = \text{Ir}, \text{Rh}$) as proposed by Zhang *et al.*³⁴ and Davies *et al.*²⁸

More recently, Alharis as part of the Davies and Macgregor collaboration, carried out a detailed experimental and computational study of steric and electronic effects on cyclometallation of *meta*-(**L2.4-R**) and *para*-(**L2.5-R**) substituted phenylpyrazoles with $[\text{MCl}_2\text{Cp}^*]_2$ ($\text{M} = \text{Ir}, \text{Rh}$) (**Scheme 2.4**).³⁵ In general, the reactions were shown to be sensitive to steric effects with *para*-isomers being formed exclusively observed for larger substituents (**L2.4-R**, $\text{R} = \text{NMe}_2, \text{CF}_3$) for both metals. For **L2.4-F** the *ortho* regioisomer was the major one as expected due to “*ortho* effect”.³⁰⁻³² For **L2.4-OMe** and **NO₂** both isomers were formed. Significantly some of the isomer ratios, changed over time, particularly those with Rh suggesting the initial ratios may have indicated kinetic selectivity but the later ones were showing thermodynamic selectivity. In addition, H/D exchange reactions showed that reactions with electron-donating substituents are more reversible than with electron-withdrawing groups. Surprisingly in some cases H/D exchange was observed in the *ortho* position even though none of that isomer was isolated in the products suggesting that *ortho* C–H activation is possible but very reversible in some cases. The DFT calculations demonstrated that instead of *ortho*-isomers having a higher barrier to the reaction, they are often kinetically favoured with lower transition states for C–H activation than for *para*-isomers however, the *para*-isomers are often favoured thermodynamically. The calculations for the reactions with **L2.4-F** for both metals showed that the *ortho*-isomer is both kinetically and thermodynamically favoured.



Scheme 2.4: Cyclometallation of *meta*-substituted phenylpyrazoles **L2.4-R** with $[\text{MCl}_2\text{Cp}^*]_2$ (M = Ir, Rh).³⁶

Alharis also assessed the electronic effects by employing competition experiments (**Scheme 2.5**) and DFT calculations.³⁵ The relative proportions of products formed were used to get relative rates of reactions with different substituents which were compared with Hammett plots. Both, experimental data and DFT calculations demonstrated that substrates with electron-donating groups are favoured kinetically consistent with results of Jones *et al.*²⁹ However, surprisingly the thermodynamic selectivity was entirely opposite with ligands with electron-withdrawing groups being favoured. Additionally, reactions with Ir were relatively irreversible and generally under kinetic control, whilst reactions with Rh were reversible and often showed thermodynamic selectivity after longer reaction times.



Scheme 2.5: Competition experiments of *para*-substituted phenylpyrazoles with $[\text{MCl}_2\text{Cp}^*]_2$ (M = Ir, Rh).³⁵

From the kinetic results linear Hammett plots with good correlations (≥ 0.96) with slopes (ρ) of -2.7 for Ir, and -2.3 for Rh, were produced. The negative slopes are relatively small compared to usual values obtained for $\text{S}_{\text{E}}\text{Ar}$ (-5 to -9)³⁶ and the transition states showed

little evidence for build-up of positive charge in the phenyl being activated.³⁵ Hence the reaction was proposed to go via an AMLA-6 mechanism.

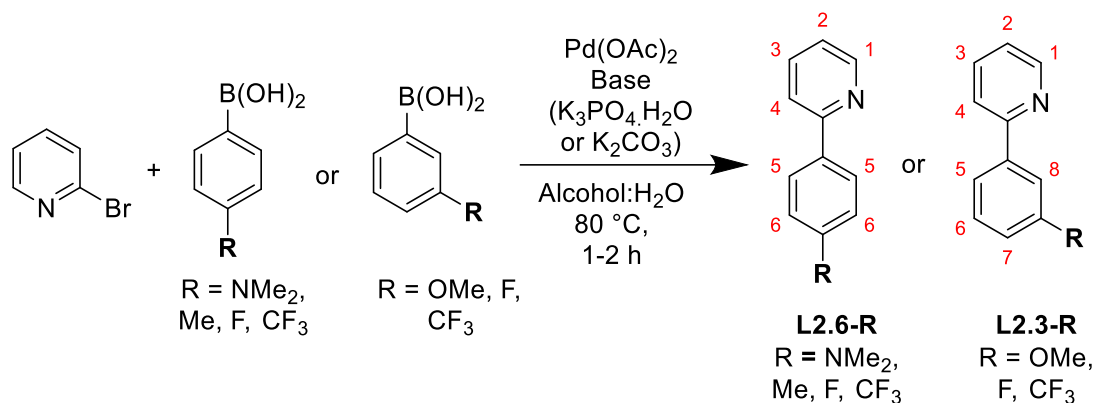
The aim of this chapter is to investigate electronic and steric effects on acetate-assisted C–H activation with phenylpyridines with Ir and Rh half-sandwich complexes to assess whether (i) the donor group plays a significant role in determining product selectivity (ii) the donor group has a significant effect on reversibility and hence whether kinetic or thermodynamic selectivity is observed (iii) the kinetic and thermodynamic selectivities are different for phenylpyridines than was found for phenylpyrazoles.

2.2 Results and Discussion

This section will describe the preparation and characterisation of Ir(III) and Rh(III) half-sandwich cyclometallated complexes with *para*-substituted 2-phenylpyridines (**L2.6-R**, R = NMe₂, Me, H, F, CF₃) and *meta*-substituted ones (**L2.3-R**, R = OMe, F, CF₃). Intermolecular competition experiments between differently substituted ligands are utilised to study electronic effects on the C–H activation with both metals. The complexes **2.6a-R** (R = H, CF₃) were prepared by Joanna Barker, and complexes **2.6b-R** (R = NMe₂, Me, H, F, CF₃) by Geena Saini both under my guidance. All the data analysis, competition and deuteration experiments were carried out by myself. Unless otherwise stated the ligands were characterised by ¹H NMR, ¹³C NMR, COSY, HSQC spectroscopy and ESIMS spectrometry. All new compounds were characterised by ¹H and ¹³C NMR spectroscopy, alongside appropriate 2-D NMR techniques (COSY, NOESY, HSQC) and HRMS spectrometry or microanalysis; some complexes were characterised by single crystal X-ray diffraction (Note, these were performed by Mr K. Singh).

2.2.a Synthesis of substituted phenylpyridines

Para-(**L2.6-R**) and *meta*-(**L2.3-R**) substituted 2-phenylpyridines were prepared employing a Suzuki cross-coupling by a literature procedure (**Scheme 2.6**).³⁷ The reactions between 2-bromopyridine and substituted boronic acids were heated to 80 °C in *i*PrOH:H₂O or EtOH:H₂O mixture in the presence of a base (K₃PO₄·H₂O or K₂CO₃) and Pd(OAc)₂ catalyst. Reactions proceeded with high conversions (>90%) and after purification by column chromatography **L2.6-R** (R = NMe₂, Me, F, CF₃), **L2.3-R** (R = OMe, F, CF₃) were obtained in moderate to good yields (45-88%).



Scheme 2.6: Preparation and labelling of substituted 2-phenylpyridines.

All of the ligands have been previously reported and their ^1H NMR spectra agree with the literature and are discussed briefly below.³⁷⁻³⁹ For example, the ^1H NMR spectrum of **L2.6-NMe₂** shows four signals for the pyridine; a doublet of doublets of doublets at δ 7.11 for H², a 2H multiplet at δ 7.66 due to overlap of H³ and H⁴ and H¹ as the most downfield signal a doublet of triplets at δ 8.62. The AA'BB' system shows two mutually coupled doublets at δ 6.80 and δ 7.92 for H⁶ and H⁵ respectively. Additionally, a 6H singlet at δ 3.05 is observed for the NMe₂ group. The ^1H NMR spectra of the other ligands **L2.6-R** (R = Me, F, CF₃) show very similar signals for the pyridine, chemical shifts within 0.2 ppm of those of **L2.6-NMe₂**. Phenyl protons H⁵ do not show significant variation (all within 0.2 ppm), whilst signals for H⁶ with **L2.6-CF₃** (at *ca.* δ 7.80) *ca.* 1 ppm downfield compared to **L2.6-NMe₂** (at δ 6.80) indicating a deshielding effect of a strongly electron-withdrawing group with **L2.6-R** (R = Me, F) in between the two (at δ 7.27 and 7.16 for **L2.6-Me** and **L2.6-F** respectively) (see Chapter 6 for details).

For the *meta*-substituted ligands **L2.3-R** (R = OMe, F, CF₃) the ^1H NMR spectra show pyridine protons within 0.2 ppm of the respective ones of **L2.6-R** whilst the phenyls show four inequivalent protons. The ^{13}C NMR spectra show the expected number of signals for all quaternary and CH carbons for **L2.6-R** (R = NMe₂, Me, F, CF₃) and **L2.3-R** (R = OMe, F, CF₃) (see Chapter 6 for details).

2.2.b Cyclometallation of *para*-substituted phenylpyridines

The ligands (**L2.6-R**, R = H, NMe₂, Me, F, CF₃) were reacted with the appropriate metal dimer $[\text{MCl}_2\text{Cp}^*]_2$ (M = Ir, Rh) in the presence of NaOAc in DCM:MeOH 4:1 mixture for Ir and in MeOH for Rh following a procedure developed in the group (reported by

protons did not show a significant change in chemical shift (<0.3 ppm). The three phenyl protons are a doublet of doublet at δ 6.44, a narrow doublet at δ 7.15 and a doublet at δ 7.46. In the NOESY spectrum the narrow doublet δ 7.15 shows an NOE with the NMe₂ and Cp* singlets so is assigned as H^{6a}, whilst the signal at δ 7.46 shows an NOE with the pyridine signal H⁴ at δ 7.57 so is assigned as H^{5b} leaving the doublet of doublets at δ 6.44 as H^{6b}. Compared to the free ligand protons (δ 6.80 and δ 7.92 for H⁶ and H⁵ respectively) H^{5b} and H^{6b} in the complex are shifted upfield by about 0.4 ppm in agreement with increased electron density on the ring upon cyclometallation, whilst H^{6a} is shifted downfield by about 0.4 ppm possibly due to the close proximity to the chloride. The ¹³C NMR spectra for **2.6b-NMe₂** show the expected number of signals with the cyclometallated carbon C^{5a} as a doublet at δ 180.2 (J_{C-Rh} = 31.1 Hz) downfield compared to the free ligand at δ 127.7. In addition, for **2.6b-NMe₂** the signal for the C₅Me₅ appears as a doublet at δ 95.6 (J_{C-Rh} = 6.0 Hz). The HRMS(ESI) spectra show ions at m/z 525.1880 due to [M-Cl]⁺ for **2.6a-NMe₂** and at m/z 476.1569 due to [M-Cl+MeCN]⁺ for **2.6b-NMe₂**.

The reactions of **L2.6-Me** with [IrCl₂Cp*]₂ and [RhCl₂Cp*]₂ after precipitation gave **2.6a-Me** and **2.6b-Me** in 90% and 73% yields respectively. The ¹H NMR spectrum of **2.6a-Me** agrees with the literature.⁴² The Rh complex **2.6b-Me** is new and shows singlets for Cp* and Me at δ 1.62 and δ 2.40 respectively. The signals for the pyridine group appear within 0.2 ppm of the signals of the free ligand. The phenyl protons show the same pattern as for **2.6b-NMe₂**, a doublet of doublets at δ 6.86 H^{6b}, a doublet at δ 7.49 H^{5b} and a signal at δ 7.61 due to H^{6a}. All the resonances **2.6b-Me** are within 0.2 ppm of the corresponding ones of **2.6a-Me**. The ¹³C NMR spectra for **2.6b-Me** shows the cyclometallated carbon C^{5a} as a doublet at δ 178.7 (J_{C-Rh} = 32.1 Hz) which is downfield compared to the free ligand at δ 129.5. The HRMS(ESI) spectra show ions at m/z 537.1890 and at m/z 447.1309 due to [M-Cl+MeCN]⁺ for **2.6a-Me** and **2.6b-Me** respectively.

Complexes **2.6a-F** and **2.6b-F** were prepared as described above in 61% and 82% yields respectively. Both complexes have been reported, for **2.6a-F** the data are in a different solvent to the literature but there is reasonable agreement with the reported data.⁴³ However for **2.6b-F** the phenyl protons were previously incorrectly reported as singlets.⁴⁴ The ¹H NMR spectrum of **2.6b-F** shows three signals for the phenyl and each show

additional coupling to the fluorine substituent: an apparent triplet of doublets ($J_{\text{H-H}} = 8.6$, 2.6 Hz, $J_{\text{H-F}} = 8.6$ Hz) at δ 6.75 for H^{6b}, a doublet of doublets ($J_{\text{H-H}} = 8.5$ Hz, $J_{\text{H-F}} = 5.4$ Hz) at δ 7.58 for H^{5b} and a doublet of doublets ($J_{\text{H-H}} = 2.6$ Hz, $J_{\text{H-F}} = 8.8$ Hz) at δ 7.50 for H^{6a}. The ¹³C NMR spectra for **2.6a-F** and **2.6b-F** show the expected number of signals for quaternary and CH carbons. The phenyl carbons, except the one attached to pyridine, were split into doublets due to coupling to the fluorine which also aided the assignment. For example for **2.6b-F** doublets are observed for C-F at δ 164.4 ($^1J_{\text{C-F}} = 254.0$ Hz), C^{6b} at δ 110.1 ($^2J_{\text{C-F}} = 24.1$ Hz), C^{6a} at δ 122.7 ($^2J_{\text{C-F}} = 18.1$ Hz), C^{5b} at δ 124.6 ($^3J_{\text{C-F}} = 9.0$ Hz) and cyclometallated carbon C^{5a} is a doublet of doublets (due to coupling to both Rh and F) at δ 181.3 ($J_{\text{C-Rh}} = 33.1$ Hz, $^3J_{\text{C-F}} = 4.3$ Hz). The ¹⁹F NMR spectra for **2.6a-F** and **2.6b-F** show singlets at *ca.* δ -111. The HRMS(ESI) spectra show ions at m/z 541.1641 due to $[\text{M-Cl+MeCN}]^+$ for **2.6a-F** and at m/z 410.0794 due to $[\text{M-Cl}]^+$ for **2.6b-F**.

Complexes **2.6a-CF₃** and **2.6b-CF₃** are both new, the reactions reached high conversions (>80%) and after precipitation the complexes were isolated in 72% and 48% yields respectively. The ¹H NMR spectrum of **2.6b-CF₃** shows the same pattern as for **2.6b-NMe₂** with phenyl signals as a doublet of doublets at δ 7.30 for H^{6b}, a doublet at δ 7.67 for H⁵ and a narrow doublet at δ 8.06 for H^{6a}. The ¹H NMR spectrum of Ir complex **2.6a-CF₃** is very similar to that of Rh analogue with all signals within 0.1 ppm of the corresponding ones in **2.6b-CF₃**. The ¹³C NMR spectra for both complexes show the expected number of signals, coupling with the CF₃ substituent was observed with several carbon signals being split into quartets. For example quartets are observed for **2.6b-CF₃** for CF₃ at 124.5 ($^1J_{\text{C-F}} = 273.1$ Hz), C-CF₃ at 130.8 ($^2J_{\text{C-F}} = 31.1$ Hz), C^{6b} at δ 119.8 ($^3J_{\text{C-F}} = 3.0$ Hz) and C^{6a} at 133.2 ($^3J_{\text{C-F}} = 4.0$ Hz). The cyclometallated carbon C^{5a} is a doublet at δ 178.4 ($J_{\text{C-Rh}} = 33.1$ Hz) for **2.6b-CF₃** and a singlet at δ 163.1 for **2.6a-CF₃**. The ¹⁹F NMR spectra for **2.6a-CF₃** and **2.6b-CF₃** show singlets at about δ -63. The HRMS(ESI) spectra show ions at m/z 550.1356 and at m/z 460.0750 due to $[\text{M-Cl}]^+$ for **2.6a-CF₃** and **2.6b-CF₃** respectively.

Two Ir complexes **2.6a-F** and **2.6a-CF₃** gave crystals suitable for the X-ray diffraction and the structures are shown below in **Figure 2.1** with selected bond distances and angles in **Table 2.3**. Data for **2.6a-H** reported by Davies *et al.*⁴⁵ is included for comparison. The structures of **2.6a-F** and **2.6a-CF₃** show the expected piano stool geometry. The data show that varying the substituent from H to F to CF₃ does not have a significant effect on

Table 2.3: Selected bond distances (Å) and bond angles [°] for **2.6a-H**,⁴⁵ **2.6a-F** and **2.6a-CF₃**.

	2.6a-H	2.6a-F	2.6a-CF₃
Ir—C(11)	2.058(5)	2.049(6)	2.043(8)
Ir—N	2.074(5)	2.099(5)	2.091(7)
Ir—Cl	2.405(2)	2.401(2)	2.401(2)
C(11)—Ir—N	78.0(2)	77.9(2)	78.1(3)

the geometry at the metal with the Ir—C(11) [2.058(5), 2.049(6) and 2.043(8) Å], Ir—Cl bond distances [2.405(2), 2.401(2) and 2.401(2) Å] and C—Ir—N bite angles [78.0(2), 77.9(2) and 78.1(3)°] for **2.6a-H**, **2.6a-F** and **2.6a-CF₃** respectively being statistically the same. Only the N—Ir bond distance [2.074(5), 2.099(5) and 2.091(7) Å for **2.6a-H**, **2.6a-F** and **2.6a-CF₃** respectively] shows a slightly bigger variation, however even this is too small to be chemically significant.

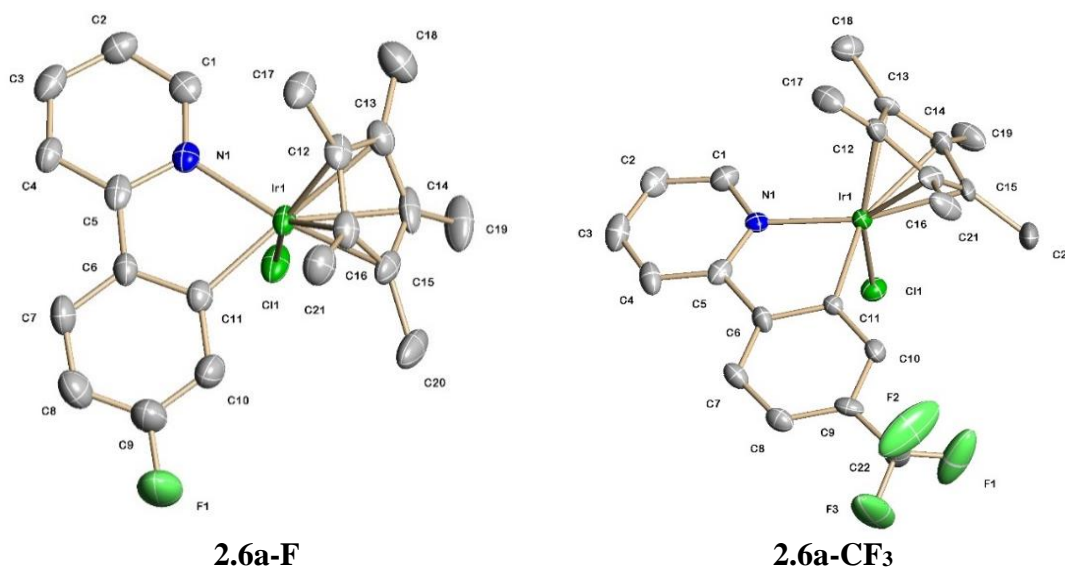
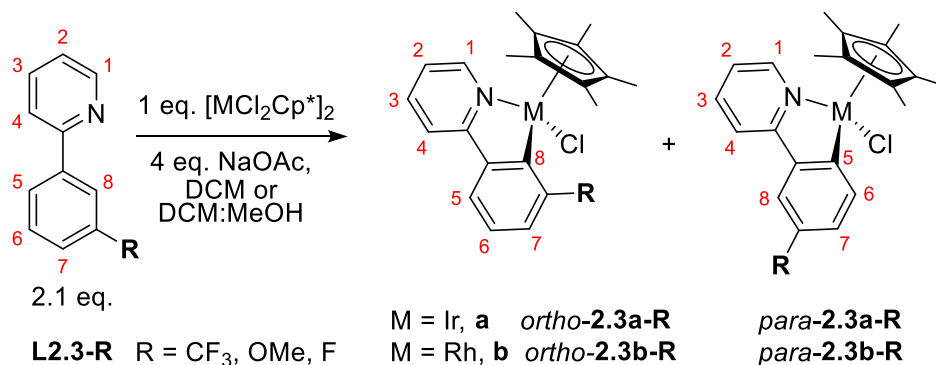


Figure 2.1: X-ray structures of **2.6a-F** and **2.6a-CF₃** showing 50% displacement ellipsoids. Hydrogen atoms have been omitted for clarity.

2.2.c Cyclometallation of *meta*-substituted phenylpyridines

The steric effects on the C—H activation were investigated by utilising the reactions of *meta*-substituted ligands (**L2.3-R**, R = OMe, F, CF₃) with [MCl₂Cp*]₂ (M = Ir, Rh) in the presence of NaOAc (**Scheme 2.8**). All of the reactions were carried out in DCM:MeOH (4:1) with reactions with Ir also repeated in DCM, and were monitored by ¹H NMR

spectroscopy after 15 minutes and again after 2 hours, and the observed isomer ratios are summarised in **Tables 2.4**. In some cases individual isomers were isolated after work up and this helped in identification of individual isomers in the mixtures. The characterisation of individual isomers will be described first then the isomer ratios will be discussed.



Scheme 2.8: Cyclometallation and labelling of **L2.3-R** with [MCl₂Cp*]₂ M = Ir, Rh.

The reactions of **L2.3-R** (R = CF₃, OMe) with [MCl₂Cp*]₂ (M = Ir, Rh) (**Scheme 2.8**) have been reported previously (**Table 2.2**),²⁹ and the NMR spectra agree with the literature but some key signals are discussed below. Complexes **2.3a-F** and **2.3b-F** are new. From the reactions of **L2.3-CF₃** with [MCl₂Cp*]₂ (M = Ir, Rh) complexes *para*-**2.3a-CF₃** and *para*-**2.3b-CF₃** were isolated after work up in 45 and 48% yields respectively. The ¹H NMR spectrum of *para*-**2.3a-CF₃** shows pyridine protons all within 0.2 ppm of the corresponding ones of the free ligand (see Chapter 6 for details). The signals for the three phenyl protons are a doublet of doublets at δ 7.40 for H⁷, a narrow doublet at δ 7.86 (*J* = 1.4 Hz) for H⁸ and a doublet at 7.93 due to H⁶. These clearly agree with the *para*-isomer rather than *ortho*. The ¹H NMR spectrum of *para*-**2.3b-CF₃** is very similar to the Ir analogue with all signals within 0.1 ppm of *para*-**2.3a-CF₃**. The ¹³C NMR spectra for *para*-**2.3a-CF₃** and *para*-**2.3b-CF₃** show the cyclometallated carbons as a singlet at δ 166.1 and as a doublet at 184.6 (*J*_{C-Rh} = 33.1 Hz) respectively. The ¹⁹F NMR spectra for both complexes show singlets at about δ -62. The HRMS(ESI) spectrum shows ions at *m/z* 550.1356 due to [M-Cl]⁺ for **2.3a-CF₃** and at *m/z* 460.0754 due to [M-Cl]⁺ for **2.3b-CF₃**.

From the reaction of **L2.3-OMe** with [RhCl₂Cp*]₂, **2.3b-OMe** was initially formed as a mixture (**Table 2.4**) but the *para*-isomer was isolated pure in 35% yield after crystallisation; the reported data is for a mixture of two isomers.²⁹ Mixture of two isomers

was isolated for the reaction of **L2.3-OMe** with $[\text{IrCl}_2\text{Cp}^*]_2$ and agrees with the reported data.²⁹ The ^1H NMR spectra of *para*-**2.3a/b-OMe** each show the same pattern as *para*-**2.3a/b-CF₃** and this aids the assignment of the ^1H NMR spectrum of the mixture of isomers *ortho*-**2.3a-OMe** and *para*-**2.3a-OMe**. For *ortho*-**2.3a-OMe** the phenyl shows two doublet of doublets at δ 6.76 H⁵ and 7.35 H⁷ and a triplet at 7.03 H⁶. The HRMS(ESI) spectrum show ions at m/z 512.158 due to $[\text{M-Cl}]^+$ for **2.3a-OMe** and at m/z 422.0985 due to $[\text{M-Cl}]^+$ for **2.3b-OMe**.

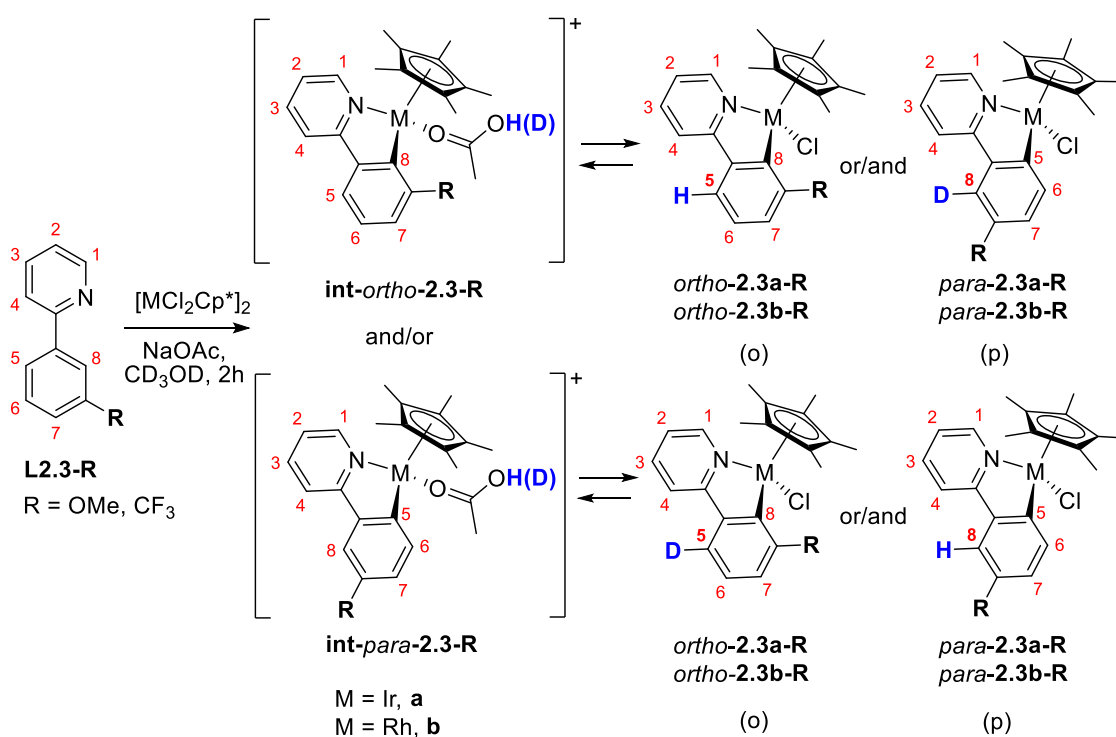
The reactions of **L2.3-F** with $[\text{MCl}_2\text{Cp}^*]_2$ (M = Ir, Rh) both led to a mixture of *ortho* and *para* isomers. For Ir the mixture of isomers was obtained in combined 92% yield, whilst for Rh recrystallisation allowed isolation of a single isomer in 43% yield. The ^1H NMR spectrum of the isolated Rh isomer shows phenyl signals as apparent triplets of doublets at δ 6.95 and 7.04 and a broad doublet at δ 7.46 which are assigned to H⁷, H⁶ and H⁵ respectively in *ortho*-**2.3b-F**. The assignment is confirmed by the observation of the cyclometallated carbon C⁵ at δ 159.7 as a doublet of doublets coupling to Rh and F with a large $J(\text{C-F})$ coupling constant ($^2J_{\text{C-F}} = 44.2$ Hz). For Ir the ^1H NMR spectrum of the mixture showed that the major isomer is *ortho*-**2.3a-F** with all signals within 0.1 ppm of the respective Rh complex, leaving the minor isomer as *para*-**2.3a-F**. The phenyl signals of *para*-**2.3a-F** are a multiplet at δ 6.97, and two doublet of doublets at δ 7.35 and 7.72. The signal at δ 7.35 has an NOE with H⁴ indicating it is H⁸ and the signal at 7.72 shows a correlation with Cp* in NOESY spectrum indicating it is H⁶, leaving the signal at δ 6.97 as H⁷. The ^{13}C NMR spectra for mixture of *ortho*-**2.3a-F** and *para*-**2.3a-F** and for *ortho*-**2.3b-F** showed the expected number of quaternary and CH carbons and the $J(\text{C-F})$ couplings provided confirmation of the assignment. For the mixture of *ortho*-**2.3a-F** and *para*-**2.3a-F** the cyclometallated carbons are doublets at δ 146.2 ($^2J_{\text{C-F}} = 42.2$ Hz) and at δ 166.4 ($^4J_{\text{C-F}} = 5.0$ Hz) respectively. The ^{19}F NMR spectra of the **2.3a-F** mixture and *ortho*-**2.3b-F** show singlets at δ -123.3 for *para*-**2.3a-F** and at δ ca. -94 for *ortho*-**2.3a/b-F**. The HRMS(ESI) spectrum show ions at m/z 541.1636 due to $[\text{M-Cl+MeCN}]^+$ for **2.3a-F** and at m/z 410.0783 due to $[\text{M-Cl}]^+$ for *ortho*-**2.3b-F**.

For the reactions of **L2.3-R** (R = OMe, CF₃, F) with Ir and Rh the ratios between two isomers were determined by ^1H NMR spectroscopy based on the relative integrations of the signals for H⁵ of the *ortho*-isomer and H⁷ of the *para*-isomer for **2.3a/b-OMe** mixtures, the signals for H⁵ of the *ortho*-isomer with signal for H⁶ of the *para*-isomer for

2.3a/b-F. The results for reactions with Ir and Rh are summarised in **Table 2.4** and the relevant results reported by Jones *et al.* also included.²⁹ In the case two isomers were observed at room temperature, the reactions were repeated and heated at 50 °C for two days.

As mentioned above, with the large CF₃ substituent only the less sterically hindered *para*-isomer is observed for both metals with only traces (less than 2%) of possible *ortho* isomer present in ¹⁹F NMR spectrum. The exclusive observation of only *para*-isomer for cyclometallation of **L2.3-CF₃** is not consistent with the value of 1:6.4 (*ortho:para*) reported by Jones *et al.* where *ortho*-isomer was still observed.²⁹ Note, the data provided for **L2.3-CF₃** reaction with Ir and Rh in the supplementary information of the paper does not agree with the data published in the paper – only the *para*-isomers are present in the ¹H NMR spectra of **2.3a/b-CF₃** in the supplementary information hence it is not possible to verify Jones' data.. With the smaller OMe group the *para*-isomer is slightly favoured over the *ortho*-isomer for Ir (*o:p* 1:1.3) but slightly more so for Rh (*o:p* 1:2.7). Heating the reactions of **L2.3-OMe** with Ir at 50 °C led to the significant increase in the preference for the *para*-isomer for Ir suggesting that reaction is reversible upon heating and at room temperature the results are kinetic, whilst thermodynamically the *para*-isomer is favoured. However, heating the reaction of **L2.3-OMe** with Rh at 50 °C only resulted in a small change in favour of the *para*-isomer (*o:p* 1:3.0), therefore, it is not clear if the initial ratios are kinetic or thermodynamic or both. The biggest difference between the two metals is seen with **L2.3-F**. The *ortho*-isomer is favoured over the *para* (*o:p* 3.4:1) for Ir but by a much larger ratio (*o:p* 11:1) for Rh. The preference for the *ortho*-isomer over the *para* with F substituent has been observed previously (phenylimines **Table 2.1**,²⁹ phenylpyrazoles)³⁵ and is further discussed below.³⁰⁻³² Heating the reactions of **L2.3-F** with Ir and Rh did not result in a change in ratios therefore, it is not clear if the initial ratios are kinetic or thermodynamic or both.

For the results shown in **Table 2.4**, with the exception of the reactions with **L2.3-OMe**, no significant change (all within experimental error) in *ortho:para* ratios were observed when reactions were monitored after 15 minutes or heating. This suggests that either the reactions are irreversible and are under kinetic control or are reversible and have already reached equilibrium upon monitoring. Therefore, to test if the reactions are reversible, cyclometallation reactions of **L2.3-R** (R = OMe, CF₃) with Ir and Rh were carried out in CD₃OD in the presence of NaOAc to see if deuterium exchange occurs (**Scheme 2.10**). If C–H activation is reversible then D-incorporation may be observed at site 8 of the *para*-isomer or at site 5 of the *ortho*-isomer. The ¹H NMR spectra for the reactions of **L2.3-OMe** were recorded after 15 minutes and 2 hours and for reactions of **L2.3-CF₃** after 2 hours. The relative D-incorporation was measured by comparing the relative integrations of signals H⁷ with H⁵ for the *ortho*-isomers and H⁶ with H⁸ for the *para*-isomers and the results are summarised in **Table 2.5**. The D-incorporation was confirmed in each case by running a ²H NMR spectrum.



Scheme 2.10: Deuterium incorporation experiments with **L2.3-R** (R = OMe, CF₃) with Ir and Rh.

Table 2.5: Deuteration of **L2.3-R** with Ir and Rh (in CD₃OD).

Entry	R	M	Time	<i>o:p</i>	% D in site 5 (<i>ortho</i> -isomer)	%D in site 8 (<i>para</i> -isomer)
1	CF ₃	Ir	2 h	<i>para</i> -only ^a	-	N.D.
2	CF ₃	Rh	2 h	<i>para</i> -only ^a	-	N.D.
3	OMe	Ir	15 min.	1.1:1	N.D.	N.D.
4	OMe	Ir	2 h	1.1:1	N.D.	N.D.
5	OMe	Rh	15 min.	1:2.2	N.D.	20
6	OMe	Rh	2 h	1:2.5	50	>80

N.D. not detected by ¹H and ²H NMR spectroscopy

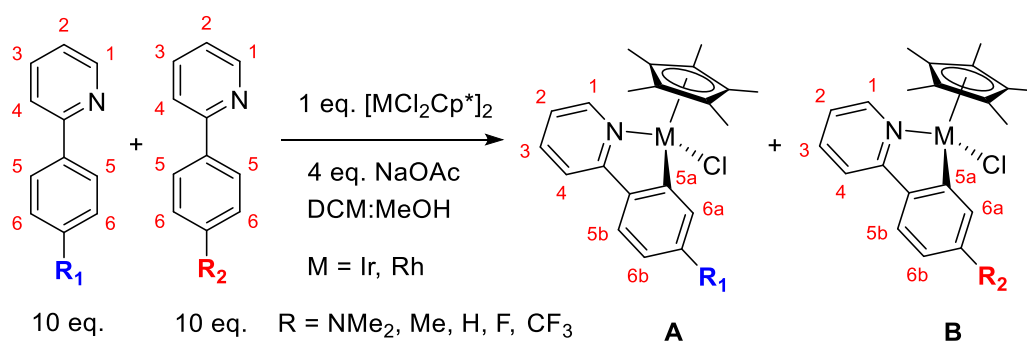
^aNo *ortho*-isomer was detected by ¹⁹F NMR spectroscopy

No D-incorporation was observed for cyclometallation of **L2.3-CF₃** with Ir and Rh (entries 1 and 2 respectively) or for cyclometallation of **L2.3-OMe** with Ir (entries 3 and 4). This suggests that these reactions are irreversible under these conditions and the regioselectivity is likely to be kinetic in origin. However, for cyclometallation of **L2.3-OMe** with Rh, D-incorporation was observed after 15 minutes in the *para*-isomer (*ca.* 20%) this means formation of *ortho*-isomer **int-ortho-2.3b-OMe** has occurred, undergone H/D exchange and then recyclometallated to form the *para*-**2.3b-OMe** with some incorporation of D in position 8. After 2 hours both the *ortho* (*ca.* 50%) and *para*-isomer (>80%) show D-incorporation indicating that C–H activation of both **2.3b-OMe** isomers is reversible. The observation of an increased amount of *para*-**2.3b-OMe** relative to the *ortho* suggests that the *para*-isomer is the thermodynamically favoured product. The initial observation of D-incorporation only in the *para*-isomer which has to go through the *ortho*-isomer first, suggests that the *ortho*-isomer may be kinetically favoured but is thermodynamically less stable so its formation is more reversible. Further experiments would be needed to confirm this. This suggests that the initially observed isomer ratio is possibly not a kinetic one and maybe at least some way towards equilibrium and the thermodynamic ratio. Overall, the results show that the reaction with Rh and **L2.3-OMe** is reversible, whilst that with the more electron-withdrawing substituent (R = CF₃) is irreversible at room temperature in MeOH. With either **L2.3-R** R = CF₃ or OMe each reaction with Ir is irreversible under these conditions hence are likely to be under kinetic control which is consistent with previous observations by Davies *et al.*²⁶ and Alharis.³⁵ Finally, the ratios observed for cyclometallation of **L2.3-**

OMe with Ir and Rh in CD₃OD (**Table 2.5**, entries 3-6) were slightly different from the results in DCM:MeOH mixture (**Table 2.4**) in all cases giving an increased proportion of the *ortho*-isomer which is now slightly favoured for Ir (1.1:1). The minor differences in ratios in different solvents may be due to solvent effects or may partially reflect the degree of reversibility in different solvents and hence the extent to which equilibration has taken place.

2.2.d Competition experiments with *para*-substituted phenylpyridines

In order to assess the electronic effects of the substituents on the C–H activation, the relative rates of the reactions were investigated. Problems with the solubility of NaOAc in organic solvents and the hydration state of the NaOAc may hamper the reproducibility of individual reactions, therefore, to ensure consistency and reproducibility the relative rates were measured by carrying out competition experiments between two substrates and measuring the relative proportions of the two formed products (**Scheme 2.11**).



Scheme 2.11: Competition experiments of **L2.6-R** with [MCl₂Cp*]₂ (M = Ir, Rh).

A fivefold excess of ligands compared to the metal centre was used to ensure that concentration of ligands remains relatively constant as the reaction progresses. Ratios of the two products formed were measured by ¹H NMR spectroscopy and/or, where applicable, ¹⁹F NMR spectroscopy. The drawback of using a large excess of the ligands is that small signals of products may overlap large peaks of ligands, however at least one set of the same signals (usually H^{6b}) (**Scheme 2.11**) was sufficiently isolated to be used to measure the relative ratios. Competition experiments were carried out in DCM:MeOH mixture and the ratio of products were measured at rt at short reaction times (15 minutes) and again after longer reaction times (2 hours) as well as after heating (reactions repeated in TFE as a solvent, 60-90 °C for 2 hours) to investigate whether there was any change in ratios and so whether the selectivity is kinetic or thermodynamic. It was decided to not

use *meta*-substituted ligands **L2.3-R** (R = OMe, F) in the competition experiments, due to the complication of formation of two isomers. In general, after 15 minutes the only {MCp*}(M = Ir, Rh) species observed in the ¹H NMR spectra were cyclometallated species **A** and **B** indicating a full conversion. The results for Ir are summarised in **Table 2.6**, and those for Rh in **Table 2.7** (see below).

Table 2.6: Results of competition experiments to form *meta*-substituted complexes of {IrCp*}.

Entry	R ₁	R ₂	A:B, 15 min, rt,	A:B, 15 min, rt,	A:B, 2 h, 60°C,
			DCM:MeOH	TFE	TFE
1	Me	NMe ₂	1:1.4	-	-
2	H	NMe ₂	-	1:1.2	1.3:1
3	H	Me	1:1.3	1.1:1	1.3:1
4	F	H	1:2.9	1:1.3	1.3:1 ^a
5	CF ₃	H	1:5.0	1:1.4	1.7:1 ^a
6	CF ₃	F	1:1.8	-	-

^a 90 °C, 2 hours

Table 2.7: Results of competition experiments to form *meta*-substituted complexes of {RhCp*}.

Entry	R ₁	R ₂	DCM:MeOH		TFE	
			A:B, 15 min., rt	A:B, 3 days, 50°C	A:B, 15 min., rt,	A:B, 2h, 60 °C
1	H	NMe ₂	1:2.9	1:1.2 ^a	1.2:1	1.4:1
2	H	Me	1:1.1	1.2:1	1.2:1	1.2:1
3	F	H	1:3.8	1.1:1 ^b	2.8:1	2.8:1
4	CF ₃	F	1:2.1	1:1.7	-	-
5	CF ₃	H	-	-	3.2:1	3.2:1

^a 2 days;

^b 2 hours

From the initial ratios (15 minutes, in DCM:MeOH) the relative rates of formation of *meta*-substituted complexes **2.6a/b-R** compared to the unsubstituted complex **2.6a/b-H** were calculated (k_R/k_H) and are presented in the **Table 2.8** together with the appropriate Hammett constants (σ_m). The Hammett plots are shown in **Figure 2.2**.

Table 2.8: Relative rates of formation of *meta*-substituted complexes of {IrCp*} and {RhCp*}.

M	Group	NMe ₂	Me	H	F	CF ₃
	σ_m	-0.15	-0.07	0	0.34	0.43
Ir	k_R/k_H	1.8 ^a	1.3	1	0.35	0.2
	$\log(k_R/k_H)$	0.26	0.11	0	-0.46	-0.70
Rh	k_R/k_H	2.9	1.1	1	0.26	0.13 ^b
	$\log(k_R/k_H)$	0.46	0.04	0	-0.59	-0.89

^a Calculated from **Table 2.6** first entries for 1 and 3: $1.4 \times 1.3 = 1.8$,

^b Calculated from **Table 2.7** first entries for 3 and 4: $1 : (3.8 \times 2.1) = 0.13$

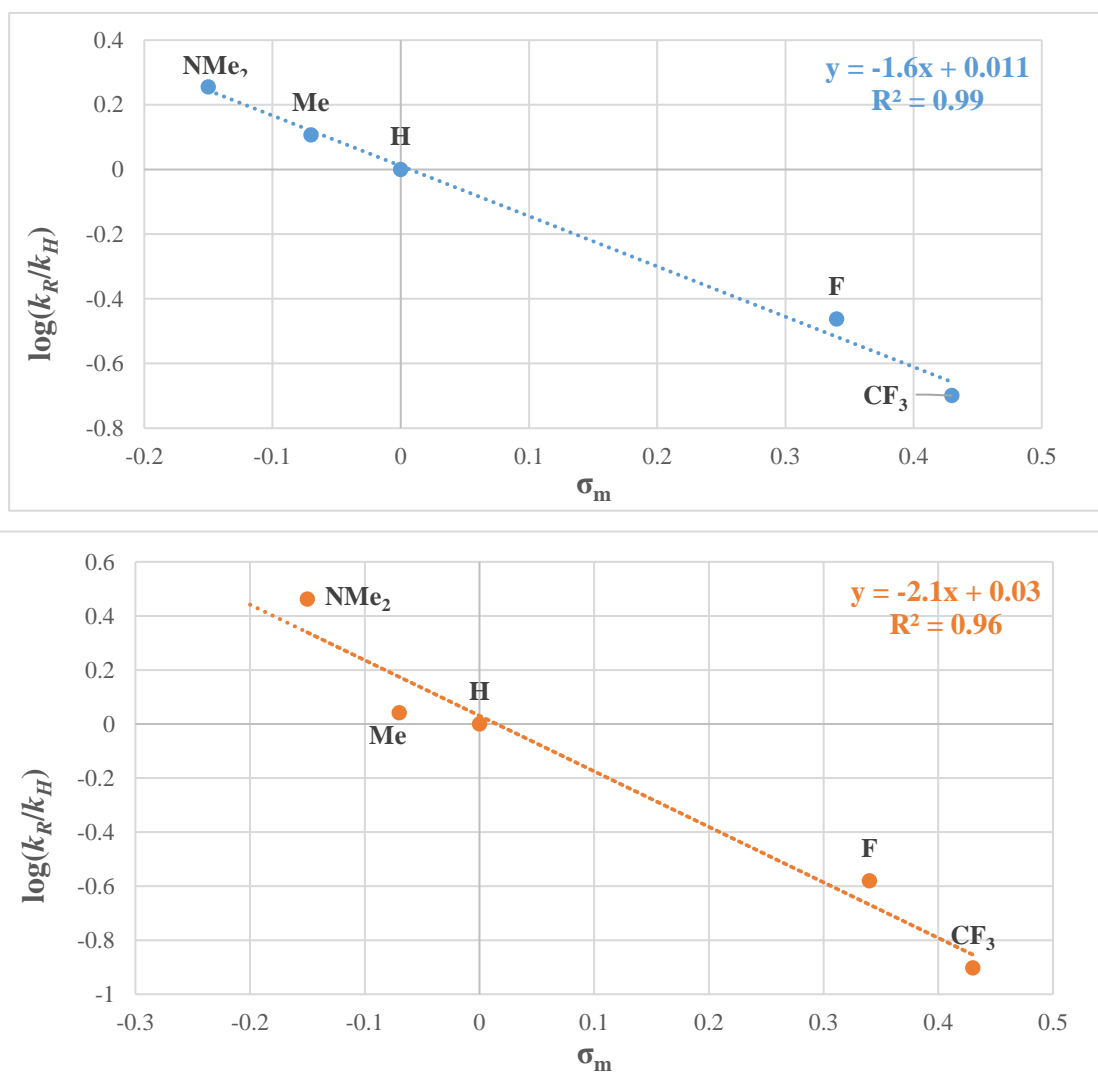


Figure 2.2: Hammett plot for formation of *meta*-cyclometallated complexes of Ir (top) and Rh (bottom), $\log(k_R/k_H)$ against σ_m .

The Hammett plots are straight lines with very good correlation for Ir ($R^2 = 0.99$) and a good correlation for Rh (0.96) which overall suggests that plotted results are kinetic in nature. However, slightly worse correlation for Rh compared to Ir could suggest that Rh reactions are starting to equilibrate at room temperature. The slopes are -1.6 and -2.3 for Ir and Rh respectively. The negative slopes are in agreement with an “electrophilic-type” mechanism with some build-up of positive charge in the transition state and facilitation of the reactions with electron-donating groups. Broadly speaking this is consistent with both a S_{EAr} and an AMLA mechanism. However, the slopes are significantly smaller than the usual values obtained for S_{EAr} reactions (-5 to -9)³⁶ suggesting an AMLA mechanism over S_{EAr} . The slope is similar to that obtained by Ryabov (-1.6)⁴⁸ for a Pd cyclometallation and that obtained for cyclometallation of substituted phenylpyrazoles with Ir (-2.7) and Rh (-2.3) all of which were proposed to go via an AMLA mechanism.²⁷

35

As seen in **Table 2.6** for Ir, using TFE as a solvent at room temperature gave slightly different ratios to those in DCM:MeOH. Upon heating in TFE the ratios changed further and favoured the product with the more electron-withdrawing substituent. As can be seen, (**Table 2.7**) for reactions with Rh in DCM:MeOH the ratios changed over time in favour of products with more electron-withdrawing substituents. When reactions with Rh were repeated in TFE and heated the selectivity was even more in favour of electron-withdrawing groups compared to DCM:MeOH (15 min., rt). Overall, the change in ratios upon heating for both Ir and Rh indicates that under these conditions, reactions are reversible showing thermodynamic selectivity and supports that the initial results (15 min., DCM:MeOH) are kinetic. The final ratios (**Tables 2.6** and **2.7**) were used to calculate the relative equilibrium constants for formation of **2.6a/b-R** and **2.6a/b-H**. The data are presented in **Table 2.9** and the corresponding Hammett plots ($\log(K_R/K_H)$ against σ_m for Ir(top) and Rh(bottom)) are shown in **Figure 2.3**.

Table 2.9: Relative equilibrium constants of formation of *meta*-substituted phenylpyridine complexes of {IrCp*} and {RhCp*}.

Group	NMe ₂	Me	H	F	CF ₃	
σ_m	-0.15	-0.07	0	0.34	0.43	
Ir	K_R/K_H	0.77	0.77	1	1.3	1.7
	$\log(K_R/K_H)$	-0.11	-0.11	0	0.11	0.23
Rh	K_R/K_H	0.71	0.83	1	2.8	3.2
	$\log(K_R/K_H)$	-0.15	-0.081	0	0.45	0.51

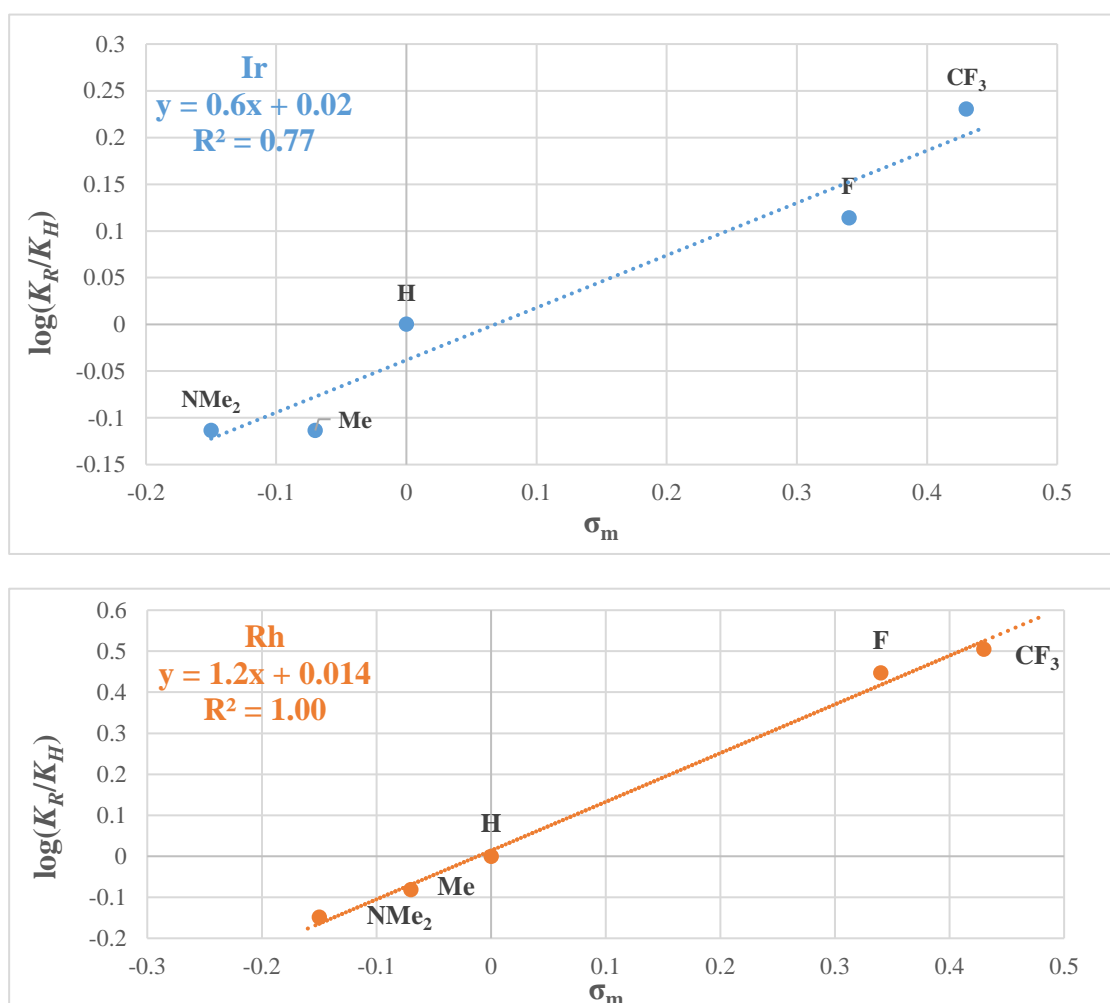


Figure 2.3: Hammett plot for final results of formation of *meta*-cyclometallated complexes with Ir (top) and Rh (bottom), $\log(K_R/K_H)$ against σ_m .

The plot for Rh shows an excellent correlation ($R^2 = 1.00$), whilst correlation for Ir is much poorer (0.77). This is likely because Ir is less reversible compared to Rh and possibly has not reached thermodynamic equilibrium under the reaction conditions.³⁵

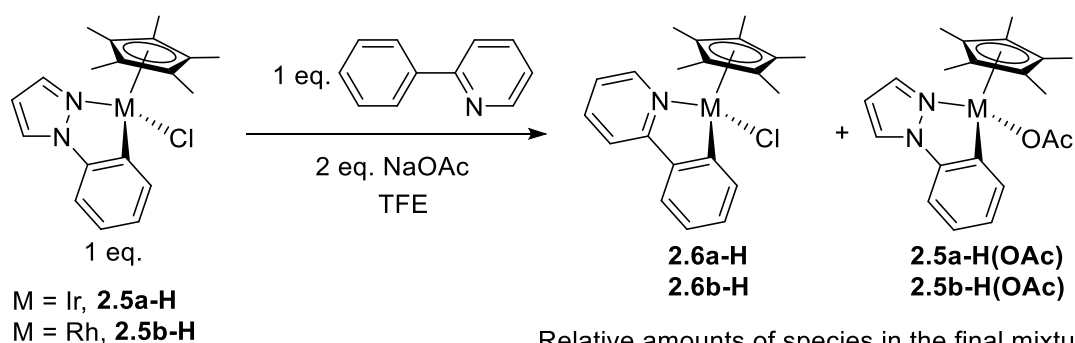
However, it was attempted to promote reversibility of Ir reactions by adding 1 equivalent of PivOH and heating reactions further (60-90 °C, 2 hours, TFE), which led to decomposition before the ratio stopped changing. Therefore, it was not possible to reach thermodynamic equilibrium with Ir in this study. The overall trend for Ir (from Hammett plot, **Figure 2.3**) is the same as for Rh indicating that the overall selectivity should still apply. The slopes for Ir and Rh were positive (1.2 and 0.6 respectively) indicating preference for the electron-withdrawing groups. Overall thermodynamic selectivity for electron-withdrawing groups substituted complexes has been seen before in related systems for Re complexes,^{30, 31} Pd⁴⁷ as well as Ir, Rh half-sandwich complexes³¹ including phenylpyrazole complexes ($\rho = 1.6$ for Ir, $\rho = 1.5$ for Rh)³⁵ and was attributed to a stronger M–C bond in these cases.^{30, 31, 35}

In conclusion, reactions with Ir allow us to observe kinetic selectivity whilst reactions with Rh are more reversible than with Ir and start to equilibrate even at room temperature in DCM:MeOH. Carrying out reactions in a more polar solvent (TFE) with heating allows observation of thermodynamic selectivity under those conditions for Rh however with Ir the approach to equilibrium with more electron-withdrawing groups is slow even under these conditions. Thermodynamic selectivity for both metals is in favour of products with electron-withdrawing groups and is opposite to that of the kinetic selectivity which is consistent with the results observed for phenylpyrazoles.³⁵

2.2.e Phenylpyrazole to phenylpyridine exchange at Ir and Rh

As discussed above the Hammett plots of competition experiments of phenylpyridines (**L2.5-R**, **L2.6-R**) with Ir and Rh using initial ratios gave smaller slopes (-1.6 for Ir and -2.1 for Rh) compared to the phenylpyrazoles (-2.7 for Ir and -2.3 for Rh). Overall this suggests that the donor group (pyridine compared to pyrazole) is having some effect on the cyclometallation and electronic effects. To try and assess the effect of the donor group, complexes **2.5a/b-H** were stirred in TFE in presence of NaOAc with 1 equivalent of 2-phenylpyridine (**Scheme 2.12**). The reactions were followed by ¹H NMR spectroscopy and within 1 hour the ¹H NMR spectra of the reaction mixtures for both Ir and Rh showed that in addition to **2.5a/b-H**, **2.6a/b-H**, free 1-phenylpyrazole and 2-phenylpyridine, additional species that were identified to be acetate complexes **2.5a/b-H(OAc)** were present in <15% of total complexes. The ratios were determined from the

relative integrations of the Cp* signals of **2.5a/b-H** (and **2.5a/b-H(OAc)**) compared to **2.6a/b-H**.



Relative amounts of species in the final mixtures:

M	2.5a/b-H	2.6a/b-H	2.5a/b-H(OAc)
Ir	1	5.5	0.5
Rh	1	4.8	0.2

Scheme 2.12: Exchange of phenylpyrazole of **2.5a/b-H** with phenylpyridine to form complexes **2.6a/b-H** and the relative amounts of each species in the final mixtures.

Within 1 hour of reaction with Ir, *ca.* 8% of **2.6a-H** was present, after stirring overnight the conversion to **2.6a-H** increased to 25% and after heating to 50 °C for 4 hours about 80% conversion to **2.6a-H** was reached. For reaction with Rh within 1 hour about 35% conversion of **2.5b-H** to **2.6b-H** was observed and after stirring overnight about 75% conversion to **2.6b-H** was reached. Overall, the results suggest that pyridine is better donor group than pyrazole leading to more thermodynamically stable complexes **2.6a/b-H**. The reaction with Ir (of **2.5a-H**) is less reversible (C–H activation of phenylpyrazole has to reverse for **2.6a-H** to form) and so required harsher conditions to reach good conversions than the equivalent reaction with Rh (of **2.5b-H**).²⁸

2.3 Conclusions

In conclusion, cyclometallation reactions of **L2.6-R** (R = NMe₂, Me, H, F, CF₃) and **L2.3-R** (R = CF₃, OMe, F) with [MCl₂Cp*]₂ (M = Ir, Rh) in the presence of NaOAc have been discussed. Overall, for cyclometallation of *meta*-substituted ligands **L2.3-R** steric hindrance has a big impact on the regioselectivity with the large substituent R = CF₃ favouring exclusively the *para*-isomer with both Ir and Rh. For less bulky R = OMe, with Ir no significant kinetic preference was observed for either isomer, whilst the *para*-isomer was favoured thermodynamically. For reaction of **L2.3-OMe** with Rh H/D exchange

experiments suggested the *para*-isomer was favoured thermodynamically, whilst the *ortho*-isomer was shown to be favoured kinetically. With R = F the *ortho*-isomer was favoured over *para* with both metals due to the “*ortho* effect”.³⁰⁻³²

Competition experiments were carried out to measure relative rates of cyclometallation of substituted phenylpyridines **L2.6-R** (R = NMe₂, Me, H, F, CF₃) with [MCl₂Cp*]₂ (M = Ir, Rh) and these were compared using a Hammett plot. They showed relatively good correlations with a negative slope for both metals (-1.6 for Ir and -2.1 for Rh). The negative slope is indicative of faster reaction rates with electron-donating substituents and is consistent with formation of a cationic intermediate during C–H activation via an AMLA mechanism. The slope is somewhat smaller than ones obtained by Alharis³⁵ for phenylpyrazole ligands (-2.7 for Ir and -2.3 for Rh),³⁵ however, with the same sign indicating that both phenylpyridines and phenylpyrazoles substituted with electron-donating groups react faster.

The thermodynamic selectivity observed with Ir and Rh was opposite to that of the kinetic selectivity with both metals showing a preference for electron-withdrawing groups. This is consistent with increased M–C bond strength and so formation of more stable complexes with electron-withdrawing substituents as observed in other systems such as Pd,⁴⁷ Ir and Rh half-sandwich complexes³¹ including phenylpyrazole complexes.³⁵ Overall, kinetic and thermodynamic selectivities were consistent with those observed for phenylpyrazoles (electron-donating groups favoured kinetically, electron-withdrawing groups favoured thermodynamically).³⁵ Reactions with Ir were shown to be harder to reverse upon heating (TFE) not reaching thermodynamic equilibrium (as evident by poor correlation $R^2 = 0.77$ in Hammett plot of thermodynamic data, **Figure 2.3**) compared to reactions with Rh whose reached thermodynamic equilibrium upon heating in TFE ($R^2 = 1.00$).

For equivalent ligands - phenylpyrazoles studied by Alharis, the overall acetate assisted cyclometallation with [MCl₂Cp*]₂ (M = Ir, Rh) consists of four steps (i) ligand binding, (ii) loss of acetate to give a cation (iii) AMLA C–H activation and finally (iv) exchange of acetic acid with chloride to form the final complex.³⁵ The results in this Chapter show that increasing the donor strength of the directing group, i.e. changing from pyrazole to pyridine leads to a reduction in the electronic effects (smaller magnitude of Hammett plot slopes). It may be that steps (i) and (ii) for a stronger donor group constitute a smaller

part and so lead to the reduced overall barrier to cyclometallation, as such reducing the extent of the electronic effects (for further discussion see Chapter 5). Therefore, the electronic effects observed from these intermolecular competitions are affected by the donor group and do not represent electronic selectivity of just the C–H activation step, but rather the combination of multiple steps for the overall cyclometallation process.

2.4 Bibliography

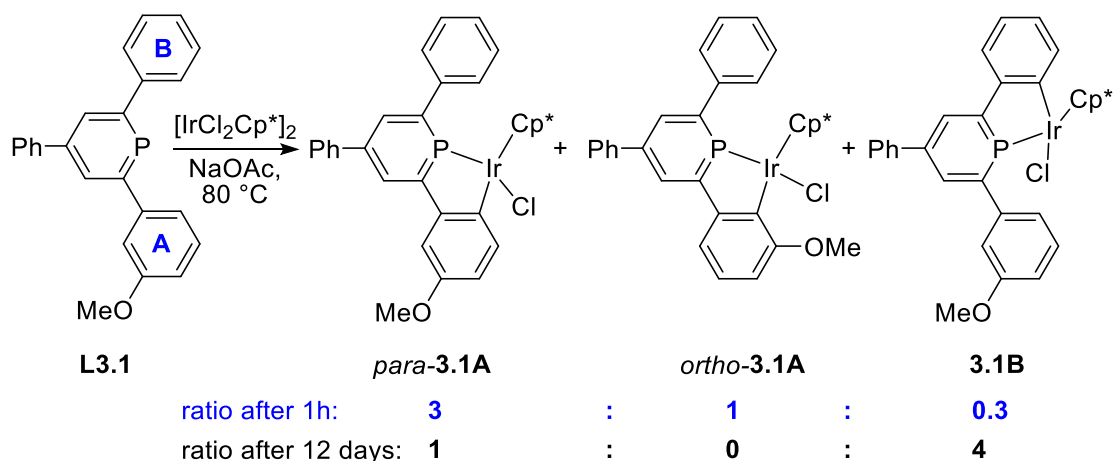
1. J. P. Kleiman and M. Dubeck, *J. Am. Chem. Soc.*, 1963, **85**, 1544-1545.
2. S. Trofimenko, *Inorg. Chem.*, 1973, **12**, 1215-1221.
3. L. Wang, W. He and Z. Yu, *Chem. Soc. Rev.*, 2013, **42**, 599-621.
4. J. R. Chen, X. Q. Hu, L. Q. Lu and W. J. Xiao, *Acc. Chem. Res.*, 2016, **49**, 1911-1923.
5. Y. Park, Y. Kim and S. Chang, *Chem. Rev.*, 2017, **117**, 9247-9301.
6. Y. Yang, J. Lan and J. You, *Chem. Rev.*, 2017, **117**, 8787-8863.
7. Z. Huang, H. N. Lim, F. Mo, M. C. Young and G. Dong, *Chem. Soc. Rev.*, 2015, **44**, 7764-7786.
8. K. Sordakis, C. Tang, L. K. Vogt, H. Junge, P. J. Dyson, M. Beller and G. Laurenczy, *Chem. Rev.*, 2018, **118**, 372-433.
9. C. K. Prier, D. A. Rankic and D. W. C. MacMillan, *Chem. Rev.*, 2013, **113**, 5322-5363.
10. J. Twilton, C. Le, P. Zhang, M. H. Shaw, R. W. Evans and D. W. C. MacMillan, *Nat. Rev. Chem.*, 2017, **1**, 19.
11. K. L. Skubi, T. R. Blum and T. P. Yoon, *Chem. Rev.*, 2016, **116**, 10035-10074.
12. I. Omae, *Coord. Chem. Rev.*, 2016, **310**, 154-169.
13. J. Kalinowski, V. Fattori, M. Cocchi and J. A. G. Williams, *Coord. Chem. Rev.*, 2011, **255**, 2401-2425.
14. I. Omae, *J. Organomet. Chem.*, 2016, **823**, 50-75.
15. Z. P. Liu, W. J. He and Z. J. Guo, *Chem. Soc. Rev.*, 2013, **42**, 1568-1600.
16. X. Jiang, J. Peng, J. Wang, X. Guo, D. Zhao and Y. Ma, *ACS Applied Materials & Interfaces*, 2016, **8**, 3591-3600.
17. M. R. Gill and J. A. Thomas, *Chem. Soc. Rev.*, 2012, **41**, 3179-3192.
18. M. Mauro, A. Aliprandi, D. Septiadi, N. S. Kehra and L. De Cola, *Chem. Soc. Rev.*, 2014, **43**, 4144-4166.
19. K. Y. Zhang, Q. Yu, H. J. Wei, S. J. Liu, Q. Zhao and W. Huang, *Chem. Rev.*, 2018, **118**, 1770-1839.
20. C. F. Markwalter, A. G. Kantor, C. P. Moore, K. A. Richardson and D. W. Wright, *Chem. Rev.*, 2018, **119**, 1456-1518.
21. X. Wang, X. Wang, S. Jin, N. Muhammad and Z. Guo, *Chem. Rev.*, 2018, **47**, 6603-6743.
22. G. Gasser, I. Ott and N. Metzler-Nolte, *J. Med. Chem.*, 2011, **54**, 3-25.
23. L. Ackermann, *Chem. Rev.*, 2011, **111**, 1315-1345.
24. X. Qi, Y. Li, R. Bai and Y. Lan, *Acc. Chem. Res.*, 2017, **50**, 2799-2808.
25. Y.-F. Han and G.-X. Jin, *Chem. Soc. Rev.*, 2014, **43**, 2799-2823.
26. A. D. Ryabov, I. K. Sakodinskaya and A. K. Yatsimirsky, *J. Chem. Soc., Dalton Trans.*, 1985, 2629-2638.
27. D. L. Davies, S. M. A. Donald and S. A. Macgregor, *J. Am. Chem. Soc.*, 2005, **127**, 13754-13755.
28. K. J. T. Carr, D. L. Davies, S. A. Macgregor, K. Singh and B. Villa-Marcos, *Chem. Sci.*, 2014, **5**, 2340-2346.
29. L. Li, W. W. Brennessel and W. D. Jones, *Organometallics*, 2009, **28**, 3492-3500.
30. E. Clot, M. Besora, F. Maseras, C. Mégret, O. Eisenstein, B. Oelckers and R. N. Perutz, *Chem. Commun.*, 2003, 490-491.
31. E. Clot, C. Mégret, O. Eisenstein and R. N. Perutz, *J. Am. Chem. Soc.*, 2009, **131**, 7817-7827.

32. A. D. Selmeçzy, W. D. Jones, M. G. Partridge and R. N. Perutz, *Organometallics*, 1994, **13**, 522-532.
33. A. D. Ryabov, *Inorg. Chem.*, 1987, **26**, 1252-1260.
34. J. Li, W. Hu, Y. Peng, Y. Zhang, J. Li and W. Zheng, *Organometallics*, 2014, **33**, 2150-2159.
35. R. A. Alharis, C. L. McMullin, D. L. Davies, K. Singh and S. A. Macgregor, *J. Am. Chem. Soc.*, 2019, **141**, 8896-8906.
36. J. Clayden, N. Greeves and S. Warren, *Organic Chemistry*, 2nd edn., Oxford: Oxford University Press, Oxford, 2012.
37. C. Liu, N. Han, X. Song and J. Qiu, *Eur. J. Org. Chem.*, 2010, **2010**, 5548-5551.
38. M. L. N. Rao and R. J. Dhanorkar, *Tetrahedron*, 2015, **71**, 338-349.
39. B. Yang and Z.-X. Wang, *Org. Lett.*, 2017, **19**, 6220-6223.
40. Y. Boutadla, O. Al-Duaij, D. L. Davies, G. A. Griffith and K. Singh, *Organometallics*, 2009, **28**, 433-440.
41. J.-P. Djukic, W. Iali, M. Pfeffer and X.-F. Le Goff, *Chem. Eur. J.*, 2012, **18**, 6063-6078.
42. Z. Liu, A. Habtemariam, A. M. Pizarro, G. J. Clarkson and P. J. Sadler, *Organometallics*, 2011, **30**, 4702-4710.
43. A. J. Millett, A. Habtemariam, I. Romero-Canelón, G. J. Clarkson and P. J. Sadler, *Organometallics*, 2015, **34**, 2683-2694.
44. M. Brasse, J. Cámpora, J. A. Ellman and R. G. Bergman, *J. Am. Chem. Soc.*, 2013, **135**, 6427-6430.
45. Y. Boutadla, D. L. Davies, R. C. Jones and K. Singh, *Chem. Eur. J.*, 2011, **17**, 3438-3448.
46. J. Milani, N. E. Pridmore, A. C. Whitwood, I. J. S. Fairlamb and R. N. Perutz, *Organometallics*, 2015, **34**, 4376-4386.
47. A. Petit, J. Flygare, A. T. Miller, G. Winkel and D. H. Ess, *Org. Lett.*, 2012, **14**, 3680-3683.

Chapter Three

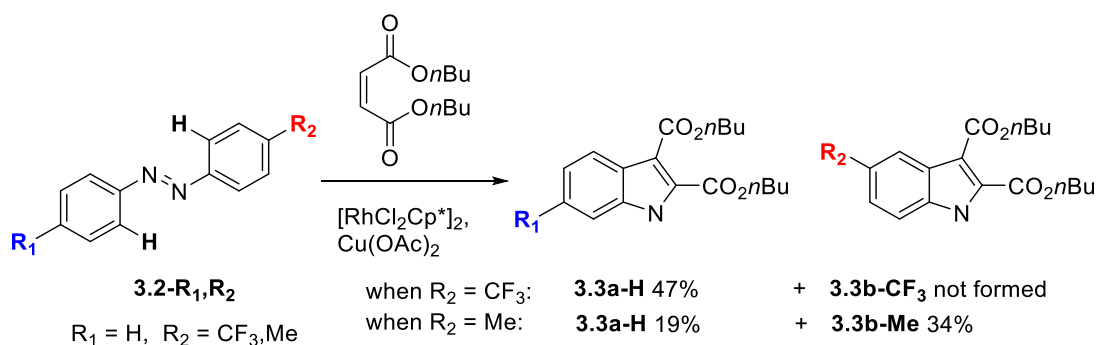
3.1 Introduction

Chapter 2 showed that for the intermolecular competition the nature of the donor group (changing from pyrazole to pyridine i.e. increasing the donor strength) affects the electronic effects (reduced slopes for kinetic results for phenylpyridines $\rho = -1.6$ for Ir, -2.1 for Rh compared to phenylpyrazoles $\rho = -2.7$ for Ir, -2.3 for Rh) suggesting that not just the C–H activation step controls the overall rate of cyclometallation. An intramolecular competition (discussed in Chapter 1) could provide more insight into selectivity of the actual C–H activation step as it will be the product determining step and so product selectivity should only reflect that step. Muller *et al.* investigated the cyclometallation of phosphinines **L3.1** with $[\text{IrCl}_2\text{Cp}^*]_2$ (**Scheme 3.1**).¹ After 1 hour **L3.1** gave preferentially cyclometallation of ring A with *para*-**3.1A** being favoured over *ortho*-**3.1A** with even less of product (**3.1B**) formed by cyclometallation of ring B. Over several days the ratios changed in favour of cyclometallation on the unsubstituted phenyl, hence **3.1B** became the major species with *ortho*-**3.1A** disappearing altogether. The authors concluded that **3.1A** formed by cyclometallation on OMe-substituted ring is the kinetic product (faster reaction with electron-donating groups) whilst cyclometallation on the unsubstituted ring gives **3.1B**, the thermodynamic product which according to authors is favoured due to the steric effects. However, it is not immediately clear why *para*-**3.1A** has more steric hindrance than **3.1B**. Based on the recent work by Alharis with phenylpyrazoles (discussed in Chapter 2)² cyclometallation is thermodynamically favoured by the more electron-withdrawing groups which is in agreement with **3.1B** being favoured over **3.1A** (OMe group at the *para* position is an electron-donating $\sigma_p(\text{OMe}) = -0.27$ *cf.* $\sigma_p(\text{H}) = 0$).



Scheme 3.1: Intramolecular competition of phosphinines **L3.1** to form irridacycles.¹

Another example of an intramolecular competition was reported for {RhCp*}-catalysed formation of indoles from azobenzenes (**Scheme 3.2**).³ Note, strictly the different N atoms each act as a directing group for C–H activation of one of the phenyls and their donor strengths are likely to be similar but not identical. Competition between reaction at the CF₃-substituted and the unsubstituted phenyl of **3.2-H**, CF₃ led to product formation exclusively on the unsubstituted phenyl (only **3.3a-H** formed), whilst for **3.2-H**, Me product formation was favoured on the Me-substituted ring (**3.3a-H** minor, **3.3b-Me** major). These results show that the reactions are favoured by electron-donating groups.



Scheme 3.2: Competitions between two phenyls on the azobenzene to form indoles.³

In this chapter electronic and steric effects on C–H activation will be assessed using an intramolecular competition between differently substituted diphenyl N-heterocyclic carbenes (NHCs). NHCs have been established as organocatalysts,⁴ coordinating compounds to the main group elements⁵ and ligands for transition metals.^{6, 7} Common ways to prepare the M–NHC complexes are deprotonation of an imidazolium salt to form

a free carbene which then reacts with an appropriate metal complex⁸ or by formation of an Ag-NHC complex followed by carbene transfer to the desired metal.^{9, 10} The largest application of M-NHC complexes is in homogeneous catalysis¹¹ and two commercially available examples, Pd-PEPPSI-*i*Pr^{12, 13} and the Hoveyda-Grubbs-II catalyst^{14, 15} are shown in **Figure 3.1**.

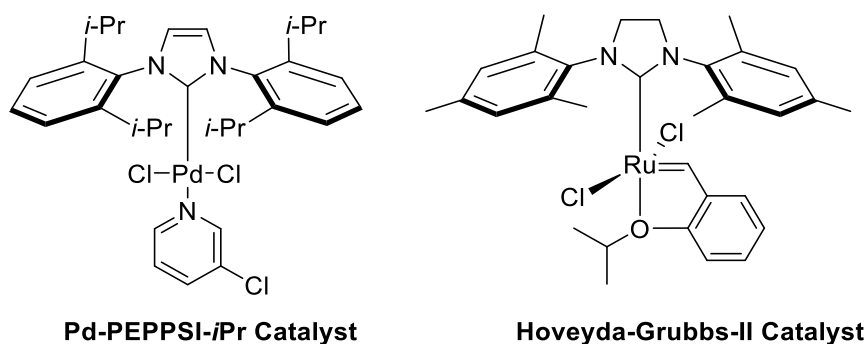
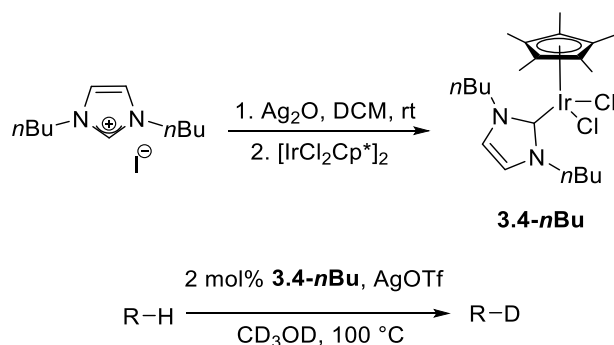


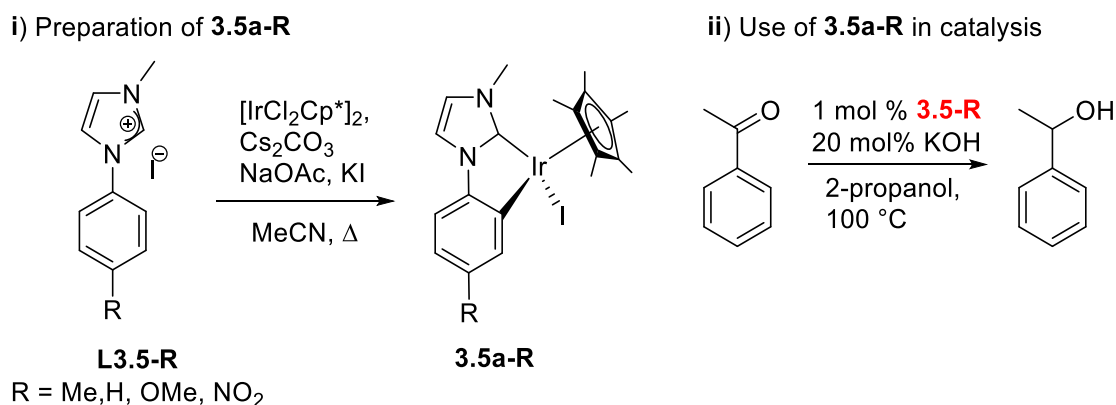
Figure 3.1: Examples of commercially available M-NHC catalysts.

Half-sandwich Ir-NHC complex **3.4-*n*Bu** has been prepared by *in situ* transmetalation from Ag (**Scheme 3.3**).¹⁶ Complex **3.4-*n*Bu** is able to catalyse H/D exchange of CD₃OD and organic compounds (e.g. Et₂O, THF, and styrene).¹⁷



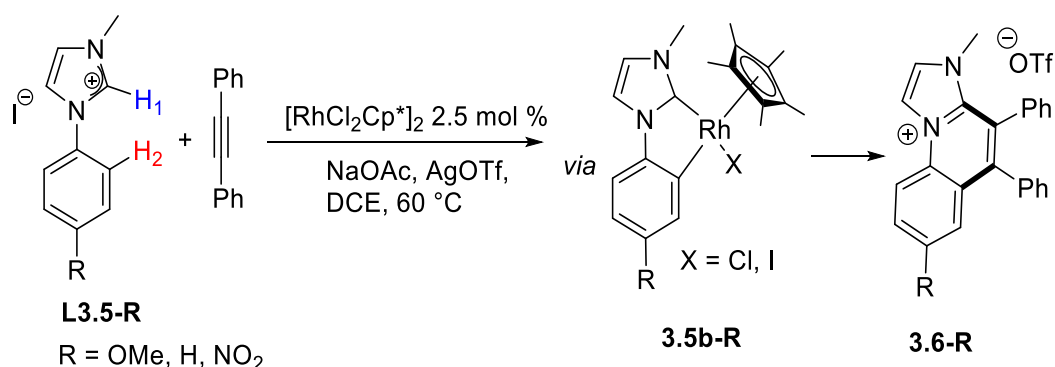
Scheme 3.3: Preparation of **3.4-*n*Bu** complex and **3.4-*n*Bu** catalysed H/D exchange.¹⁶

Cyclometallated Ir-NHC complexes **3.5a-R** (R = Me, H, OMe, NO₂) are also known (**Scheme 3.4 i**).¹⁸ They were prepared by direct C–H activation of **L3.5-R** with [IrCl₂Cp*]₂ in the presence of NaOAc and were shown to catalyse transfer hydrogenation reactions (**Scheme 3.4 ii**).



Scheme 3.4: i) Preparation of complexes **3.5a-R** and ii) their use in catalysis¹⁸

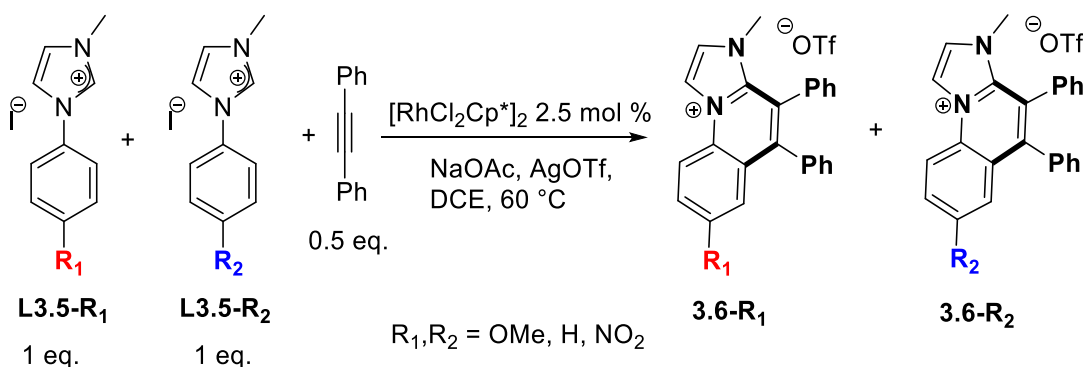
In 2016 (coincidental with work in this thesis) Choudhury *et al.* reported a {RhCp*}-catalysed functionalisation of imidazolium salts (**Scheme 3.5**).¹⁹ The reactions were proposed to go via a double AMLA/CMD C–H activation first of the imidazolium C–H₁ and then phenyl C–H₂ to form cyclometallated intermediates **3.5b-R** which after alkyne insertion and reductive elimination led to the final products (**3.6-R**).



Scheme 3.5: Rh catalysed annulation of imidazolium salts.¹⁹

One-pot intermolecular competition experiments between two imidazolium salts (**L3.5-R₁** and **L3.5-R₂**) lead to a mixture of products **3.6-R₁** and **3.6-R₂** favouring the salt with the more electron-withdrawing group (**Scheme 3.6**, **Table 3.1**). This selectivity is consistent with a CMD mechanism. However, the results are for the formation of the final compound **3.6-R** which involves two C–H activation events and alkyne insertion and so C–H activation of the phenyl may not be the product determining step (and hence the selectivity determining step). In fact, the first order dependence of the rate on the

concentration of **L3.5-R** combined with DKIE experiments, showed that the first C–H activation (non-directed activation of imidazolium) is the rds.

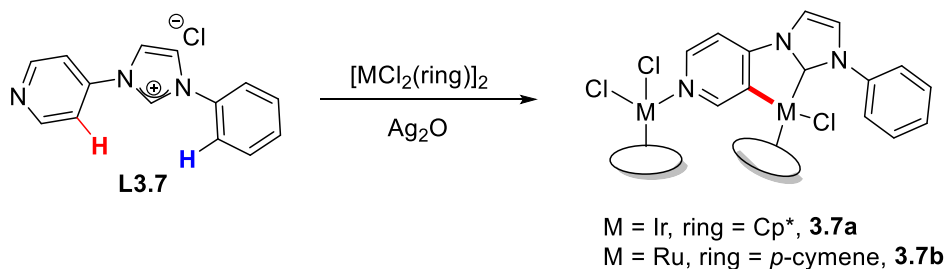


Scheme 3.6: Intermolecular competitions with phenylimidazolium salts **L3.5-R**.

Table 3.1: Intermolecular competition results with phenylimidazolium salts **L3.5-R**

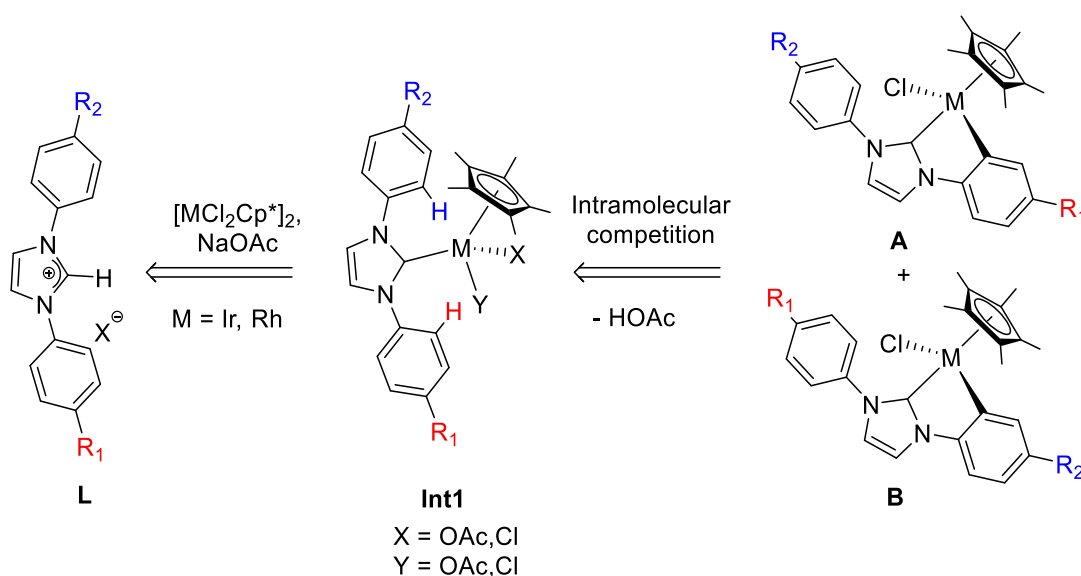
L3.5-R₁	L3.5-R₂	3.6-R₁:R₂
OMe	H	1:1.4
NO ₂	H	2.4:1
OMe	NO ₂	1:3.7

Intramolecular competition between phenyl and pyridine rings with an NHC directing group (**L3.7**) have been reported with {IrCp*} and {Ru(*p*-cymene)} (**Scheme 3.7**). Cyclometallation on the pyridine was favoured over the phenyl and the products contained an additional {IrCp*} or {Ru(*p*-cymene)} fragment coordinated to the pyridine. The authors concluded that the reaction proceeds via a CMD mechanism and activation on the pyridine is due to the higher acidity of these protons compared to those of the phenyl and this effect is enhanced when the pyridine coordinates to a metal.



Scheme 3.7: Intramolecular competition between C–H activation at pyridine and phenyl rings with {IrCp*} and {Ru(*p*-cymene)}.²⁰

In conclusion, NHCs are easily cyclometallated at {MCp*} (M = Ir, Rh) hence they are ideal substrates to study electronic and steric effects on C–H activation via an intramolecular competition of differently substituted phenyl groups. The proposed reactions for studying electronic effects are shown in **Scheme 3.8**. The reactions involve two steps: non-directed C–H of the imidazolium salt to form an NHC complex **Int1** followed by directed C–H activation of one of the two phenyl rings. The NHC acts as a common directing group for both phenyl rings hence if the non-cyclometallated M–NHC **Int1** can be isolated the C–H activation step can be studied in isolation from ligand binding. Therefore, Chapter 3 will include the preparation of the diphenylimidazolium salts and *meta*-substituted monophenylimidazolium salts and discuss their reactions with Ir and Rh half-sandwich complexes.



Scheme 3.8: Proposed strategy for intramolecular competition experiments.

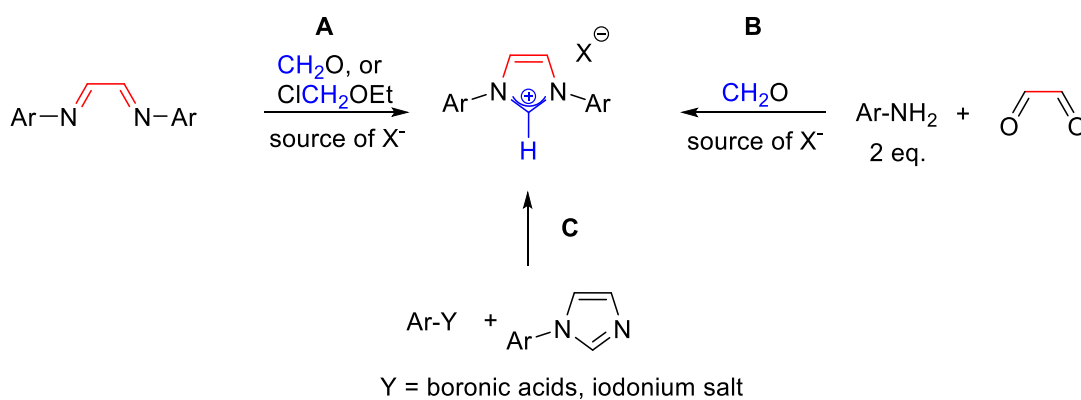
3.2 Results and discussion

All new compounds were characterised by ^1H and ^{13}C NMR spectroscopy, alongside with appropriate 2-D NMR techniques (COSY, NOESY, TOCSY, HSQC, HMBC) and HRMS spectrometry or microanalysis; some complexes were characterised by single crystal X-ray diffraction (Note, these were performed by Mr K. Singh).

3.2a. Preparation of diphenylimidazolium salts

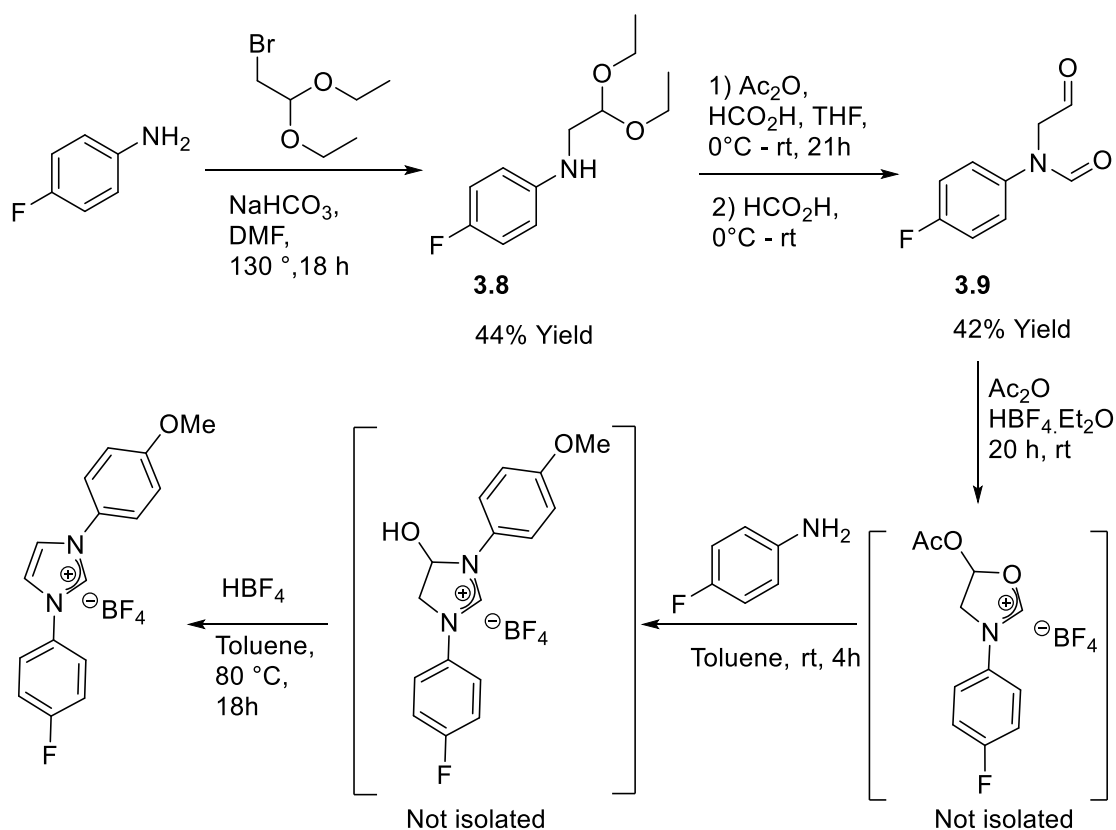
Common routes to prepare diarylimidazolium salts are (i) cyclisation of diaryl-diazadienes with either formic acid or chloromethyl-ethyl ether (**Scheme 3.9 A**),^{21, 22} (ii)

condensation of glyoxal with two equivalents of aromatic amines (**Scheme 3.9 B**)^{21, 22} or (iii) direct quaternisation of an arylimidazole (**Scheme 3.9 C**).^{23, 24}



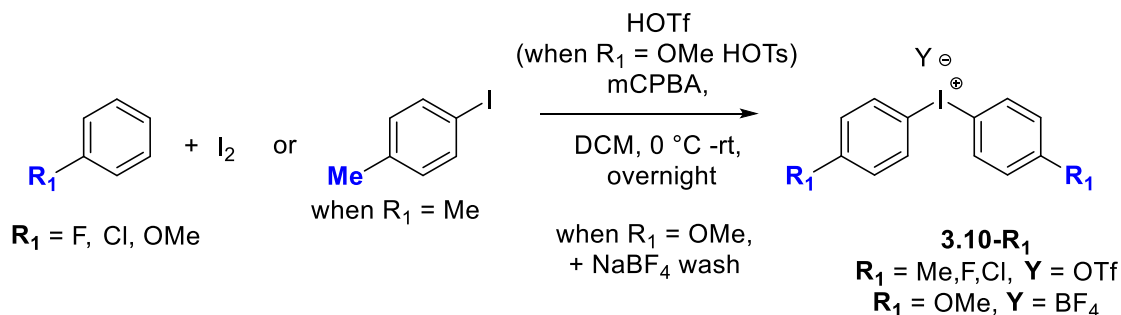
Scheme 3.9: Common methods to prepare symmetrical arylimidazolium salts, **A** from diazadienes,^{21, 22} **B** from glyoxal,^{21, 22} or from an arylimidazole **C**.^{23, 24}

The majority of published procedures involve preparation of symmetrical imidazolium salts, whilst methods to prepare unsymmetrical imidazolium salts are relatively sparse. The first method attempted to prepare unsymmetrical imidazolium salt involved cyclisation of anilines following a literature procedure (**Scheme 3.10**).²⁵ *N*-alkylation of 4-fluoroaniline gave **3.8** in only 44% yield, partly due to some losses during purification. *N*-formylation of **3.8** then gave **3.9** in 42% yield. Cyclisation of **3.9** in acetic anhydride and reaction with *p*-anisidine and then HBF₄ gave imidazolium salt in 10% yield. It is possible that the poor yield is due to the instability of the oxazolium intermediate, examples in literature were stabilised by bulky groups (mesityl, 2,6-di-isopropylphenyl) on the N, or R groups on the oxazolium ring which is not the case here. This procedure was deemed unsatisfactory, therefore an alternative method to imidazolium salts, arylation of an *N*-aryl imidazole was investigated.



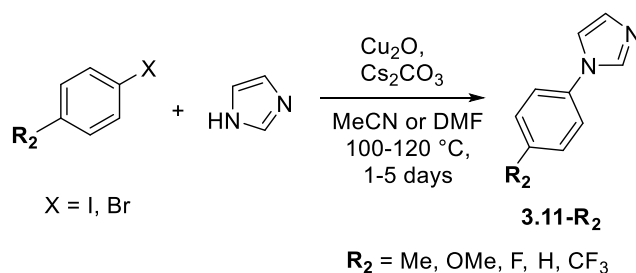
Scheme 3.10: Attempted imidazolium salt synthesis from cyclisation of anilines adapted from reference 25.²⁵

First, the aryliodonium salts **3.10-R₁** = F, Cl, Me, OMe were prepared following appropriate literature methods (**Scheme 3.11**) (see Chapter 6 for details).^{26,27} Note, **3.10-R₁** R₁ = F, Cl, Me were prepared as OTf salts, whilst R₁ = OMe was prepared as BF₄ salt. All of the compounds have been reported previously in the literature and their respective ¹H NMR spectra and ESI-MS agree with the reported data.^{24,26}



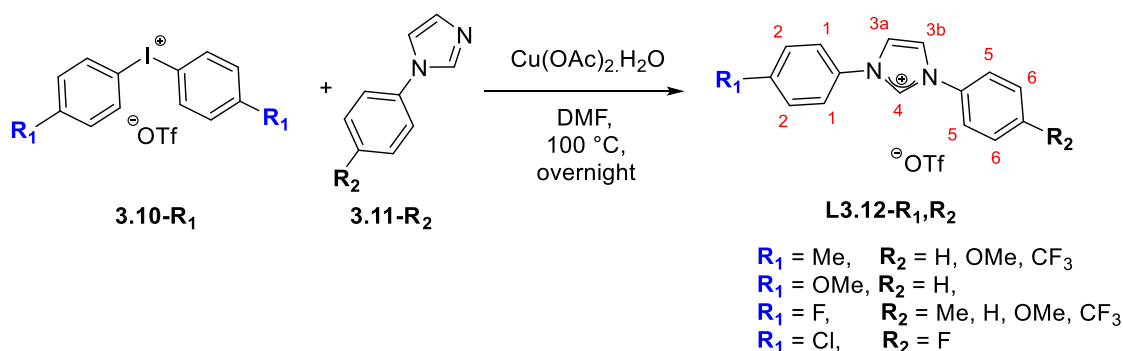
Scheme 3.11: Preparation of aryliodonium salts **3.10-R₁**.^{24,26}

Phenylimidazoles (**3.11-R₂**) were prepared by Cu₂O catalysed coupling of aryl halide with imidazole (**Scheme 3.12**).²⁸ After work up and column chromatography **3.11-R₂** (R₂ = Me, H, OMe, F, CF₃) were obtained in moderate to good yields. All of the compounds have been reported previously in the literature and their respective ¹H and ¹³C NMR spectra and ESI-MS agree with the reported data.^{28, 29}



Scheme 3.12: Preparation of phenylimidazoles **3.11-R₂**.

The phenylimidazoles **3.11-R₂** were then coupled with arylidonium salts (**Scheme 3.13**).²³ Rather than using column chromatography as in the literature,²³ the diaryl imidazolium salts **L3.12-R₁,R₂** were purified by precipitation from DCM/Et₂O or MeOH/Et₂O and washing with Et₂O which gave compounds of high purity (>95%) in good yields. The salts **L3.12-OMe,H**, **L3.12-Me,H** and **L3.12-F,H** are known²³ whilst **L3.12-Me,OMe**, **L3.12-Me,CF₃**, **L3.12-F,Me**, **L3.12-F,OMe**, **L3.12-F,CF₃**, **L3.12-Cl,F** are new compounds. The counter ion is OTf unless otherwise specified.



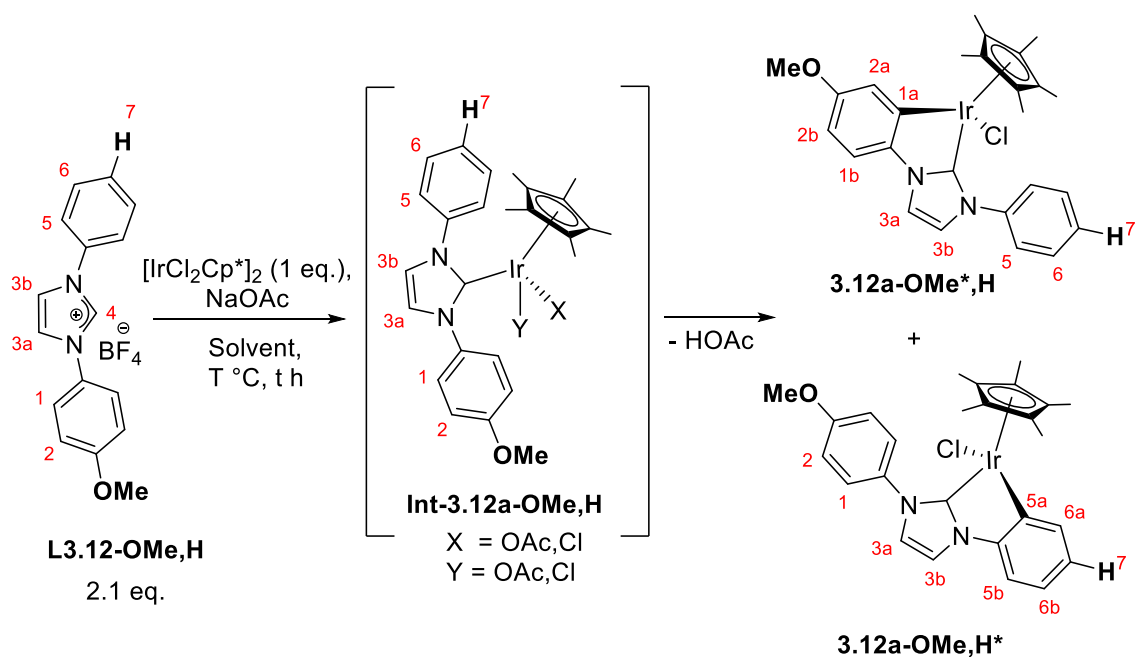
Scheme 3.13: Preparation of diarylimidazolium salts **L3.12-R₁,R₂** and labelling scheme.

Formation of the diaryl imidazolium salts was most apparent from the shifts of the imidazole signals in the ¹H NMR spectra. The most downfield signal at δ 9.1-10.0 is a broad singlet corresponding to H⁴ which is 1-2 ppm downfield from the corresponding signal in **3.11-R₂** (at about δ 7.8) due to formation of a cationic imidazolium salt. The

other two imidazolium signals are also downfield (about 0.8 ppm) compared to the precursor phenylimidazoles and appear as narrow doublets. The ^1H NMR spectra show two AA'BB' patterns except when R = H or F which both have additional coupling to the H or F respectively. The ^{13}C NMR spectra for all the salts **L3.12-R₁,R₂** show the expected number of CH and quaternary carbons with the imidazolium C⁴ present at δ 134-137. For R = F or CF₃ some signals are split into doublets or quartets respectively, additionally, a signal for OTf is observed as a quartet at *ca.* δ 122.0. ^{19}F NMR spectra show signals for OTf at δ -80.0, additionally, when R = F a signal at *ca.* δ -112.0 is observed and at *ca.* δ -64.0 when R = CF₃. The HRMS (ESI) show ions for the imidazolium cation in each case.

3.2bi Preparation of Ir and Rh half-sandwich NHC complexes by direct C-H activation

The reaction of **L3.12-OMe,H(BF₄)** with $[\text{IrCl}_2\text{Cp}^*]_2$ and NaOAc was examined varying the solvent and the temperature (**Scheme 3.14, Table 3.2**) and was monitored by ^1H NMR spectroscopy. The initial reaction (entry 1) used three equivalents of NaOAc per dimer in DCM at room temperature. After 20 hours the ^1H NMR spectrum showed no formation of Ir-NHC species, just unreacted **L3.12-OMe,H** and a broad signal for $\{\text{IrCp}^*\}$ at about δ 1.7 (note, the dimer had reacted with NaOAc to give $[\text{Ir}(\text{OAc})_2\text{Cp}^*]$ and possibly some mixed Cl/OAc complexes as discussed in Chapter 1 **Section 1.4b**).³⁰ Addition of MeOH to the reaction mixture to promote the C-H activation reaction (as discussed in Chapter 2) or increase in the equivalents of NaOAc did not result in the formation of any Ir-NHC species (entries 2-3). Changing the solvent to DCE and heating to 75 °C for 1 hour led to over 90% conversion (entry 4) to two new species formed in about 1:2 ratio (based on two new OMe and Cp* signals). Separation of the two products was attempted by precipitation from DCM/ hexane or DCM/Et₂O, however, the mixture precipitated together. Column chromatography on silica provided a fraction heavily biased to the major product (minor:major 1:10) in 27% combined yield.



Scheme 3.14: Proposed reaction pathway and possible products of test reactions of **L3.12-OMe,H** with $[\text{IrCl}_2\text{Cp}^*]_2$ in the presence of NaOAc.

Table 3.2: Test reactions of **L3.12-OMe,H** with $[\text{IrCl}_2\text{Cp}^*]_2$ in the presence of NaOAc.

Entry	Eq. of NaOAc ^a	Solvent	Temperature	Time, h	Conversion to the products
1	3	DCM	rt	20	N.D.
2	3	DCM:MeOH (5:3)	rt	18	N.D.
3	8	DCM:MeOH (5:3)	rt	18	N.D.
4	8	DCE	75 °C	1	>90%

N.D. not detected by ^1H NMR spectroscopy

^a Per Ir dimer

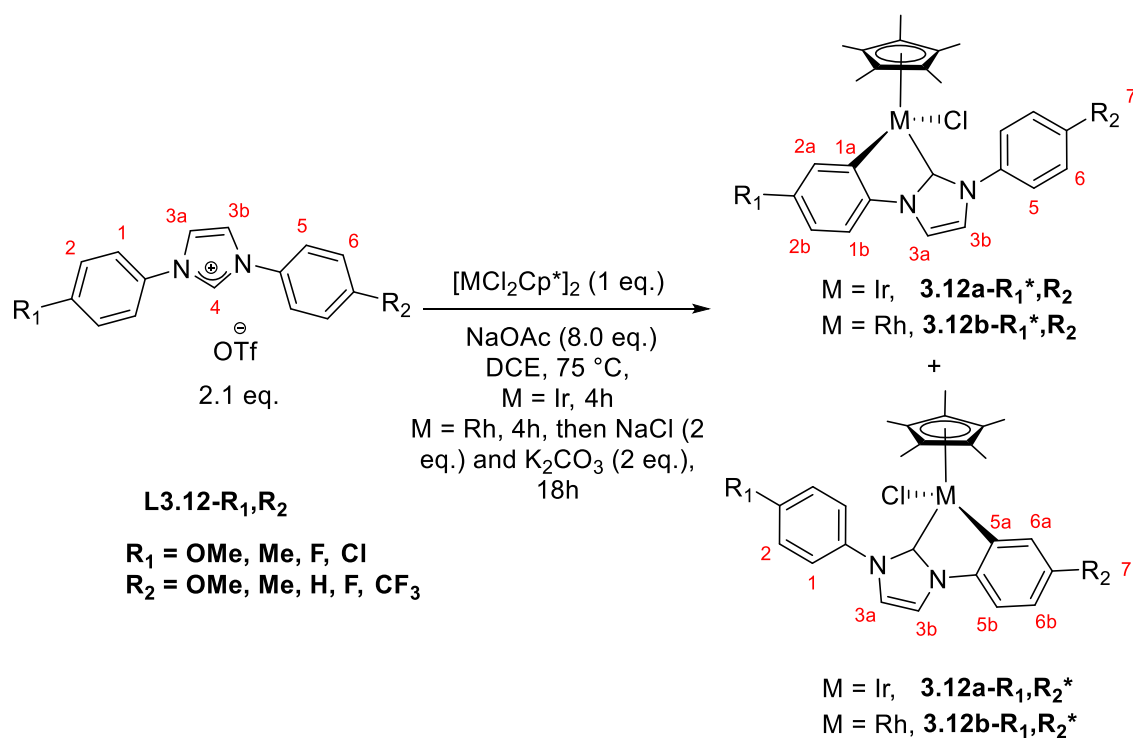
The ^1H NMR spectrum of the major product shows singlets at δ 1.47 and 3.88 corresponding to a Cp* and OMe group respectively. The most apparent change from **L3.12-OMe,H** in the ^1H NMR spectrum is the absence of the most downfield signal H⁴ confirming formation of an Ir–NHC species. Signals for ten protons are observed in the aromatic region, indicating formation of a cyclometallated species either **3.12a-OMe*,H**

or **3.12a-OMe,H*** (Scheme 3.14). An AA'BB' pattern is observed with doublets at δ 7.04 and 7.87 with the former showing an NOE with the OMe signal, showing that the OMe ring has not been cyclometallated. The four inequivalent protons are on one ring as shown by the COSY spectrum (see Chapter 6 for details). One of these, a doublet of doublets at δ 7.74 shows an NOE with Cp* indicating that this ring is cyclometallated and the signal is assigned to H^{6a}. Finally, two mutually coupled narrow doublets present at δ 7.14 and 7.47 with the former showing an NOE with H¹ are assigned to imidazole-2-ylidene protons H^{3a} and H^{3b} respectively. Therefore, overall the ¹H NMR spectrum is consistent with the major product being cyclometallated on the unsubstituted phenyl ring i.e. **3.12a-OMe,H***. The asterisk refers to the ring that was cyclometallated and this notation will be used in Chapters 3 and 4.

Whilst the minor product was not isolated it was possible to extract its signals from the ¹H NMR spectrum of the 1:2 product mixture. The ¹H NMR spectrum shows singlets at δ 1.45 and 3.86 corresponding to a Cp* and OMe group respectively with no signals above δ 8 ppm indicating loss of H⁴ and formation of an Ir-NHC complex. In the aromatic region three inequivalent protons are on the same ring (as shown by the COSY spectrum) one of which, a narrow doublet at δ 7.33, shows an NOE with a Cp* indicating that it is on the cyclometallated ring and an NOE with an OMe shows that it is on the OMe-substituted ring. These data, indicate that the minor product has cyclometallated on the OMe-substituted ring i.e. **3.12a-OMe*,H**. The ¹³C NMR spectrum of **3.12a-OMe,H*** shows the expected number of signals with the C^{5a} at δ 145.9 and C⁴ at δ 163.7 (shows a cross peak with Cp* and H^{3a/3b} in ¹H-¹³C HMBC spectrum) and is in agreement with previously reported Ir half-sandwich NHCs.¹⁶ The HRMS(ESI) spectrum shows ions at m/z 618.2108 due to [M-Cl+MeCN]⁺.

Having carried out test reactions, the triflate salts **L3.12-R₁,R₂** were reacted with the appropriate metal dimer [MCl₂Cp*]₂ (M = Ir, Rh) in the presence of NaOAc (4 equivalents per metal centre) in DCE at 75 °C (Scheme 3.15). For reactions with Ir, high conversions (>90%) were reached after heating for 1 hour, whilst for reactions with Rh conversions of about 60% were reached within 2-4 hours and these did not increase after heating overnight; possibly due to the reversibility of the Rh reactions as discussed in Chapter 2. To try and increase conversions NaCl and K₂CO₃ (2 equivalents per metal centre for both) were added to the mixtures after reactions reached about 60% conversion

and were heated at 75 °C overnight reaching over 80% conversions. Isomer ratios were measured by ^1H NMR spectroscopy and/or where applicable ^{19}F NMR spectroscopy within 1 hour and before workup and are discussed later. The characterisation of a few complexes is given in detail whilst for the other complexes full data is in chapter 6 including details of isomer ratios. Two complexes **3.12a-F*,OMe** and **3.12a-F*,H**, as well as a complex prepared later in the chapter **3.12a-OMe*,OMe** gave crystals suitable for X-ray diffraction and are discussed later.



Scheme 3.15: Cyclometallation and labelling of **L3.12-R₁,R₂** with $[\text{MCl}_2\text{Cp}^*]_2$ M = Ir, Rh.

The reaction of **L3.12-Me,CF₃** with $[\text{IrCl}_2\text{Cp}^*]_2$ resulted in isolation of a complex in modest yield, due to difficulties in removing excess of **L3.12-Me,CF₃**. The ^1H NMR spectrum of the complex shows an AA'BB' pattern with signals at δ 7.31 and 7.83, former of which shows an NOE with Me indicating this ring is not cyclometallated. The CF₃-substituted ring shows signals for three protons one of which the narrow doublet shows an NOE with Cp* indicating that CF₃-substituted ring is cyclometallated and that the complex is **3.12a-Me,CF₃***. The ^{13}C NMR spectrum shows the expected number of signals with the C^{6a} at δ 148.8 and C⁴ at δ 164.7. The ^{19}F NMR shows a singlet at δ -61.2 for CF₃. The HRMS(ESI) spectrum shows ions at m/z 670.2029 due to $[\text{M-Cl}+\text{MeCN}]^+$.

The reaction of **L3.12-F,Me** with $[\text{IrCl}_2\text{Cp}^*]_2$ after 1 hour of heating resulted in formation of two isomers which after crystallisation were obtained in good yield. The major isomer in the ^1H NMR spectrum shows an AA'BB' pattern with doublets at δ 7.12 for H^6 and 7.80 for H^5 the former of which shows an NOE with the Me group. However, the F-substituted ring shows three signals a triplet of doublets at δ 6.65 ($J_{\text{H-F}} = 8.6$ Hz), doublets of doublets at δ 7.11 ($J_{\text{H-F}} = 4.8$ Hz) and 7.43 ($J_{\text{H-F}} = 9.0$ Hz) consistent with cyclometallation on this ring to form **3.12a-F*,Me**. The signal at δ 7.43 shows an NOE with Cp^* indicating it is H^{2a} . H^{1b} and H^{2b} are distinguished by the magnitude of $J(\text{HF})$ (larger for H^{2b}). The minor isomer was not isolated, but it was possible to extract signals for it from the ^1H NMR spectrum of the mixture, which for the minor isomer in the aromatic region shows three signals on the same ring (as shown by COSY spectrum) of which a narrow doublet at δ 7.54 shows an NOE with Cp^* and Me consistent with the minor isomer being cyclometallation on the Me-substituted ring product **3.12a-F,Me***. The fraction of the **3.12a-F,Me*** in the mixture was too little to allow assignment of the ^{13}C NMR spectrum, however, all of the signals could be assigned for the major isomer **3.12a-F*,Me** with C^{1a} seen as a doublet at δ 145.7 ($^3J_{\text{C-F}} = 5.0$ Hz) and C^4 as a singlet at δ 162.7. The ^{19}F NMR spectrum shows singlets at -118.7 and -113.3 for F for **3.12a-F*,Me** and **3.12a-F,Me*** respectively. The HRMS(ESI) spectrum shows ions at m/z 579.1806 due to $[\text{M-Cl}]^+$.

The reaction of **L3.12-F,OMe** with $[\text{IrCl}_2\text{Cp}^*]_2$ after work up gave a mixture of two isomers in modest yield. The ^1H NMR spectrum of the major product shows an AA'BB' pattern for the OMe-substituted ring. The F-substituted ring gives three signals at δ 6.67 for H^{2b} , 7.14 for H^{1b} and 7.45 for H^{2a} implying cyclometallation on the F-substituted ring i.e. product **3.12a-F*,OMe**. The minor isomer was not isolated but signals could be extracted from the ^1H NMR spectrum of mixture and the product shows a narrow doublet that shows an NOE with Cp^* and OMe indicating that this isomer is cyclometallation on OMe-substituted phenyl product **3.12a-F,OMe***. The ^{13}C and ^{19}F NMR spectra of **3.12a-F*,OMe** shows the same features as **3.12a-F*,Me** with the expected number of signals. The HRMS(ESI) spectrum shows ion at m/z 595.1757 due to $[\text{M-Cl}]^+$.

The reaction of **L3.12-F,H** with $[\text{IrCl}_2\text{Cp}^*]_2$ formed two isomers and after crystallisation were obtained in modest yield. The ^1H NMR spectrum for the major isomer shows three multiplets for the F-substituted ring with each showing coupling to F, indicating that the

major isomer is **3.12a-F*,H** which has cyclometallated on the F-substituted ring. The minor isomer signals were extracted from the ^1H NMR spectrum of the mixture (additionally, this isomer was isolated and characterised from transmetallation reaction with Cu, section **3.bii**, see Chapter 6 for details) with four phenyl signals showing the same pattern as for **3.12a-OMe,H*** indicating that the minor isomer is the product of cyclometallation of the non-substituted ring **3.12a-F,H***. The HRMS(ESI) spectrum shows ions at m/z 604.1874 due to $[\text{M-Cl+MeCN}]^+$. Reaction of the same ligand **L3.12-F,H** with $[\text{RhCl}_2\text{Cp}^*]_2$ resulted in formation of two isomers and the major isomer was isolated in moderate yield. The major isomer for Rh was assigned to have cyclometallated on the F-substituted ring **3.12b-F*,H**. The ^{13}C spectrum of **3.12b-F*,H** shows the expected number of signals. The cyclometallated phenyl C^{1a} is present as a doublet of doublets δ 162.8 ($^1J_{\text{C-Rh}} = 34.6$, $^3J_{\text{C-F}} = 3.5$ Hz) and C^4 is present as a doublet at 180.5 ($^1J_{\text{C-Rh}} = 57.2$ Hz). The ^{19}F NMR spectrum for **3.12b-F*,H** shows one signals at δ -118.2. The HRMS(ESI) spectrum shows ions at m/z 475.1057 due to $[\text{M-Cl}]^+$.

The reaction of **L3.12-Me,H** with $[\text{IrCl}_2\text{Cp}^*]_2$ formed two isomers which were obtained in good yield. The major isomer has undergone cyclometallation on the unsubstituted phenyl to give **3.12a-Me,H***. Whilst the minor isomer is **3.12a-Me*,H**. The HRMS(ESI) spectrum show ions at m/z 602.2150 due to $[\text{M-Cl+MeCN}]^+$. The reaction of **L3.12-Me,H** with $[\text{RhCl}_2\text{Cp}^*]_2$ gave, after precipitation from DCM/hexane, a mixture of isomers in a combined moderate yield. From the ^1H NMR spectrum, the major isomer is assigned to be cyclometallated on the unsubstituted phenyl i.e. **3.12b-Me,H***. The HRMS(ESI) spectrum show ions at m/z 471.1291 due to $[\text{M-Cl+MeCN}]^+$.

The reaction of **L3.12-Me,OMe** with $[\text{MCl}_2\text{Cp}^*]_2$ ($\text{M} = \text{Ir, Rh}$) resulted in isolation of almost equimolar isomeric mixtures for Ir and Rh. The slightly major isomers for both Ir and Rh and were assigned as **3.12a/b-Me,OMe***, whilst the slightly minor isomers were identified as **3.12a/b-Me*,OMe**. The HRMS(ESI) spectra for the Ir complexes show ions at m/z 632.2265 due to $[\text{M-Cl+MeCN}]^+$ whilst the Rh complexes show ions at m/z 501.1413 due to $[\text{M-Cl}]^+$.

The reaction of **L3.12-Cl,F** with $[\text{MCl}_2\text{Cp}^*]_2$ ($\text{M} = \text{Ir, Rh}$) resulted in formation of two isomers in good yields. From the ^1H NMR spectra of the mixtures the major isomers were assigned to be the **3.12a/b-Cl*,F** and the minor ones as **3.12a/b-Cl,F***. The HRMS(ESI)

spectra show ions at m/z 640.1508 due to $[M-Cl+MeCN]^+$ for the Ir complexes and ions at m/z 550.0939 due to $[M-Cl]^+$ for the Rh complexes.

The reaction of **L3.12-F,CF₃** with $[MCl_2Cp^*]_2$ (M = Ir, Rh) formed two isomers in each case in moderate yields for Ir and for Rh. From the ¹H NMR spectra the major isomers for both Ir and Rh were assigned as cyclometallation of CF₃-substituted phenyl products **3.12a/b-F,CF₃***. The HRMS(ESI) spectra shows ions at m/z 674.1793 for Ir complexes due to $[M-Cl+MeCN]^+$ and ions at m/z 543.0935 due to $[M-Cl]^+$ for Rh complexes.

Three Ir complexes **3.12a-F*,OMe**, **3.12a-F*,H** and **3.12a-OMe*,OMe** (preparation discussed later in the section) gave crystals suitable for the X-ray diffraction and the structures are shown below in **Figure 3.2** with selected bond distances and angles in **Table 3.3**. All three structures show the expected piano stool geometry. For all three complexes **3.12a-F*,OMe**, **3.12a-F*,H** and **3.12a-OMe*,OMe**, the Ir—C(1) carbene distance [2.009(4), 2.011(8) and 2.022(6) Å respectively] is very similar to the Ir—C(11) [2.056(4), 2.032(11) and 2.064(6), Å respectively]. The Ir—C(1) carbene distance is similar to that observed in the literature and lies within the reported range [1.98-2.06 Å] for Ir half-sandwich NHC complexes.^{16,31} The Ir—C(11) distance for all three complexes is consistent with the equivalent distance in phenylpyridine complexes **2.6a-R** (R = H, F, CF₃) [2.058(5), 2.049(6) and 2.043(8) Å for **2.6a-H**, **2.6a-F**, **2.6a-CF₃** respectively]. The bite angles of 77-78° for all three complexes are also consistent with the bite angles of *ca.* 78° observed for phenylpyridines **2.6a-R** (R = H, F, CF₃) (Chapter 2, **Table 2.3**) and five-membered cyclometallated complexes in the literature (**3.5a-R**, **Scheme 3.4**).^{18,32}

For **3.12a-F*,OMe** the angle between imidazole plane (defined by C(1), N(1),C(2),C(3), N(2)) and cyclometallated phenyl plane (defined by C(10)-C(15)) is 10.3° indicating that these two rings are coplanar and suggesting conjugation. Whilst the angle between the imidazole and the non-cyclometallated phenyl plane is 51.1° indicating that they are not coplanar. The other two structures **3.12a-F*,H** and **3.12a-OMe*,OMe** show similar features.

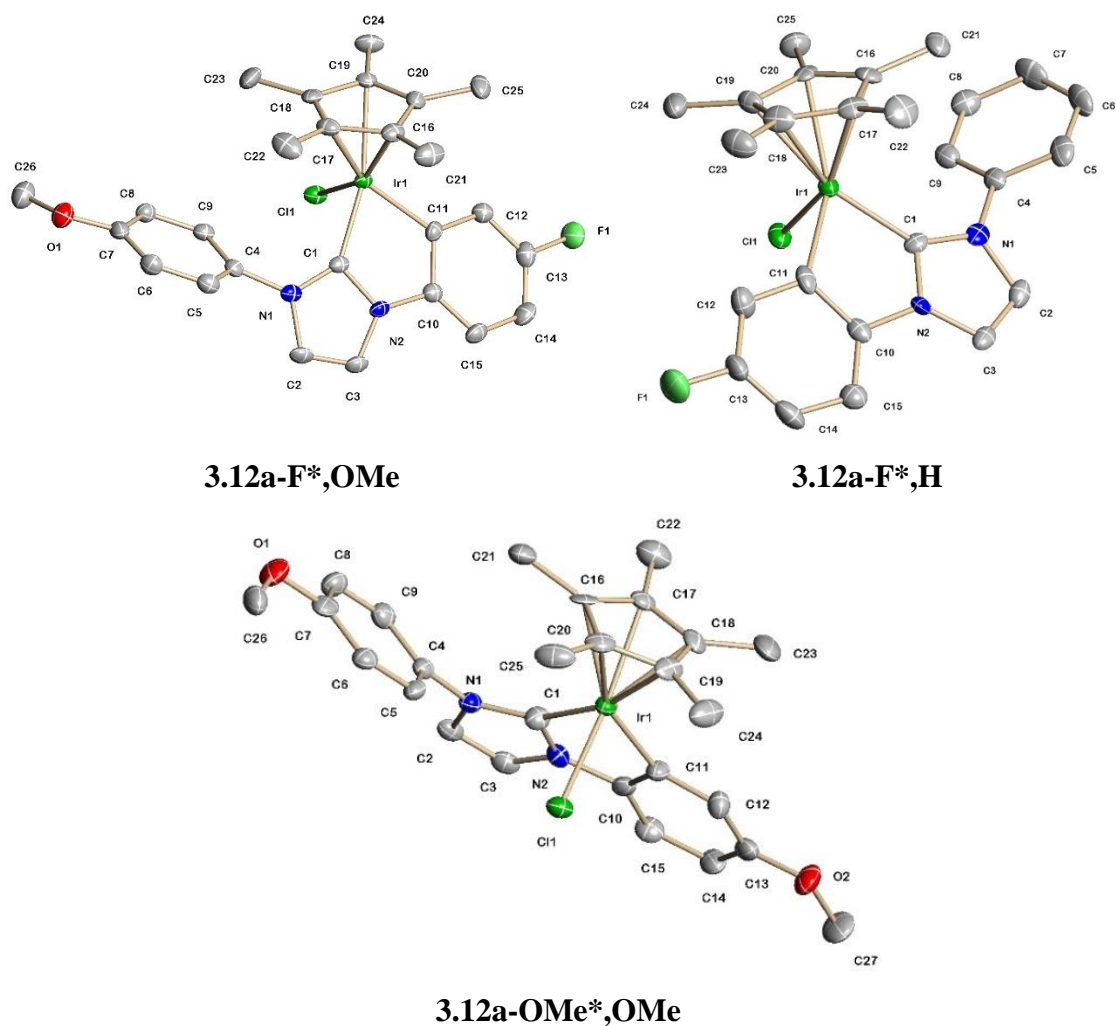


Figure 3.2: X-ray structures of **3.12a-F*,OMe**, **3.12a-F*,H** and **3.12a-OMe*,OMe** showing 50% displacement ellipsoids. Hydrogen atoms have been omitted for clarity.

Table 3.3: Selected bond distances (Å) and bond angles [°] for **3.12a-F*,OMe**, **3.12a-F*,H** and **3.12a-OMe*,OMe**.

	3.12a-F*,OMe	3.12a-F*,H	3.12a-OMe*,OMe
Ir—C(1)	2.009(4)	2.011(8)	2.022(6)
Ir—C(11)	2.056(4)	2.032(11)	2.064(6)
Ir—Cl	2.419(1)	2.414(3)	2.407(2)
C(11)—Ir—C(1)	77.6(2)	76.9(4)	78.0(2)

As mentioned above, all reactions were monitored in less than 1 hour to obtain initial isomer ratios, and again after several hours or overnight. In all cases two isomers were obtained and the ratios did not change significantly (>10%), therefore, only the initial

ratios are shown in **Table 3.4**. The reactions with very electron-withdrawing substituents (Cl,F and F,CF₃) proceeded slowly even at room temperature reaching *ca.* 20% conversions within 4-24 hours for both Ir and Rh (**Table 3.4**, entries 8 and 9). This agrees with the literature observation that the imidazolium C–H (H⁴ for **L3.12-R₁,R₂**) is more acidic with electron-withdrawing substituents.³³

Table 3.4: Initial isomer ratios for cyclometallation of **L3.12-R₁,R₂** with Ir and Rh.

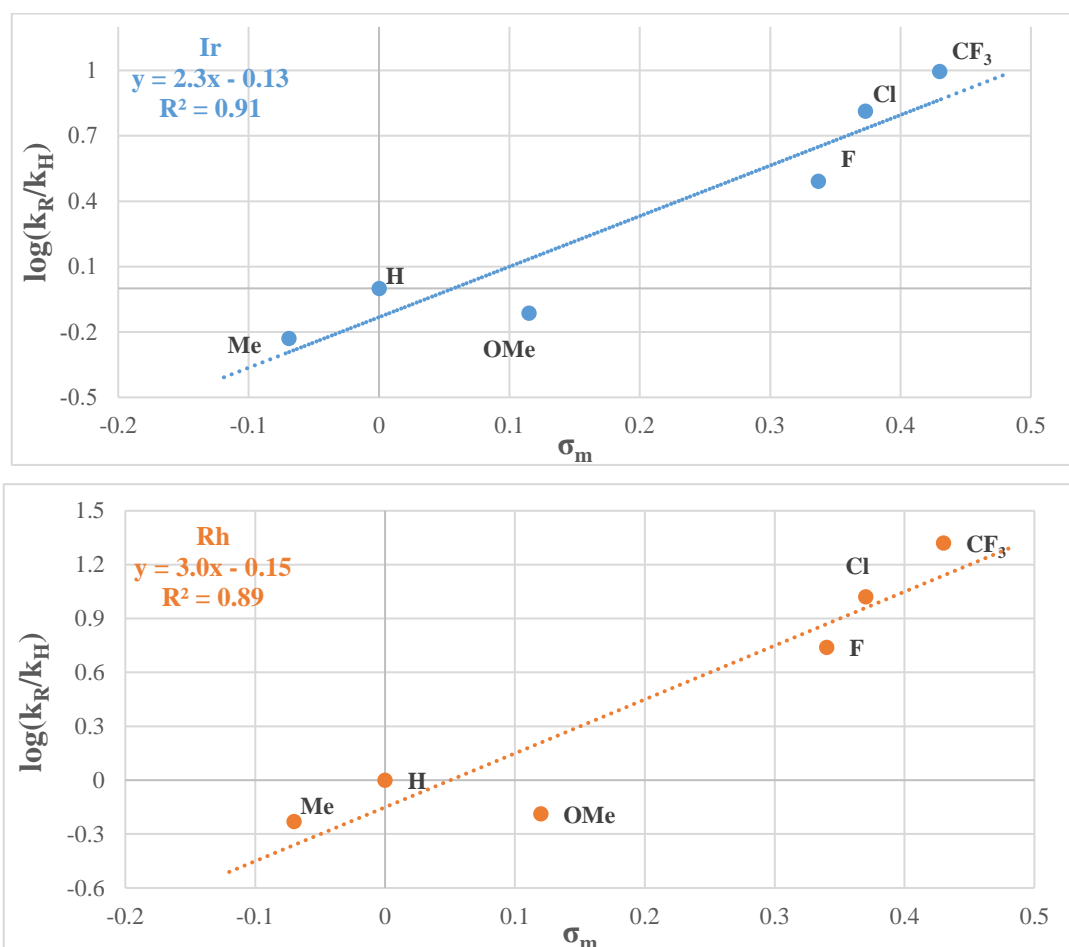
Entry	R ₁	R ₂	Ir, R ₁ *:R ₂ *	Rh, R ₁ *:R ₂ * ^a
1	OMe	H	1:1.3	-
2	Me	CF ₃	1:15	-
3	F	Me	5.3:1	-
4	F	OMe	4.1:1	-
5	F	H	3.1:1	5.5:1
6	Me	H	1:1.7	1:1.7
7	Me	OMe	1:1.2	1:1.1
8^a	Cl	F	2.1:1(2.1:1) ^a	1.9:1(1.9:1) ^a
9^a	F	CF ₃	1:3.2(1:2.8) ^a	1:3.8(1:3.8) ^a

^a ratios at rt at *ca.* 20% conversion.

The ratios shown above were used to calculate the relative rates of formation (k_R/k_H) compared to the unsubstituted phenyl and are presented in the **Table 3.5** together with the appropriate Hammett constants (σ_m) and the Hammett plot is shown in **Figure 3.3**. To check the consistency of the data, some of the observed ratios from intramolecular competitions (**Table 3.4**) were used to predict the expected ratios for other combinations (for example observed ratio of R₁*:R₂* for F,OMe pair for Ir is 4:1 the observed ratio for F,H is 3.1:1 and OMe,H is 1:1.3, therefore, predicted ratio of F,OMe is $3.1 \times (1 \div 1.3) = 4:1$) which were found to be within experimental error of the observed ratios indicating that the data is fairly self-consistent (appendix, **Table S1**).

Table 3.5: Relative rates of intramolecular competition of {IrCp*} and {RhCp*}.

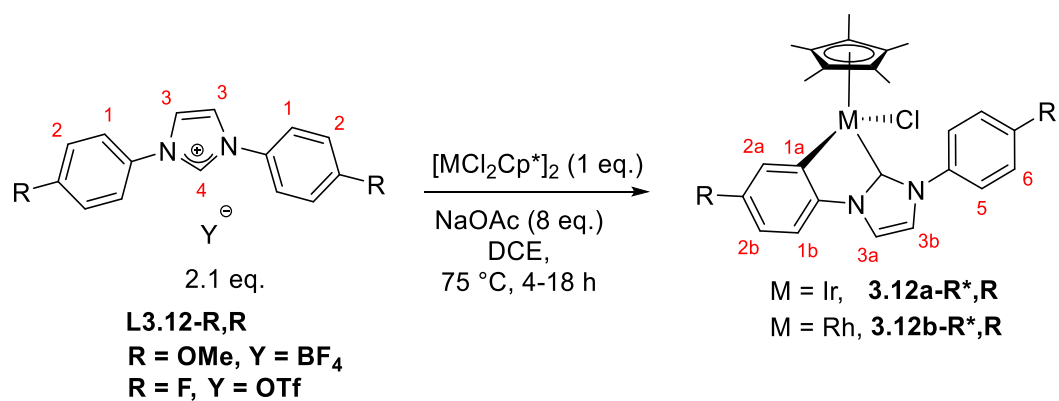
Group	Me	H	OMe	F	Cl	CF ₃	
σ_m	-0.07	0	0.12	0.34	0.37	0.43	
Ir	k_R/k_H	0.59	1	0.77	3.1	6.5	9.9
	$\log(k_R/k_H)$	-0.23	0	-0.11	0.49	0.81	1.0
Rh	k_R/k_H	0.59	1	0.65	5.5	10.5	20.9
	$\log(k_R/k_H)$	-0.23	0	-0.19	0.74	1.02	1.32

**Figure 3.3:** Hammett plots for initial results of cyclometallation of **L3.12-R₁,R₂** with Ir (top) and Rh (bottom), $\log(k_R/k_H)$ against σ_m .

As can be seen from the Hammett plot the slopes for both Ir (2.3) and Rh (3.0) are positive indicating a preference for electron-withdrawing groups with Rh having a slightly larger slope. However the correlations ($R^2 = 0.91$ and 0.89 for Ir and Rh respectively) are a little low, the data for OMe substituted rings seems to have the largest difference to the plotted lines. An OMe group at the *meta*-position is electron-withdrawing ($\sigma_m = 0.12$), however

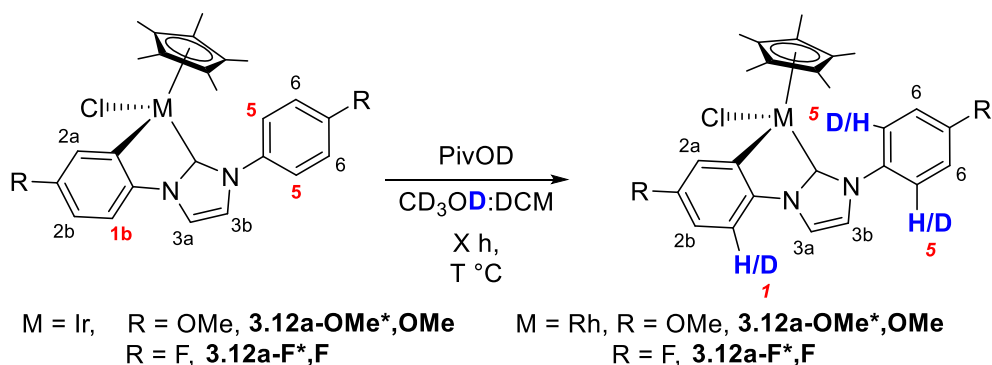
in a *para*-position it is electron donating ($\sigma_p = -0.27$). In this case the $\log(k_R/k_H)$ value for OMe is similar to that for Me. The slopes are very different to those for phenylpyridines ($\rho = -1.6$ and -2.1 for Ir and Rh respectively) discussed in Chapter 2 and those for phenylpyrazoles ($\rho = -2.7$ and -2.3 for Ir and Rh respectively).² However, positive slopes could suggest the thermodynamic selectivity as observed for phenylpyridines (Chapter 2, $\rho = 0.6$ and 1.2 for Ir and Rh respectively) and phenylpyrazoles ($\rho = 1.6$ and 1.5 for Ir and Rh respectively).²

As mentioned above no change in ratios was observed when reactions were monitored after longer times or with heating indicating that either the cyclometallations are irreversible under the reaction conditions or they are reversible but have already reached equilibrium at the time of first monitoring. Hence it is important to try and establish if the measured ratios are showing kinetic or thermodynamic preference. To test whether the cyclometallation is reversible H/D exchange experiments were carried out. Use of the complexes prepared from unsymmetrical imidazolium salts could result in difficulty in observing H/D exchange due to possible isomerisation and overlap of signals from the two isomers. Therefore, two symmetrical imidazolium salts **L3.12-OMe,OMe** and **L3.12-F,F** were prepared by the same method as before (**Scheme 3.13**). The salts **L3.12-OMe,OMe** and **L3.12-F,F** were then reacted with $[MCl_2Cp^*]$ ($M = Ir, Rh$) in the presence of NaOAc in DCE for 4 hours with Ir and 18 hours with Rh (**Scheme 3.16**). Complexes **3.12a/b-OMe*,OMe** and **3.12a/b-F*,F** were isolated, characterised and the 1H NMR spectra assigned in the same way as the complexes above (see Chapter 6 for details). The cyclometallated and non-cyclometallated rings show different environments for the substituents; thus in the 1H NMR spectra for **3.12a/b-OMe*,OMe** the two OMe groups give signals at *ca.* δ 3.87 and 3.89 and two signals are seen in the ^{19}F NMR spectra of **3.12a/b-F*,F** at about δ -113.0 and -118.3.



Scheme 3.16: Cyclometallation of **L3.12-R,R** (R = OMe, F) with Ir and Rh.

As discussed in Chapter 1 (**Figure 1.12**) after AMLA C–H activation coordinated acetic acid is exchanged with chloride to form the cyclometallated product. Therefore, for the reverse reaction to happen acid has to replace chloride. If the cyclometallation is reversible then D-incorporation is possible in all *ortho* positions available (1 and 5) (**Scheme 3.17**). Deuteration experiments were carried out by dissolving the complexes in CD₃OD (*ca.* 0.5 mL and with *ca.* 0.05 mL of DCM) with PivOD to promote the reverse of C–H activation (**Scheme 3.17**). The reactions were monitored by ¹H NMR spectroscopy and deuterium incorporation was calculated by comparing integrations of the *ortho* signals (H^{1b}, H⁵) with the other signals (H^{2a}, H^{2b}, H⁶) and the results are summarised in **Table 3.6**. The presence of deuterium was confirmed by ²H NMR spectroscopy.



Scheme 3.17: Deuterium incorporation experiments with **3.12a/b-R,R** (R = OMe, F).

Table 3.6: Results of D-incorporation experiments.

Entry	R	M	Temperature, °C	Time, h	% D in site 1	%D in site 5
1	OMe	Ir	rt	48	N.D.	N.D.
2	OMe	Rh	rt	48	N.D.	N.D.
3	OMe	Ir	70	1	90	80
4	OMe	Rh	70	1	80	80
5	F	Ir	70	2	N.D.	N.D.
6	F	Rh	rt	24	N.D.	N.D.
7	F	Rh	70	2	20	10
8	F	Rh	70	24	95	80

N.D. not detected by ¹H NMR spectroscopy

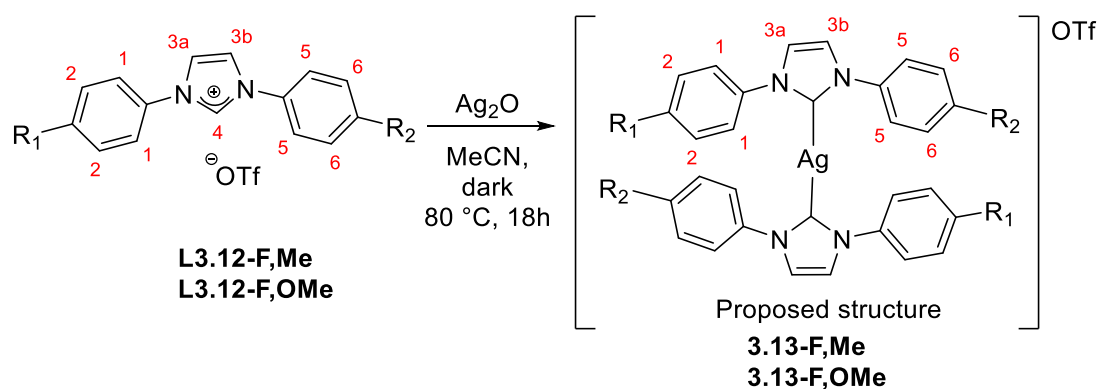
For **3.12a-OMe*,OMe** no D-incorporation was observed at room temperature with Ir and Rh (entries 1 and 2). Heating the complexes at 70 °C for an hour resulted in high D-incorporation (>80%) for both complexes (entries 3 and 4) indicating that the cyclometallations for these complexes are reversible. Complexes containing more electron-withdrawing substituents are less reversible; Ir complex **3.12a-F*,F** shows no H/D exchange within 2 hours at 70 °C (entry 5) and Rh complex **3.12a/b-F*,F** requires heating for a day to show high D-incorporation (entries 6 - 8). Overall, the results indicate that C–H activation of a phenyl for **L3.12a/b-R,R** can be reversible at 70 °C in the presence of acid with those with the more electron-withdrawing substituent (F) being less reversible than those with OMe-substituents. Presumably the more electron-withdrawing group gives a more thermodynamically stable complex as found for phenylpyridines (Chapter 2) and phenylpyrazoles.² In addition, the Rh reactions are more easily reversible than Ir as has been found previously.³⁴ These results suggest that in many cases the observed ratios may already be equilibrium ratios (or certainly not purely kinetic ones) especially with Rh. It should be noted that acid is needed to reverse the C–H activation and the concentration of acid in the preparative reactions is likely to be lower than in the D-incorporation experiments. The reversibility will be discussed further in the DFT section **3.2d**.

To summarise, the reactions of **L3.12-R₁,R₂** with [MCl₂Cp*]₂ (M = Ir, Rh) in the presence of NaOAc led directly to the formation of two isomeric cyclometallated

complexes, and the non-cyclometallated intermediate complexes **int-3.12a/b-R₁,R₂** were not observed. The reactions with electron-withdrawing pairs (Cl,F and F,CF₃) were found to take place at room temperature, likely due to the increased acidity of the imidazolium H⁴ with electron-withdrawing substituents, whilst the others required heating.³³ The non-directed C–H activation of the imidazolium proton takes place prior to the C–H activation of the phenyl, the subsequent NHC directed C–H activation of the phenyl is easier and hence prevents build-up of the intermediate. Since the reactions were conducted at 75 °C and based on the deuteration experiments it is likely that the selectivity is thermodynamic. In order to try and observe kinetic selectivity it is therefore necessary to try and make the intermediate non-cyclometallated NHC complexes at lower temperature hence transmetallation reactions were attempted as discussed below.

3.bii Preparation of Ir and Rh half-sandwich NHC complexes by transmetallations

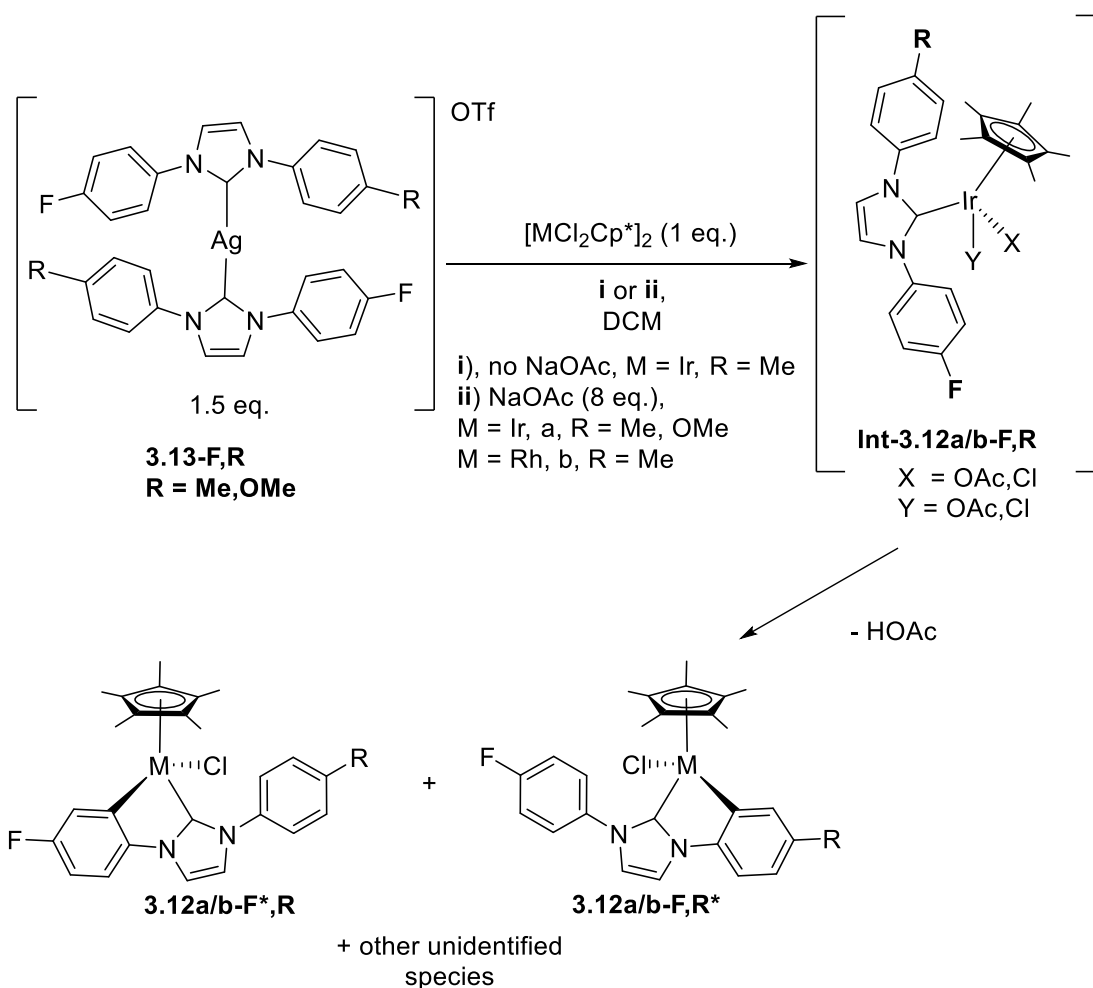
Transmetallations from Ag and Cu were attempted as a route to non-cyclometallated NHC complexes. First, Ag complexes **3.13-F,Me** and **3.13-F,OMe** were prepared by heating **L3.12-F,Me** or **L3.12-F,OMe** with excess Ag₂O (Scheme 3.18).⁹ This gives di-carbene Ag complexes with weakly or non-coordinating ions (OTf, BF₄, PF₆).^{33, 35} The reaction mixtures were filtered through celite and solvent removed to give **3.13-F,Me** and **3.13-F,OMe** both of which are novel compounds. The ESI-MS for each show ions corresponding to the cation. Both complexes show two AA'BB' patterns in the ¹H NMR spectra indicating that complexes **3.13-F,OMe** and **3.13-F,Me** are not cyclometallated whilst the ¹³C NMR spectra each show a broad signal at *ca.* δ 180 which is characteristic for Ag-NHCs (see Chapter 6 for details).³⁵ Both complexes start to decompose in solution (after several hours) as well as when left open to air; the instability of some Ag-NHC complexes has been reported previously.³³



Scheme 3.18: Preparation of Ag-NHCs from unsymmetrical imidazolium salts.

Reaction of **3.13-F,Me** with $[\text{IrCl}_2\text{Cp}^*]_2$ in DCM in the absence of NaOAc (**Scheme 3.19**) and protected from the light led to the formation of a complex mixture after 15 minutes. From the ^{19}F NMR spectrum the mixture contained traces of unreacted **3.13-F,Me** (<10%) and **L3.12-F,Me** (*ca.* 20%) presumably formed by hydrolysis of **3.13-F,Me**, and two very broad signals that had very similar shifts to and so assigned to cyclometallated complexes **3.12a-F*,Me** and **3.12a-F,Me*** (*ca.* 70%). However, the ^1H NMR spectra showed broad unresolved signals including for the possible **3.12a-F*,Me** with Cp* region showing several broad signals and the spectra did not change significantly when the mixture was stirred for a further day. Hence, the non-cyclometallated **int-3.12a-F,Me** complex could only be at most a very minor component of the mixture.

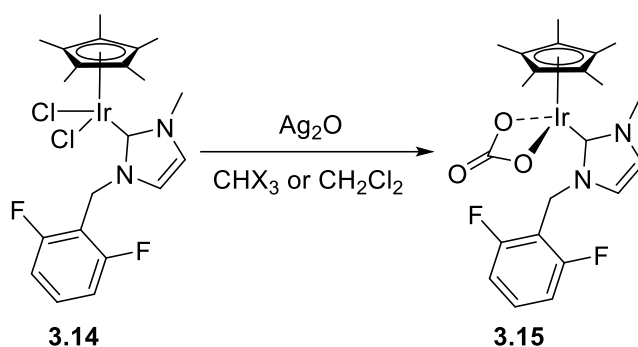
The reaction of **3.13-F,Me** with $[\text{IrCl}_2\text{Cp}^*]_2$ was repeated in the presence of NaOAc (**Scheme 3.19**). The ^1H NMR spectrum after an hour of the reaction showed the formation of several species with three major species being **L3.12-F,Me** and **3.12a-F*,Me** and **3.12a-F,Me*** in a 1.2:1:2 ratio. The reaction of **3.13-F,Me** in the presence of NaOAc was also tried with $[\text{RhCl}_2\text{Cp}^*]_2$ and **3.13-F,OMe** was also reacted with $[\text{IrCl}_2\text{Cp}^*]_2$ but the major species observed were cyclometallated products and imidazolium salts.



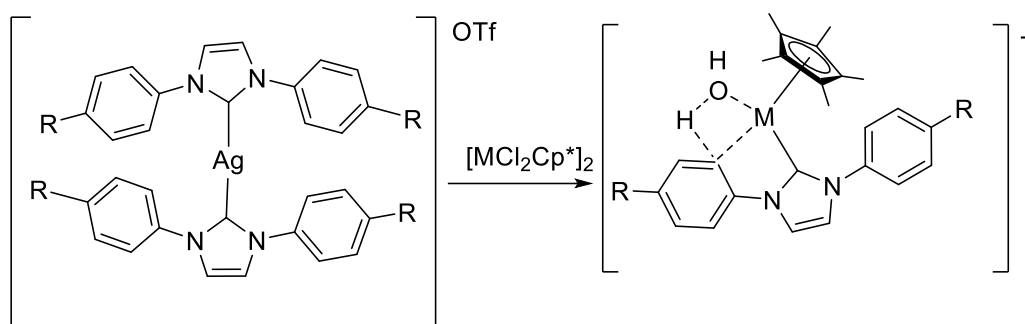
Scheme 3.19: Attempted transmetalations with **3.13-F,R** (R = OMe, Me) with Ir and Rh.

Recently it has been reported that IrNHC complex **3.14** (**Scheme 3.20 i**) in the presence of Ag_2O can convert haloforms ($CHCl_3$, $CHBr_3$, CH_2Cl_2) to carbonates to form **3.15**. Such species may also be forming in the reactions attempted above.³⁶ In addition, it was shown that Ag nanoparticles can promote cyclometallation of Ir-NHCs, which could explain the observed cyclometallation in the absence of NaOAc (discussed in more detail in Chapter 4, **Scheme 4.4 ii**).³⁷ Also, since Ag_2O is basic it may deprotonate the phenyl or give rise to a coordinated OH which could result in an AMLA-4 C–H activation and could also explain the cyclometallation (**Scheme 3.20 ii**).

i) Reaction of haloform with Ir-NHCs and Ag₂O

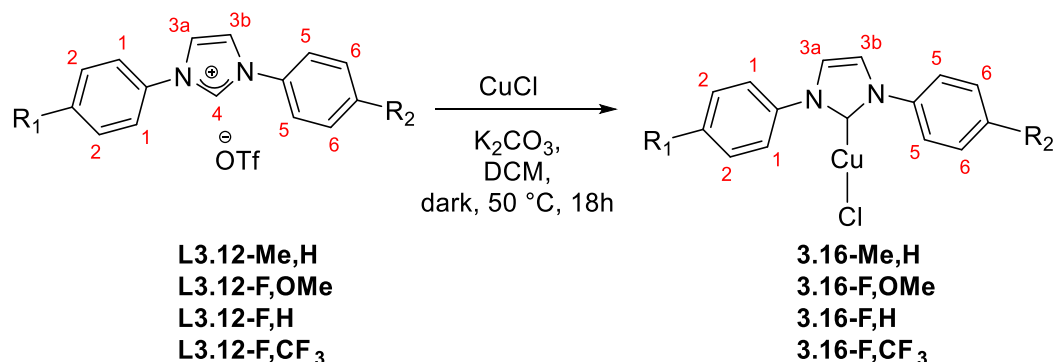


ii) AMLA-4 activation



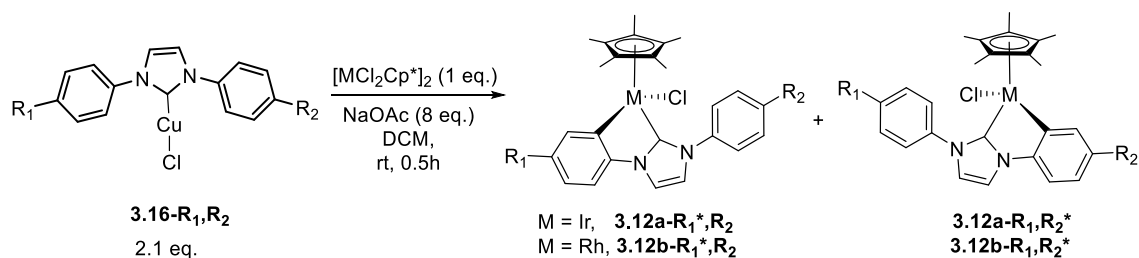
Scheme 3.20: Possible involvement of Ag in C–H activation **i)** Ag-promoted formation of **3.15**,³⁶ **ii)** Possible AMLA-4 activation.

As the transmetalations with Ag proved to be unsuccessful in giving **int-3.12a-R1,R2**, transmetalation with Cu was tried as an alternative. First of all, Cu-NHC complexes **3.16-R1,R2** (**R1,R2** = **Me,H**; **F,OMe**; **F,H**; **F,CF₃**) were prepared by a literature method (**Scheme 3.21**)³⁸ in high yields. The ESI-MS show ions corresponding to [M-Cl].³⁸ The ¹H NMR spectra of the **3.16-R1,R2** show ¹H NMR spectra as expected; similar to the free ligand but without the H⁴ proton and the ¹³C NMR spectra show C⁴ as a broad signal at about δ 180 which is characteristic for a Cu bound NHC.³⁸ Partial decomposition (turning green releasing Cu) in solution and as a solid when open to air was also observed within several hours.



Scheme 3.21: Preparation of Cu-NHCs **3.16-R₁,R₂** from **L3.12-R₁,R₂**.

The Cu-NHC complex **3.16-F,OMe** was reacted with $[\text{IrCl}_2\text{Cp}^*]_2$ in DCM at room temperature in the absence of NaOAc and after 15 minutes five signals were observed in the ^{19}F NMR spectrum, one of which was unreacted **3.16-F,OMe** (*ca.* 15%), two unidentified species (*ca.* 20% combined) and two broad signals at δ -118.6 and -113.2 assigned to **3.12a-F*,OMe** and **3.12a-F,OMe*** (*ca.* 65% combined). However, the ^1H NMR spectrum was broad and hence unhelpful. The ^1H and ^{19}F NMR spectra did not change significantly when mixture was left to stand for 2 days. As it was not possible to isolate any intermediate non-cyclometallated complexes, it was decided to move on from trying to prepare the intermediate and to investigate cyclometallation from Cu-transmetallation at room temperature to assess the kinetic selectivity. Therefore, **3.16-R₁,R₂** were reacted with $[\text{MCl}_2\text{Cp}^*]_2$ (M = Ir, Rh) in DCM at rt in the presence of NaOAc (**Scheme 3.22**) and the results are shown in **Table 3.7**. The reactions were clean and gave two cyclometallated products in high conversions (>90%) as observed by the ^1H or ^{19}F NMR spectra.



Scheme 3.22: Cu-transmetallation with Ir and Rh.

Table 3.7: Cyclometallation selectivity from Cu-transmetallation with Ir and Rh.

Entry	R ₁	R ₂	Ir, R ₁ *:R ₂ *	Rh, R ₁ *:R ₂ *
1	Me	H	1:1.2 (1:1.7)	1:1.4 (1:1.7)
2	F	H	1:2.9 (3.1:1)	5.2:1 (5.5:1)
3	F	OMe	1:1 (4.1:1)	7.7:1
4	F	CF ₃	1:2.7 (1:3.2)	1:3.7 (1:3.8)

Values in parentheses correspond to the ratios observed in direct C–H activation (**Table 3.4**)

The selectivities observed by transmetallation from Cu (entries 1-4) showed an increased preference for more electron-donating groups compared to the direct C–H activation reactions at 75 °C particularly in the case of Ir, entry 2 showing a complete switch in selectivity. These changes provide further evidence that the ratios obtained at 75 °C are at least partially if not fully equilibrated. The transmetallation ratios observed after 0.5 hour (>90% conversion) were then used to calculate the relative rates of formation (k_R/k_H) compared to the unsubstituted phenyl and are presented in the **Table 3.8** together with the appropriate Hammett constants (σ_m) and the Hammett plots are shown in **Figure 3.4**.

Table 3.8: Relative rates of intramolecular competition of Ir and Rh from Cu-transmetallations.

Group	Me	H	OMe	F	CF ₃	
σ_m	-0.07	0	0.12	0.34	0.43	
Ir	k_R/k_H	0.83	1	0.35	0.35	0.95
	$\log(k_R/k_H)$	-0.08	0	-0.46	-0.46	-0.02
Rh	k_R/k_H	0.71	1	0.71	5.2	19.2
	$\log(k_R/k_H)$	-0.15	0	-0.15	0.71	1.28

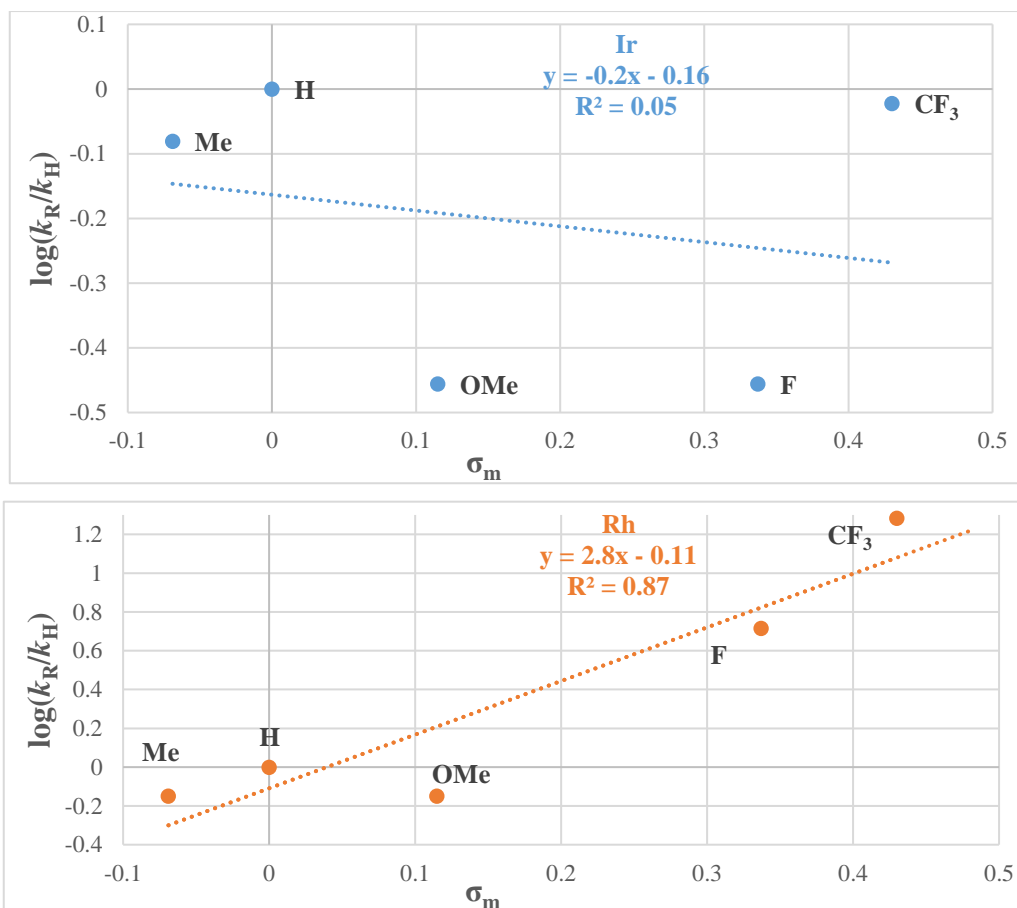
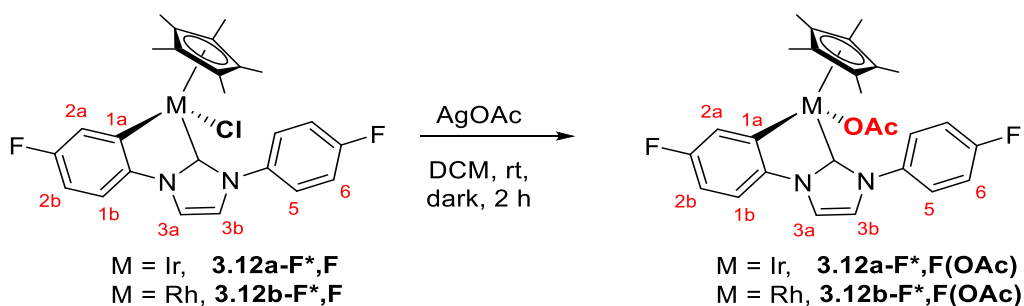


Figure 3.4: Hammett plot for transmetallation of **3.16-R₁,R₂** with Ir (top) and Rh (bottom), $\log(k_R/k_H)$ against σ_m .

As can be seen, the results for Rh show a modest correlation ($R^2 = 0.87$) whilst those for Ir, show no correlation at all ($R^2 = 0.05$) and are very different from the results observed from the direct C–H activation ($R^2 = 0.91$, $\rho = 2.3$, **Figure 3.3**). The selectivities observed for Rh are similar to those observed from the direct C–H activation discussed previously with slopes of 2.8 and 3.0 respectively (**Figure 3.3**). These results are consistent with the cyclometallation reactions with Rh being more reversible than for Ir. Hence reactions with Rh show something close to thermodynamic selectivity even at room temperature whilst reactions with Ir may be showing a mixture of kinetic and thermodynamic selectivity leading to almost no correlation between relative rate and substituent Hammett parameter. As it is unclear if the transmetallation reactions resulted in kinetic selectivity, conditions that would allow the direct C–H activation reactions to take place at room temperature and so hopefully allowing assessment of kinetic selectivity were investigated next.

3.2c Influence of chloride concentration

The final metal complexes isolated from the direct C–H activation and transmetalation have chloride bound to the metal. However, in all cases there was a relatively high acetate ion concentration (4 equivalents per metal centre) and so acetate complexes could potentially form instead. Hence, it was decided to investigate whether acetate complexes may be forming and if so how fast substitution by chloride occurs. Complexes **3.12a-F*,F** and **3.12b-F*,F** were each reacted with AgOAc in the dark at room temperature (Scheme 3.23). After two hours in each case, both ^1H NMR and ^{19}F NMR spectroscopy showed new species were formed and after work up **3.12a-F*,F(OAc)** and **3.12b-F*,F(OAc)** were isolated in 95% and 96% yields respectively.



Scheme 3.23: Preparation of acetate complexes from **3.12a-F*,F** and **3.12b-F*,F**.

The ^1H NMR spectrum of the **3.12a-F*,F(OAc)** is similar to the chloride complex **3.12a-F*,F** but has an additional 3H singlet at δ 1.78 corresponding to OAc. There is a slight change in chemical shifts of the protons closest to the OAc, H^{2a} and H^5 , which are at δ 7.63 and 7.81 respectively (*cf.* δ 7.42 and 7.95 for H^{2a} and H^5 respectively for **3.12a-F*,F**). These signals also show an NOE with the OAc signal at δ 1.78 indicating close proximity to it. Similar observations are observed for the Rh analogue **3.12b-F*,F(OAc)**. The ^{13}C NMR spectra for both **3.12a-F*,F(OAc)** and **3.12b-F*,F(OAc)** show the expected number of signals with two new signals for OAc at *ca.* δ 24 and 177. The change in shifts is also observed for fluorine signals in ^{19}F NMR spectra for **3.12a-F*,F(OAc)** with signals present at δ -118.9 and -113.6 (*cf.* δ -118.4 and -113.0 for **3.12a-F*,F**) and for **3.12b-F*,F(OAc)** at δ -118.7 and -113.6 (*cf.* δ -118.2 and -112.9 for **3.12b-F*,F**).

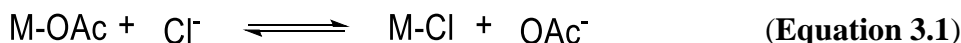
The exchange of acetate by chloride was then investigated. Complexes **3.12a-F*,F(OAc)** or **3.12b-F*,F(OAc)** were dissolved in deuterated solvent (CDCl_3 or CD_2Cl_2) in an NMR tube and Et_4NCl was added in portions. The reactions were monitored by ^1H NMR and

^{19}F NMR spectroscopy at time intervals (5 and 30 minutes). The relative percentage of the chloride complexes **3.12a-F*,F** or **3.12b-F*,F** were calculated by comparing the integrations of $\text{H}^{2\text{a}}$ and $\text{H}^{3\text{a}}$ signals for the acetate complex **3.12a/b-F*,F(OAc)** with the corresponding signals of the growing chloride complex **3.12a/b-F*,F**. The results are summarised in **Table 3.9**.

Table 3.9: Percentage of chloride complex **3.12a/b-F*,F** formed from **3.12a/b-F*,F(OAc)** in the presence of Et_4NCl .

Entry	Time after addition of Et_4NCl	Percentage of 3.12a-F*,F , %, (Et ₄ NCl eq)		Percentage of 3.12b-F*,F , %, (Et ₄ NCl eq)	
		CDCl_3	CD_2Cl_2	CDCl_3	CD_2Cl_2
1	5 min.	8(0.28)	15(0.25)	20(0.22)	29(0.35)
2	30 min.	10(0.28)	18(0.25)	22(0.22)	35(0.35)
3	+5 min.	38(2.56)	21(1.3)	79(1.6)	65(0.8)
4	+30 min.	42(2.56)	22(1.3)	86(1.6)	71(0.8)
5	overnight	83(2.56)	-	>95(1.6)	-
6	+30 min.	-	>95(1.3) + drop of CD_3OD	-	>95(1.0) + drop of CD_3OD

As seen in the **Table 3.9**, the exchange of the acetate ion by chloride was relatively slow in CDCl_3 for both Ir and Rh complexes with an excess of chloride (entries 1-4). Entry 5 after leaving overnight for Ir and Rh, shows that significantly more chloride has coordinated compared to entries 4, particularly for Ir. Thus, for Ir it requires overnight for the reactions to reach equilibrium whereas it is much faster for Rh, as expected, requiring something in the region of a few hours. Similar results are seen in CD_2Cl_2 . However, upon addition of a small amount of the more polar solvent CD_3OD (0.1 mL) (entry 6) over 95% conversions of **3.12a/b-F*,F(OAc)** to the chloride complexes **3.12a/b-F*,F** were observed within 30 minutes showing that anion exchange is much faster in more polar solvents (CD_3OD). This is supported by the larger equilibrium constants for the exchange in $\text{CD}_2\text{Cl}_2:\text{CD}_3\text{OD}$ compared to CDCl_3 (**Table 3.10**). The equilibrium constants for the equilibrium results (entries 5 and 6) were calculated by expressing the chloride-acetate exchange by **Equation 3.1** and using formula **3.1** and **3.2**.



M-Cl = the corresponding chloride complex **3.12a-F*,F** or **3.12b-F*,F**.

M-OAc = the acetate complex **3.12a-F*,F(OAc)** or **3.12b-F*,F(OAc)**,

Cl⁻ = ‘free’ chloride ion

OAc⁻ = ‘free’ acetate ion

$$K = \frac{[\text{M-Cl}][\text{OAc}]}{[\text{M-OAc}][\text{Cl}]} \quad (3.1)$$

$$K = \frac{[x][x]}{[1-x][y-x]} \quad (3.2)$$

If all concentrations are expressed as fractions of the starting concentration of [M-OAc].

Then, after some time the concentration of [M-Cl] formed = x = [OAc];

[M-OAc] = 1-x;

[Cl] = y-x, where y = (the total concentration of Et₄NCl added).

Table 3.10: Equilibrium constants for acetate ion to chloride ion exchange in different solvents using the last reading from **Table 3.9** (in bold) for the appropriate solvent.

K_{eq}	Ir	Rh
K(CDCl₃)	2.34	27.8
K(CD₂Cl₂:CD₃OD)	51.6	361

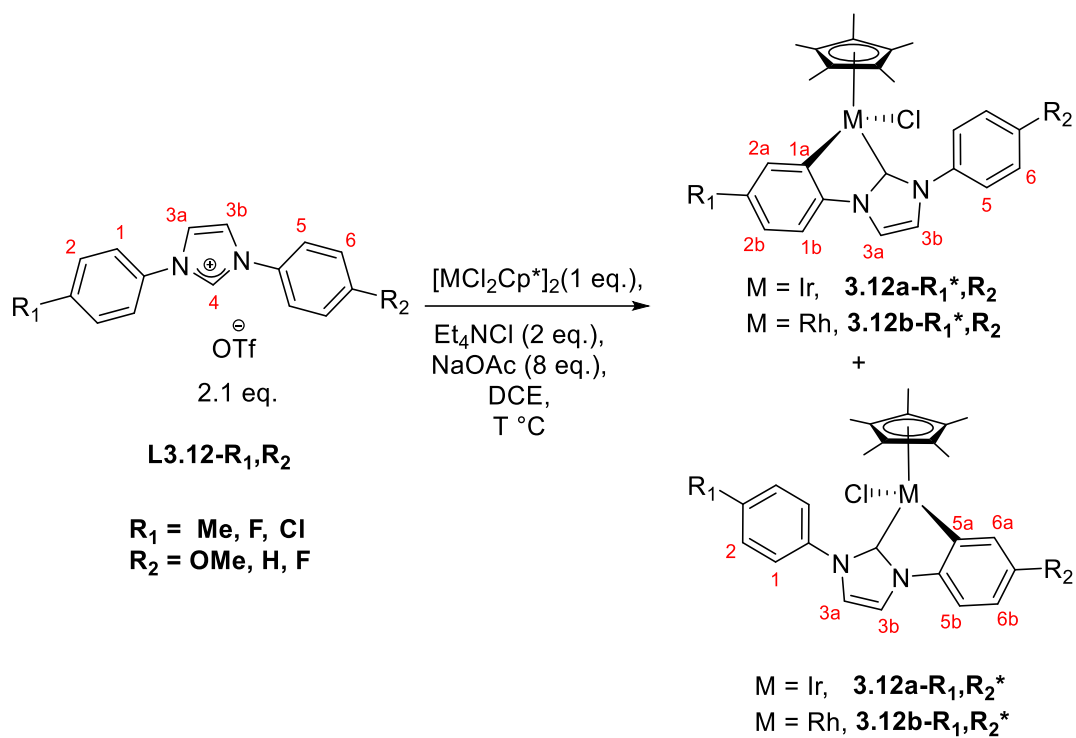
Note, the values are minimum values for K_{eq}, it is assumed the reactions have reached equilibrium. This is almost certainly the case for Rh, but may not be for Ir in CDCl₃.

Overall, for Ir and Rh the chloride complexes **3.12a/b-F*,F** are thermodynamically preferred over acetate complexes suggesting that if acetate complexes are formed first they should be converted to chloride complexes but this is likely to be slow in DCE. Therefore, traces of acetate complexes might have been present in some of the direct C-H activation as well as transmetallation reactions.

Given the results above, it was decided to test the direct C-H activation reactions with added Et₄NCl anticipating that this might favour formation of the final chloride complexes. The chloride may also increase the acidity of the imidazolium salts (proton H⁴) allowing easier deprotonation.³³ The ligands **L3.12-Me,H**, **L3.12-F,H**, **L3.12-F,OMe**, **L3.12-Cl,F** were reacted with [MCl₂Cp*]₂ (M = Ir, Rh) with added Et₄NCl (2 eq. per metal dimer) and NaOAc (8 eq.) with starting Cl:OAc ratio of 6:8. The reactions

were monitored by ^1H NMR spectroscopy and where applicable by ^{19}F NMR spectroscopy. This time all of the reactions took place at the room temperature reaching about 20% conversion within 2 hours at which point the ratios between two isomers were noted. The reversibility of the reactions and the effect of the temperature on the ratios were investigated by heating the reactions to 50 °C for 1 hour and then further to 75 °C overnight with added PivOH to try and ensure that the thermodynamic equilibrium is reached. The results are summarised in **Table 3.11**.

Table 3.11: Cyclometallation of **L3.12-R₁,R₂** in the presence of NaOAc and Et₄NCl.



Entry	M	Conditions	Me,H	F,H	F,OMe	Cl,F
1		rt, 1-4 h ^a	1:1.1	1:3.2	1:1.1	1.9:1
2		50 °C, 1h	1:1.2	1:3.2	1.5:1	2.0:1
3	Ir	75°C, overnight with PivOH	1:1.3	6.6:1	6.0:1 ^b	2.1:1
4		75°C, without Et ₄ NCl ^c	1:1.7	3.1:1	4.1:1	2.1:1
5		rt, 1-4 h, ^a	1:1.2	1:1.8	1.3:1	1.9:1
6		50 °C, 1h	1:1.5	3.0:1	6.0:1	2.0:1
7	Rh	75°C, overnight with PivOH	1:1.7	5.9:1	7.0:1 ^b	2.0:1
8		75°C, without Et ₄ NCl ^c	1:1.7	5.5:1	-	1.9:1

^a at <25% conversion,

^b after 3h,

^c results from heating directly without Et₄NCl (**table 3.4**).

Reactions for entries 1-3 and 5-7 (Ir and Rh) at room temperature with added Et₄NCl showed ratios more in favour of electron-donating groups compared to the reactions at 75°C without Et₄NCl suggesting these (entries 1-3, 5-7, **Table 3.11**) may be more reflective of kinetic rather than thermodynamic selectivity. Reactions with Rh (entries 5-7) were found to be more reversible with ratios changing upon heating, whilst reactions with Ir (entries 1-3) were found to require heating to 75 °C with PivOH for the ratios to change significantly. For entries 1-3 and 5-7 the ratios after heating at 75 °C overnight generally show good agreement (particularly with Rh) with ratios without Et₄NCl at 75 °C. Hence these ratios are likely to be thermodynamic. For entries 4 and 8 the ratios did not change significantly upon heating with added PivOH compared to room temperature, therefore, it is unclear if these ratios are kinetic or thermodynamic. However, from the results for phenylpyridines (Chapter 2) and phenylpyrazoles,² reactions with electron-withdrawing groups tend to be less reversible so for entries 4 and 8 it is possible that they are not easily reversible under the conditions tested.

The ratios at early conversions (20%) were used to calculate the relative rates of cyclometallation of *meta*-substituted phenyls compared to the unsubstituted phenyl (k_R/k_H). The relative rates are represented in **Table 3.12** together with the appropriate Hammett constants and the corresponding Hammett plots are shown in **Figure 3.5**.

Table 3.12: Relative rates of cyclometallation of imidazolium salts with Ir and Rh.

Group		Me	H	OMe	F	Cl
	σ_m	-0.07	0	0.12	0.34	0.37
Ir	k_R/k_H	0.91	1	0.34	0.31	0.59
	$\log(k_R/k_H)$	-0.04	0	-0.47	-0.51	-0.23
Rh	k_R/k_H	0.83	1	0.43	0.56	1.06
	$\log(k_R/k_H)$	-0.08	0	-0.46	-0.25	0

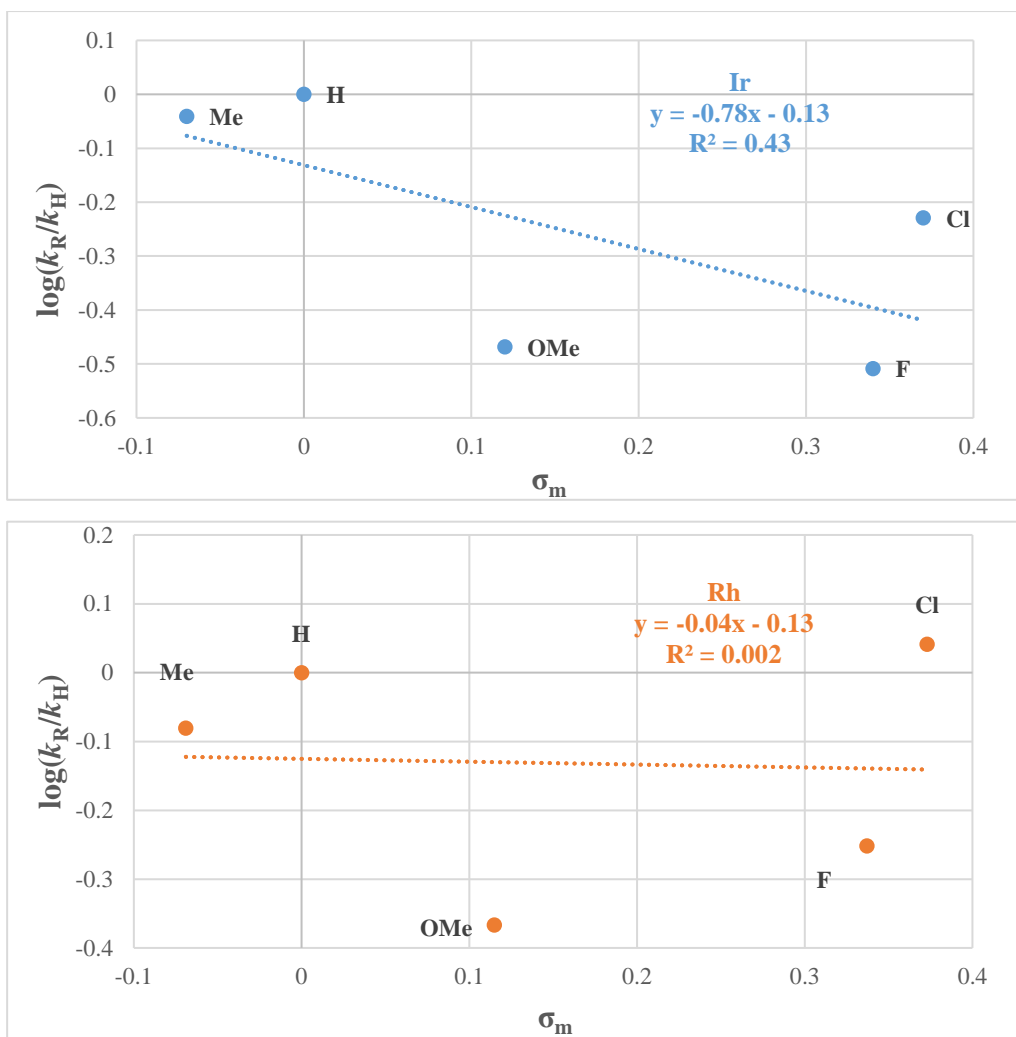


Figure 3.5: Hammett plots for intramolecular competitions of **L3.12-R₁,R₂** with Ir (top) and Rh (bottom) in the presence of added Et₄NCl.

As can be seen from the plots the correlations are very poor for both Ir and Rh. Compared to the Hammett plots obtained from heating at 75°C without Et₄NCl (**Figure 3.3**) which had a reasonable correlation ($R^2 \geq 0.89$) and positive slopes (2.3 for Ir and 3.0 for Rh) the plots shown in **Figure 3.5** are completely different, suggesting that previous results were thermodynamic. Additionally, compared to the plots obtained from Cu-transmetallation reactions (**Figure 3.4**) plot for Ir results is similar ($R^2 = 0.05$, $\rho = 0.2$) to the one in **Figure 3.5** suggesting that with Ir the results may have shown small degree of equilibration at room temperature. However, the Cu-transmetallation reaction results with Rh (**Figure 3.4**) gave a plot ($R^2 = 0.87$, $\rho = 2.8$) very similar to that of the direct C–H activation rather than one in **Figure 3.5** indicating that with Rh at room temperature the results from Cu-transmetallation have already equilibrated and were showing thermodynamic selectivity.

Overall, the results plotted in **Figure 3.5** should be the kinetic results. However, it is possible that even though the reactions with Et₄NCl were monitored at room temperature at early conversions, the reactions were already starting to equilibrate and so observed ratios may not be true kinetic (especially with Rh) and therefore Hammett plots produced do not show good correlation (discussed further in section **3.2d**). Alternatively, a linear free energy relationship (LFER) is only observed if the substituent has a much more significant effect on one position (*meta* or *para*) over the other (if $\rho_m\sigma_m \gg \rho_p\sigma_p$ or $\rho_p\sigma_p \gg \rho_m\sigma_m$) for a kinetically relevant step.^{39 40} As discussed for the electronic effects of substituted benzoates on Ru-catalysed arylation of fluorobenzenes (Chapter 1, **section 1.4bii**)⁴⁰ in some cases a substituent can exert electronic effects on both *meta* (σ_m , in this case C–H activation) and *para* (σ_p , in this case directing group) sites of the reaction centre. In such cases both σ_m and σ_p should be considered at the same time⁴⁰ which can be done by Jaffé’s analysis (see appendix).⁴¹ Therefore, to test if the poor-correlations in Hammett plots are caused by a substituent having both *meta* and *para* influence, Jaffé’s analysis was carried out using the relative rates shown in **Table 3.12**, the resulting plots are shown in **Figure 3.6** and averages of the obtained ρ_m and ρ_p are given in the **Table 3.13**. Note, the Jaffè modifications are shown in **Table S2**.

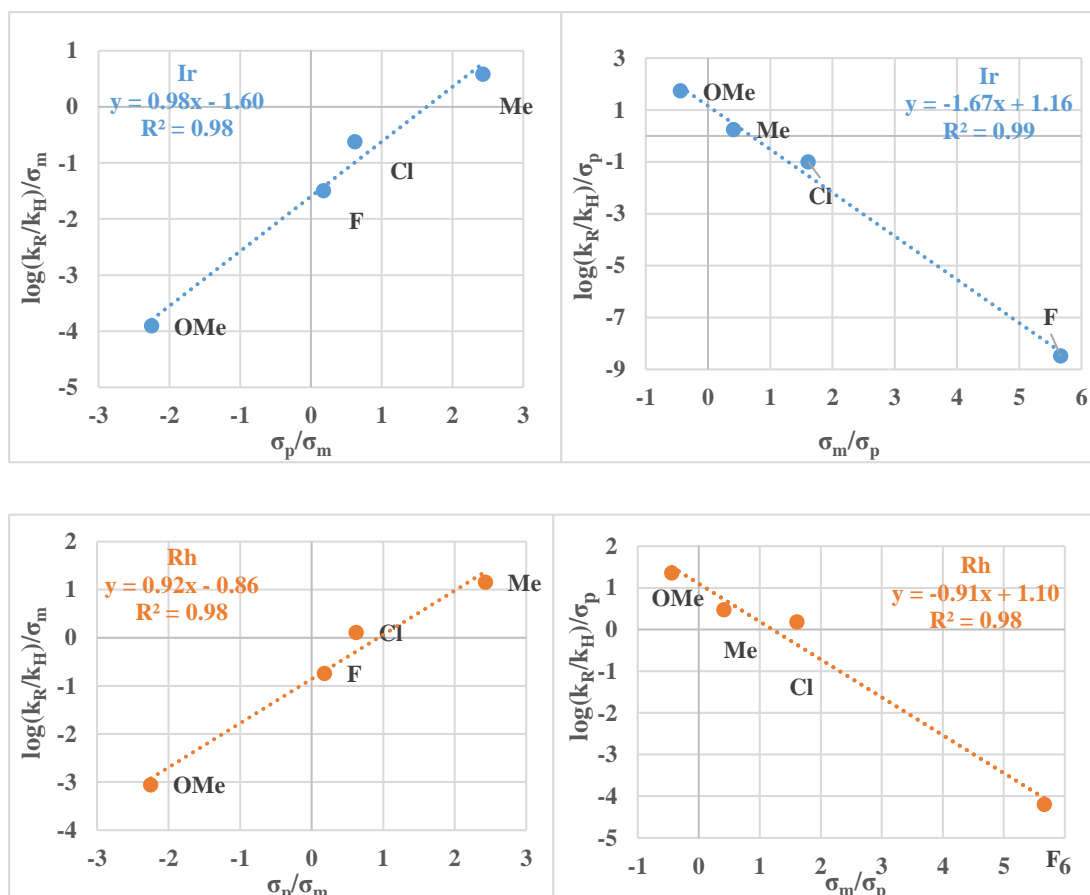


Figure 3.6: Jaffé plots for cyclometallation of **L3.12-R₁,R₂** with Ir (top) and Rh (bottom) in the presence of added Et₄NCl.

Table 3.13: Average ρ_m and ρ_p values from Jaffè plots for cyclometallation of Ir and Rh complexes **3.12a/b-R₁,R₂** in the presence of added Et₄NCl.^a

M	ρ_{m1}	ρ_{m2}	$\rho_{m(\text{average})}$	ρ_{p1}	ρ_{p2}	$\rho_{p(\text{average})}$
Ir	-1.60	-1.67	-1.6	0.98	1.16	1.1
Rh	-0.86	-0.91	-0.9	0.92	1.10	1.0

^a For plots $\log(k_R/k_H)/\sigma_m$ vs. σ_p/σ_m $y = \rho_p x + \rho_m$, for plots $\log(k_R/k_H)/\sigma_p$ vs. σ_m/σ_p $y = \rho_m x + \rho_p$.

The resulting Jaffé plots show good linear correlations for both Ir and Rh ($R^2 = 0.98$ - 0.99). Similar ρ values were obtained for both *meta* (ρ_m) and *para* (ρ_p) effects with both metals indicating a LFER and presence of both *meta* and *para* effect of the substituent. The *meta* effect has a negative slope ($\rho_m = -1.6$ and -0.9 for Ir and Rh respectively) whilst

the *para*-effect has a similar magnitude but a positive slope ($\rho_p = 1.1$ and 1.0 for Ir and Rh respectively). These similar magnitude but opposite sign effects lead to the poor correlations in the simple Hammett plots. The *para* effect has a positive slope indicating improved rate with electron-withdrawing groups, possibly suggesting that removing electron density from the imidazole ring promotes the reaction rate. The *meta* substituent effect is on the actual C–H activation step and the negative slope indicates increased reaction rate with electron-donating substituents. The slopes for Ir and Rh are relatively small, and as discussed in Chapter 2, are smaller than expected for S_EAr (-5 to -9)⁴² but still consistent with AMLA/CMD mechanism taking place via a cationic intermediate. Note, care has to be taken when comparing slopes acquired from Hammett plots with ones obtained from Jaffé plots due to the former assuming there is only a single effect whilst the latter separating *meta* and *para* effects meaning the slopes obtained are not necessarily directly comparable.

The ratios after heating to $75\text{ }^\circ\text{C}$ were used to calculate the relative equilibrium constants of cyclometallation of *meta*-substituted phenyls compared to the unsubstituted phenyl (K_R/K_H) with Ir and Rh from intramolecular competition and the Hammett plot ($\log(K_R/K_H)$ against σ_m) shown in **Figure 3.7** (for the relative equilibrium constants see appendix **Table S3**).

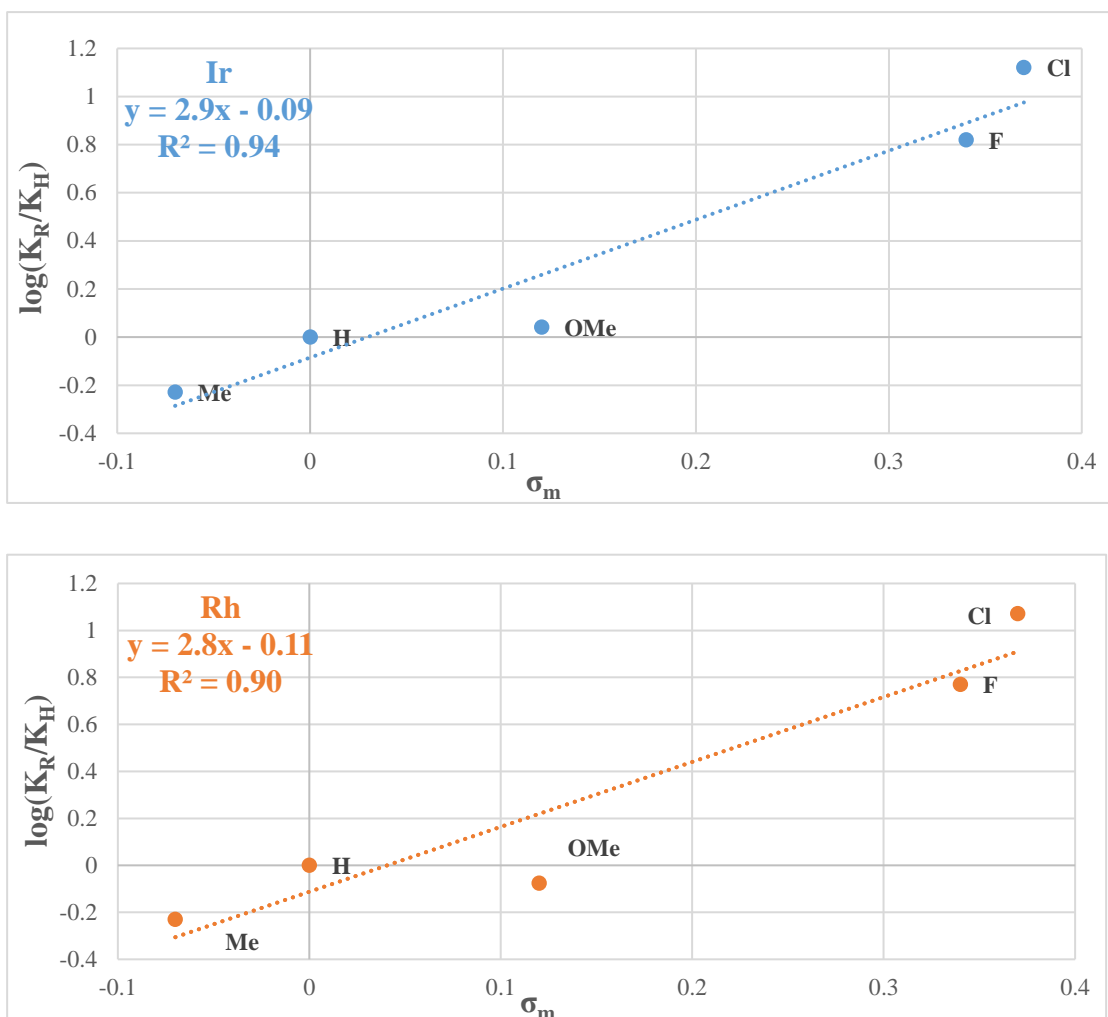


Figure 3.7: Hammett plot of thermodynamic results for intramolecular competition of **L3.12-R₁,R₂** with Ir (top) and Rh (bottom), $\log(K_R/K_H)$ against σ_m .

The resulting Hammett plots show moderate correlation for Ir (0.94) and Rh (0.90) and are very similar to the ones produced from the reactions carried out at 75 °C without added Et₄NCl ($\rho = 2.9$ for Ir and 2.8 for Rh, **Figure 3.7** cf. $\rho = 2.3$ for Ir and 3.0 for Rh, **Figure 3.3**) indicating that under these conditions the reactions have reached equilibrium. The positive slopes indicate preference for electron-withdrawing groups which is consistent with the increased M–C bond strength in these cases.^{2, 43, 44} As observed previously OMe is an outlier for both Ir and Rh, which could be due to σ_m and σ_p for OMe being of opposite sign and there being some *para*-effect on the overall stability. The thermodynamic selectivity observed favours electron-withdrawing groups for both Ir and Rh and is consistent with the selectivity observed for phenylpyridines ($\rho = 0.6$ for Ir, 1.2 for Rh, **Figure 2.3**, Chapter 2) and phenylpyrazoles ($\rho = 1.6$ for Ir, 1.5 for Rh).²

3.2d Preliminary DFT studies with Ir

To get some insight into the observed selectivity patterns DFT calculations for cyclometallations of the imidazolium salts at $[\text{MCl}_2\text{Cp}^*]_2$ have been carried out by the group of Prof. S.A. Macgregor. The C–H activation was computed via an AMLA mechanism. The example is shown in **Figure 3.8** for **L3.12-F,CF₃**. First, acetate opens the dimer $[\text{IrCl}_2\text{Cp}^*]_2$ **A** which produces $[\text{Ir}(\text{OAc})_2\text{Cp}^*]$ **B**. The ligand then binds *via* a non-directed C–H activation giving a neutral complex **C**. Loss of acetic acid gives cationic intermediate **D**. Starting at **D** intramolecular competition between two phenyl rings occurs via AMLA transition states **TS_{D-E}** to give acetic acid adducts **E**. These undergo substitution of acetic acid by chloride via 16-electron species **I_{E-F}** to form the final product **F**. In principle the kinetic product will be determined by the lower **TS_{D-E}**, whilst the thermodynamic product will be determined by the most stable **F**. The computed selectivities based on **TS_{D-E}** and the products **F** as well as experimentally observed selectivities at room temperature (kinetic selectivity, **Table 3.11**) and upon heating (thermodynamic selectivity, **Table 3.11**), are shown in **Table 3.14**.

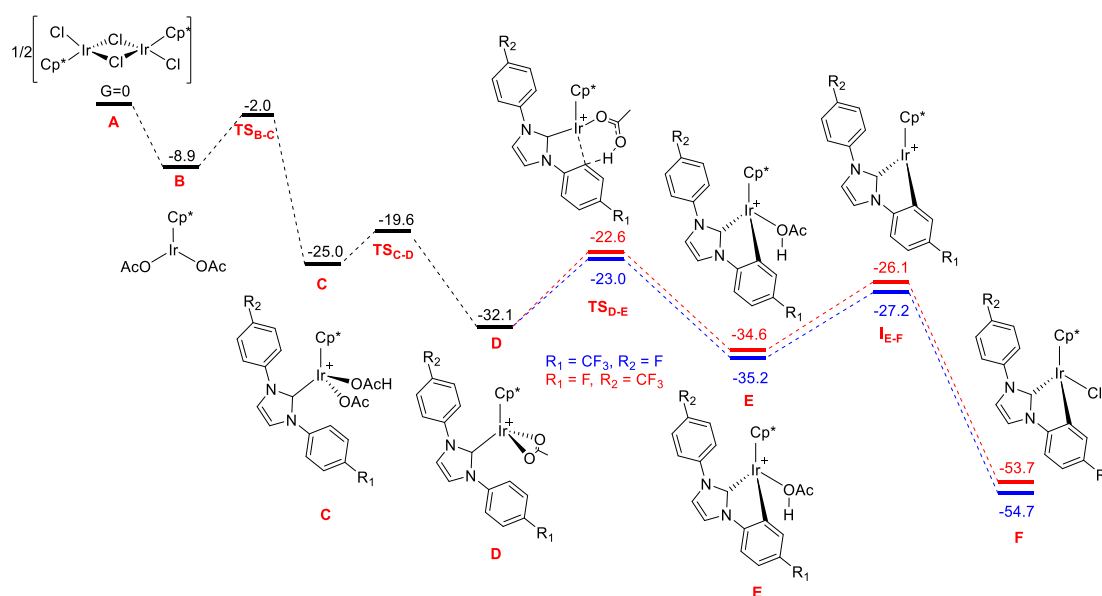


Figure 3.8: The reaction profile for activation of **L3.12-F,CF₃** with $[\text{IrCl}_2\text{Cp}^*]_2$, energies are in kcal mol⁻¹.

The DFT calculations show that the differences in energy between **TS_{D-E}** for the two possible C–H activations are very small (< than 1 kcal mol⁻¹), with similarly small differences between species **E** (< 1.0 kcal mol⁻¹) and between final products **F** (< 2.6 kcal

mol⁻¹)(see appendix, **Table S4**). This is in agreement with relative small ratios observed for the intramolecular competitions both for kinetic and thermodynamic selectivity.

Table 3.14: Computationally calculated favoured regioisomers for cyclometallation of **L3.12-R₁,R₂** with Ir and the experimentally observed selectivity.

Entry	R₁,R₂	TS_{D-E}	F	Kin.^a	Thermod.^b
1	F,CF ₃	CF ₃	CF ₃	CF ₃ ^c	CF ₃
2	Cl,F	Cl ≈F ^c	Cl	Cl	Cl
3	F,OMe	OMe	F	OMe≈F	F
4	F,H	H	F	H	F
5	Me,H	Me ≈H ^d	H ≈Me ^d	Me≈H	H

^a kinetic selectivity based on the ratios measured at rt from direct C–H activation with added chloride,

^b thermodynamic selectivity based on the ratios measured at 75 °C from direct C–H activation -without added chloride,

^c from room temperature results shown in **Table 3.4**,

^d the substituent in bold is the marginally favoured isomer, values are regarded as almost equal if the difference between them is less than 0.3 kcal mol⁻¹

As can be seen in all cases there is quite good agreement between the DFT and the experimental results with the exception for pairs OMe,H and Me,OMe (appendix **table S5**) for which the difference between the two TS/products is less than 0.3 kcal mol⁻¹. For entries 1 and 2 (**Table 3.14**) cyclometallation on the same ring had a lower energy transition state **TS_{D-E}**, intermediate **E** and final product **F** indicating that in these cases the kinetic and thermodynamic selectivity is the same. For entries 3-5 there is a switch in selectivity computed for **TS_{D-E}** which shows electron-donating groups being favoured kinetically and those for **F**, which favour electron-withdrawing groups thermodynamically. An example of this is shown for (F,OMe) in **Figure 3.9**.

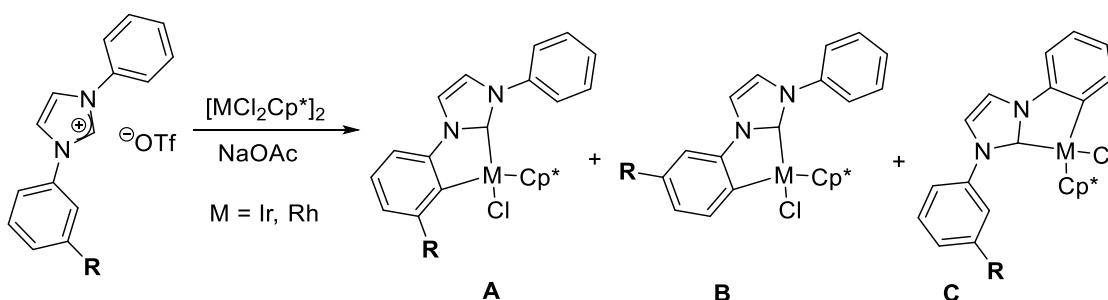
I is higher than **TS_{D-E}** the reaction may reverse at that point and shuttle between **D** and the **TS_{E-I}** for ligand exchange (see **Figure 3.9**). D-exchange could also occur in **E** without going all the way to **F**.

In conclusion, isolating a simple NHC bound complex with no cyclometallation of a phenyl proved impossible. As a result it was difficult to find conditions that provided exclusively kinetic selectivity particularly with Rh, and even with the results obtained at room temperature it is not entirely clear if the selectivity observed is purely kinetic. The Hammett plot of the results from direct C–H activation reactions with Et₄NCl showed no correlation for either Ir or Rh. Jaffé analysis suggested that two factors may contribute to the kinetic selectivity; a *meta* electronic effect on the C–H activation step that is in favour of electron-donating groups and a *para*-effect that favours electron-withdrawing groups that affects the directing group. However, the reason for a *para*-effect is not clear and may suggest that good fits in Jaffé plots are just fortuitous and the problem is that the data reflects some thermodynamic contribution. The thermodynamic selectivity was in favour of electron-withdrawing groups which reflects the increased M–C bond strength for these complexes.² In agreement with the experimental results, DFT calculations showed good agreement with experiment in both kinetic and thermodynamic selectivity. However, distinguishing which transition state is product determining and is actually influencing kinetic selectivity was difficult with the C–H activation TS and acetic acid by chloride exchange barriers being similar in energy. Furthermore, in some cases there may be some equilibration between cyclometallation at the two differently substituted rings leading to a lower selectivity (isomer ratios) than might be expected on the basis of the relative TS energies for just the C–H activation step. In these cases the actual meaning of “kinetic” selectivity is less clear since both C–H activation and acetic acid loss affect the overall rate.

Having investigated the electronic effects on cyclometallation with imidazolium salts it was then moved onto investigation of steric effects. This was done by preparing mono-phenylimidazolium salts containing *meta*-substituents as described below.

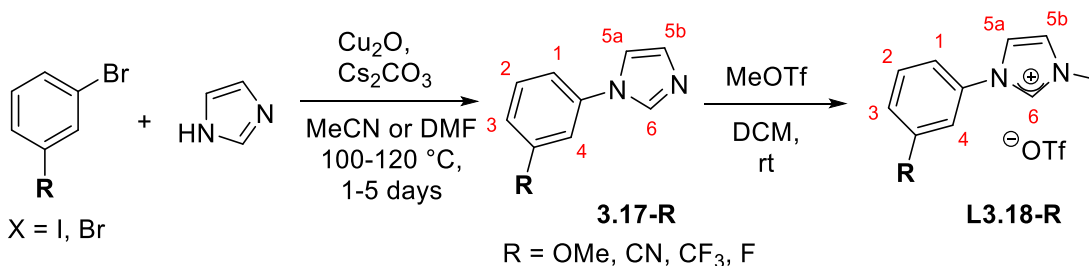
3.2e Synthesis of *meta*-substituted phenylimidazolium salts

It was anticipated that using unsymmetrical *meta*-substituted diaryl imidazolium salts to investigate steric effects could lead to the formation of three potential regioisomers (**Scheme 3.24**). The characterisation of an individual isomer would likely to be difficult due to large overlap in the ^1H and ^{13}C NMR spectra. Therefore, it was decided to use *N*-phenyl,*N'*-methyl imidazolium salts **L3.18-R** ($\text{R} = \text{OMe}, \text{F}, \text{CF}_3, \text{CN},$) as these can only give two regioisomers.



Scheme 3.24: Possible cyclometallation products of *meta*-substituted unsymmetrical diaryl imidazolium salts with Ir and Rh.

Meta-substituted phenylimidazoles **3.17-R** are known compounds and were prepared by Cu-catalysed arylation of imidazole with arylhalides (**Scheme 3.25**) by the same method as the *para*-substituted phenylimidazoles **3.11-R₂**; and the data agree with the literature.⁴⁶⁻⁴⁹ The salts **L3.18-R** ($\text{R} = \text{OMe}, \text{CN}, \text{CF}_3, \text{F}$) were then prepared by methylation of **3.17-R** with MeOTf (**Scheme 3.25**). The salts **L3.18-R** were obtained in high yields (72-98%) after precipitation from DCM with Et₂O. **L3.18-OMe**, **L3.18-F** and **L3.18-CN** are new compounds, whilst **L3.18-CF₃** is known as the iodide salt.⁵⁰



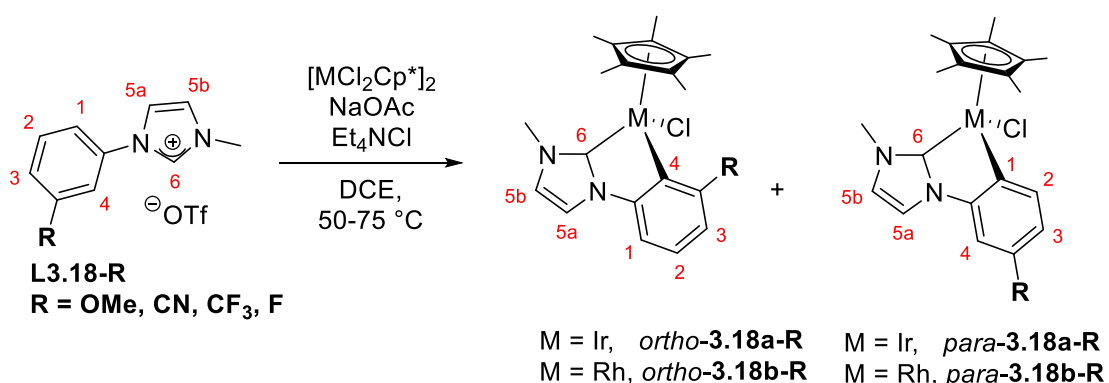
Scheme 3.25: Preparation and labelling of *meta*-substituted phenylimidazolium salts.

The salts **L3.18-R** ($\text{R} = \text{OMe}, \text{CN}, \text{CF}_3, \text{F}$) all show a singlet for the Me group at about δ 4.0 in the ^1H NMR spectra confirming methylation. The most downfield signal is the

imidazolium proton H⁶ at about δ 9.4-10.0 which is 1.5 ppm downfield from the precursor phenylimidazole **3.17-R** (R = OMe, CN, CF₃, F) due to formation of cationic imidazolium salts. In each case the phenyl group shows four inequivalent protons. The ¹³C NMR spectra show the expected number of signals for all quaternary and CH carbons with imidazolium C⁶ at δ ca. 137. The HRMS (ESI) show ions for the imidazolium cations in each case.

3.2f Cyclometallations of *meta*-substituted phenylimidazolium salts with Ir and Rh

The reactions of **L3.18-OMe** with [MCl₂Cp*]₂ (M = Ir, Rh) were first attempted in the presence of NaOAc, however, after heating at 75 °C overnight the ¹H NMR spectra of the reaction mixtures showed only traces of possible product formation for both Ir and Rh with multiple unidentified species in both the aromatic and Cp* regions suggesting decomposition. Therefore, the reactions were repeated with added Et₄NCl, which worked well but still required heating to reach high conversions. The reactions were first heated to 50 °C for 1 hour and then at 75 °C for 1-6 hours (**Scheme 3.26**), then the reactions were worked up to isolate the products in moderate to good yields (50-90%). All of the prepared complexes **3.18a/b-R** (R = OMe, CN, CF₃, F) are new and were fully characterised. Subsequently, reactions were repeated in DCM:MeOH and monitored at room temperature (ca. 20% conversion) and upon heating (50 °C overnight) to further investigated if ratios change and so whether selectivity is kinetic or thermodynamic (see later).



Scheme 3.26: Reactions of **L3.18-R** with [MCl₂Cp*]₂ (M = Ir, Rh) and labelling scheme.

The reaction of **L3.18-OMe** with [IrCl₂Cp*]₂ and NaOAc after 6 hours at 70 °C gave a mixture of two products. The ¹H NMR spectrum of the mixture, shows singlets at δ 1.79,

3.80 and 3.98 for the major product and singlets at δ 1.85, 3.82 and 3.97 for the minor product corresponding to Cp*, OMe and N-Me groups respectively. For the major product three phenyl protons are present as a doublet of doublets at δ 6.65, a narrow doublet at δ 6.76 and a doublet at δ 7.60. This pattern is typical of the *para*-isomer (the same as for *para*-**2.3a/b-R** R = OMe, CF₃, discussed in Chapter 2). The doublet at δ 7.60 has an NOE with the Cp* and so is assigned to H² that at δ 6.76 has an NOE with OMe and H^{5a} and so is assigned to H⁴ leaving the signal at δ 6.65 as H³. The minor product shows three aromatic protons two doublets of doublets at δ 6.54 and 6.83 and a triplet at 6.93 and this pattern agrees with the *ortho*-isomer. The signal at δ 6.54 has an NOE with the OMe group and is assigned to H³, the triplet at δ 6.93 based on multiplicity is assigned to H², leaving the signal at δ 6.83 as H¹. This is consistent with the minor product being the *ortho*-**3.18a-OMe**. The imidazole protons overlap for the two isomers, giving two mutually coupled narrow doublets at δ 7.30 and 6.95 respectively and the latter shows an NOE with Me group in both isomers and so assigned to H^{5b} with the signal at δ 7.30 assigned to H^{5a}.

The reaction of **L3.18-OMe** with [RhCl₂Cp*]₂ after 6 hours at 70 °C also gave a mixture of isomers. The ¹H NMR spectrum of the mixture of isomers *ortho*-**3.18b-OMe** and *para*-**3.18b-OMe** is very similar to the Ir analogues described above with all the signals within 0.2 ppm and with the *para*-isomer also being the major species. The ¹³C NMR spectra for the major isomers *para*-**3.18a-OMe** and *para*-**3.18b-OMe** show the expected number of signals, however, signals of the minor isomers were too weak to be assigned fully. The phenyl cyclometallated carbons C¹ are at δ 146.9 (singlet) and 146.6 (doublet, J_{C-Rh} = 35.7 Hz) for *para*-**3.18a-OMe** and *para*-**3.18b-OMe** respectively. The C⁶ are a singlet at δ 166.6 for *para*-**3.18a-OMe** and as doublet at δ 184.2 (J_{C-Rh} = 55.5 Hz) for *para*-**3.18b-OMe** and are significantly downfield from the C⁶ for **L3.18-OMe** at δ 136.6 which is consistent with formation of an Ir/Rh-NHC.¹⁶ The HRMS(ESI) spectra shows ions at m/z 515.1675 due to [M-Cl]⁺ for **3.18a-OMe** mixture and also ions at m/z 425.1100 due to [M-Cl]⁺ for the **3.18b-OMe** mixture.

The reactions of **L3.18-CN** with Ir and Rh after heating at 70 °C for 1 hour resulted in the formation of a mixture of two isomers with both metals. The ¹H NMR spectra for the Ir and Rh complexes showed the major isomers were *para*-**3.18a-CN** and *para*-**3.18b-CN** respectively and the signals for the minor isomers are consistent with *ortho*-**3.18a-**

CN and *ortho*-**3.18b-CN** respectively. The HRMS(ESI) spectra shows ions at m/z 510.1523 due to $[M-Cl]^+$ for the mixture of **3.18a-CN** and ions at m/z 420.0947 due to $[M-Cl]^+$ for the mixture of **3.18b-CN**.

The reactions of **L3.18-CF₃** resulted in isolation of single products whose ¹H NMR spectra agree with *para*-**3.18a-CF₃** and *para*-**3.18b-CF₃** respectively. The HRMS(ESI) spectra shows ions at m/z 553.1445 due to $[M-Cl]^+$ for **3.18a-CF₃** and ions at m/z 463.0862 due to $[M-Cl]^+$ for the mixture of **3.18b-CN**.

For **L3.18-F** the reaction with $[RhCl_2Cp^*]_2$ gave mainly one isomer, whilst reaction of **L3.18-F** with $[IrCl_2Cp^*]_2$ led to formation of mixture of isomers. The ¹H-¹⁹F HMBC spectrum for the major isomer for Ir shows a cross-peak between the F and Cp* suggesting the *ortho*-isomer. The ¹H NMR data (see Chapter 6 for details) agree with the major isomer being *ortho*-**3.18a-F** rather than *para*. The minor isomer is then the *para*-isomer which shows a doublets of doublets at δ 7.64 for H² which shows an NOE with the Cp* confirming the assignment. The ¹H NMR spectrum of the major Rh isomer shows the same pattern as the Ir analogue with signals within 0.1 ppm of the respective ones in *ortho*-**3.18a-F**. The ¹⁹F NMR spectra show signals at δ -94.9 and -122.9 for *ortho*-**3.18a-F** and *para*-**3.18a-F** respectively and at δ -93.9 for *ortho*-**3.18b-F**. The HRMS(ESI) spectra shows ion at m/z 551.1790 due to $[M-Cl]^+$ for **3.18a-F** mixture and ions at m/z at 413.0902 due to $[M-Cl]^+$ for **3.18b-F**.

As mentioned above, the reactions were repeated to establish the initial and final ratios of isomers and the data are presented in **Table 3.15**. As the preparative reactions in DCE required heating to reach good conversions, the reactions to establish ratios were repeated in DCM:MeOH with the anticipation that this may allow for reactions to take place at room temperature.

Table 3.15: Regioselectivity of cyclometallation of **L3.18-R** with Ir and Rh in DCM:MeOH.

Entry	R	Ir		Rh	
		r.t., <i>o:p</i>	50 °C, <i>o:p</i>	r.t., <i>o:p</i>	50 °C, <i>o:p</i>
1	OMe	1:1.5 ^a	1:3.0 ^b	1:3.0 ^a	1:3.0 ^b
2	CN	1:1.3	1:2.2	1.2:1	1:2.0
3	CF ₃	1:3 ⁵¹	1:>20 ⁵¹	1:6 ⁵¹	1:>40 ⁵¹
4	F	2.2:1	2.2:1	6.0:1	10:1

^a in DCE, at 50 °C, 1 hour,

^b in DCE, 70 °C, 6 hours,

Most of the initial ratios changed upon heating (with the exceptions of the reactions of **L3.18-OMe** with Rh and of **L3.18-F** with Ir) suggesting that under these conditions the reactions are reversible. The reaction of **L3.18-OMe** with Rh did not show a change in ratio change whilst the equivalent reaction with Ir did. Since these cyclometallation reactions with Rh tend to be more reversible than with Ir it suggests that with **L3.18-OMe** the initial ratio with has already equilibrated and corresponds to the thermodynamic ratio.

For the reaction of **L3.18-R** (R = CF₃, CN, OMe) with both Ir and Rh the same trend was observed – a mixture of the *ortho* and *para*-isomer initially with increasing fraction of the *para*-isomer overtime (entries 1-3). This indicates that thermodynamically the *para*-isomer is favoured, whilst kinetically there is no clear preference for either *para* or *ortho*-isomers (except for R = CF₃). For the reaction of **L3.18-F** with Rh the increase in the *ortho*-isomer upon heating indicates that it is favoured thermodynamically and possibly kinetically (ratio at rt *o:p* 6:1), whilst no change is observed for Ir so it is not clear if the *ortho*-isomer is favoured kinetically or thermodynamically or both. Interestingly for **L3.18-CN** reaction with Rh (entry 2) at room temperature a minor preference for the *ortho*-isomer was observed indicating that this isomer is slightly favoured kinetically. This selectivity could indicate that “ortho effect” observed for reactions with **L3.18-F** with Ir and Rh (entry 4) may not be exclusive to the F substituent. The preference for the *ortho*-isomer over the *para* with F substituent has been observed previously for phenylpyridines (Chapter 2), phenylimines (Chapter 2 **Table 2.1**),⁵² phenylpyrazoles;^{2 43, 44, 53} Note, the reactions of **L3.18-OMe** with Ir and Rh were attempted in DCM:MeOH at room temperature and heating, however, after several hours additional species (that

had signals equivalent to the products but slightly shifted) started to form and due to the overlap between products and new species it was not possible to obtain reliable ratios.

Overall, the steric bulk mainly controls the regioselectivities in agreement with the results observed with phenylimines (Jones et al.,⁵² Chapter 2, **Table 2.1**), phenylpyridines (Chapter 2, **Table 2.4**) and phenylpyrazoles.² However, for the phenylimines or phenylpyridines the *ortho*-isomer was not observed for the reactions when R = CF₃, whilst it was present in the substantial quantities for the reactions of **L3.16-CF₃** suggesting that there is less steric bulk at the metal centre at **3.16a/b-R** compared to the phenylpyridines (Chapter 2), phenylimines,⁵² and phenylpyrazoles.²

3.2g Conclusions

Unsymmetrically substituted diphenylimidazolium salts were prepared and used in intramolecular competition reactions of acetate-assisted cyclometallation with [MCl₂Cp*]₂ (M = Ir, Rh). The initial conditions required heating to 75 °C in most cases and led directly to cyclometallated complexes **3.12a/b-R₁,R₂** and no intermediate non-cyclometallated complexes **int-3.12a/b-R₁,R₂** were observed. Attempts to prepare non-cyclometallated Ir/Rh NHCs via transmetalation from Ag and Cu were unsuccessful with only cyclometallated complexes **3.12a/b-R₁,R₂** isolated though these reactions did proceed at room temperature. However, the transmetalation reactions particularly with Ag were not clean giving some unidentified species. Overall the results indicate that the non-directed C–H activation of imidazolium salts is the rds (which is in agreement with the observations by Choudhury *et al.*)¹⁹ whilst the following NHC directed C–H activation of phenyl is much easier and is fast under the reaction conditions.

Addition of a soluble chloride source allowed the direct C–H activation reactions to be repeated at room temperature to investigate kinetic selectivity. These reactions were used to measure the relative rates of cyclometallation of different diphenylimidazolium salts **L3.12-R₁,R₂** and the data were compared using a Hammett plot. The Hammett plot showed very poor correlation between the σ_m value of the substituent and the relative rate of cyclometallation for either Ir or Rh. A Jaffé analysis produced linear plots and demonstrated that poor correlation in Hammett plots may be due to substituents exerting not only *meta* effects on the C–H activation step ($\rho_m = -1.6$ and -0.9 for Ir and Rh respectively) but also *para* effects on the directing group ($\rho_p = 1.1$ and 1.0 for Ir and Rh

respectively). These effects have similar magnitude slopes but of opposite signs. The *meta* effect gives increased reaction rate with electron-donating substituents, whilst the *para* effect shows improved reaction rate with electron-withdrawing groups. However, understanding the reason for this selectivity is not clear and it is possible that the good fits in Jaffé plots are just fortuitous. It is also possible that the data is still not reflective of exclusively kinetic selectivity especially with Rh. The resulting Hammett plots of the thermodynamic selectivity showed linear plots with positive slopes ($\rho = 2.9$ for Ir and 2.8 for Rh). The thermodynamic selectivity observed favours electron-withdrawing groups for both Ir and Rh and is consistent with the selectivity observed for phenylpyridines (Chapter 2) and phenylpyrazoles² and is consistent with the increased M–C bond strength in these cases.^{2, 43, 44}

Computational studies (carried out in Heriot-Watt University by the group of Prof. S.A. Macgregor) for Ir with **L3.12-R₁,R₂** showed a good agreement with the experimental results. The thermodynamic selectivity was in favour of electron-withdrawing groups. Determining kinetic selectivity proved complicated, because the transition state for C–H activation of phenyl had very similar barrier to the lowest possible barrier for acetic acid substitution by chloride making this step kinetically relevant. Therefore, it is likely that both steps are contributing to the selectivity observed at room temperature. Furthermore, the reverse barrier for C–H activation of phenyl before the formation of final chloride species is comparable with the barrier for the forward reaction, hence reactions could be equilibrating before acetic acid by chloride exchange and so before formation of the final product. This would lead to a lower selectivity than might be expected on the basis of the relative TS energies for just the C–H activation step. In such cases the actual meaning of “kinetic” selectivity is less clear since both C–H activation and acetic acid loss affect the overall rate.

The *meta*-substituted phenylimidazolium salts **L3.18-R** (R = OMe, CN, CF₃, F) were prepared and used to study steric effects on the cyclometallation. The *para*-isomers were favoured thermodynamically over the *ortho* for R = OMe, CN, CF₃, with both metals. Kinetically, for the smaller R = OMe, CN groups there was a slight preference for the *para*-isomers with Ir and Rh (with exception of R = OMe for Rh) and a significant preference for the *para*-isomers for the bulky R = CF₃ with both metals. The reaction of **L3.18-F** with Rh showed preference for the *ortho*-isomer both kinetically and

thermodynamically, for Ir the *ortho*-isomer was also favoured, but no change in ratio was observed for Ir so it is not clear if the *ortho*-isomer is favoured kinetically or thermodynamically or both. Overall, the regioselectivity was not as pronounced as for the phenylpyridines (Chapter 2), phenylimines,⁵² and phenylpyrazoles² suggesting reduced steric bulk at the metal centre for the complexes **3.18a/b-R**.

3.3 Bibliography

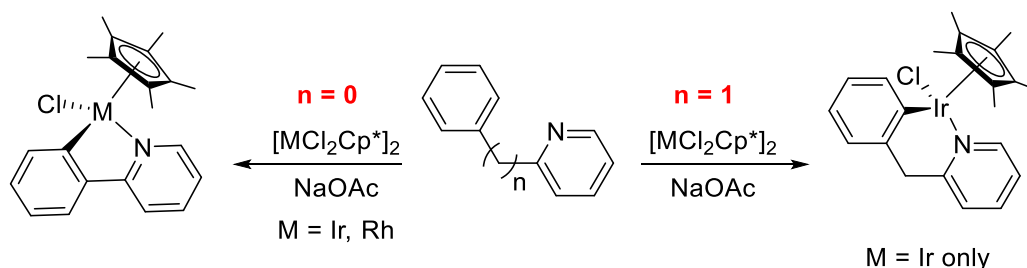
1. L. E. E. Broeckx, S. Güven, F. J. L. Heutz, M. Lutz, D. Vogt and C. Müller, *Chem. Eur. J.*, 2013, **19**, 13087-13098.
2. R. A. Alharis, C. L. McMullin, D. L. Davies, K. Singh and S. A. Macgregor, *J. Am. Chem. Soc.*, 2019, **141**, 8896-8906.
3. Y. Oh, S. H. Han, N. K. Mishra, U. De, J. Lee, H. S. Kim, Y. H. Jung and I. S. Kim, *Eur. J. Org. Chem.*, 2017, **2017**, 6265-6273.
4. D. M. Flanigan, F. Romanov-Michailidis, N. A. White and T. Rovis, *Chem. Rev.*, 2015, **115**, 9307-9387.
5. V. Nesterov, D. Reiter, P. Bag, P. Frisch, R. Holzner, A. Porzelt and S. Inoue, *Chem. Rev.*, 2018, **118**, 9678-9842.
6. E. Peris, *Chem. Rev.*, 2018, **118**, 9988-10031.
7. M. N. Hopkinson, C. Richter, M. Schedler and F. Glorius, *Nature*, 2014, **510**, 485.
8. D. J. Nelson, *Eur. J. Inorg. Chem.*, 2015, **2015**, 2012-2027.
9. J. C. Garrison and W. J. Youngs, *Chem. Rev.*, 2005, **105**, 3978-4008.
10. I. J. B. Lin and C. S. Vasam, *Coord. Chem. Rev.*, 2007, **251**, 642-670.
11. S. Díez-González, N. Marion and S. P. Nolan, *Chem. Rev.*, 2009, **109**, 3612-3676.
12. G. C. Fortman and S. P. Nolan, *Chem. Soc. Rev.*, 2011, **40**, 5151-5169.
13. N. Marion and S. P. Nolan, *Acc. Chem. Res.*, 2008, **41**, 1440-1449.
14. R. K. M. Khan, S. Torker and A. H. Hoveyda, *J. Am. Chem. Soc.*, 2013, **135**, 10258-10261.
15. O. M. Ogba, N. C. Warner, D. J. O'Leary and R. H. Grubbs, *Chem. Soc. Rev.*, 2018, **47**, 4510-4544.
16. R. Corberán, M. Sanaú and E. Peris, *J. Am. Chem. Soc.*, 2006, **128**, 3974-3979.
17. S. Ibanez, M. Poyatos and E. Peris, *Dalton Trans.*, 2016, **45**, 14154-14159.
18. S. Semwal, I. Mukkatt, R. Thenarukandiyil and J. Choudhury, *Chem. Eur. J.*, 2017, **23**, 13051-13057.
19. R. Thenarukandiyil, S. K. Gupta and J. Choudhury, *ACS Catal.*, 2016, **6**, 5132-5137.
20. S. Semwal, D. Ghorai and J. Choudhury, *Organometallics*, 2014, **33**, 7118-7124.
21. L. Benhamou, E. Chardon, G. Lavigne, S. Bellemin-Laponnaz and V. César, *Chem. Rev.*, 2011, **111**, 2705-2733.
22. L. Hintermann, *Beilstein Journal of Organic Chemistry*, 2007, **3**, 22.
23. T. Lv, Z. Wang, J. You, J. Lan and G. Gao, *J. Org. Chem.*, 2013, **78**, 5723-5730.
24. S. Li, F. Yang, T. Lv, J. Lan, G. Gao and J. You, *Chem. Commun.*, 2014, **50**, 3941-3943.
25. A. Fürstner, M. Alcarazo, V. César and C. W. Lehmann, *Chem. Commun.*, 2006, 2176-2178.
26. M. Bielawski, M. Zhu and B. Olofsson, *Adv. Synth. Catal.*, 2007, **349**, 2610-2618.
27. M. Zhu, N. Jalalian and B. Olofsson, *Synlett*, 2008, **2008**, 592-596.
28. X. Wang, M. Wang and J. Xie, *Synth. Commun.*, 2017, **47**, 1797-1803.
29. H.-C. Ma and X.-Z. Jiang, *J. Org. Chem.*, 2007, **72**, 8943-8946.
30. D. L. Davies, O. Al-Duaij, J. Fawcett, M. Giardiello, S. T. Hilton and D. R. Russell, *Dalton Trans.*, 2003, 4132-4138.
31. R. Corberán, M. Sanaú and E. Peris, *Organometallics*, 2006, **25**, 4002-4008.

32. Y. Boutadla, D. L. Davies, R. C. Jones and K. Singh, *Chem. Eur. J.*, 2011, **17**, 3438-3448.
33. J. C. Y. Lin, R. T. W. Huang, C. S. Lee, A. Bhattacharyya, W. S. Hwang and I. J. B. Lin, *Chem. Rev.*, 2009, **109**, 3561-3598.
34. K. J. T. Carr, D. L. Davies, S. A. Macgregor, K. Singh and B. Villa-Marcos, *Chem. Sci.*, 2014, **5**, 2340-2346.
35. A. J. Arduengo, H. V. R. Dias, J. C. Calabrese and F. Davidson, *Organometallics*, 1993, **12**, 3405-3409.
36. A. C. Marr, P. J. Morgan, G. C. Saunders and H. P. Thomas, *Dalton Trans.*, 2019, **48**, 1947-1949.
37. A. C. Marr, G. C. Saunders, H. P. Thomas and Y.-M. Wang, *Inorg. Chim. Acta*, 2019, **486**, 1-7.
38. O. Santoro, A. Collado, A. M. Z. Slawin, S. P. Nolan and C. S. J. Cazin, *Chem. Commun.*, 2013, **49**, 10483-10485.
39. K. H. Jensen, J. D. Webb and M. S. Sigman, *J. Am. Chem. Soc.*, 2010, **132**, 17471-17482.
40. M. Simonetti, R. Kuniyil, S. A. Macgregor and I. Larrosa, *J. Am. Chem. Soc.*, 2018, **140**, 11836-11847.
41. H. H. Jaffé, *J. Am. Chem. Soc.*, 1954, **76**, 4261-4264.
42. J. Clayden, N. Greeves and S. Warren, *Organic Chemistry*, 2nd edn., Oxford: Oxford University Press, Oxford, 2012.
43. E. Clot, M. Besora, F. Maseras, C. Mégret, O. Eisenstein, B. Oelckers and R. N. Perutz, *Chem. Commun.*, 2003, 490-491.
44. E. Clot, C. Mégret, O. Eisenstein and R. N. Perutz, *J. Am. Chem. Soc.*, 2009, **131**, 7817-7827.
45. R. A. Alharis, C. L. McMullin, D. L. Davies, K. Singh and S. A. Macgregor, *Faraday Discuss.*, 2019, DOI: 10.1039/C9FD00063A.
46. X. Ge, X. Chen, C. Qian and S. Zhou, *RSC Advances*, 2016, **6**, 58898-58906.
47. D. P. Phillips, X.-F. Zhu, T. L. Lau, X. He, K. Yang and H. Liu, *Tetrahedron Lett.*, 2009, **50**, 7293-7296.
48. Q. Zhang, J. Luo and Y. Wei, *Synth. Commun.*, 2012, **42**, 114-121.
49. A. V. Nakhate and G. D. Yadav, *ChemistrySelect*, 2017, **2**, 2395-2405.
50. T.-Y. Li, X. Liang, L. Zhou, C. Wu, S. Zhang, X. Liu, G.-Z. Lu, L.-S. Xue, Y.-X. Zheng and J.-L. Zuo, *Inorg. Chem.*, 2015, **54**, 161-173.
51. It is not possible conclusively rule out that minor species are not just carbene bound, but this has not been observed previously
52. L. Li, W. W. Brennessel and W. D. Jones, *Organometallics*, 2009, **28**, 3492-3500.
53. A. D. Selmecky, W. D. Jones, M. G. Partridge and R. N. Perutz, *Organometallics*, 1994, **13**, 522-532.

Chapter Four

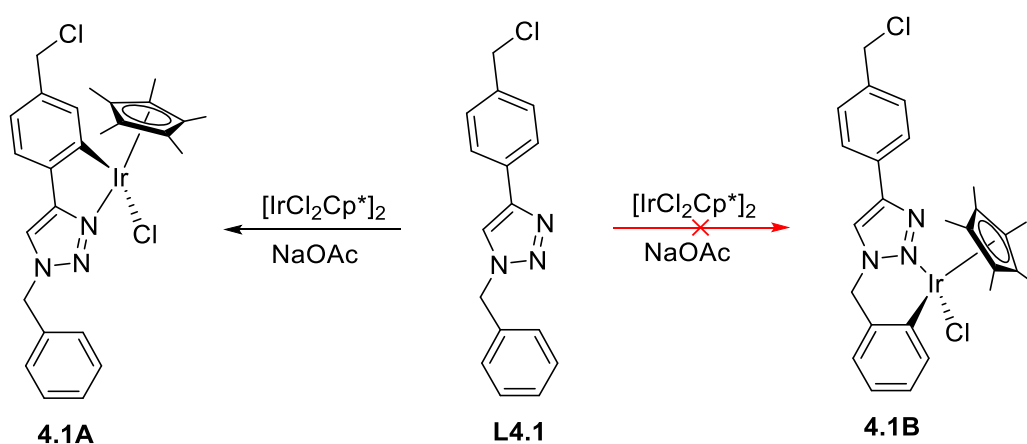
4.1. Introduction

As shown in Chapter 3, since the NHC-directed C–H activation is much easier than the non-directed C–H activation of the imidazolium salt, isolation of the proposed non-cyclometallated M–NHC complexes was not successful. It is known that cyclometallations to form six-membered rings are more difficult than formation of five-membered rings. For example, the Davies group reported that cyclometallation of 2-phenylpyridine with $[\text{IrCl}_2\text{Cp}^*]_2$ is complete within 4 hours,¹ whilst the cyclometallation of 2-benzylpyridine with $[\text{IrCl}_2\text{Cp}^*]_2$ takes 20 hours (**Scheme 4.1**).² In addition, 2-phenylpyridines react with both Ir and Rh,¹ whilst 2-benzylpyridine was only shown to give a complex with Ir and not Rh.³



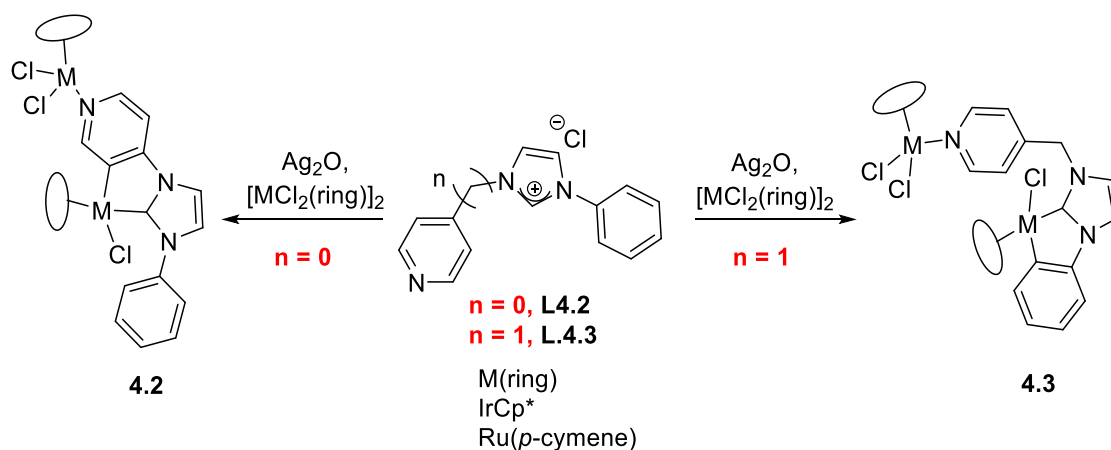
Scheme 4.1: Reaction of phenylpyridine¹ and benzylpyridine³ with $[\text{MCl}_2\text{Cp}^*]_2$ (M = Ir, Rh).

Davies *et al.* reported that reaction of **L4.1** with $[\text{IrCl}_2\text{Cp}^*]_2$ formed exclusively five-membered iridacycle **4.1A** in preference to six-membered iridacycle **4.1B** (**Scheme 4.2**).²



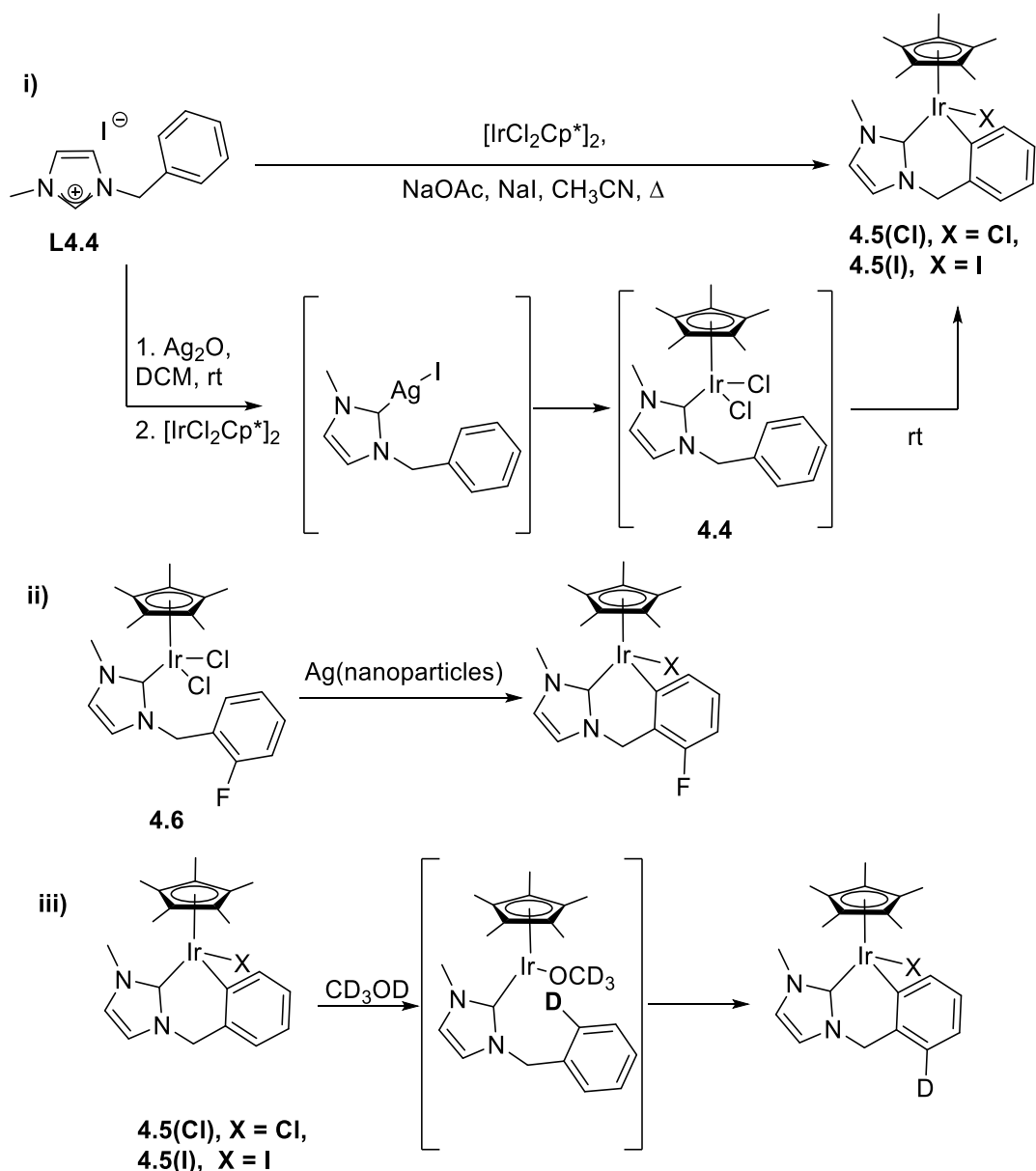
Scheme 4.2: Reaction of triazole **L4.1** with $[\text{IrCl}_2\text{Cp}^*]_2$.²

Choudhury *et al.*⁴ reported an intramolecular competition between phenyl and pyridine rings using an NHC as a directing group with $[MCl_2(\text{ring})]_2$ ($M = \text{Ir}$, ring = Cp*, $M = \text{Ru}$, ring = *p*-cymene) (**Scheme 4.3**, **L4.2**) and the metallacycle formed exclusively on the pyridine (i.e. more electron deficient ring) to give **4.2**. However, when **L4.3** ($n = 1$) containing CH₂Py was used instead, the cyclometallation was observed exclusively on the phenyl ring giving five-membered ring product **4.3**, showing that in this case preference for formation of a five- over six-membered metallacycle is stronger than the electronic selectivity.



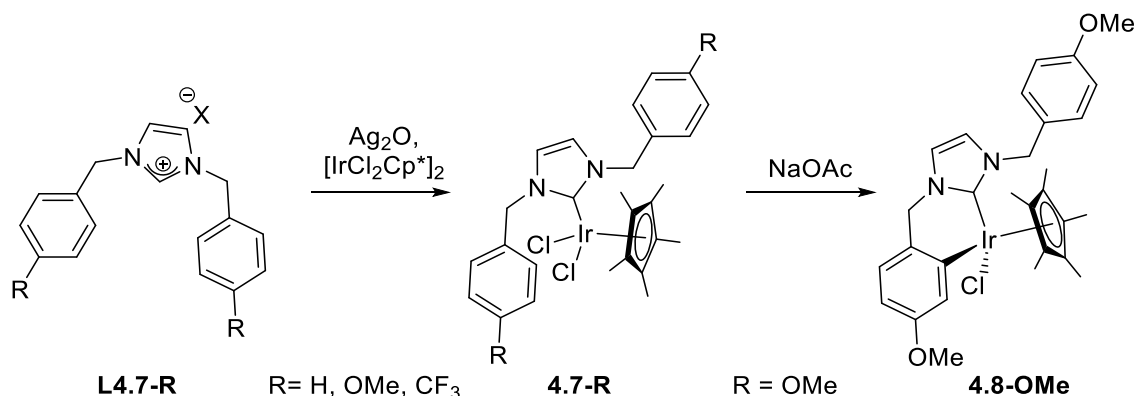
Scheme 4.3: Selectivities between pyridine and phenyl ring and five- and six-membered metallocycle formation.⁴

Although the formation of six-membered metallocycles is less favourable than five-membered ones, examples of cyclometallation to form six-membered rings with NHCs as directing groups have been reported (**Scheme 4.4 i**).^{5, 6} The cyclometallated complex **4.5(I)** was obtained from direct C–H activation reactions in the presence of NaOAc and NaI. Using transmetalation with the *in situ* prepared Ag–NHC for **L4.4** an intermediate non-cyclometallated Ir–NHC complex **4.4** was observed, however, it cyclometallated in solution within 5 hours to form **4.5(Cl)**. This cyclometallation appears not to require any additional reagents, however, Ag nanoparticles present in the solution have recently been reported to promote *ortho* C–H activation of Ir–NHC complex **4.6** (**Scheme 4.4 ii**).⁷ When the isolated complexes **4.5(Cl)** or **4.5(I)** were refluxed in CD₃OD quantitative D incorporation was observed after 24 hours indicating that this cyclometallation is reversible (**Scheme 4.4 iii**).



Scheme 4.4: i) Preparation of cyclometallated Ir-NHC complexes **4.5**,^{5,6} ii) *ortho* C–H activation of Ir-benzyl-NHC **4.6** in the presence of Ag nanoparticles,⁷ and iii) D incorporation with **4.5(Cl)** and **4.5(I)**.^{5,6}

During the course of this work, Xiao *et al.* reported the synthesis of stable Ir-NHC complexes **4.7-R** (R = H, OMe, CF₃) from the reaction of symmetrical dibenzylimidazolium salts **L4.7-R** with Ag₂O and [IrCl₂Cp*]₂ (**Scheme 4.5**). Complex **4.7-OMe** was shown to require addition of NaOAc to form six-membered iridacycle **4.8-OMe**.



Scheme 4.5: The reactions of symmetrical dibenzylimidazolium salts **L4.7-R** with $[\text{IrCl}_2\text{Cp}^*]_2$ to form **4.7-R**, cyclometallation of **4.7-OMe** in the presence of NaOAc.⁸

In conclusion, the formation of six-membered metallacycles is possible but is more difficult than formation of five-membered metallacycles. Therefore, benzyylimidazolium salts that should lead to the six-membered metallacycles may be ideal substrates for this study, particularly since, unlike phenyl imidazolium salts, the isolation of non-cyclometallated intermediate M-NHC complexes (M = Ir, Rh) should be possible. This should allow the electronic and steric effects on the C–H activation step to be studied in isolation from binding of the NHC to the metal. Therefore, the aims of this chapter are (i) to prepare unsymmetrical dibenzylimidazolium salts and their respective $\{\text{IrCp}^*\}$ and $\{\text{RhCp}^*\}$ complexes to study electronic effects effects on C–H activation and (ii) to prepare *meta*-substituted monobenzylimidazolium salts to study steric effects on C–H activation.

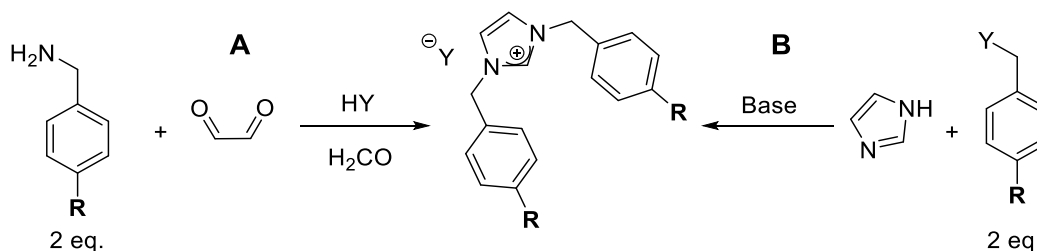
4.2 Results and discussion

All new compounds were characterised by ¹H and ¹³C NMR spectroscopy, alongside appropriate 2-D NMR techniques (COSY, NOESY, HSQC, HMBC) and HRMS spectrometry. Some complexes were characterised by single crystal X-ray diffraction (Note, these were performed by Mr K. Singh). The dibenzylimidazolium salts, their respective non-cyclometallated complexes **4.10a-OMe,H**, **4.10a/b-OMe,CF₃**, **4.10a/b-CF₃,F**, were prepared by Jessica Winter under my supervision. All the data interpretation has been done by myself.

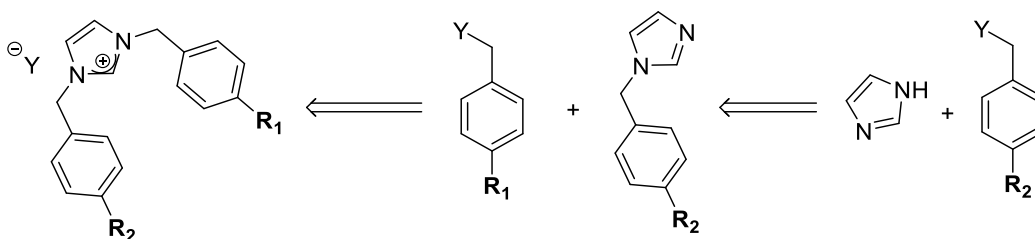
4.2a Preparation of dibenzylimidazolium salts

Preparation of symmetrical dibenzylimidazolium salts has been reported previously by cyclisation of benzylamines with glyoxal and formaldehyde with HY (Y = Cl, BF₄) as a source of counter ion (**Scheme 4.6 i(A)**).⁹ An alternative is deprotonation of imidazole and alkylation with benzyl halides (**Scheme 4.6 i(B)**).¹⁰ It was envisioned that method **B** could be adapted to prepare unsymmetrical dibenzylimidazolium salts by sequential reaction of imidazole with two different benzyl halides (**Scheme 4.6 ii**).

i) Methods to prepare symmetrical dibenzylimidazolium salts

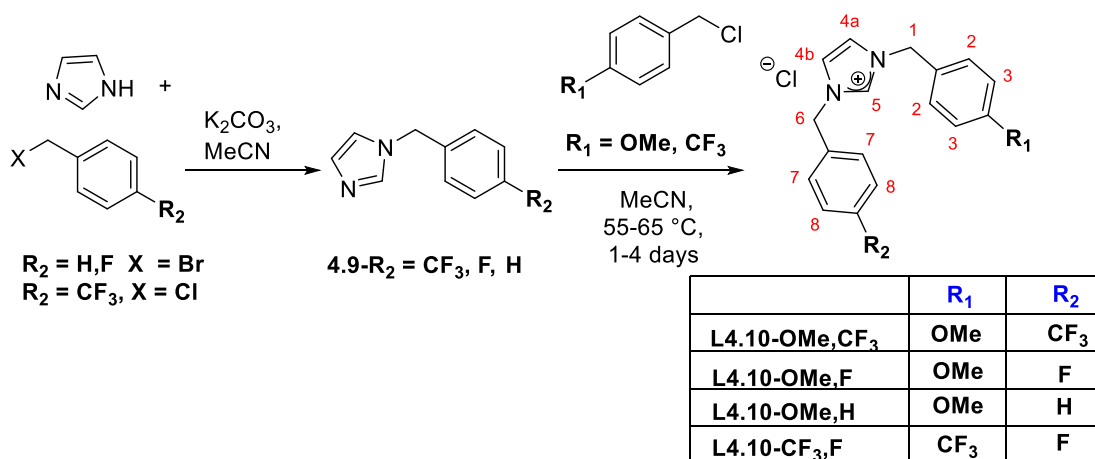


ii) Approach used to prepare unsymmetrical dibenzylimidazolium salts



Scheme 4.6: i) Two common routes to prepare symmetrical benzyimidazolium salts,^{9,10} ii) envisioned strategy to prepare unsymmetrical benzyimidazolium salts

First, benzyimidazoles **4.9-R₂** (R₂ = H, F, CF₃) were prepared by stirring imidazole with K₂CO₃ for 2 hours, followed by the addition of just 1 equivalent of the appropriate benzyl halide and stirring at room temperature for 1 hour (**Scheme 4.7**). After work up benzyimidazoles **4.9-R₂** were obtained in moderate to good yields (58-64%). All three benzyimidazoles have been reported previously and their respective ¹H and ¹³C NMR and ESI-MS agree with the reported data.^{11, 12} The benzyimidazoles **4.9-R₂** were then coupled with another benzyl chloride by heating in MeCN for 1-4 days (**Scheme 4.7**). The reaction with the most electron-withdrawing substituents CF₃,F was the slowest and took four days to go to completion. After the work up the corresponding unsymmetrical imidazolium salts **L4.10-OMe,H**, **L4.10-OMe,F**, **L4.10-OMe,CF₃**, **L4.10-CF₃,F** were obtained in moderate to good yields (56-73%). All four salts are new compounds.



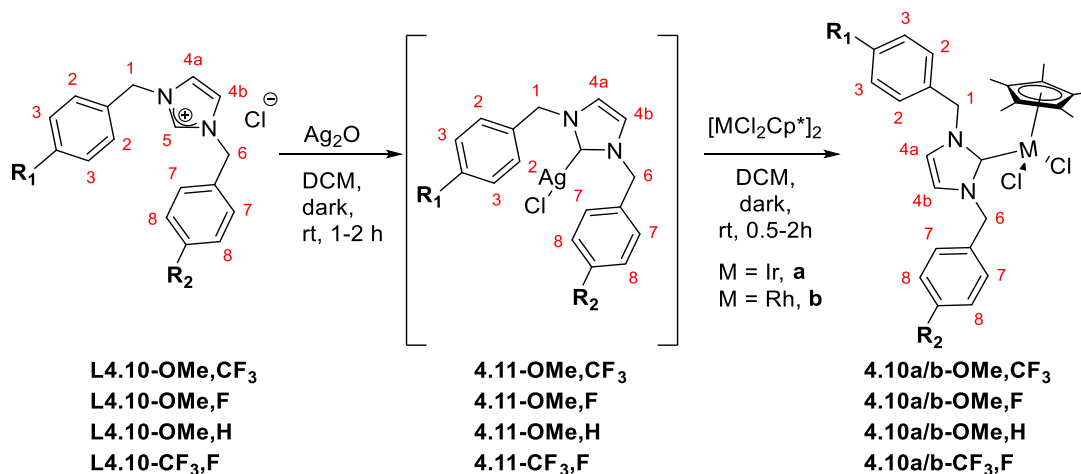
Scheme 4.7: Preparation and labelling scheme of benzylimidazolium salts.

Formation of the dibenzylimidazolium salts was most evident by the shifts of the imidazolium H⁵ signal in the ¹H NMR spectra. Proton H⁵ gives a broad singlet which is the most downfield signal at δ 10.9-11.4 which is *ca.* 3.5 ppm downfield from the corresponding signal in **4.9-R₂** (at *ca.* δ 7.5) due to formation of a cationic imidazolium salt. In the aromatic region an AA'BB' pattern is observed for the phenyl groups, except when **R₂** = H or F which both have additional coupling to the H or F respectively. Two 2H singlets are observed at δ 5.4-5.8 for H¹ and H⁶. The ¹³C NMR spectra for all dibenzylimidazolium salts show the expected number of signals with the imidazolium carbon C⁵ present at about δ 137. The HRMS(ESI) spectra show ions for the dibenzylimidazolium cation in each case (see Chapter 6 for details).

4.2bi Complexation of dibenzylimidazolium salts

As discussed in the introduction, non-cyclometallated benzyl-NHC complexes can be prepared by transmetalation from the corresponding silver complex (**Schemes 4.4, 4.5**).^{5,8} Therefore, the salts **L4.10-R₁,R₂** were stirred with Ag₂O at room temperature in the dark for 1-2 hours to form Ag NHC complexes **4.11-R₁,R₂** (**Scheme 4.8**). The absence of signals above δ 9 (disappearance of the H⁵ signal) in the ¹H NMR spectrum was used as an indicator that the reactions were complete. Based on the literature reports **4.11-R₁,R₂** are mono-carbene species.¹³ The reaction mixtures were filtered through celite a few times to ensure complete removal of Ag salts. The resulting Ag-complexes **4.11-R₁,R₂** were reacted with [MCl₂Cp*]₂ (M = Ir, Rh) in DCM. Within 2 hours a single new species was formed in high conversion in each case as observed by ¹H NMR spectroscopy (determined by the replacement of two 2H singlets for H¹ and H⁶ with four 1H doublets)

(Scheme 4.8). The resulting complexes **4.10a/b-R₁,R₂** were isolated by precipitation from DCM with hexane in moderate to good yields (57-90%) with the yields varying depending on solubility of complexes (see Chapter 6 for details). Some of the complexes gave crystals suitable for X-ray diffraction which are discussed later.



Scheme 4.8: Synthesis and labelling of **4.10a/b-R₁,R₂**.

The ¹H NMR spectrum of **4.10a-OMe,CF₃** shows singlets at δ 1.65 and 3.81 for Cp* and OMe groups respectively. The aromatic region shows two AA'BB' patterns one showing doublets at δ 6.89 and 7.35 the former of which shows an NOE with the OMe group so is assigned to H³ hence the other doublet at 7.35 is assigned as H². The other AA'BB' pattern at δ 7.53 and 7.61 is assigned to H⁸ and H⁷ respectively, the former shows a cross peak in the HSQC to a carbon at δ 125.6 that is a quartet (³J_{C-F} = 4.0 Hz). The presence of two AA'BB' patterns indicates that neither phenyl is cyclometallated. Two mutually coupled narrow doublets at δ 6.61 and 6.69 are assigned to H^{4b} and H^{4a} respectively based on NOE with H² and H⁷ respectively. The benzylic protons, which give two singlets in imidazolium salt **L4.10-OMe,CF₃** give rise to 1H doublets at δ 5.10, 5.24, 6.09, and 6.26 due to loss of the mirror plane upon formation of IrCp* complex **4.10a-R₁,R₂**. A cross-peak between doublets at δ 5.10 and 6.09 is observed in the COSY spectrum indicating they are on the same carbon, as both of these signals show an NOE to H² so they are assigned to H¹ protons. Analogously, the mutually coupled doublets at δ 5.24 and 6.26 are assigned to H⁶ protons due to an NOE with H⁷.

The ^1H NMR spectrum of the **4.10b-OMe,CF₃** complex is very similar to that of the Ir analogue with all signals within 0.2 ppm of the corresponding signals in **4.10a-OMe,CF₃**. The ^{13}C NMR spectra for **4.10a-OMe,CF₃** and **4.10b-OMe,CF₃** complexes show the expected number of signals with the M-NHC carbons C⁵ at δ 157.6 as a singlet and at δ 171.3 as a doublet ($J_{\text{C-Rh}} = 57.2$ Hz) for Ir and Rh respectively. These signals are downfield compared to **L4.10-OMe,CF₃** at δ 137.2 which is consistent with formation of the Ir/Rh carbene.⁸ The ^{19}F NMR spectra of **4.10a-OMe,CF₃** and **4.10b-OMe,CF₃** each show a signal at δ -62.6. The HRMS(ESI) spectra show ions at m/z 709.1783 due to $[\text{M-Cl}]^+$ for **4.10a-OMe,CF₃** and at m/z 619.1210 due to $[\text{M-Cl}]^+$ for **4.10b-OMe,CF₃**.

The ^1H NMR spectrum of **4.10a-OMe,F** shows the same main features as observed for **4.10a-OMe,CF₃** discussed above: in the aromatic region an AA'BB' pattern is present, with doublets at 6.88 for H³ and 7.33 for H², and an AA'BB'X pattern with a 2H triplet at δ 7.03 for H⁸ and a 2H doublet of doublets at δ 7.42 for H⁷ which shows an NOE with some benzylic and imidazole protons. The ^1H NMR spectrum of **4.10b-OMe,F** shows the same features as the Ir analogue with the corresponding signals within 0.2 ppm of **4.10a-OMe,F**. The ^{13}C NMR spectra for **4.10a-OMe,F** and **4.10b-OMe,F** show the expected number of signals with the M-NHC carbons C⁵ a singlet at δ 156.8 and a doublet at δ 170.5 ($J_{\text{C-Rh}} = 56.2$ Hz) for Ir and Rh respectively. The ^{19}F NMR spectra of **4.10a-OMe,F** and **4.10b-OMe,F** each show a signal at *ca.* δ -114. The HRMS(ESI) spectra show ions at m/z 659.1817 due to $[\text{M-Cl}]^+$ for **4.10a-OMe,F** and at m/z 569.1240 due to $[\text{M-Cl}]^+$ for **4.10b-OMe,F**.

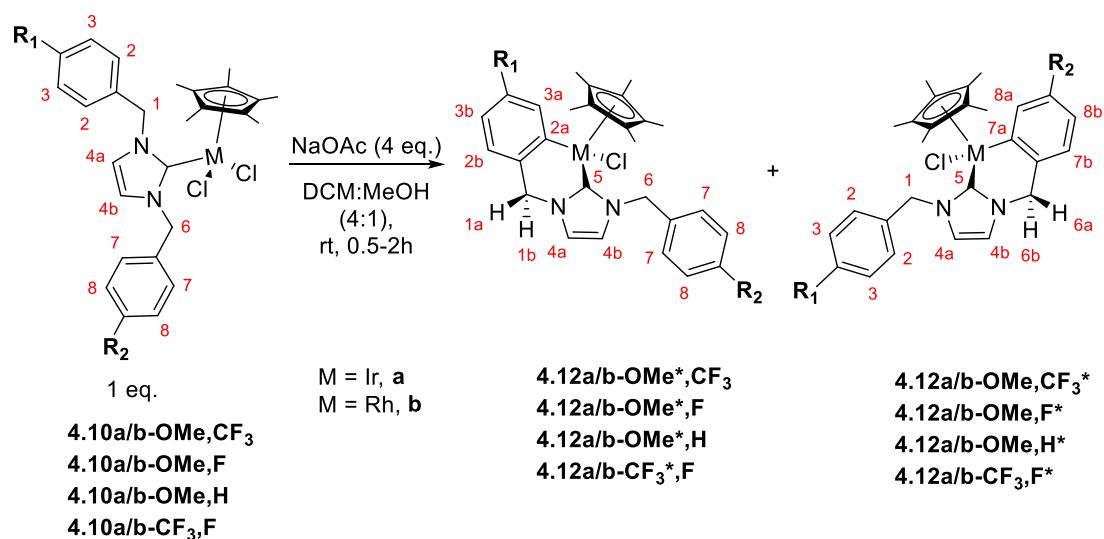
The complexes **4.10a-OMe,H** and **4.10b-OMe,H** and **4.10a-CF₃,F** and **4.10b-CF₃,F** were prepared by the method described above. The ^1H NMR spectra show the same general features as the complexes above (see Chapter 6 for details). The HRMS(ESI) spectra show ions at m/z 641.1899 and 551.1340 due to $[\text{M-Cl}]^+$ for **4.10a-OMe,H** and **4.10b-OMe,H** respectively, whilst **4.10a-CF₃,F** and **4.10b-CF₃,F** show ions at m/z 697.1571 and 619.1210 due to $[\text{M-Cl}]^+$ respectively.

Two Ir complexes **4.10a-OMe,CF₃** and **4.10a-CF₃,F** and Rh complex **4.10b-OMe,H** gave crystals suitable for X-ray diffraction and the structures are shown below in **Figure 4.1** with selected bond distances. For the Ir complexes the structures show disorder at C⁷ (X-ray labelling) with 50% occupancy by OMe and CF₃ at each site in **4.10a-OMe,CF₃** and 50% occupancy by CF₃ and F for **4.10a-CF₃,F**. The structures for all three complexes

OMe,F with Ag₂O and [IrCl₂Cp*]₂ was left to stand for a longer time without work up (2 days) the formation of cyclometallated complexes **4.12a-OMe*,F** and **4.12a-OMe,F*** in combined 10% conversion was observed. However, if the mixture was filtered through celite within 6 hours to remove Ag species then no cyclometallation of **4.10a-OMe,F** was observed in the ¹H NMR spectrum. In addition, isolated **4.10a-OMe,F** is stable in solution and only traces of cyclometallation (*ca.* 1%) were observed after the complex was left in CDCl₃ overnight. This suggests that the Ag species present in the reaction mixture after transmetallation are responsible for the cyclometallation which is consistent with the reports that Ag nanoparticles promote *ortho* C–H activation of Ir-benzyl-NHC complex **4.6** (Scheme 4.4 ii).⁷ In conclusion, the non-cyclometallated complexes **4.10a/b-R₁,R₂** were prepared and isolated as stable complexes and fully characterised. Unlike the phenyl-NHC complexes of **L3.12-R₁,R₂** (Chapter 3) the benzyl complexes do not undergo immediate cyclometallation presumably because formation of a six-membered ring is less favoured compared to a five-membered ring.

4.2bii Cyclometallation of dibenzylimidazolium salts

The cyclometallations of Ir and Rh-complexes **4.10a/b-R₁,R₂** (OMe,CF₃; OMe,F; OMe,H; CF₃,F) were investigated in the presence of NaOAc. The reactions were monitored by ¹H NMR spectroscopy and where applicable ¹⁹F NMR spectroscopy. Stirring **4.10a-OMe,F** with NaOAc in DCM at room temperature gave two cyclometallated complexes after 2 hours but it took over 40 hours for the reaction to reach full conversion. Repeating the reaction in DCM:MeOH (4:1) full conversion to the cyclometallated products was observed within 1 hour at rt. This is consistent with cyclometallation taking place via a cationic intermediate which is favoured in more polar solvents (as discussed in Chapter 1, Scheme 1.35).¹⁴ Therefore, further reactions were carried out in DCM:MeOH (4:1) (Scheme 4.9).



Scheme 4.9: Cyclometallation of the Ir and Rh-NHCs **4.10a/b-R₁R₂** and their labelling.

To start, preparative reactions were carried out to isolate and characterise products. All of the reactions proceeded in high conversions (>80%) and mixtures of isomers were isolated in moderate to good yields (48-90%). The results and characterisation of products of the cyclometallation of **4.10a/b-O_{Me},CF₃** will be discussed in detail, the others will be described more briefly and all details are given in chapter 6. The ratios of isolated complexes from the preparative reactions are after purification and are not necessarily indicative of the reaction selectivity due to possible preferential loss of one isomer during work-up, therefore, will not be discussed. Several complexes **4.12a-O_{Me}^{*},CF₃**, **4.12a-O_{Me}^{*},H**, **4.12b-O_{Me},CF₃^{*}**, **4.12b-O_{Me},F^{*}** and **4.12b-O_{Me},H^{*}** gave crystals suitable for X-ray diffraction and these will be discussed later. The reactions were then repeated to measure the isomer ratios and these results are discussed after the characterisation. The asterisks in the complexes labels refers to the ring that was cyclometallated.

Stirring **4.10a-O_{Me},CF₃** with NaOAc in DCM:MeOH (4:1) for 0.5 hours led to complete conversion to the two cyclometallated products. Recrystallisation from DCM/hexane gave a small amount of crystals which were suitable for X-ray diffraction (see below) and some powdered solid. The ¹H NMR spectra showed that these were of the minor and major isomer respectively. The ¹H NMR spectrum of the major isomer shows singlets at δ 1.68 and 3.79 for the Cp* and OMe groups respectively. In the aromatic region, only one AA'BB' pattern is observed with doublets at δ 6.85 and 7.36. The signal at δ 6.85 shows an NOE with the OMe group and so is assigned to H³, which indicates that the

OMe-substituted ring is not cyclometallated. The CF₃-substituted ring shows three inequivalent protons; a doublet of doublets at δ 7.04, coupled to a doublet at δ 7.08 and a narrow doublet at δ 7.92. The latter shows an NOE to the Cp* indicating it is H^{8a} consistent with the CF₃ ring having been cyclometallated. The imidazole protons are observed as two narrow doublets at δ 6.63 (H^{4a}) and 6.90 (H^{4b}) with the former showing an NOE with H². For the benzylic protons two pairs of mutually coupled doublets are seen at δ 5.92 and 5.02, and at δ 4.87 and 4.73, the former pair show an NOE to H² and so are assigned to H¹ protons the latter pair then being H⁶ protons. The H⁶ protons can be distinguished since H^{6a} shows an NOE with the Cp* whilst H^{6b} shows an NOE with H^{4b} and H^{7b}. Overall, the ¹H NMR spectrum indicates that the major isomer is cyclometallated on the CF₃-substituted ring i.e. **4.12a-OMe,CF₃***.

The ¹H NMR spectrum of the minor isomer shows singlets at δ 1.68 and 3.81 for Cp* and OMe groups respectively. A very second order AA'BB' 4H signal is present at δ 7.54 for the CF₃ substituted ring. A doublet of doublets at δ 6.42, a doublet at 6.93 and a narrow doublet at δ 7.27, are assigned to the OMe-substituted ring protons and the signal at δ 7.27 shows an NOE with Cp* and so is assigned as H^{3a}. This is consistent with **4.12a-OMe*,CF₃** which is cyclometallated on the OMe-substituted ring. The imidazole and benzylic protons are similar to those of the major isomer (see Chapter 6 for details).

The ¹³C NMR spectrum of the mixture of **4.12a-OMe*,CF₃**:**4.12a-OMe,CF₃*** shows the C⁵ at δ 158.0 and 156.3 for **4.12a-OMe*,CF₃** and **4.12a-OMe,CF₃*** respectively whilst the cyclometallated carbons C^{2a} and C^{7a} are also very similar at δ 145.8 and 145.4 for **4.12a-OMe*,CF₃** and **4.12a-OMe,CF₃*** respectively. The ¹⁹F NMR spectrum of the mixture show signals for the CF₃ groups at δ -62.6 for **4.12a-OMe*,CF₃** and δ -61.7 for **4.12a-OMe,CF₃***. The HRMS(ESI) spectrum shows ions at m/z 673.2021 due to [M-Cl]⁺.

Stirring Rh complex **4.10b-OMe,CF₃** with NaOAc for 1 hour and subsequent work up gave an isomeric mixture of **4.12b-OMe*,CF₃**:**4.12b-OMe,CF₃***. The ¹H NMR spectra of the isomers show the same features as the Ir analogues with the corresponding signals within 0.2 ppm. The ¹³C NMR spectrum allowed assignment of the signals for **4.12b-OMe,CF₃*** with C⁵ and C⁷ seen as doublets at δ 174.2 ($J_{C-Rh} = 55.2$ Hz) and at δ 162.0 ($J_{C-Rh} = 33.1$ Hz) respectively but is too weak to allow assignment of all quaternary carbon signals of **4.12b-OMe*,CF₃**. The ¹⁹F NMR spectrum of the mixture show signals for the

CF₃ groups at δ -62.6 for **4.12b-OMe*,CF₃** and δ -61.7 for **4.12b-OMe,CF₃***. The HRMS(ESI) spectrum shows an ion at m/z 583.1445 due to [M-Cl]⁺.

The cyclometallation of **4.10a-OMe,F** resulted in formation of two isomers. The ¹H NMR spectrum for the mixture for one of the isomers shows that the cyclometallated ring is similar to **4.13-OMe*,CF₃** therefore is **4.12a-OMe*,F** cyclometallated on the OMe-substituted ring. The other isomer in the aromatic region shows an AA'BB' pattern for OMe-substituted ring but the F-substituted ring shows three inequivalent protons so is cyclometallated on the F-substituted ring and is assigned as **4.12a-OMe,F***. The ¹⁹F NMR spectrum of the mixture shows signals at δ -114.2 for **4.12a-OMe*,F** and at δ -118.5 for **4.12a-OMe,F***. The HRMS(ESI) show ion m/z 623.2065 due to [M-Cl]⁺. The cyclometallation of Rh complex **4.10b-OMe,F** by the same method, after work up yielded two isomers, **4.12b-OMe*,F** and **4.12b-OMe,F***. The ¹H NMR spectrum of the mixture is very similar to that for Ir. The ¹⁹F NMR spectrum of the mixture shows signals at δ -114.1 for **4.12b-OMe*,F** and at δ -117.8 for **4.12b-OMe,F***. The HRMS(ESI) spectrum show ions at m/z 533.1472 due to [M-Cl]⁺.

The cyclometallation of **4.10a-OMe,H**, **4.10b-OMe,H**, **4.10a-CF₃,F**, **4.10b-CF₃,F** yielded two isomers each. The ¹H NMR spectra of whose show general features as for the complexes above. The HRMS(ESI) spectra all show ions due to [M-Cl] (see Chapter 6 for details).

Two Ir complexes **4.12a-OMe*,CF₃** and **4.12a-OMe*,H** and three Rh complexes **4.12b-OMe,CF₃***, **4.12b-OMe,F*** and **4.12b-OMe,H*** gave crystals suitable for the X-ray diffraction and the structures are shown below in **Figure 4.2** with selected bond distances and angles in **Table 4.1**. All of the structures show the expected piano stool geometry. The metallocycles in **4.12a-OMe*,CF₃**, **4.12a-OMe*,H**, **4.12b-OMe,CF₃***, **4.12b-OMe,F*** and **4.12b-OMe,H** all are non-planar and exhibit boat-like conformation with metal and C(11) present on the same side of a plane defined by C(1), N(2), C(12), C(13).¹⁵ Ir—C(1) distances for **4.12a-OMe*,CF₃** and **4.12a-OMe*,H** [2.012(6) and 2.017(9) Å respectively] are very similar to the Ir—C(1) distances for five-membered complexes **3.12a-F*,OMe** and **3.12a-OMe*,OMe** [2.009(4) and 2.022(6) Å respectively]. The Rh—C(1) distances for **4.12b-OMe,CF₃***, **4.12b-OMe,F*** and **4.12b-OMe,H*** are statistically the same as well. The Ir—C(13) distances for **4.12a-OMe*,CF₃** and **4.12a-OMe*,H** [2.058(5) and 2.062(9) Å respectively] are statistically the same as the

equivalent Ir—C(11) distances for **3.12a-F*,OMe** and **3.12a-OMe*,OMe** (Chapter 3, [2.056(4)-2.064(6) Å respectively]) suggesting that the Ir—C distances in the cyclometallated complexes are not affected by ring size.

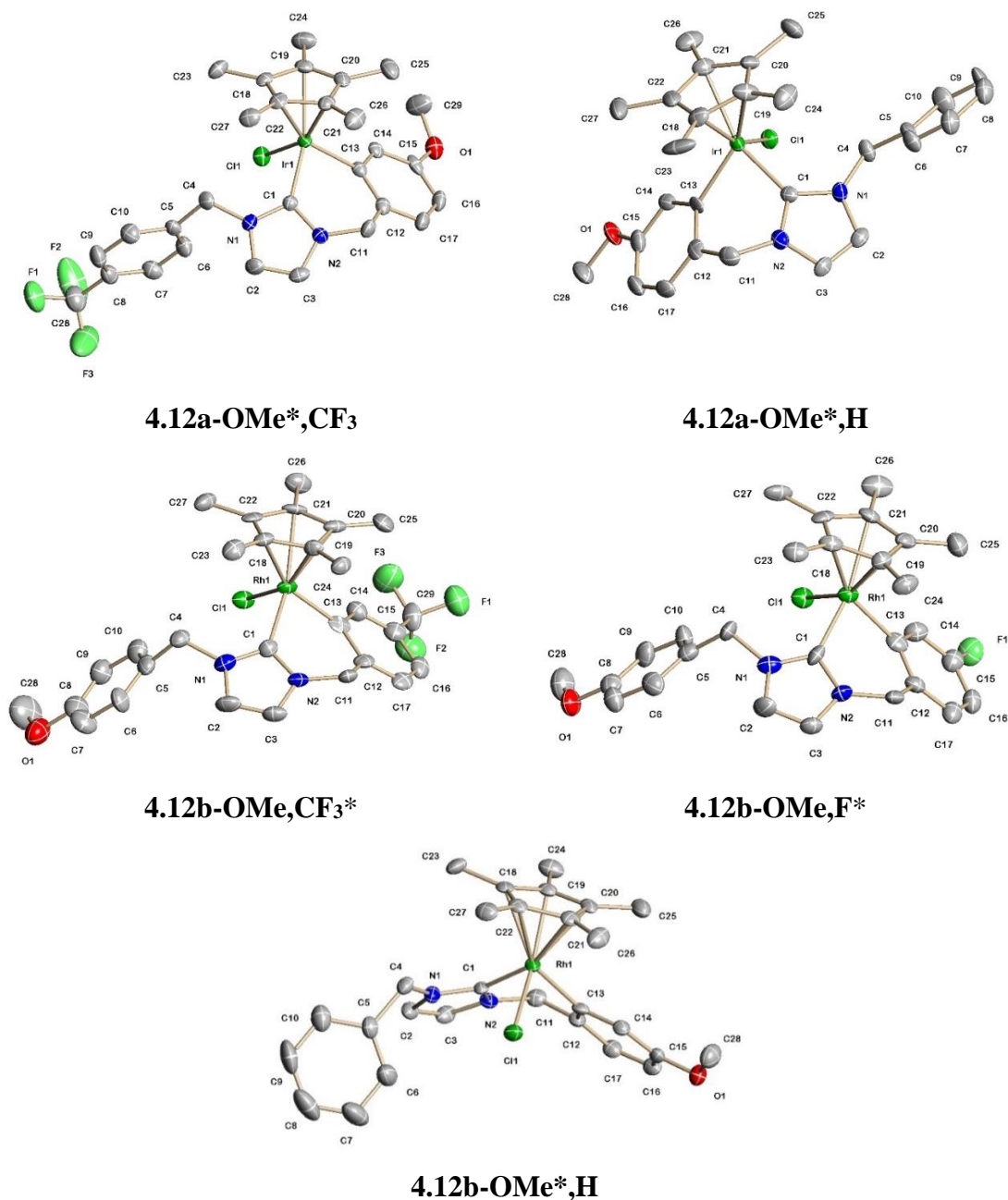


Figure 4.2: X-ray structures of **4.12a-OMe*,CF₃**, **4.12a-OMe,H***, **4.12b-OMe,CF₃***, **4.12b-OMe,F** and **4.12b-OMe,H***, showing 50% displacement ellipsoids. Hydrogen atoms have been omitted for clarity.

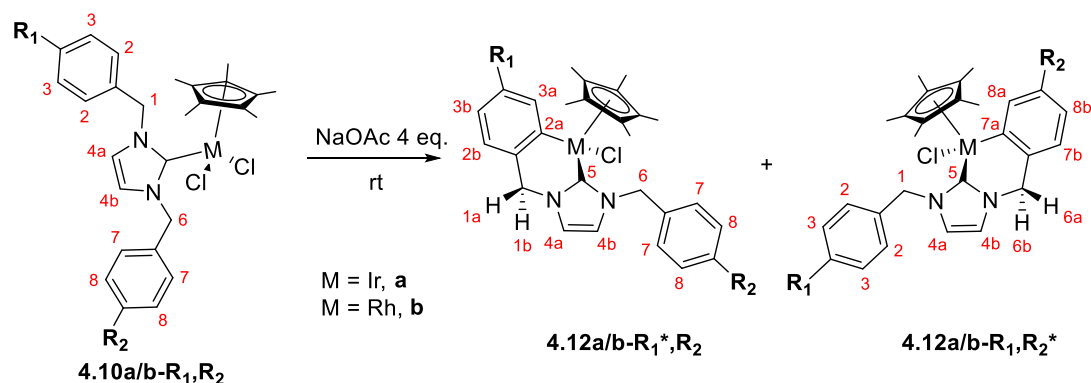
Table 4.1: Selected bond distances (Å) and bond angles [°] for **4.12a-OMe*,CF₃**, **4.12a-OMe,H***, **4.12b-OMe,CF₃***, **4.12b-OMe,F*** and **4.12b-OMe,H***.

	4.12a- OMe*,CF₃	4.12a- OMe*,H	4.12b- OMe,CF₃*	4.12b- OMe,F*	4.12b- OMe*,H
M—C(1)	2.012(6)	2.017(9)	2.010(9)	2.005(9)	2.004(4)
M—C(13)	2.058(5)	2.062(9)	2.006(10)	2.031(8)	2.045(4)
C(13)—M—C(1)	86.0(2)	83.5(4)	84.4(4)	85.2(3)	86.4(2)

The C(13)—M—C(1) chelate bite angle for these six-membered Ir and Rh complexes are 83.5-86.4° which are consistent with reported values of 85-88° for six-membered Ir-NHC cyclometallated complexes.^{5,8,16} These bite angles are significantly bigger than equivalent chelate bite angles for the five-membered complexes [76-77°] see Chapter 3 (**Table 3.5**) or published elsewhere [77-78°].^{6, 16} The results are consistent with increased chelate angle due to increased ring size.²

As shown above, cyclometallation of NHC-complexes **4.10a/b-R₁,R₂** takes place in the presence of NaOAc. After the products were characterised the reactions were repeated to obtain isomer ratios of these intramolecular competition reactions. To facilitate easy monitoring of the reaction progress by NMR spectroscopy, the intramolecular competition reactions were carried out in NMR tube using *ca.* 5 mg of non-cyclometallated **4.10a/b-R₁,R₂** in the presence of NaOAc in CDCl₃. Note, all of the complexes **4.10a/b-R₁,R₂** were fully dissolved in CDCl₃, but some of the NaOAc was not. All of the competition reactions were followed by ¹H NMR spectroscopy and where applicable, ¹⁹F NMR spectroscopy and the summarised results are presented in **Table 4.2**. Additionally, the reactions of **4.10a/b-R₁,R₂** were repeated in DCM:MeOH (4:1) and monitored at early conversions (<25%) (**Table 4.5**).

Table 4.2: Results of intramolecular competition between R₁ and R₂ for cyclometallation of **4.10a/b-R₁,R₂** in CDCl₃ at <25% conversion.



Entry	R ₁ ,R ₂	Ir,	Rh,
		R ₁ *:R ₂ *	R ₁ *:R ₂ *
1	OMe,H	1:1.4	1:1.4
2	OMe,F	1.3:1	1.4:1
3	OMe,CF ₃	1:1.1	1:1.1
4	CF ₃ ,F	1.2:1	1.3:1

The cyclometallation reactions in CDCl₃ took 4-24 hours to reach high enough conversion (>5%) to give reliable ratios between two isomers, whilst the reactions in the DCM:MeOH mixture reached about 20% conversion within 5-30 minutes. There are two possible factors contributing to this significant difference in timescales: the lower polarity solvents create less favourable cyclometallation conditions;¹⁷ and NaOAc is less soluble in CDCl₃. It is notable that no isomer ratio is bigger than 1:1.5 for Ir or Rh. The relative rates of cyclometallation of the substituted ring compared to the unsubstituted ring (k_R/k_H) in CDCl₃ were calculated and are presented in **Table 4.3** together with the appropriate Hammett constants (σ_m). Hammett plots produced from this data are shown in **Figure 4.3**. The results in DCM:MeOH were very similar to those in CDCl₃ and are shown in appendix in **Table S6** and **Figure S1**.

Table 4.3: Relative rates of R₁ vs. R₂ intramolecular competition for cyclometallation of **4.10a/b-R₁,R₂** complexes in CDCl₃.

Group		H	OMe	F	CF ₃
	σ_m	0	0.12	0.34	0.43
Ir	k_R/k_H	1	0.71	0.55	0.79
	$\log(k_R/k_H)$	0	-0.15	-0.26	-0.10
Rh	k_R/k_H	1	0.71	0.51	0.79
	$\log(k_R/k_H)$	0	-0.15	-0.29	0.10

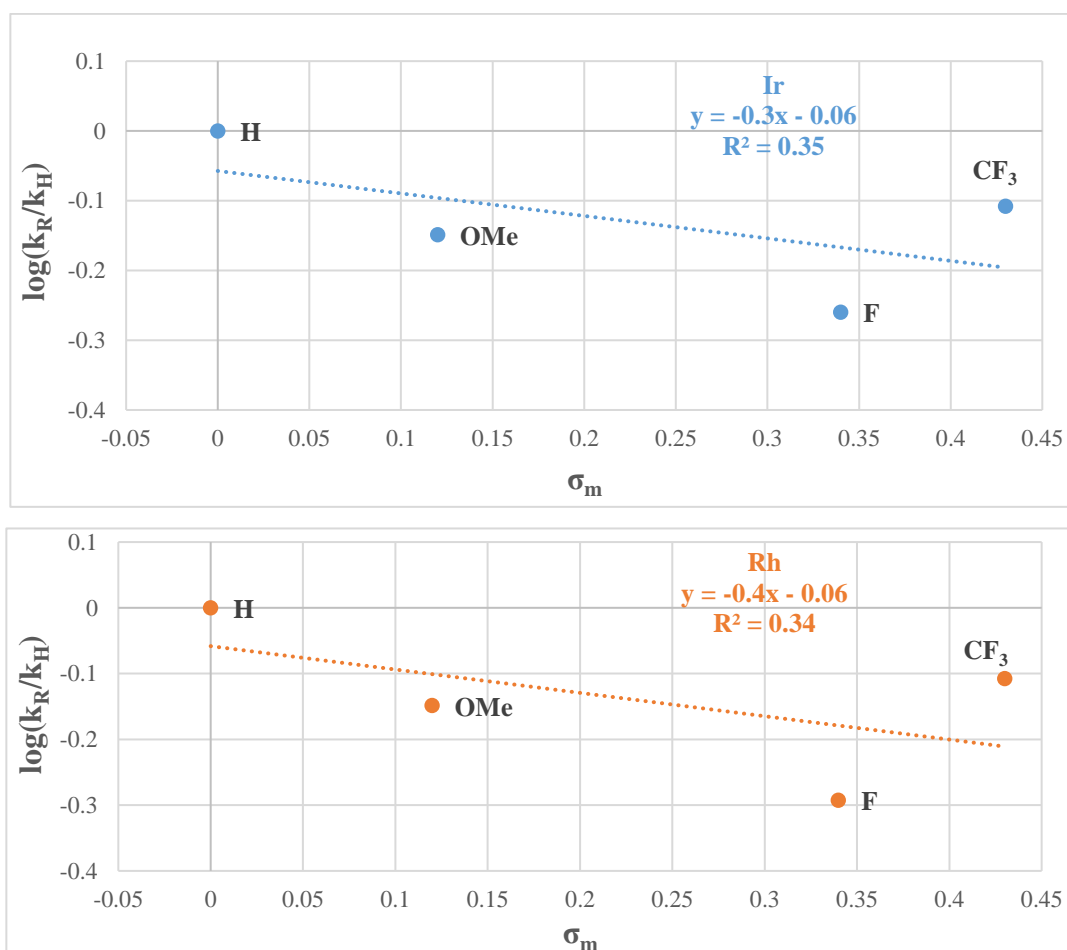


Figure 4.3: Hammett plot for intramolecular competitions of R₁ vs. R₂ for cyclometallation of Ir (top) and Rh (bottom) complexes **4.10a/b-R₁,R₂**, $\log(k_R/k_H)$ against σ_m in CDCl₃.

The resulting Hammett plots show very poor correlation between $\log(k_R/k_H)$ and σ_m in CDCl₃ ($R^2 = 0.37$ and 0.36 for Ir and Rh respectively) with both metals. As discussed in

Chapter 3, this could be either due to reactions already equilibrating and true kinetic selectivity not observed or the substituent could have an effect on the sites both *para* and *meta* to the reaction centre as this can also lead to non-linear Hammett plots. These can be assessed by employing Jaffè analysis,¹⁸ therefore, Jaffè plots were produced (**Figure 4.4**) (for results in DCM:MeOH see **Table S8**, **Figure S2** in the appendix). The resulting Jaffè plots show good linear correlation ($R^2 \geq 0.88$) and the averages of the resulting slopes for Ir and Rh (ρ_m , ρ_p) are shown in **Table 4.4** (**Table S9** for results in DCM:MeOH). Note, the Jaffè modifications are shown in **Table S7**.

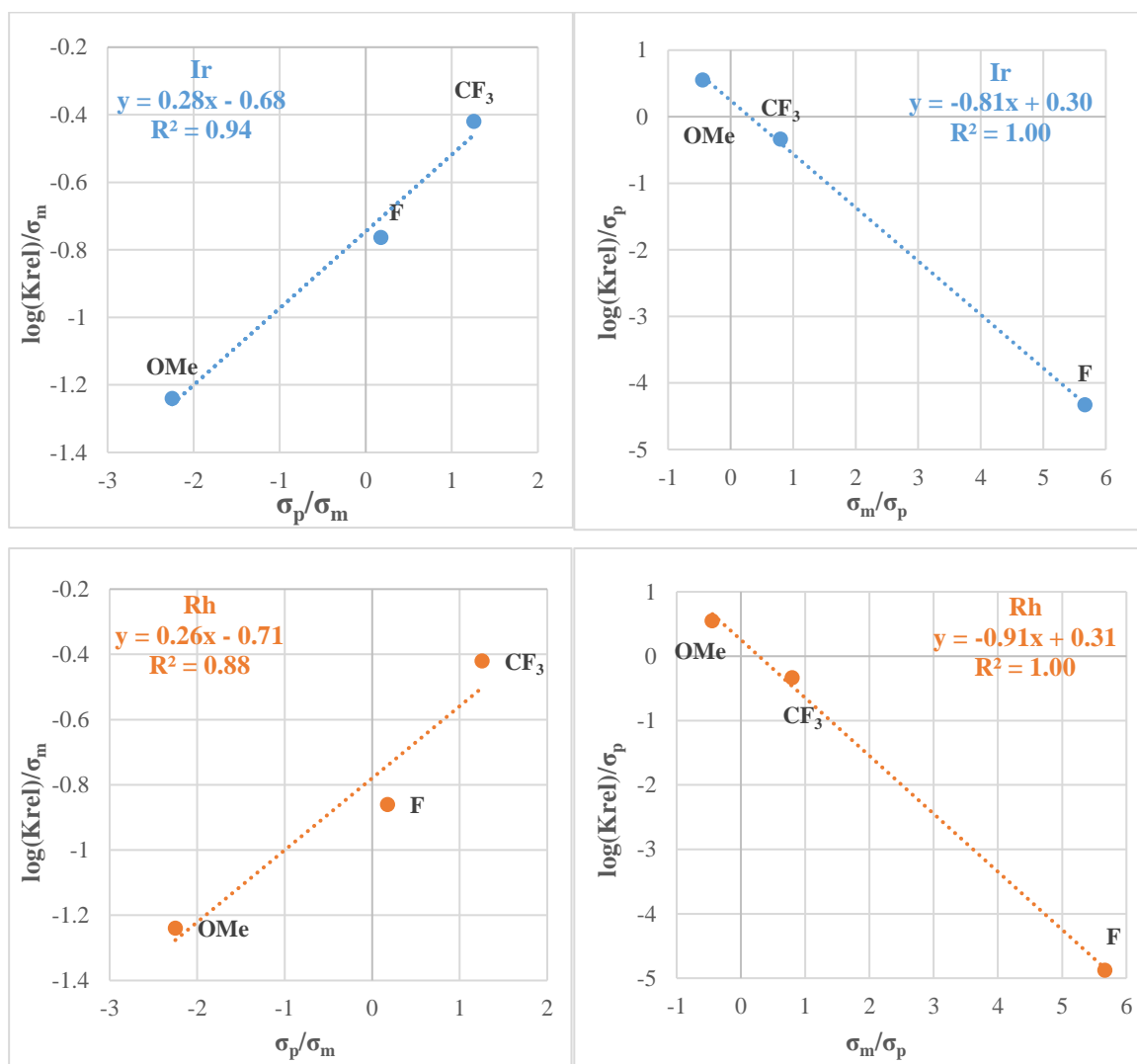


Figure 4.4: Jaffè plots for intramolecular competitions of R₁ vs. R₂ for cyclometallation of Ir (top) and Rh (bottom) complexes **4.10a/b-R₁,R₂** in CDCl₃.

Table 4.4: Average ρ_m and ρ_p values from Jaffé plots for cyclometallation of **4.10a/b-R₁,R₂** in CDCl₃.^a

M	ρ_{m1}	ρ_m	$\rho_{m(\text{average})}$	ρ_{p1}	ρ_{p2}	$\rho_{p(\text{average})}$
Ir	-0.68	-0.81	-0.7	0.28	0.30	0.3
Rh	-0.71	-0.91	-0.8	0.26	0.31	0.3

^a For plots $\log(k_R/k_H)/\sigma_m$ vs. σ_p/σ_m $y=\rho_p x+\rho_m$, for plots $\log((k_R/k_H)/\sigma_p)$ vs. σ_m/σ_p $y=\rho_m x+\rho_p$.

The results show a small *para* effect ($\rho_p = 0.3$) presumably affecting the directing group and a slightly bigger *meta* effect (-0.7 for Ir, -0.8 for Rh) affecting the actual C-H activation step for both Ir and Rh. Thus, the presence of both *para* and *meta* effects explains the poor correlations in the Hammett plots. The positive slope for the *para* effect is indicating a preference for more electron-withdrawing groups. The slope of the *para* effect for benzyl-NHCs is smaller compared to one observed for phenyl-NHCs **3.12a/b-R₁,R₂** discussed in Chapter 3 ($\rho_p = 1.1$ for Ir and $\rho_p = 1.0$ for Rh), which is consistent with the loss of conjugation between the directing group (NHC) and substituent. A similar effect was observed by Hammett for the ionisation of benzoic and phenylacetic acids where a slope of 1 was obtained for benzoic acids but only 0.5 for ionisation of phenylacetic acids.¹⁹ The *meta* effects (ρ_m) have negative slopes ($\rho_m = -0.7$ and -0.8 for Ir and Rh respectively) both indicating a preference for more electron-donating groups as found with phenyl pyridines (Chapter 2), phenyl-NHCs **3.12a/b-R₁,R₂** (Chapter 3) and phenylpyrazoles.²⁰ The slopes for the *meta* effect are significantly smaller in magnitude compared to those expected for S_EAr (-5 to -9),²¹ therefore, the results are inconsistent with an S_EAr mechanism. The magnitudes of the slopes ρ_m are slightly smaller than that of -1.6 obtained for Ir phenyl-NHCs **3.12a-R₁,R₂** and are very similar to the one obtained for Rh phenyl-NHCs **3.12b-R₁,R₂** ($\rho_m -0.9$). Note, care has to be taken when comparing slopes acquired from Hammett plots with ones obtained from Jaffé plots due to the former assuming there is only a single effect whilst the latter separating *meta* and *para* effects making slopes obtained not necessarily directly comparable. Overall, the *meta* effect is consistent with an AMLA C-H activation taking place via a cationic intermediate. However, the reactions are not very sensitive to electronic effects since none of the ratios for cyclometallation of **4.10a/b-R₁,R₂** are larger than 1:1.5.

To see if ratios between cyclometallated products change and so whether the reactions are reversible and to investigate possible thermodynamic selectivity the cyclometallation reactions of **4.10a/b-R₁,R₂** were heated overnight at 60 °C in DCM:MeOH (4:1). The reactions were monitored as above and the results are summarised in **Table 4.5**.

Table 4.5: Intramolecular competition results of R₁ vs. R₂ for cyclometallation of **4.10a/b-R₁,R₂** in DCM:MeOH at room temperature and 60 °C.

Entry	M	R ₁ ,R ₂	R ₁ *:R ₂ * at <25% conversion	R ₁ *:R ₂ * at rt, >80% conversion	R ₁ *:R ₂ * at 60 °C
1		OMe,H	1:1.4	1.4:1	1.4:1
2	Ir	OMe,F	1.3:1	1:1.2	1:5.0
3		CF ₃ ,F	1.1:1	1.3:1	1.6:1 ^a
4		OMe,H	1:1.4	1.2:1	1.5:1
5	Rh	OMe,F	1.4:1	1:1	1:6 ^b
6		CF ₃ ,F	1.2:1	1.2:1	1.5:1 ^a

^a added PivOH, overnight at 60 °C,

^b from ¹⁹F NMR spectrum

Overall, comparing the initial results (<25% conversion) with those at high conversions (>80%) and upon heating overnight a change in ratios was observed for entries 1, 2 and 4, 5 in favour of more electron-withdrawing groups with a slight change for entries 3 and 6 upon heating. The change is particularly noticeable in entries 1, 2 and 4, 5 where the selectivity switches from cyclometallation on one ring to the other. This suggests that the reactions are reversible, indicating thermodynamic control under the harsher conditions. The ratios obtained from heating overnight were used to calculate the equilibrium constants (K_R/K_H) for Ir and Rh complexes and these are presented in the **Table 4.6** together with the appropriate Hammett constants (σ_m), whilst the resulting Hammett plot is shown in **Figure 4.5**.

Table 4.6: Equilibrium constants of intramolecular competition of R₁ vs. R₂ for formation of **4.12a/b-R₁,R₂** upon heating.

Group		H	OMe	F	CF ₃
	σ_m	0	0.12	0.34	0.43
Ir	K _R /K _H	1	1.4	7	11.2
	log(K _R /K _H)	0	0.15	0.85	1.05
Rh	K _R /K _H	1	1.5	9	13.5
	log(K _R /K _H)	0	0.18	0.95	1.13

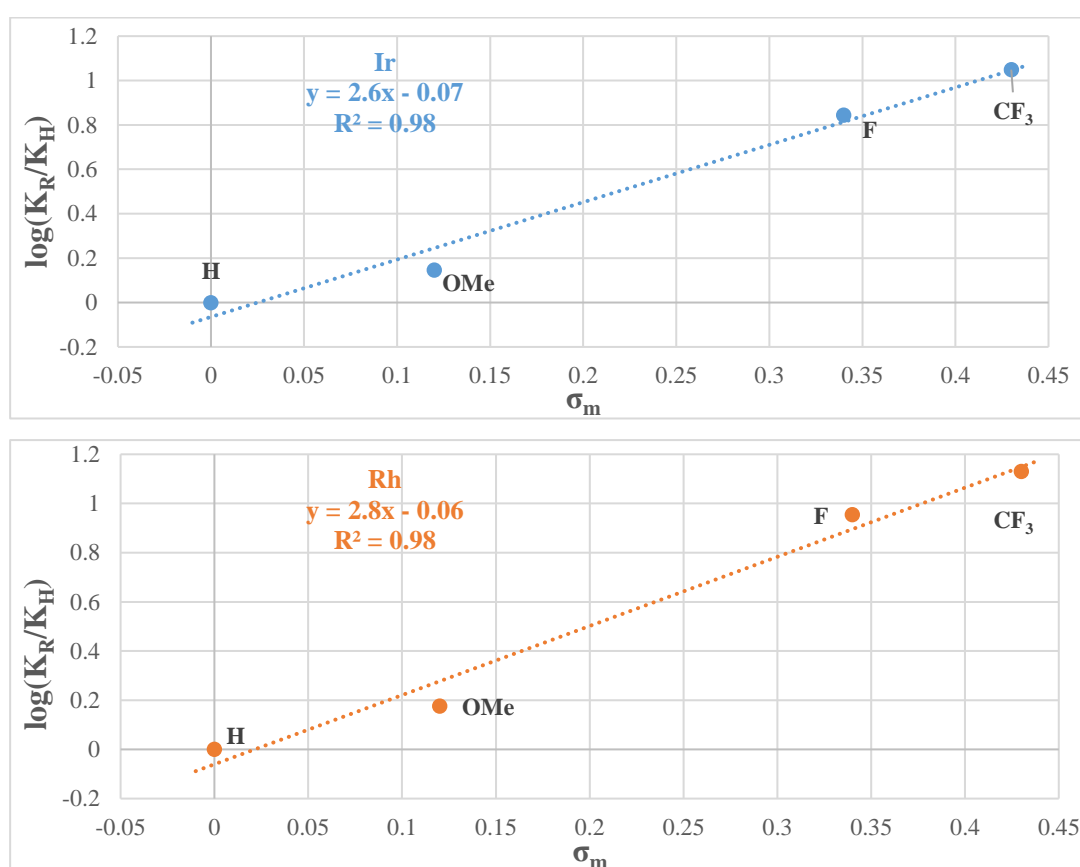
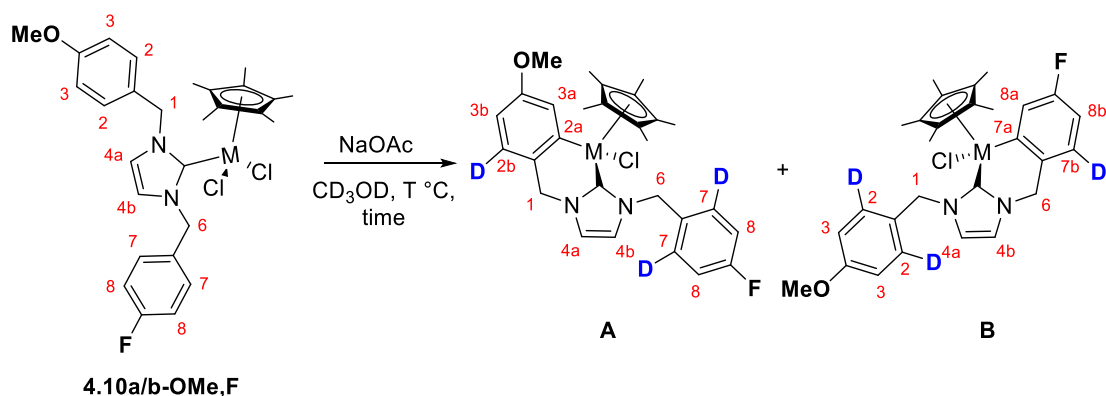


Figure 4.5: Hammett plot for thermodynamic results of intramolecular competitions of R₁ vs. R₂ for formation of Ir (top) and Rh (bottom) complexes **4.12a/b-R₁,R₂**, log(K_R/K_H) against σ_m .

The resulting Hammett plots of the thermodynamic ratios show good correlations ($R^2 = 0.99$ for Ir and Rh) with positive slopes similar in magnitude for Ir ($\rho = 2.6$) and Rh ($\rho = 2.8$) indicating a preference for more electron-withdrawing groups. This is in agreement with the thermodynamic preference for electron-withdrawing groups observed for diphenylimidazolium salts (Chapter 3), phenylpyridines (Chapter 2) and phenylpyrazoles

as reported by Alharis;²⁰ which is consistent with increased M–C bond strength in these cases, as observed for phenylpyrazoles²⁰ and related Re and Ir, Rh systems.^{22, 23} However, the low number of data points and the fact that the ratio for the OMe,F pair was used in combination with the CF₃,F pair to calculate the K_{CF_3}/K_H means the good fit may be fortuitous. However the general trend favouring electron-withdrawing groups thermodynamically should be reliable.

The reversibility of cyclometallation was also investigated by carrying out deuteration experiments. The cyclometallation of **4.10a-OMe,F** and **4.10b-OMe,F** in the presence of NaOAc was attempted in CD₃OD. If the C–H activation reactions are reversible D-incorporation is expected in *ortho* C–H positions (H² and H⁷) of the benzyl rings (**Scheme 4.10**). The reactions were monitored by ¹H NMR spectroscopy and the D-incorporation (**Table 4.7**) was determined by comparing the integrations for the *ortho* signals H² and H⁷ with H^{3a-b} and H^{8a-b}. The D-incorporation was confirmed in each case by running a ²H NMR spectrum.



Scheme 4.10: D incorporation experiments with **4.10a/b-OMe,F**.

Table 4.7: % D-incorporation in **4.12a/b-OMe,F** in CD₃OD at 70 °C with PivOD.

M	Time, h,	D% in A		D% in B	
		Site 7	Site 2b	Site 2	Site 7b
Ir,	48 h	40	30	30	10
Rh	4 h	>95	^a	>60	-

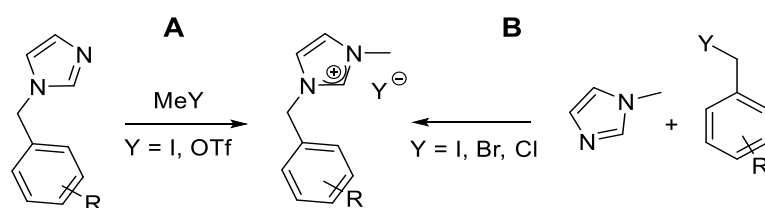
^a Due to overlap of the signals it was not possible to determine the percentage D-incorporation

effect it is unclear and so good fits in Jaffé plots maybe fortuitous, whilst poor correlation in Hammett plots could be due to the data reflecting some thermodynamic contribution. Heating cyclometallation reactions of **4.10a/b-R₁,R₂** (if necessary with PivOH) led to changes of ratios (**Table 4.5**) in favour of the more electron-withdrawing groups indicating that the reactions are reversible under these conditions. The Hammett plot analysis of the thermodynamic ratios (**Figure 4.5**) gave slopes of 2.6 and 2.8 for Ir and Rh respectively showing preference for the electron-withdrawing groups which reflects the increased M–C bond strength for these complexes.

Having investigated the electronic effects on cyclometallation with benzyliimidazolium salts it was then moved onto investigation of steric effects. This was done by preparing mono-benzyliimidazolium salts containing *meta*-substituents as described below.

4.2c Preparation of *meta*-substituted monobenzyliimidazolium salts

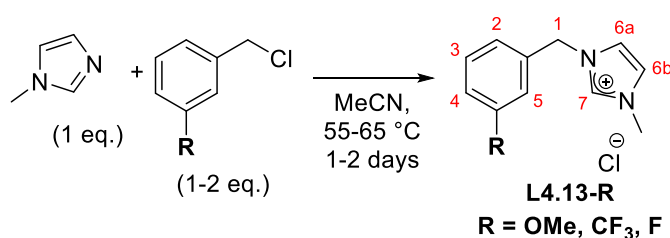
As discussed in Chapter 3, using *meta*-substituted diphenylimidazolium salts (when one ring is unsubstituted) could lead to up to three possible cyclometallated isomers (Chapter 3, **Scheme 3.24**) whose characterisation is likely to be challenging. The same would apply to dibenzyliimidazolium salts. Therefore, *N*-methyl *N*-benzyliimidazolium salts were selected to study steric effects on C–H activation. These salts can be prepared either by methylation of benzyliimidazole (**Scheme 4.12 A**)¹⁶ or benzylation of *N*-methyl imidazole (**Scheme 4.12 B**).²⁴



Scheme 4.12: Possible routes to *N*-methyl benzyliimidazolium salts: **A** methylation of benzyliimidazoles,¹⁶ **B** benzylation of *N*-methyl imidazole.²⁴

It was anticipated that having another halide (e.g. I⁻) rather than Cl⁻ as a counter ion for the salts could lead to ion exchange at the metal (during reactions with [MCl₂Cp*]₂) and subsequently bias the steric selectivity. Therefore, it was decided to select a method that allows preparation of benzyl imidazolium chlorides and as MeCl is a gas, method **B** was chosen as the most straightforward approach to prepare **L4.13-R** (R = OMe, CF₃, F) (**Scheme 4.13**). Hence, *N*-methyl imidazole was heated with an excess of appropriately

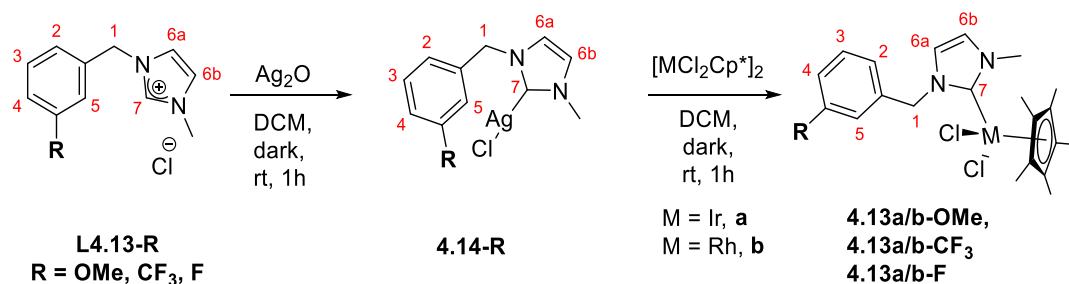
meta-substituted benzyl chloride for 1-2 days. All three salts **L4.13-R** (R = OMe, CF₃, F) were obtained in moderate to good yields (55-87%) and have been reported previously,²⁵ however, they have not been fully characterised. The ¹H NMR spectra of **L4.13-R** show H⁷ as a broad singlet which is the most downfield signal at δ 9-10 and the aromatic ring protons give rise to four inequivalent signals. The ¹³C NMR spectra for all three benzylimidazolium salts show the expected number of signals with the imidazolium carbon C⁷ present at about δ 137-138. The HRMS(ESI) show ions for the cation in each case.



Scheme 4.13: Preparation and labelling of *meta*-substituted benzylimidazolium chlorides **L4.13-R** (R = OMe, CF₃, F).

4.2di Complexation of *meta*-substituted monobenzylimidazolium salts

The reactions of **L4.13-R** with [MCl₂Cp*]₂ (M = Ir, Rh) followed the same procedure (**Scheme 4.14**) as for complexes **4.10a/b-R₁,R₂**. First, **L4.13-R** (R = OMe, CF₃, F) was stirred with Ag₂O in the dark for 1 hour to give **4.14-R**. The reactions were monitored by ¹H NMR spectroscopy and this step was regarded as complete when the signal due to H⁷ had disappeared, at which point, the reactions were filtered through celite to remove the excess of Ag salts, and the resulting filtrate was reacted with [MCl₂Cp*]₂ (M = Ir, Rh) (**Scheme 4.14**) which after work up gave the final complexes **4.13a/b-R** (R = OMe, CF₃, F), which are all new, in moderate to excellent yields (67-92%) (see Chapter 6 for details). Complex **4.13a-OMe** gave crystals suitable for X-ray diffraction which is discussed later.



Scheme 4.14: Synthesis and labelling of **4.13a/b-R**.

The ^1H NMR spectrum of **4.13a-OMe** shows singlets at δ 1.62, 3.78 and 4.00 for Cp*, OMe and Me groups respectively. The benzylic protons H¹ give two mutually coupled doublets at δ 5.22 and 5.93. The aromatic region shows two mutually coupled narrow doublets at δ 6.72 for H^{6a} and 6.90 for H^{6b} which are assigned from the NOE between H^{6b} and the Me group. For the phenyl, four signals are observed between δ 6.84, and 7.25; protons H⁴ and H⁵ show NOEs with the OMe group allowing assignment of all the phenyl protons. The ^1H NMR spectrum of Rh complex **4.13b-OMe** is very similar to the Ir analogue with all the signals within 0.1 ppm of the corresponding signals in **4.13a-OMe**. The ^{13}C NMR spectra for **4.13a-OMe** and **4.13b-OMe** show the expected number of signals with the M-NHC carbons C⁷ at δ 156.9 as a singlet and at δ 170.3 as a doublet ($J_{\text{Rh-C}} = 56.2$ Hz) for Ir and Rh respectively. The HRMS(ESI) show ions at m/z 565.1591 due to $[\text{M-Cl}]^+$ for **4.13a-OMe** and at m/z 475.1016 due to $[\text{M-Cl}]^+$ for **4.13b-OMe**.

The ^1H NMR spectra of **4.13a-CF₃** and **4.13b-CF₃** had the same key features as **4.13a-OMe** and **4.13b-OMe** (see Chapter 6 for details). The ^{19}F NMR spectra for **4.13a-CF₃** and **4.13b-CF₃** show a signal at δ -62.5 for CF₃ for both complexes. The HRMS(ESI) show ions at m/z 603.1360 due to $[\text{M-Cl}]^+$ for **4.13b-CF₃** and at m/z 513.0786 due to $[\text{M-Cl}]^+$ for **4.13b-CF₃**.

The reactions of **L4.13-F** with Ir and Rh gave **4.13a-F** and **4.13b-F** and the ^1H NMR spectra had similar features to the ones discussed above but the phenyl protons show additional coupling to the fluorine substituent (see Chapter 6 for details). The ^{19}F NMR spectra for **4.13a-F** and **4.13b-F** each show a signal at about δ -112.4. The HRMS(ESI) show ions at m/z 553.1394 due to $[\text{M-Cl}]^+$ for **4.13a-F** and at m/z 427.102 due to $[\text{M-HCl}_2]^+$ for **4.13b-F**. Note, the loss of HCl₂ in the HRMS(ESI) spectrum may reflect cyclometallation in the mass spectrometer. The loss of HCl₂ in the HRMS(ESI) spectra for non-cyclometallated benzyl Ir-NHCs has been observed in the literature.⁸

Complex **4.13a-OMe** gave crystals suitable for X-ray diffraction and the structure is shown in **Figure 4.6**. The structure confirms that it is not cyclometallated and shows the expected piano stool geometry. The Ir—C(1) bond distance 2.047(9) Å is statistically the same as for **4.10a-OMe,CF₃** and **4.10a-CF₃,F** [2.058(8) and 2.053(6) Å] (**Table 4.1**) suggesting this distance is not significantly affected by changing the *N*-Me substituent for an *N*-benzyl group one.

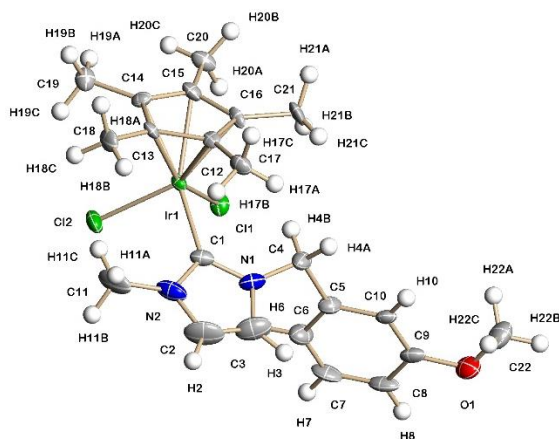
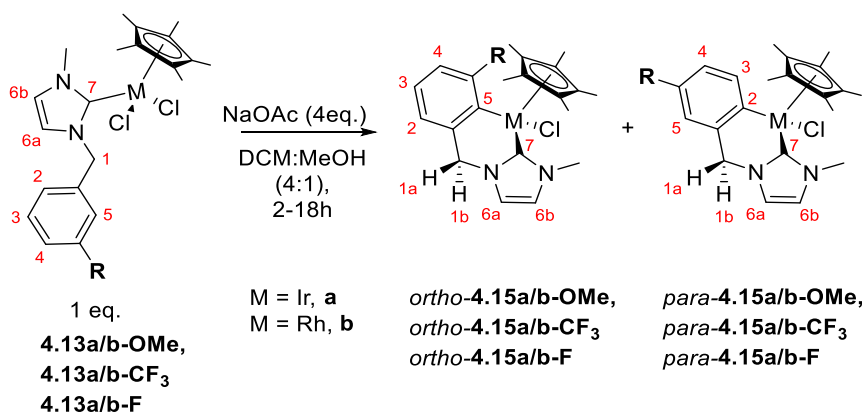


Figure 4.6: X-ray structure of **4.13a-OMe** showing 50% displacement ellipsoids.

4.2dii Cyclometallation of *meta*-substituted monobenzylimidazolium salts

The cyclometallation of **4.13a/b-R** (R = OMe, CF₃, F) in the presence of NaOAc was investigated by stirring in DCM:MeOH (4:1) at room temperature (**Scheme 4.15**). The reaction progression was monitored by ¹H NMR spectroscopy and the mixtures were filtered through celite and precipitated from DCM with hexane to give the final complexes (which are all new) in moderate to excellent yields (68-96%). A brief characterisation of the cyclometallated complexes will be discussed first, followed by a discussion of the ratios from the repeated reactions of **4.13a/b-R** (R = OMe, CF₃, F) with NaOAc in CDCl₃.



Scheme 4.15: Cyclometallation of **4.13a/b-R** (R = OMe, CF₃,F) and their labelling.

The reactions of **4.13a/b-OMe** with NaOAc gave single products in each case. The ¹H NMR spectrum for **4.13a-OMe** shows singlets at δ 1.68, 3.75 and 3.92 for the Cp*, OMe and Me respectively. The benzylic protons give two mutually coupled doublets at δ 4.60

for H^{1b} and 4.84 for H^{1a} with the former showing an NOE with the Cp*. The phenyl ring shows three signals in a pattern that is typical for a *para*-isomer (as observed for *para*-**2.3a/b-R** (R = OMe, CF₃) in Chapter 2, and *para*-**3.18-R** (R = OMe, CN, CF₃) in Chapter 3), a narrow doublet at δ 6.61, a doublet of doublets at δ 6.67 and a doublet at δ 7.47. The signals at δ 6.61 and 6.67 show NOEs with the OMe group and are assigned to H⁵ and H⁴ respectively. For Rh, the ¹H NMR spectrum of the complex also agrees with *para*-**4.15b-OMe**. The ¹³C NMR spectra of *para*-**4.15a-OMe** and *para*-**4.15b-OMe** show the expected number of carbons with C² as a singlet at δ 132.5 and C⁷ as a singlet at δ 157.3 for Ir whilst for Rh C² and C⁷ are doublets at δ 147.8 ($J_{\text{Rh-C}} = 32.1$ Hz) and 175.0 ($J_{\text{Rh-C}} = 55.2$ Hz) respectively. The HRMS(ESI) show ions at m/z 527.1804 due to [M-Cl]⁺ for *para*-**4.15a-OMe** and at m/z 439.1246 due to [M-Cl]⁺ for *para*-**4.15b-OMe**.

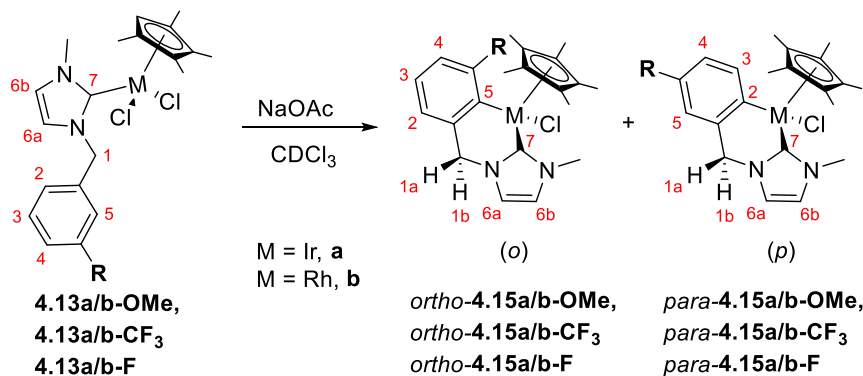
The cyclometallation of **4.13a/b-CF₃** each yielded single products and the ¹H NMR spectra of the complexes agree with *para*-**4.15a/b-CF₃**. (see Chapter 6 for details). The ¹⁹F NMR spectra for *para*-**4.15a/b-CF₃** each show a signal at *ca.* δ -61.5 for CF₃. The HRMS(ESI) show ions at m/z 565.1574 due to [M-Cl]⁺ for *para*-**4.15a-CF₃** and at m/z 477.1025 due to [M-Cl]⁺ for *para*-**4.15b-CF₃**.

The cyclometallation of **4.13a-F** and **4.13b-F** both led to the isolation of isomeric mixtures in a 10:1 ratio for both Ir and Rh. The ¹H-¹⁹F HMBC spectrum for the Rh major isomer shows a correlation between the F and Cp*, indicating that the major isomer is *ortho*-**4.15b-F**. The ¹H NMR spectrum for *ortho*-**4.15b-F**, shows three aryl protons at δ 6.76 for H² and H⁴ and a signal at δ 6.82 for H³. The major isomer for Ir was also identified as *ortho*-**4.15a-F** with the corresponding signals within 0.1 ppm of those of *ortho*-**4.15b-F**. The small proportion of minor isomers and additional complexity due to coupling to fluorine meant that full characterisation of the minor isomers was not possible, however some signals could be assigned to the *para*-isomers (see Chapter 6 for details). The ¹⁹F NMR spectra of *ortho*-**4.15b-F** and *ortho*-**4.15b-F** show signals for fluorine substituents at δ -87.8 and -84.7 respectively and at about δ -125 for *para*-**4.15a/b-F**. The HRMS(ESI) show ions at m/z 517.1631 due to [M-Cl]⁺ for **4.15a-F** and at m/z 427.1049 due to [M-Cl]⁺ for **4.15b-F**.

The steric effects on cyclometallation were then studied in more detail by repeating the reactions of **4.13a/b-R** (R = OMe, CF₃, F) with NaOAc in an NMR tube in CDCl₃. The reactions were monitored by ¹H NMR spectroscopy, conversions and isomer ratios were

determined from signals for H¹ for starting materials **4.13a/b-R** (R = OMe, CF₃, F) and products **4.15a/b-R** and the results are summarised in **Table 4.8**.

Table 4.8: Steric effect studies of cyclometallation of **4.13a/b-R**.



Entry	R	M	1 day, <20% conversion,	10 days, (conversion %),
			<i>o:p</i>	<i>o:p</i>
1	OMe	Ir	1:1	1:10 (95)
2	OMe	Rh	1:1	1:>30(50)
3	CF ₃	Ir	<i>para</i> -only ^a	<i>para</i> -only (33) ^a
4	CF ₃	Rh	<i>para</i> -only ^a	<i>para</i> -only (15) ^a
5	F	Ir	10:1	10:1 (60) ^{c,d}
6	F	Rh	10:1 ^b	9:1 (60) ^{c,d}

^a traces (<1%) of species that could be the *ortho*-isomer were detected by ¹⁹F NMR spectroscopy,

^b 6 hours,

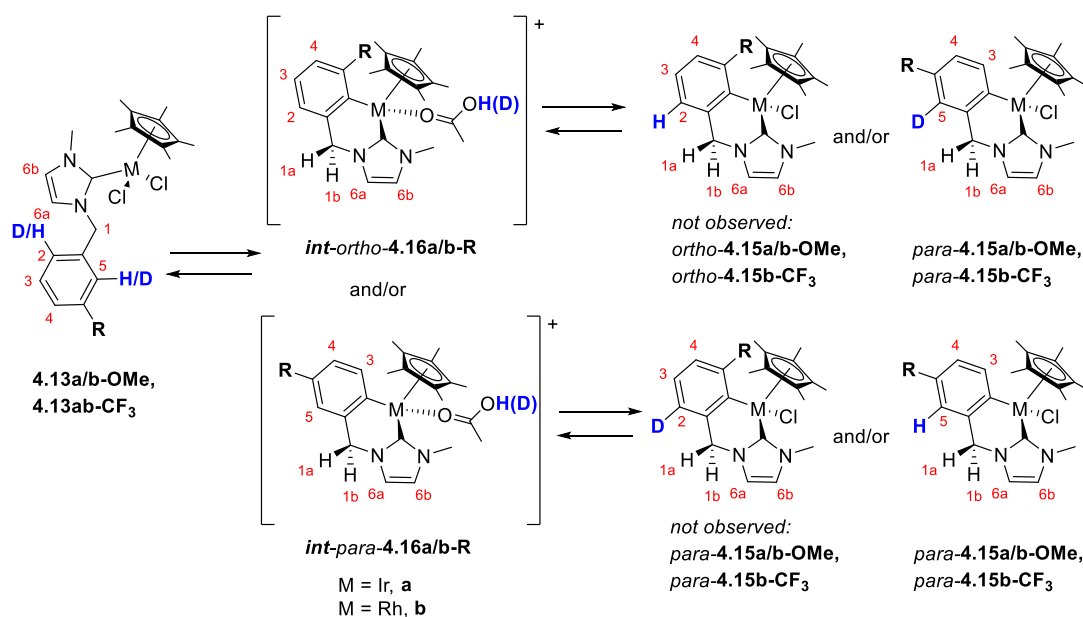
^c 7 days,

^d *o:p* ratio 10:1 after reaching full conversion and heating in DCM:MeOH at 50 °C for 2 days

Reactions in CDCl₃ in the NMR tube were significantly slower compared to reactions in DCM:MeOH taking at least 5 days to reach over 50% conversions for **4.13a/b-R** (R = OMe, F) and for R = CF₃ not even reaching 50% conversion in 10 days. For the cyclometallation of **4.13a-OMe** and **4.13b-OMe** (entries 1 and 2) at low conversions (<20%), the *ortho* and *para*-isomers **4.15a/b-OMe** were observed in 1:1 ratio. As the conversion increased (50% for Rh and 95% for Ir reaction), the ratio between the two isomers increased significantly in favour of the *para*-isomer for both Ir (*ortho:para* 1:10) and Rh which showed only traces of the *ortho*-isomer. These results indicate that the *para*-isomer is favoured thermodynamically, whilst there is almost no kinetic preference

for either *ortho* or *para*. This is consistent with the isolation of only the *para*-isomers **4.15a/b-OMe** from the preparative reactions in DCM:MeOH (4:1) as they both reached high conversions (>80%). In the case of **4.13a-CF₃** and **4.13b-CF₃** all the ¹H NMR spectra irrespective of percentage conversion only showed the *para*-isomer (even when high conversions were reached for preparative reactions). In the absence of further data it is not possible to prove if this is a kinetic and/or thermodynamic preference for the *para*-isomer. The cyclometallations of **4.13a-F** and **4.13b-F** led to the formation of **4.15a/b-F** in 10:1 *ortho:para* ratio for both Ir and Rh, (entries 5 and 6) irrespective of percentage conversion and upon heating. The *ortho*-isomer was favoured due to “ortho effect”^{22, 23, 26} and as the ratios did not change it is unclear whether this selectivity is kinetic and/or thermodynamic in nature.

To get greater insight into the reversibility of the cyclometallation reactions and formation of the *ortho*-isomers, deuteration experiments were carried out with **4.13a-OMe**, **4.13b-OMe**, **4.13b-CF₃** in CD₃OD with NaOAc. As discussed in Chapter 2 for cyclometallation of **L2.3-OMe** with Rh, even if the *ortho*-isomer is not observed/isolated at all it is possible that it has formed in significant proportion. This has been shown to be the case for phenypyrazoles by Alharis.²⁰ As discussed in Chapter 3 (**Section 3.2d**), the reaction can reverse after C–H activation before substitution of acetic acid by chloride which in this case is at intermediate **int-4.16a/b-R** (**Scheme 4.16**) leading to deuterated starting complex **4.13a/b-R** (given that HOAc has undergone H/D exchange with CD₃OD). Alternatively, formed product **4.15a/b-R** can reverse to either intermediate **4.16a/b-R** or even starting complex **4.13a/b-R**. As *ortho*-isomers were not observed above (when R = OMe, CF₃) the D-incorporation is expected at site 5 of the *para*-isomer (or sites 2 and 5 of non-cyclometallated complex **4.13a/b-R**) as shown in **Scheme 4.16** and **Table 4.9**.



Scheme 4.16: D incorporation experiments with **4.13a/b-OMe** and **4.13b-CF₃**.

Table 4.9: Summary of D-incorporation experiments with **4.13a/b-OMe** and **4.13b-CF₃**, overnight at rt.

Entry	R	M	% D-incorporation in <i>para</i> - 4.15a/b-R	% D-incorporation in 4.13a/b-R
1	OMe	Ir	>90	- ^a
2	OMe	Rh	80	> 95 (at both H ² and H ⁵)
3	CF ₃	Rh	N.D.	- ^a

N.D. not detected by ¹H and ²H NMR spectroscopy

^a reactions reached completion

Attempts to follow the cyclometallation reactions by ¹H NMR spectroscopy were made but the signals were broad and unresolved. Therefore, the reactions were left to stand at room temperature in the NMR tube overnight, then solvent was removed and the residue was re-dissolved in CDCl₃. The percentage D-incorporation at position 5 was determined by comparing integrations of signals H¹ and H⁴ with H⁵. The presence of deuterium was confirmed by running a ²H NMR spectrum. For entries 1 and 2, the cyclometallated products *para*-**4.15a/b-OMe** were observed as the major species in the ¹H NMR spectrum, with *ortho*-**4.15a/b-OMe** being present in trace quantities (*ortho:para* 1:>20 for Ir and Rh). A high D-incorporation (>70%) was observed for both *para*-**4.15a-OMe** and *para*-**4.15b-OMe** confirming that formation of the *ortho*-isomer via formation of *int*-

ortho-**4.16a/b-OMe** had occurred but was easily reversible ultimately leading to the formation of the thermodynamically favoured *para*-isomer. Note, cyclometallation of **4.13b-OMe** did not reach completion after overnight with 55% of the mixture being the *para*-**4.15b-OMe** and another 45% of the mixture being the deuterated at sites 2 and 5 of **4.13b-OMe**. No D-incorporation was detected for the cyclometallation of **4.13b-CF₃** (entry 3) suggesting that either the formation of the *ortho*-isomer has a significantly higher activation barrier than formation of the *para*-isomer and/or it is so easily reversible that there is no time for D-exchange.

The regioselectivity is more pronounced compared to the phenyl-NHC complexes **3.18a/b-R** (R = OMe, CN, CF₃, F) discussed in Chapter 3 where some *ortho*-isomer (25 and 14% for Ir and Rh respectively) was observed with R = CF₃ and about 30% *ortho*-isomer was seen for R = OMe with both metals after heating. This could be possibly due to a less sterically hindered metal centre for the five-membered phenyl-NHCs **3.18a/b-R** compared to the six-membered ones **4.15a/b-R**. This is consistent with the longer distance between H of the cyclometallated ring adjacent to the Ir (*ortho*-H, shown in **Figure 4.7**) for the equivalent five-membered complexes **3.12a-R₁,R₂** (Chapter 3) [3.21-3.26 Å] compared to the six membered complexes **4.12a/b-R₁,R₂** [2.97-3.03 Å].

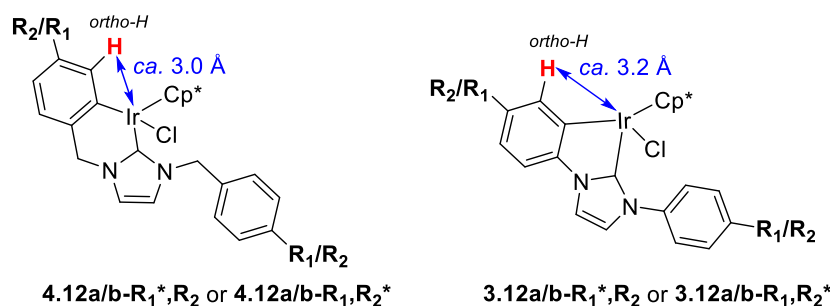


Figure 4.7: Structures of **4.12a/b-R₁^{*},R₂** and **3.12a/b-R₁^{*},R₂** showing *ortho*-H.

4.2e Conclusions

Para-substituted dibenzylimidazolium chlorides **L4.10-R₁,R₂** were prepared and reacted with {IrCp*} and {RhCp*} via transmetalations with Ag giving non-cyclometallated Ir and Rh half-sandwich complexes **4.10a/b-R₁,R₂**. This contrasts with diphenylimidazolium salts **L3.12-R₁,R₂** for which transmetalation from intermediate Ag complexes (**3.13-R₁,R₂**) with {IrCp*} and {RhCp*} lead to cyclometallated complexes

(Chapter 3, section 3.bii). The increased stability of **4.10a/b-R₁,R₂** is due to less favourable formation of a six-membered metallocycle compared to a five-membered metallocycle. Isolated complexes **4.10a/b-R₁,R₂** cyclometallate upon addition of NaOAc to form **4.12a/b-R₁^{*},R₂:4.12a/b-R₁,R₂^{*}**. The ratios of these pairs of complexes allows calculation of the relative rates of acetate-assisted cyclometallation for differently substituted (H, OMe, F, CF₃) complexes (k_R/k_H) under kinetic conditions. Comparison of these results using Hammett and Jaffé plots showed a minor *para* influence of the substituents on the directing group ($\rho_p = 0.2-0.3$) in favour of electron-withdrawing groups, but a more significant *meta* influence on the C–H activation step in favour of more electron-donating groups, $\rho_m = -0.7$ and -0.8 for Ir and Rh respectively (**Figure 4.4**). The magnitude of the slope for the *para* effect for the formation of complexes **4.12a/b-R₁,R₂** is less than that observed for the phenyl-NHCs **3.12a/b-R₁,R₂** ($\rho_p = 1.1$ for Ir and $\rho_p = 1.0$ for Rh) presumably due to loss of conjugation between the NHC and the substituted phenyl in **4.10a/b-R₁,R₂**. The magnitude of the slope for the *meta* effects is rather small ($\rho_m = -0.7$ for Ir and -0.8 for Rh, **Figure 4.4**) so are inconsistent with the S_EAr mechanism (expected slopes -5 to -9),²¹ but are consistent with the AMLA C–H activation occurring via a cationic intermediate. The observed slopes for cyclometallation of **4.10a/b-R₁,R₂** (-0.7 for Ir, -0.8 for Rh) are similar compared to previously observed results for phenylimidazolium salts (-1.6 for Ir, -0.9 for Rh, **Figure 3.6**, Chapter 3) and smaller compared to cyclometallation of phenylpyridines (-1.6 for Ir and -2.1 for Rh, **Figure 2.2**, Chapter 2) and phenylpyrazoles (-2.7 for Ir and -2.4 for Rh).²⁰ Results show that for kinetic selectivity there is little electronic effect on the actual C–H activation step for formation of **4.12a/b-R₁,R₂** (See Chapter 5 for further discussion). As discussed in Chapter 3 the reason for a *para* effect it is unclear and so good fits in Jaffé plots are maybe fortuitous, whilst poor correlation in Hammett plots could be due to the data reflecting some thermodynamic contribution.

Longer reaction times and heating, if necessary with PivOH, led to changes of ratios (**Table 4.5**) in favour of the more electron-withdrawing groups indicating that the reactions are reversible under these conditions and the thermodynamically favoured products are those with more electron-withdrawing groups. The Hammett plot analysis of the thermodynamic ratios (**Figure 4.5**) gave slopes of 2.6 and 2.8 for Ir and Rh respectively both of which are similar in magnitude to the results of the phenyl-NHCs **3.12a/b-R₁,R₂** ($\rho = 2.9$ and 2.8 for Ir and Rh respectively, **Figure 3.7**, Chapter 3) and

bigger in magnitude than those for phenylpyridines ($\rho = 0.6$ and 1.2 for Ir and Rh respectively, **Figure 2.3**, Chapter 3) and phenylpyrazoles ($\rho = 1.6$ and 1.5 for Ir and Rh respectively).²⁰ The preference for more electron-withdrawing groups could be a reflection of the greater M–C bonding in the products and so leading to more thermodynamically stable products.^{20, 22, 23} Note, for more robust conclusions a larger range of substituents with bigger range of $\sigma(p,m)$ should be explored and DFT calculations should be done to provide information on the electronic effects on the transition states. The kinetic selectivity favours electron-donating substituents whilst the thermodynamic selectivity favours electron-withdrawing groups which is consistent with the results for phenylpyridines (Chapter 2), phenyl-NHCs **3.12a/b-R₁,R₂** (Chapter 3) and phenylpyrazoles.²⁰

The steric effects on C–H activation of benzyimidazolium salts were assessed using *meta*-substituted benzyimidazolium salts and their respective Ir and Rh complexes **4.13a/b-R** (R = OMe, CF₃, F). The cyclometallation of **4.13a/b-OMe** resulted in formation of the *ortho* and *para* isomers initially (<20 % conversion) in equal quantities. At high conversions the relative percentages of the *ortho*-isomer diminished with less than 10% being observed for Ir and none for Rh indicating a thermodynamic preference for the *para*-isomer. The reversibility of cyclometallation reactions of **4.13a/b-OMe** and formation of the *ortho*-isomers were confirmed by D-incorporation experiments. For cyclometallation of **4.13a/b-CF₃** none of the *ortho*-isomer could be detected even at low conversions likely due to the bulkier CF₃ group. Therefore, steric effects control regioselectivity with the *para*-isomer being the major one for cyclometallation of **4.13a/b-R** (R = OMe, CF₃). The selectivity for the *para*-isomer observed for the cyclometallation of **4.13a/b-R** is larger compared to the five-membered metallacycle formation with ligands **L3.18-R** (R = OMe, CF₃, Chapter 3). This is possibly caused by the closer proximity of the substituent to the metal centre for the six- compared to the five-membered metallacycles as evident by *ca.* 0.2 Å shorter M (M = Ir, Rh) distance to the *ortho* hydrogen for cyclometallated ring for **4.13a/b-R₁,R₂** compared to **3.12a-R₁,R₂**. For cyclometallation of **4.13a/b-F** the “*ortho* effect”^{22, 23, 26} was observed with substantial selectivity for *ortho*-isomer (>90%) over the *para*-isomer formed for Ir and Rh.

4.3 Bibliography

1. Y. Boutadla, O. Al-Duaij, D. L. Davies, G. A. Griffith and K. Singh, *Organometallics*, 2009, **28**, 433-440.
2. Y. Boutadla, D. L. Davies, R. C. Jones and K. Singh, *Chem. Eur. J.*, 2011, **17**, 3438-3448.
3. L. Li, W. W. Brennessel and W. D. Jones, *Organometallics*, 2009, **28**, 3492-3500.
4. S. Semwal, D. Ghorai and J. Choudhury, *Organometallics*, 2014, **33**, 7118-7124.
5. R. Corberán, M. Sanaú and E. Peris, *J. Am. Chem. Soc.*, 2006, **128**, 3974-3979.
6. R. Corberán, M. Sanaú and E. Peris, *Organometallics*, 2006, **25**, 4002-4008.
7. A. C. Marr, G. C. Saunders, H. P. Thomas and Y.-M. Wang, *Inorg. Chim. Acta*, 2019, **486**, 1-7.
8. S. Gülcemal, D. Gülcemal, G. F. S. Whitehead and J. Xiao, *Chem. Eur. J.*, 2016, **22**, 10513-10522.
9. C. Huerta-Aguilar, J. M. Talamantes Gómez, P. Thangarasu, I. Camacho-Arroyo, A. González-Arenas, J. Narayanan and R. Srivastava, *Appl. Organomet. Chem.*, 2013, **27**, 578-587.
10. S. Patil, J. Claffey, A. Deally, M. Hogan, B. Gleeson, L. M. Menéndez Méndez, H. Müller-Bunz, F. Paradisi and M. Tacke, *Eur. J. Inorg. Chem.*, 2010, **2010**, 1020-1031.
11. G. Lv, L. Guo, L. Qiu, H. Yang, T. Wang, H. Liu and J. Lin, *Dalton Trans.*, 2015, **44**, 7324-7331.
12. N. Jiang, X. Zhai, Y. Zhao, Y. Liu, B. Qi, H. Tao and P. Gong, *Eur. J. Med. Chem.*, 2012, **54**, 534-541.
13. J. C. Y. Lin, R. T. W. Huang, C. S. Lee, A. Bhattacharyya, W. S. Hwang and I. J. B. Lin, *Chem. Rev.*, 2009, **109**, 3561-3598.
14. D. L. Davies, C. E. Ellul, S. A. Macgregor, C. L. McMullin and K. Singh, *J. Am. Chem. Soc.*, 2015, **137**, 9659-9669.
15. D. Lionetti, V. W. Day and J. Blakemore, *Dalton Trans.*, 2019, **48**, 12396-12406.
16. S. Semwal, I. Mukkatt, R. Thenarukandiyil and J. Choudhury, *Chem. Eur. J.*, 2017, **23**, 13051-13057.
17. K. J. T. Carr, D. L. Davies, S. A. Macgregor, K. Singh and B. Villa-Marcos, *Chem. Sci.*, 2014, **5**, 2340-2346.
18. H. H. Jaffé, *J. Am. Chem. Soc.*, 1954, **76**, 4261-4264.
19. L. P. Hammett, *J. Am. Chem. Soc.*, 1937, **59**, 96-103.
20. R. A. Alharis, C. L. McMullin, D. L. Davies, K. Singh and S. A. Macgregor, *J. Am. Chem. Soc.*, 2019, **141**, 8896-8906.
21. J. Clayden, N. Greeves and S. Warren, *Organic Chemistry*, 2nd edn., Oxford: Oxford University Press, Oxford, 2012.
22. E. Clot, M. Besora, F. Maseras, C. Mégret, O. Eisenstein, B. Oelckers and R. N. Perutz, *Chem. Commun.*, 2003, 490-491.
23. E. Clot, C. Mégret, O. Eisenstein and R. N. Perutz, *J. Am. Chem. Soc.*, 2009, **131**, 7817-7827.
24. L. Canovese, F. Visentin, C. Levi, C. Santo and V. Bertolasi, *J. Organomet. Chem.*, 2013, **732**, 27-39.
25. I. Kilpeläinen, H. Xie, A. King, M. Granstrom, S. Heikkinen and D. S. Argyropoulos, *J. Agric. Food. Chem.*, 2007, **55**, 9142-9148.
26. A. D. Selmezy, W. D. Jones, M. G. Partridge and R. N. Perutz, *Organometallics*, 1994, **13**, 522-532.

Chapter Five

5.1 Conclusions and Future Directions for Steric Effects on C–H Activation

This thesis describes studies of steric and electronic effects on the cyclometallation via C–H activation of some *meta*- and *para*-substituted ligands. Intermolecular competition experiments were used with phenylpyridines (Chapter 2) and intramolecular competition experiments with NHC ligands forming five (Chapter 3) and six-membered (Chapter 4) metallocycles at Ir and Rh.

Steric effects were investigated using *meta*-substituted ligands. For phenylpyridine substituted with the bulky R = CF₃, exclusive preference for the less sterically hindered *para*-isomer was observed with both Ir and Rh, with no H/D exchange observed in CD₃OD suggesting that the selectivity is kinetic in origin. For R = OMe the initial kinetic ratio (*o:p* 1:1.3) with Ir showed almost no preference, however after heating the *para*-isomer was favoured (*o:p* 1:2.5) showing that it is thermodynamically preferred. H/D exchange experiments showed that for R = OMe with Rh the reaction starts to equilibrate even at room temperature with the *ortho*-isomer favoured kinetically but with the *para*-isomer (*o:p* 1:3.0) being preferred thermodynamically. For R = F the *ortho*-isomer was favoured (*o:p* 3.4:1 for Ir and 11:1 for Rh) due to the “ortho effect”.¹⁻³ However, no change in ratio was observed upon heating for both Ir and Rh so it is not clear if this preference is kinetic or thermodynamic or both, as was found for phenylpyrazoles.⁴

For phenyl NHCs substituted with less sterically bulky groups (R = OMe, CN) there was a small kinetic preference for the *para*-isomer (*o:p* 1:≤1.5) with Ir or Rh; however, as with phenylpyridines, the *para*-isomers were favoured (*o:p* 1:≥2.0) thermodynamically. The ligand with R = CF₃ showed a moderate kinetic preference for the *para*-isomers over the *ortho*-isomers (*o:p* 1:3 ratios for Ir and *o:p* 1:6 Rh), with the thermodynamic preference for the *para*-isomer being even greater (<5% of the *ortho*-isomer). Again with R = F the *ortho*-isomer is favoured kinetically for both Ir and Rh (*o:p* 2.2:1 for Ir and 6.0:1 for Rh), and as preference for the *ortho*-isomer increased further upon heating for Rh (*o:p* 10:1) indicating that it was also favoured thermodynamically. However, no change in ratio was observed with Ir and so it is not proven that the *ortho*-isomer is also favoured thermodynamically.

For the benzyl NHCs for R = OMe the *ortho-para* ratio was 1:1 for both Ir and Rh at early conversions (<20%) indicating that there is no kinetic preference for either isomer. However, thermodynamically, high selectivity for formation of the *para*-isomers (<10% of the *ortho*-isomer) was observed. For R = CF₃ only the *para*-isomer was observed at early conversions (< 15%) and when reaction reached completion for both metals. For R = F the *ortho*-isomer was substantially favoured (*o:p* 10:1 for both Ir and Rh) kinetically with both metals (conversions <20%) but as these ratios did not change upon heating, it is not clear if they were favoured thermodynamically as well.

When comparing five-membered phenylNHC complexes with six-membered benzylNHC complexes, the *ortho-para*-selectivity for five-membered complexes was found to be less pronounced (smaller ratios), likely due to less steric encumbrance at the metal centre. To conclude, steric factors are important both kinetically and thermodynamically. The kinetic selectivity shows a slight preference for the *para*-isomer for smaller groups (except for R = F which favour the *ortho*-isomers) whilst for bulkier R = CF₃ the *para*-isomer is preferred. Additionally, thermodynamic selectivity favours the *para*-isomers, except when R = F which favour the *ortho*-isomers. In general, the results are similar to those observed with phenylpyrazoles⁴ and phenylimines.⁵

In the future, a wider range of R groups such as CN, Me, NMe₂ could be studied to gain a further insight into the overall selectivity. Additionally, other NHC precursors with larger ring sizes i.e. ring-expanded NHCs (examples of which are shown in **Figure 5.1**) could be utilised. One of the key features of the ring-expanded NHCs is a wider N-C-N angle compared to the five-membered NHCs.⁶⁻⁸ This results in N-substituted wingtips being pushed more toward the metal, therefore, these could be interesting ligands to investigate the steric effects on cyclometallation, due to changed proximity of the substituent to the metal centre and possibly the conformation of the metal complex.

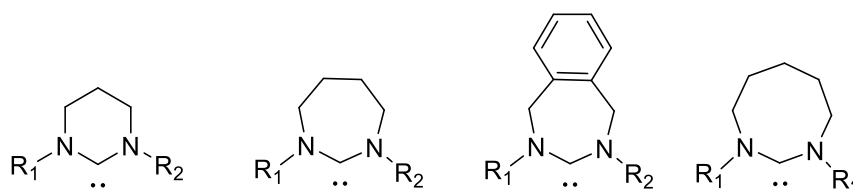


Figure 5.1: Examples of ring-expanded NHCs.⁶⁻⁸

5.2 Conclusions and Future Directions for Electronic Effects on C–H Activation

Electronic effects were assessed by employing *para*-substituted phenylpyridines, diphenylimidazolium salts and dibenzylimidazolium salts. Chapter two described the intermolecular competition experiments of *para*-substituted phenylpyridines with Ir and Rh and showed that kinetically, substrates with electron-donating groups reacted faster ($\rho = -1.6$ and -2.1 for Ir and Rh respectively). However, the thermodynamic selectivity was opposite, favouring substrates with electron-withdrawing groups ($\rho = 0.6$ for Ir,⁹ $\rho = 1.2$ for Rh). This change in selectivity is in agreement with the results reported for similar experiments with phenylpyrazoles.⁴ As these competition experiments were intermolecular, the overall selectivity observed for phenylpyridines is for the whole cyclometallation process and not just the C–H activation step with ligand binding being a component. Therefore, Chapter three and four explored intramolecular competition experiments in an attempt to study just the C–H activation step, because the ligand binding step should be the exactly the same for both competing arenes.

Chapter three showed that because the formation of five-membered metallacycles with phenylimidazolium salts is relatively easy, finding conditions that allow observation of the kinetic selectivity for their reactions is difficult. The results in Chapter three showed that at room temperature there is no correlation in the Hammett plot between the ratios observed and σ_m values, however, a Jaffé analysis suggested that this could be due to a very similar in magnitude *meta* effect (on the actual C–H activation step) ($\rho_m = -1.6$ and -0.9 for Ir and Rh respectively) and *para* effect (on the directing group) ($\rho_p = 1.1$ and 1.0 for Ir and Rh respectively). The *meta* effect favours electron-donating groups consistent with AMLA C–H activation taking place via a cationic intermediate. However the *para* effect favours electron-withdrawing groups suggesting that removal of electron density from the imidazole ring promotes the reaction. It is not clear why this may be and without further detailed DFT calculations it is not possible to explain this phenomenon. The lack of a clear Hammett correlation and the low electronic sensitivity as judged by the Jaffé analysis all point to cyclometallation not taking place via S_EAr . However, the failure to stop at the NHC bound species before cyclometallation leaves some doubt as to whether these data are purely “kinetic” in origin (see below for further discussion). Thermodynamic selectivity for cyclometallation of diphenylimidazolium salts at both Ir and Rh favours more electron-withdrawing groups ($\rho = 2.9$ for Ir, $\rho = 2.8$ for Rh) which

could be due to stronger M–C bonds in these complexes.⁴ Qualitatively, DFT calculations showed good agreement with experimental results, correctly predicting at which ring cyclometallation is favoured, except for pairs OMe,H and Me,OMe (appendix, **Table S6**) for which the calculated differences in TS energies and final energies are less than 0.3 kcal mol⁻¹. These calculations also demonstrated that the exchange of acetic acid by chloride, which occurs after the C–H activation step, becomes competitive with the phenyl C–H activation step. Hence, in some cases there may be some equilibration between cyclometallation at the two differently substituted rings prior to final product formation by exchange with chloride, leading to a lower selectivity (isomer ratio) than might be expected on the basis of the relative TS energies of just the C–H activation step alone. In these cases the actual meaning of “kinetic” selectivity is less clear since both C–H activation and acetic acid loss affect the overall rate.

The increase in ring size from five to six-membered complexes (Chapter four) by employing dibenzylimidazolium salts allowed isolation of non-cyclometallated Ir and Rh intermediates whose cyclometallation was then studied upon addition of NaOAc. The kinetic selectivity was shown to be small for both Ir and Rh with little electronic effects (no ratio bigger than 1:1.5 for the two isomers). Jaffé analysis again showed a very small *para* effect ($\rho_p = 0.3$ for Ir and Rh) in favour of electron-withdrawing groups, with a slightly bigger *meta* effect ($\rho_m = -0.7$ and -0.8 for Ir and Rh respectively) in favour of electron-donating substituents. The low electronic selectivity for the six-membered species further corroborates the fact that the reactions do not take place via S_EAr mechanism but is consistent with an AMLA C–H activation mechanism. The thermodynamic selectivity was consistent with previous results and in favour of electron-withdrawing substituents ($\rho = 2.6$ for Ir, $\rho = 2.8$ for Rh). Overall, for six-membered complexes the non-cyclometallated intermediates were isolated, however, they showed a small electronic effect indicating that change in ring size has not had a large effect on the degree of electronic selectivity.

The overall magnitude of electronic effect on kinetic selectivity (based on Hammett/Jaffé plot slopes) for Ir and Rh follows the order phenylpyrazoles > phenylpyridines > phenylNHCs \approx benzylNHCs. The overall cyclometallation of the ligands takes place via four key steps: (i) ligand binding, (ii) loss of acetate to give a cation (iii) AMLA C–H activation and finally (iv) exchange of acetic acid with chloride to form the final

complex.⁴ The overall electronic effects observed are a combination of all of these steps for intermolecular competition reactions with phenylpyridines and a combination of steps (iii) and (iv) for the intramolecular competition reactions with diphenyl and dibenzylimidazolium salts. Increasing strength of the donor group should promote the ligand binding, anion exchange and acetic acid substitution steps and hence decrease the overall barrier to cyclometallation. This reduced barrier may mean that the variations with substituent are also reduced leading to less electronic sensitivity for better donor ligands. Consistent with this, phenylpyrazole being the weakest donor group out of all those studied shows the biggest electronic effects. On the other hand, the NHCs with the highest donor strength show relatively small electronic sensitivity. Overall, multiple factors contribute to the electronic selectivity observed and these vary between the systems.

The range of substituent Hammett parameter σ in this study was somewhat restricted for ease of measurement as formation of diarylNHC complexes substituted at the *para*-position would make measurements more challenging, however, using *meta*-substituted NHCs would allow a wider range of σ values and perhaps allow clearer trends. As it is likely that increasing the donor strength of the directing group leads to diminished electronic effects these could be studied using a weaker directing group than NHCs, for example, 2,6-diphenylpyridines could be a useful candidate (**Figure 5.2 A**). However, attempts to make unsymmetrical differently substituted 2,6-diphenylpyridines proved to be challenging.¹⁰ Notably, all of the C–H activation processes studied here involved a neutral ligand, whereby C–H activation takes place via a cationic intermediate. If an anionic directing group were used (examples of which are shown in **Figure 5.2 B, C**) then the C–H activation step may occur at a neutral complex (as shown in Chapter 1 **Figure 1.13**). Under these conditions it is possible that the kinetic electronic selectivity may favour electron-withdrawing groups in contrast to the electron-donating groups favoured in this study.

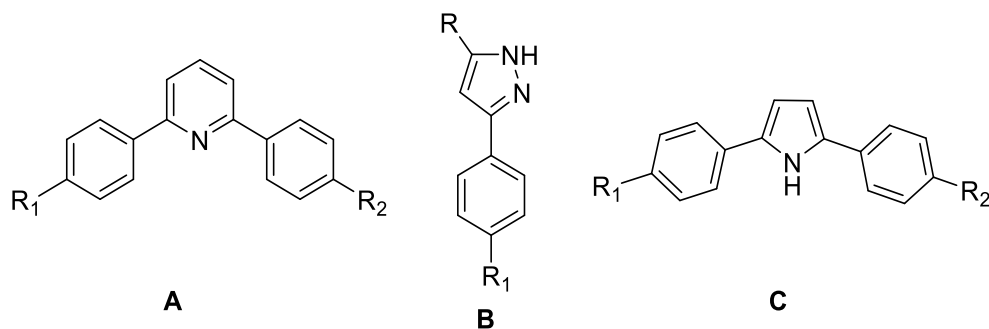


Figure 5.2: Potential ligands to study electronic effects on C–H activation.

5.3 Overall Conclusions

As suggested previously by Fagnou¹¹ and independently by Davies and Macgregor,¹² AMLA and CMD are essentially the same. It is also likely that given the similarity in the transition states BIES¹³ is also the same. Whether a particular reaction favours electron-donating or withdrawing groups will depend on the nature of the directing group, if there is one, and on the overall charge on the catalyst before the C–H activation step (i.e. neutral as for some Pd(II) examples, or cationic as described in this thesis) and on the reaction conditions (i.e. whether it is under kinetic or thermodynamic control). Furthermore, it should be borne in mind that if the electronic data is measured in a catalytic process it is vital to prove that C–H activation is the rds. This study has confirmed that the electronic selectivity should not be used on its own to determine the mechanism of the C–H activation, because different conditions can lead to different electronic preferences, even for the same reactions.

5.4 Bibliography

1. E. Clot, M. Besora, F. Maseras, C. Mégret, O. Eisenstein, B. Oelckers and R. N. Perutz, *Chem. Commun.*, 2003, 490-491.
2. E. Clot, C. Mégret, O. Eisenstein and R. N. Perutz, *J. Am. Chem. Soc.*, 2009, **131**, 7817-7827.
3. A. D. Selmecky, W. D. Jones, M. G. Partridge and R. N. Perutz, *Organometallics*, 1994, **13**, 522-532.
4. R. A. Alharis, C. L. McMullin, D. L. Davies, K. Singh and S. A. Macgregor, *J. Am. Chem. Soc.*, 2019, **141**, 8896-8906.
5. L. Li, W. W. Brennessel and W. D. Jones, *Organometallics*, 2009, **28**, 3492-3500.
6. M. J. Page, W. Y. Lu, R. C. Poulten, E. Carter, A. G. Algarra, B. M. Kariuki, S. A. Macgregor, M. F. Mahon, K. J. Cavell, D. M. Murphy and M. K. Whittlesey, *Chem. Eur. J.*, 2013, **19**, 2158-2167.
7. J. W. Hall, D. M. L. Unson, P. Brunel, L. R. Collins, M. K. Cybulski, M. F. Mahon and M. K. Whittlesey, *Organometallics*, 2018, **37**, 3102-3110.
8. N. Phillips, R. Tirfoin and S. Aldridge, *Chem. Eur. J.*, 2014, **20**, 3825-3830.
9. The reactions with Ir have not reached thermodynamic equilibrium
10. Unpublished results
11. L. David and F. Keith, *Chem. Lett.*, 2010, **39**, 1118-1126.
12. D. L. Davies, S. A. Macgregor and C. L. McMullin, *Chem. Rev.*, 2017, **117**, 8649-8709.
13. W. Ma, R. Mei, G. Tenti and L. Ackermann, *Chem. Eur. J.*, 2014, **20**, 15248-15251.

Chapter Six

6.1 General information and materials

1D and 2D NMR spectra were recorded on a Bruker DRX400 or AV400 spectrometer operating at 400 (^1H), 376 (^{19}F) and 100 MHz (^{13}C) or Bruker DRX500 spectrometer at 500 (^1H) and 125 MHz (^{13}C) at ambient temperature. ^2H NMR spectra were recorded on a Bruker AV400 spectrometer 61 MHz. Chemical shifts were recorded in ppm and are referred to the residual protic solvent peaks, and coupling constants are expressed in Hertz (Hz). Assignments of ^1H NMR and ^{13}C NMR were made where possible, using COSY, TOCSY, NOESY, HSQC and HMBC experiments.

The electrospray (ESI) mass spectra were recorded using a micromass Quattro LC mass spectrometer in HPLC grade acetonitrile. Mass accuracy was carried out by Mr Mick Lee and Dr Sharad Mistry by using a reference lock mass scan, once every 10 seconds in ESI mode. For the imidazolium salts **L3.12-R₁,R₂**, **L3.18-R**, **L4.10-R₁,R₂** and **L4.13-R** the HRMS (ESI) given ion $[\text{M}]^+$ corresponds to the imidazolium cation in each case.

X-ray diffraction of single crystals was performed by Mr. Kuldip Singh at the University of Leicester using a Bruker APEX 2000 CCD diffractometer. The data were corrected for Lorentz and polarisation effects and empirical absorption corrections applied. Structure solution by direct methods and structure refinement were based on full-matrix least-squares on F^2 employed SHELXTL version 6.10.1. Hydrogen atoms were included in calculated positions ($\text{C-H} = 0.96 - 1.00 \text{ \AA}$) riding on the bonded atom with isotropic displacement parameters set to $1.5 U_{\text{eq}}(\text{C})$ for methyl H atoms and $1.2 U_{\text{eq}}(\text{C})$ for all other H atoms. All non-H atoms were refined with anisotropic displacement parameters.

Elemental analysis (combustion analysis) of carbon, hydrogen, and nitrogen was performed on dry, clean and microcrystalline products at the Science Technical Support Unit, London Metropolitan University.

All starting materials were acquired from the commercial sources and were used without purification unless specified otherwise. $[\text{IrCl}_2\text{Cp}^*]_2$ and $[\text{RhCl}_2\text{Cp}^*]_2$ were prepared according to the literature procedure.¹ *p*-(dimethylamino)phenyl and *m*-fluorophenyl boronic acids were prepared following a literature procedure.²

6.2 Experimental procedures for Chapter 2

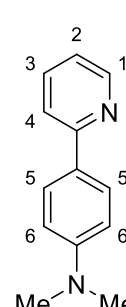
6.2a Synthesis of *para* and *meta*-substituted phenylpyridines

General procedure for preparation of *para*-(L2.6-R) and *meta*-(L2.3-R) substituted phenylpyridines

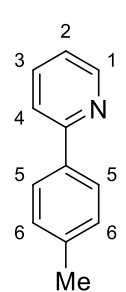
para- and *meta*-Substituted phenylpyridines were prepared following literature procedures.^{3,4} A Schlenk flask was charged with magnetic stirrer bar, 2-bromopyridine (1 eq.), appropriate boronic acid (1.5 eq.), base (2 eq.), Pd(OAc)₂ (1.5 mol%), ⁱPrOH (8 mL), H₂O (8 mL) and heated to 80 °C whilst vigorously stirring to ensure even mixing of the two layers for 1 h. The solvent was concentrated on a rotary evaporator, the resulting oil/solid dissolved in DCM (50 mL), filtered through celite, concentrated on a rotary evaporator and purified by column chromatography.

Preparation of *para*-(L2.6-R) substituted phenylpyridines

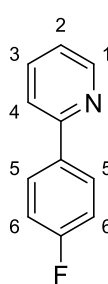
L2.6-NMe₂

 Purification by column chromatography (EtOAc:Pet.Ether 2:8, on Biotage Isolera) yielded **L2.6-NMe₂** as an off-white powder (350 mg, 68%). ¹H NMR (500 MHz, CDCl₃): δ 3.05 (s, 6H, NMe₂), 6.80 (d, *J* = 8.9 Hz, 2H, *H*⁶), 7.11 (ddd, *J* = 6.8, 5.0, 1.6 Hz, 1H, *H*²), 7.66 (m, 2H, *H*³, *H*⁴), 7.92 (d, *J* = 8.9 Hz, 2H, *H*⁵), 8.62 (dt, *J* = 4.5, 1.4 Hz, 1H, *H*¹), ¹³C{¹H} NMR (126 MHz, CDCl₃): δ 40.4 (NMe₂), 112.2 (*C*⁶), 119.2 (*C*⁴), 120.6 (*C*²), 127.0, 127.7 (*C*⁵), 136.6 (*C*³), 149.2 (*C*¹), 151.1, 157.5. ESIMS: *m/z* 199 [M+H]⁺. Data agrees with the literature.⁵

L2.6-Me

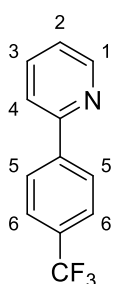
 Purification by column chromatography (EtOAc:Pet.Ether 1:9, on Biotage Isolera) yielded **L2.6-Me** as a colourless oil (334 mg, 78%). ¹H NMR (400 MHz, CDCl₃): δ 2.40 (s, 3H, Me), 7.18 (ddd, *J* = 6.5, 4.6, 2.2 Hz, 1H, *H*²), 7.27 (d, *J* = 8.0 Hz, 2H, *H*⁶), 7.64 - 7.76 (m, 2H, *H*³, *H*⁴), 7.89 (d, *J* = 8.2 Hz, 2H, *H*⁵), 8.67 (dt, *J* = 4.7, 1.5 Hz, 1H, *H*¹), ¹³C{¹H} NMR (126 MHz, CDCl₃): δ 21.2 (Me), 120.2 (*C*²), 121.8 (*C*⁴), 126.8 (*C*⁵), 129.5 (*C*⁶), 136.6 (*C*³), 136.6, 138.9, 149.5 (*C*¹), 157.47. ESIMS: *m/z* 170 [M+H]⁺. Data agrees with the literature.³

L2.6-F



Purification by column chromatography (EtOAc:Pet.Ether 1:9, on Biotage Isolera) yielded **L2.6-F** as a colourless oil (310 mg, 70%). $^1\text{H NMR}$ (400 MHz, CDCl_3): δ 7.16 (t, $J = 8.7$ Hz, 2 H, H^6), 7.22 (ddd, $J = 7.4, 4.8, 1.3$ Hz, 1H, H^2), 7.68 (m, 1H, H^4), 7.74 (m, 1H, H^3), 7.98 (m, 2H, H^5), 8.68 (dd, $J = 4.0, 0.7$ Hz, 1H, H^1), $^{13}\text{C}\{^1\text{H}\}$ NMR (126 MHz, CDCl_3): δ 115.6 (d, $^2J_{\text{C-F}} = 21.1$ Hz, C^6), 120.2 (C^4), 122.0 (C^2), 128.7 (d, $^3J_{\text{C-F}} = 8.0$ Hz, C^5), 135.5 (d, $^4J_{\text{C-F}} = 2.0$ Hz), 136.8 (C^3), 149.7 (C^1), 156.5, 163.5 (d, $^1J_{\text{C-F}} = 249.0$ Hz, C-F), $^{19}\text{F}\{^1\text{H}\}$ NMR (376 MHz, CDCl_3): δ -113.2 (F). ESIMS: m/z 174 $[\text{M}+\text{H}]^+$. Data agrees with the literature.³

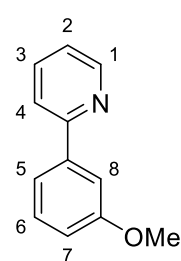
L2.6-CF₃



Purification by column chromatography (EtOAc:Pet.Ether 2:8) yielded **L2.6-CF₃** as a white powder (340 mg, 61%). $^1\text{H NMR}$ (400 MHz, CDCl_3): δ 7.30 (ddd, $J = 6.9, 5.0, 1.6$ Hz, 1H, H^2), 7.71 - 7.80 (m, 4H, H^3, H^4, H^6), 8.10 (d, $J = 8.2$ Hz, 2H, H^5), 8.72 (d, $J = 4.6$ Hz, 1H, H^1), $^{13}\text{C}\{^1\text{H}\}$ NMR (126 MHz, CDCl_3): δ 120.8 (C^4), 122.9 (C^2), 124.2 (d, $^1J_{\text{C-F}} = 272.0$ Hz, CF_3), 125.6 (q, $^3J_{\text{C-F}} = 4.0$ Hz, C^6), 127.1 (C^5), 130.8 (q, $^2J_{\text{C-F}} = 32.1$ Hz, C- CF_3), 136.9, 142.6, 149.9 (C^1), 155.8, $^{19}\text{F}\{^1\text{H}\}$ NMR (376 MHz, CDCl_3): δ -62.6 (CF_3). ESIMS: m/z 224 $[\text{M}+\text{H}]^+$. Data agrees with the literature.⁵

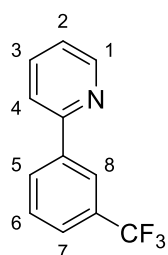
Preparation of *meta*-(L2.3-R) substituted phenylpyridines

L2.3-OMe



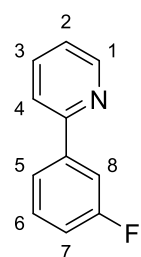
Purification by column chromatography (EtOAc:Pet.Ether 1:9, on Biotage Isolera) yielded **L2.3-OMe** as a colourless oil (384 mg, 82%). $^1\text{H NMR}$ (400 MHz, CDCl_3): δ 3.90 (s, 3H, OMe), 6.97 (ddd, $J = 8.2, 2.6, 1.0$ Hz, 1H, H^7), 7.23 (ddd, $J = 6.7, 4.8, 2.0$ Hz, 1H, H^2), 7.38 (t, $J = 7.9$ Hz, 1H, H^6), 7.55 (dt, $J = 7.6, 1.3$ Hz, 1H, H^5), 7.59 (dd, $J = 2.5, 1.6$ Hz, 1H, H^8), 7.69 - 7.78 (m, 2H, H^3, H^4), 8.69 (dt, $J = 4.8, 1.4$ Hz, 1H, H^1), $^{13}\text{C}\{^1\text{H}\}$ NMR (126 MHz, CDCl_3): δ 55.3 (OMe), 112.0 (C^8), 115.0 (C^7), 119.3 (C^5), 120.7 (C^4), 122.2 (C^2), 129.7 (C^6), 136.7 (C^3), 140.8, 149.6 (C^1), 157.2, 160.0. ESIMS: m/z 186 $[\text{M}+\text{H}]^+$. Data agrees with the literature.⁶

L2.3-CF₃



Purification by column chromatography (EtOAc:Pet.Ether 1:9) yielded **L2.3-CF₃** as a white powder (261 mg, 45%). ¹H NMR (400 MHz, CDCl₃): δ 7.29 (ddd, *J* = 6.8, 4.9, 1.8 Hz, 1H, *H*²), 7.60 (t, *J* = 7.7 Hz, 1H, *H*⁶), 7.67 (d, *J* = 7.6 Hz, 1H, *H*⁷), 7.74 - 7.87 (m, 2H, *H*³, *H*⁴), 8.18 (d, *J* = 7.8 Hz, 1H, *H*⁸), 8.29 (br. s, 1H, *H*⁸), 8.73 (dt, *J* = 4.7, 1.4 Hz, 1H, *H*¹), ¹³C{¹H} NMR (126 MHz, CDCl₃): δ 120.6 (*C*⁴), 122.8 (*C*²), 123.8 (q, ³*J*_{C-F} = 4.0 Hz, *C*⁸), 123.8 (q, ¹*J*_{C-F} = 273.1 Hz, CF₃), 125.5 (q, ³*J*_{C-F} = 4.0 Hz, *C*⁷), 129.2 (*C*⁵), 130.1 (*C*⁶), 131.2 (q, ²*J*_{C-F} = 32.1 Hz, C-CF₃), 137.0 (*C*³), 140.1, 149.9 (*C*¹), 155.9, ¹⁹F{¹H} NMR (376 MHz, CDCl₃): δ -62.6 (CF₃). ESIMS: *m/z* 224 [M+H]⁺. Data agrees with the literature.⁶

L2.3-F



Purification by column chromatography (EtOAc:Pet.Ether 2:8, on Biotage Isolera) yielded **L2.3-F** as a colourless oil (200 mg, 45%). ¹H NMR (400 MHz, CDCl₃): δ 7.11 (tdd, *J* = 8.4, 8.4, 2.6, 0.9 Hz, 1H, *H*⁷), 7.26 (m, 1H, *H*²), 7.43 (td, *J* = 8.0, 6.0 Hz, 1H, *H*⁶), 7.67 - 7.83 (m, 4H, *H*³, *H*⁴, *H*⁵, *H*⁸), 8.70 (ddd, *J* = 4.8, 1.6, 0.9 Hz, 1H, *H*¹), ¹³C{¹H} NMR (126 MHz, CDCl₃): δ 113.8 (d, ²*J*_{C-F} = 23.1 Hz, *C*⁸), 115.8 (d, ²*J*_{C-F} = 21.1 Hz, *C*⁷), 120.6 (*C*⁴), 122.4 (d, ⁴*J*_{C-F} = 2.0 Hz, *C*⁵), 122.6 (*C*²), 130.2 (d, ³*J*_{C-F} = 8.0 Hz, *C*⁶), 136.9 (*C*³), 141.7 (d, ³*J*_{C-F} = 7.0 Hz), 149.7 (*C*¹), 156.0 (d, ⁴*J*_{C-F} = 2.0 Hz), 163.3 (d, ¹*J*_{C-F} = 245.9 Hz, C-F), ¹⁹F{¹H} NMR (376 MHz, CDCl₃): δ -112.9 (*F*). ESIMS: *m/z* 174 [M+H]⁺. Data agrees with the literature.⁶

6.2b Cyclometallation of *para*-substituted phenylpyridines **L2.6-R** with {IrCp*} and {RhCp*}

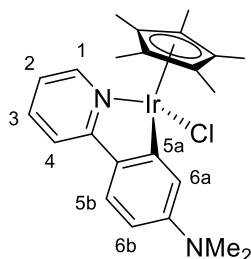
General procedure for cyclometallation of *para*-phenylpyridines **L2.6-R** with {IrCp*} and {RhCp*}

A Schlenk flask was charged with [MCl₂Cp*]₂ (M = Ir, Rh) (1 eq.), NaOAc (4 eq.) and magnetic stirrer bar, capped, evacuated for 15 mins, then purged with N₂ three times. Dry DCM:MeOH mixture (4:1) (when M = Ir) or dry MeOH (when M = Rh) was added and the solution stirred at rt for 15 mins, followed by addition of an appropriate substituted phenylpyridine **L2.6-R** (2.1 eq.). The mixture was stirred for 1 h to overnight before

being filtered through celite and the solvent removed by rotary evaporation. Pure products were obtained by precipitation from DCM/hexane mixture.

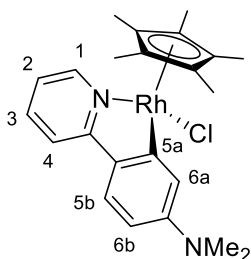
Cyclometallation of *para*-phenylpyridines **L2.6-R** with {IrCp*} and {RhCp*}

2.6a-NMe₂



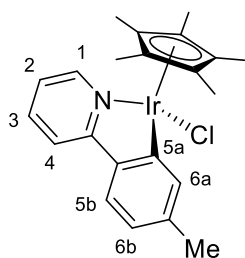
Following the general procedure, a mixture of [IrCl₂Cp*]₂ (20 mg, 0.025 mmol), **L2.6-NMe₂** (10 mg, 0.051 mmol) and NaOAc (8 mg, 0.100 mmol) in dry DCM (1.6 mL) and dry MeOH (0.4 mL) was stirred at rt for 1.5 h. The product was precipitated from DCM/hexane mixture to give **2.6a-NMe₂** as a yellow powder (25 mg, 89%). ¹H NMR (400 MHz, CDCl₃): δ 1.68 (s, 15H, C₅Me₅), 3.08 (s, 6H, NMe₂), 6.46 (dd, *J* = 8.5, 1.7 Hz, 1H, H^{6b}), 6.86 (m, 1H, H²), 7.16 (br s, 1H, H^{6a}), 7.46 - 7.55 (m, 2H, H³, H^{5:b}), 7.57 (d, *J* = 8.1 Hz, 1H, H⁴), 8.55 (d, *J* = 5.6 Hz, 1H, H¹), ¹³C{¹H} NMR (101 MHz, CDCl₃): δ 8.9 (C₅Me₅), 40.4 (NMe₂), 88.1 (C₅Me₅), 107.0 (C^{6b}), 117.4 (C⁴), 118.3 (C^{6a}), 119.7 (C²), 125.0 (C^{5b}), 133.0, 136.3 (C³), 150.8 (C¹), 152.0, 164.8 (C^{5a}), 167.4. ESIMS: *m/z* 525 [M-Cl]⁺. HRMS (ESI): Calcd for C₂₃H₂₈N₂¹⁹³Ir [M-Cl]⁺ 525.1882, found 525.1880. The data agrees with the literature.⁷

2.6b-NMe₂



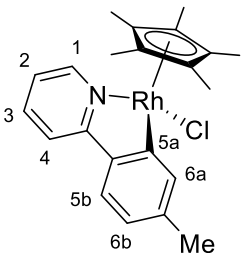
Following the general procedure, a mixture of [RhCl₂Cp*]₂ (41 mg, 0.066 mmol), **L2.6-NMe₂** (29 mg, 0.145 mmol) and NaOAc (14 mg, 0.170 mmol) in dry MeOH (6 mL) was stirred at rt overnight. The product was crystallised from DCM/hexane mixture to yield **2.6b-NMe₂** as red - orange crystals (33 mg, 53%). ¹H NMR (400 MHz, CDCl₃): δ 1.63 (s, 15H, C₅Me₅), 3.08 (s, 6H, NMe₂), 6.44 (dd, *J* = 8.6, 2.5 Hz, 1H, H^{6b}), 6.92 (ddd, *J* = 6.9, 5.5, 1.9 Hz, 1H, H²), 7.15 (d, *J* = 2.5 Hz, 1H, H^{6a}), 7.46 (d, *J* = 8.6 Hz, 1H, H^{5b}), 7.53 (ddd, *J* = 8.4, 4.0, 0.6 Hz, 1H, H⁴), 7.56 (ddd, *J* = 8.2, 6.9, 1.6 Hz, 1H, H³), 8.59 (dd, *J* = 5.3, 1.2 Hz, 1H, H¹), ¹³C{¹H} NMR (126 MHz, CDCl₃): δ 9.2 (C₅Me₅), 40.4 (NMe₂), 95.6 (d, ¹*J*_{C-Rh} = 6.0 Hz, C₅Me₅), 107.7 (C^{6b}), 117.5 (C⁴), 119.1 (C^{6a}), 119.5 (C²), 124.3 (C^{5b}), 132.6, 136.4 (C³), 150.9 (C¹), 151.4, 165.7, 180.2 (d, ¹*J*_{C-Rh} = 31.1 Hz, C^{5a}). ESIMS: *m/z* 476 [M-Cl+MeCN]⁺. HRMS (ESI): Calcd for C₂₅H₃₁N₃¹⁰³Rh [M-Cl+MeCN]⁺ 476.1572, found 476.1569.

2.6a-Me



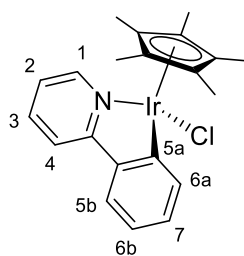
Following the general procedure, a mixture of $[\text{IrCl}_2\text{Cp}^*]_2$ (20 mg, 0.025 mmol), **L2.6-Me** (9 mg, 0.054 mmol) and NaOAc (9 mg, 0.110 mmol) in dry DCM (4 mL) and dry MeOH (1 mL) was stirred at rt for 3 h. The product was precipitated from DCM/hexane mixture to yield **2.6a-Me** as a yellow powder (24 mg, 90%). ^1H NMR (400 MHz, CDCl_3): δ 1.68 (s, 15H, C_5Me_5), 2.41 (s, 3H, *Me*), 6.85 (dd, $J = 7.9, 1.1$ Hz, 1H, H^{6b}), 7.02 (ddd, $J = 7.2, 5.9, 1.4$ Hz, 1H, H^3), 7.56 (d, $J = 7.8$ Hz, 1H, H^{5b}), 7.59 - 7.66 (m, 2H, H^3, H^{6a}), 7.75 (d, $J = 8.0$ Hz, 1H, H^4), 8.66 (dt, $J = 5.2, 1.0$ Hz, 1H, H^1), $^{13}\text{C}\{^1\text{H}\}$ NMR (126 MHz, CDCl_3): δ 8.9 (C_5Me_5), 21.8 (*Me*), 88.4 (C_5Me_5), 118.5 (C^4), 121.7 (C^2), 123.2 (C^{6b}), 123.6 (C^{5a}), 136.4 (C^3), 136.8 (C^{6a}), 140.7, 141.5, 151.2 (C^1), 163.3 (C^{5a}), 167.4. ESIMS: m/z 537 $[\text{M}-\text{Cl}+\text{MeCN}]^+$. HRMS (ESI): Calcd for $\text{C}_{24}\text{H}_{28}\text{N}_2^{193}\text{Ir} [\text{M}-\text{Cl}+\text{MeCN}]^+$ 537.1882, found 537.1890. The data agrees with the literature.⁴

2.6b-Me



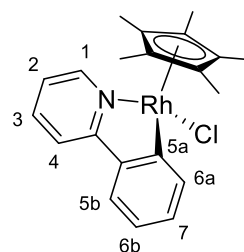
Following the general procedure, a mixture of $[\text{RhCl}_2\text{Cp}^*]_2$ (70 mg, 0.113 mmol), **L2.6-Me** (42 mg, 0.249 mmol) and NaOAc (24 mg, 0.293 mmol) in dry MeOH (10 mL) was stirred at rt overnight. The product was crystallised from DCM/hexane mixture to yield **2.6b-Me** as red - orange crystals (74 mg, 74%). ^1H NMR (400 MHz, CDCl_3): δ 1.62 (s, 15H, C_5Me_5), 2.40 (s, 3H, *Me*), 6.86 (dd, $J = 7.8, 1.0$ Hz, 1H, H^{6b}), 7.08 (ddd, $J = 7.0, 5.5, 1.8$ Hz, 1H, H^2), 7.49 (d, $J = 7.8$ Hz, 1H, H^{5b}), 7.61 (d, $J = 0.9$ Hz, 1H, H^{6a}), 7.67 (ddd, $J = 8.4, 6.8, 1.8$ Hz, 1H, H^3), 7.70 (d, $J = 7.0$ Hz, 1H, H^4), 8.70 (d, $J = 5.6$ Hz, 1H, H^1), $^{13}\text{C}\{^1\text{H}\}$ NMR (126 MHz, CDCl_3): δ 9.1 (C_5Me_5), 21.9 (*Me*), 95.9 (d, $^1J_{\text{C}-\text{Rh}} = 6.0$ Hz, C_5Me_5), 119.0 (C^4), 121.9 (C^2), 122.7 (C^{6b}), 123.4 (C^{5b}), 130.4 (C^7), 136.9 (C^{6a}), 137.0 (C^3), 143.7, 151.3 (C^1), 165.4, 178.7 (d, $^1J_{\text{C}-\text{Rh}} = 32.1$ Hz, C^{5a}). ESIMS: m/z 447 $[\text{M}-\text{Cl}+\text{MeCN}]^+$. HRMS (ESI): Calcd for $\text{C}_{24}\text{H}_{28}\text{N}_2^{103}\text{Rh} [\text{M}-\text{Cl}+\text{MeCN}]^+$ 447.1308, found 447.1309.

2.6a-H



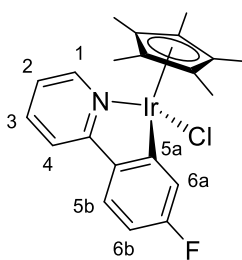
Following the general procedure, a mixture of $[\text{IrCl}_2\text{Cp}^*]_2$ (40.1 mg, 0.050 mmol), 2-phenylpyridine (18.3 mg, 0.118 mmol) and NaOAc (16.4 mg, 0.200 mmol) in dry DCM (4 mL) and dry MeOH (1 mL) was stirred at rt for 3 h. The product was precipitated from DCM/hexane mixture to yield **2.6a-H** as a yellow powder (45.8 mg, 89%). ^1H NMR (400 MHz, CDCl_3): δ 1.68 (s, 15H, C_5Me_5), 6.99 - 7.11 (m, 2H, H^2 , H^{6b}), 7.20 (td, $J = 7.4, 1.4$ Hz, 1H, H^7), 7.61 - 7.69 (m, 2H, H^3 , H^{5b}), 7.81 (m, 2H, H^4 , H^{6a}), 8.70 (ddd, $J = 5.8, 1.4, 0.8$ Hz, 1H, H^1), $^{13}\text{C}\{^1\text{H}\}$ NMR (101 MHz, CDCl_3): δ 8.9 (C_5Me_5), 88.5 (C_5Me_5), 118.9 (C^4), 122.0 (C^{6b}), 122.2 (C^2), 123.8 (C^{5b}), 131.0 (C^7), 135.8 (C^{6a}), 136.9 (C^3), 144.0, 151.3 (C^1), 163.3 (C^{5a}), 167.4. ESIMS: m/z 482 $[\text{M}-\text{Cl}+\text{MeCN}]^+$. HRMS (ESI): Calcd for $\text{C}_{21}\text{H}_{23}\text{N}^{193}\text{Ir}$ $[\text{M}-\text{Cl}]^+$. 482.1460, found 482.1487. The data agrees with the literature.⁸

2.6b-H



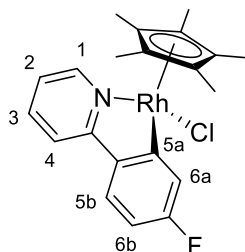
Following the general procedure a mixture of $[\text{RhCl}_2\text{Cp}^*]_2$ (102 mg, 0.165 mmol), 2-phenylpyridine (66 mg, 0.426 mmol) and NaOAc (32 mg, 0.390 mmol) in dry MeOH (10 mL) was stirred at rt overnight. The product was crystallised from DCM/hexane mixture to yield **2.6b-H** as red - orange crystals (87.0 mg, 62%). ^1H NMR (400 MHz, CDCl_3): δ 1.63 (s, 15H, C_5Me_5), 7.06 (td, $J = 7.4, 1.2$ Hz, 1H, H^{6b}), 7.13 (ddd, $J = 7.2, 5.6, 1.5$ Hz, 1H, H^2), 7.25 (td, $J = 7.5, 1.4$ Hz, 1H, H^7), 7.60 (dd, $J = 7.8, 1.4$ Hz, 1H, H^{5b}), 7.72 (ddd, $J = 8.8, 7.2, 1.6$ Hz, 1H, H^3), 7.77 (d, $J = 7.9$ Hz, 1H, H^4), 7.81 (dd, $J = 7.6, 1.2$ Hz, 1H, H^{6a}), 8.74 (dt, $J = 5.6, 0.8$ Hz, 1H, H^1), $^{13}\text{C}\{^1\text{H}\}$ NMR (126 MHz, CDCl_3): δ 9.1 (C_5Me_5), 95.8 (d, $^1J_{\text{C}-\text{Rh}} = 6.0$ Hz, C_5Me_5), 118.6 (C^4), 121.4 (C^2), 123.1 (C^{5b}), 123.9 (C^{6b}), 136.9 (C^3), 137.4 (C^{6a}), 140.2, 141.1, 151.2 (C^1), 165.4, 178.5 (d, $^1J_{\text{C}-\text{Rh}} = 31.1$ Hz, C^{5a}). ESIMS: m/z 392 $[\text{M}-\text{Cl}]^+$. HRMS (ESI): Calcd for $\text{C}_{21}\text{H}_{23}\text{N}^{103}\text{Rh}$ $[\text{M}-\text{Cl}]^+$ 392.0886, found 392.0892. The data agrees with the literature.⁸

2.6a-F



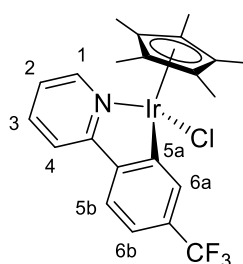
Following the general procedure, a mixture of $[\text{IrCl}_2\text{Cp}^*]_2$ (79.8 mg, 0.100 mmol), **L2.6-F** (39.0 mg, 0.225 mmol) and NaOAc (35.0mg, 0.427 mmol) in dry DCM (4 mL) and dry MeOH (1 mL) was stirred at rt for 3 h. The product was precipitated from DCM/hexane mixture to yield **2.6a-F** as a yellow powder (65.5 mg, 61%). ^1H NMR (400 MHz, CDCl_3): δ 1.68 (s, 15H, C_5Me_5), 6.74 (td, $J = 8.7, 2.5$ Hz, 1H, H^{6b}), 7.07 (ddd, $J = 7.2, 5.8, 1.5$ Hz, 1H, H^2), 7.48 (dd, $J = 9.4, 2.5$ Hz, 1H, H^{6a}), 7.65 (m, 2 H, H^3, H^{5b}), 7.74 (d, $J = 8.0$ Hz, 1H, H^4), 8.66 (ddd, $J = 5.6, 1.4, 0.8$ Hz, 1H, H^1), $^{13}\text{C}\{^1\text{H}\}$ NMR (126 MHz, CDCl_3): δ 8.9 (C_5Me_5), 88.7 (C_5Me_5), 109.4 (d, $^2J_{\text{C-F}} = 23.1$ Hz, C^{6b}), 118.8 (C^4), 121.5 (d, $^2J_{\text{C-F}} = 18.1$ Hz, C^{6a}), 122.0 (C^2), 125.4 (d, $^3J_{\text{C-F}} = 9.0$ Hz, C^5), 137.1 (C^3), 140.4, 151.3 (C^1), 164.3 (d, $^1J_{\text{C-F}} = 253.0$ Hz, C-F), 166.1 (d, $^3J_{\text{C-F}} = 5.0$ Hz, C^{5a}), 166.3, $^{19}\text{F}\{^1\text{H}\}$ NMR (376 MHz, CDCl_3): δ -111.0 (F). ESIMS: m/z 541 $[\text{M}-\text{Cl}+\text{MeCN}]^+$. HRMS (ESI): Calcd for $\text{C}_{23}\text{H}_{25}\text{N}_2\text{F}^{193}\text{Ir} [\text{M}-\text{Cl}+\text{MeCN}]^+$. 541.1631, found 541.1641. The data agrees with the literature.⁹

2.6b-F



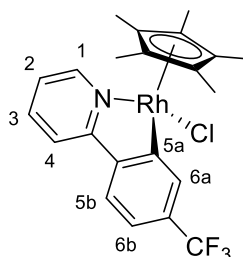
Following the general procedure, a mixture of $[\text{RhCl}_2\text{Cp}^*]_2$ (71 mg, 0.115 mmol), **L2.6-F** (43 mg, 0.249 mmol) and NaOAc (25 mg, 0.305 mmol) in dry MeOH (10 mL) was stirred at rt overnight. The product was crystallised from DCM/hexane mixture to yield **2.6b-F** as red - orange crystals (84 mg, 82%). ^1H NMR (400 MHz, CDCl_3): δ 1.63 (s, 15H, C_5Me_5), 6.75 (td, $J = 8.6, 2.5$ Hz, 1H, H^{6b}), 7.12 (ddd, $J = 7.1, 5.9, 2.5$ Hz, 1H, H^2), 7.50 (dd, $J = 8.8, 2.5$ Hz, 1H, H^{6a}), 7.58 (dd, $J = 8.5, 5.4$ Hz, 1H, H^{5b}), 7.64 - 7.74 (m, 2 H, H^3, H^4), 8.70 (d, $J = 5.7$ Hz, 1H, H^1), $^{13}\text{C}\{\text{H}\}$ NMR (126 MHz, CDCl_3): δ 9.1 (C_5Me_5), 96.0 (d, $^1J_{\text{C-Rh}} = 6.0$ Hz, C_5Me_5), 110.1 (d, $^2J_{\text{C-F}} = 24.1$ Hz, C^{6b}), 118.9 (C^4), 121.8 (C^2), 122.7 (d, $^2J_{\text{C-F}} = 18.1$ Hz, C^{6a}), 124.6 (d, $^3J_{\text{C-F}} = 9.0$ Hz, C^{5b}), 137.2 (C^3), 139.9, 151.2 (C^1), 164.4 (d, $^1J_{\text{C-F}} = 254.0$ Hz, C-F), 181.3 (d, $^1J_{\text{C-Rh}} = 33.1$ Hz, C^{5a}), $^{19}\text{F}\{^1\text{H}\}$ NMR (376 MHz, CDCl_3): δ -110.8 (F). ESIMS: m/z 410 $[\text{M}-\text{Cl}]^+$. HRMS (ESI): Calcd for $\text{C}_{21}\text{H}_{22}\text{NF}^{103}\text{Rh} [\text{M}-\text{Cl}]^+$ 410.0791, found 410.0794. The signal multiplicities for the ^1H NMR data in the literature is incorrect.¹⁰

2.6a-CF₃



Following the general procedure, a mixture of [IrCl₂Cp*]₂ (80.5 mg, 0.101 mmol), **L2.6-CF₃** (53.5 mg, 0.240 mmol) and NaOAc (34.6 mg, 0.422 mmol) in dry DCM (4 mL) and dry MeOH (1 mL) was stirred at rt for 3 h. The product was precipitated from DCM/hexane mixture to yield **2.6a-CF₃** as a yellow powder (85.1 mg, 72%). ¹H NMR (400 MHz, CDCl₃): δ 1.68 (s, 15H, C₅Me₅), 7.17 (ddd, *J* = 7.3, 5.8, 1.4 Hz, 1H, *H*²), 7.27 (ddd, *J* = 7.0, 1.8, 0.6 Hz, 1H, *H*^{6b}), 7.65 - 7.76 (m, 2H, *H*³, *H*^{5b}), 7.87 (d, *J* = 8.0 Hz, 1H, *H*⁴), 8.05 (d, *J* = 1.2 Hz, 1H, *H*^{6a}), 8.73 (ddd, *J* = 5.7, 1.6, 0.8 Hz, 1H, *H*¹), ¹³C{¹H} NMR (126 MHz, CDCl₃): δ 8.9 (C₅Me₅), 88.9 (C₅Me₅), 119.0 (q, ³*J*_{C-F} = 3.0 Hz, C^{6b}), 119.6 (C⁴), 123.4 (C²), 123.5 (C^{5b}), 124.5 (q, ¹*J*_{C-F} = 272.0 Hz, CF₃), 131.4 (q, ²*J*_{C-F} = 30.1 Hz, C-CF₃), 132.1 (q, ³*J*_{C-F} = 4.0 Hz, C^{6a}), 137.3 (C³), 147.4, 151.6 (C¹), 163.1 (C^{5a}), 165.9, ¹⁹F{¹H} NMR (376 MHz, CDCl₃): δ -63.2 (CF₃). ESIMS: *m/z* 591 [M-Cl+MeCN]⁺. HRMS (ESI): Calcd for C₂₂H₂₂NF₃¹⁹³Ir [M-Cl]⁺ 550.1334, found 550.1356.

2.6b-CF₃



Following the general procedure a mixture of [RhCl₂Cp*]₂ (41 mg, 0.066 mmol), **L2.6-CF₃** (32 mg, 0.143 mmol) and NaOAc (14 mg, 0.170 mmol) in dry MeOH (6 mL) was stirred at rt overnight. The product was crystallised from DCM/hexane mixture to yield **2.6b-CF₃** as red - orange crystals (31 mg, 48%). ¹H NMR (400 MHz, CDCl₃): δ 1.63 (s, 15H, C₅Me₅), 7.23 (ddd, *J* = 7.2, 5.7, 1.6 Hz, 1H, *H*²), 7.30 (dd, *J* = 8.0, 1.2 Hz, 1H, *H*^{6b}), 7.67 (d, *J* = 8.0 Hz, 1H, *H*^{5b}), 7.79 (ddd, *J* = 9.0, 7.4, 1.6 Hz, 1H, *H*³), 7.83 (d, *J* = 7.6 Hz, 1H, *H*⁴), 8.06 (d, *J* = 0.8 Hz, 1H, *H*^{6a}), 8.77 (ddd, *J* = 7.2, 6.4, 0.9 Hz, 1H, *H*¹), ¹³C{¹H} NMR (126 MHz, CDCl₃): δ 9.1 (C₅Me₅), 96.3 (d, ¹*J*_{C-Rh} = 6.0 Hz, C₅Me₅), 119.8 (C⁴, C^{6b}), 123.0 (C^{5b}), 123.1 (C²), 124.5 (q, ¹*J*_{C-F} = 273.1 Hz, CF₃), 130.8 (q, ²*J*_{C-F} = 31.1 Hz, C-CF₃), 133.2 (q, ³*J*_{C-F} = 4.0 Hz, C^{6a}), 137.4 (C³), 146.9, 151.5 (C¹), 164.0, 178.4 (d, ¹*J*_{C-Rh} = 33.1 Hz, C^{5a}), ¹⁹F{¹H} NMR (376 MHz, CDCl₃): δ -62.2 (CF₃). ESIMS: *m/z* 460 [M-Cl]⁺. HRMS (ESI): Calcd for C₂₂H₂₂NF₃¹⁰³Rh [M-Cl]⁺ 460.0759, found 460.0750.

6.2c Cyclometallation of *meta*-substituted phenylpyridines **L2.3-R** with {IrCp*} and {RhCp*}

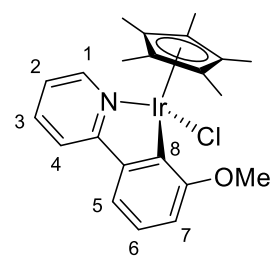
General procedure for cyclometallation of *meta*-phenylpyridines **L2.3-R** with {IrCp*} and {RhCp*}

A Schlenk flask was charged with [MCl₂Cp*]₂ (M = Ir, Rh) (1 eq.), NaOAc (4 eq.) and magnetic stirrer bar, capped, evacuated for 15 mins, then purged with N₂ three times. A dry DCM:MeOH mixture (4:1) was added and the solution stirred at rt for 15 mins, followed by the addition of the appropriate substituted phenylpyridine **L2.3-R** (2.1 eq.). The mixture was stirred for 1 h to overnight before being filtered through celite and the solvent removed by rotary evaporation. Pure products were obtained by precipitation from DCM/hexane mixture.

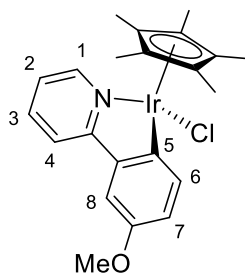
Cyclometallation of *meta*-phenylpyridines **L2.3-R** with {IrCp*} and {RhCp*}

2.3a-OMe

Following the general procedure, a mixture of [IrCl₂Cp*]₂ (25 mg, 0.032 mmol), **L2.3-OMe** (13 mg, 0.069 mmol) and NaOAc (10 mg, 0.122 mmol) in dry DCM (2 mL) and dry MeOH (0.5 mL) was stirred at rt for 2 h. The product was precipitated from DCM/hexane mixture to yield **2.3a-OMe** (*ortho:para* 1:1.1) as a yellow powder (30 mg, 88%).



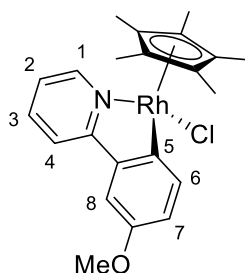
ortho-**2.3a-OMe**. ¹H NMR (400 MHz, CDCl₃): δ 1.65 (s, 15H, C₅Me₅), 3.84 (s, 3H, OMe), 6.76 (dd, *J* = 8.0, 1.0 Hz, 1H, H⁵), 7.03 (t, *J* = 7.7 Hz, 1H, H⁶), 7.06 (m, 1H, H²), 7.35 (dd, *J* = 7.8, 0.8 Hz, 1H, H⁷), 7.65 (m, 1H, H³), 7.79 (d, *J* = 8.0 Hz, 1H, H⁴), 8.70 (m, H¹), ¹³C{¹H} NMR (126 MHz, CDCl₃): δ 9.1 (C₅Me₅), 88.9 (C₅Me₅), 113.3 (C⁵), 117.5 (C⁷), 119.1 (C⁴), 122.0 (C²), 123.5 (C⁶), 136.9 (C³), 145.1, 151.4 (C¹), 152.5 (C⁸), 162.8 (C-OMe), 167.8. ESIMS: *m/z* 512 [M-Cl]⁺. HRMS (ESI): Calcd for C₂₃H₂₅NO¹⁹³Ir [M-Cl]⁺ 512.1566, found 512.1584. Data agrees with the literature.¹¹



para-**2.3-OMe**. ^1H NMR (400 MHz, CDCl_3): δ 1.68 (s, 15H, C_5Me_5), 3.83 (s, 3H, OMe), 6.92 (dd, $J = 8.2, 2.7$ Hz, 1H, H^7), 7.06 (m, 1H, H^2), 7.22 (d, $J = 2.7$ Hz, 1H, H^8), 7.65 (m, 1H, H^3), 7.69 (d, $J = 8.2$ Hz, 1H, H^6), 7.77 (d, $J = 7.8$ Hz, 1H, H^4), 8.70 (d, 1H, $J = 4.4$ Hz, H^1), $^{13}\text{C}\{^1\text{H}\}$ NMR (126 MHz, CDCl_3): δ 8.9 (C_5Me_5), 88.2 (C_5Me_5), 109.2 (C^8), 118.3 (C^7), 118.9 (C^4), 122.3 (C^2), 136.0 (C^6), 136.9 (C^3), 144.3, 151.4 (C^1), 153.1 (C^5), 155.9 (C-OMe), 167.1. ESIMS: m/z 512 $[\text{M}-\text{Cl}]^+$. HRMS (ESI): Calcd for $\text{C}_{23}\text{H}_{25}\text{NO}^{193}\text{Ir}$ $[\text{M}-\text{Cl}]^+$ 512.1566, found 512.1584. Data agrees with the literature.¹¹

2.3b-OMe

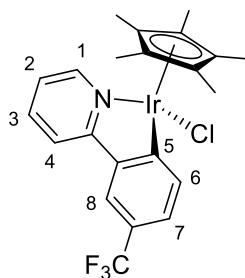
Following the general procedure, a mixture of $[\text{RhCl}_2\text{Cp}^*]_2$ (70 mg, 0.113 mmol), **L2.3-OMe** (46 mg, 0.250 mmol) and NaOAc (24 mg, 0.294 mmol) in dry MeOH (10 mL) was stirred at rt overnight. The product was crystallised from DCM/hexane mixture to yield single regioisomer *para*-**2.3b-OMe** as orange crystals (37 mg, 35%).



para-**2.3b-OMe**. ^1H NMR (400 MHz, CDCl_3): δ 1.63 (s, 15H, C_5Me_5), 3.83 (s, 3H, OMe), 6.95 (dd, $J = 8.4, 2.7$ Hz, 1H, H^7), 7.13 (td, $J = 6.0, 2.5$ Hz, 1H, H^2), 7.19 (d, $J = 2.8$ Hz, 1H, H^8), 7.68 (d, $J = 8.3$ Hz, 1H, H^6), 7.70 - 7.76 (m, 2H, H^3, H^4), 8.75 (d, $J = 5.5$ Hz, 1H, H^1), $^{13}\text{C}\{^1\text{H}\}$ NMR (126 MHz, CDCl_3): δ 9.2 (C_5Me_5), 95.7 (d, $^1J_{\text{C-Rh}} = 6.0$ Hz, C_5Me_5), 109.1 (C^8), 117.7 (C^7), 119.1 (C^4), 122.0 (C^2), 136.9 (C^6), 137.0 (C^3), 143.6, 151.4 (C^1), 156.5, 165.2, 167.6 (d, $^1J_{\text{C-Rh}} = 33.1$ Hz, C^5). ESIMS: m/z 422 $[\text{M}-\text{Cl}]$ HRMS (ESI): Calcd for $\text{C}_{22}\text{H}_{25}\text{NO}^{103}\text{Rh}$ $[\text{M}-\text{Cl}]^+$ 422.099, found 422.0985. Data agrees with the literature.¹¹

2.3a-CF₃

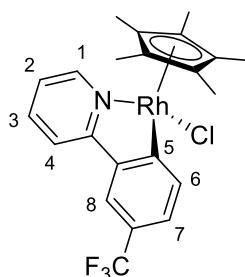
Following the general procedure, a mixture of $[\text{IrCl}_2\text{Cp}^*]_2$ (15 mg, 0.019 mmol), **L2.3-CF₃** (10 mg, 0.045 mmol) and NaOAc (8 mg, 0.100 mmol) in dry DCM (5 mL) was stirred at rt for 5 h. The product was precipitated from DCM/hexane mixture to yield single regioisomer *para*-**2.3a-CF₃** as yellow powder (10 mg, 45%).



para-**2.3a-CF₃**. ¹H NMR (400 MHz, CDCl₃): δ 1.68 (s, 15H, C₅Me₅), 7.16 (ddd, *J* = 7.3, 5.8, 1.4 Hz, 1H, *H*²), 7.40 (dd, *J* = 8.0, 1.4 Hz, 1H, *H*⁷), 7.72 (ddd, *J* = 8.3, 7.2, 1.6 Hz, 1H, *H*³), 7.86 (br.s, 1H, *H*⁸), 7.88 (d, *J* = 8.2 Hz, 1H, *H*⁴), 7.93 (d, *J* = 7.8 Hz, 1H, *H*⁶), 8.72 (ddd, *J* = 5.9, 1.5, 0.8 Hz, 1H, *H*¹), ¹³C{¹H} NMR (126 MHz, CDCl₃): δ 8.9 (C₅Me₅), 89.1 (C₅Me₅), 119.2 (C⁴), 120.2 (q, ³*J*_{C-F} = 3.0 Hz, C⁸), 123.1 (C²), 124.4 (q, ²*J*_{C-F} = 32.1 Hz, C-CF₃), 125.0 (q, ¹*J*_{C-F} = 271.0 Hz, CF₃), 126.8 (q, ³*J*_{C-F} = 3.0 Hz, C⁷), 136.1 (C⁶), 137.4 (C³), 144.5, 151.5 (C¹), 166.1 (C⁵), 169.0, ¹⁹F{¹H} NMR (376 MHz, CDCl₃): δ -61.8 (CF₃). ESIMS: *m/z* 591 [M-Cl+MeCN]⁺. HRMS (ESI): Calcd for C₂₂H₂₂NF₃¹⁹³Ir [M-Cl]⁺ 550.1334, found 550.1356. Data agrees with the literature.¹¹

2.3b-CF₃

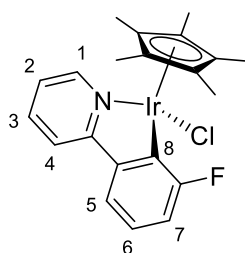
Following the general procedure, a mixture of [RhCl₂Cp*]₂ (40 mg, 0.065 mmol), **L2.3-CF₃** (32 mg, 0.143 mmol) and NaOAc (14 mg, 0.167 mmol) in dry DCM (4 mL) and dry MeOH (1 mL) was stirred at rt overnight. The product was crystallised from DCM/hexane mixture to yield single regioisomer *para*-**2.3b-CF₃** as orange crystals (34 mg, 53%).



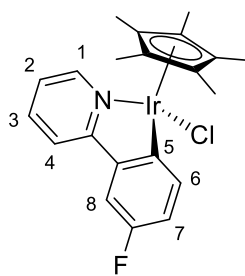
para-**2.3b-CF₃**. ¹H NMR (400 MHz, CDCl₃): δ 1.63 (s, 15H, C₅Me₅), 7.22 (ddd, *J* = 7.2, 5.7, 1.6 Hz, 1H, *H*²), 7.46 (dd, *J* = 8.0, 1.4 Hz, 1H, *H*⁷), 7.78 (m, 1H, *H*³), 7.79 (br.s, 1H, *H*⁸), 7.85 (d, *J* = 8.0 Hz, 1H, *H*⁴), 7.94 (d, *J* = 8.0 Hz, 1H, *H*⁶), 8.76 (d, *J* = 5.7 Hz, 1H, *H*¹), ¹³C{¹H} NMR (126 MHz, CDCl₃): δ 9.2 (C₅Me₅), 96.4 (d, ¹*J*_{C-Rh} = 7.0 Hz, C₅Me₅), 119.4 (C⁴), 119.6 (q, ³*J*_{C-F} = 3.0 Hz, C⁸), 122.8 (C²), 124.7 (q, ¹*J*_{C-F} = 273.1 Hz, CF₃), 125.3 (q, ²*J*_{C-F} = 32.1 Hz, C-CF₃), 126.0 (q, ³*J*_{C-F} = 3.0 Hz, C⁷), 137.2 (C⁶), 137.4 (C³), 143.9, 151.4 (C¹), 164.2, 184.6 (br d, ¹*J*_{C-Rh} = 33.1 Hz, C⁵), ¹⁹F{¹H} NMR (376 MHz, CDCl₃): δ -62.2 (CF₃). ESIMS: *m/z* 460 [M-Cl]⁺. HRMS (ESI): Calcd for C₂₂H₂₂NF₃¹⁰³Rh [M-Cl]⁺ 460.0759, found 460.0754. Data agrees with the literature.¹¹

2.3a-F

Following the general procedure, a mixture of $[\text{IrCl}_2\text{Cp}^*]_2$ (40 mg, 0.050 mmol), **L2.3-F** (19 mg, 0.109 mmol) and NaOAc (10 mg, 0.127 mmol) in dry DCM (2.25 mL) and dry MeOH (0.75 mL) was stirred at rt for 2 h. The product was precipitated from DCM/hexane mixture to yield **2.3a-F** (*ortho:para* 3.4:1) as a yellow powder (49 mg, 92%).



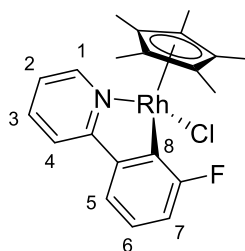
ortho-**2.3a-F**. ^1H NMR (400 MHz, CDCl_3): δ 1.71 (s, 15H, C_5Me_5), 6.94 (td, $J = 8.4, 1.2$ Hz, 1H, H^7), 7.00 (td, $J = 10.4, 5.3$ Hz, 1H, H^6), 7.11 (ddd, $J = 7.3, 5.8, 1.4$ Hz, 1H, H^2), 7.50 (d, $J = 7.4$ Hz, 1H, H^5), 7.68 (td, $J = 7.7, 1.5$ Hz, 1H, H^3), 7.82 (d, $J = 8.0$ Hz, 1H, H^4), 8.71 (d, $J = 5.9, 1.5, 0.7$ Hz, 1H, H^1), $^{13}\text{C}\{^1\text{H}\}$ NMR (126 MHz, CDCl_3): δ 9.2 (C_5Me_5), 89.2 (C_5Me_5), 116.7 (d, $^2J_{\text{C-F}} = 30.1$ Hz, C^7), 119.5 (C^4), 120.1 (d, $^4J_{\text{C-F}} = 3.0$ Hz, C^5), 122.7 (C^2), 123.7 (d, $^3J_{\text{C-F}} = 7.0$ Hz, C^6), 137.2 (C^3), 146.2 (d, $^2J_{\text{C-F}} = 42.2$ Hz, C^8), 146.6 (d, $^3J_{\text{C-F}} = 14.1$ Hz), 151.4 (C^1), 166.2 (d, $^1J_{\text{C-F}} = 234.9$ Hz, C-F), 166.9, $^{19}\text{F}\{^1\text{H}\}$ NMR (376 MHz, CDCl_3): δ -94.1 (F). ESIMS: m/z 541 $[\text{M-Cl+MeCN}]^+$. HRMS (ESI): Calcd for $\text{C}_{23}\text{H}_{25}\text{N}_2\text{F}^{193}\text{Ir} [\text{M-Cl+MeCN}]^+$ 541.1631, found 541.1636. Anal Calcd for $\text{C}_{22}\text{H}_{22}\text{DNCl}_4\text{Ir} [\text{M+CDCl}_3]$: C, 40.31; H, 3.69; N, 2.14; found C, 39.96; H, 3.61; N, 2.32 %.



para-**2.3a-F**. ^1H NMR (400 MHz, CDCl_3): δ 1.67 (s, 15 H, C_5Me_5), 6.97 (m, 1H, H^7), 7.11 (ddd, $J = 7.3, 5.8, 1.4$ Hz, 1H, H^2), 7.35 (dd, $J = 10.2, 2.7$ Hz, 1H, H^8), 7.68 (td, $J = 7.7, 1.5$ Hz, 1H, H^3), 7.72 (dd, $J = 8.1, 2.1$ Hz, 1H, H^6), 7.75 (d, $J = 7.8$ Hz, 1H, H^4), 8.71 (d, $J = 5.9, 1.5, 0.7$ Hz, 1H, H^1), $^{13}\text{C}\{^1\text{H}\}$ NMR (126 MHz, CDCl_3): δ 8.9 (C_5Me_5), 88.5 (C_5Me_5), 110.3 (d, $^2J_{\text{C-F}} = 21.1$ Hz, C^8), 118.2 (d, $^2J_{\text{C-F}} = 20.1$ Hz, C^7), 119.1 (C^4), 122.4 (C^2), 136.3 (d, $^3J_{\text{C-F}} = 7.0$ Hz, C^6), 137.2 (C^3), 144.9 (d, $^3J_{\text{C-F}} = 6.0$ Hz), 151.5 (C^1), 160.0 (d, $^1J_{\text{C-F}} = 237.9$ Hz, C-F), 166.4 (d, $^4J_{\text{C-F}} = 5.0$ Hz, C^5), 166.9, $^{19}\text{F}\{^1\text{H}\}$ NMR (376 MHz, CDCl_3): δ -123.3 (F). ESIMS: m/z 541 $[\text{M-Cl+MeCN}]^+$. HRMS (ESI): Calcd for $\text{C}_{23}\text{H}_{25}\text{N}_2\text{F}^{193}\text{Ir} [\text{M-Cl+MeCN}]^+$ 541.1631, found 541.1636. Anal Calcd for $\text{C}_{22}\text{H}_{22}\text{DNCl}_4\text{Ir} [\text{M+CDCl}_3]$: C, 40.31; H, 3.69; N, 2.14; found C, 39.96; H, 3.61; N, 2.32 %.

2.3b-F

Following the general procedure, a mixture of $[\text{RhCl}_2\text{Cp}^*]_2$ (40 mg, 0.065 mmol), **L2.3-F** (25 mg, 0.145 mmol) and NaOAc (14 mg, 0.170 mmol) in dry DCM (4 mL) and dry MeOH (1 mL) was stirred at rt overnight. The product crystallised from DCM/hexane mixture to yield single regioisomer *ortho*-**2.3b-F** as red - orange crystals (25 mg, 43%).



ortho-**2.3b-F**. ^1H NMR (400 MHz, CDCl_3): δ 1.65 (s, 15H, C_5Me_5), 6.95 (td, $J = 7.5, 0.8$ Hz, 1H, H^7), 7.04 (td, $J = 7.7, 5.3$ Hz, 1H, H^6), 7.15 (ddd, $J = 7.1, 5.6, 1.6$ Hz, 1H, H^2), 7.46 (d, $J = 7.4$ Hz, 1H, H^5), 7.73 (ddd, $J = 8.6, 7.1, 1.5$ Hz, 1H, H^3), 7.77 (d, $J = 7.6$ Hz, 1H, H^4), 8.73 (d, $J = 5.5$ Hz, 1H, H^1), $^{13}\text{C}\{^1\text{H}\}$ NMR (126 MHz, CDCl_3): δ 9.3 (C_5Me_5), 96.6 (d, $^1J_{\text{C-Rh}} = 7.0$ Hz, C_5Me_5), 116.7 (d, $^2J_{\text{C-F}} = 29.1$ Hz, C^7), 119.6 (C^4), 119.7 (C^5), 122.3 (C^2), 124.4 (d, $^3J_{\text{C-F}} = 7.0$ Hz, C^6), 137.3 (C^3), 146.1 (d, $^3J_{\text{C-F}} = 15.1$ Hz), 151.5 (C^1), 159.7 (dd, $^2J_{\text{C-F}} = 44.2$, $^1J_{\text{C-Rh}} = 35.1$ Hz, C^8) 166.9 (d, $^1J_{\text{C-F}} = 233.9$ Hz, C-F), $^{19}\text{F}\{^1\text{H}\}$ NMR (376 MHz, CDCl_3): δ -93.6 (F). ESIMS: m/z 410 $[\text{M-Cl}]^+$. HRMS (ESI): Calcd for $\text{C}_{21}\text{H}_{22}\text{NF}^{103}\text{Rh} [\text{M-Cl}]^+$ 410.0791, found 410.0783.

6.2d General procedure for measuring steric effects with *meta*-substituted phenylpyridines L2.3-R

An oven-dried Schlenk flask was charged with $[\text{MCl}_2\text{Cp}^*]_2$ (M = Ir, Rh) (1 eq.), NaOAc (4 eq.) and magnetic stirrer bar, capped, evacuated for 15 mins, then purged with N_2 three times. Dry DCM:MeOH mixture (4:1) was added and the solution stirred at rt for 15 mins, followed by addition of the appropriate substituted 2-phenylpyridine (2.1 eq.). Mixture was stirred at rt for 2 h and then if two isomers were observed heated to 50 °C for 2 days. The reactions were monitored and ratios between the two isomers were determined by ^1H NMR spectroscopy by comparing relative integrations of the appropriate signals for the *para*-isomers (H^7) with the *ortho*-isomers (H^5) and where appropriate ^{19}F NMR spectroscopy.

6.2e General procedure for deuterium incorporation experiments

A vial was charged with $[\text{MCl}_2\text{Cp}^*]_2$ (M = Ir, Rh) (0.0251 mmol, 20.0 mg (Ir), 15.5 mg (Rh), NaOAc (0.100 mmol, 8.2 mg) and CD_3OD (0.5 mL) and allowed to sit at rt for 15 mins. Then substituted 2-phenylpyridine (0.0527 mmol) in CD_3OD (0.5 mL) was added. The percentage of deuteration was monitored and determined by ^1H NMR spectroscopy

by comparing relative integrations for the signal for H⁷ for the *para*-isomers to H⁵ for the *ortho*-isomers. The deuterium incorporation was additionally confirmed by ²H NMR spectroscopy.

6.2f General procedure for competition experiments

An oven-dried Schlenk tube equipped with a stirrer bar was degassed three times and left under N₂ atmosphere. The reagents and solvent were added in the following order: [MCl₂Cp*]₂ (M = Ir, Rh) (1 eq., 0.0125 mmol, 10.0 mg for Ir) (1 eq., 0.0162 mmol, 10.0 mg for Rh); NaOAc (4 eq., 0.051 mmol, 4.2 mg for Ir), (4 eq., 0.064 mmol, 5.3 mg for Rh), dry solvent (MeOH 1 mL+ DCM 3 mL) and the mixture stirred for 15 mins. Then **L2.6-R₁** (10 eq., 0.125 mmol for Ir) (10 eq., 0.162 mmol for Rh) + **L2.6-R₂** (10 eq., 0.125 mmol for Ir) (10 eq., 0.162 mmol for Rh) were dissolved in DCM (1 mL) before adding them to Schlenk tube. The Schlenk tube was then sealed and left stirring at rt. The reaction was monitored by integration of appropriate signals (either H^{6a} or H^{6b}) in the ¹H NMR spectrum. After 2 h the reactions were heated to 50 °C for 1-3 days. Alternatively the reaction was repeated on the same scale in TFE (5 mL) first stirring at rt for 2 h, then heating to 60 °C for 2 h and further heating to 90 °C for 2 h. After this PivOH (0.0125 mmol for Ir) (0.0162 mmol for Rh) was added and heated overnight, but at this point reactions have decomposed.

6.2g Procedure for phenylpyrazole to phenylpyridine exchange

An oven-dried Schlenk tube equipped with a stirrer bar was degassed three times and left under an N₂ atmosphere. To which the appropriate Ir or Rh half-sandwich phenylpyrazole complex **2.5a/b-H** (0.0395 mmol), NaOAc (0.080 mmol) and TFE (2 mL) and 2-phenylpyridine (0.083 mmol) were added and stirred at rt overnight. The reaction with Ir reached 25% conversion and so was heated to 50 °C for 4 h at which point 80% conversion to **2.6a-H** was reached. The reaction with Rh reached 75% conversion to **2.6b-H** after stirring at rt overnight. The percentage conversion was monitored and determined by ¹H NMR spectroscopy by comparing relative integrations for the signals for Cp* and H⁵ for **2.6a/b-H**.

6.3 Experimental procedures for Chapter 3

6.3a Preparation of diphenylimidazolium salts L3.12-R₁,R₂ and their starting reagents 3.10-R₁, 3.11-R₂

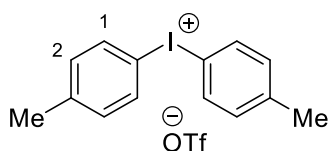
6.3ai Synthesis of aryliodonium salts 3.10-R₁

General procedure for synthesis of aryliodonium salts 3.10-R₁

Aryliodonium salts **3.10-R** (R = F, Cl, OMe) were prepared following literature procedures.^{12, 13} mCPBA (70% purity, 2-3 eq.) was placed in a Schlenk flask and evacuated for 2 h, then the flask placed under N₂ atmosphere and I₂ (1 eq.) and DCM (10-25 mL) were added resulting in a dark purple solution. The flask was cooled in ice, followed by addition of appropriate arene (4-10 eq.) and then TfOH (for R = F, Cl) or TsOH (for R = OMe) and stirred at rt overnight. Afterwards the solvent was removed by rotary evaporation, Et₂O was added and the mixture stirred at rt for 10 minutes. To ensure full precipitation, the flask was stored in a freezer for several hours and then the resulting powder collected by filtration and washed with Et₂O and dried under vacuum to give the aryliodonium salt.

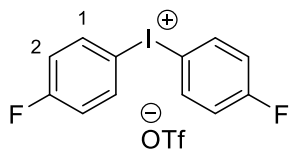
Preparation of aryliodonium salts 3.10-R₁

3.10-Me



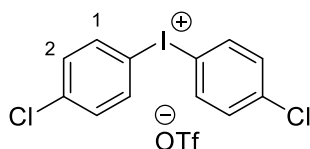
Following the literature procedure,¹² mCPBA (0.649 g, 3.75 mmol) was placed in a Schlenk flask and evacuated for 2 h, then toluene (0.255 g, 2.77 mmol), *p*-iodotoluene (0.507 g, 2.33 mmol) and DCM (10 mL) were added under N₂ atmosphere, followed by dropwise addition of TfOH (0.4 mL, 0.676 g, 4.51 mmol). The solution was stirred at rt for 15 mins, then the solvent was removed by rotary evaporation, Et₂O (15 mL) was added and the mixture was placed overnight in a freezer to yield **3.10-Me** as grey crystals (0.580 g, 55%). ¹H NMR (500 MHz, (CD₃)₂SO): δ 2.33 (s, 6H, *Me*), 7.32 (d, *J* = 8.5 Hz, 4H, *H*²), 8.09 (d, *J* = 8.3 Hz, 4H, *H*¹). ESIMS: *m/z* 309 [M]⁺. Data agrees with the literature.¹²

3.10-F



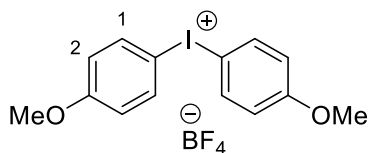
Following the general procedure,¹² mCPBA (3.01g, 17.45 mmol), fluorobenzene (2.79 mL, 2.857 g, 29.8 mmol), I₂ (0.757 g, 2.98 mmol) and TfOH (1 mL, 1.69 g, 11.26 mmol) and DCM (25 mL) were placed in a Schlenk flask and stirred at rt for 18 h. Precipitation from Et₂O gave **3.10-F** as a pale yellow powder (1.83g, 66%). ¹H NMR (400 MHz, CD₃OD): δ 7.30 (t, *J* = 8.7 Hz, 4H, *H*²), 8.23 (dd, *J* = 9.1, 4.8 Hz, 4H, *H*¹), ¹⁹F{¹H} NMR (376 MHz, CD₃OD): δ -80.02 (*OTf*), -107.05 (*F*). ESIMS: *m/z* 317 [M]⁺. Data agrees with the literature.¹²

3.10-Cl



Following the general procedure,¹² mCPBA (1.608 g, 9.3 mmol), chlorobenzene (1.5 mL, 1.659 g, 14.74 mmol), I₂ (0.380 g, 1.497 mmol) and TfOH (0.4 mL, 0.676 g, 4.51 mmol) and DCM (25 mL) were placed in a Schlenk flask and stirred at rt for 18 h. Precipitation from Et₂O gave **3.10-Cl** as an off-white powder (0.67 g, 45%). ¹H NMR (400 MHz, (CD₃)₂CO): δ 7.67 (d, *J* = 8.7 Hz, 4H, *H*²), 8.39 (d, *J* = 8.9 Hz, 4H, *H*¹). ESIMS: *m/z* 349 [M]⁺. Data agrees with the literature.¹²

3.10-OMe(BF₄)



Following the general procedure,¹³ mCPBA (1.04 g, 6.03 mmol), anisole (0.7 mL, 0.697 g, 6.44 mmol), I₂ (0.381 g, 1.5 mmol) and TsOH (1.514 g, 7.96 mmol) and DCM (12.5 mL) were placed in a Schlenk flask and stirred at rt for 18 h. Then the DCM was removed by rotary evaporation, Et₂O added, the resulting thick oil was collected into a flask, dissolved in DCM (100 mL) and washed with aqueous NaBF₄ (5x20 mL), then the solvent was removed by rotary evaporation and the resulting residue was washed with Et₂O to give **3.10-OMe(BF₄)** as an off-white powder (0.746 g, 58%). ¹H NMR (500 MHz, (CD₃)₂CO) δ 3.89 (s, 6H, *OMe*), 7.13 (d, *J* = 9.1 Hz, 4H, *H*²), 8.23 (d, *J* = 9.1 Hz, 4H, *H*¹). ESIMS: *m/z* 341 [M]⁺. Data agrees with the literature.¹³

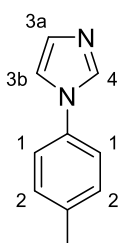
6.3aai Synthesis of phenylimidazoles 3.11-R₂

General procedure for synthesis of phenylimidazoles 3.11-R₂

N-arylated imidazoles were prepared according to a modified literature procedure.¹⁴ Arylhalide (1 eq.), imidazole (1.5 eq.), Cs₂CO₃ (2 eq.), CuO₂ (10 mol%) and MeCN or DMF (5-10 mL) were added to a Schlenk flask, sealed with a screw-cap, placed under N₂ atmosphere, partially evacuated, transferred to an oil bath and stirred at 100-120 °C for 1-5 days behind a blast shield. Afterwards the reaction mixture was cooled to rt, followed by filtration through celite. The solvent was removed by rotary evaporation and pure phenylimidazole was obtained by column chromatography (EtOAc:Pet. Ether, Biotage Isolera).

Preparation of phenylimidazoles

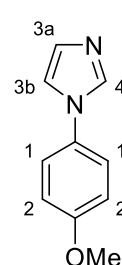
3.11-Me



Purification by column chromatography (EtOAc:Pet. Ether 5:5, Biotage Isolera) yielded **3.11-Me** as a yellow oil (418 mg, 53%). ¹H NMR (500 MHz, CDCl₃): δ 2.41 (s, 3H, *Me*), 7.19 (s, 1H, *H*^{3a}), 7.25 (s, 1H, *H*^{3b}), 7.28 (br. s, 4H, *H*¹, *H*²), 7.82 (s, 1H, *H*⁴), ¹³C{¹H} NMR (126 MHz, CDCl₃): δ 20.9 (*Me*), 118.4 (*C*^{3b}), 121.5 (*C*²), 130.3 (*C*^{3a}), 130.4 (*C*¹), 132.5, 135.6, 137.4 (*C*⁴).

ESIMS: *m/z* 159 [M+H]. Data agrees with the reported data.¹⁵

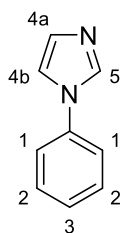
3.11-OMe



Purification by column chromatography (DCM:MeOH, 98:2, Biotage Isolera) yielded **3.11-OMe** as a pale brown solid (357 mg, 82%). ¹H NMR (500 MHz, CDCl₃): δ 3.85 (s, 3H, *OMe*), 6.98 (d, *J* = 8.9 Hz, 2H, *H*²), 7.18 (br. s, 1H, *H*^{3a/3b}), 7.20 (br. s, 1H, *H*^{3a/3b}), 7.30 (d, *J* = 8.9 Hz, 2H, *H*¹), 7.76 (br s, 1H, *H*⁴), ¹³C{¹H} NMR (126 MHz, CDCl₃): δ 55.5 (*OMe*), 114.8 (*C*²), 118.7 (*C*^{3a}), 123.1 (*C*¹), 130.0 (*C*^{3b}), 130.6, 135.8 (*C*⁴), 158.9.

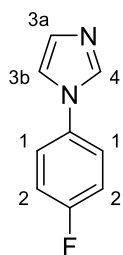
ESIMS: *m/z* 175 [M+H]. Data agree with the reported data.¹⁵

3.11-H



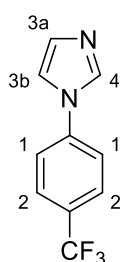
Purification by column chromatography (DCM:MeOH 9:1, Biotage Isolera) yielded **3.11-H** as a colourless oil (655 mg, 89%). ^1H NMR (500 MHz, CDCl_3): δ 7.20 (br. s, 1H, H^{4a}), 7.28 (br. s, 1H, H^{4b}), 7.37 (m, 1H, H^3), 7.38 (d, $J = 7.5$ Hz, 2H, H^1) 7.47 (m, 2H, H^2), 7.85 (s, 1H, H^5), $^{13}\text{C}\{^1\text{H}\}$ NMR (126 MHz, CDCl_3): δ 118.2 (C^{4b}), 121.5 (C^1), 127.4 (C^3), 129.8 (C^2), 130.4 (C^{4a}), 135.6, 137.4 (C^5). ESIMS: m/z 145 [$\text{M}+\text{H}$]. Data agree with the reported data.¹⁵

3.11-F



Purification by column chromatography (DCM:MeOH 9:1, Biotage Isolera) yielded **3.11-F** as a colourless oil (516 mg, 64%). ^1H NMR (500 MHz, CDCl_3): δ 7.18(t, $J = 8.6$ Hz, 2H, H^2), 7.20 (br. s, 1H, H^{3a}), 7.22 (br. s, 1H, H^{3b}), 7.37 (m, 1H, H^3), 7.36 (dd, $J = 8.9, 4.6$ Hz, 2H, H^1), 7.78 (s, 1H, H^4), $^{19}\text{F}\{^1\text{H}\}$ NMR (376 MHz, CDCl_3): δ -115.3 ESIMS: m/z 163 [$\text{M}+\text{H}$]. Data agree with the reported data.¹⁵

3.11-CF₃



Purification by column chromatography (DCM:MeOH, 98:2, Biotage Isolera) yielded **3.11-CF₃** as a white powder (357 mg, 60%). ^1H NMR (500 MHz, CDCl_3): δ 7.25 (s, 1H, H^{3a}), 7.33 (s, 1H, H^{3b}), 7.53 (d, $J = 8.3$ Hz, 2H, H^1), 7.76 (d, $J = 8.3$ Hz, 2H, H^2), 7.92 (s, 1H, H^4), $^{13}\text{C}\{^1\text{H}\}$ NMR (126 MHz, CDCl_3): δ 117.7 (C^{3a}), 121.1 (C^1), 123.5 (q, $^1J = 272.0$ Hz, CF_3), 127.1 (q, $^3J = 3.3$ Hz, C^2), 129.3 (q, $^2J = 33.1$ Hz, $\text{C}-\text{CF}_3$), 130.9 (C^{3b}), 135.3 (C^4), 139.9, $^{19}\text{F}\{^1\text{H}\}$ NMR (376 MHz, CDCl_3): δ -62.5 (CF_3). ESIMS: m/z 213 [$\text{M}+\text{H}$]. Data agree with the reported data.¹⁶

6.3aiii Synthesis of diphenylimidazolium salts L3.12-R₁,R₂

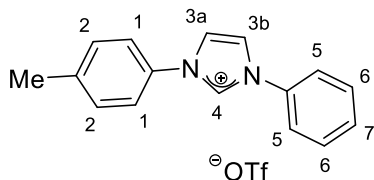
General procedure for synthesis of diphenylimidazolium salts L3.12-R₁,R₂

Arylimidazole **3.11-R₂** (1 eq.), bisaryliodonium salt **3.10-R₁** (1.5 eq.), $\text{Cu}(\text{OAc})_2 \cdot \text{H}_2\text{O}$ (10 mol%) and DMF (4 mL) were added to a Schlenk flask, sealed with screw-cap, placed under N_2 atmosphere, transferred to an oil bath and stirred at 100 °C for 18-22 h. The reaction mixture was cooled to rt with continuous stirring. The mixture was transferred to a round bottom flask and DMF was removed by co-evaporation with toluene. The

residue was dissolved in DCM and precipitated with Et₂O. The precipitate was filtered, washed with Et₂O and dried to yield pure imidazolium salt.¹⁷

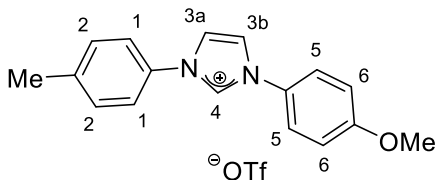
Preparation of diphenylimidazolium salts **L3.12-R₁,R₂**

L3.12-Me,H



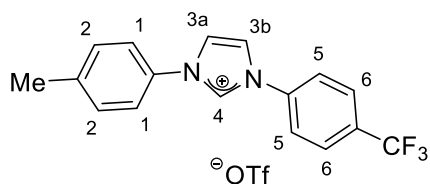
Following the general procedure, a mixture of **3.11-H** (143 mg, 0.996 mmol), **3.10-Me** (692.0 mg, 1.511 mmol), Cu(OAc)₂·H₂O (19 mg, 0.098 mmol) and DMF (4 mL) was stirred at 100 °C overnight. The product was precipitated from DCM/Et₂O to give **L3.12-Me,H** as an off-white powder (340.6 mg, 89%). ¹H NMR (400 MHz, CD₃OD): δ 2.46 (s, 3H, *Me*), 7.49 (d, 2H, *J* = 8.0 Hz, *H*²), 7.7 (m, 5H, *H*¹, *H*⁶, *H*⁷), 7.82 (d, *J* = 8.2 Hz, 2H, *H*⁵), 8.22 (br. s, 1H, *H*^{3a}), 8.26 (br. s, 1H, *H*^{3b}), 10.01 (s, 1H, *H*⁴), ¹³C{¹H} NMR (126 MHz, CD₃OD): 21.1 (*Me*), 121.7(q, ¹*J*_{C-F} = 318.2 Hz, *OTf*), 123.3 (*C*¹), 123.5 (*C*⁵), 123.6 (*C*^{3b}), 123.7 (*C*^{3a}), 131.6 (*C*⁶, *C*⁷), 132.0 (*C*²), 134.0, 135.5 (*C*⁴), 136.4, 142.4 (*C-Me*), ¹⁹F{¹H} NMR (376 MHz, CD₃OD): δ -79.7 (*OTf*). ESIMS: *m/z* 235 [M]⁺. HRMS (ESI): Calcd for C₁₆H₁₅N₂ [M]⁺ 235.1235, found 235.1243.

L3.12-Me,OMe



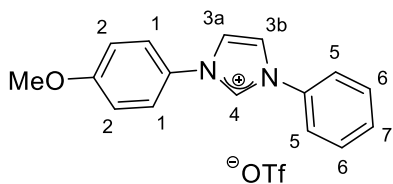
Following the general procedure, a mixture of **3.110-OMe** (175 mg, 1.005 mmol), **3.10-Me** (703 mg, 1.534 mmol), Cu(OAc)₂·H₂O (20 mg, 0.100 mmol) and DMF (4 mL) was stirred at 100 °C overnight. The product was precipitated from DCM/Et₂O to give **L3.12-Me,OMe** as an off-white powder (341 mg, 82%). ¹H NMR (400 MHz, CD₃OD): δ 2.47 (s, 3H, *Me*), 3.89 (s, 3H, *OMe*), 7.19 (d, *J* = 9.2 Hz, 2H, *H*⁶), 7.48 (d, *J* = 8.2 Hz, 2H, *H*²), 7.68 (d, *J* = 8.6 Hz, 2H, *H*¹), 7.72 (d, *J* = 9.0 Hz, 2H, *H*⁵), 8.16 (d, *J* = 2.0 Hz, 1H, *H*^{3a/b}), 8.20 (d, *J* = 2.0 Hz, 1H, *H*^{3a/b}), 9.88 (t, *J* = 1.7 Hz, 1H, *H*⁴), ¹³C{¹H} NMR (126 MHz, CD₃OD): δ 21.1 (*Me*), 56.3(*OMe*), 116.4 (*C*⁶), 121.9 (q, ¹*J*_{C-F} = 318.2 Hz, *OTf*), 123.2 (*C*¹), 123.4 (*C*^{3a/b}), 123.8 (*C*^{3a/b}), 125.0 (*C*⁵), 129.2, 131.9 (*C*²), 133.2, 135.1 (*C*⁴), 142.2 (*C-Me*), 162.5 (*C-OMe*). ESIMS: *m/z* 265 [M]⁺. HRMS (ESI): Calcd for C₁₇H₁₇N₂O [M]⁺ 265.1341, found 265.1351.

L3.12-Me,CF₃



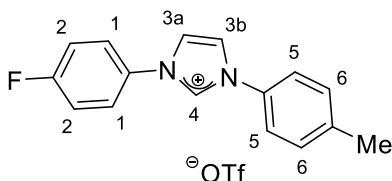
Following the general procedure, a mixture of **3.11-CF₃** (204 mg, 0.965 mmol), **3.10-Me** (697 mg, 1.522 mmol), Cu(OAc)₂·H₂O (20 mg, 0.100 mmol) and DMF (4 mL) at 100 °C overnight. The product was precipitated from DCM/Et₂O to give **L3.12-Me,CF₃** as an off-white powder (428 mg, 98%,). ¹H NMR (400 MHz, CD₃OD): δ 2.4 (s, 3H, *Me*), 7.44 (d, *J* = 8.4 Hz, 2H, *H*²), 7.66 (d, *J* = 8.4 Hz, 2H, *H*¹), 7.95 (m, 4H, *H*⁵,*H*⁶), 8.22 (d, *J* = 2.2 Hz, 1H, *H*^{3a/b}), 8.29 (d, *J* = 2.2 Hz, 1H, *H*^{3a/b}), 10.04 (br. s, 1H, *H*⁴), ¹³C{¹H} NMR (126 MHz, CD₃OD): δ 21.1 (*Me*), 122.0 (q, ¹*J*_{C-F} = 318.2 Hz, *OTf*), 123.3 (*C*¹), 123.4 (*C*^{3a/b}), 124.0 (*C*^{3a/b}), 124.3 (*C*⁵), 124.8 (q, ¹*J*_{C-F} = 272.1 Hz, *CF*₃), 128.7 (m, *C*⁶), 132.0 (*C*²), 133.1 (q, ²*J*_{C-F} = 32.5 Hz, *C*-*CF*₃), 133.8, 136.0 (*C*⁴), 139.2, 142.5 (*C*-*Me*), ¹⁹F{¹H} NMR (376 MHz, CD₃OD): δ 80.0 (*OTf*), -64.3 (*CF*₃). ESIMS: *m/z* 303 [M]⁺. HRMS (ESI): Calcd for C₁₇H₁₄N₂F₃ [M]⁺ 303.1109, found 303.1113.

L3.12-OMe,H



Following the general procedure, a mixture of **3.11-H** (80 mg, 0.055 mmol), **3.10-OMe(BF₄)** (357 mg, 0.833 mmol), Cu(OAc)₂·H₂O (11 mg, 0.055 mmol) and DMF (2mL) at 100 °C overnight. The product was precipitated from DCM/Et₂O to give **L3.12-OMe,H** as an off-white powder (183 mg, 98%,). ¹H NMR (500 MHz, CD₃OD): δ 3.88 (s, 3H, *OMe*), 7.17 (d, *J* = 9.1 Hz, 2H, *H*²), 7.64 (m, 3H, *H*⁶, *H*⁷), 7.73 (d, *J* = 8.9 Hz, 2H, *H*¹), 7.81 (d, *J* = 7.6 Hz, 2H, *H*⁵), 8.16 (br.s, 1H, *H*^{3a}), 8.23 (br.s, 1H, *H*^{3b}), 9.88 (s, 1H, *H*⁴), ¹³C{¹H} NMR (126 MHz, CD₃OD): δ 56.3 (*OMe*), 116.4 (*C*²), 123.5 (*C*^{3b}, *C*⁵), 124.0 (*C*^{3a}), 125.1 (*C*¹), 129.2, 131.5 (*C*⁶, *C*⁷), 135.4 (*C*⁴), 136.4, 162.6 (*C*-*OMe*), ¹⁹F{¹H} NMR (376 MHz, CD₃CN): δ -151.9 (*BF*₄). ESIMS: *m/z* 251 [M]⁺. HRMS (ESI): Calcd for C₁₆H₁₅N₂O [M]⁺ 251.1184, found 251.1189.

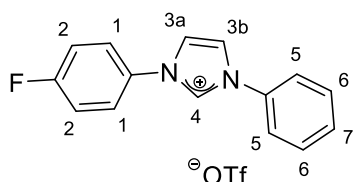
L3.12-F,Me



Following the general procedure, a mixture of **3.11-Me** (165 mg, 1.042 mmol), **3.10-F** (700 mg, 1.502 mmol), Cu(OAc)₂·H₂O (21 mg, 0.109 mmol) and DMF (4 mL) at 100 °C overnight. The product was precipitated from DCM/Et₂O to give **L3.12-F,Me** as an off-white powder

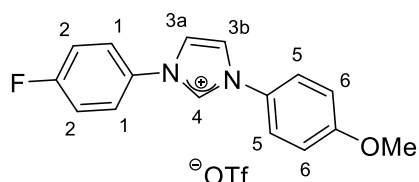
(351 mg, 84%). ^1H NMR (400 MHz, $(\text{CD}_3)_2\text{CO}$): δ 2.48 (s, 3H, *Me*), 7.51 (m, 4H, H^2 , H^6), 7.84 (d, $J = 8.5$ Hz, 2H, H^5), 8.04 (dd, $J = 9.2, 4.5$ Hz, 2H, H^5), 8.43 (m, 2H, H^{3a} , H^{3b}), 10.08 (t, $J = 1.7$ Hz, 1H, H^4), $^{13}\text{C}\{^1\text{H}\}$ NMR (126 MHz, CD_3OD): δ 21.1(*Me*), 118.2 (d, $^2J_{\text{C-F}} = 24.1$ Hz, C^2), 123.1 (q, $^1J_{\text{C-F}} = 318.2$ Hz, *OTf*), 123.2 (C^6), 123.6 ($C^{3a/3b}$), 123.8 ($C^{3a/3b}$), 126.1 (d, $^1J_{\text{C-F}} = 9.0$ Hz, C^1), 131.9 (C^5), 132.6 (d, $^3J_{\text{C-F}} = 3.0$ Hz), 133.8, 135.5 (C^4), 142.21 (*C-Me*), 164.7 (d, $^1J_{\text{C-F}} = 249.0$ Hz, *C-F*), $^{19}\text{F}\{^1\text{H}\}$ NMR (376 MHz $(\text{CD}_3)_2\text{CO}$): δ -111.8 (*F*), -78.5 (*OTf*). ESIMS: m/z 253[M] $^+$. HRMS (ESI): Calcd for $\text{C}_{16}\text{H}_{14}\text{N}_2\text{F}$ [M] $^+$ 253.1141, found 253.1155.

L3.12-F,H



Following the general procedure, a mixture of **3.11-H** (212 mg, 1.475 mmol), bis-(4-fluorophenyl) **3.10-F** (1000 mg, 2.145 mmol), $\text{Cu}(\text{OAc})_2 \cdot \text{H}_2\text{O}$ (31 mg, 0.156 mmol) and DMF (6mL) at 100 °C overnight. The product was precipitated from DCM/Et₂O to give **L3.12-F,H** as an off-white powder (354 mg, 62%). ^1H NMR (400 MHz, CD_3OD): δ 7.45 (t, $J = 8.6$ Hz, 2H, H^2), 7.68 (m, 3H, H^6 , H^7), 7.85 (d, $J = 7.0$ Hz, 2H, H^5), 7.90 (dd, $J = 9.1, 4.4$ Hz, 2H, H^2), 8.26 (d, $J = 1.8$ Hz, 1H, H^{3a}), 8.30 (d, $J = 1.6$ Hz, 1H, H^{3b}), 10.03 (br.s, 1H, H^4), $^{13}\text{C}\{^1\text{H}\}$ NMR (126 MHz, CD_3OD): δ 118.5 (d, $^2J_{\text{C-F}} = 24.1$ Hz, C^2), 122.0 (q, $^1J_{\text{C-F}} = 318.2$ Hz, *OTf*), 123.5 (C^5), 123.7 (C^{3b}), 124.1 (C^{3a}), 126.3 (d, $^3J_{\text{C-F}} = 9.0$ Hz, C^1), 131.7 (C^6), 131.8 (C^7), 132.8, 136.0 (C^4), 136.4, 165.0 (d, $^1J_{\text{C-F}} = 250.0$ Hz, *C-F*), $^{19}\text{F}\{^1\text{H}\}$ NMR (376 MHz, CD_3OD): δ -111.9 (*F*), -80.0 (*OTf*). ESIMS: m/z 239 [M] $^+$. HRMS (ESI): Calcd for $\text{C}_{15}\text{H}_{12}\text{N}_2\text{F}$ [M] $^+$ 239.0985, found 239.0996.

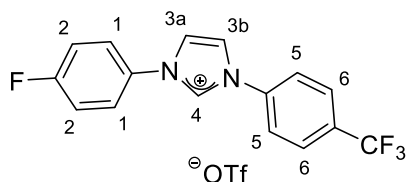
L3.12-F,OMe



Following the general procedure, a mixture of **3.11-OMe** (174 mg, 1.000 mmol), **3.10-F** (702 mg, 1.506 mmol), $\text{Cu}(\text{OAc})_2 \cdot \text{H}_2\text{O}$ (19 mg, 0.095 mmol) and DMF (4 mL) at 100 °C overnight. The product was precipitated from DCM/Et₂O to give **L3.12-F,OMe** as an off-white powder (304 mg, 73%). ^1H NMR (400 MHz, CD_3OD): δ 3.90 (s, 3H, *OMe*), 7.20 (d, $J = 9.2$ Hz, 2H, H^5), 7.44 (t, $J = 8.4$ Hz, 2H, H^2), 7.73 (d, $J = 9.2$ Hz, 2H, H^6), 7.86 (dd, $J = 9.1, 4.4$ Hz, 2H, H^1), 8.19 (m, 1H, H^{3b}), 8.22 (m, 1H, H^{3a}), 9.92 (br. s, 1H, H^4), $^{13}\text{C}\{^1\text{H}\}$ NMR (126 MHz, CD_3OD): δ 56.3 (*OMe*), 116.4 (C^5), 118.3 (d, $^2J_{\text{C-F}} = 24.1$

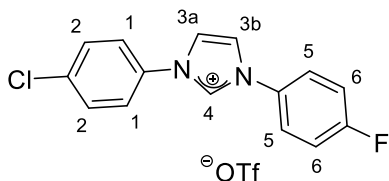
Hz, C^2), 121.9 (q, $^1J_{C-F} = 318.2$ Hz, *OTf*), 123.7 (C^{3a}), 123.9 (C^{3b}), 125.1 (C^6), 126.1 (br d, $^3J_{C-F} = 9.0$ Hz, C^1), 129.2, 132.7 (d, $^3J_{C-F} = 3.0$ Hz), 135.6 (C^4), 162.6 (*C-OMe*), 164.7 (d, $^1J_{C-F} = 249.0$ Hz, *C-F*), $^{19}\text{F}\{^1\text{H}\}$ NMR (376 MHz, CD_3OD): δ -111.9 (*F*), -80.0 (*OTf*). ESIMS: m/z 269 $[\text{M}]^+$. HRMS (ESI): Calcd for $\text{C}_{16}\text{H}_{14}\text{N}_2\text{OF}$ $[\text{M}]^+$ 269.1090, found 269.1097.

L3.12-F,CF₃



Following the general procedure, a mixture of **3.11-CF₃** (219mg, 1.036 mmol), **3.10-F** (705 mg, 1.513 mmol), $\text{Cu}(\text{OAc})_2 \cdot \text{H}_2\text{O}$ (20 mg, 0.1 mmol) and DMF (4 mL) at 100 °C overnight. The product was precipitated from DCM/Et₂O to give **L3.12-F,CF₃** as an off-white powder (340.6 mg, 72%). ^1H NMR (400 MHz, CD_3OD): δ 7.45 (t, $J = 8.7$ Hz, 2H, H^2), 7.90 (dd, $J = 9.0, 4.4$ Hz, 2H, H^1), 8.01 (m, 2H, H^6), 8.07 (m, 2H, H^5), 8.30 (d, $J = 2.2$ Hz, 1H, H^{3a}), 8.38 (d, $J = 2.2$ Hz, 1H, H^{3b}), 10.14 (br.s, 1H, H^4), $^{13}\text{C}\{^1\text{H}\}$ NMR (126 MHz, CD_3OD): δ 118.4 (d, $^1J_{C-F} = 23.1$ Hz, C^2), 121.8 (q, $^1J_{C-F} = 318.2$ Hz, *OTf*), 123.5 (C^{3b}), 124.3 (C^{3a}), 124.4 (C^5), 125.0 (q, $^1J_{C-F} = 271.0$ Hz, CF_3), 126.3 (d, $^3J_{C-F} = 10.0$ Hz, C^1), 128.8 (m, C^6), 132.6 (d, $^4J_{C-F} = 3.0$ Hz), 133.3 (q, $^2J_{C-F} = 32.5$ Hz, *C-CF₃*), 136.2 (C^4), 139.2, 165.0 (d, $^1J_{C-F} = 250.0$ Hz, *C-F*), $^{19}\text{F}\{^1\text{H}\}$ NMR (376 MHz, CD_3OD): δ -111.7 (*F*), -80.0 (*OTf*), -64.3 (CF_3). ESIMS: m/z 307 $[\text{M}]^+$. HRMS (ESI): Calcd for $\text{C}_{15}\text{H}_{11}\text{N}_2\text{F}_4$ $[\text{M}]^+$ 307.0858, found 307.0858.

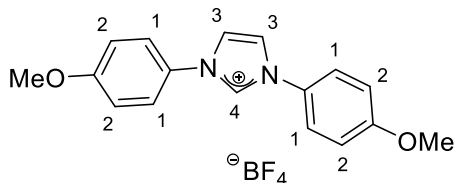
L3.12-Cl,F



Following the general procedure, a mixture of **3.11-F** (112 mg, 0.690 mmol), **3.10-Cl** (519 mg, 1.039 mmol), $\text{Cu}(\text{OAc})_2 \cdot \text{H}_2\text{O}$ (14 mg, 0.073 mmol) and DMF (3 mL) at 100 °C overnight. The product was precipitated from DCM/Et₂O to give **L3.12-Cl,F** as an off-white powder (140 mg, 48%). ^1H NMR (400 MHz, CD_3OD): δ 7.44 (t, $J = 8.6$ Hz, 2H, H^6), 7.71 (d, $J = 8.9$ Hz, 2H, H^2), 7.84 (d, $J = 8.9$ Hz, 2H, H^1), 7.88 (dd, $J = 9.0, 4.5$ Hz, 2H, H^5), 8.26 (d, $J = 2.2$ Hz, 1H, H^{3b}), 8.28 (d, $J = 2.2$ Hz, 1H, H^{3a}), 10.02 (s, 1H, H^4), $^{13}\text{C}\{^1\text{H}\}$ NMR (126 MHz, CD_3OD): δ 118.3 (d, $^2J_{C-F} = 24.1$ Hz, C^6), 121.7 (q, $^1J_{C-F} = 318.9$ Hz, *OTf*), 123.6 (C^{3a}), 124.0 (C^{3b}), 125.1 (C^1), 126.1 (br d, $^3J_{C-F} = 9.0$ Hz, C^1), 131.5 (C^2), 134.9 (d, $^4J_{C-F} = 3.0$ Hz), 135.9 (C^4), 137.3 (*C-Cl*), 164.74 (d, $^1J_{C-F} = 250.0$ Hz, *C-F*), $^{19}\text{F}\{^1\text{H}\}$ NMR

(376 MHz, (CD₃)₂CO): δ -111.7 (*F*), -78.9 (*OTf*). ESIMS: m/z 273 [M]⁺. HRMS (ESI): Calcd for C₁₅H₁₁N₂FCl [M]⁺ 275.0565, found 275.0586.

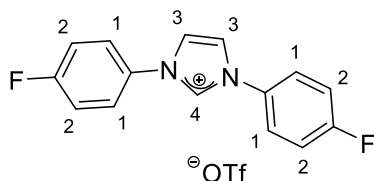
L3.12-OMe,OMe



Following the general procedure, a mixture of **3.11-OMe** (165 mg, 0.950 mmol), **3.10-OMe(BF₄)** (679 mg, 1.586 mmol), Cu(OAc)₂·H₂O (22 mg, 0.110 mmol) and DMF (4 mL) at 100 °C overnight.

The product was precipitated from DCM/Et₂O to give **L3.12-OMe,OMe** as an off-white powder (334 mg, 96%). ¹H NMR (400 MHz, CD₃CN): δ 3.88 (s, 6H, *OMe*), 7.17 (d, $J = 9.2$ Hz, 4H, H^2), 7.63 (d, $J = 9.2$ Hz, 4H, H^1), 7.86 (d, $J = 1.8$ Hz, 2H, H^3), 9.14 (t, $J = 1.8$ Hz, 1H, H^4), ¹³C{¹H} NMR (126 MHz, CD₃CN): 56.6 (*OMe*), 116.3 (C^2), 123.5 (C^3), 125.1 (C^1), 128.7, 134.4 (C^4), 162.1 (*C-OMe*), ¹⁹F{¹H} NMR (376 MHz, CD₃CN): δ -151.5 (BF_4^-). ESIMS: m/z 281 [M]⁺. HRMS (ESI): Calcd for C₁₇H₁₇N₂O₂ [M]⁺ 281.1290, found 281.1277.

L3.12-F,F



Following the general procedure, a mixture of **3.11-F** (67 mg, 0.417 mmol), **3.10-F** (293 mg, 0.628 mmol), Cu(OAc)₂·H₂O (10 mg, 0.050 mmol) and DMF (4 mL) at 100 °C overnight. The product was precipitated from DCM/Et₂O to give **L3.12-F,F** as an off-white powder

(143 mg, 85%). ¹H NMR (500 MHz, CD₃OD): δ 7.42 (t, $J = 8.4$, 4H, H^2), 7.86 (m, 4H, H^1), 8.21 (s, 2H, H^3), 9.94 (s, 1H, H^4), ¹³C{¹H} NMR (126 MHz, CD₃OD): δ 118.3 (d, ² $J_{C-F} = 24.1$ Hz, C^2), 121.8 (q, ¹ $J_{C-F} = 319.2$ Hz, *OTf*), 123.9 (C^3), 126.2 (d, ³ $J_{C-F} = 9.0$ Hz, C^1), 132.5, 136.1 (C^4), 164.8 (d, ¹ $J_{C-F} = 250.0$ Hz, *C-F*), ¹⁹F{¹H} NMR (376 MHz, CD₃OD): δ -112.1 (*F*), -80.0 (*OTf*). ESIMS: m/z 257 [M]⁺. HRMS (ESI): Calcd for C₁₅H₁₁N₂F₂ [M]⁺ 257.0890, found 257.0893.

6.3b Cyclometallation of diphenylimidazolium salts L3.12-R₁,R₂ with {IrCp*} and {RhCp*}

General procedure for cyclometallation of diphenylimidazolium salts L3.12-R₁,R₂ with {IrCp*}

[IrCl₂Cp*]₂ (1 eq.), NaOAc (8 eq.) were placed in a Schlenk flask, sealed with screw-cap, evacuated for 15 mins and placed under an N₂ atmosphere. DCE (5 mL) was added and the mixture stirred for another 15 mins. The appropriate imidazolium salt **L3.12-R₁,R₂** (2.1 eq.) added, and the Schlenk flask transferred to a preheated oil bath and stirred at 75 °C for 4 h. The reaction mixture was cooled to rt with continuous stirring, diluted with DCM (10 mL), filtered through celite, then a silica plug and the solvent removed by rotary evaporation.

General procedure for cyclometallation of diphenylimidazolium salts L3.12-R₁,R₂ with {RhCp*}

[RhCl₂Cp*]₂ (40 mg, 0.065 mmol, 1 eq.), NaOAc (8 eq.) were placed in an oven-dried Schlenk flask, sealed with screw-cap, evacuated for 15 mins and placed under N₂ atmosphere. DCE (5 mL) was added and the mixture stirred for another 15 mins. The appropriate imidazolium salt **L3.12-R₁,R₂** (2.1 eq.) was added, the Schlenk flask transferred to a preheated oil bath and stirred at 50 °C for 1-4 h, then heated at 75 °C for further 1-4 h, followed by the addition of K₂CO₃ (2 eq.) and NaCl (2 eq.) and further heating of reaction mixture at 75 °C overnight. The reaction mixture was cooled to rt with continuous stirring, diluted with DCM (10 mL), filtered through celite, silica plug and the solvent removed by rotary evaporation.

General procedure for measuring ratios for cyclometallation of diphenylimidazolium salts L3.12-R₁,R₂ with {IrCp*} and {RhCp*}

The direct C–H activation reactions were monitored at time intervals at 1 h, 4 h (and overnight for reactions with Rh). The reactions were monitored by ¹H NMR spectroscopy by comparing the integrations of the appropriate signals of the complexes (H^{2b} with H^{6b}, OMe, Me groups) and/or where applicable by ¹⁹F NMR spectroscopy.

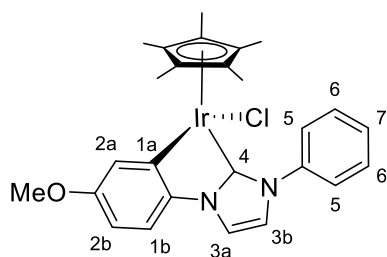
General procedure for cyclometallation of diphenylimidazolium salts **L3.12-R₁,R₂** with {MCp*} (M = Ir, Rh) in the presence of Et₄NCl

[MCl₂Cp*]₂ (M = Ir, Rh) (1 eq., 0.0125-0.025 mmol), NaOAc (8 eq.) were placed in an oven-dried Schlenk flask, sealed with screw-cap, evacuated for 15 mins and placed under an N₂ atmosphere. DCE (1-2 mL) added and mixture stirred for another 15 mins. Appropriate imidazolium salt **L3.12-R₁,R₂** (2.1 eq.) and Et₄NCl (2 eq.) were added and stirred at rt overnight, then heated to 50°C for 1 h, then further 75°C for 1 h, and PivOH (1 eq.) added and heated further at 75°C for 3 h to overnight. The reactions were monitored after 1-2 h, 4 h, overnight at rt, then 1 h at 50°C, 1 h at 75 °C, 3 h to overnight at 75 °C with PivOH by ¹H NMR spectroscopy by comparing the integrations of the appropriate complexes signals (H^{2b} with H^{6b}, OMe, Me groups) and/or where applicable by ¹⁹F NMR spectroscopy.

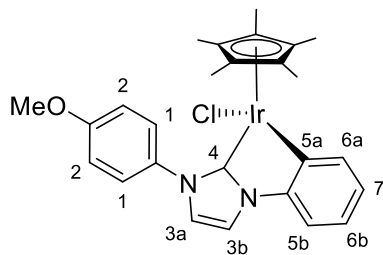
Cyclometallation of diphenylimidazolium salts **L3.12-R₁,R₂** with {IrCp*} and {RhCp*}

3.12a-OMe*,H and **3.12a-OMe,H***

Following the general procedure, a mixture of [IrCl₂Cp*]₂ (50. mg, 0.063 mmol), NaOAc (41 mg, 0.503 mmol), imidazolium salt **L3.12a-OMe,H** (52 mg, 0.130 mmol) in DCE (5 mL) was heated to 75 °C for 4 h. The product was purified by filtration through celite and short column chromatography (DCM:MeOH 9:1) to yield **3.12a-OMe*,H:3.12a-OMe,H*** in 1:10 ratio as a yellow solid (21 mg, 27%).



3.12a-OMe*,H. ¹H NMR (400 MHz, CDCl₃): δ 1.45 (s, 15H, C₅Me₅), 3.86 (s, 3H, OMe), 6.54 (dd, *J* = 8.4, 2.7 Hz, 1H, H^{2b}), 7.11 (d, *J* = 8.4 Hz, 1H, H^{1b}), 7.04 (m, 1H, H^{6b}), 7.14 (d, *J* = 2.1Hz, 1H, H^{3a}), 7.33 (d, *J* = 2.7 Hz, 1H, H^{2a}), 7.43 (d, *J* = 2.1 Hz, 1H, H^{3b}), 7.52 (m, 3H, H⁶, H⁷), 7.96 (br d, *J* = 7.6 Hz, 2H, H⁵). ESIMS: *m/z* 618 [M-Cl+MeCN]⁺. HRMS (ESI): Calcd for C₂₈H₃₁N₃O¹⁹³Ir [M-Cl+MeCN]⁺ 618.2097, found 618.2108.

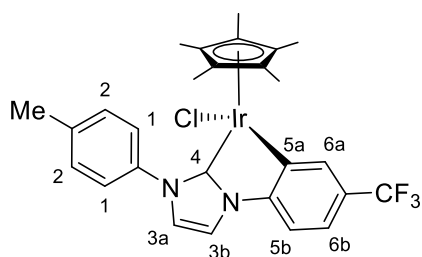


3.12a-OMe,H*. ^1H NMR (400 MHz, CDCl_3): δ 1.47 (s, 15H, C_5Me_5), 3.88 (s, 3H, *OMe*), 6.98 (td, $J = 7.4, 1.4$ Hz, 1H, H^7), 7.04 (d, $J = 9.3$ Hz, 2H, H^2), 7.04 (m, 1H, H^{6b}), 7.14 (d, $J = 2.1$ Hz, 1H, H^{3a}), 7.17 (dd, $J = 7.5, 1.3$ Hz, 1H, H^{5b}), 7.47 (d, $J = 2.1$ Hz, 1H, H^{3b}), 7.74 (dd, $J = 7.3, 1.3$ Hz, 1H, H^{6a}), 7.87 (br d, $J = 8.5$ Hz, 2H, H^1),

$^{13}\text{C}\{^1\text{H}\}$ NMR (126 MHz, CDCl_3): δ 9.1 (C_5Me_5), 55.7 (*OMe*), 91.4 (C_5Me_5), 110.3 (C^{5b}), 114.5 (C^2), 114.9 (C^{3b}), 121.9 (C^{3a}), 122.0 (C^7), 126.1 (C^{6b}), 127.1 (C^1), 133.6, 137.2 (C^7), 143.1, 145.9 (C^{5a}), 159.28 (*C-OMe*), 163.7 (C^4). ESIMS: m/z 618 [*M-Cl+MeCN*] $^+$. HRMS (ESI): Calcd for $\text{C}_{28}\text{H}_{31}\text{N}_3\text{O}^{193}\text{Ir}$ [*M-Cl+MeCN*] $^+$ 618.2097, found 618.2108.

3.12a-Me,CF₃*

Following the general procedure, a mixture of [*IrCl*₂*Cp**]₂ (51 mg, 0.064mmol), NaOAc (47 mg, 0.580 mmol), imidazolium salt **L3.12-Me,CF₃**. (62 mg, 0.137 mmol) and DCE (5 mL) was heated to 75 °C for 4 h. The product was purified by filtration through celite and then silica plug to yield **3.12a-Me*,CF₃** as a yellow solid (29 mg, 34%).



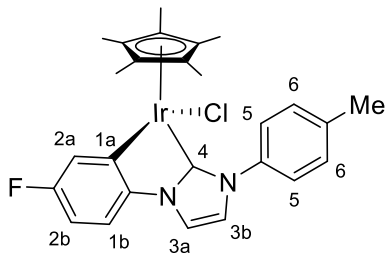
3.12a-Me*,CF₃. ^1H NMR (400 MHz, CD_2Cl_2): δ 1.44 (s, 15H, C_5Me_5), 2.46 (s, 3H, *Me*), 7.11 (d, $J = 2.2$ Hz, 1H, H^{3a}), 7.16 (dd, $J = 8.4, 1.5$ Hz, 1H, H^{6b}), 7.24 (d, $J = 8.1$ Hz, 1H, H^{5b}), 7.31 (d, $J = 8.5$ Hz, 2H, H^2), 7.58 (d, $J = 2.2$ Hz, 1H, H^{3b}), 7.83 (d, $J = 8.4$ Hz, 2H, H^1),

7.93 (d, $J = 1.5$ Hz, 1H, H^{6a}), $^{13}\text{C}\{^1\text{H}\}$ NMR (126 MHz, CDCl_3): δ 9.1 (C_5Me_5), 21.2 (*Me*), 91.9 (C_5Me_5), 109.9 (C^{5b}), 115.2 (C^{3b}), 119.8 (q, $^3J_{\text{C-F}} = 4.0$ Hz, C^{6b}), 122.5 (C^{3a}), 124.8 (q, $^1J_{\text{C-F}} = 272.1$ Hz, CF_3), 125.7 (C^1), 127.2 (q, $^2J_{\text{C-F}} = 31.1$ Hz, *C-CF₃*), 130.0 (C^2), 133.6 (q, $^3J_{\text{C-F}} = 4.0$ Hz, C^{6a}), 137.6 (*C-Me*), 138.3, 143.6, 148.8 (C^{5a}), 164.6 (C^4), $^{19}\text{F}\{^1\text{H}\}$ NMR (376 MHz, CDCl_3): δ -61.2. ESIMS: m/z 670 [*M-Cl+MeCN*] $^+$. HRMS (ESI): Calcd for $\text{C}_{29}\text{H}_{30}\text{F}_3\text{N}_3^{193}\text{Ir}$ [*M-Cl+MeCN*] $^+$ 670.2021 found 670.2029.

3.12a-F*,Me and 3.12a-F,Me*

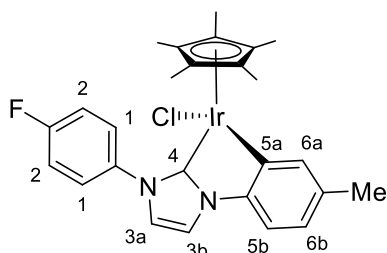
Following the general procedure, a mixture of [*IrCl*₂*Cp**]₂ (50 mg, 0.063 mmol), NaOAc (43 mg, 0.524 mmol), imidazolium salt **L3.12-F,Me** (52 mg, 0.129 mmol) and DCE (5 mL) was heated to 75 °C for 4 h. The product was purified by filtration through celite and then silica plug to yield **3.12a-F*,Me** as a yellow solid (67 mg, 86%) with traces of minor isomer (1:20).

3.12a-F*,Me. ^1H NMR (400 MHz, CDCl_3): δ 1.45 (s, 15H, C_5Me_5), 2.46 (s, 3H, *Me*),



6.65 (td, $J = 8.6, 2.6$ Hz, 1H, H^{2b}), 7.11 (dd, $J = 8.5, 4.8$ Hz, 1H, H^{1b}), 7.12 (d, $J = 2.0$ Hz, 1H, H^{3b}), 7.31 (d, $J = 8.2$ Hz, 2H, H^6), 7.42 (d, $J = 2.0$ Hz, 1H, H^{3a}), 7.43 (dd, $J = 9.0, 2.7$ Hz, 1H, H^{2a}), 7.80 (br. d, $J = 8.1$ Hz, 2H, H^5), $^{13}\text{C}\{^1\text{H}\}$ NMR (126 MHz, CDCl_3): δ 9.0 (C_5Me_5), 21.2

(*Me*), 91.5 (C_5Me_5), 108.1 (d, $^2J_{\text{C-F}} = 24.1$ Hz, C^{2b}), 110.8 (d, $^3J_{\text{C-F}} = 9.0$ Hz, C^{1b}), 115.1 (C^{3a}), 122.0 (C^{3b}), 123.2 (d, $^2J_{\text{C-F}} = 19.1$ Hz, C^{2a}), 125.7 (C^6), 130.0 (C^5), 137.8, 138.1 (C-Me), 142.2, 145.7 (d, $^3J_{\text{C-F}} = 5.0$ Hz, C^{1a}), 160.6 (d, $^1J_{\text{C-F}} = 244.9$ Hz, C-F), 162.7 (C^4), $^{19}\text{F}\{^1\text{H}\}$ NMR (376 MHz, CDCl_3): δ -118.7(*F*). ESIMS: m/z 579 [M-Cl] $^+$. HRMS (ESI): Calcd for $\text{C}_{26}\text{H}_{27}\text{N}_2\text{OF}^{193}\text{Ir}$ [M-Cl] $^+$ 579.1788 found 579.1806. ESIMS: m/z 620 [M-Cl+MeCN] $^+$. HRMS (ESI): Calcd for $\text{C}_{28}\text{H}_{30}\text{FN}_3\text{O}^{193}\text{Ir}$ [M-Cl+MeCN] $^+$ 620.2053 found 620.2079.

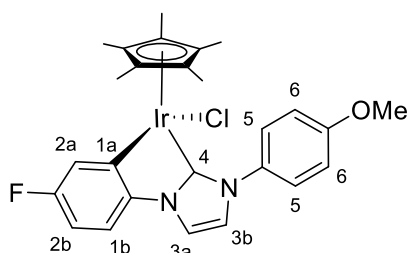


3.12a-F,Me*. ^1H NMR (400 MHz, CDCl_3): δ 1.46 (s, 15H, C_5Me_5), 2.38 (s, 3H, *Me*), 6.78 (dd, $J = 7.5, 0.7$ Hz, 1H, H^{6b}), 7.05 (d, $J = 7.9$ Hz, 1H, H^{5b}), 7.12 (d, $J = 2.0$ Hz, 1H, H^{3b}), 7.20 (t, $J = 8.7$ Hz, 2H, H^2), 7.42 (d, $J = 2.0$ Hz, 1H, H^{3a}), 7.54 (d, $J = 0.7$ Hz, 1H, H^{6a}),

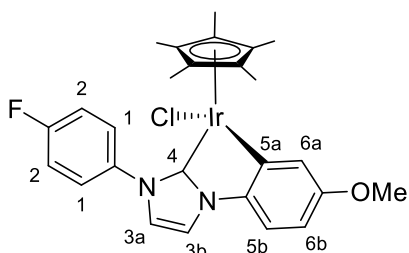
7.80 (dd, $J = 8.4, 4.5$ Hz, 2H, H^1), $^{19}\text{F}\{^1\text{H}\}$ NMR (376 MHz, CDCl_3): δ -113.3 (*F*). ESIMS: m/z 579 [M-Cl] $^+$. HRMS (ESI): Calcd for $\text{C}_{26}\text{H}_{27}\text{N}_2\text{OF}^{193}\text{Ir}$ [M-Cl] $^+$ 579.1788 found 579.1806. ESIMS: m/z 620 [M-Cl+MeCN] $^+$. HRMS (ESI): Calcd for $\text{C}_{28}\text{H}_{30}\text{N}_3\text{OF}^{193}\text{Ir}$ [M-Cl+MeCN] $^+$ 620.2053 found 620.2079.

3.12a-F*,OMe and 3.12a-F,OMe*

Following the general procedure, a mixture of $[\text{IrCl}_2\text{Cp}^*]_2$ (50 mg, 0.063mmol), NaOAc (44 mg, 0.536mmol), imidazolium salt **L3.12a-F,OMe** (58 mg, 0.139mmol) and DCE (5 mL) was heated to 75 °C for 4 h. The product was purified by filtration through celite and then silica plug to yield **3.12a-F*,OMe:3.12a-F,OMe*** in 10:1 ratio as a yellow solid (32mg, 47%).



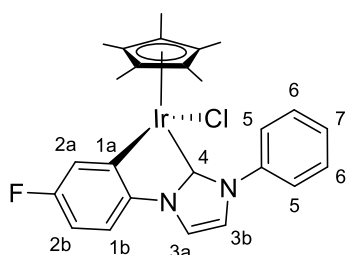
3.12a-F*,OMe. ^1H NMR (400 MHz, CDCl_3): δ 1.47 (s, 15H, C_5Me_5), 3.88 (s, 3H, OMe), 6.67 (td, $J = 8.6, 2.6$ Hz, 1H, H^{2b}), 7.03 (d, $J = 9.2$ Hz, 2H, H^6), 7.14 (dd, $J = 8.4, 4.6$ Hz, 1H, H^{1b}), 7.15 (d, $J = 2.2$ Hz, 1H, H^{3b}), 7.44 (d, $J = 2.1$ Hz, 1H, H^{3a}), 7.45 (dd, $J = 9.0, 2.7$ Hz, 1H, H^{2a}), 7.85 (br. d, $J = 8.6$ Hz, 2H, H^5), $^{13}\text{C}\{^1\text{H}\}$ NMR (126 MHz, CDCl_3): δ 9.1 (C_5Me_5), 55.7 (OMe), 91.6 (C_5Me_5), 108.2 (d, $^2J_{\text{C-F}} = 26.1$ Hz, C^{2b}), 110.8 (d, $^3J_{\text{C-F}} = 9.0$ Hz, C^{1b}), 114.5 (C^6), 115.0 (C^{3a}), 122.2 (C^{3b}), 123.2 (d, $^2J_{\text{C-F}} = 19.1$ Hz, C^{2a}) 127.1 (C^5) 133.5, 142.2, 145.7 (d, $^3J_{\text{C-F}} = 4.0$ Hz, C^{1a}) 159.4 (C-OMe), 160.7 (d, $^1J_{\text{C-F}} = 244.9$ Hz, C-F), 162.8 (C^4), $^{19}\text{F}\{^1\text{H}\}$ NMR (376 MHz, CDCl_3): δ -118.7 (F). ESIMS: m/z 595 $[\text{M-Cl}]^+$. HRMS (ESI): Calcd for $\text{C}_{26}\text{H}_{27}\text{N}_2\text{OF}^{193}\text{Ir} [\text{M-Cl}]^+$ 595.1737, found 595.1757. ESIMS: m/z 636 $[\text{M-Cl+MeCN}]^+$. HRMS (ESI): Calcd for $\text{C}_{28}\text{H}_{30}\text{N}_3\text{OF}^{193}\text{Ir} [\text{M-Cl+MeCN}]^+$ 636.2002, found 636.2029.



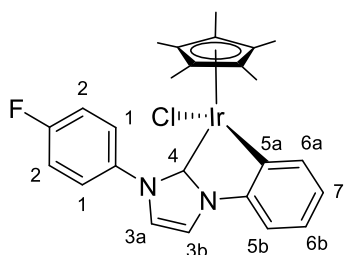
3.12a-F,OMe*: ^1H NMR (400 MHz, CDCl_3): δ 1.47 (s, 15H, C_5Me_5), 3.85 (s, 3H, OMe), 6.53 (dd, $J = 8.3, 2.7$ Hz, 1H, H^{6b}), 7.10 (d, $J = 8.5$ Hz, 1H, H^{5b}), 7.12 (d, $J = 2.2$ Hz, 1H, H^{3b}), 7.21 (t, $J = 8.7$ Hz, 2H, H^2), 7.32 (d, $J = 2.7$ Hz, 1H, H^{6a}), 7.44 (d, $J = 2.1$ Hz, 1H, H^{3a}), 7.45 (dd, $J = 9.0, 2.7$ Hz, 1H, H^{2a}), 7.96 (dd, $J = 8.7, 4.8$ Hz, 2H, H^1), $^{13}\text{C}\{^1\text{H}\}$ NMR (101 MHz, CDCl_3): δ 9.1 (C_5Me_5), 55.4 (OMe), 91.4 (C_5Me_5), 106.9 (C^{6b}), 110.8 (C^{5b}), 115.0 (C^{3b}), 116.3 (d, $^2J_{\text{C-F}} = 22.3$ Hz, C^2), 121.6 (C^{3a}), 122.7 (C^{6a}), 127.7 (br.d, $^3J_{\text{C-F}} = 6.4$ Hz, C^1), 133.4, 142.2, 145.7, 160.5 (d, $^1J_{\text{C-F}} = 244.9$ Hz, C-F), 161.5 (C-OMe), 162.8 (C^4), $^{19}\text{F}\{^1\text{H}\}$ NMR (376 MHz, CDCl_3): δ -113.3 (F). ESIMS: m/z 595 $[\text{M-Cl}]^+$. HRMS (ESI): Calcd for $\text{C}_{26}\text{H}_{27}\text{N}_2\text{OF}^{193}\text{Ir} [\text{M-Cl}]^+$ 595.1737, found 595.1757. ESIMS: m/z 636 $[\text{M-Cl+MeCN}]^+$. HRMS (ESI): Calcd for $\text{C}_{28}\text{H}_{30}\text{N}_3\text{OF}^{193}\text{Ir} [\text{M-Cl+MeCN}]^+$ 636.2002, found 636.2029.

3.12a-F*,H and 3.12a-F,H*

Following the general procedure, a mixture of $[\text{IrCl}_2\text{Cp}^*]_2$ (50 mg, 0.063 mmol), NaOAc (43 mg, 0.529 mmol), imidazolium salt **L3.12-F,H** (52 mg, 0.133 mmol) and DCE (5 mL) was heated to 75 °C for 4 h. The product was purified by filtration through celite and then silica plug to yield **3.12a-F*,H:3.12a-F,H*** in 10:1 ratio as a yellow solid (26 mg, 34%).



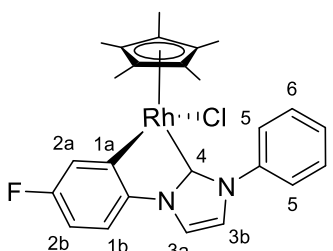
3.12a-F*,H. ^1H NMR (400 MHz, CDCl_3): δ 1.44 (s, 15H, C_5Me_5), 6.67 (td, $J = 8.6, 2.7$ Hz, 1H, H^{2b}), 7.06 (dd, $J = 8.4, 4.7$ Hz, 1H, H^{1b}), 7.21 (d, $J = 2.1$ Hz, 1H, H^{3b}), 7.46 (m, 1H, H^7), 7.50 (dd, $J = 9.2, 2.6$ Hz, 1H, H^{2a}), 7.52 (d, $J = 2.1$ Hz, 1H, H^{3a}), 7.55 (t, $J = 8.0$, 2H, H^6), 8.06 (br d, $J = 7.6$ Hz, 2H, H^5), $^{13}\text{C}\{^1\text{H}\}$ NMR (126 MHz, CDCl_3): δ 9.0 (C_5Me_5), 91.6 (C_5Me_5), 108.2 (d, $^2J_{\text{C-F}} = 24.1$ Hz, C^{2b}), 110.9 (d, $^3J_{\text{C-F}} = 9.0$ Hz, C^{1b}), 115.3 (C^{3a}), 121.9 (C^{3b}), 123.2 (d, $^2J_{\text{C-F}} = 19.1$ Hz, C^{2a}), 125.9 (C^5), 128.1 (C^7), 129.5 (C^6), 140.2, 142.1, 145.7 (d, $^3J_{\text{C-F}} = 5.0$ Hz, C^{1a}), 160.7 (d, $^3J_{\text{C-F}} = 244.9$ Hz, C-F), 162.9 (C^4), $^{19}\text{F}\{^1\text{H}\}$ NMR (376 MHz, CDCl_3): δ -118.5 (F). ESIMS: m/z 565 $[\text{M-Cl}]^+$. HRMS (ESI): Calcd for $\text{C}_{25}\text{H}_{25}\text{N}_2\text{F}^{193}\text{Ir} [\text{M-Cl}]^+$ 565.1631, found 565.1652. ESIMS: m/z 604 $[\text{M-Cl+MeCN}]^+$. HRMS (ESI): Calcd for $\text{C}_{27}\text{H}_{28}\text{N}_3\text{F}^{193}\text{Ir} [\text{M-Cl+MeCN}]^+$ 604.1873, found 604.1874.



3.12a-F,H*. ^1H NMR (400 MHz, CDCl_3): δ 1.47 (s, 15H, C_5Me_5), 6.98 (td, $J = 7.6, 1.5$ Hz, 1H, H^{6b}), 7.04 (td, $J = 7.4, 1.5$ Hz, 1H, H^7), 7.15 (d, $J = 2.0$ Hz, 1H, H^{3a}), 7.17 (br dd, $J = 7.6, 1.5$ Hz, 1H, H^{5b}), 7.22 (t, $J = 8.6$ Hz, 2H, H^2), 7.50 (d, $J = 2.2$ Hz, 1H, H^{3a}), 7.74 (dd, $J = 7.3, 1.2$ Hz, 1H, H^{6a}), 7.95 (dd, $J = 8.7, 4.4$ Hz, 2H, H^1), $^{13}\text{C}\{^1\text{H}\}$ NMR (101 MHz, CDCl_3): δ 9.1 (C_5Me_5), 91.5 (C_5Me_5), 110.5 (C^{5b}), 115.3 (C^{3b}), 116.3 (d, $^2J_{\text{C-F}} = 22.3$ Hz, C^2), 121.7 (C^{3a}), 122.1 (C^{6b}), 126.3 (C^7), 127.7 (d, $^3J_{\text{C-F}} = 7.2$ Hz, C^1), 136.5 (d, $^3J_{\text{C-F}} = 2.4$ Hz), 137.2 (C^{6a}), 143.0 (C^{5a}), 145.7, 162.2 (d, $^1J_{\text{C-F}} = 248.0$ Hz, C-F), 162.9 (C^4), $^{19}\text{F}\{^1\text{H}\}$ NMR (376 MHz, CDCl_3): δ -113.2 (F). ESIMS: m/z 565 $[\text{M-Cl}]^+$. HRMS (ESI): Calcd for $\text{C}_{25}\text{H}_{25}\text{N}_2\text{F}^{193}\text{Ir} [\text{M-Cl}]^+$ 565.1631, found 565.1652. ESIMS: m/z 604 $[\text{M-Cl+MeCN}]^+$. HRMS (ESI): Calcd for $\text{C}_{27}\text{H}_{28}\text{N}_3\text{F}^{193}\text{Ir} [\text{M-Cl+MeCN}]^+$ 604.1873, found 604.1874.

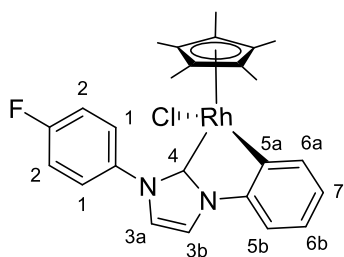
3.12b-F*,H and 3.12b-F,H*

Following the general procedure, a mixture of $[\text{RhCl}_2\text{Cp}^*]_2$ (50 mg, 0.081 mmol), NaOAc (54 mg, 0.657 mmol), imidazolium salt **L3.12-F,H** (67 mg, 0.172 mmol) and DCE (5 mL) was heated to 75 °C for 20 h. The product was purified by filtration through celite and then precipitated from DCM/hexane to yield major regioisomer **3.12b-F*,H** (the minor:major isomer ratio 1:6) as an orange solid (51 mg, 61%).



3.12b-F*,H. ^1H NMR (400 MHz, CDCl_3): δ 1.38 (s, 15H, C_5Me_5), 6.67 (td, $J = 8.5, 2.7$ Hz, 1H, H^{2b}), 7.09 (dd, $J = 8.4, 4.5$ Hz, 1H, H^{1b}), 7.21 (d, $J = 2.1$ Hz, 1H, H^{3b}), 7.44-7.51 (m, 2 H, H^{2a}, H^7), 7.52 (d, $J = 2.2$ Hz, 1H, H^{3a}), 7.55 (t, $J = 8.2$ Hz, 2H, H^6), 8.06 (d, $J = 7.7$ Hz, 2H, H^5),

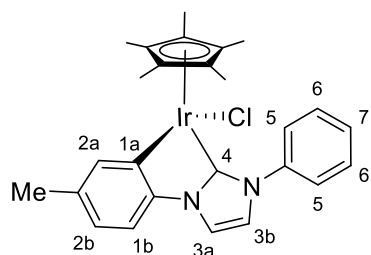
$^{13}\text{C}\{^1\text{H}\}$ NMR (126 MHz, CDCl_3): δ 9.3 (C_5Me_5), 98.1 (d, $^1J_{\text{Rh-C}} = 5.0$ Hz, C_5Me_5), 109.0 (d, $^2J_{\text{C-F}} = 24.1$ Hz, C^{2b}), 111.1 (d, $^3J_{\text{C-F}} = 9.0$ Hz, C^{1b}), 115.6 (C^{3a}), 122.4 (C^{3b}), 124.6 (d, $^2J_{\text{C-F}} = 20.1$ Hz, C^{2a}), 125.3 (C^5), 128.2 (C^7), 129.5 (C^6), 140.0, 141.6, 160.0 (d, $^1J_{\text{C-F}} = 246.0$ Hz, C-F), 162.8 (dd, $^1J_{\text{Rh-C}} = 34.6$ Hz, $^3J_{\text{F-C}} = 3.5$ Hz, C^{1a}), 180.5 (d, $^1J_{\text{Rh-C}} = 57.2$ Hz, C^4), $^{19}\text{F}\{^1\text{H}\}$ NMR (376 MHz, CDCl_3): δ -118.2 (F). ESIMS: m/z 457 $[\text{M-Cl}]^+$. HRMS (ESI): Calcd for $\text{C}_{25}\text{H}_{25}\text{N}_2\text{F}^{103}\text{Rh} [\text{M-Cl}]^+$ 475.1057, found 475.1057



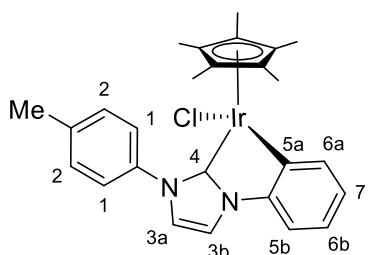
3.12b-F,H*. ^1H NMR (400 MHz, CDCl_3): δ 1.40 (s, 15H, C_5Me_5), 7.02 (td, $J = 7.4, 1.6$ Hz, 1H, H^{6b}), 7.09 (m, 1H, H^7), 7.11 (dd, $J = 7.5, 1.3$ Hz, 1H, H^{5b}), 7.19 (d, $J = 2.0$ Hz, 1H, H^{3a}), 7.25 (m, 2H, H^2), 7.54 (d, $J = 2.2$ Hz, 1H, H^{3b}), 7.78 (dd, $J = 7.3, 1.1$ Hz, 1H, H^{6a}), 8.10 (dd, $J = 8.8, 4.7$ Hz, 2H, H^1), $^{19}\text{F}\{^1\text{H}\}$ NMR (376 MHz, CDCl_3): δ -113.1 (F). ESIMS: m/z 457 $[\text{M-Cl}]^+$. HRMS (ESI): Calcd for $\text{C}_{25}\text{H}_{25}\text{N}_2\text{F}^{103}\text{Rh} [\text{M-Cl}]^+$ 475.1057, found 475.1057.

3.12a-Me*,H and 3.12a-Me,H*

Following the general procedure, a mixture of $[\text{IrCl}_2\text{Cp}^*]_2$ (30 mg, 0.037 mmol), NaOAc (25 mg, 0.299 mmol), imidazolium salt **L3.12-Me,H** (30 mg, 0.079 mmol) and DCE (3 mL) was heated to 75 °C for 4 h. The product was purified by filtration through celite and then silica plug to yield mixture of **3.12a-Me*,H**:**3.12a-Me,H*** in 1:1.7 ratio as a yellow solid (32 mg, 71%).



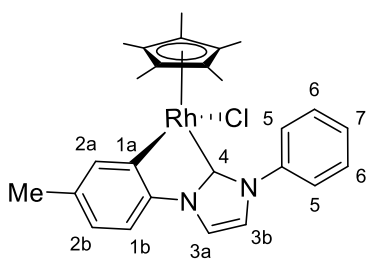
3.12a-Me*,H. ^1H NMR (400 MHz, CDCl_3): δ 1.45 (s, 15H, C_5Me_5), 2.39 (s, 3H, *Me*), 6.80 (dd, $J = 7.8, 1.2$ Hz, 1H, H^{2b}), 7.08 (d, $J = 7.8$ Hz, 1H, H^{1b}), 7.19 (d, $J = 2.1$ Hz, 1H, H^{3b}), 7.43 (m, 1H, H^7), 7.47 (d, $J = 2.0$ Hz, 1H, H^{3a}), 7.53 (td, $J = 7.8, 0.9$ Hz, 2H, H^6), 7.56 (d, $J = 1.2$ Hz, 1H, H^{2a}), 7.97 (br. d, $J = 7.6$ Hz, 2H, H^5), $^{13}\text{C}\{^1\text{H}\}$ NMR (126 MHz, CDCl_3): δ 9.0 (C_5Me_5), 21.3 (*Me*), 91.4 (C_5Me_5), 110.0 (C^{1b}), 115.1 (C^{3a}), 121.6 (C^{3b}), 122.6 (C^{2b}), 125.9 (C^5), 127.9 (C^7), 129.4 (C^6), 135.1 (*C-Me*), 137.9 (C^{2a}), 140.4, 142.8, 143.6 (C^{1a}), 163.2 (C^4). ESIMS: m/z 602 $[\text{M}-\text{Cl}+\text{MeCN}]^+$. HRMS (ESI): Calcd for $\text{C}_{28}\text{H}_{31}\text{N}_3^{193}\text{Ir} [\text{M}-\text{Cl}+\text{MeCN}]^+$ 602.2147, found 602.2150. Anal Calcd for $\text{C}_{27}\text{H}_{29}\text{N}_2\text{Cl}_2\text{Ir} [\text{M}+\text{CHCl}_3]$: C, 45.32; H, 4.09; N, 3.91; found C, 45.55; H, 4.32; N, 4.13%



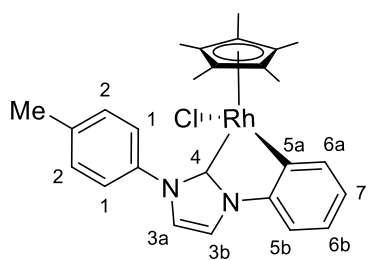
3.12a-Me,H*. ^1H NMR (400 MHz, CDCl_3): δ 1.46 (s, 15H, C_5Me_5), 2.45 (s, 3H, *Me*), 6.99 (td, $J = 7.4, 1.7$ Hz, 1H, H^{6b}), 7.04 (td, $J = 7.2, 1.6$ Hz, 1H, H^7), 7.17 (d, $J = 2.2$ Hz, 1H, H^{3a}), 7.18 (d, $J = 7.8$ Hz, 1H, H^{5b}), 7.31 (d, $J = 7.9$ Hz, 2H, H^2), 7.49 (d, $J = 2.2$ Hz, 1H, H^{3b}), 7.75 (dd, $J = 7.3, 1.4$ Hz, 1H, H^{6a}), 7.83 (d, $J = 8.2$ Hz, 2H, H^1), $^{13}\text{C}\{^1\text{H}\}$ NMR (126 MHz, CDCl_3): δ 9.0 (C_5Me_5), 21.2 (*Me*), 91.4 (C_5Me_5), 110.3 (C^{5b}), 115.0 (C^{3b}), 121.8 (C^{3a}), 122.0 (C^{6b}), 125.7 (C^1), 126.1 (C^7), 129.9 (C^2), 137.1 (C^{6a}), 137.9 (*C-Me*), 137.9, 143.1, 145.8 (C^{5a}), 163.6 (C^4). ESIMS: m/z 602 $[\text{M}-\text{Cl}+\text{MeCN}]^+$. HRMS (ESI): Calcd for $\text{C}_{28}\text{H}_{31}\text{N}_3^{193}\text{Ir} [\text{M}-\text{Cl}+\text{MeCN}]^+$ 602.2147, found 602.2150. Anal Calcd for $\text{C}_{27}\text{H}_{29}\text{N}_2\text{Cl}_2\text{Ir} [\text{M}+\text{CHCl}_3]$: C, 45.32; H, 4.09; N, 3.91; found C, 45.55; H, 4.32; N, 4.13%.

3.12b-Me*,H and 3.12b-Me,H*

Following the general procedure, a mixture of $[\text{RhCl}_2\text{Cp}^*]_2$ (39 mg, 0.063 mmol), NaOAc (41 mg, 0.500 mmol), imidazolium salt **L3.12b-Me,H**. (49 mg, 0.128 mmol) and DCE (5 mL) was heated to 50 °C for 2 h, then to 75 °C for 1 h, then K_2CO_3 (35 mg, 0.25 mmol) and NaCl (15.7 mg, 0.268 mmol) added and the mixture was heated to 75 °C for further 15 h. The product was purified by filtration through celite and then precipitated from DCM/hexane several times to yield regioisomers **3.12b-Me*,H**:**3.12b-Me,H*** in 1:2.0 ratio as a yellow solid (51 mg, 79%).



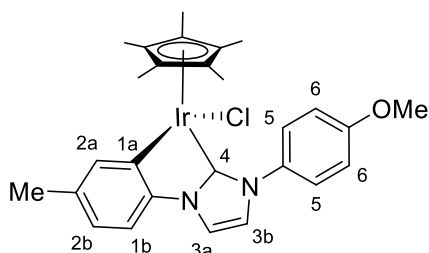
3.12b-Me*,H. ^1H NMR (400 MHz, CDCl_3) 1.38 (s, 15 H, C_5Me_5), 2.38 (s, 3H, *Me*), 6.81 (dd, $J = 7.8, 1.8$ Hz, 1H, H^{2b}), 7.02 (d, $J = 7.6$ Hz, 1H, H^{1b}), 7.23 (d, $J = 2.1$ Hz, 1H, H^{3b}), 7.45 (m, 1H, H^7), 7.55 (d, $J = 2.1$ Hz, 1H, H^{3a}), 7.53 (m, 2H, H^6), 7.60 (d, $J = 1.8$ Hz, 1H, H^{2a}), 8.09 (d, $J = 7.4$ Hz, 2H, H^5), $^{13}\text{C}\{^1\text{H}\}$ NMR (101MHz, CDCl_3): δ 9.3 (C_5Me_5), 21.3 (*Me*), 97.7 (d, $^1J_{\text{Rh-C}} = 4.7$ Hz, C_5Me_5), 110.4 (C^{1b}), 115.4 (C^{3a}), 122.2 (C^{3b}), 123.3 (C^{2b}), 125.3 (C^5 , C^6), 127.8 (C^7), 134.8 (*C-Me*), 139.0 (C^{2a}), 140.2, 143.1 159.3 (d, $^1J_{\text{Rh-C}} = 34.2$ Hz, C^{1a}), 180.3 (d, $^1J_{\text{Rh-C}} = 58.0$ Hz, C^4). ESIMS: m/z 471 $[\text{M-Cl}]^+$. HRMS (ESI): Calcd for $\text{C}_{26}\text{H}_{28}\text{N}_2^{103}\text{Rh} [\text{M-Cl}]^+$ 471.1308, found 471.1291.



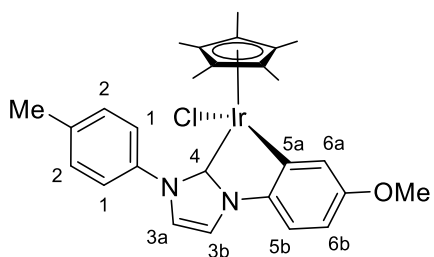
3.12b-Me,H*. ^1H NMR (400 MHz, CDCl_3) δ : 1.39 (s, 15H, C_5Me_5), 2.46 (s, 3H, *Me*), 7.00 (td, $J = 7.3, 1.5$ Hz, 1H, H^{6b}), 7.07 (td, $J = 7.3, 1.5$ Hz, H^7), 7.12 (dd, $J = 7.5, 1.3$ Hz, 1H, H^{5b}), 7.19 (d, $J = 2.0$ Hz, 1H, H^{3a}), 7.33 (d, $J = 7.8$ Hz, 2H, H^2), 7.54 (d, $J = 2.2$ Hz, 1H, H^{3b}), 7.80 (dd, $J = 6.4, 1.0$ Hz, 1H, H^{6a}), 7.94 (d, $J = 8.3$ Hz, 2H, H^1), $^{13}\text{C}\{^1\text{H}\}$ NMR (101 MHz, CDCl_3) δ : 9.3 (C_5Me_5), 21.2 (*Me*), 97.9 (d, $^1J_{\text{Rh-C}} = 4.8$ Hz, C_5Me_5), 110.8 (C^{5b}), 115.3 (C^{3b}), 122.3 (C^{3a}), 122.6 (C^{6b}), 125.1 (C^2), 125.7 (C^7), 129.9 (C^1), 137.7, 138.0 (*C-Me*), 138.4 (C^{6a}), 145.4, 159.7 (d, $^1J_{\text{Rh-C}} = 34.2$ Hz, C^{5a}), 181.4 (d, $^1J_{\text{Rh-C}} = 58.0$ Hz, C^4). ESIMS: m/z 471 $[\text{M-Cl}]^+$. HRMS (ESI): Calcd for $\text{C}_{26}\text{H}_{28}\text{N}_2^{103}\text{Rh} [\text{M-Cl}]^+$ 471.1308, found 471.1291.

3.12a-Me*,OMe and 3.12a-Me,OMe*

Following the general procedure, a mixture of $[\text{IrCl}_2\text{Cp}^*]_2$ (53 mg, 0.067 mmol), NaOAc (42 mg, 0.506 mmol), imidazolium salt **L3.12-Me,OMe** (54 mg, 0.131 mmol) and DCE (5 mL) was heated to 75 °C for 4 h. The product was purified by filtration through celite and then silica plug to yield mixture of **3.12a-Me*,OMe** and **3.12a-Me,OMe*** 1:1.1 as a yellow solid (15 mg, 17%).



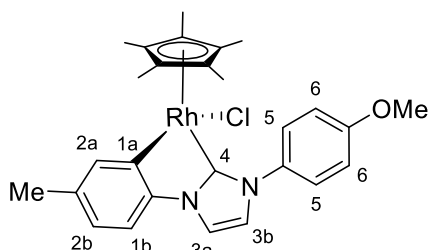
3.12a-Me*,OMe. ^1H NMR (400 MHz, CDCl_3): δ 1.47 (s, 15 H, C_5Me_5), 2.38 (s, 3H, *Me*), 3.88 (s, 3 H, *OMe*), 6.78 (dd, $J = 7.7, 1.1$ Hz, 1H, H^{2b}), 7.01 (d, $J = 9.0$ Hz, 2H, H^6), 7.07 (d, $J = 7.8$ Hz, 1H, H^{1b}), 7.13 (d, $J = 2.1$ Hz, 1H, H^{3b}), 7.44 (d, $J = 2.2$ Hz, 1H, H^{3a}), 7.56 (br.s, 1H, H^{2a}), 7.87 (d, $J = 8.8$ Hz, 2H, H^5), $^{13}\text{C}\{^1\text{H}\}$ NMR (101 MHz, CDCl_3): δ 9.1 (C_5Me_5), 21.3 (*Me*), 55.7 (*OMe*), 91.3 (C_5Me_5), 110.0 (C^{1b}), 114.4 (C^6), 114.9 (C^{3a}), 121.8 (C^{3b}), 122.6 (C^{2b}), 127.1 (C^5), 133.7, 135.0 (*C-Me*), 137.9 (C^{2a}), 142.9, 143.7 (C^{1a}), 159.3 (*C-OMe*), 163.1 (C^4). ESIMS: m/z 632 $[\text{M-Cl+MeCN}]^+$. HRMS (ESI): Calcd for $\text{C}_{29}\text{H}_{33}\text{N}_3\text{O}^{193}\text{Ir} [\text{M-Cl+MeCN}]^+$ 632.2253, found 632.2265.



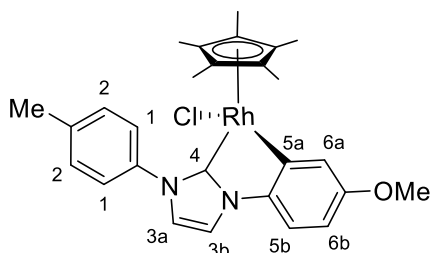
3.12a-Me,OMe*. ^1H NMR (400 MHz, CDCl_3): δ 1.46 (s, 15H, C_5Me_5), 2.45 (s, 3H, *Me*), 3.86 (s, 3H, *OMe*), 6.54 (dd, $J = 8.4, 2.6$ Hz, 1H, H^{6b}), 7.10 (d, $J = 8.4$ Hz, 1H, H^{5b}), 7.13(d, $J = 2.1$ Hz, 1H, H^{3a}), 7.31 (d, $J = 7.8$ Hz, 2 H, H^2), 7.33 (d, $J = 2.7$ Hz, 1H, H^{6a}), 7.42 (d, $J = 2.2$ Hz, 1H, H^{3b}), 7.81 (d, $J = 8.2$ Hz, 2H, H^1), $^{13}\text{C}\{^1\text{H}\}$ NMR (101 MHz, CDCl_3): δ 9.1 (C_5Me_5), 21.2 (*Me*), 55.4 (*OMe*), 91.4 (C_5Me_5), 106.8 (C^{6b}), 110.6 (C^{5b}), 114.9 (C^{3b}), 121.8 (C^{3a}), 122.7 (C^{6a}), 125.8 (C^1), 129.9 (C^2), 137.9, 138.0 (*C-Me*), 140.0 (C^{5a}), 144.8, 157.4 (*C-OMe*), 162.1 (C^4). ESIMS: m/z 632 $[\text{M-Cl+MeCN}]^+$. HRMS (ESI): Calcd for $\text{C}_{29}\text{H}_{33}\text{N}_3\text{O}^{193}\text{Ir} [\text{M-Cl+MeCN}]^+$ 632.2253, found 632.2265.

3.12b-Me*,OMe and 3.12b-Me,OMe*

Following the general procedure, a mixture of $[\text{RhCl}_2\text{Cp}^*]_2$ (39 mg, 0.063 mmol), NaOAc (41 mg, 0.504 mmol), imidazolium salt **L3.12b-Me,OMe**. (55 mg, 0.132 mmol) and DCE (5 mL) was heated to 50 °C for 2 h, then to 75 °C for 2 h, then K_2CO_3 (35 mg, 0.250 mmol) and NaCl (15 mg, 0.261 mmol) added and the mixture was heated to 75 °C for further 18 h. The product was purified by several precipitations from a MeOH/hexane to yield regioisomers **3.12b-Me*,OMe:3.12b-Me,OMe*** in 1:1.7 ratio as a yellow solid (39 mg, 57%).



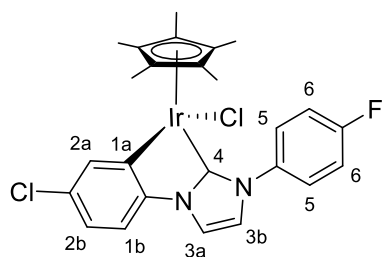
3.12b-Me*,OMe. ^1H NMR (400 MHz, CDCl_3) 1.40 (s, 15 H, C_5Me_5), 2.38 (s, 3H, *Me*), 3.88 (s, 3H, *OMe*), 6.79 (dd, $J = 7.8, 1.7$ Hz, 1H, H^{2b}), 6.99 (d, $J = 7.8$ Hz, 1H, H^{1b}), 7.04 (d, $J = 9.2$ Hz, 2H, H^6), 7.14 (d, $J = 2.1$ Hz, 1H, H^{3b}), 7.49 (d, $J = 2.1$ Hz, 1H, H^{3a}), 7.59 (d, $J = 1.1$ Hz, 1H, H^{2a}), 7.98 (d, $J = 8.8$ Hz, 2H, H^5), $^{13}\text{C}\{^1\text{H}\}$ NMR (101MHz, CDCl_3): δ 9.3 (C_5Me_5), 21.2 (*Me*), 55.6 (*OMe*), 97.7 (d, $^1J_{\text{Rh-C}} = 4.7$ Hz, C_5Me_5), 110.3 (C^{1b}), 114.3 (C^6), 115.3 (C^{3a}), 122.2 (C^{3b}), 123.1 (C^{2b}), 126.3 (C^5), 133.4, 134.5 (*C-Me*), 139.5 (C^{2a}), 143.2, 159.6 (*C-OMe*), 159.3 (d, $^1J_{\text{Rh-C}} = 34.2$ Hz, C^{1a}), 180.3 (d, $^1J_{\text{Rh-C}} = 58.0$ Hz, C^4). ESIMS: m/z 501 $[\text{M-Cl}]^+$. HRMS (ESI): Calcd for $\text{C}_{27}\text{H}_{30}\text{N}_2\text{OCl}^{103}\text{Rh} [\text{M-Cl}]^+$ 501.1413, found 501.1413.



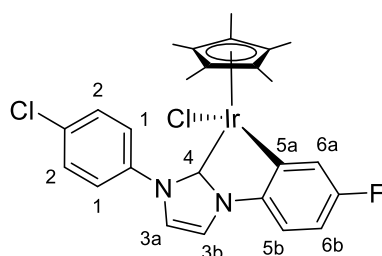
3.12b-Me,OMe*. ^1H NMR (400 MHz, CDCl_3) δ : 1.39 (s, 15 H, C_5Me_5), 2.46 (s, 3H, *Me*), 3.85 (s, 3H, *OMe*), 6.52 (dd, $J = 8.3, 2.7$ Hz, 1H, H^{6b}), 7.02 (d, $J = 8.4$ Hz, 1H, H^{5b}), 7.14 (d, $J = 2.1$ Hz, 1H, H^{3a}), 7.32 (d, $J = 8.0$ Hz, 2H, H^2), 7.38 (d, $J = 2.5$ Hz, 1H, H^{6a}), 7.46 (d, $J = 2.1$ Hz, 1H, H^{3b}), 7.92 (d, $J = 8.3$ Hz, 2H, H^1), $^{13}\text{C}\{^1\text{H}\}$ NMR (101MHz, CDCl_3): δ 9.3 (C_5Me_5), 21.1 (*Me*), 55.3 (*OMe*), 97.8 (d, $^1J_{\text{Rh-C}} = 5.6$ Hz, C_5Me_5), 107.4 (C^{6b}), 110.8 (C^{5b}), 115.3 (C^{3b}), 122.1 (C^{3a}), 123.8 (C^{6a}), 125.0 (C^2), 129.8 (C^1), 137.7, 137.8 (*C-Me*), 139.0, 159.1 (*C-OMe*), 161.2 (d, $^1J_{\text{Rh-C}} = 34.2$ Hz, C^{5a}), 179.2 (d, $^1J_{\text{Rh-C}} = 58.0$ Hz, C^4). ESIMS: m/z 501 $[\text{M-Cl}]^+$. HRMS (ESI): Calcd for $\text{C}_{27}\text{H}_{30}\text{ON}_2\text{Cl}^{103}\text{Rh} [\text{M-Cl}]^+$ 501.1413, found 501.1413.

3.12a-Cl*,F and 3.12a-Cl,F*

Following the general procedure, a mixture of $[\text{IrCl}_2\text{Cp}^*]_2$ (50 mg, 0.063 mmol), NaOAc (42 mg, 0.513 mmol), imidazolium salt **L3.12-Cl,F** (56 mg, 0.133 mmol) and DCE (5 mL) was heated to 75 °C for 4 h. The product was purified by filtration through celite and then silica plug to yield **3.12a-Cl*,F**: **3.12a-Cl,F*** in 2:1 ratio as a yellow solid (50 mg, 62%).



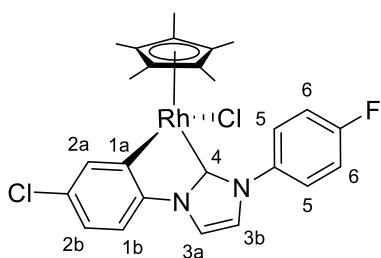
3.12a-Cl*,F. ^1H NMR (400 MHz, CDCl_3): δ 1.46 (s, 15H, C_5Me_5), 6.91 (dd, $J = 8.3, 2.2$ Hz, 1H, H^{2b}), 7.08 (d, $J = 8.2$ Hz, 1H, H^{1b}), 7.10 (d, $J = 2.2$ Hz, 1H, H^{3b}), 7.22 (dd, $J = 9.2, 8.1$ Hz, 2H, H^6), 7.44 (d, $J = 2.2$ Hz, 1H, H^{3a}), 7.64 (d, $J = 2.2$ Hz, 1H, H^{2a}), 7.95 .95 (dd, $J = 8.7, 4.4$ Hz, 2H, H^5), $^{13}\text{C}\{^1\text{H}\}$ NMR (126 MHz, CDCl_3): δ 9.1 (C_5Me_5), 91.8 (C_5Me_5), 111.4 (C^{1b}), 115.5 (C^{3a}), 116.4 (d, $^2J_{\text{C-F}} = 22.3$ Hz, C^6), 122.0 (C^{2b}), 122.1 (C^{3b}), 127.7 (br.d, $^3J_{\text{C-F}} = 8.0$ Hz, C^5), 130.6, 136.3 (d, $^4J_{\text{C-F}} = 3.2$ Hz), 136.5 (C^{2a}), 144.6 (C-Cl), 145.2 (C^{1a}), 162.2 (d, $^1J_{\text{C-F}} = 248.8$ Hz, C-F), 163.8 (C^4), $^{19}\text{F}\{^1\text{H}\}$ NMR (376 MHz, CDCl_3): δ -112.9 (F). ESIMS: m/z 640 $[\text{M-Cl+MeCN}]^+$. HRMS (ESI): Calcd for $\text{C}_{27}\text{H}_{27}\text{N}_3\text{FCl}^{193}\text{Ir} [\text{M-Cl+MeCN}]^+$ 640.1507, found 640.1508.



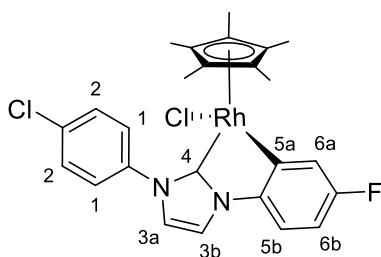
3.12a-Cl,F*. ^1H NMR (400 MHz, CDCl_3): δ 1.46 (s, 15 H, C_5Me_5), 6.64 (td, $J = 8.6, 2.7$ Hz, 1H, H^{6a}), 7.10 (d, $J = 2.2$ Hz, 1H, H^{3a}), 7.11 (m, 1H, H^{5b}), 7.41 (dd, $J = 9.3, 2.7$ Hz, 1H, H^{6a}), 7.44 (d, $J = 2.2$ Hz, 1H, H^{3b}), 7.50 (d, $J = 8.9$ Hz, 2H, H^2), 7.95 (d, $J = 8.9$ Hz, 2H, H^1), $^{13}\text{C}\{^1\text{H}\}$ NMR (126 MHz, CDCl_3): δ 9.1 (C_5Me_5), 91.8 (C_5Me_5), 108.3 (d, $^2J_{\text{C-F}} = 24.6$ Hz, C^{6b}), 110.0 (d, $^3J_{\text{C-F}} = 8.7$ Hz, C^{5b}), 115.6 (C^{3b}), 121.7 (C^{3a}), 123.3 (d, $^2J_{\text{C-F}} = 19.1$ Hz, C^{6a}), 127.2 (C^2), 129.6 (C^1), 134.1, 138.7 (C-Cl), 142.0, 145.6 (d, $^3J_{\text{C-F}} = 8.7$ Hz, C^{5a}), 160.7 (d, $^1J_{\text{C-F}} = 245.6$ Hz, C-F), 163.2 (C^4), $^{19}\text{F}\{^1\text{H}\}$ NMR (376 MHz, CDCl_3): δ 118.3 (F). ESIMS: m/z 640 $[\text{M-Cl+MeCN}]^+$. HRMS (ESI): Calcd for $\text{C}_{27}\text{H}_{27}\text{N}_3\text{FCl}^{193}\text{Ir} [\text{M-Cl+MeCN}]^+$ 640.1507, found 640.1508.

3.12b-Cl*,F and 3.12b-Cl,F*

Following the general procedure, a mixture of $[\text{RhCl}_2\text{Cp}^*]_2$ (39 mg, 0.063 mmol), NaOAc (41 mg, 0.504 mmol), imidazolium salt **L3.12-Cl,F** (56 mg, 0.132 mmol) and DCE (5 mL) was stirred at rt for 23h, then heated to 50 °C for 2 h, then to 75 °C for 1 h, then K_2CO_3 (35 mg, 0.253 mmol) and NaCl (15 mg, 0.248 mmol) were added and the mixture was heated to 75 °C for further 18 h. The product was purified by filtration through celite and then precipitated from DCM/hexanes several times to yield regioisomers **3.12b-Cl*,F**:**3.12b-Cl,F*** in 2:1 ratio as a yellow solid (51 mg, 80%).



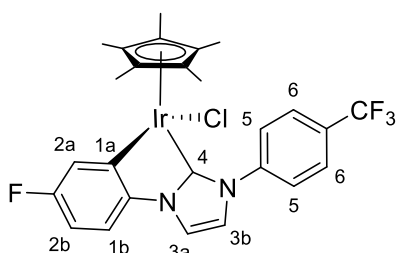
3.12b-Cl*,F. ^1H NMR (400 MHz, CDCl_3): δ 1.40 (s, 15H, C_5Me_5), 6.92 (dd, $J = 8.1, 2.2$ Hz, 1H, H^{2b}), 7.03 (d, $J = 8.1$ Hz, 1H, H^{1b}), 7.14 (d, $J = 2.2$ Hz, 1H, H^{3b}), 7.24 (t, $J = 8.6$ Hz, 2H, H^6), 7.52 (d, $J = 2.2$ Hz, H^{3a}), 7.69 (d, $J = 2.0$ Hz, 1H, H^{2a}), 8.06 (dd, $J = 8.4, 4.7$ Hz, 2H, H^5), $^{13}\text{C}\{^1\text{H}\}$ NMR (101MHz, CDCl_3): δ 9.3 (C_5Me_5), 98.1 (d, $^1J_{\text{C-Rh}} = 5.6$ Hz, C_5Me_5), 111.8 (C^{1b}), 116.0 (C^{3a}), 116.3 (d, $^2J_{\text{C-F}} = 22.3$ Hz, C^6), 122.5 (C^{3b}), 122.6 (C^{2b}), 127.0 (d, $^3J_{\text{C-F}} = 8.0$ Hz, C^4), 130.1, 136.1 (d, $^4J_{\text{C-F}} = 2.4$ Hz), 137.5 (C^{2a}), 144.0 (C-Cl), 161.8 (d, $^1J_{\text{C-Rh}} = 35.0$ Hz, C^{1a}), 162.2 (d, $^1J_{\text{C-F}} = 248.8$ Hz, C-F), 180.9 (d, $^1J_{\text{C-Rh}} = 58.0$ Hz, C^4). $^{19}\text{F}\{^1\text{H}\}$ NMR (376 MHz, CDCl_3): δ -112.8 (F). ESIMS: m/z 543 $[\text{M-Cl}]^+$. HRMS (ESI): Calcd for $\text{C}_{25}\text{H}_{24}\text{N}_2\text{FCl}^{103}\text{Rh}$ $[\text{M-Cl}]^+$ 550.0933, found 550.0939.



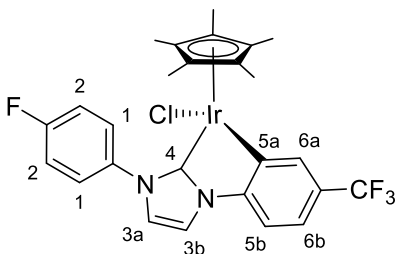
3.12b-Cl,F*. ^1H NMR (400 MHz, CDCl_3) δ : 1.40 (s, 15H, C_5Me_5), 6.66 (td, $J = 8.5, 2.6$ Hz, 1H, H^{6b}), 7.05 (dd, $J = 8.3, 4.4$ Hz, 1H, H^{5b}), 7.16 (d, $J = 2.2$ Hz, 1H, H^{3a}), 7.48 (dd, $J = 8.8, 2.5$ Hz, 1H, H^{6a}), 7.52 (m, 3H, H^2, H^{3b}), 8.06 (d, $J = 8.8$ Hz, 2H, H^1), $^{13}\text{C}\{^1\text{H}\}$ NMR (101MHz, CDCl_3): δ 9.3 (C_5Me_5), 98.1 (d, $^1J_{\text{C-Rh}} = 5.6$ Hz, C_5Me_5), 109.0 (d, $^2J_{\text{C-F}} = 23.8$ Hz, C^{6b}), 111.3 (d, $^3J_{\text{C-F}} = 8.7$ Hz, C^{5b}), 116.0 (C^{3b}), 122.2 (C^{3a}), 124.5 (d, $^2J_{\text{C-F}} = 19.1$ Hz, C^{6a}), 126.4 (C^1), 129.5 (C^2), 134.0, 138.5 (C-Cl), 141.5, 159.9 (d, $^1J_{\text{C-F}} = 247.2$ Hz, C-F), 162.4 (dd, $^1J_{\text{C-Rh}} = 35.0$ Hz, $^3J_{\text{C-F}} = 4.0$ Hz, C^{5a}), 180.4 (d, $^1J_{\text{C-Rh}} = 57.2$ Hz, C^4), $^{19}\text{F}\{^1\text{H}\}$ NMR (376 MHz, CDCl_3): δ -117.8 (F). ESIMS: m/z 543 $[\text{M-Cl}]^+$. HRMS (ESI): Calcd for $\text{C}_{25}\text{H}_{24}\text{N}_2\text{FCl}^{103}\text{Rh}$ $[\text{M-Cl}]^+$ 550.0933, found 550.0939.

3.12a-F*,CF₃ and 3.12a-F,CF₃*

Following the general procedure, a mixture of [IrCl₂Cp*]₂ (51 mg, 0.063 mmol), NaOAc (42 mg, 0.516 mmol), imidazolium salt **L3.12-F,CF₃** (60 mg, 0.132 mmol) and DCE (5 mL) and heated to 75 °C for 4 h. The product was purified by filtration through celite and then silica plug to yield **3.12a-F*,CF₃:3.12a-F,CF₃*** in 1:3 ratio as a yellow solid (40 mg, 59%).



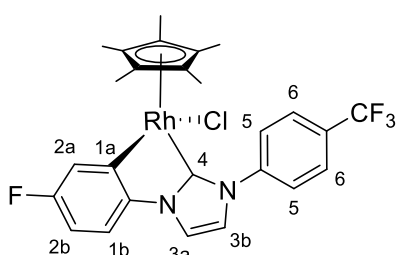
3.12a-F*,CF₃: ¹H NMR (400 MHz, CD₂Cl₂): δ 1.43 (s, 15H, C₅Me₅), 6.62 (td, *J* = 8.6, 2.7 Hz, 1H, H^{2b}), 7.12 (m, 2H, H^{3b}, H^{1b}), 7.42 (dd, *J* = 9.3, 2.6 Hz, 1H, H^{2a}), 7.47 (d, *J* = 2.2 Hz, 1H, H^{3a}), 7.80 (d, *J* = 8.8 Hz, 2H, H⁶), 8.15 (d, *J* = 8.4 Hz, 2H, H⁵), ¹³C{¹H} NMR (126 MHz, CDCl₃): δ 9.0 (C₅Me₅), 91.8 (C₅Me₅), 108.4 (d, ²*J*_{C-F} = 25.1 Hz, C^{2b}), 111.1 (d, ³*J*_{C-F} = 9.0 Hz, C^{1b}), 116.0 (C^{3a}), 121.5 (C^{3b}), 123.3 (d, ²*J*_{C-F} = 19.1 Hz, C^{2a}), 126.0 (q, ¹*J*_{C-F} = 250.0 Hz, CF₃), 126.1 (C⁵), 126.6 (q, ³*J*_{C-F} = 3.0 Hz, C⁶), 130.3 (q, ²*J*_{C-F} = 33.1 Hz, C-CF₃), 141.9, 142.9, 145.6 (d, ³*J*_{C-F} = 5.0 Hz, C^{1a}), 160.8 (d, ³*J*_{C-F} = 246.0 Hz, C-F), 163.6 (C⁴), ¹⁹F{¹H} NMR (376 MHz, CDCl₃): δ -118.1 (F), -62.4 (CF₃). ESIMS: *m/z* 674 [M-Cl+MeCN]⁺. HRMS (ESI): Calcd for C₂₈H₂₇N₃F₄¹⁹³Ir [M-Cl+MeCN]⁺ 674.1771 found 674.1793.



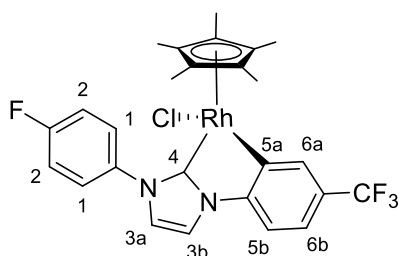
3.12a-F,CF₃*: ¹H NMR (400 MHz, CDCl₃): δ 1.46 (s, 15H, C₅Me₅), 7.04 (d, *J* = 2.2 Hz, 1H, H^{3a}), 7.11 (br. d, *J* = 8.3 Hz, 1H, H^{6b}), 7.19 (br. d, *J* = 8.1 Hz, 1H, H^{5b}), 7.24 (t, *J* = 8.1 Hz, 2H, H²), 7.51 (d, *J* = 2.2 Hz, 1H, H^{3b}), 7.95 (1H, br.s, 1H, H^{6a}), 7.98 (m, 2H, H¹), ¹³C{¹H} NMR (126 MHz, CDCl₃): δ 9.0 (C₅Me₅), 91.9 (C₅Me₅), 110.0 (C^{5b}), 115.7 (C^{3b}), 116.4 (d, ²*J*_{C-F} = 23.1 Hz, C²), 119.8 (q, ³*J*_{C-F} = 4.0 Hz, C^{6b}), 122.3 (C^{3a}), 124.7 (q, ¹*J*_{C-F} = 272.1 Hz, CF₃), 127.2 (q, ²*J*_{C-F} = 31.1 Hz, C-CF₃), 127.6 (d, ³*J*_{C-F} = 7.0 Hz, C¹), 133.6 (q, ³*J*_{C-F} = 3.0 Hz, C^{6a}), 136.2 (d, ³*J*_{C-F} = 3.0 Hz), 143.4, 148.7 (C^{5a}), 162.3 (d, ¹*J*_{C-F} = 250.0 Hz, C-F), 164.8 (C⁴), ¹⁹F{¹H} NMR (376 MHz, CDCl₃): δ -112.7 (F), -61.2 (CF₃). ESIMS: *m/z* 674 [M-Cl+MeCN]⁺. HRMS (ESI): Calcd for C₂₈H₂₇N₃F₄¹⁹³Ir [M-Cl+MeCN]⁺ 674.1771 found 674.1793.

3.12b-F*,CF₃ and 3.12b-F,CF₃*

Following the general procedure, a mixture of [RhCl₂Cp*]₂ (39 mg, 0.062 mmol), NaOAc (41 mg, 0.504 mmol), imidazolium salt **L3.12-F,CF₃** (61 mg, 0.133 mmol) and DCE (5 mL) was heated to 50 °C for 2 h, then to 75 °C for 1 h, then K₂CO₃ (35 mg, 0.252 mmol) and NaCl (15 mg, 0.248 mmol) were added and the mixture was heated to 75 °C for further 18 h. The product was purified by filtration through celite and then precipitated from DCM/hexane several times to yield regioisomers **3.12b-F*,CF₃**:**3.12b-F,CF₃*** in 1:3 ratio as a yellow solid (44 mg, 60%).



3.12b-F*,CF₃. ¹H NMR (400 MHz, CDCl₃) δ: 1.37 (s, 15H, C₅Me₅), 6.62 (td, *J* = 8.6, 2.7 Hz, 1H, H^{2b}), 7.04 (dd, *J* = 8.4, 4.4 Hz, 1H, H^{1b}), 7.17 (d, *J* = 2.0 Hz, 1H, H^{3b}), 7.47 (dd, *J* = 8.7, 2.3 Hz, 1H, H^{2a}), 7.54 (d, *J* = 2.2 Hz, 1H, H^{3a}), 7.82 (d, *J* = 8.6 Hz, 2H, H⁶), 8.26 (d, *J* = 8.1 Hz, 2H, H¹), ¹³C{¹H} NMR (101MHz, CDCl₃): δ 9.3 (C₅Me₅), 98.2 (d, ¹*J*_{Rh-C} = 4.8 Hz, C₅Me₅), 109.2 (d, ²*J*_{C-F} = 23.8 Hz, C^{2b}), 111.4 (d, ³*J*_{C-F} = 8.7 Hz, C^{1b}), 116.3 (C^{3a}), 122.0 (C^{3b}), 124.6 (d, ²*J*_{C-F} = 19.1 Hz, C^{2a}), 125.1 (q, ¹*J*_{C-F} = 274.0 Hz, C-CF₃), 125.5 (C⁵), 126.6 (q, ³*J*_{C-F} = 3.2 Hz, C⁶), 130.4 (q, ²*J*_{C-F} = 33.1Hz, C-CF₃), 141.4, 142.7, 160.1 (d, ¹*J*_{C-F} = 248.0 Hz, C-F), 162.5 (dd, ¹*J*_{Rh-C} = 35.0 Hz, ³*J*_{C-F} = 4.0 Hz, C^{1a}), 181.3 (d, ¹*J*_{Rh-C} = 58.0 Hz, C⁴), ¹⁹F{¹H} NMR (376 MHz, CDCl₃): δ -117.7 (F), -62.4 (CF₃). ESIMS: *m/z* 543[M-Cl]⁺. HRMS (ESI): Calcd for C₂₆H₂₄N₂F₄¹⁰³Rh [M-Cl]⁺ 543.0931, found 543.0935. Anal Calcd for C₂₆H₂₄N₂ClF₄Rh [M]: C, 53.95; H, 4.18; N, 4.84; found C, 53.83; H, 4.20; N, 4.83%.

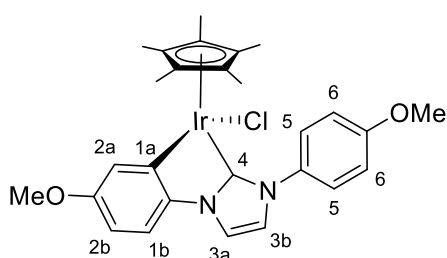


3.12b-F,CF₃*. ¹H NMR (400 MHz, CDCl₃): δ 1.39 (s, 15H, C₅Me₅), 7.00 (d, *J* = 2.2 Hz, 1H, H^{3a}), 7.08 (br. d, *J* = 8.2 Hz, H^{6b}), 7.13 (br. d, *J* = 8.2 Hz, H^{5b}), 7.26 (t, *J* = 8.6 Hz, 2H, H²), 7.60 (d, *J* = 2.2 Hz, 1H, H^{3b}), 8.00 (s, 1H, H^{6a}), 8.08 (dd, *J* = 8.4, 4.6 Hz, 2H, H¹), ¹³C{¹H} NMR (101MHz, CDCl₃): δ 9.3 (C₅Me₅), 98.4 (d, ¹*J*_{Rh-C} = 4.8 Hz, C₅Me₅), 110.5 (C^{5b}), 116.2 (C^{3b}), 116.4 (d, ²*J*_{C-F} = 23.1 Hz, C²), 120.4 (q, ³*J*_{C-F} = 4.0 Hz, C^{6b}), 122.7 (C^{3a}), 124.7 (q, ¹*J*_{C-F} = 273.4 Hz, C-CF₃), 126.8 (q, ²*J*_{C-F} = 31.8 Hz, C-CF₃), 127.0 (d, ³*J*_{C-F} = 8.0 Hz, C¹), 134.8 (q, ³*J*_{C-F} = 3.2 Hz, C^{6a}), 136.0 (d, ⁴*J*_{C-F} = 2.4 Hz), 148.2, 160.1 (d, ¹*J*_{Rh-C} = 35.0 Hz, C^{5a}), 162.3 (d, ¹*J*_{C-F} = 248.8 Hz, C-F), 182.2 (d, ¹*J*_{Rh-C} = 58.0 Hz, C⁴), ¹⁹F{¹H}

NMR (376 MHz, CDCl₃): δ -112.5 (*F*), -61.2 (*CF*₃). ESIMS: *m/z* 543[M-Cl]⁺. HRMS (ESI): Calcd for C₂₆H₂₄N₂F₄¹⁰³Rh [M-Cl]⁺ 543.0931, found 543.0935. Anal Calcd for C₂₆H₂₄N₂ClF₄Rh [M]: C, 53.95; H, 4.18; N, 4.84; found C, 53.83; H, 4.20; N, 4.83%.

3.12a-OMe*,OMe

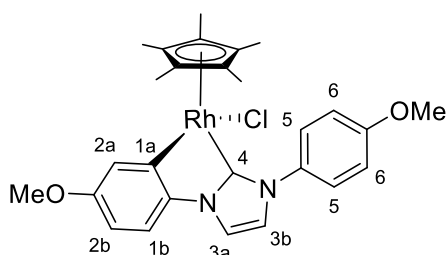
Following the general procedure, a mixture of [IrCl₂Cp*]₂ (51 mg, 0.063 mmol), NaOAc (41 mg, 0.497 mmol), imidazolium salt **L3.12-OMe,OMe** (52 mg, 0.140 mmol) and DCE (5 mL) was heated to 75 °C for 4 h. The product was purified by filtration through celite and then silica plug to yield **3.12a-OMe*,OMe** as a yellow solid (41 mg, 51%).



3.12a-OMe*,OMe. ¹H NMR (400 MHz, CDCl₃): δ 1.48 (s, 15H, C₅Me₅), 3.86 (s, 3H, OMe), 3.88 (s, 3H, OMe), 6.55 (dd, *J* = 2.5, 8.4 Hz, 1H, *H*^{2b}), 7.03 (d, *J* = 9.2 Hz, 2H, *H*⁶), 7.10 (d, *J* = 8.4 Hz, 1H, *H*^{1b}), 7.13 (d, *J* = 2.2 Hz, 1H, *H*^{3b}), 7.33 (d, *J* = 2.5 Hz, 1H, *H*^{2a}), 7.41 (d, *J* = 2.2, 1H, *H*^{3a}), 7.86 (br. d, *J* = 8.6 Hz, 2H, *H*⁵), ¹³C{¹H} NMR (126 MHz, CDCl₃): δ 9.1 (C₅Me₅), 55.4 (OMe), 55.6 (OMe), 91.3 (C₅Me₅), 106.8 (C^{2b}), 110.6 (C^{1b}), 114.5 (C⁶), 114.8 (C^{3a}), 121.8 (C^{2a}), 122.7 (C^{3b}), 127.1 (C¹), 133.6, 140.0 (C^{1a}), 144.6, 157.3 (C-OMe), 159.2 (C-OMe), 162.1 (C⁴). ESIMS: *m/z* 607 [M-Cl]⁺. HRMS (ESI): Calcd for C₂₇H₃₀¹⁹³IrN₂O₂ [M-Cl]⁺ 607.1937, found 607.1942. ESIMS: *m/z* 648 [M-Cl+MeCN]⁺. HRMS (ESI): Calcd for C₂₉H₃₃N₃O₂¹⁹³Ir [M-Cl+MeCN]⁺ 648.2202, found 648.2225.

3.12b-OMe*,OMe

Following the general procedure, a mixture of [RhCl₂Cp*]₂ (40 mg, 0.065 mmol), NaOAc (42 mg, 0.506 mmol), imidazolium salt **L3.12-OMe,OMe** (51 mg, 0.138 mmol) and DCE (5 mL) was heated to 75 °C for 20 h. The product was purified by filtration through celite and precipitated from DCM/hexane to yield **3.12b-OMe*,OMe** as an orange solid (70 mg, 97%).

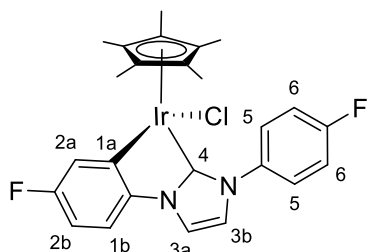


3.12b-OMe*,OMe. ¹H NMR (400 MHz, CDCl₃) δ : 1.42 (s, 15H, C₅Me₅), 3.87 (s, 3H, OMe), 3.89 (s, 3H, OMe), 6.56 (dd, *J* = 8.4, 2.5 Hz, 1H, *H*^{2b}), 7.05 (m, 3H, *H*^{1b}, *H*⁶), 7.18 (d, *J* = 2.2 Hz, 1H, *H*^{3b}), 7.39 (d, *J* = 2.5 Hz, 1H, *H*^{2a}), 7.48 (d, *J* = 2.2 Hz, 1H,

H^{3a}), 7.98 (d, $J = 8.6$ Hz, 2H, H^5), $^{13}\text{C}\{^1\text{H}\}$ NMR (126 MHz, CDCl_3): δ 9.4 (C_5Me_5), 55.4 (OMe), 55.6 (OMe), 97.8 (d, $^1J_{\text{Rh-C}} = 5.0$ Hz C_5Me_5), 107.6 (C^{2b}), 110.9 (C^{1b}), 114.4 (C^6), 115.2 (C^{3a}), 122.3 (C^{3b}), 123.9 (C^{2a}), 126.4 (C^5), 133.5, 139.5, 156.7 (C-OMe), 156.7 (C-OMe), 162.8 (d, $^1J_{\text{Rh-C}} = 34.1$ Hz, C^{1a}), 180.5 (d, $^1J_{\text{Rh-C}} = 57.2$ Hz, C^4). ESIMS: m/z 558 $[\text{M-Cl+MeCN}]^+$. HRMS (ESI): Calcd for $\text{C}_{27}\text{H}_{30}\text{N}_2\text{O}_2^{103}\text{Rh} [\text{M-Cl}]^+$ 517.1362, found 517.1359.

3.12a-F*,F

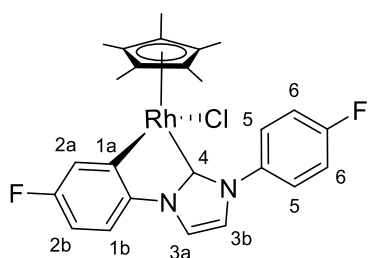
Following the general procedure, a mixture of $[\text{IrCl}_2\text{Cp}^*]_2$ (40 mg, 0.05 mmol), NaOAc (35 mg, 0.431 mmol), imidazolium salt **L3.12-F,F** (44 mg, 0.108 mmol) and DCE (5 mL) was heated to 75 °C for 4 h. The product was purified by filtration through celite and then silica plug to yield **3.12a-F*,F** as a yellow solid (39 mg, 63%).



3.12a-F*,F. ^1H NMR (400 MHz, CDCl_3): δ 1.45 (s, 15H, C_5Me_5), 6.68 (td, $J = 8.6, 2.7$ Hz, 1H, H^{2b}), 7.13 (dd, $J = 8.5, 4.6$ Hz, 1H, H^{1b}), 7.16 (d, $J = 2.1$ Hz, 1H, H^{3b}), 7.22 (t, $J = 8.6$ Hz, 2H, H^6), 7.42 (dd, $J = 9.2, 2.6$ Hz, 1H, H^{2a}), 7.45 (d, $J = 2.2$ Hz, 1H, H^{3a}), 7.95 (br dd, $J = 8.5, 4.76$ Hz, 2H, H^5), $^{13}\text{C}\{^1\text{H}\}$ NMR (126 MHz, CDCl_3): δ 9.0 (C_5Me_5), 91.6 (C_5Me_5), 108.3 (d, $^2J_{\text{C-F}} = 24.1$ Hz, C^{2b}), 110.9 (d, $^3J_{\text{C-F}} = 9.0$ Hz, C^{1b}), 115.4 (C^{3a}), 116.3 (d, $^2J_{\text{C-F}} = 22.1$ Hz, C^6), 121.9 (C^{3b}), 123.2 (d, $^2J_{\text{C-F}} = 19.1$ Hz, C^{2a}), 127.7 (br d, $^3J_{\text{C-F}} = 8.0$ Hz, C^5), 136.36 (d, $^4J_{\text{C-F}} = 2.0$ Hz), 141.7, 145.60 (d, $^3J_{\text{C-F}} = 5.02$ Hz, C^{1a}), 160.7 (d, $^1J_{\text{C-F}} = 244.9$ Hz, C-F), 162.2 (d, $^1J_{\text{C-F}} = 249.0$ Hz, C-F), 163.2 (C^4). $^{19}\text{F}\{^1\text{H}\}$ NMR (376 MHz, CDCl_3): δ -118.4 (F), -113.0 (F). ESIMS: m/z 624 $[\text{M-Cl+MeCN}]^+$. HRMS (ESI): Calcd for $\text{C}_{27}\text{H}_{27}\text{N}_3\text{F}_2^{193}\text{Ir} [\text{M-Cl+MeCN}]^+$ 624.1802, found 624.1812.

3.12b-F*,F

Following the general procedure, a mixture of $[\text{RhCl}_2\text{Cp}^*]_2$ (30.0 mg, 0.049 mmol), NaOAc (32.0 mg, 0.390 mmol), imidazolium salt **L3.12-F,F** (41.0 mg, 0.101 mmol) and DCE (4 mL) was heated to 75 °C for 2 h, then K_2CO_3 (27.8 mg, 0.201 mmol) and NaCl (12.1 mg, 0.205 mmol) added and mixture heated to 75 °C for further 18 h. The product was purified by filtration through celite and then precipitated from DCM/hexane to yield **3.12b-F*,F** as a yellow solid (40.7 mg, 79%).



3.12b-F*,F ^1H NMR (400 MHz, CDCl_3) δ : 1.40 (s, 15H, C_5Me_5), 6.68 (td, $J = 8.5, 2.6$ Hz, 1H, H^{2b}), 7.06 (dd, $J = 8.4, 4.5$ Hz, 1H, H^{1b}), 7.17 (d, $J = 2.0$ Hz, 1H, H^{3b}), 7.25 (t, $J = 8.6$ Hz, 2H, H^6), 7.48 (dd, $J = 8.8, 2.2$ Hz, 1H, H^{2a}), 7.51 (d, $J = 2.2$ Hz, 1H, H^{3a}), 8.07 (dd, $J = 8.7, 4.5$ Hz, 1H, 2H, H^5), $^{13}\text{C}\{^1\text{H}\}$ NMR (101MHz, CDCl_3) δ : 9.3 (C_5Me_5), 98.1 (d, $^1J_{\text{C-Rh}} = 4.8$ Hz, C_5Me_5), 109.0 (d, $^2J_{\text{C-F}} = 24.0$ Hz, C^{2b}), 111.2 (d, $^3J_{\text{C-F}} = 8.0$ Hz, C^{1b}), 115.8 (C^{3a}), 116.3 (d, $^2J_{\text{C-F}} = 22.4$ Hz, C^6), 122.4 (C^{3b}), 124.4 (d, $^2J_{\text{C-F}} = 19.2$ Hz, C^{2a}), 127.0 (d, $^3J_{\text{C-F}} = 8.0$ Hz, C^5), 136.2, 141.6, 159.8 (d, $^1J_{\text{C-F}} = 225.3$ Hz, C-F), 162.3 (d, $^1J_{\text{C-F}} = 225.3$ Hz, C-F), 162.4 (dd, $^1J_{\text{C-Rh}} = 34.4$ Hz, $^3J_{\text{C-F}} = 4.0$ Hz, C^{1a}), 180.4 (d, $^1J_{\text{C-Rh}} = 57.5$ Hz, C^4), $^{19}\text{F}\{^1\text{H}\}$ NMR (376 MHz, CDCl_3): δ -118.2 (F), -112.9 (F). ESIMS: m/z 543[M-Cl] $^+$. HRMS (ESI): Calcd for $\text{C}_{25}\text{H}_{24}\text{N}_2\text{F}_2^{103}\text{Rh}$ [M-Cl] $^+$ 493.0963, found 493.0954.

6.3c General procedure for D-incorporation experiments

An NMR tube was charged with the appropriate metal complex **3.12a/b-R,R** (R = OMe, F) (5 mg, 0.008 mmol for Ir, 0.009 mmol for Rh), PivOD (*ca.* 1 eq.) and CD_3OD (0.5 mL) as well as few drops of DCM (*ca.* 0.1 mL) (until all of the complex dissolved) and allowed to sit at rt for 24-48 h, then heated to 70 °C for 1-24 h. The percentage of deuteration was monitored and determined by ^1H NMR spectroscopy by comparing the relative integrations for signals for H^1 , H^5 , H^{2b} . The deuterium incorporation was additionally confirmed by ^2H NMR spectroscopy.

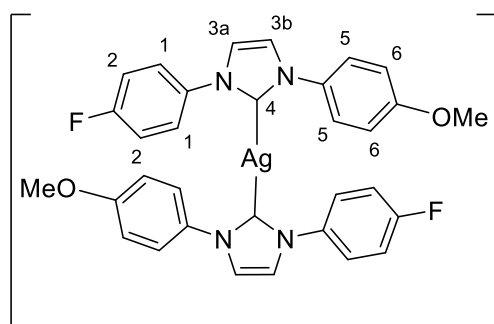
6.3d Transmetalation from Ag and Cu-NHCs with {IrCp*} and {RhCp*}

General procedure for synthesis of Ag-NHCs **3.13-F,R₁**

An oven-dried Schlenk flask was wrapped in foil and charged with imidazolium salt (1 eq.), Ag_2O (1.5 eq.) and MeCN (5 mL), then sealed with a screw-cap, placed under N_2 atmosphere, transferred to a preheated oil bath and stirred at 80 °C for 18 h. The reaction mixture was cooled to rt with continuous stirring. The mixture was filtered through celite and the solvent was removed by rotary evaporation, the resulting brown residue was redissolved several times in DCM and filtered through celite until the final product was obtained as an off-white powder.

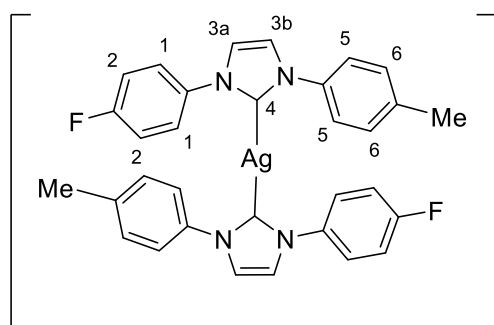
Synthesis of Ag-NHCs 3.13-F,R1

3.13-F,OMe



OTf Following the general procedure, the mixture of **L3.12-F,OMe** (38.7 mg, 0.093 mmol), Ag₂O (24.1 mg, 0.104 mmol) and MeCN (5 mL) was heated at 80 °C overnight. **3.13-F,OMe** was obtained as an off-white powder (35.0 mg, 95%). ¹H NMR (500 MHz, CDCl₃): δ 3.85 (s, 6H, OMe), 6.84 (d, *J* = 8.9 Hz, 4H, *H*⁶), 7.06 (t, *J* = 8.4 Hz, 4H, *H*²), 7.37 (d, *J* = 8.7 Hz, 4H, *H*⁵), 7.39 (d, *J* = 1.8 Hz, 2H, *H*^{3a/3b}), 7.43 (d, *J* = 2.0 Hz, 2H, *H*^{3a/3b}), 7.46 (dd, *J* = 8.9, 4.6 Hz, 4H, *H*¹), ¹³C{¹H} NMR (126 MHz, CDCl₃): δ 55.6 (OMe), 114.7 (*C*⁶), 116.5 (d, ²*J*_{C-F} = 23.1 Hz, *C*²), 122.7 (*C*^{3a/3b}), 123.2 (*C*^{3a/3b}), 125.4 (*C*¹), 126.0 (d, ³*J*_{C-F} = 9.0 Hz, *C*¹), 132.5, 135.7 (d, ⁴*J*_{C-F} = 3.0 Hz), 159.9 (C-OMe) 162.4 (d, ¹*J*_{C-F} = 250.0 Hz, C-F), 178.8 (m, *C*⁴), ¹⁹F{¹H} NMR (376 MHz, CDCl₃): δ -75.2 (OTf), -108.8 (F). ESIMS: *m/z* 645 [M]⁺. HRMS (ESI): Calcd for C₃₂H₂₆N₄O₂F₂¹⁰⁹Ag [M]⁺ 645.1071, found 645.1082.

3.13-F,Me



OTf Following the general procedure, the mixture of **L3.12-F,Me** (130.0 mg, 0.323 mmol), Ag₂O (118.8 mg, 0.510 mmol) and MeCN (10 mL) was heated at 80 °C overnight. **3.13-F,Me** was obtained off-white powder (106.4 mg, 87%). ¹H NMR (400 MHz, CDCl₃): δ 2.44 (s, 6H, Me), 7.14 (t, *J* = 8.5 Hz, 4H, *H*²), 7.26 (d, *J* = 8.1 Hz, 4H, *H*⁶), 7.42 (d, *J* = 8.4 Hz, 4H, *H*⁵), 7.44 (s, 4H, *H*^{3a}, *H*^{3b}), 7.54 (dd, *J* = 9.0, 4.5 Hz, 4H, *H*¹), ¹³C{¹H} NMR (101 MHz, CDCl₃): δ 21.1 (Me), 116.9 (d, ²*J*_{C-F} = 23.4 Hz, *C*²), 122.8 (*C*^{3a/3b}), 123.0 (*C*^{3a/3b}), 123.8 (*C*⁶), 126.0 (d, ³*J*_{C-F} = 8.6 Hz, *C*¹), 130.5 (*C*⁵), 135.7 (d, ⁴*J*_{C-F} = 3.1 Hz), 137.0, 139.6, 162.7 (d, ¹*J*_{C-F} = 250.0 Hz, C-F), 177.7 (m, *C*⁴), ¹⁹F{¹H} NMR (376 MHz, CDCl₃): δ -77.6 (OTf), -111.0 (F). ESIMS: *m/z* 611 [M]⁺.

General procedure for transmetallations from Ag-NHC **3.13-F,R** with {IrCp*} and {RhCp*}

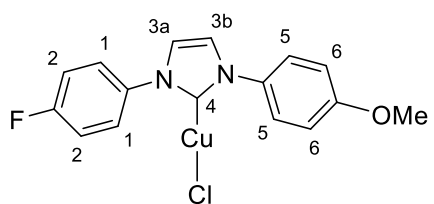
An aluminium foil-wrapped Schlenk flask charged with $[MCl_2Cp^*]_2$ (M = Ir, Rh) (1 eq.), NaOAc (8 eq.) and DCM (1-4 mL) and purged with N₂ three times and stirred at rt for 15 min. Then Ag-NHC **3.13-F,R** was added and the mixture stirred at rt overnight with measurements taken after 0.5 h, 1 h and 2 h.

General procedure for synthesis of Cu-NHCs **3.16-R₁,R₂**

The Cu-NHCs **3.16-R₁,R₂** were prepared as *per* modified literature procedure.¹⁸ The appropriate imidazolium salt **L3.12-R₁,R₂** (1 eq.), CuCl (1.2 eq.) and K₂CO₃ (2 eq.) were placed in an aluminium-foil wrapped Schlenk flask, purged with N₂ three times, then dry DCM (2-4 mL) was added, the mixture heated at 50 °C overnight. Afterwards, the mixture was allowed to cool to rt and was filtered through celite and the solvent was removed by rotary evaporation. Note, heating the reaction mixture in acetone and open to air as *per* literature procedure was found to lead to oxidation of imidazolium salts instead of formation of Cu-NHCs.

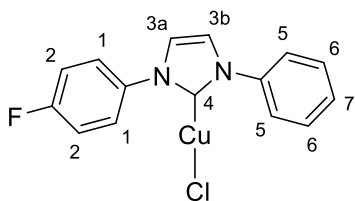
Synthesis of Cu-NHCs **3.16-R₁,R₂**

3.16-F,OMe



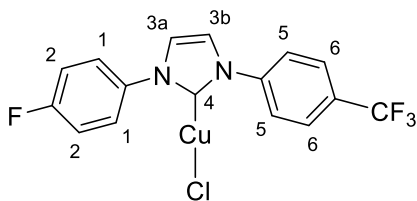
Following the general procedure, a Schlenk flask was loaded with **L3.12-F,OMe** (40.8 mg, 0.098 mmol), CuCl (14.6 mg, 0.147 mmol), K₂CO₃ (29.8 mg, 0.216 mmol) and DCM (4 mL) and heated to 50 °C overnight. The product was purified by filtration through cotton wool to yield **3.16-F,OMe** as an off-white powder (30.2 mg, 81%). ¹H NMR (400 MHz, CDCl₃): δ 3.79 (s, 3H, OMe), 6.86 (br d, *J* = 8.3 Hz, 2H, H⁶), 7.04 (br t, *J* = 8.2 Hz, 2H, H²), 7.28 (s, 2H, H^{3a}, H^{3b}), 7.43 (br d, *J* = 8.6 Hz, 2H, H⁵), 7.51 (br dd, *J* = 8.7, 4.5 Hz, 2H, H¹), ¹³C{¹H} NMR (101 MHz, CDCl₃): δ 55.6 (OMe), 114.9 (C⁶), 116.8 (d, ²*J*_{C-F} = 23.0 Hz, C²), 121.8 (C^{3a/3b}), 122.4 (C^{3a/3b}), 125.0 (C⁵), 125.7 (d, ³*J*_{C-F} = 8.7 Hz, C¹), 132.3, 135.5 (d, ⁴*J*_{C-F} = 3.2 Hz), 160.0 (C-OMe), 162.1 (d, ¹*J*_{C-F} = 250.3 Hz, C-F), ¹⁹F{¹H} NMR (376 MHz, CDCl₃): δ -111.7 (F). N.B. ¹³C NMR spectra was too weak to assign C⁴.

3.16-F,H



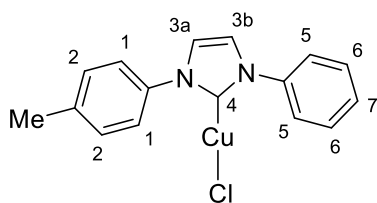
Following the general procedure, a Schlenk flask was loaded with **L3.12-F,H** (50.0 mg, 0.129 mmol), CuCl (15.1 mg, 0.153 mmol), K₂CO₃ (41.3 mg, 0.299 mmol) and DCM (2.4 mL) and heated to 50 °C overnight. The product was purified by filtration through cotton wool to yield **3.16-F,H** as an off-white powder (35.7 mg, 82%). ¹H NMR (400 MHz, CDCl₃): δ 7.09 (br t, *J* = 8.4 Hz, 2H, *H*²), 7.40 (d, *J* = 2.0 Hz, *H*^{3a/3b}), 7.42 (d, *J* = 2.0 Hz, *H*^{3a/3b}), 7.45 (m, 3H, *H*⁶, *H*⁷), 7.52 - 7.68 (m, 4H, *H*¹, *H*⁵), ¹³C{¹H} NMR (101 MHz, CDCl₃): δ 116.8 (d, ²*J*_{C-F} = 23.0 Hz, *C*²), 122.2 (*C*^{3a/3b}), 122.2 (*C*^{3a/3b}), 123.7 (*C*⁶), 125.7 (d, ³*J*_{C-F} = 8.7 Hz, *C*²), 129.1 (*C*⁷), 129.9 (*C*⁵), 135.5 (d, ⁴*J*_{C-F} = 3.2 Hz), 139.2, 162.5 (d, ¹*J*_{C-F} = 249.5 Hz, C-F), 175.0 (br s, *C*⁴), ¹⁹F{¹H} NMR (376 MHz, CDCl₃): δ -111.6 (*F*).

3.16-F,CF₃



Following the general procedure, a Schlenk flask was loaded with **L3.12-F,CF₃** (52.6 mg, 0.115 mmol), CuCl (14.6 mg, 0.147 mmol), K₂CO₃ (36.5 mg, 0.265 mmol) and DCM (2.4 mL) and heated to 50 °C overnight. The product was purified by filtration through cotton wool to yield **3.16-F,CF₃** as an off-white powder (43.4 mg, 93%). ¹H NMR (400 MHz, CDCl₃): δ 7.07 (br t, *J* = 8.4 Hz, 2H, *H*¹), 7.38 (d, *J* = 2.0 Hz, 1H, *H*^{3a/3b}), 7.42 (d, *J* = 1.7 Hz, *H*^{3a/3b}), 7.62 (dd, *J* = 8.9, 4.5 Hz, 2H, *H*¹), 7.66 (br d, *J* = 8.6 Hz, 2H, *H*⁵), 7.80 (d, *J* = 8.3 Hz, 2H, *H*⁶), ¹³C{¹H} NMR (101 MHz, CDCl₃): δ 116.8 (d, ²*J*_{C-F} = 23.8 Hz, *C*²), 121.9 (*C*^{3a/3b}), 122.8 (*C*^{3a/3b}), 124.2 (*C*⁵), 125.8 (d, ³*J*_{C-F} = 8.7 Hz, *C*¹), 127.1 (q, ³*J*_{C-F} = 4.0 Hz, *C*⁶), 131.1 (q, ²*J*_{C-F} = 32.6 Hz, C-CF₃), 135.3 (d, ⁴*J*_{C-F} = 3.2 Hz), 141.9, 162.5 (d, ¹*J*_{C-F} = 250.3 Hz, C-F), 175.5 (br s, *C*⁴), ¹⁹F{¹H} NMR (376 MHz, CDCl₃): δ -62.7 (CF₃), -111.2 (*F*).

3.16-Me,H



Following the general procedure, a Schlenk flask was loaded with **L3.12-Me,H** (35.3 mg, 0.092 mmol), CuCl (11.9 mg, 0.120 mmol), K₂CO₃ (26.9 mg, 0.195 mmol) and DCM (3 mL) and heated to 60 °C overnight. The product was purified by filtration through cotton wool to yield **3.16-Me,H** as an off-white powder (28.5 mg, 93%). ¹H NMR (400 MHz, CDCl₃):

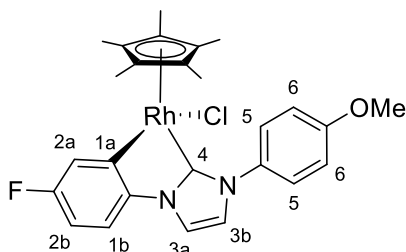
δ 2.38 (s, 3H, *Me*), 7.14 (br d, $J = 7.6$ Hz, 2H, H^2), 7.37 (m, 5H, H^{3a} , H^{3b} , H^6 , H^7), 7.46 (d, $J = 7.5$ Hz, 2H, H^1) 7.50 (br d, $J = 6.1$ Hz, 2H, H^5), $^{13}\text{C}\{^1\text{H}\}$ NMR (101 MHz, CDCl_3): δ 21.1 (*Me*), 122.3 ($C^{3a/3b}$), 122.5 ($C^{3a/3b}$), 123.5 (C^6), 123.7 (C^1), 129.0 (C^7), 129.8 (C^5), 130.3 (C^2), 136.9, 139.1, 139.3, 174.0 (br.s, C^4).

General procedure for transmetallations from Cu-NHC **3.16-R₁,R₂** with {IrCp*} and {RhCp*}

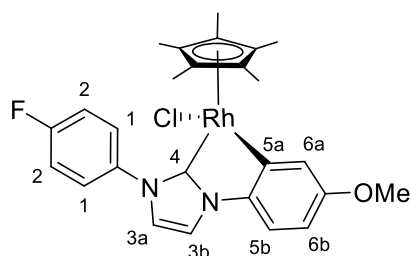
An aluminium foil-wrapped Schlenk flask charged with $[\text{MCl}_2\text{Cp}^*]_2$ (M = Ir, Rh) (1 eq.), NaOAc (8 eq.) and DCM (1-2 mL) and purged with N_2 three times and stirred at rt for 15 min. Then Cu-NHC **3.16-R₁,R₂** was added and the mixture stirred at rt overnight with measurements taken after 0.5, 1 and 2 h.

3.12b-F,OMe

Following the general procedure, a Schlenk flask was loaded with $[\text{RhCl}_2\text{Cp}^*]_2$ (8 mg, 0.0126 mmol), NaOAc (8.2mg, 0.100 mmol), imidazolium salt **3.16b-F,OMe** (10 mg, 0.028 mmol) and DCM (1 mL) and stirred at rt for 30 mins. The product was purified by filtration through celite and then precipitated from DCM/hexane several times to yield **3.12b-F*,OMe:3.12b-F,OMe*** in 9.3:1 ratio as a yellow solid (10 mg, 74%).



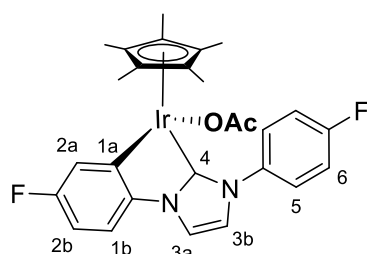
3.12b-F*,OMe. ^1H NMR (400 MHz, CDCl_3): δ 1.40 (s, 15 H, C_5Me_5), 3.88 (s, 3H, *OMe*), 6.65 (td, $J = 8.5, 2.7$ Hz, 1H, H^{2b}), 7.04 (d, $J = 9.2$ Hz, 2H, H^6), 7.04 (m, 1H, H^{1b}), 7.14 (d, $J = 2.0$ Hz, 1H, H^{3b}), 7.47 (dd, $J = 8.1, 0.6$ Hz, 1H, H^{2a}), 7.48 (d, $J = 2.1$ Hz, 1H, H^{3a}), 7.95 (d, $J = 8.8$ Hz, 2H, H^6), $^{13}\text{C}\{^1\text{H}\}$ NMR (101MHz, CDCl_3): δ 9.3 (C_5Me_5), 55.6 (*OMe*), 98.0 (d, $^1J_{\text{Rh-C}} = 5.0$ Hz, C_5Me_5), 109.0 (d, $^2J_{\text{C-F}} = 24.4$ Hz, C^{2b}), 111.1 (d, $^3J_{\text{C-F}} = 9.5$ Hz, C^{1b}), 114.7 (C^6), 115.4 (C^{3a}), 122.6 (C^{3b}), 124.5 (d, $^2J_{\text{C-F}} = 19.1$ Hz, C^{2a}), 126.5 (C^5), 133.6, 141.7 (d, $J = 1.7$ Hz), 159.4 (*C-OMe*), 159.9 (d, $^1J_{\text{C-F}} = 248.0$ Hz, *C-F*), 162.6 (dd, $^1J_{\text{Rh-C}} = 34.9$ Hz, $^3J_{\text{C-F}} = 4.0$ Hz, C^{1a}), 180.0 (d, $^1J_{\text{Rh-C}} = 57.8$ Hz, C^4), $^{19}\text{F}\{^1\text{H}\}$ NMR (376 MHz, CDCl_3): δ -118.1 (*F*), ESIMS: m/z 505 $[\text{M-Cl}]^+$. HRMS (ESI): Calcd for $\text{C}_{26}\text{H}_{27}\text{N}_2\text{OF}^{103}\text{Rh} [\text{M-Cl}]^+$ 505.1162, found 505.1162.



3.12b-F,OMe*. ¹H NMR (400 MHz, CDCl₃): δ 1.40 (s, 15H, C₅Me₅), 3.81 (s, 3H, OMe), 6.51 (dd, *J* = 8.4, 2.6 Hz, 1H, H^{6b}), 7.04 (m, 1H, H^{5b}), 7.14 (d, *J* = 2.0 Hz, 1H, H^{3a}), 7.21 (t, *J* = 8.2 Hz, H²), 7.36 (d, *J* = 2.2 Hz, H^{6a}), 7.48 (d, *J* = 2.0 Hz, 1H, H^{3b}), 8.06 (dd, *J* = 9.1, 4.9 Hz, 2H, H¹), ¹⁹F{¹H} NMR (376 MHz, CDCl₃): δ -111.7 (F). ESIMS: *m/z* 505 [M-Cl]⁺. HRMS (ESI): Calcd for C₂₆H₂₇N₂O¹⁰³Rh [M-Cl]⁺ 505.1162, found 505.1162.

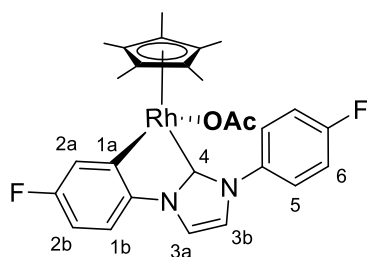
6.3e Preparation and study of acetate complexes 3.12a/b-R,R(OAc)

3.12a-F*,F(OAc)



An aluminium foil wrapped, N₂ purged Schlenk flask was charged with **3.12a-F*,F** (18 mg, 0.028 mmol), AgOAc (7 mg, 0.042 mmol) and DCM (2 mL) capped, and stirred in the dark for 2 h. Afterwards the reaction mixture was filtered through celite, 0.2 mL of hexane added and the solution was allowed to sit for 1 h, filtered through celite again (to ensure removal of excess of Ag), and the solvent removed by rotary evaporation to give **3.12a-F*,F(OAc)** as a purple solid (17.7 mg, 95%). ¹H NMR (400 MHz, CDCl₃): δ 1.40 (s, 15H, C₅Me₅), 1.78 (s, 3H, OCOCH₃), 6.68 (td, *J* = 8.6, 2.7 Hz, 1H, H^{2b}), 7.09 (dd, *J* = 8.4, 4.7 Hz, 1H, H^{1b}), 7.18 (d, *J* = 2.0 Hz, 1H, H^{3b}), 7.22 (t, *J* = 8.6 Hz, 2H, H⁶), 7.44 (d, *J* = 2.0 Hz, 1H, H^{3a}), 7.63 (dd, *J* = 9.3, 2.7 Hz, 1H, H^{2a}), 7.81 (dd, *J* = 8.8, 4.8 Hz, 2H, H⁵), ¹³C{¹H} NMR (101 MHz, CDCl₃): δ 9.2 (C₅Me₅), 23.5 (OCOCH₃), 90.3 (C₅Me₅), 108.2 (d, ²*J*_{C-F} = 24.6 Hz, C^{2b}), 110.3 (d, ³*J*_{C-F} = 8.7 Hz, C^{2a}), 115.2 (C^{3a}), 116.3 (d, ²*J*_{C-F} = 22.3 Hz, C⁶), 121.6 (C^{3b}), 123.4 (d, ²*J*_{C-F} = 19.9 Hz, C^{2a}), 127.4 (d, ³*J*_{C-F} = 8.7 Hz, C⁵), 136.7 (d, ⁴*J*_{C-F} = 3.2 Hz), 142.9, 146.0 (d, ³*J*_{C-F} = 4.8 Hz, C^{1a}), 160.3 (d, ¹*J*_{C-F} = 244.8 Hz, C-F), 162.0 (d, ¹*J*_{C-F} = 248.8 Hz, C-F), 166.0 (C⁴), 177.4 (OCOCH₃), ¹⁹F{¹H} NMR (376MHz, CDCl₃): δ -118.9 (F), -113.6 (F).

3.12b-F*,F(OAc)



An aluminium foil wrapped, N₂ purged Schlenk flask was charged with **3.12b-F*,F** (20.2 mg, 0.0383 mmol), AgOAc (8 mg, 0.048 mmol) and DCM (2 mL) and stirred in the dark for 2 h. Afterwards the reaction mixture was filtered through celite, 0.2 mL of hexane added and the solution was allowed to sit for 1h, filtered through celite again (to ensure removal of excess of Ag), the solvent removed by rotary evaporation to give **3.12b-F*,F(OAc)** as an orange solid (20.3 mg, 96%). ¹H NMR (400 MHz, CDCl₃): δ 1.35 (s, 15H, C₅Me₅), 1.75 (s, 3H, OCOCH₃), 6.70 (td, *J* = 8.6, 2.7 Hz, 1H, H^{2b}), 7.04 (dd, *J* = 8.4, 4.5 Hz, 1H, H^{1b}), 7.22 (d, *J* = 2.1Hz, 1H, H^{3b}), 7.23 (t, *J* = 8.6 Hz, 2H, H⁶), 7.50 (d, *J* = 2.2 Hz, 1H, H^{3a}), 7.64 (dd, *J* = 8.8, 2.7 Hz, 1H, H^{2a}) 7.89 (dd, *J* = 9.0, 4.8 Hz, 2H, H⁵), ¹³C{H} NMR (101 MHz, CDCl₃): δ 9.3 (C₅Me₅), 24.7 (OCOCH₃), 97.0 (d, ¹*J*_{C-Rh} = 5.6 Hz C₅Me₅), 109.0 (d, ²*J*_{C-F} = 24.6 Hz, C^{2b}), 110.7 (d, ³*J*_{C-F} = 8.7 Hz, C^{2a}), 115.6 (C^{3a}), 116.2 (d, ³*J*_{C-F} = 22.3 Hz, C⁵), 122.1 (C^{3b}), 124.4 (d, ²*J*_{C-F} = 19.9 Hz, C^{2a}), 126.7 (d, ³*J*_{C-F} = 7.9 Hz, C⁵), 136.6 (d, ⁴*J*_{C-F} = 3.2 Hz), 142.4, (d, ⁴*J*_{C-F} = 1.6 Hz), 158.6 (d, ¹*J*_{C-F} = 241.6 Hz, C-F), 161.8 (d, ¹*J*_{C-F} = 243.2 Hz, C-F), 162.9 (dd, ¹*J*_{C-Rh} = 35.6, ³*J*_{C-F} = 4.0 Hz, C^{1a}), 176.9 (OCOCH₃), 183.4 (d, ¹*J*_{C-Rh} = 58.0 Hz, C⁴), ¹⁹F{¹H} NMR (376MHz, CDCl₃): δ -118.7 (F), -113.6 (F).

General procedure for acetate to chloride exchange with 3.12a/b-F*,F(OAc)

An NMR tube was charged with the appropriate **3.12a/b-F*,F(OAc)** complex (1.0 eq., ca. 5 mg.) and CDCl₃ or CD₂Cl₂ (0.5 mL). The reference ¹H NMR and ¹⁹F NMR spectra recorded. To this Et₄NCl was added in portions and the ¹H NMR and ¹⁹F NMR spectra were recorded after 5 mins and 30 mins after every addition of Et₄NCl. The reaction was monitored at time intervals (1 h, 4 h, 24 h, several days) and the relative percentage of formed chloride complex was determined by the integration of H^{2a} and H^{3b} signals of the **3.12a/b-F*,F(OAc)** and formed chloride **3.12a/b-F*,F** complexes in the ¹H NMR spectrum.

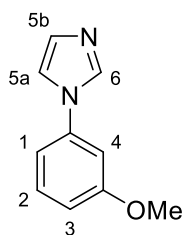
6.3f Synthesis of *meta*-substituted phenylimidazolium salts L3.18-R and their precursors 3.17-R

6.3fi Synthesis of *meta*-substituted phenylimidazoles 3.17-R

General procedure for synthesis of *meta*-substituted phenylimidazoles 3.17-R

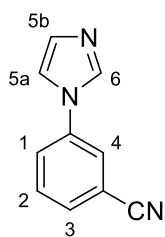
3.17-R were prepared according to a modified literature procedure.¹⁴ *meta*-Substituted arylhalide (1 eq.), imidazole (1.5 eq.), Cs₂CO₃ (2 eq.), CuO₂ (10 mol%) and MeCN or DMF (5-10 mL) were added to a Schlenk flask, sealed with a screw-cap, placed under N₂ atmosphere, partially evacuated, transferred to an oil bath and stirred at 100-120 °C for 1-5 days behind a blast shield. Afterwards the reaction mixture was cooled to rt, followed by filtration through celite. The solvent was removed by rotary evaporation and pure phenylimidazole was obtained by column chromatography (EtOAc:Pet. Ether, Biotage Isolera).

3.17-OMe



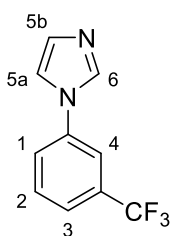
Following the general procedure, a mixture of 1-bromo-3-methoxybenzene (0.65 mL, 960 mg, 5.133 mmol), imidazole (525 mg, 7.362 mmol), Cs₂CO₃ (3362 mg, 10.313 mmol), Cu₂O (74 mg, 0.520 mmol, 10 mol%) and MeCN (10 mL) was heated to 110 °C for 5 days. Purification by column chromatography (DCM to DCM:MeOH 9:1, Biotage Isolera) yielded **3.17-OMe** as a colourless oil (768 mg, 86%). ¹H NMR (500 MHz, CDCl₃): δ 3.86 (s, 3H, OMe), 6.88 - 6.94 (m, 2H, H¹, H⁴), 6.98 (ddd, *J* = 7.9, 2.1, 1.0 Hz, 1H, H³), 7.20 (t, *J* = 1.2 Hz, 1H, H^{5b}), 7.27 (m, 1H, H^{5a}), 7.38 (t, *J* = 8.0 Hz, 1H, H²), 7.85 (t, *J* = 1.1 Hz, 1H, H⁶), ¹³C{¹H} NMR (126 MHz, CDCl₃): δ 55.4 (OMe), 107.6 (C³), 112.5 (C¹), 113.6 (C⁴), 118.1 (C^{5a}), 130.3 (C^{5b}), 130.6 (C²), 135.5 (C⁶), 138.4, 160.6. ESIMS: *m/z* 175 [M+H].

3.17-CN



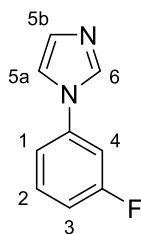
Following the general procedure, a mixture of 1-bromo-3-benzonitrile (911 mg, 5.004 mmol), imidazole (510 mg, 7.506 mmol), Cs₂CO₃ (3255 g, 9.984 mmol), Cu₂O (72 mg, 0.506 mmol, 10 mol%) and DMF (10 mL) was heated to 110 °C for 4 days. Purification by column chromatography (DCM to DCM:MeOH 95:5, Biotage Isolera) yielded **3.17-CN** as a white solid (689 mg, 81%). ¹H NMR (500 MHz, CDCl₃): δ 7.26 (s, 1H, *H*^{5b}), 7.31 (s, 1H, *H*^{5a}), 7.57 - 7.69 (m, 3H, *H*¹⁻³), 7.70 (d, *J* = 1.8 Hz, 1H, *H*⁴), 7.90 (s, 1H, *H*⁶), ¹³C{¹H} NMR (126 MHz, CDCl₃): δ 114.3, 117.4, 117.8 (*C*^{5a}), 124.6 (*C*⁴), 125.5 (*C*¹) 130.8 (*C*^{5b}), 131.0 (*C*²), 131.4 (*C*³), 135.4 (*C*⁶), 138.0. ESIMS: *m/z* 170 [M+H].

3.17-CF₃



Following the general procedure, a mixture of 1-bromo 3-trifluoromethylbenzene (0.55 mL, 877 mg, 5.001 mmol), imidazole (510 mg, 7.500 mmol), Cs₂CO₃ (3331 mg, 10.218 mmol), Cu₂O (74 mg, 0.520 mmol, 10 mol%) and MeCN (10 mL) was heated to 110 °C for 1 day. Purification by column chromatography (DCM to DCM:MeOH 9:1, Biotage Isolera) yielded **3.17-CF₃** as a colourless oil (386 mg, 1.821 mmol, 36%). ¹H NMR (500 MHz, CDCl₃): δ 7.24 (s, 1H, *H*^{5b}), 7.27 (s, 1H, *H*^{5a}), 7.58 - 7.69 (m, 4H, *H*¹⁻⁴), 7.88 (s, 1H, *H*⁶), ¹³C{¹H} NMR (126 MHz, CDCl₃): δ 118.0 (*C*^{5a}), 118.3 (q, ³*J*_{C-F} = 3.0 Hz, *C*³), 123.3 (br d, ¹*J*_{C-F} = 272.0 Hz, CF₃), 124.1 (q, ³*J*_{C-F} = 4.0 Hz, *C*⁴), 124.6 (*C*²), 130.7 (*C*^{5b}), 131.1 (*C*¹), 132.5 (q, ²*J*_{C-F} = 32.5 Hz, C-CF₃), 135.5 (*C*⁶), 137.8, ¹⁹F{¹H} NMR (376 MHz, CDCl₃): δ -62.8 (CF₃). ESIMS: *m/z* 213 [M+H].

3.17-F



Following the general procedure, a mixture of 1-Iodo- 3-fluorobenzene (540 mg, 2.433 mmol), imidazole (260 mg, 3.826 mmol), Cs₂CO₃ (1534 mg, 4.706 mmol), Cu₂O (42 mg, 0.295 mmol, 12 mol%) and MeCN (5 mL) was heated to 105 °C for 2 days. Purification by column chromatography (DCM to DCM:MeOH 98:2, Biotage Isolera) yielded **3.17-F** as a colourless oil (236 mg, 60%). ¹H NMR (400 MHz, CDCl₃): δ 7.07 (tdd, *J* = 8.3, 8.3, 2.4, 0.9 Hz, 1H, *H*³), 7.12 (dt, *J* = 9.5, 2.2 Hz, 1H, *H*⁴), 7.17 - 7.24 (m, 2H, *H*^b, *H*¹), 7.28 (s, 1H, *H*^{5a}), 7.45 (td, *J* = 8.2, 6.1Hz, 1H, *H*²), 7.87 (s, 1H, *H*⁶), ¹³C{¹H} NMR (126 MHz, CDCl₃): δ 108.7 (d, ²*J*_{C-F} = 25.1Hz, *C*⁴), 114.1 (d, ²*J*_{C-F} = 21.1 Hz, *C*³), 116.7 (d, ⁴*J*_{C-F} = 3.0 Hz, *C*¹), 117.9

(C^{5a}), 130.5 (C^{5b}), 131.1 (d, $^3J_{C-F} = 10.0$ Hz, C^2), 135.3 (C^6), 138.5 (d, $^3J_{C-F} = 10.0$ Hz), 163.0 (d, $^1J_{C-F} = 248.0$ Hz, C-F), $^{19}\text{F}\{^1\text{H}\}$ NMR (376 MHz, CDCl_3): δ -110.0 (F). ESIMS: m/z 163 [M+H].

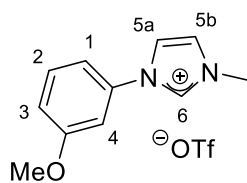
6.3fii Synthesis of *meta*-substituted phenylimidazolium salts L3.18-R

General procedure for methylation of *meta*-substituted phenylimidazoles L3.18-R

A nitrogen flushed Schlenk flask was charged with magnetic stirrer, *meta*-substituted phenylimidazole (1 eq.), dry DCM (4-6 mL), methyl trifluoromethanesulfonate (1.1 eq.), capped and stirred at rt for 2-4 h. Then solvent was removed by rotary evaporation and the product was either precipitated from DCM/ Et_2O mixture or washed with Et_2O to yield imidazolium salt L3.18-R.

Preparation of *meta*-substituted phenylimidazolium salts L3.18-R

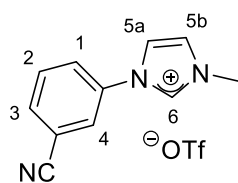
L3.18-OMe



Following the general procedure, a mixture **3.17-OMe** (174 mg, 1.002 mmol), dry DCM (4 mL), methyl trifluoromethanesulfonate (0.125 mL, 181 mg, 1.105 mmol), capped was stirred at rt for 4 h.

The formed oil was washed with Et_2O (3 x 5 mL) to yield **L3.18-OMe** as a colourless oil (244 mg, 72%). ^1H NMR (400 MHz, CD_3CN): δ 3.88 (s, 3H, OMe), 3.97 (s, 3H, Me), 7.14 (m, 1H, H), 7.19 - 7.24 (m, 2H, H^l , H^d), 7.51 (t, $J = 8.4$ Hz, 1H, H^2), 7.57 (t, $J = 1.9$ Hz, 1H, H^{5b}), 7.80 (t, $J = 2.0$ Hz, 1H, H^{5a}), 9.23 (s, 1H, H^6), $^{13}\text{C}\{^1\text{H}\}$ NMR (126 MHz, CD_3CN): δ 37.3 (Me), 56.8 (OMe), 109.0 (C^4), 115.0 (C^l), 116.7 (C^3), 121.8 (d, $J=320.2$ Hz, OTf), 122.3 (C^{5a}), 125.3 (C^{5b}), 132.2 (C^2), 136.6 (C^6), 136.8, 161.8. $^{19}\text{F}\{^1\text{H}\}$ NMR (376 MHz, CD_3CN): δ -79.3 (OTf). ESIMS: m/z 189 [M] $^+$. HRMS (ESI): Calcd for $\text{C}_{11}\text{H}_{13}\text{N}_2\text{O}$ [M] $^+$ 189.1028, found 189.1028.

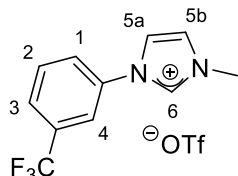
L3.18-CN



Following the general procedure, a mixture of **3.17-CN** (253 mg, 1.497 mmol), dry DCM (6 mL), methyl trifluoromethanesulfonate (0.19 mL, 278 mg, 1.680 mmol) was stirred at rt for 2.5 h. The product was precipitated from a DCM/ Et_2O to yield **L3.18-CN** as a white solid (412 mg, 1.237 mmol, 83%). ^1H NMR (400 MHz, CD_3OD): δ 4.08 (s, 3H, Me), 7.84 (m, 2H, H^d , H^{5b}), 7.97 (dt, $J = 7.9, 1.3$ Hz, 1H, H^l), 8.05 (ddd, $J = 8.3, 2.4, 1.1$

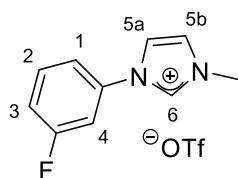
Hz, 1H, H^3), 8.12 (t, $J = 1.8$ Hz, 1H, H^{5b}), 8.20 (t, $J = 1.7$ Hz, 1H, H^4) 9.51 (s, 1H, H^6), $^{13}\text{C}\{^1\text{H}\}$ NMR (101 MHz, CD_3OD): δ 37.2 (*Me*), 115.6, 118.3, 121.9 (d, $^1J_{\text{C-F}} = 318.7$ Hz, *OTf*), 123.0 (C^{5a}), 126.1 (C^{5b}), 127.3 (C^4), 128.2 (C^3), 132.9 (C^2), 134.9 (C^1), 137.2, 137.8 (C^6), $^{19}\text{F}\{^1\text{H}\}$ NMR (376 MHz, CD_3OD): δ -80.0 (*OTf*). ESIMS: m/z 227 [M] $^+$. HRMS (ESI): Calcd for $\text{C}_{11}\text{H}_{10}\text{N}_3$ [M] $^+$ 184.0875, found 184.0883.

L3.18-CF₃



Following the general procedure, a mixture of **3.17-CF₃** (213 mg, 1.007 mmol), dry DCM (4 mL), methyl trifluoromethanesulfonate (0.130 mL, 189 mg, 1.150 mmol) was stirred at rt for 3 h. The product was precipitated from a DCM/Et₂O to yield **L3.18-CF₃** as a white solid (306 mg, 81%). ^1H NMR (400 MHz, CD_3OD): δ 4.06 (s, 3H, *Me*), 7.81 (d, $J = 2.2$ Hz, 1H, H^{5b}), 7.88 (m, 1H, H^2), 7.94 (d, $J = 7.8$ Hz, 1H, H^3), 8.01 (d, $J = 8.2$ Hz, 1H, H^1), 8.11 (s, 1H, H^4), 8.15 (d, $J = 1.2$ Hz, 1H, H^{5a}), 9.55 (s, 1H, H^6), $^{13}\text{C}\{^1\text{H}\}$ NMR (126 MHz, CD_3OD): δ 37.1 (*Me*), 120.9 (q, $^3J_{\text{C-F}} = 4.2$ Hz, C^4), 121.8 (q, $^1J_{\text{C-F}} = 319.2$ Hz, *OTf*), 123.1 (C^{5a}), 124.8 (q, $^1J_{\text{C-F}} = 272.0$ Hz, CF_3), 126.0 (C^{5b}), 127.5 (C^1), 128.1 (q, $^3J_{\text{C-F}} = 4.0$ Hz, C^3), 132.8 (C^2) 133.8 (q, $^2J_{\text{C-F}} = 33.5$ Hz, C-CF_3), 137.2 (q, $^4J_{\text{C-F}} = 3.0$ Hz), 137.9 (C^6), $^{19}\text{F}\{^1\text{H}\}$ NMR (376 MHz, CD_3OD): δ -80.1 (*OTf*), -64.3 (CF_3). ESIMS: m/z 227 [M] $^+$. HRMS (ESI): Calcd for $\text{C}_{11}\text{H}_{10}\text{N}_2\text{F}_3$ [M] $^+$ 227.0796, found 227.0796.

L3.18-F



Following the general procedure, a mixture of **3.17-F** (166 mg, 1.022 mmol), dry DCM (4 mL), methyl trifluoromethanesulfonate (0.130 mL, 189 mg, 1.150 mmol) was stirred at rt for 2.5 h. The formed oil was washed with Et₂O (3 x 5mL) to yield **L3.18-F** as a colourless oil (325 mg, 98%). ^1H NMR (400 MHz, CD_3OD): δ 4.04 (s, 3H, *Me*), 7.34 (tdd, $J = 8.4, 8.4, 2.4, 1.0$ Hz, 1H, H^3), 7.57 (m, 2H, H^1, H^4), 7.65 (td, $J = 8.3, 5.6$ Hz, 1H, H^2), 7.76 (t, $J = 1.8$ Hz, 1H, H^{5b}), 8.05 (t, $J = 2.0$ Hz, 1H, H^{5a}), 9.47 (s, 1H, H^6), $^{13}\text{C}\{^1\text{H}\}$ NMR (126 MHz, CD_3OD): δ 37.1 (*Me*), 111.2 (d, $^2J_{\text{C-F}} = 27.1$ Hz, C^4), 118.2 (d, $^2J_{\text{C-F}} = 21.1$ Hz, C^3), 119.3 (d, $^4J_{\text{C-F}} = 3.0$ Hz, C^1), 121.9 (d, $^1J_{\text{C-F}} = 318.2$ Hz, *OTf*), 122.8 (C^{5a}), 125.9 (C^{5b}), 133.4 (d, $^3J = 9.0$ Hz, C^2), 137.5 (C^6), 137.6 (d, $^3J_{\text{C-F}} = 10.0$ Hz), 164.5 (d, $^1J_{\text{C-F}} = 249.0$ Hz, C-F), $^{19}\text{F}\{^1\text{H}\}$ NMR (376 MHz, CD_3OD): δ -111.0 (*F*), -80.0 (*OTf*). ESIMS: m/z 177 [M] $^+$. HRMS (ESI): Calcd for $\text{C}_{10}\text{H}_{10}\text{N}_2\text{F}$ [M] $^+$ 177.0828, found 177.0832.

6.3g Cyclometallation of *meta*-substituted phenylimidazolium salts L3.18-R with {IrCp*} and {RhCp*}

General procedure for cyclometallation of *meta*-substituted phenylimidazolium salts L3.18-R with {IrCp*} and {RhCp*} in DCE

[MCl₂Cp*]₂ (M = Ir, Rh) (1 eq.), NaOAc (8 eq.) were placed in an oven-dried Schlenk flask, sealed with a screw-cap, evacuated for 15 mins and placed under N₂ atmosphere. DCE (2 mL) added and mixture stirred for another 15 mins. The appropriate imidazolium salt **L3.18-R** (2.1 eq.) and Et₄NCl (2 eq.) was added, and the Schlenk flask transferred to a preheated oil bath and stirred at 50 °C for 1-2 h, then at 70 °C for 1-6 h. The reaction mixture was cooled to rt with continuous stirring, diluted with DCM (10 mL), filtered through celite and solvent removed by rotary evaporation. The pure products were isolated by several precipitations from DCM/hexane.

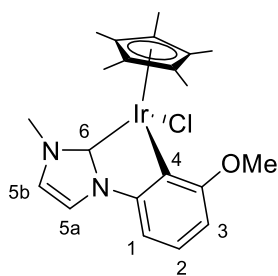
General procedure for cyclometallation of *meta*-substituted phenylimidazolium salts L3.18-R with {IrCp*} and {RhCp*} in DCM:MeOH

[MCl₂Cp*]₂ (M = Ir, Rh) (1 eq., 0.0251 mmol), NaOAc (8 eq.) were placed in an oven-dried Schlenk flask, sealed with a screw-cap, evacuated for 15 mins and placed under N₂ atmosphere. Dry DCM (1.6 mL) and MeOH (0.4 mL) were added and the mixture stirred for another 15 mins. The appropriate imidazolium salt (2.1 eq.) and Et₄NCl (2 eq.) was added and the mixture stirred at rt overnight and then heated to 50 °C overnight. The reactions were monitored by ¹H NMR spectroscopy by comparing the relative integrations of the appropriate signals (H³ of the *ortho*-isomers compared to the H³ of the *para*-isomers).

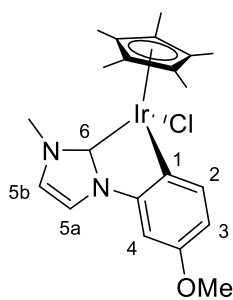
Cyclometallation of *meta*-substituted phenylimidazolium salts L3.18-R with {IrCp*} and {RhCp*}

3.18a-OMe

Following the general procedure, a mixture of [IrCl₂Cp*]₂ (20 mg, 0.0251 mmol), NaOAc (17 mg, 0.207 mmol), **L3.18-OMe** (18 mg, 0.0533 mmol), Et₄NCl (9 mg, 0.053 mmol), DCE (2 mL) was heated to 50 °C for 2 h, then heated further at 70 °C for 6 h. The product was purified by crystallisation from DCM/hexane to yield **3.18a-OMe** (*ortho:para* ratio 1:2.2) as a yellow powder (29.9 mg, 94%).



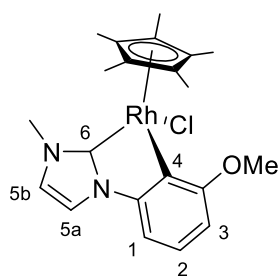
ortho-3.18a-OMe. ^1H NMR (400 MHz, CDCl_3): δ 1.85 (s, 15H, C_5Me_5), 3.82 (s, 3H, *OMe*), 3.97 (s, 3H, *Me*), 6.54 (dd, $J = 7.9$, 1.1 Hz, 1H, H^3), 6.83 (dd, $J = 7.7$, 1.1 Hz, 1H, H^1), 6.93 (t, $J = 8.3$ Hz, 1H, H^2), 6.95 (d, $J = 2.2$ Hz, 1H, H^{5b}), 7.31 (d, $J = 2.2$ Hz, 1H, H^{5a}). ESIMS: m/z 513 $[\text{M}-\text{Cl}]^+$. HRMS (ESI): Calcd for $\text{C}_{21}\text{H}_{26}\text{N}_2\text{O}^{193}\text{Ir} [\text{M}-\text{Cl}]^+$ 515.1674, found 515.1675.



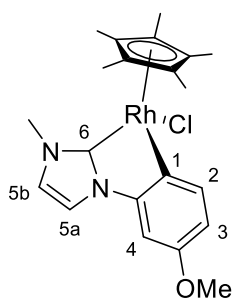
para-3.18a-OMe. ^1H NMR (400 MHz, CDCl_3): δ 1.79 (s, 15H, C_5Me_5), 3.80 (s, 3H, *OMe*), 3.98 (s, 3H, *Me*), 6.65 (dd, $J = 8.2$, 2.6 Hz, 1H, H^3), 6.76 (d, $J = 2.4$ Hz, 1H, H^4), 6.97 (d, $J = 2.2$ Hz, 1H, H^{5b}), 7.29 (d, $J = 2.2$ Hz, 1H, H^{5a}), 7.60 (d, $J = 8.3$ Hz, 1H, H^2), $^{13}\text{C}\{^1\text{H}\}$ NMR (101MHz, CDCl_3): δ 9.74 (C_5Me_5), 37.0 (*Me*), 55.5 (*OMe*), 90.6 (C_5Me_5), 98.6 (C^4), 110.8 (C^3), 114.8 (C^{5a}), 121.3 (C^{5b}), 131.2, 136.1 (C^2), 146.9 (C^1), 156.3, 166.6 (C^6). ESIMS: m/z 513 $[\text{M}-\text{Cl}]^+$. HRMS (ESI): Calcd for $\text{C}_{21}\text{H}_{26}\text{N}_2\text{O}^{193}\text{Ir} [\text{M}-\text{Cl}]^+$ 515.1674, found 515.1675.

3.18b-OMe

Following the general procedure, a mixture of $[\text{RhCl}_2\text{Cp}^*]_2$ (15 mg, 0.025 mmol), NaOAc (17 mg, 0.207 mmol), **L3.18-OMe** (18 mg, 0.053 mmol), Et_4NCl (9 mg, 0.054 mmol), DCE (2 mL) was stirred at 50 $^\circ\text{C}$ for 1 h, then heated to 70 $^\circ\text{C}$ for 6 h. The product was purified by precipitation from DCM/hexane to yield **3.18b-OMe** (*ortho:para* 1:1.9 ratio) as an orange-yellow powder (14 mg, 61%).



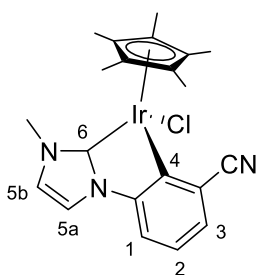
ortho-3.18b-OMe. ^1H NMR (400 MHz, CDCl_3): δ 1.68 (s, 15H, C_5Me_5), 3.83 (s, 3H, *OMe*), 3.97 (s, 3 H, *Me*), 6.58 (dd, $J = 8.0$, 0.9 Hz, 1H, H^3), 6.78 (dd, $J = 7.7$, 1.0 Hz, 1H, H^1), 6.98 (d, $J = 2.0$ Hz, 1H, H^{5b}), 6.99 (t, $J = 7.8$ Hz, 1H, H^2), 7.37 (d, $J = 2.0$ Hz, 1H, H^{5a}), $^{13}\text{C}\{^1\text{H}\}$ NMR (101MHz, CDCl_3): δ 9.9 (C_5Me_5), 37.0 (*Me*), 56.3 (*OMe*), 97.9 (d, $^1J_{\text{C}-\text{Rh}} = 5.2$ Hz, C_5Me_5), 104.9 (C^1), 108.9 (C^3), 115.9 (C^{5a}), 121.9 (C^{5b}), 124.0 (C^2), 146.1, 145.6 (d, $^1J_{\text{C}-\text{Rh}} = 42.1$ Hz, C^4), 156.7, 184.2 (d, $^1J_{\text{C}-\text{Rh}} = 55.5$ Hz, C^6). ESIMS: m/z 425 $[\text{M}-\text{Cl}]^+$. HRMS (ESI): Calcd for $\text{C}_{21}\text{H}_{26}\text{N}_2\text{O}^{103}\text{Rh} [\text{M}-\text{Cl}]^+$ 425.1100, found 425.1100.



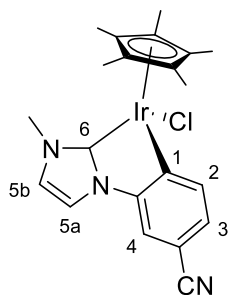
para-3.18b-OMe. ^1H NMR (400 MHz, CDCl_3): δ 1.70 (s, 15H, C_5Me_5), 3.78 (s, 3H, OMe), 4.01 (s, 3H, Me), 6.66 (dd, $J = 8.3, 2.6$ Hz, 1H, H^3), 6.71 (d, $J = 2.5$ Hz, 1H, H^4), 6.98 (d, $J = 2.1$ Hz, 1H, H^{5b}), 7.35 (d, $J = 2.0$ Hz, 1H, H^{5a}), 7.63 (d, $J = 8.3$ Hz, 1H, H^2), $^{13}\text{C}\{^1\text{H}\}$ NMR (101MHz, CDCl_3): δ 9.9 (C_5Me_5), 37.0 (Me), 55.5 (OMe), 97.2 (d, $^1J_{\text{C-Rh}} = 5.0$ Hz, C_5Me_5), 99.0 (C^4), 110.5 (C^3), 115.1 (C^{5a}), 122.2 (C^{5b}), 137.2 (C^2), 146.1, 146.6 (d, $^1J_{\text{C-Rh}} = 35.7$ Hz, C^1), 165.0, 184.2 (d, $J_{\text{C-Rh}} = 55.5$ Hz, C^6). ESIMS: m/z 425 $[\text{M-Cl}]^+$. HRMS (ESI): Calcd for $\text{C}_{21}\text{H}_{26}\text{N}_2\text{O}^{103}\text{Rh} [\text{M-Cl}]^+$ 425.1100, found 425.1100.

3.18a-CN

Following the general procedure, a mixture of $[\text{IrCl}_2\text{Cp}^*]_2$ (20 mg, 0.025 mmol), NaOAc (16 mg, 0.196 mmol), **L3.18-CN** (18 mg, 0.0526 mmol), Et_4NCl (9 mg, 0.053 mmol), DCE (2 mL) was stirred at 50 °C for 1.5 h, then heated further to 70 °C for 1 h. The product was purified by crystallisation from DCM/hexane to yield **3.18a-CN** (*ortho:para* ratio 1:2.0) as an orange-yellow powder (24 mg, 90%).



ortho-3.18a-CN. ^1H NMR (400 MHz, CDCl_3): δ 1.83 (s, 15H, C_5Me_5), 3.98 (s, 3H, Me), 7.00 (t, $J = 7.8$ Hz, 1H, H^2), 7.01 (d, $J = 2.6$ Hz, 1H, H^{5b}), 7.21 (dd, $J = 7.8, 1.2$ Hz, 1H, H^1), 7.33 (d, $J = 2.2$ Hz, 1H, H^{5a}), 7.37 (dd, $J = 7.7, 1.2$ Hz, 1H, H^3), $^{13}\text{C}\{^1\text{H}\}$ NMR (101MHz, CDCl_3): δ 9.6 (C_5Me_5), 36.8 (Me), 92.6 (C_5Me_5), 94.8, 112.5 (C^1), 115.6 (C^{5a}), 120.3, 121.6 (C^2), 122.0 (C^{5b}), 131.2 (C^3), 148.0, 151.1 (C^4), 167.9 (C^6). ESIMS: m/z 510 $[\text{M-Cl}]^+$. HRMS (ESI): Calcd for $\text{C}_{21}\text{H}_{23}^{193}\text{IrN}_3 [\text{M-Cl}]^+$ 510.1521, found 510.1523. ESIMS: m/z 551 $[\text{M-Cl+MeCN}]^+$. HRMS (ESI): Calcd for $\text{C}_{23}\text{H}_{26}\text{N}_4^{193}\text{Ir} [\text{M-Cl+MeCN}]^+$ 551.1787, found 551.1790.

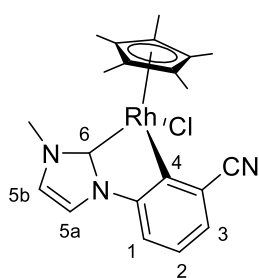


para-3.18a-CN. ^1H NMR (400 MHz, CDCl_3): δ 1.79 (s, 15H, C_5Me_5), 3.99 (s, 3H, Me), 7.03 (d, $J = 2.2$ Hz, 1H, H^{5b}), 7.21 (dd, $J = 7.7$ Hz, 1.7, 1H, H^3), 7.32 (d, $J = 1.7$ Hz, 1H, H^4), 7.34 (d, $J = 2.1$ Hz, 1H, H^{5a}), 7.88 (d, $J = 7.7$ Hz, 1H, H^2), $^{13}\text{C}\{^1\text{H}\}$ NMR (101MHz, CDCl_3): δ 9.7 (C_5Me_5), 37.0 (Me), 91.8 (C_5Me_5), 104.6, 112.6 (C^4), 114.9 (C^{5a}), 122.2 (C^{5b}), 122.6, 129.0 (C^3), 137.2 (C^2), 147.3, 153.4 (C^1), 166.2 (C^6). ESIMS: m/z 510 $[\text{M-Cl}]^+$. HRMS (ESI): Calcd for $\text{C}_{21}\text{H}_{23}^{193}\text{IrN}_3 [\text{M-Cl}]^+$

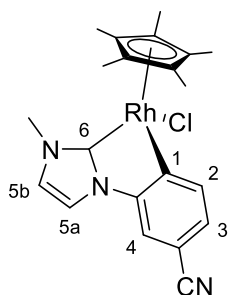
510.1521, found 510.1523. ESIMS: m/z 551 [M-Cl+MeCN]⁺. HRMS (ESI): Calcd for C₂₃H₂₆N₄¹⁹³Ir [M-Cl+MeCN]⁺ 551.1787, found 551.1790.

3.18b-CN

Following the general procedure, a mixture of [RhCl₂Cp*]₂ (15 mg, 0.025 mmol), NaOAc (17 mg, 0.207 mmol), **L3.18-CN** (18 mg, 0.054 mmol), Et₄NCl (9 mg, 0.054 mmol), DCE (2 mL) was stirred at 50 °C for 1.5 h, then heated to 70 °C for 1 h. The product was purified by precipitation from DCM/hexane to yield **3.18b-CN** (*ortho:para* ratio 1:1.9) as an orange-yellow powder (13 mg, 58%).



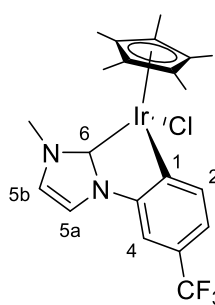
ortho-**3.18b-CN**. ¹H NMR (400 MHz, CDCl₃): δ 1.75 (s, 15H, C₅Me₅), 3.99 (s, 3H, Me), 7.01 (d, $J = 2.2$ Hz, 1H, H^{5b}), 7.05 (t, $J = 7.7$ Hz, 1H, H^2), 7.17 (dd, $J = 7.8, 1.3$ Hz, 1H, H^1), 7.40 (m, 1H, H^3), 7.41 (d, $J = 2.0$ Hz, 1H, H^{5a}), ¹³C{¹H} NMR (101MHz, CDCl₃): δ 9.7 (C₅Me₅), 37.1 (Me), 94.0, 98.8 (d, $^1J_{C-Rh} = 4.8$ Hz, C₅Me₅), 113.1 (C¹), 116.1 (C^{5a}), 122.0, 123.1 (C²), 123.3 (C^{5b}), 130.7 (C³), 147.3, 167.4 (d, $^1J_{C-Rh} = 38.2$ Hz, C⁴), 185.1 (d, $^1J_{C-Rh} = 54.8$ Hz, C⁶). ESIMS: m/z 420 [M-Cl]⁺. HRMS (ESI): Calcd for C₂₁H₂₃N₃¹⁰³Rh [M-Cl]⁺ 420.0947, found 420.0947. ESIMS: m/z 461 [M-Cl+MeCN]⁺. HRMS (ESI): Calcd for C₂₃H₂₆N₄¹⁰³Rh [M-Cl+MeCN]⁺ 461.1213, found 461.1213.



para-**3.18b-CN**. ¹H NMR (400 MHz, CDCl₃): δ 1.71 (s, 15H, C₅Me₅), 4.00 (s, 3H, Me), 7.03 (d, $J = 2.2$ Hz, 1H, H^{5b}), 7.27 (m, 1H, H^3), 7.27 (br.s, 1H, H^4), 7.41 (d, $J = 2.1$ Hz, 1H, H^{5a}), 7.94 (dd, $J = 8.1, 0.9$ Hz, 1H, H^2), ¹³C{¹H} NMR (101MHz, CDCl₃): δ 9.8 (C₅Me₅), 37.1 (Me), 98.2 (d, $^1J_{C-Rh} = 5.6$ Hz, C₅Me₅), 105.5, 112.8 (C⁴), 115.4 (C^{5a}), 120.1, 123.1 (C^{5b}), 128.0 (C³), 138.4 (C²), 146.6, 170.3 (d, $^1J_{C-Rh} = 35.8$ Hz, C¹), 183.7 (d, $^1J_{C-Rh} = 55.6$ Hz, C⁶). Calcd for C₂₁H₂₃N₃¹⁰³Rh [M-Cl]⁺ 420.0947, found 420.0947. ESIMS: m/z 461 [M-Cl+MeCN]⁺. HRMS (ESI): Calcd for C₂₃H₂₆N₄¹⁰³Rh [M-Cl+MeCN]⁺ 461.1213, found 461.1213.

3.18a-CF₃

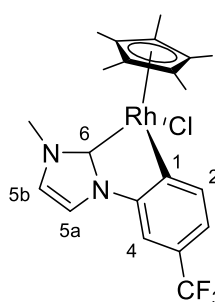
Following the general procedure, a mixture of [IrCl₂Cp*]₂ (20 mg, 0.025 mmol), NaOAc (17 mg, 0.207 mmol), **L3.18-CF₃** (20 mg, 0.0532 mmol), Et₄NCl (9 mg, 0.055 mmol), DCE (2 mL) was stirred first at rt for 24 h, then heated to 50 °C for 1 h and then at 70 °C for a further 1 h. The product was purified by crystallisation from DCM/hexane to yield single regioisomer *para*-**3.18a-CF₃** as orange crystals (19 mg, 64%).



para-**3.18a-CF₃**. ¹H NMR (400 MHz, CDCl₃): δ 1.80 (s, 15H, C₅Me₅), 3.97 (s, 3H, Me), 7.02 (d, *J* = 2.2 Hz, 1H, H^{5b}), 7.22 (br. d, *J* = 7.8 Hz, 1H, H³), 7.30 (d, *J* = 1.2 Hz, 1H, H⁴), 7.38 (d, *J* = 2.2 Hz, 1H, H^{5a}), 7.87 (d, *J* = 7.8 Hz, 1H, H²), ¹³C{¹H} NMR (101MHz, CDCl₃): δ 9.7 (C₅Me₅), 37.0 (Me), 91.4 (C₅Me₅), 106.8 (q, ³*J*_{C-F} = 4.0 Hz, C⁴), 114.9 (C^{5a}), 121.8 (C^{5b}), 122.1 (q, ³*J*_{C-F} = 3.2 Hz, C³), 124.4 (q, ²*J*_{C-F} = 31.2 Hz, C-CF₃), 125.0 (q, ¹*J*_{C-F} = 271.0, CF₃), 136.6 (C²), 146.9, 148.9 (C¹), 166.3 (C⁶), ¹⁹F{¹H} NMR (376MHz, CDCl₃): δ -61.5 (CF₃). ESIMS: *m/z* 553 [M-Cl]⁺. HRMS (ESI): Calcd for C₂₁H₂₃N₂F₃¹⁹³Ir [M-Cl]⁺ 553.1643, found 553.1645.

3.18b-CF₃

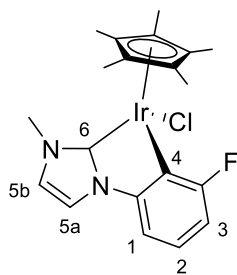
Following the general procedure, a mixture of [RhCl₂Cp*]₂ (20 mg, 0.032 mmol), NaOAc (21 mg, 0.259 mmol), **L3.18-CF₃** (25 mg, 0.066 mmol), dry DCM (2.5 mL) was stirred first at rt for 24 h, then heated to 50 °C for 1 h and then at 70 °C for a further 1 h. The product was purified by crystallisation from DCM/hexane to yield *para*-**3.18b-CF₃** as yellow crystals (25 mg, 78%).



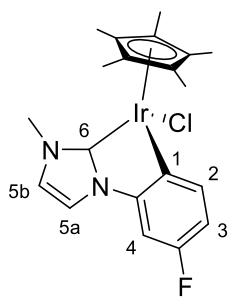
para-**3.18b-CF₃**. ¹H NMR (400 MHz, CD₂Cl₂): δ 1.71 (s, 15H, C₅Me₅), 4.00 (s, 3H, Me), 7.10 (d, *J* = 2.2 Hz, 1H, H^{5b}), 7.28 (d, *J* = 7.8 Hz, 1H, H³), 7.33 (d, *J* = 1.5 Hz, 1H, H⁴), 7.49 (d, *J* = 2.0 Hz, 1H, H^{5a}), 7.92 (d, *J* = 7.8 Hz, 1H, H²), ¹³C{¹H} NMR (101MHz, CD₂Cl₂): δ 10.2 (C₅Me₅), 37.6 (Me), 98.5 (d, ¹*J*_{C-Rh} = 4.8 Hz, C₅Me₅), 107.5 (q, ³*J*_{C-F} = 4.0 Hz, C⁴), 115.7 (C^{5a}), 121.5 (q, ⁴*J*_{C-F} = 2.4 Hz, C³), 123.6 (C^{5b}), 125.4 (q, ²*J*_{C-F} = 31.8 Hz, C-CF₃), 125.6 (q, ¹*J*_{C-F} = 271.0, CF₃), 138.5 (C²), 147.1, 167.1 (d, ¹*J*_{C-Rh} = 36.6 Hz, C¹), 184.7 (d, ¹*J*_{C-Rh} = 55.6 Hz, C⁶), ¹⁹F{¹H} NMR (376MHz, CD₂Cl₂): δ -61.8 (CF₃). ESIMS: *m/z* 463 [M-Cl]⁺. HRMS (ESI): Calcd for C₂₁H₂₃N₂F₃¹⁰³Rh [M-Cl]⁺ 463.0868, found 463.0862. Anal Calcd for C₂₁H₂₃N₂F₃ClRh [M]: C, 50.57; H, 4.65; N, 5.62; found C, 50.44; H, 4.77; N, 5.47 %.

3.18a-F

Following the general procedure, a mixture of $[\text{IrCl}_2\text{Cp}^*]_2$ (20 mg, 0.025 mmol), NaOAc (16 mg, 0.200 mmol), **L3.18-F** (18 mg, 0.055 mmol), Et_4NCl (9 mg, 0.055 mmol), DCE (2 mL) was heated to 70 °C for 3 h. The product was purified by crystallisation from DCM/hexane to yield **3.18a-F** (*ortho:para* ratio 2.1:1) as a yellow powder (18 mg, 67%).



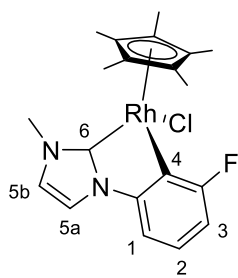
ortho-**3.18a-F**. ^1H NMR (400 MHz, CDCl_3): δ 1.80 (d, 15 H, C_5Me_5), 3.97 (s, 3H, Me), 6.72 (m, 1H, H^3), 6.94 (m, 2H, H^1, H^2), 6.97 (d, $J = 2.1$ Hz, 1H, H^{5b}), 7.32 (d, $J = 2.1$ Hz, 1H, H^{5a}), $^{13}\text{C}\{^1\text{H}\}$ NMR (101 MHz, CDCl_3): δ 9.9 (d, $J_{\text{C-F}} = 2.7$ Hz, C_5Me_5), 36.9 (Me), 91.6 (C_5Me_5), 106.6 (d, $^4J_{\text{C-F}} = 2.7$ Hz, C^1), 112.1 (d, $^2J_{\text{C-F}} = 29.4$ Hz, C^3), 115.5 (C^{5a}), 121.4 (C^{5b}), 123.8 (d, $^3J_{\text{C-F}} = 8.2$ Hz, C^2), 126.3 (d, $^2J_{\text{C-F}} = 44.6$ Hz, C^4), 148.5 (d, $^3J_{\text{C-F}} = 18.3$ Hz), 166.5 (C^6), 167.8 (d, $^1J_{\text{C-F}} = 235.0$ Hz, C-F), $^{19}\text{F}\{^1\text{H}\}$ NMR (376 MHz, CDCl_3): δ -94.9 (F). ESIMS: m/z 503 $[\text{M-Cl}]^+$. HRMS (ESI): Calcd for $\text{C}_{20}\text{H}_{23}\text{N}_2\text{F}^{193}\text{Ir}$ $[\text{M-Cl}]^+$ 503.1674, found 503.1676. ESIMS: m/z 544 $[\text{M-Cl+MeCN}]^+$. HRMS (ESI): Calcd for $\text{C}_{22}\text{H}_{26}\text{N}_3\text{F}^{193}\text{Ir}$ $[\text{M-Cl+MeCN}]^+$ 544.1740, found 544.1744.



para-**3.18a-F**. ^1H NMR (400 MHz, CDCl_3): δ 1.79 (s, 15H, C_5Me_5), 3.99 (s, 3H, Me), 6.78 (ddd, $J = 9.8, 8.3, 2.7$ Hz, 1H, H^3), 6.87 (dd, $J = 9.5, 2.6$ Hz, 1H, H^4), 6.97 (d, $J = 2.1$ Hz, 1H, H^{5b}), 7.27 (d, $J = 2.1$ Hz, 1H, H^{5a}), 7.64 (dd, $J = 8.3, 6.5$ Hz, 1H, H^2), $^{19}\text{F}\{^1\text{H}\}$ NMR (376 MHz, CDCl_3): δ -122.9 (F). ESIMS: m/z 503 $[\text{M-Cl}]^+$. HRMS (ESI): Calcd for $\text{C}_{20}\text{H}_{23}^{193}\text{IrN}_2\text{F}$ $[\text{M-Cl}]^+$ 503.1674, found 503.1676. ESIMS: m/z 544 $[\text{M-Cl+MeCN}]^+$. HRMS (ESI): Calcd for $\text{C}_{22}\text{H}_{26}\text{N}_3\text{F}^{193}\text{Ir}$ $[\text{M-Cl+MeCN}]^+$ 544.1740, found 544.1744.

3.18b-F

Following the general procedure, a mixture of $[\text{RhCl}_2\text{Cp}^*]_2$ (15 mg, 0.025 mmol), NaOAc (17 mg, 0.207 mmol), **L3.18-F** (17 mg, 0.052 mmol), Et_4NCl (9 mg, 0.053 mmol), DCE (2 mL) was heated to 70 °C for 3 h. The product was purified by precipitation from DCM/hexane to yield **3.18b-F** (*ortho:para* ratio 10:1) as an orange-yellow powder (13 mg, 59%).



ortho-**3.18b-F**. ^1H NMR (400 MHz, CDCl_3): δ 1.75 (s, 15H, C_5Me_5), 3.98 (s, 3H, *Me*), 6.72 (td, $J = 8.0, 1.0$ Hz, 1H, H^3), 6.92 (dd, $J = 7.6, 1.0$ Hz, 1H, H^1), 6.98 (td, $J = 7.8, 5.4$ Hz, 1H, H^2), 6.98 (d, $J = 2.1$ Hz, 1H, H^{5b}), 7.39 (d, $J = 2.1$ Hz, 1H, H^{5a}), $^{13}\text{C}\{^1\text{H}\}$ NMR (101MHz, CDCl_3): δ 10.0 (d, $^1J_{\text{C-F}} = 1.6$ Hz, C_5Me_5), 37.1 (*Me*), 98.2 (d, $^1J_{\text{C-Rh}} = 5.6$ Hz, C_5Me_5), 107.1 (C^1), 112.3 (d, $^2J_{\text{C-F}} = 29.4$ Hz, C^3), 115.9 (C^{5a}), 122.3 (C^{5b}), 124.4 (d, $^3J_{\text{C-F}} = 7.9$ Hz) 141.1 (dd, $^2J_{\text{C-Rh,C-F}} = 39.7, 10.3$ Hz, C^4), 147.9 (d, $^2J_{\text{C-F}} = 19.1$ Hz), 168.3 (d, $^1J_{\text{C-F}} = 232.9$ Hz, C-F), 183.9 (d, $^1J_{\text{C-Rh}} = 54.8$ Hz, C^6), $^{19}\text{F}\{^1\text{H}\}$ NMR (376MHz, CDCl_3): δ -93.9 (*F*). ESIMS: m/z 413 [M-Cl] $^+$. HRMS (ESI): Calcd for $\text{C}_{20}\text{H}_{23}\text{N}_2\text{FRh}$ [M-Cl] $^+$ 413.0900, found 413.0902.

6.4 Experimental procedures for Chapter 4

6.4a Synthesis of dibenzylimidazolium salts L4.10-R₁,R₂ and their precursors 4.9-R₂

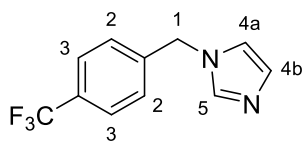
6.4ai Synthesis of benzylimidazoles 4.9-R₂

General procedure for preparation of benzylimidazoles 4.9-R₂

A Schlenk flask was charged with a magnetic stirrer bar, imidazole (1.5 eq.), K_2CO_3 (3 eq.) and MeCN (5-10 mL), capped and stirred at rt for 2 h, followed by addition of the appropriate benzyl chloride or bromide (1 eq.) and stirred for a further 1 h. Then the mixture was filtered through celite, the solvent removed by rotary evaporation, the residue dissolved in EtOAc (50 mL) and washed with water (20 mL) and then brine (20mL), EtOAc layer collected, dried over MgSO_4 , filtered and the solvent removed by rotary evaporation to yield the final product.

Synthesis of benzylimidazoles 4.9-R₂

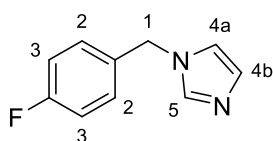
4.9-CF₃



Following the general procedure a mixture of imidazole (320 mg, 4.706 mmol), K_2CO_3 (1239 mg, 8.98 mmol), 4-trifluoromethylbenzyl chloride (585 mg, 3.006 mmol) and MeCN (5 mL) was stirred for a total of 3 h. **4.9-CF₃** was obtained as a clear oil (394 mg, 58%). ^1H NMR (400 MHz, CDCl_3): δ 5.19 (s, 2H, H^1),

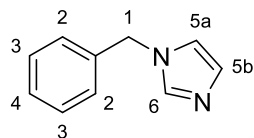
6.91 (t, $J = 1.3$ Hz, 1H, H^{4b}), 7.11 (s, 1H, H^{5a}), 7.25 (d, $J = 8.0$ Hz, 2H, H^2), 7.55 (s, 1H, H^5), 7.60 (d, $J = 8.0$ Hz, 2H, H^3), $^{13}\text{C}\{^1\text{H}\}$ NMR (125 MHz, CDCl_3): δ 49.8 (C^1), 119.1 (C^{4a}), 123.6 (q, $^1J_{\text{C-F}} = 273.1$ Hz, CF_3), 125.6 (q, $^3J_{\text{C-F}} = 3.0$ Hz, C^3), 127.1 (C^2), 129.9 (C^{4b}), 130.1 (q, $^2J_{\text{C-F}} = 32.1$ Hz, C-CF_3), 137.2 (C^5), 140.2, $^{19}\text{F}\{^1\text{H}\}$ NMR (376MHz, CDCl_3): δ -62.7 (CF_3). ESIMS: m/z 227 $[\text{M}+\text{H}]^+$. HRMS (ESI): Calcd for $\text{C}_{11}\text{H}_{10}\text{N}_2\text{F}_3$ $[\text{M}+\text{H}]^+$ 227.0796, found 227.0798.

4.9-F



Following the general procedure a mixture of imidazole (547 mg, 8.044 mmol), K_2CO_3 (2218 mg, 16.072 mmol), 4-fluorobenzylbromide (1008 mg, 5.333 mmol) and MeCN (10 mL) was stirred for a total of 3 h. **4.9-F** was obtained as a yellow oil (580 mg, 62%). ^1H NMR (400 MHz, CDCl_3): δ 5.08 (s, 2H, H^1), 6.88 (d, $J = 1.2$ Hz, 1H, H^{4b}), 7.04 (t, $J = 8.6$ Hz, 2H, H^3), 7.09 (s, 1H, H^{4a}), 7.14 (m, 2H, H^2), 7.53 (s, 1H, H^5), $^{13}\text{C}\{^1\text{H}\}$ NMR (125 MHz, CDCl_3): δ 49.9 (C^1), 115.8 (d, $^2J_{\text{C-F}} = 22.1$ Hz, C^3), 119.0 (C^{4a}), 129.0 (d, $^3J_{\text{C-F}} = 8.0$ Hz, C^2), 129.8 (C^{4b}), 131.9 (d, $^4J_{\text{C-F}} = 3.0$ Hz), 137.2 (C^5), 162.4 (d, $^1J_{\text{C-F}} = 247.0$ Hz, C-F), $^{19}\text{F}\{^1\text{H}\}$ NMR (376MHz, CDCl_3): δ -113.6 (F). ESIMS: m/z 177 $[\text{M}+\text{H}]^+$. HRMS (ESI): Calcd for $\text{C}_{10}\text{H}_{10}\text{N}_2\text{F}$ $[\text{M}+\text{H}]^+$ 177.0828, found 177.0833

4.9-H



Following the general procedure a mixture of imidazole (331 mg, 4.868 mmol), K_2CO_3 (1322 mg, 9.58 mmol), benzylbromide (551 mg, 3.222 mmol) and MeCN (5 mL) was stirred for a total of 3 h. **4.9-H** was obtained as a white crystalline solid (324 mg, 64%). ^1H NMR (400 MHz, CDCl_3): δ 5.11 (s, 2H, H^1), 6.90 (t, $J = 1.2$ Hz, 1H, H^{5b}), 7.09 (t, $J = 1.0$ Hz, 1H, H^{5a}), 7.15 (m, 2H, H^2), 7.35 (m, 3H, H^3 , H^4), 7.54 (s, 1H, H^6), $^{13}\text{C}\{^1\text{H}\}$ NMR (125 MHz, CDCl_3): δ 50.7 (C^1), 119.2 (C^{5a}), 127.2 (C^2), 128.2 (C^4), 128.9 (C^3) 129.8 (C^{5b}), 136.1, 137.4 (C^6). ESIMS: m/z 159 $[\text{M}+\text{H}]^+$. HRMS (ESI): Calcd for $\text{C}_{10}\text{H}_{11}\text{N}_2$ $[\text{M}+\text{H}]^+$ 159.0922, found 159.0917.

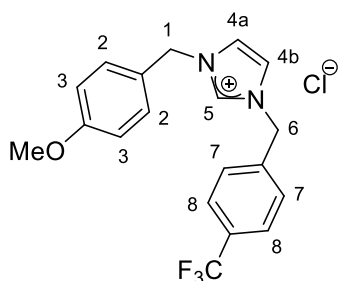
6.4aai Synthesis of dibenzylimidazolium salts **L4.10-R₁**,**R₂**

General procedure for preparation of dibenzylimidazolium salts **L4.10-R₁**,**R₂**

A Schlenk flask was charged with the appropriate benzyimidazole (1 eq.), substituted benzyl chloride (1.5 eq.) and MeCN (5 mL), capped and heated to 55 °C for 1-5 days. Afterwards the reaction mixture was allowed to cool down to rt, Et₂O added, the formed top layer collected and precipitated from DCM/hexane to yield imidazolium salts **L4.10-R₁**,**R₂** as white solids that become sticky overtime.

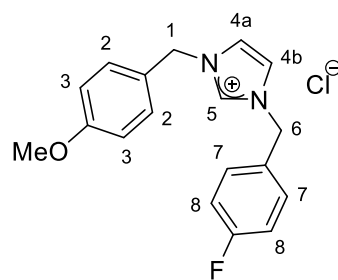
Preparation of dibenzylimidazolium salts **L4.10-R₁**,**R₂**

L4.10-OMe,CF₃



Following the general procedure, the mixture of 1-(4-trifluoromethylbenzyl)-1H-imidazole (239 mg, 1.058 mmol), 4-methoxybenzyl chloride (256 mg, 1.635 mmol) and MeCN (5 mL) was stirred at 55 °C for 20 h, then heated to 65 °C for additional 6 h. **L4.10-OMe,CF₃** was obtained as a crystalline solid that became sticky in air (227 mg, 56%). ¹H NMR (400 MHz, CDCl₃): δ 3.81 (s, 3H, OMe), 5.45 (s, 2H, H¹), 5.75 (s, 2H, H⁶), 6.84 (br d, *J* = 8.2 Hz, 2H, H³), 7.32 (br s, 1H, H^{4a}), 7.40 (br d, *J* = 8.2 Hz, 2H, H²), 7.56 (br d, *J* = 7.8 Hz, 2H, H⁸), 7.61 (br s, 1H, H^{4b}), 7.73 (br d, *J* = 7.6 Hz, 2H, H⁷) 10.89 (br. s, 1H, H⁵), ¹³C{¹H} NMR (125 MHz, CDCl₃): δ 52.3 (C⁶), 52.9 (C¹), 55.2 (OMe), 114.6 (C³), 121.7 (C^{4a}), 122.2 (C^{4b}), 122.4, 124.6, 125.0 (q, ¹*J*_{C-F} = 272.1 Hz, CF₃), 126.0 (q, ³*J*_{C-F} = 3.0 Hz, C⁸), 129.4 (C²), 130.4 (C⁷), 131.2 (q, ²*J*_{C-F} = 32.1 Hz, C-CF₃), 137.2 (C⁵), ¹⁹F{¹H} NMR (376MHz, CDCl₃): δ -62.8 (CF₃). ESIMS: *m/z* 347 [M]⁺. HRMS (ESI): Calcd for C₁₉H₁₈N₂OF₃ [M]⁺ 347.1371, found 347.1375.

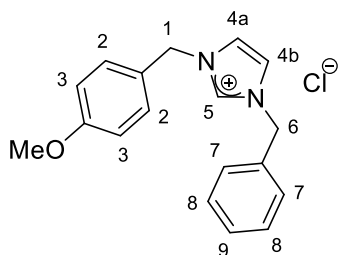
L4.10-OMe,F



Following the general procedure, the mixture of 1-(4-fluorobenzyl)-1H-imidazole (178 mg, 1.01 mmol), 4-methoxybenzyl chloride (238 mg, 1.52 mmol) and MeCN (5 mL) was stirred at 55 °C for 24 h. **L4.10-OMe,F** was obtained as a crystalline solid that became sticky in air (260 mg, 77%). ¹H NMR (400 MHz, CDCl₃): δ 3.76 (s, 3H, OMe), 5.43 (s, 2H, H¹), 5.57 (s, 2H, H⁶), 6.85 (d, *J* = 8.6 Hz, 2H, H³), 7.02 (t, *J* = 8.6 Hz,

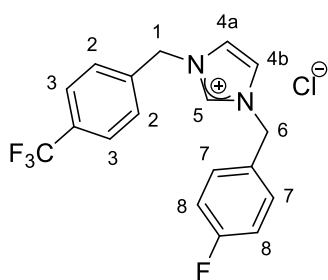
2H, H^8), 7.17 (s, 1H, H^{4a}), 7.29 (s, 1H, H^{4b}), 7.37 (d, $J = 8.6$ Hz, 2H, H^2), 7.52 (dd, $J = 8.6, 5.3$ Hz, 2H, H^7), 10.99 (s, 1H, H^5), $^{13}\text{C}\{^1\text{H}\}$ NMR (125 MHz, CDCl_3): δ 52.5 (C^6), 53.0 (C^1), 55.3 (OMe), 114.7 (C^3), 116.4 (d, $^2J_{\text{C-F}} = 22.1$ Hz, C^8), 121.5 (C^{4b}), 121.6 (C^{4a}), 124.6, 129.0, 130.6 (C^2), 131.2 (d, $^3J_{\text{C-F}} = 9.0$ Hz, C^7), 137.4 (C^5), 160.4, 163.1 (d, $^1J_{\text{C-F}} = 249.0$ Hz, C-F). $^{19}\text{F}\{^1\text{H}\}$ NMR (376MHz, CDCl_3): δ -111.3 (F). ESIMS: m/z 297 $[\text{M}]^+$. HRMS (ESI): Calcd for $\text{C}_{18}\text{H}_{18}\text{N}_2\text{OF}$ $[\text{M}]^+$ 297.1403, found 297.1418.

L4.10-OMe,H



Following the general procedure, the mixture of 1-benzyl-1H-imidazole (188 mg, 1.190 mmol), 4-methoxybenzyl chloride (297 mg, 1.90 mmol) and MeCN (5 mL) was stirred at 55 °C for 24 h. **L4.10-OMe,H** was obtained as a white powder (236 mg, 63%). ^1H NMR (400 MHz, CDCl_3): δ 3.79 (s, 3H, OMe), 5.47 (s, 2H, H^1), 5.55 (s, 2H, H^6), 6.90 (d, $J = 8.6$, 2H, H^3), 7.05 (br. s, 2H, H^{4a} , H^{4b}), 7.38 – 7.46 (m, 7H, H^2 , H^7 , H^8 , H^9), 11.34 (s, 1H, H^5), $^{13}\text{C}\{^1\text{H}\}$ NMR (125 MHz, CDCl_3): δ 52.8 (C^1), 53.2 (C^6), 55.2 (OMe), 114.6 (C^3), 121.7 ($C^{4a/4b}$), 121.8 ($C^{4a/4b}$), 124.9 (C^5), 128.9 (C^7), 129.3 (C^9), 130.5 (C^2), 133.0, 137.1 (C^5), 160.3. ESIMS: m/z 279 $[\text{M}]^+$. HRMS (ESI): Calcd for $\text{C}_{18}\text{H}_{19}\text{N}_2\text{O}$ $[\text{M}]^+$ 279.1497, found 279.1505.

L4.10-F,CF₃



Following the general procedure, the mixture of 1-(4-fluorobenzyl)-1H-imidazole (186 mg, 1.057 mmol), 4-trifluoromethylbenzyl chloride (327 mg, 1.680 mmol) and MeCN (5 mL) was stirred at 55 °C for 4 days, then heated to 65 °C for an additional day. **L4.10-F,CF₃** was obtained as a crystalline solid that became sticky in air (286 mg, 73%). ^1H NMR (400 MHz, CDCl_3): δ 5.54 (s, 2H, H^1), 5.71 (s, 2H, H^5), 7.01 (t, $J = 8.6$ Hz, 2H, H^8), 7.33 (t, $J = 1.8$ Hz, 1H, H^{4b}), 7.43 (t, $J = 1.8$ Hz, 1H, H^{4a}), 7.49 (dd, $J = 8.8, 5.1$ Hz, 2H, H^7), 7.56 (d, $J = 8.2$ Hz, 2H, H^3), 7.66 (d, $J = 8.0$ Hz, 2H, H^2), 11.07 (s, 1H, H^5), $^{13}\text{C}\{^1\text{H}\}$ NMR (125 MHz, CDCl_3): δ 52.5 (C^5), 52.6 (C^1), 116.5 (d, $^2J_{\text{C-F}} = 22.1$ Hz, C^8), 121.9 (C^{4a}), 122.1 (C^{4b}), 123.5 (q, $^1J_{\text{C-F}} = 272.0$ Hz, CF_3), 126.3 (q, $^3J_{\text{C-F}} = 4.0$ Hz, C^3), 128.7 (d, $^4J_{\text{C-F}} = 3.0$ Hz), 129.4 (C^2), 131.1 (d, $^3J_{\text{C-F}} = 8.0$ Hz, C^7), 131.5 (q, $^2J_{\text{C-F}} = 33.1$ Hz, C- CF_3), 137.0, 137.7 (C^5), 163.2 (d, $^1J_{\text{C-F}} = 250.0$ Hz, C-F), $^{19}\text{F}\{^1\text{H}\}$ NMR (376MHz,

CDCl₃): δ -110.9 (*F*), -62.9 (*CF*₃). ESIMS: *m/z* 335 [M]⁺. HRMS (ESI): Calcd for C₁₈H₁₅N₂F₄ [M]⁺ 335.1181, found 335.1171.

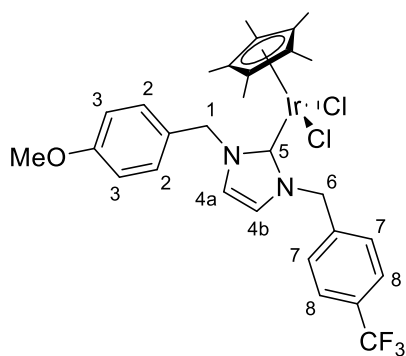
6.4b Complexation of dibenzylimidazolium salts **L4.10-R₁,R₂** with {IrCp*} and {RhCp*}

General procedure for complexation of dibenzylimidazolium salts **L4.10-R₁,R₂** with {IrCp*} and {RhCp*}

An aluminium foil wrapped Schlenk flask was charged with a magnetic stirrer bar, the appropriate benzylimidazolium salt (2.1 eq.) and Ag₂O (2.2 eq.), capped, purged with N₂. Dry DCM (2.5 mL) was added and the mixture stirred at rt for 1-2 h. Then the reaction mixture was filtered through celite and the solvent removed by rotary evaporation. Residue re-dissolved in dry DCM (2.5 mL) and added to an N₂ purged and aluminium foil wrapped Schlenk flask, followed by addition of [MCl₂Cp*]₂ (M = Ir, Rh) (1 eq.). The reaction mixture was stirred at rt for 0.5 to 2 h. Then it was filtered through celite, solvent removed by rotary evaporation and the final **4.10a/b-R₁,R₂** obtained by precipitation/crystallisation from DCM/Et₂O or DCM/hexane.

Complexation of dibenzylimidazolium salts **4.10-R₁,R₂** with {IrCp*} and {RhCp*}

4.10a-OMe,CF₃

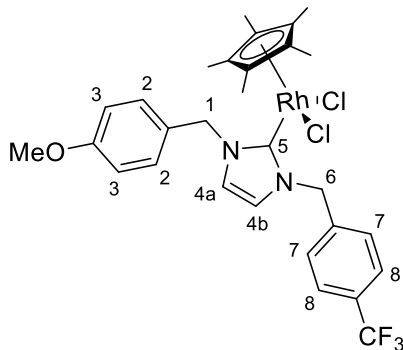


Following the general procedure, the mixture of **L4.10-OMe,CF₃** (108 mg, 0.282 mmol), Ag₂O (66 mg, 0.285 mmol), dry DCM (2.5 mL), stirred at rt for 1 h, then [IrCl₂Cp*]₂ (101 mg, 0.127 mmol) and dry DCM (2.5 mL) were added and stirred for 1 h. Crystallisation from DCM/hexane yielded **4.10a-OMe,CF₃** as yellow crystals (109 mg, 57%). ¹H NMR (400 MHz, CDCl₃):

δ 1.65 (s, 15 H, C₅Me₅), 3.81 (s, 3 H, OMe), 5.10 (d, *J* = 14.7 Hz, 1H, H¹), 5.24 (d, *J* = 15.1 Hz, 1H, H⁶), 6.09 (d, *J* = 14.5 Hz, 1H, H¹), 6.26 (d, *J* = 15.1 Hz, 1H, H⁶), 6.61 (d, *J* = 2.2 Hz, 1H, H^{4b}), 6.69 (d, *J* = 2.2 Hz, 1H, H^{4a}), 6.89 (d, *J* = 8.8 Hz, 2 H, H³), 7.35 (d, *J* = 8.8 Hz, 2 H, H²), 7.53 (d, *J* = 8.0 Hz, 2 H, H⁸), 7.61 (d, *J* = 8.2 Hz, 2 H, H⁷), ¹³C{¹H} NMR (125 MHz, CDCl₃): δ 9.3 (C₅Me₅), 54.1 (C¹), 54.2 (C⁶), 55.3 (OMe), 89.1 (C₅Me₅), 114.1 (C³), 121.3 (C^{4b}), 122.1 (C^{4a}), 124.0 (q, ¹*J*_{C-F} = 272.1 Hz, CF₃), 125.6 (q, ¹*J*_{C-F} = 4.0 Hz, C⁸), 128.2, 128.8 (C⁷), 130.1 (C²), 130.2 (q, ²*J*_{C-F} = 33.1 Hz, C-CF₃), 140.8, 157.6

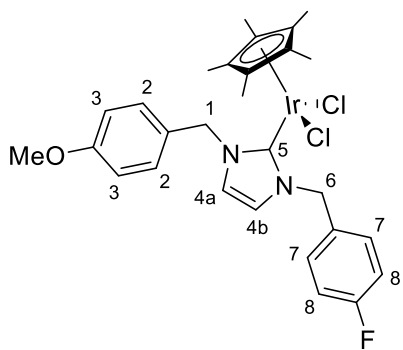
(C^5), 159.5, $^{19}\text{F}\{^1\text{H}\}$ NMR (376MHz, CDCl_3): δ -62.6 (CF_3). ESIMS: m/z 709 $[\text{M}-\text{Cl}]^+$. HRMS (ESI): Calcd for $\text{C}_{29}\text{H}_{32}\text{N}_2\text{OF}_3\text{Cl}^{193}\text{Ir}$ $[\text{M}-\text{Cl}]^+$ 709.1784, found 709.1783.

4.10b-OMe,CF₃



Following the general procedure, the mixture of **L4.10-OMe,CF₃** (21 mg, 0.055 mmol), Ag_2O (13 mg, 0.056 mmol), dry DCM (2.5 mL) was stirred at rt for 1 h, then $[\text{RhCl}_2\text{Cp}^*]_2$ (16 mg, 0.026 mmol) and dry DCM (2.5 mL) were added and stirred for 1 h. Crystallisation from DCM/hexane yielded **4.10b-OMe,CF₃** as orange-red crystals (31 mg, 90%). ^1H NMR (400 MHz, CDCl_3): δ 1.64 (s, 15H, C_5Me_5), 3.80 (s, 3H, OMe), 5.13 (br d, $J = 14.1$ Hz, 1H, H^l), 5.27 (br d, $J = 15.1$ Hz, 1H, H^6), 6.18 (br d, $J = 14.3$ Hz, 1H, H^l), 6.37 (br d, $J = 14.9$ Hz, 1H, H^6), 6.69 (d, $J = 1.8$ Hz, 1H, H^{4a}), 6.76 (d, $J = 1.8$ Hz, 1H, H^{4b}), 6.89 (br d, $J = 8.5$ Hz, 2H, H^3), 7.37 (br d, $J = 8.3$ Hz, 2H, H^2), 7.54 (br d, $J = 7.9$ Hz, 2H, H^8), 7.60 (br d, $J = 8.1$ Hz, 2H, H^7), $^{13}\text{C}\{^1\text{H}\}$ NMR (125 MHz, CDCl_3): δ 9.6 (C_5Me_5), 54.3 (C^l), 54.4 (C^6), 55.3 (OMe), 96.5 (d, $^1J_{\text{C}-\text{Rh}} = 7.0$ Hz, C_5Me_5), 114.1 (C^3), 122.4 ($C^{4a/4b}$), 123.0 ($C^{4a/4b}$), 123.9 (q, $^1J_{\text{C}-\text{F}} = 272.1$ Hz, CF_3), 125.6 (q, $^4J_{\text{C}-\text{F}} = 4.0$ Hz, C^8), 128.2, 128.9 (C^7), 130.2 (C^2), 130.3 (q, $^2J_{\text{C}-\text{F}} = 32.1$ Hz, $\text{C}-\text{CF}_3$), 140.7, 159.5, 171.3 (d, $^1J_{\text{C}-\text{Rh}} = 57.2$ Hz, C^5), $^{19}\text{F}\{^1\text{H}\}$ NMR (376MHz, CDCl_3): δ -62.6 (CF_3). ESIMS: m/z 619 $[\text{M}-\text{Cl}]^+$. HRMS (ESI): Calcd for $\text{C}_{29}\text{H}_{32}\text{N}_2\text{OF}_3\text{Cl}^{103}\text{Rh}$ $[\text{M}-\text{Cl}]^+$ 619.1210, found 619.1210.

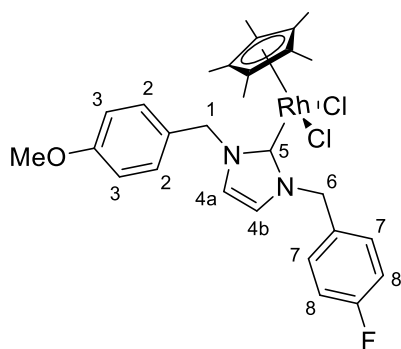
4.10a-OMe,F



Following the general procedure, the mixture of **L4.10-OMe,F** (77 mg, 0.231 mmol), Ag_2O (56 mg, 0.242 mmol), dry DCM (2.5 mL) was stirred at rt for 1h, then $[\text{IrCl}_2\text{Cp}^*]_2$ (86 mg, 0.108 mmol) and dry DCM (2.5 mL) were added and stirred for 1 h. Crystallisation from DCM/hexane yielded **4.10a-OMe,F** as yellow crystals (125 mg, 83%). ^1H NMR (400 MHz, CDCl_3): δ 1.65 (s, 15H, C_5Me_5), 3.80 (s, 3H, OMe), 5.07 (m, 2H, H^l , H^6), 6.06 (d, $J = 14.5$ Hz, 1H, H^l), 6.18 (d, $J = 14.7$ Hz, 1H, H^6), 6.60 (d, $J = 2.2$ Hz, 1H, H^{4b}), 6.65 (d, $J = 2.2$ Hz, 1H, H^{4a}), 6.88 (d, $J = 8.8$ Hz, 2H, H^3), 7.03 (t, $J = 8.7$ Hz, 2H, H^8), 7.33 (d, $J = 8.6$, 2H, H^2), 7.42 (dd, $J = 8.7, 5.3$ Hz, 2H, H^7), $^{13}\text{C}\{^1\text{H}\}$ NMR (125 MHz, CDCl_3): δ 9.3 (C_5Me_5), 53.7 (C^6),

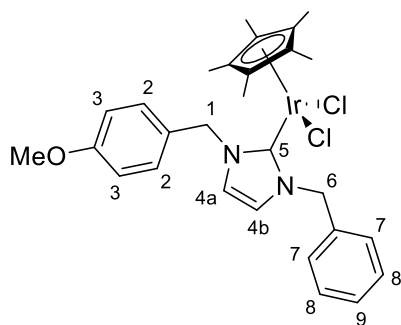
54.1 (C^1), 55.3 (OMe), 89.0 (C_5Me_5), 114.1 (C^3), 115.6 (d, $^2J_{C-F} = 21.1$ Hz, C^8), 121.4 (C^{4b}), 121.8 (C^{4a}), 128.4, 130.1 (C^2), 130.6 (d, $^3J_{C-F} = 8.0$ Hz, C^7), 132.3 (d, $^4J_{C-F} = 3.0$ Hz), 156.8 (C^5), 159.4, 162.5 (d, $^1J_{C-F} = 247.0$ Hz, C-F), $^{19}F\{^1H\}$ NMR (376MHz, $CDCl_3$): δ -114.0 (F). ESIMS: m/z 659 $[M-Cl]^+$. HRMS (ESI): Calcd for $C_{28}H_{32}N_2OFCl$ ^{193}Ir $[M-Cl]^+$ 659.1849, found 659.1817.

4.10b-OMe,F



Following the general procedure, the mixture of **L4.10-OMe,F** (33 mg, 0.099 mmol), Ag_2O (24 mg, 0.104 mmol), dry DCM (2.5 mL) was stirred at rt for 1 h, then $[RhCl_2Cp^*]_2$ (29 mg, 0.047 mmol) and dry DCM (2.5 mL) were added and stirred for 0.5 h. Crystallisation from DCM/hexane yielded **4.10b-OMe,F** as orange-red crystals (52 mg, 91%). 1H NMR (400 MHz, $CDCl_3$): δ 1.65 (s, 15H, C_5Me_5), 3.81 (s, 3H, OMe), 5.11 (m, 2H, H^1 , H^6), 6.17 (br d, $J = 13.7$ Hz, 1H, H^1), 6.31 (br d, $J = 14.5$ Hz, 1H, H^6), 6.69 (d, $J = 2.2$ Hz, 1H, H^{4a}), 6.73 (d, $J = 2.2$ Hz, 1H, H^{4b}), 6.88 (d, $J = 8.6$ Hz, 2H, H^3), 7.04 (t, $J = 8.6$ Hz, 2H, H^8), 7.35 (d, $J = 8.6$ Hz, 2H, H^2), 7.44 (dd, $J = 8.7, 5.4$ Hz, 2H, H^7), $^{13}C\{^1H\}$ NMR (125 MHz, $CDCl_3$): δ 9.6 (C_5Me_5), 53.9 (C^6), 54.3 (C^1), 55.3 (OMe), 96.4 (d, $^1J_{C-Rh} = 7.0$ Hz, C_5Me_5), 114.1 (C^3), 115.6 (d, $^2J_{C-F} = 21.1$ Hz, C^8), 122.3 ($C^{4a/4b}$), 122.7 ($C^{4a/4b}$), 128.3, 130.2 (C^2), 130.7 (d, $^3J_{C-F} = 8.0$ Hz, C^6), 132.3 (d, $^4J_{C-F} = 3.0$ Hz), 159.4, 162.5 (d, $^1J_{C-F} = 247.0$ Hz, C-F), 170.5 (d, $^1J_{C-Rh} = 56.2$ Hz, C^5), $^{19}F\{^1H\}$ NMR (376MHz, $CDCl_3$): δ -113.9 (F). ESIMS: m/z 569 $[M-Cl]^+$. HRMS (ESI): Calcd for $C_{28}H_{32}N_2OFCl^{103}Rh$ $[M-Cl]^+$ 569.1242, found 569.1240.

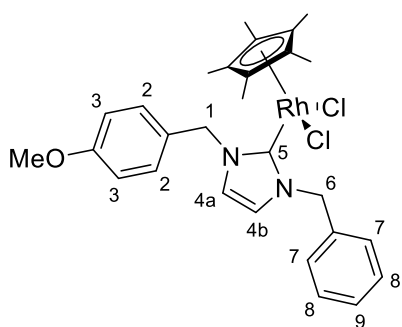
4.10a-OMe,H



Following the general procedure, the mixture of **L4.1-OMe,H** (25 mg, 0.080 mmol), Ag_2O (19 mg, 0.078 mmol), dry DCM (2.5 mL) was stirred at rt for 1 h, then $[IrCl_2Cp^*]_2$ (30 mg, 0.038 mmol) and dry DCM (2.5 mL) were added and stirred for 1 h. Crystallisation from DCM/hexane yielded **4.10a-OMe,H** as yellow crystals (42 mg, 82%). 1H NMR (400 MHz, $CDCl_3$): δ 1.65 (s, 15H, C_5Me_5), 3.81 (s, 3H, OMe), 5.10 (d, $J = 14.3$ Hz, 1H, H^1), 5.35 (d, $J = 15.1$ Hz, 1H,

H^6), 6.00 (d, $J = 15.1$ Hz, 1H, H^6), 6.07 (d, $J = 14.7$ Hz, 1H, H^1), 6.65 (m, 2H, H^{4a} , H^{4b}), 6.89 (d, $J = 8.8$, Hz, 2H, H^3), 7.28-7.35 (m, 7H, H^2 , H^7 , H^8 , H^9), $^{13}\text{C}\{^1\text{H}\}$ NMR (125 MHz, CDCl_3): δ 9.3 (C_5Me_5), 54.1 (C^1), 54.6 (C^6), 55.3 (OMe), 89.0 (C_5Me_5), 114.1 (C^3), 121.6 ($\text{C}^{4a/4b}$), 121.7 ($\text{C}^{4a/4b}$), 127.9 (C^9), 128.4 ($\text{C}^{7/8}$), 128.5, 128.7 ($\text{C}^{7/8}$), 130.1 (C^2), 136.8, 156.9 (C^5), 159.4. ESIMS: m/z 641 $[\text{M}-\text{Cl}]^+$. HRMS (ESI): Calcd for $\text{C}_{28}\text{H}_{33}\text{N}_2\text{OCl}^{193}\text{Ir}$ $[\text{M}-\text{Cl}]^+$ 641.1911, found 641.1899.

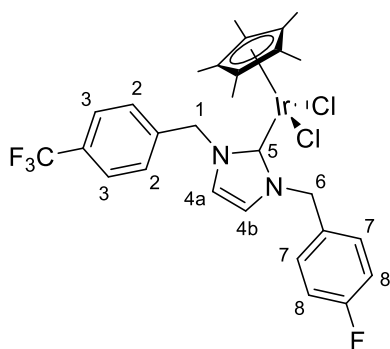
4.10b-OMe,H



Following the general procedure, the mixture of **L4.10-OMe,H** (64 mg, 0.204 mmol), Ag_2O (45 mg, 0.194 mmol), dry DCM (2.5 mL) was stirred at rt for 1 h, then $[\text{RhCl}_2\text{Cp}^*]_2$ (30 mg, 0.087 mmol) and dry DCM (2.5 mL) were added and stirred for 1 h. Crystallisation from DCM/hexane yielded **4.10b-OMe,H** as orange crystals (87 mg, 85%). ^1H NMR (400 MHz, CDCl_3): δ 1.63 (s,

15 H, C_5Me_5), 3.80 (s, 3 H, OMe), 5.14 (br d, $J = 14.3$ Hz, 1H, H^1), 5.40 (br d, $J = 14.3$ Hz, 1H, H^6), 6.08 (br d, $J = 15.1$ Hz, 1H, H^6), 6.17 (br d, $J = 14.3$ Hz, 1H, H^1), 6.73 (m, 2H, H^{4a} , H^{4b}), 6.88 (d, $J = 8.8$, Hz, 2H, H^3), 7.27-7.37 (m, 7H, H^2 , H^7 , H^8 , H^9), $^{13}\text{C}\{^1\text{H}\}$ NMR (125 MHz, CDCl_3): δ 9.5 (C_5Me_5), 54.3 (C^1), 54.9 (C^6), 55.3 (OMe), 96.4 (d, $^1J_{\text{C-Rh}} = 7.0$ Hz, C_5Me_5), 114.1 (C^3), 122.5 ($\text{C}^{4a/4b}$), 122.6 ($\text{C}^{4a/4b}$), 127.9 (C^9), 128.0 (C^8), 128.4 (C^3), 128.5, 128.7 (C), 130.1 (C^7), 136.7, 159.4, 170.6 (d, $^1J_{\text{C-Rh}} = 57.2$ Hz, C^5). ESIMS: m/z 551 $[\text{M}-\text{Cl}]^+$. HRMS (ESI): Calcd for $\text{C}_{28}\text{H}_{33}\text{N}_2\text{OCl}^{103}\text{Rh}$ $[\text{M}-\text{Cl}]^+$ 551.1336, found 551.1340.

4.10a-CF₃,F

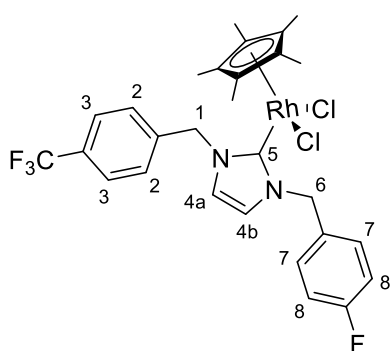


Following the general procedure, the mixture of **L4.10-CF₃,F** (68 mg, 0.183 mmol), Ag_2O (46 mg, 0.198 mmol), dry DCM (2.5 mL), stirred at rt for 1 h, then $[\text{IrCl}_2\text{Cp}^*]_2$ (70 mg, 0.087 mmol) was dry DCM (2.5 mL) were added and stirred for 1 h. Crystallisation from DCM/hexane yielded **4.10a-CF₃,F** as yellow crystals (72 mg, 56%). ^1H NMR (400 MHz, CDCl_3): δ 1.65 (s,

15H, C_5Me_5), 5.04 (d, $J = 14.3$ Hz, 1H, H^6), 5.22 (d, $J = 14.9$ Hz, 1H, H^1), 6.24 (m, 2H, H^1 , H^6), 6.64 (d, $J = 2.2$ Hz, 1H, H^{4a}), 6.67 (d, $J = 2.0$ Hz, 1H, H^{4b}), 7.05 (t, $J = 8.7$ Hz,

2H, H^8), 7.44 (dd, $J = 8.7, 5.3$ Hz, 2H, H^7), 7.54 (d, $J = 8.0$, 2H, H^3), 7.61 (d, $J = 8.2$ Hz, 2H, H^2), $^{13}\text{C}\{^1\text{H}\}$ NMR (125 MHz, CDCl_3): δ 9.3 (C_5Me_5), 53.8 (C^5), 54.1 (C^6), 89.2 (C_5Me_5), 115.7 (d, $^2J_{\text{C-F}} = 22.1$ Hz, C^8), 121.9 (C^{4a}), 122.0 (C^{4b}), 123.9 (q, $^1J_{\text{C-F}} = 272.1$ Hz, CF_3), 125.6 (q, $^3J_{\text{C-F}} = 3.0$ Hz, C^3), 128.9 (C^2), 130.3 (q, $^2J_{\text{C-F}} = 32.1$ Hz, C-CF_3), 130.7 (d, $^3J_{\text{C-F}} = 8.0$ Hz, C^7), 132.0 (d, $^4J_{\text{C-F}} = 3.0$ Hz), 140.6, 157.9 (C^5), 162.6 (d, $^1J_{\text{C-F}} = 247.0$ Hz, C-F), $^{19}\text{F}\{^1\text{H}\}$ NMR (376MHz, CDCl_3): δ -113.6 (F), -62.5 (CF_3). ESIMS: m/z 697 $[\text{M-Cl}]^+$. HRMS (ESI): Calcd for $\text{C}_{28}\text{H}_{29}\text{N}_2\text{OF}_4\text{Cl}^{193}\text{Ir} [\text{M-Cl}]^+$ 697.1585, found 697.1571.

4.10b- CF_3, F



Following the general procedure, the mixture of **L4.10- CF_3, F** (51 mg, 0.137 mmol), Ag_2O (33 mg, 0.142 mmol), dry DCM (2.5 mL) was stirred at rt for 1 h, then $[\text{RhCl}_2\text{Cp}^*]_2$ (41 mg, 0.066 mmol) and dry DCM (2.5 mL) were added and stirred for 1 h. Crystallisation from DCM/hexane yielded **4.10b- CF_3, F** as orange-red crystals (70 mg, 83%). ^1H NMR (400 MHz, CDCl_3): δ

1.62 (s, 15H, C_5Me_5), 5.04 (d, $J = 14.1$ Hz, 1H, H^6), 5.21 (d, $J = 14.5$ Hz, 1H, H^1), 6.35 (d, $J = 14.1$ Hz, 1H, H^6), 6.40 (d, $J = 14.5$ Hz, H^1), 6.71 (br s, 1H, H^{4b}), 6.75 (br s, 1H, H^{4a}), 7.01 (br t, $J = 8.4$ Hz, 2H, H^8), 7.45 (dd, $J = 8.5, 5.2$ Hz, 2H, H^7), 7.56 (m, 4H, H^3, H^4), $^{13}\text{C}\{^1\text{H}\}$ NMR (125 MHz, CDCl_3): δ 9.5 (C_5Me_5), 53.9 (C^6), 54.2 (C^1), 96.5 (d, $^1J_{\text{C-Rh}} = 7.0$ Hz, C_5Me_5), 115.6 (d, $^2J_{\text{C-F}} = 22.1$ Hz, C^8), 122.7 (C^{4a}), 122.9 (C^{4b}), 124.0 (q, $^1J_{\text{C-F}} = 232.9$ Hz, CF_3), 125.5 (q, $^3J_{\text{C-F}} = 3.0$ Hz, C^3), 129.0 (C^2), 130.2 (q, $^2J_{\text{C-F}} = 33.1$ Hz, C-CF_3), 130.8 (d, $^3J_{\text{C-F}} = 8.0$ Hz, C^7), 131.9 (br d, $^4J_{\text{C-F}} = 3.0$ Hz), 140.5, 162.5 (d, $^1J_{\text{C-F}} = 246.9$ Hz, C-F), 171.5 (d, $^1J_{\text{C-Rh}} = 56.2$ Hz, C^5), $^{19}\text{F}\{^1\text{H}\}$ NMR (376MHz, CDCl_3): δ -113.6 (F), -62.6 (CF_3). ESIMS: m/z 607 $[\text{M-Cl}]^+$. HRMS (ESI): Calcd for $\text{C}_{28}\text{H}_{29}\text{N}_2\text{OF}_4\text{Cl}^{103}\text{Rh} [\text{M-Cl}]^+$ 607.1010, found 607.1011.

6.4c Cyclometallation of 4.10a/b- R_1, R_2

General procedure for cyclometallation of 4.10a/b- R_1, R_2 in DCM:MeOH

An oven-dried Schlenk flask was charged with a magnetic stirrer bar, the appropriate **4.10a/b- R_1, R_2** complex (1.0 eq.) and NaOAc (4 eq.), capped, purged with N_2 . Dry DCM:MeOH (4:1) was added and the mixture stirred at rt for 0.5-44 h. Then the reaction

mixture was filtered through celite and the solvent was removed by rotary evaporation. The final cyclometallated complexes were obtained by precipitation/crystallisation from DCM/hexane.

General procedure for monitoring cyclometallation of 4.10a/b-R₁,R₂ in CDCl₃

An NMR tube was charged with the appropriate **4.10a/b-R₁,R₂** complex (1.0 eq., *ca.* 5 mg), NaOAc (4 eq.) and CDCl₃ (0.5 mL). The reactions were monitored by ¹H NMR spectroscopy at time intervals (1 h, 4 h, 24 h, and several days) by comparing the relative integrations of the appropriate signals (either H^{1a/1b} with H^{6a/6b} or H^{3b} with H^{8b}).

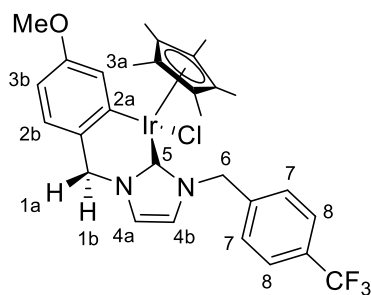
General procedure for monitoring cyclometallation of 4.10a/b-R₁,R₂ in DCM:MeOH

An oven-dried Schlenk flask was charged with a magnetic stirrer bar, the appropriate **4.10a/b-R₁,R₂** complex (1.0 eq., 10-20 mg), NaOAc (4 eq.) and dry DCM:MeOH (4:1, 1-2 mL) and stirred at rt. The reactions were monitored by ¹H NMR spectroscopy and/or where applicable ¹⁹F NMR spectroscopy at time intervals (1 h, 4 h, 24 h) by comparing the relative integrations of the appropriate signals (either H^{1a/1b} with H^{6a/6b} or H^{3b} with H^{8b}). After 1 day the reactions were heated to 60 °C overnight whilst for **4.10a/b-CF₃,F** the PivOH (1 eq.) was added after 1 day at rt and the reactions were heated to 60 °C overnight.

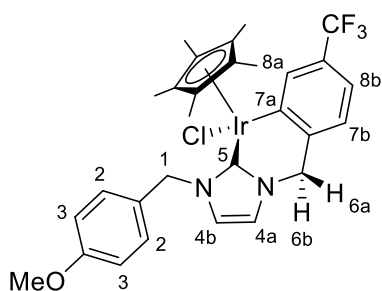
Cyclometallation of 4.10a-R₁,R₂

4.12a-OMe*,CF₃ and 4.12a-OMe,CF₃*

Following the general procedure, the mixture of **4.10a-OMe,CF₃** (75 mg, 0.100 mmol), NaOAc (40 mg, 0.488 mmol), dry DCM (2.5 mL) and MeOH (0.5 mL) was stirred at rt for 0.5 h. Precipitation from DCM/hexane yielded **4.12a-OMe*,CF₃**:**4.12a-OMe,CF₃*** in 1:2 ratio as a yellow powder (63 mg, 90%).



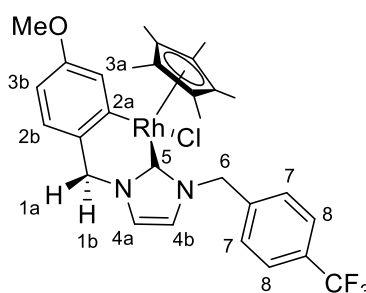
4.12a-OMe*,CF₃. ¹H NMR (400 MHz, CDCl₃): δ 1.68 (s, 15H, C₅Me₅), 3.81 (s, 3H, OMe), 4.65 (d, *J* = 13.9 Hz, 1H, H^{1b}), 4.86 (d, *J* = 13.7 Hz, 1H, H^{1a}), 5.12 (d, *J* = 14.7 Hz, 1H, H⁶), 6.14 (d, *J* = 14.7 Hz, 1H, H⁶), 6.42 (dd, *J* = 8.2, 2.7 Hz, 1H, H^{3b}), 6.59 (d, *J* = 2.0 Hz, 1H, H^{4b}), 6.93 (d, *J* = 8.0 Hz, 1H, H^{2b}), 6.94 (d, *J* = 2.0 Hz, 1H, H^{4a}), 7.27 (d, *J* = 2.7 Hz, 1H, H^{3a}), 7.55 (m, 4H, H⁷, H⁸), ¹³C{¹H} NMR (125 MHz, CDCl₃): δ 9.5 (C₅Me₅), 52.8 (C⁶), 55.1 (OMe), 56.1 (C¹), 90.4 (C₅Me₅), 108.0 (C^{3b}), 119.4 (C^{4b}), 120.8 (C^{4a}), 124.2 (q, ¹*J*_{C-F} = 272.1 Hz, CF₃), 124.6 (C^{2b}), 125.4 (q, ³*J*_{C-F} = 3.0 Hz, C⁸), 125.8 (C^{3a}), 129.3 (C⁷), 130.1 (q, ²*J*_{C-F} = 32.1 Hz, C-CF₃), 131.5, 140.8, 145.8 (C^{2a}), 158.0 (C⁵), 158.4, ¹⁹F{¹H} NMR (376MHz, CDCl₃): δ -62.6 (CF₃). ESIMS: *m/z* 673 [M-Cl]⁺. HRMS (ESI): Calcd for C₂₉H₃₁N₂OF₃¹⁹³Ir [M-Cl]⁺ 673.2018, found 673.2021.



4.12a-OMe,CF₃*. ¹H NMR (400 MHz, CDCl₃): δ 1.68 (s, 15H, C₅Me₅), 3.79 (s, 3H, OMe), 4.73 (d, *J* = 14.3 Hz, 1H, H^{6b}), 4.87 (d, *J* = 14.1 Hz, 1H, H^{6a}), 5.02 (d, *J* = 14.1 Hz, 1H, H¹), 5.92 (d, *J* = 14.3 Hz, 1H, H¹), 6.63 (d, *J* = 2.2 Hz, 1H, H^{4a}), 6.85 (d, *J* = 8.8 Hz, 2H, H³), 6.90 (d, *J* = 2.2 Hz, 1H, H^{4b}), 7.04 (d, *J* = 7.3 Hz, 1H, H^{7b}), 7.08 (dd, *J* = 8.0, 2.0 Hz Hz, 1H, H^{8b}), 7.36 (d, *J* = 8.8 Hz, 2H, H³), 7.92 (d, *J* = 1.0 Hz, 1H, H^{8a}), ¹³C{¹H} NMR (125 MHz, CDCl₃): δ 9.4 (C₅Me₅), 52.8 (C¹), 55.2 (OMe), 56.9 (C⁶), 90.5 (C₅Me₅), 114.0 (C³), 118.8 (q, *J*_{C-F} = 3.0 Hz, C^{8a}), 119.8 (C^{4a}), 120.3 (C^{4b}), 123.8 (C^{7b}), 124.9 (q, ¹*J*_{C-F} = 272.0 Hz, CF₃), 128.2, 129.0 (q, ²*J*_{C-F} = 30.1 Hz, C-CF₃), 130.5 (C²), 137.7 (q, ³*J*_{C-F} = 4.0 Hz, C^{8a}), 142.5, 145.4 (C^{7a}), 156.3 (C⁵), 159.4, ¹⁹F{¹H} NMR (376MHz, CDCl₃): δ -61.7 (CF₃). ESIMS: *m/z* 673 [M-Cl]⁺. HRMS (ESI): Calcd for C₂₉H₃₁N₂OF₃¹⁹³Ir [M-Cl]⁺ 673.2018, found: 673.2021.

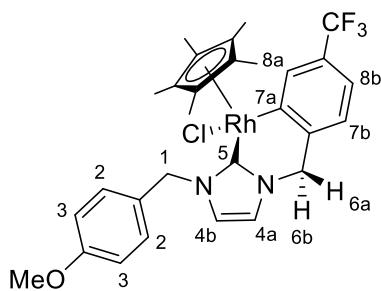
4.12b-OMe*,CF₃ and 4.12b-OMe,CF₃*

Following the general procedure, the mixture of **4.10b-OMe,CF₃** (20 mg, 0.031 mmol), NaOAc (10 mg, 0.122 mmol), dry DCM (2 mL) and MeOH (0.5 mL) was stirred at rt for 1 h. Precipitation from DCM/hexane yielded regioisomers **4.12b-OMe*,CF₃**:**4.12b-OMe,CF₃*** in 1:3.5 ratio as an orange powder (12 mg, 61%).



4.12b-OMe*,CF₃. ¹H NMR (400 MHz, CDCl₃): δ 1.62 (s, 15H, C₅Me₅), 3.82 (s, 3H, OMe), 4.74 (d, *J* = 14.1 Hz, 1H, H^{1b}), 5.00 (m, 1H, H^{1a}), 5.15 (d, *J* = 14.5 Hz, 1H, H⁶), 6.30 (d, *J* = 14.3 Hz, 1H, H⁶), 6.47 (dd, *J* = 8.1, 2.6 Hz, 1H, H^{3b}), 6.64 (d, *J* = 1.8 Hz, 1H, H^{4b}), 6.91 (d, *J* = 8.0 Hz, 1H, H²), 7.00 (d, *J* = 2.0 Hz, 1H, H^{4a}), 7.37 (d, *J* = 2.7 Hz, 1H, H^{3a}), 7.56 (m, 4H, H⁷, H⁸), ¹³C{¹H} NMR (125 MHz, CDCl₃): δ 9.7 (C₅Me₅), 53.1 (C⁶), 55.2 (OMe), 55.9 (C¹), 97.3 (d, ¹*J*_{C-Rh} = 5.0 Hz C₅Me₅), 108.5 (C^{3b}), 120.3 (C^{4b}), 121.7 (C^{4a}), 124.9 (C²), 125.1 (C^{3a}), 125.5 (q, ¹*J*_{C-F} = 4.0 Hz, C⁸), 128.4, 129.5 (C⁷), 131.7, 159.5, ¹⁹F{¹H} NMR (376 MHz, CDCl₃): δ -62.6 (CF₃). ESIMS: *m/z* 583 [M-Cl]⁺. HRMS (ESI): Calcd. for C₂₉H₃₁N₂OF₃¹⁰³Rh 583.1644 [M-Cl]⁺, found 583.1645.

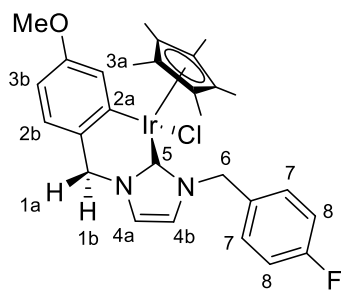
N.B. ¹³C NMR spectrum of the regioisomer was too weak to assign quartets belonging to CF₃ and C-CF₃ and multiplets belonging to C^{2a} and C⁵.



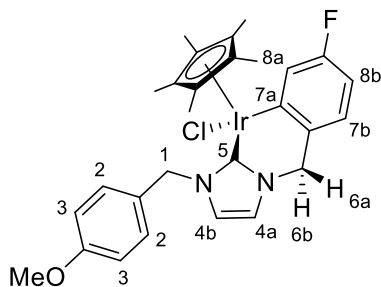
4.12b-OMe,CF₃*. ¹H NMR (400 MHz, CDCl₃): δ 1.62 (s, 15H, C₅Me₅), 3.79 (s, 3H, OMe), 4.82 (d, *J* = 14.5 Hz, 1H, H^{6b}), 5.00 (m, 1H, H^{6a}), 5.05 (d, *J* = 14.1 Hz, 1H, H¹), 6.06 (d, *J* = 14.1 Hz, 1H, H¹), 6.68 (d, *J* = 1.8 Hz, 1H, H^{4a}), 6.86 (d, *J* = 8.6 Hz, 2H, H³), 6.97 (d, *J* = 2.0 Hz, 1H, H^{4b}), 7.04 (d, *J* = 7.8 Hz, 1H, H^{7b}), 7.15 (dd, *J* = 7.7, 1.1 Hz, 1H, H^{8b}), 7.39 (d, *J* = 8.6 Hz, 2H, H²), 8.03 (s, 1H, H^{8a}), ¹³C{¹H} NMR (125 MHz, CDCl₃): δ 9.7 (C₅Me₅), 53.2 (C¹), 55.3 (OMe), 56.1 (C⁶), 97.5 (d, ¹*J*_{C-Rh} = 4.0 Hz C₅Me₅), 114.0 (C³), 119.2 (q, ³*J*_{C-F} = 4.0 Hz, C^{8b}), 120.7 (C^{4a}), 121.3 (C^{4b}), 124.2 (C⁷), 124.4 (q, ¹*J*_{C-F} = 272.1 Hz, CF₃), 128.0, 128.6 (q, ¹*J*_{C-F} = 31.1 Hz, C-CF₃), 130.8 (C²), 137.5 (C^{8a}), 142.9, 159.5, 162.0 (d, ¹*J*_{C-Rh} = 33.1 Hz, C^{7a}), 174.2 (d, ¹*J*_{C-Rh} = 55.2 Hz, C⁵), ¹⁹F{¹H} NMR (376 MHz, CDCl₃): δ -61.6 (CF₃). ESIMS: *m/z* 583 [M-Cl]⁺. HRMS (ESI): Calcd. for C₂₉H₃₁N₂OF₃¹⁰³Rh 583.1644 [M-Cl]⁺, found 583.1645.

4.12a-OMe*,F and 4.12a-OMe,F*

Following the general procedure, the mixture of **4.12a-OMe,F** (68 mg, 0.099 mmol), NaOAc (40 mg, 0.488 mmol), dry DCM (2.5 mL) was stirred at rt for 44h. Precipitation from DCM/hexane yielded **4.12a-OMe*,F:4.12a-OMe,F*** in 1.5:1 ratio as a yellow powder (31 mg, 48%).



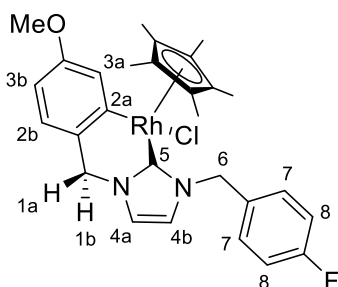
4.12a-OMe*,F. ^1H NMR (400 MHz, CDCl_3): δ 1.68 (s, 15H, C_5Me_5), 3.80 (s, 3H, OMe), 4.63 (d, $J = 13.7$ Hz, 1H, H^{1b}), 4.84 (d, $J = 13.7$ Hz, 1H, H^{1a}), 4.98 (d, $J = 14.3$ Hz, 1H, H^6), 6.06 (d, $J = 14.1$ Hz, 1H, H^6), 6.40 (dd, $J = 8.0, 2.7$ Hz, 1H, H^{3b}), 6.59 (d, $J = 2.2$ Hz, 1H, H^{4b}), 6.89 (d, $J = 2.0$ Hz, 1H, H^{4a}). 6.90 (d, $J = 7.6$ Hz, 1H, H^2), 6.99 (t, $J = 8.7$ Hz, 2H, H^8), 7.27 (d, $J = 2.8$ Hz, 1H, H^{3a}), 7.43 (dd, $J = 8.7, 5.4$ Hz, 2H, H^7), $^{13}\text{C}\{^1\text{H}\}$ NMR (125 MHz, CDCl_3): δ 9.5 (C_5Me_5), 52.6 (C^6), 55.1 (OMe), 56.7 (C^1), 90.3 (C_5Me_5), 108.0 (C^{3b}), 115.5 (d, $^2J_{\text{C-F}} = 22.1$ Hz, C^8), 119.4 (C^{4b}), 120.5 (C^{4a}), 124.6 (C^{2b}), 125.9 (C^{3a}), 130.5, 131.0 (d, $^3J_{\text{C-F}} = 8.0$ Hz, C^7), 132.4 (d, $^4J_{\text{C-F}} = 3.0$ Hz), 145.9 (C^{2a}), 158.1 (d, $^1J_{\text{C-F}} = 217.8$ Hz, C-F), 158.4 (C^5 , C-OMe), $^{19}\text{F}\{^1\text{H}\}$ NMR (376MHz, CDCl_3): δ -114.2 (F). ESIMS: m/z 623 $[\text{M-Cl}]^+$. HRMS (ESI): Calcd for $\text{C}_{28}\text{H}_{32}\text{N}_2\text{O}^{193}\text{Ir}$ $[\text{M-Cl}]^+$, 623.2050, found 623.2065.



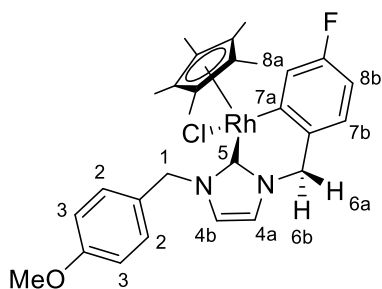
4.12a-OMe,F*. ^1H NMR (400 MHz, CDCl_3): δ 1.68 (s, 15H, C_5Me_5), 3.78 (s, 3H, OMe), 4.64 (d, $J = 13.9$ Hz, 1H, H^{6b}), 4.83 (d, $J = 13.9$ Hz, 1H, H^{6a}), 5.00 (d, $J = 14.3$ Hz, 1H, H^1), 5.92 (d, $J = 14.3$ Hz, 1H, H^1), 6.51 (td, $J = 8.5, 2.8$ Hz, 1H, H^{8b}), 6.62 (d, $J = 2.2$ Hz, 1H, H^{4a}), 6.84 (d, $J = 8.8$ Hz, 2H, H^3), 6.88 (d, $J = 2.2$ Hz, 1H, H^{4b}), 6.93 (dd, $J = 8.2, 2.3$ Hz, 1H, H^{7b}), 7.35 (d, $J = 8.8$ Hz, 2H, H^2), 7.38 (dd, $J = 10.2, 2.7$ Hz, 1H, H^{8a}), $^{19}\text{F}\{^1\text{H}\}$ NMR (376MHz, CDCl_3): δ -118.5 (F). ESIMS: m/z 623 $[\text{M-Cl}]^+$. HRMS (ESI): Calcd for $\text{C}_{28}\text{H}_{32}\text{N}_2\text{O}^{193}\text{Ir}$ $[\text{M-Cl}]^+$, 623.2050, found: 623.2065.

4.12b-OMe*,F and 4.12b-OMe,F*

Following the general procedure, the mixture of **4.10b-OMe,F** (25 mg, 0.041 mmol), NaOAc (13 mg, 0.159 mmol), dry DCM (2 mL) and MeOH (0.5 mL) was stirred at rt for 1 h. Precipitation from DCM/hexane yielded **4.12b-OMe*,F**:**4.12b-OMe,F*** in 1:3.5 ratio as an orange powder (21 mg, 90%).



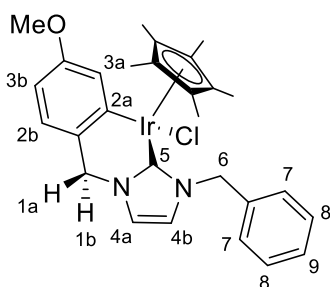
4.12b-OMe*,F. ^1H NMR (400 MHz, CDCl_3): δ 1.63 (s, 15H, C_5Me_5), 3.82 (s, 3H, OMe), 4.71 (d, $J = 14.3$ Hz, 1H, H^{1b}), 4.95 (d, $J = 14.1$ Hz, 1H, H^{1a}), 5.01 (d, $J = 13.9$ Hz, 1H, H^6), 6.24 (d, $J = 13.9$ Hz, 1H, H^6), 6.46 (dd, $J = 8.1, 2.6$ Hz, 1H, H^{3b}), 6.64 (d, $J = 7.8$ Hz, 1H, H^{4b}), 6.89 (m, 1H, H^{2b}), 6.98 (t, $J = 9.0$ Hz, 2H, H^8), 7.38 (m, 1H, H^{3a}), 7.46 (dd, $J = 8.8, 5.5$ Hz, 2H, H^7), $^{13}\text{C}\{^1\text{H}\}$ NMR (125 MHz, CDCl_3): δ 9.7 (C_5Me_5), 52.8 (C^6), 55.2 (OMe), 55.9 (C^1), 97.3 (d, $^1J_{\text{C-Rh}} = 5.0$ Hz C_5Me_5), 108.5 (C^{3b}), 115.5 (d, $^2J_{\text{C-F}} = 21.1$ Hz, C^8), 120.2 (C^{4b}), 121.4 (C^{4a}), 124.9 (C^2), 125.1 (C^{3a}), 131.2 (d, $^3J_{\text{C-F}} = 8.0$ Hz, C^7), 131.8, 132.2, 157.7, 161.4 (d, $^1J_{\text{C-F}} = 249.0$ Hz, C-F), 161.6 (d, $^1J_{\text{C-Rh}} = 33.1$ Hz, C^{2a}), 175.6 (d, $^1J_{\text{C-Rh}} = 49.2$ Hz, C^5), $^{19}\text{F}\{^1\text{H}\}$ NMR (376 MHz, CDCl_3): δ -114.1 (F). ESIMS: m/z 533 $[\text{M-Cl}]^+$. HRMS (ESI): Calcd for $\text{C}_{28}\text{H}_{31}\text{N}_2\text{OF}^{103}\text{Rh}$ 533.1675 $[\text{M-Cl}]^+$, found 533.1672.



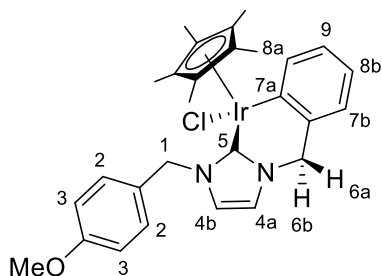
4.12b-OMe,F*. ^1H NMR (400 MHz, CDCl_3): δ 1.63 (s, 15H, C_5Me_5), 3.79 (s, 3H, OMe), 4.74 (d, $J = 14.1$ Hz, 1H, H^{6b}), 4.95 (d, $J = 14.1$ Hz, 1H, H^{6a}), 5.03 (d, $J = 14.1$ Hz, 1H, H^1), 6.06 (d, $J = 14.1$ Hz, 1H, H^1), 6.57 (td, $J = 8.4, 2.7$ Hz, 1H, H^{8b}), 6.67 (d, $J = 1.8$ Hz, 1H, H^{4a}), 6.85 (d, $J = 8.6$ Hz, 1H, H^3), 6.92 (dd, $J = 8.4, 5.3$ Hz, 1H, H^{7b}), 6.95 (d, $J = 2.0$ Hz, 1H, H^{4b}), 7.38 (d, $J = 8.6$ Hz, 2H, H^2), 7.50 (dd, $J = 9.6, 2.5$ Hz, 1H, H^{8a}), $^{13}\text{C}\{^1\text{H}\}$ NMR (125 MHz, CDCl_3): δ 9.7 (C_5Me_5), 53.1 (C^1), 55.2 (OMe), 55.8 (C^6), 97.3 (d, $^1J_{\text{C-Rh}} = 5.0$ Hz C_5Me_5), 108.8 (d, $^2J_{\text{C-F}} = 22.1$ Hz, C^{8b}), 114.0 (C^3), 120.5 (C^{4a}), 121.2 (C^{4b}), 125.0 (d, $^3J_{\text{C-F}} = 7.0$ Hz, C^{7b}), 126.7 (dd, $^3J_{\text{C-F}} = 17.1$ Hz, C^{8a}), 128.2, 130.7 (C^2), 135.0, 159.4, 161.4 (d, $^1J_{\text{C-F}} = 249.0$ Hz, C-F), 164.1 (dd, $^1J_{\text{C-Rh,C-F}} = 32.6, ^3J_{\text{C-F}} = 3.5$ Hz, C^{7a}), 174.3 (d, $^1J_{\text{C-Rh}} = 56.2$ Hz, C^5), $^{19}\text{F}\{^1\text{H}\}$ NMR (376 MHz, CDCl_3): δ -117.8 (F). ESIMS: m/z 533 $[\text{M-Cl}]^+$. HRMS (ESI): Calcd for $\text{C}_{28}\text{H}_{31}\text{N}_2\text{OF}^{103}\text{Rh}$ 533.1675 $[\text{M-Cl}]^+$, found 533.1672.

4.12a-OMe*,H and 4.12a-OMe,H*

Following the general procedure, the mixture of **4.10a-OMe,H** (70 mg, 0.104 mmol), NaOAc (44 mg, 0.537 mmol), dry DCM (2 mL) and MeOH (0.5 mL) was stirred at rt for 1 h. Precipitation from DCM/hexane yielded **4.12a-OMe*,H:4.12a-OMe,H*** in 1.5:1 ratio as a yellow powder (33 mg, 50%).



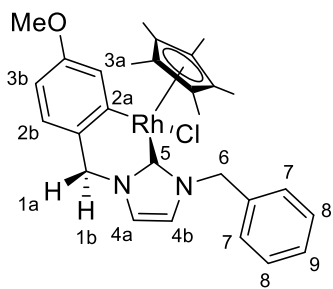
4.12a-OMe*,H. ^1H NMR (400 MHz, CDCl_3): δ 1.69 (s, 15H, C_5Me_5), 3.81 (s, 3H, *OMe*), 4.64 (d, $J = 13.7$ Hz, 1H, H^{1b}), 4.85 (d, $J = 13.7$ Hz, 1H, H^{1a}), 5.17 (d, $J = 14.5$ Hz, 1H, H^6), 5.96 (d, $J = 14.5$ Hz, 1H, H^6), 6.41 (dd, $J = 8.0, 2.7$ Hz, 1H, H^{3b}), 6.63 (d, $J = 2.2$ Hz, 1H, H^{4b}), 6.89 (d, $J = 2.2$ Hz, 1H, H^{4a}), 6.91 (d, $J = 8.0$ Hz, 1H, H^{2b}), 7.29 (d, $J = 2.7$ Hz, 1H, H^{3a}), 7.32 (m, 3H, H^8, H^9), 7.41 (dd, $J = 7.8, 1.6$ Hz, 2H, H^7), $^{13}\text{C}\{^1\text{H}\}$ NMR (125 MHz, CDCl_3): δ 9.5 (C_5Me_5), 53.4 (C^6), 55.2 (*OMe*), 56.8 (C^1), 90.3 (C_5Me_5), 108.0 (C^{3b}), 119.7 (C^{4b}), 120.3 (C^{4b}), 124.5 (C^{2b}), 125.9 (C^{3a}), 128.0 (C^9), 128.6 (C^8), 129.1 (C^7), 131.6 (C^{2a}), 136.7, 146.1, 157.2 (C^5), 158.4. ESIMS: m/z 605 $[\text{M}-\text{Cl}]^+$. HRMS (ESI): Calcd for $\text{C}_{28}\text{H}_{32}\text{N}_2\text{O}^{193}\text{Ir} [\text{M}-\text{Cl}]^+$ 605.2144, found 605.2154.



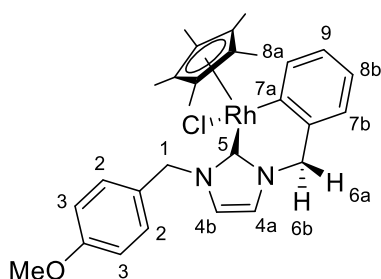
4.12a-OMe,H*. ^1H NMR (400 MHz, CDCl_3): δ 1.69 (s, 15H, C_5Me_5), 3.79 (s, 3H, *OMe*), 4.66 (d, $J = 13.9$ Hz, 1H, H^{6b}), 4.91 (d, $J = 13.9$ Hz, 1H, H^{6a}), 5.04 (d, $J = 14.3$ Hz, 1H, H^1), 5.94 (d, $J = 13.9$ Hz, 1H, H^1), 6.62 (d, $J = 2.0$ Hz, 1H, H^{4a}), 6.84 (d, $J = 9.0$ Hz, 2H, H^3), 6.83 (m, 1H, H^{8b}), 6.90 (m, 1H, H^{4b}), 7.01 (m, 2H, H^{7b}, H^9), 7.36 (d, $J = 8.6$ Hz, 2H, H^2), 7.67 (d, $J = 7.6$ Hz, 1H, H^{8a}), $^{13}\text{C}\{^1\text{H}\}$ NMR (125 MHz, CDCl_3): δ 9.5 (C_5Me_5), 52.8 (C^1), 55.2 (*OMe*), 57.2 (C^6), 90.2 (C_5Me_5), 113.9 (C^3), 119.5 (C^{4a}), 120.2 (C^{4b}), 121.9 (C^{8b}), 124.1 (C^7), 127.7 (C^9), 128.5, 130.5 (C^2), 138.7, 141.5 (C^{8a}), 144.4 (C^{7a}), 156.8 (C^5), 159.3. ESIMS: m/z 605 $[\text{M}-\text{Cl}]^+$. HRMS (ESI): Calcd for $\text{C}_{28}\text{H}_{32}\text{N}_2\text{O}^{193}\text{Ir} [\text{M}-\text{Cl}]^+$ 605.2144, found: 605.2154.

4.12b-OMe*,H and 4.12b-OMe,H*

Following the general procedure, the mixture of **4.10b-OMe,H** (54 mg, 0.092 mmol), NaOAc (40 mg, 0.488 mmol), dry DCM (2 mL) and MeOH (0.5 mL) was stirred at rt for 1 h. Precipitation from DCM/hexane yielded **4.12b-OMe*,H:4.12b-OMe,H*** in 1.2:1 ratio as an orange powder (44 mg, 87%).



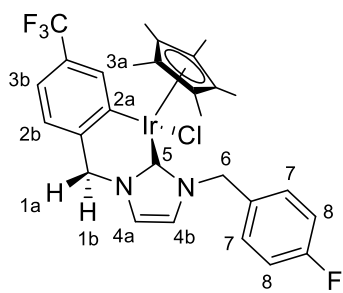
4.12b-OMe*,H. ^1H NMR (400 MHz, CDCl_3): δ 1.62 (s, 15H, C_5Me_5), 3.81 (s, 3H, *OMe*), 4.70 (d, $J = 10.2$ Hz, 1H, H^{1b}), 5.00 (d, $J = 14.3$ Hz, 1H, H^{1a}), 5.08 (d, $J = 14.1$ Hz, 1H, H^6), 6.10 (d, $J = 10.8$ Hz, 1H, H^6), 6.45 (dd, $J = 8.1, 2.6$ Hz, 1H, H^{3b}), 6.65 (d, $J = 1.5$ Hz, 1H, H^{4b}), 6.89 (d, $J = 7.6$ Hz, 1H, H^2), 6.93 (d, $J = 1.5$ Hz, 1H, H^{4a}), 7.31 (m, 1H, H^{3a}), 7.38 (m, 3H, H^8, H^9), 7.43 (dd, $J = 7.6, 1.8$ Hz, 2H, H^7), $^{13}\text{C}\{^1\text{H}\}$ NMR (125 MHz, CDCl_3): δ 9.7 (C_5Me_5), 53.1 (C^6), 55.2 (*OMe*), 56.8 (C^1), 97.2 (d, $^1J_{\text{C-Rh}} = 5.0$ Hz C_5Me_5), 108.4 (C^{3b}), 120.3 (C^{4b}), 121.3 (C^{4a}), 124.8 (C^2), 125.2 (C^{3a}), 128.0 (C^9), 128.3, 129.2 (C^7), 130.7 (C^8), 132.0, 157.6, 160.7 (d, $^1J_{\text{C-Rh}} = 32.1$ Hz, C^{2a}), 174.7 (d, $^1J_{\text{C-Rh}} = 57.2$ Hz, C^5). ESIMS: m/z 515 $[\text{M-Cl}]^+$. HRMS (ESI): Calcd for. $\text{C}_{28}\text{H}_{32}\text{N}_2\text{O}^{103}\text{Rh} [\text{M-Cl}]^+$ 515.1570, found 515.1572.



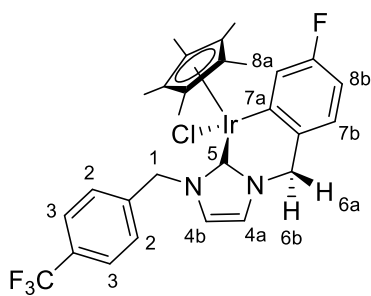
4.12b-OMe,H*. ^1H NMR (400 MHz, CDCl_3): δ 1.62 (s, 15H, C_5Me_5), 3.78 (s, 3H, *OMe*), 4.74 (d, $J = 10.2$ Hz, 1H, H^{6b}), 4.94 (d, $J = 14.1$ Hz, 1H, H^{6a}), 5.19 (d, $J = 14.3$ Hz, 1H, H^1), 6.06 (d, $J = 10.4$ Hz, 1H, H^1), 6.65 (d, $J = 1.5$ Hz, 1H, H^{4a}), 6.84 (d, $J = 8.8$ Hz, 2H, H^3), 6.89 (d, $J = 7.6$ Hz, 1H, H^{7b}), 6.93 (m, 2H, H^{4b}, H^{8b}), 7.04 (td, $J = 7.2, 1.4$ Hz, 1H, H^9), 7.30 (m, 2H, H^2), 7.55 (d, $J = 6.7$ Hz, 1H, H^{8a}), $^{13}\text{C}\{^1\text{H}\}$ NMR (125 MHz, CDCl_3): δ 9.7 (C_5Me_5), 53.7 (C^1), 55.2 (*OMe*), 55.8 (C^6), 97.2 (d, $^1J_{\text{C-Rh}} = 5.0$ Hz C_5Me_5), 113.9 (C^3), 120.4 (C^{4a}), 121.3 (C^{4b}), 122.0 ($\text{C}^{7b/8b}$), 124.6 ($\text{C}^{7b/8b}$), 127.1 (C^9), 128.6 (C^2), 136.4, 139.2, 141.1 (C^{8a}), 159.4, 162.4 (d, $^1J_{\text{C-Rh}} = 32.1$ Hz, C^{7a}), 175.0 (d, $^1J_{\text{C-Rh}} = 56.2$ Hz, C^5). ESIMS: m/z 515 $[\text{M-Cl}]^+$. HRMS (ESI): Calcd for. $\text{C}_{28}\text{H}_{32}\text{N}_2\text{O}^{103}\text{Rh} [\text{M-Cl}]^+$ 515.1570, found 515.1572.

4.12a-CF₃*F and 4.12a-CF₃F*

Following the general procedure, the mixture of **4.10a-CF₃F** (33 mg, 0.048 mmol), NaOAc (13 mg, 0.159 mmol), dry DCM (2.5 mL) was stirred at rt for 1 h. Precipitation from DCM/hexane yielded **4.12a-CF₃*F:4.12a-CF₃F*** in 1.3:1 ratio as a yellow powder (21 mg, 69%).



4.12a-CF₃*F. ¹H NMR (400 MHz, CDCl₃): δ 1.68 (s, 15H, C₅Me₅), 4.74 (d, *J* = 14.3 Hz, 1H, *H*^{1b}), 4.87 (m, 1H, *H*^{1a}), 5.00 (d, *J* = 14.3 Hz, 1H, *H*⁶), 6.02 (d, *J* = 14.1 Hz, 1H, *H*⁶), 6.62 (d, *J* = 2.1 Hz, 1H, *H*^{4b}), 6.93 (d, *J* = 2.0 Hz, 1H, *H*^{4a}), 7.00 (t, *J* = 8.7 Hz, 2H, *H*⁸), 7.05 (br. d, *J* = 7.8 Hz, 1H, *H*^{2b}), 7.09 (br. dd, *J* = 7.8, 2.0 Hz, 1H, *H*^{3b}), 7.43 (dd, *J* = 8.8, 5.3 Hz, 2H, *H*⁷), 7.90 (br d, *J* = 1.4 Hz, 1H, *H*^{3a}), ¹³C{¹H} NMR (125 MHz, CDCl₃): δ 9.5 (C₅Me₅), 52.5 (C⁶), 56.9 (C¹), 90.6 (C₅Me₅), 115.6 (d, ²*J*_{C-F} = 21.1 Hz, C⁸), 119.0 (q, ³*J*_{C-F} = 5.4 Hz, C^{3b}), 119.8 (C^{4b}), 120.6 (C^{4a}), 123.9 (C^{2b}), 131.0 (d, ³*J*_{C-F} = 8.0 Hz, C⁷), 131.0, 132.0, 137.8 (q, ³*J*_{C-F} = 3.0 Hz, C^{3a}), 142.3, 145.3 (C^{2a}), 156.9 (C⁵), 162.6 (d, ¹*J*_{C-F} = 247.0, C-F), ¹⁹F{¹H} NMR (376 MHz, CDCl₃): δ -113.9 (F), -61.6 (CF₃). ESIMS: *m/z* 661 [M-Cl]⁺. HRMS (ESI): Calcd for C₂₈H₂₈N₂F₄¹⁹³Ir [M-Cl]⁺ 661.1818, found 661.1830.

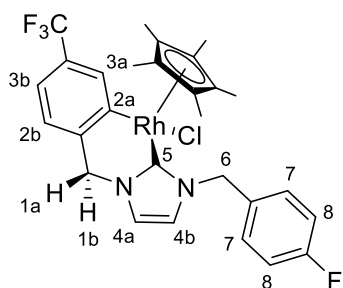


4.12a-CF₃F*. ¹H NMR (400 MHz, CDCl₃): δ 1.68 (s, 15H, C₅Me₅), 4.69 (d, *J* = 14.1 Hz, 1H, *H*^{6b}), 4.87 (d, *J* = 14.1 Hz, 1H, *H*^{6a}), 5.12 (d, *J* = 14.7 Hz, 1H, *H*¹), 6.11 (d, *J* = 14.7 Hz, 1H, *H*¹), 6.54 (td, *J* = 8.5, 2.6 Hz, 1H, *H*^{8b}), 6.62 (d, *J* = 2.1 Hz, 1H, *H*^{4a}), 6.95 (d, *J* = 2.1 Hz, 1H, *H*^{4b}), 6.96 (m, 1H, *H*^{7b}), 7.38 (dd, *J* = 10.0, 2.5 Hz, 1H, *H*^{8a}), 7.55 (q, *J* = 8.4 Hz, 4 H, *H*², *H*³), ¹³C{¹H} NMR (125 MHz, CDCl₃): δ 9.5 (C₅Me₅), 52.9 (C¹), 56.7 (C⁶), 90.6 (C₅Me₅), 108.6 (d, ²*J*_{C-F} = 22.1 Hz, C^{8b}), 119.6 (C^{4a}), 120.8 (C^{4b}), 124.8 (br d, ³*J*_{C-F} = 8.0 Hz, C^{7b}), 125.5 (q, ³*J*_{C-F} = 4.0 Hz, C³), 126.9 (br d, ²*J*_{C-F} = 17.0 Hz, C^{8a}), 129.3 (C²), 134.4, 140.6, 147.4 (C^{7a}), 157.8 (C⁵), 162.1 (d, ¹*J*_{C-F} = 247.0, C-F), ¹⁹F{¹H} NMR (376 MHz, CDCl₃): δ -118.2 (F), -62.5 (CF₃). ESIMS: *m/z* 661 [M-Cl]⁺. HRMS (ESI): Calcd for C₂₈H₂₈N₂F₄¹⁹³Ir [M-Cl]⁺, 661.1818, found 661.1830.

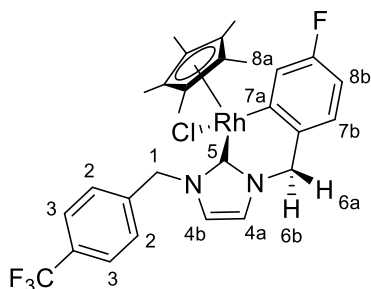
N.B. ¹³C NMR spectrum of two regioisomers was too weak and complicated to find quartets belonging to CF₃ and C-CF₃.

4.12b-CF₃*,F and 4.12b-CF₃,F*

Following the general procedure, the mixture of **4.1b-F**, CF₃ (40 mg, 0.062 mmol), NaOAc (20 mg, 0.244 mmol), dry DCM (2 mL) and MeOH (0.5 mL) was stirred at rt for 1 h. Precipitation from DCM/hexane yielded **4.12b-CF₃*,F**:**4.12b-CF₃,F*** in 1.4:1 ratio as an orange powder (29 mg, 77%).



4.12b-CF₃*,F. ¹H NMR (400 MHz, CDCl₃): δ 1.61 (s, 15H, C₅Me₅), 4.83 (d, *J* = 14.5 Hz, 1H, H^{1b}), 4.98 (m, 2H, H^{1a}, H⁶), 6.17 (br d, *J* = 14.1 Hz, 1H, H⁶), 6.67 (d, *J* = 1.8 Hz, 1H, H^{4a}), 7.00 (m, 3H, H^{4b}, H⁷), 7.05 (br d, *J* = 7.6 Hz, 1H, H^{2b}), 7.15 (br d, *J* = 7.2 Hz, 1H, H^{3b}), 7.46 (dd, *J* = 8.6, 5.3 Hz, 2H, H⁷), 8.02 (s, 1H, H^{3a}), ¹³C{¹H} NMR (125 MHz, CDCl₃): δ 9.7 (C₅Me₅), 52.8 (C⁶), 56.1 (C¹), 97.4 (d, ¹*J*_{C-Rh} = 5.0 Hz, C₅Me₅), 115.3 (d, ²*J*_{C-F} = 21.1 Hz, C⁸), 119.2 (q, ³*J*_{C-F} = 4.0 Hz, C^{3b}), 120.6 (C^{4b}), 121.6 (C^{4a}), 124.3 (C^{2b}), 124.8 (q, ¹*J*_{C-F} = 272.0 Hz, CF₃), 128.6 (q, ²*J*_{C-F} = 30.1 Hz, C-CF₃), 131.2 (d, ³*J*_{C-F} = 8.0 Hz, C⁷), 134.8, 137.4 (C^{3a}), 142.8, 161.8 (d, ¹*J*_{C-Rh} = 32.1 Hz, C^{2a}), 162.0 (d, ¹*J*_{C-F} = 237.9 Hz, C-F), 174.8 (d, ¹*J*_{C-Rh} = 56.2 Hz, C⁵), ¹⁹F{¹H} NMR (376 MHz, CDCl₃): δ -113.8 (F), -61.6 (CF₃). ESIMS: *m/z* 571 [M-Cl]⁺. HRMS (ESI): Calcd. for C₂₈H₂₈N₂F₄¹⁰³Rh [M-Cl]⁺ 571.1244, found 571.1245.



4.12b-CF₃,F* ¹H NMR (400 MHz, CDCl₃): δ 1.61 (s, 15H, C₅Me₅), 4.77 (d, *J* = 14.3 Hz, 1H, H^{6b}), 4.98 (m, 1H, H^{6a}), 5.15 (d, *J* = 14.5 Hz, 1H, H¹), 6.26 (d, *J* = 14.5 Hz, 1H, H¹), 6.58 (td, *J* = 8.4, 2.5 Hz, 1H, H^{8b}), 6.66 (d, *J* = 1.8 Hz, 1H, H^{4a}), 6.94 (dd, *J* = 7.9, 5.8 Hz, 1H, H^{7b}), 7.00 (m, 1H, H^{4b}), 7.46 (m, 1H, H^{8a}), 7.56 (m, 4H, H², H³), ¹³C{¹H} NMR (125 MHz, CDCl₃): δ 9.7 (C₅Me₅), 53.1 (C¹), 55.9 (C⁶), 97.4 (d, ¹*J*_{C-Rh} = 5.0 Hz, C₅Me₅), 108.9 (d, ²*J*_{C-F} = 22.1 Hz, C^{8b}), 120.5 (C^{4a}), 121.8 (C^{4b}), 121.8 (q, ¹*J*_{C-F} = 272.1 Hz, CF₃), 125.1 (d, ³*J*_{C-F} = 8.0 Hz, C^{7b}), 125.5 (q, ³*J*_{C-F} = 3.0 Hz, C³), 126.5 (d, ²*J*_{C-F} = 18.1 Hz, C^{8a}), 129.4 (C²), 130.3 (q, ²*J*_{C-F} = 32.1 Hz, C-CF₃), 140.4, 162.0 (d, ¹*J*_{C-F} = 230.9 Hz, C-F), 163.9 (d, ¹*J*_{C-Rh} = 33.1 Hz, C^{7a}), 175.6, 174.2 (d, ¹*J*_{C-Rh} = 56.2 Hz, C⁵), ¹⁹F{¹H} NMR (376 MHz, CDCl₃): δ -117.5 (F), -62.5 (CF₃). ESIMS: *m/z* 571 [M-Cl]⁺. HRMS (ESI): Calcd. for C₂₈H₂₈N₂F₄¹⁰³Rh [M-Cl]⁺ 571.1244, found 571.1245.

6.4d Procedures for deuterium incorporation experiments

General procedure for deuterium incorporation experiments with 4.10a/b-OMe,F

An NMR tube was charged with 4.10a/b-OMe,F (5 mg, 1 eq.) and CD₃OD (0.5 mL). The ¹H NMR spectrum was recorded and then NaOAc (4 eq.) was added. The reactions were allowed to sit at rt overnight and monitored by ¹H NMR spectroscopy. Then PivOD (1 eq.) added and reaction was allowed to sit for a further day at rt, before heating to 70 °C for 4-48 h. The percentage of deuteration was monitored and determined by ¹H NMR spectroscopy by comparing the relative integrations for signal for H⁷ for the *para*-isomers to H⁵ for the *ortho*-isomers. The deuterium incorporation was additionally confirmed by ²H NMR spectroscopy.

General procedure for deuterium incorporation experiments with 4.12a/b-OMe,CF₃*

An NMR tube was charged with 4.12a/b-OMe,CF₃* (5 mg, 1 eq.), PivOD (1 eq.) and CD₃OD (0.5 mL). The ¹H NMR spectrum was recorded and then NaOAc (4 eq.) was added. The reactions were allowed to sit at rt overnight and monitored by ¹H NMR spectroscopy, before heating to 70 °C overnight. The percentage of deuteration was monitored and determined by ¹H NMR spectroscopy by comparing relative integrations for signal for H⁷ for the *para*-isomers to H⁵ for the *ortho*-isomers. The deuterium incorporation was additionally confirmed by ²H NMR spectroscopy.

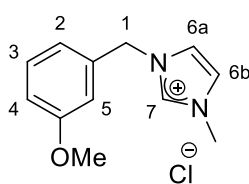
6.4e Synthesis of meta-substituted benzyimidazolium salts L4.13-R

General procedure for preparation of *meta*-substituted benzyimidazolium salts L4.13-R

A Schlenk flask was charged with *N*-methylimidazole (1 eq.), *meta*-substituted benzyl chloride (1-2 eq.) and MeCN (5mL) and stirred at 55 °C for 1 day. The resulting mixture was concentrated *in vacuo*, the residue dissolved in DCM and washed with hexane, then the solvent removed by rotary evaporation giving pure imidazolium salt as an oil or a sticky solid.

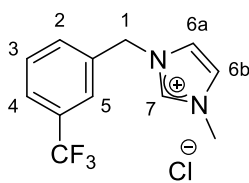
Preparation of *meta*-substituted benzylimidazolium salts L4.13-R

L4.13-OMe



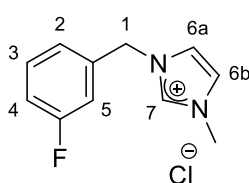
Following the general procedure, *N*-methylimidazole (250 mg, 3.049 mmol), 3-methoxybenzyl chloride (373 mg, 2.382 mmol) and MeCN (5 mL) were added to a Schlenk flask and stirred at 55 °C for 20 h. **L4.13-OMe** was obtained as a white sticky solid (480 mg, 84%). ¹H NMR (400 MHz, CDCl₃): δ 3.65 (s, 3H, OMe), 3.93 (s, 3H, Me), 5.41 (s, 2H, H¹), 6.72 (dd, *J* = 8.2, 2.3 Hz, 1H, H⁴), 6.87 (d, *J* = 7.6 Hz, 1H, H²), 6.93 (br. s, 1H, H⁵), 7.12 (t, *J* = 7.9 Hz, 1H, H³), 7.41 (s, 1H, H^{6b}), 7.56 (s, 1H, H^{6a}), 10.46 (s, 1H, H⁷), ¹³C{¹H} NMR (125 MHz, CDCl₃): δ 36.1 (Me), 52.6 (C¹), 55.1 (OMe), 114.0 (C⁵), 114.4 (C⁴), 120.5 (C⁵), 121.6 (C^{6a}), 123.4 (C^{6b}), 130.0 (C³), 134.4, 137.1 (C⁷), 159.7. ESIMS: *m/z* 203 [M-Cl]⁺. HRMS (ESI): Calcd for C₁₂H₁₅N₂O [M]⁺ 203.1184, found 203.1186.

L4.13-CF₃



Following the general procedure, *N*-methylimidazole (159 mg, 1.939 mmol), 3-trifluoromethylbenzyl chloride (563 mg, 2.893 mmol) and MeCN (5 mL) were added to a Schlenk flask and stirred at 55 °C for 1 day. Additional portion of 3-trifluoromethylbenzyl chloride (188 mg, 0.965 mmol) was added and mixture stirred at 65 °C for 1 day. **L4.13-CF₃** was obtained as a white sticky solid (294 mg, 55%). ¹H NMR (400 MHz, CDCl₃): δ 3.84 (s, 3H, Me), 5.59 (s, 2H, H¹), 7.30 (m, 1H, H³), 7.38 (m, 1H, H⁴), 7.49 (br s, 1H, H^{6b}), 7.58 (br s, 1H, H^{6a}), 7.67 (m, 2H, H², H⁵), 10.37 (m, 1H, H⁷), ¹³C{¹H} NMR (125 MHz, CDCl₃): δ 36.0 (Me), 51.6 (C¹), 122.0 (C^{6a}), 123.2 (q, ¹*J*_{C-F} = 273.1 Hz, CF₃), 123.5 (C^{6b}), 125.2 (d, ³*J*_{C-F} = 4.0 Hz, C⁵), 125.6 (C⁴), 129.5 (C³), 130.6 (q, ²*J*_{C-F} = 33.1 Hz, C-CF₃), 132.2 (C²), 134.3, 137.0 (C⁷), ¹⁹F{¹H} NMR (376MHz, CDCl₃): δ -62.4 (CF₃). ESIMS: *m/z* 241 [M-Cl]⁺. HRMS (ESI): Calcd for C₁₂H₁₂F₃N₂ [M]⁺ 241.0953, found 241.0960.

L4.13-F



Following the general procedure, *N*-methylimidazole (165 mg, 2.010 mmol), 3-fluorobenzyl chloride (404 mg, 2.793 mmol) and MeCN (5 mL) were added to a Schlenk flask and stirred at 60 °C for 24 h. **L4.13-F** was obtained as a pale yellow oil (396 mg, 87%). ¹H NMR (400 MHz, CD₃OD): δ 3.96 (s, 3H, Me), 5.48 (s, 2H, H¹), 7.16 (tdd, *J* = 8.7,

2.2, 0.7 Hz, 1H, H^4), 7.25 (dt, $J = 9.5, 2.0$ Hz, 1H, H^5), 7.30 (br. d, $J = 8.3$, 1H, H^3), 7.47 (td, $J = 8.0, 5.7$ Hz, 1H, H^2), 7.63 (d, $J = 2.0$ Hz, 1H, H^{6b}), 7.67 (d, $J = 2.0$ Hz, 1H, H^{6a}), 9.13 (s, 1H, H^7), $^{13}\text{C}\{^1\text{H}\}$ NMR (101 MHz, CD_3OD): δ 36.8 (Me), 53.4 (C^1), 116.7 (d, $^2J_{C-F} = 23.0$ Hz, C^5), 117.2 (d, $^2J_{C-F} = 20.7$ Hz, C^4), 123.8 (C^{6a}), 125.5 (C^{6b}), 125.7 (d, $^4J_{C-F} = 3.2$ Hz, C^2), 132.5 (d, $^3J_{C-F} = 7.9$ Hz, C^3), 138.0 (d, $^3J_{C-F} = 7.2$ Hz), 138.1 (C^7), 164.6 (d, $^1J_{C-F} = 246.4$ Hz, C-F). $^{19}\text{F}\{^1\text{H}\}$ NMR (376MHz, CD_3OD): δ -113.7 (F). ESIMS: m/z 191 $[\text{M}-\text{Cl}]^+$. HRMS (ESI): Calcd for $\text{C}_{11}\text{H}_{12}\text{FN}_2$ $[\text{M}]^+$ 191.0985, found 191.0982.

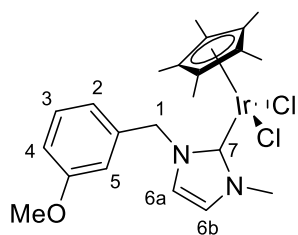
6.4f Complexation of *meta*-substituted benzylimidazolium salts **L4.13-R** with $\{\text{IrCp}^*\}$ and $\{\text{RhCp}^*\}$

General procedure for complexation of *meta*-substituted benzylimidazolium **L4.13-R** salts with $\{\text{IrCp}^*\}$ and $\{\text{RhCp}^*\}$

An aluminium foil wrapped Schlenk flask was charged with a magnetic stirrer bar, the appropriate *meta*-substituted benzylimidazolium salt **L4.13-R** (2.1 eq.) and Ag_2O (2.2 eq.), capped, purged with N_2 . Dry DCM (2.5 mL) was added and the mixture stirred at rt for 1-2 h. Then the reaction mixture was filtered through celite and the solvent removed by rotary evaporation. The residue re-dissolved in dry DCM (2.5 mL) and added to an N_2 purged and aluminium foil wrapped Schlenk flask, followed by addition of $[\text{MCl}_2\text{Cp}^*]_2$ ($\text{M} = \text{Ir, Rh}$) (1 eq.). The reaction mixture was stirred at rt for 1-2 h. Then it was filtered through celite, the solvent removed by rotary evaporation and the final **4.13a/b-R₁,R₂** obtained by precipitation/crystallisation from DCM/ Et_2O or DCM/hexane.

Complexation of *meta*-substituted benzylimidazolium salts **L4.13-R** with $\{\text{IrCp}^*\}$ and $\{\text{RhCp}^*\}$

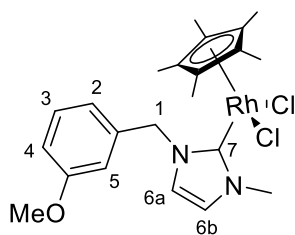
4.13a-OMe



Following the general procedure, a mixture of **L4.13-OMe** (58 mg, 0.243 mmol), Ag_2O (59 mg, 0.254 mmol), dry DCM (2.5 mL), stirred at rt for 1 h, then $[\text{IrCl}_2\text{Cp}^*]_2$ (91 mg, 0.114 mmol) and dry DCM (2.5 mL) were added and the mixture was stirred for 1 h. Crystallisation from DCM/hexane yielded **4.13a-OMe** as yellow crystals (99 mg, 72%). ^1H NMR (400 MHz, CDCl_3): δ 1.62 (s, 15H, C_5Me_5), 3.78 (s, 3H, OMe), 4.00 (s, 3H, Me), 5.22 (d, $J = 14.9$ Hz, 1H, H^1), 5.93 (d, $J = 14.9$ Hz,

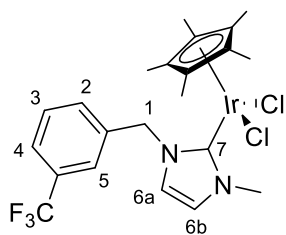
1H, H^1), 6.72 (d, $J = 2.2$ Hz, 1H, H^{6a}), 6.84 (dd, $J = 7.9, 2.2$ Hz, 1H, H^4), 6.88 (d, $J = 7.6$ Hz, 1H, H^2), 6.90 (d, $J = 2.2$ Hz, 1H, H^{6b}), 6.95 (d, $J = 2.2$ Hz, 1H, H^5), 7.25 (t, $J = 7.9$ Hz, 1H, H^3), $^{13}\text{C}\{^1\text{H}\}$ NMR (125 MHz, CDCl_3): δ 9.3 (C_5Me_5), 38.7 (*Me*), 54.5 (C^1), 55.4 (*OMe*), 88.9 (C_5Me_5), 113.7 (C^5), 113.9 (C^4), 120.7 (C^2), 121.9 (C^{6a}), 123.3 (C^{6b}), 129.7 (C^3), 138.3, 156.9 (C^7), 159.9. ESIMS: m/z 565 $[\text{M}-\text{Cl}]^+$. HRMS (ESI): Calcd for $\text{C}_{22}\text{H}_{29}\text{N}_2\text{OCl}^{193}\text{Ir} [\text{M}-\text{Cl}]^+$ 565.1598, found 565.1591.

4.13b-OMe



Following the general procedure, a mixture of **L4.13-OMe** (51 mg, 0.214 mmol), Ag_2O (52 mg, 0.224 mmol), dry DCM (2.5 mL), stirred at rt for 1 h, then $[\text{RhCl}_2\text{Cp}^*]_2$ (62 mg, 0.100 mmol) and dry DCM (2.5 mL) were added and the mixture was stirred for 1 h. Crystallisation from DCM/hexane yielded **4.13b-OMe** as yellow/orange crystals (94 mg, 92%). ^1H NMR (400 MHz, CDCl_3): δ 1.61 (s, 15H, C_5Me_5), 3.78 (s, 3H, *OMe*), 4.05 (s, 3 H, *Me*), 5.27 (br d, $J = 14.7$ Hz, 1H, H^1), 6.03 (br d, $J = 14.5$ Hz, 1H, H^1), 6.80 (d, $J = 2.0$ Hz, 1H, H^{6a}), 6.84 (dd, $J = 8.2, 2.3$ Hz, 1H, H^4), 6.89 (br d, $J = 7.5$ Hz, 1H, H^2), 6.97 (m, 2 H, H^5 , H^{6b}), 7.24 (t, $J = 7.8$ Hz, 1H, H^3), $^{13}\text{C}\{^1\text{H}\}$ NMR (125 MHz, CDCl_3): δ 9.5 (C_5Me_5), 39.2 (*Me*), 54.6 (C^1), 55.3 (*OMe*), 96.2 (d, $^1J_{\text{C-Rh}} = 6.0$ Hz, C_5Me_5), 113.7 (C^5), 113.9 (C^4), 120.6 (C^2), 122.7 (C^{6a}), 124.1 (C^{6b}), 129.6 (C^3), 138.2, 159.9, 170.3 (d, $^1J_{\text{C-Rh}} = 56.2$ Hz, C^7). ESIMS: m/z 475 $[\text{M}-\text{Cl}]^+$. HRMS (ESI): Calcd for $\text{C}_{22}\text{H}_{29}\text{N}_2\text{OCl}^{103}\text{Rh} [\text{M}-\text{Cl}]^+$ 475.1023, found 475.1016.

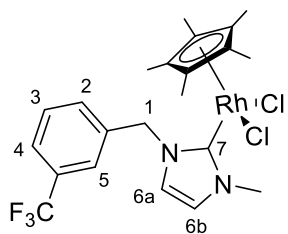
4.13a-CF₃



Following the general procedure, a mixture of **L4.13-CF₃** (52 mg, 0.188 mmol), Ag_2O (46 mg, 0.211 mmol), dry DCM (2.5 mL), stirred at rt for 1 h, then $[\text{IrCl}_2\text{Cp}^*]_2$ (71 mg, 0.089 mmol) and dry DCM (2.5 mL) were added and the mixture was stirred for 1 h. Crystallisation from DCM/hexane yielded **4.13a-CF₃** as yellow crystals (81 mg, 71%). ^1H NMR (400 MHz, CDCl_3): δ 1.63 (s, 15H, C_5Me_5), 4.01 (s, 3H, *Me*), 5.14 (br d, $J = 14.7$ Hz, 1H, H^1), 6.23 (br d, $J = 14.9$ Hz, 1H, H^1), 6.66 (d, $J = 2.2$ Hz, 1H, H^{6a}), 6.94 (d, $J = 2.0$ Hz, 1H, H^{6b}), 7.46 (t, $J = 7.7$ Hz, 1H, H^3), 7.55 (br. s, 1H, H^5), 7.56 (br. d, $J = 7.8$ Hz, 1H, H^4), 7.71 (br. d, $J = 7.6$ Hz, 1H, H^2), $^{13}\text{C}\{^1\text{H}\}$ NMR (125 MHz, CDCl_3): δ 9.1 (C_5Me_5), 38.7 (*Me*), 53.9 (C^1), 88.9 (C_5Me_5), 121.6 (C^{6b}), 123.7 (C^{6a}), 124.0 (q, $^1J_{\text{C-F}} = 245.0$ Hz, CF_3), 124.8 (q, $^3J_{\text{C-F}} = 3.0$ Hz, $\text{C}^{4/5}$), 124.9 (q, $^3J_{\text{C-}}$

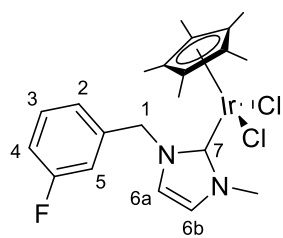
$F = 4.0$ Hz, $C^{4/5}$), 129.4 (C^2), 130.7 (q, ${}^2J_{C-F} = 33.1$ Hz, $C-CF_3$), 132.4 (C^3), 137.8, 157.3 (C^7), ${}^{19}F\{^1H\}$ NMR (376 MHz, $CDCl_3$): δ -62.5 (CF_3). ESIMS: m/z 603 $[M-Cl]^+$. HRMS (ESI): Calcd for $C_{22}H_{26}N_2F_3Cl^{193}Ir [M-Cl]^+$ 603.1366, found 603.1360.

4.13b-CF₃



Following the general procedure, a mixture of **L4.13-CF₃** (53 mg, 0.191 mmol), Ag_2O (57 mg, 0.245 mmol), dry DCM (2.5 mL), stirred at rt for 1 h, then $[RhCl_2Cp^*]_2$ (69 mg, 0.112 mmol) and dry DCM (2.5 mL) were added and the mixture was stirred for 1 h. Crystallisation from DCM/hexane yielded **4.13b-CF₃** as yellow/orange crystals (89 mg, 85%). 1H NMR (400 MHz, $CDCl_3$): δ 1.60 (s, 15H, C_5Me_5), 4.05 (s, 3H, Me), 5.17 (br d, $J = 14.5$ Hz, 1H, H^1), 6.36 (br d, $J = 14.5$ Hz, 1H, H^1), 6.73 (d, $J = 2.0$ Hz, 1H, H^{6a}), 7.02 (d, $J = 2.0$ Hz, 1H, H^{6b}), 7.44 (t, $J = 8.0$ Hz, 1H, H^3), 7.55 (m, 2H, H^4 , H^5), 7.70 (d, $J = 7.6$ Hz, 1H, H^2), ${}^{13}C\{^1H\}$ NMR (125 MHz, $CDCl_3$): δ 9.5 (C_5Me_5), 39.3 (Me), 54.1 (C^1), 96.3 (d, ${}^1J_{C-Rh} = 6.0$ Hz, C_5Me_5), 125.5 (C^{6a}), 123.8 (q, ${}^1J_{C-F} = 246.0$ Hz, CF_3), 124.7 (C^{6b}), 124.8 (q, ${}^3J_{C-F} = 4.0$ Hz, C^4/C^5), 125.0 (q, ${}^3J_{C-F} = 4.0$ Hz C^4/C^5), 129.5 (C^3), 130.7 (q, ${}^2J_{C-F} = 32.1$ Hz, $C-CF_3$), 132.6 (C^2), 137.7, 171.0 (d, ${}^1J_{C-Rh} = 56.2$ Hz, C^7), ${}^{19}F\{^1H\}$ NMR (376 MHz, $CDCl_3$): δ -62.5 (CF_3). m/z 513 $[M-Cl]^+$. HRMS (ESI): Calcd for $C_{22}H_{26}N_2F_3Cl^{103}Rh [M-Cl]^+$ 513.0792, found: 513.0786.

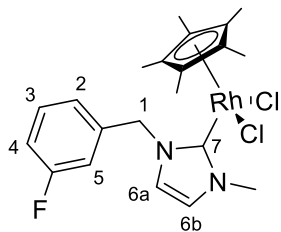
4.13a-F



Following the general procedure, a mixture of **L4.13-F** (50 mg, 0.218 mmol), Ag_2O (50 mg, 0.216 mmol), dry DCM (2.5 mL), stirred at rt for 1 h, then $[IrCl_2Cp^*]_2$ (79 mg, 0.099 mmol) and dry DCM (2.5 mL) was added and the mixture was stirred for 1 h. Crystallisation from DCM/hexane yielded **4.13a-F** as yellow crystals (86 mg, 73%). 1H NMR (400 MHz, $CDCl_3$): δ 1.63 (s, 15H, C_5Me_5), 4.00 (s, 3H, Me), 5.16 (d, $J = 14.8$ Hz, 1H, H^1), 5.93 (d, $J = 14.8$ Hz, 1H, H^1), 6.69 (d, $J = 2.0$ Hz, 1H, H^{6a}), 6.94 (d, $J = 2.1$ Hz, 1H, H^{6b}), 6.99 (td, $J = 8.3, 2.3$ Hz, 1H, H^4), 7.08 (td, $J = 9.6, 2.1$ Hz, 1H, H^5), 7.16 (d, $J = 7.8$ Hz, 1H, H^2), 7.31 (m, 1H, H^3), ${}^{13}C\{^1H\}$ NMR (125 MHz, $CDCl_3$): δ 9.1 (C_5Me_5), 38.7 (Me), 53.9 (C^1), 88.8 (C_5Me_5), 114.9 (d, ${}^2J_{C-F} = 21.1$ Hz, C^4), 115.3 (d, ${}^2J_{C-F} = 23.1$ Hz, C^5), 121.7 (C^{6a}), 123.5 (C^{6b}), 124.2 (d, ${}^4J_{C-F} = 2.0$ Hz, C^2), 130.2 (d, ${}^3J_{C-F} = 8.0$ Hz, C^3), 139.3 (d, ${}^3J_{C-F} = 7.0$ Hz, C), 157.1 (C^7), 162.9 (d, ${}^1J_{C-F} =$

247.0 Hz, C-F), $^{19}\text{F}\{^1\text{H}\}$ NMR (376 MHz, CDCl_3): δ -112.4 (*F*). ESIMS: m/z 553 [$\text{M}-\text{Cl}$] $^+$. HRMS (ESI): Calcd for $\text{C}_{21}\text{H}_{26}\text{N}_2\text{Cl}^{193}\text{Ir}$ [$\text{M}-\text{Cl}$] $^+$ 553.1398, found 553.1394.

4.13b-F



Following the general procedure, a mixture of **4.13b-F** (50 mg, 0.221 mmol), Ag_2O (52 mg, 0.223 mmol), dry DCM (2.5 mL), stirred at rt for 1 h, then $[\text{RhCl}_2\text{Cp}^*]_2$ (62 mg, 0.101 mmol) and dry DCM (2.5 mL) were added and the mixture was stirred for 1 h. Crystallisation from DCM/hexane yielded **4.13b-F** as yellow crystals (67 mg, 67%). ^1H NMR (400 MHz, CDCl_3): δ 1.63 (s, 15H, C_5Me_5), 4.06 (s, 3H, *Me*), 5.22 (d, $J = 14.1\text{ Hz}$, 1H, H^1), 6.19 (d, $J = 14.1\text{ Hz}$, 1H, H^1), 6.78 (d, $J = 2.0\text{ Hz}$, 1H, H^{6a}), 7.00 (m, 2H, H^3 , H^{6b}), 7.09 (td, $J = 9.6, 1.9\text{ Hz}$, 1H, H^5), 7.17 (dd, $J = 7.6, 0.6\text{ Hz}$, 1H, H^2), 7.31 (td, $J = 7.9, 5.9\text{ Hz}$, 1H, H^3), $^{13}\text{C}\{^1\text{H}\}$ NMR (125 MHz, CDCl_3): δ 9.5 (C_5Me_5), 39.2 (*Me*), 54.1 (C^1), 96.3 (d, $J_{\text{C-Rh}} = 6.0\text{ Hz}$, C_5Me_5), 115.0 (d, $^2J_{\text{C-F}} = 20.1\text{ Hz}$, C^4), 115.4 (d, $^2J_{\text{C-F}} = 22.1\text{ Hz}$, C^5), 122.6 (C^{6a}), 124.3 (d, $^4J_{\text{C-F}} = 2.0\text{ Hz}$, C^2), 124.5 (C^{6b}), 130.3 (d, $^3J_{\text{C-F}} = 8.0\text{ Hz}$, C^3), 139.3 (d, $^3J_{\text{C-F}} = 8.0\text{ Hz}$, C), 162.9 (d, $^1J_{\text{C-F}} = 250.0\text{ Hz}$, C-F), 170.8 (d, $J_{\text{C-Rh}} = 56.2\text{ Hz}$, C^7), $^{19}\text{F}\{^1\text{H}\}$ NMR (376 MHz, CDCl_3): δ -112.3 (*F*). ESIMS: m/z 463 [$\text{M}-\text{Cl}$] $^+$. HRMS (ESI): Calcd for $\text{C}_{21}\text{H}_{25}\text{N}_2\text{F}^{103}\text{Rh}$ [$\text{M}-\text{HCl}_2$] $^+$ 427.1057, found 427.1052.

6.4g Cyclometallation of 4.13a/b-R

General procedure for cyclometallation of 4.13a/b-R

An oven-dried and N_2 purged Schlenk flask was charged with a magnetic stirrer bar, **4.13a/b-R** (1 eq.), NaOAc (5 eq.) and dry DCM (2 mL) and MeOH (0.5 mL) and stirred at rt for indicated time. The reaction mixture was filtered through celite, which was washed with additional DCM (5-10 mL), the solvent removed by rotary evaporation and the residue purified by precipitation from DCM/hexane.

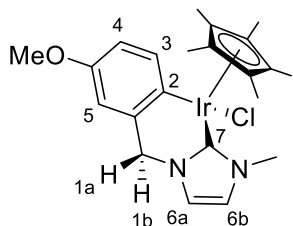
General procedure for monitoring cyclometallation of 4.13a/b-R in CDCl_3

An NMR tube was charged with appropriate **4.13a/b-R** complex (1.0 eq., ca. 5 mg.), NaOAc (4 eq.) and CDCl_3 (0.5 mL). The reaction was monitored at time intervals (1 h, 4 h, 24 h, and several days) by ^1H NMR spectroscopy (and where applicable ^{19}F NMR spectroscopy) by comparing the relative integrations of the appropriate H^1 signals.

Cyclometallation of 4.13a/b-R

4.15a-OMe

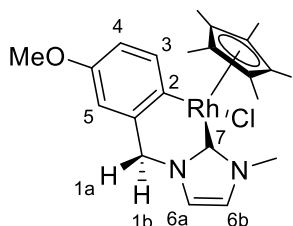
Following general procedure, a mixture of **4.13a-OMe** (15 mg, 0.025 mmol), NaOAc (8 mg, 0.098 mmol), dry DCM (2 mL) and dry MeOH (0.5 mL) was stirred at rt overnight. Precipitation from DCM/hexane yielded regioisomer *para*-**4.15a-OMe** as a yellow powder (12 mg, 84%).



para-**4.15a-OMe**. ¹H NMR (400 MHz, CDCl₃): δ 1.68 (s, 15H, C₅Me₅), 3.75 (s, 3H, OMe), 3.92 (s, 3H, Me), 4.60 (d, *J* = 13.9 Hz, 1H, *H*^{1b}), 4.84 (d, *J* = 13.9 Hz, 1H, *H*^{1a}), 6.61 (d, *J* = 2.7 Hz, 1H, *H*⁵), 6.67 (dd, *J* = 8.3, 2.6 Hz, 1H, *H*⁴), 6.89 (d, *J* = 1.4 Hz, 1H, *H*^{6b}), 6.94 (d, *J* = 1.4 Hz, 1H, *H*^{6a}), 7.47 (br d, *J* = 8.2 Hz, 1H, *H*³), ¹³C{¹H} NMR (125 MHz, CDCl₃): δ 9.4 (C₅Me₅), 36.9 (Me), 55.3 (C¹), 57.1 (OMe), 90.0 (C₅Me₅), 111.1 (C⁵), 113.6 (C⁴), 120.3 (C^{6a}), 121.1 (C^{6a}), 132.5 (C²), 138.5, 141.4 (C³), 155.8, 157.3 (C⁷). ESIMS: *m/z* 529 [M-Cl]⁺. HRMS (ESI): Calcd for C₂₂H₂₈N₂O¹⁹¹Ir [M-Cl]⁺ 527.1808, found 527.1804.

4.15b-OMe

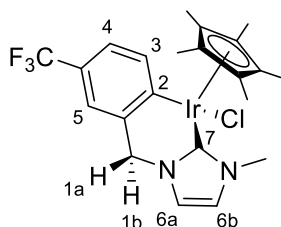
Following the general procedure, a mixture of **4.13b-OMe** (19 mg, 0.037 mmol), NaOAc (12 mg, 0.146 mmol), dry DCM (2 mL) and dry MeOH (0.5 mL) was stirred at rt overnight. Precipitation from DCM/hexane yielded *para*-**4.15b-OMe** as a yellow/orange powder (12 mg, 68%).



para-**4.15b-OMe**. ¹H NMR (400 MHz, CDCl₃): δ 1.60 (s, 15H, C₅Me₅), 3.74 (s, 3H, OMe), 4.00 (s, 3H, Me), 4.68 (d, *J* = 14.3 Hz, 1H, *H*^{1b}), 4.94 (d, *J* = 14.3 Hz, 1H, *H*^{1a}), 6.61 (d, *J* = 2.5 Hz, 1H, *H*⁵), 6.71 (dd, *J* = 8.4, 2.7 Hz, 1H, *H*⁴), 6.95 (d, *J* = 1.8 Hz, 1H, *H*^{6b}), 7.02 (d, *J* = 1.6 Hz, 1H, *H*^{6a}), 7.56 (d, *J* = 8.4 Hz, 1H, *H*³), ¹³C{¹H} NMR (125 MHz, CDCl₃): δ 9.6 (C₅Me₅), 37.5 (Me), 55.3 (C¹), 56.3 (OMe), 97.0 (d, ¹*J*_{C-Rh} = 5.0 Hz, C₅Me₅), 111.6 (C⁵), 113.3 (C⁴), 121.4 (C^{6a}), 122.0 (C^{6b}), 139.1, 141.0 (C³), 147.8 (d, ¹*J*_{C-Rh} = 32.1 Hz, C²), 156.1, 175.0 (d, ¹*J*_{C-Rh} = 55.2 Hz, C⁷). ESIMS: *m/z* 439[M-Cl]⁺. HRMS (ESI): Calcd for C₂₂H₂₈N₂O¹⁰³Rh [M-Cl]⁺ 439.1257, found 439.1246.

4.15a-CF₃

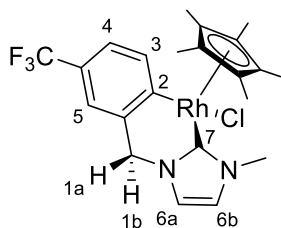
Following the general procedure, a mixture of **4.13a-CF₃** (27 mg, 0.042 mmol), NaOAc (14 mg, 0.171 mmol), dry DCM (2 mL) and dry MeOH (0.5 mL) was stirred at rt overnight. Precipitation from DCM/hexane yielded *para*-**4.15a-CF₃** as a yellow powder (21 mg, 83%).



para-**4.15a-CF₃**. ¹H NMR (400 MHz, CDCl₃): δ 1.68 (s, 15H, C₅Me₅), 3.90 (s, 3H, Me), 4.72 (br d, *J* = 13.7 Hz, 1H, H^{1b}), 4.86 (br d, *J* = 14.1 Hz, 1H, H^{1a}), 6.92 (br s, 1H, H^{6b}), 6.98 (br s, 1H, H^{6a}), 7.18 (m, 2H, H⁴, H⁵), 7.75 (m, 1H, H³), ¹³C{¹H} NMR (125 MHz, CDCl₃): δ 9.4 (C₅Me₅), 36.9 (Me), 55.3 (C¹), 90.5 (C₅Me₅), 120.3 (q, ³*J*_{C-F} = 3.0 Hz, C^{4/5}), 120.4 (C^{6a}), 121.4 (C^{6b}), 123.6 (q, ³*J*_{C-F} = 3.0 Hz, C^{4/5}), 124.1 (q, ²*J*_{C-F} = 31.1 Hz, C-CF₃), 125.2 (q, ¹*J*_{C-F} = 271.1 Hz, CF₃), 138.9, 141.8 (C³), 152.1 (C²), 156.6 (C⁷). ¹⁹F{¹H} NMR (376MHz, CDCl₃): δ -61.4 (CF₃). ESIMS: *m/z* 567 [M-Cl]⁺. HRMS (ESI): Calcd for C₂₂H₂₅N₂F₃¹⁹¹Ir [M-Cl]⁺ 565.1574, found 565.1576.

4.15b-CF₃

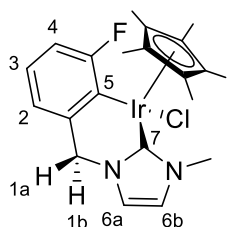
Following the general procedure, a mixture of **4.13b-CF₃** (50 mg, 0.091 mmol), NaOAc (30 mg, 0.366 mmol), dry DCM (2 mL) and dry MeOH (0.5 mL) was stirred at rt overnight. Precipitation from DCM/hexane yielded *para*-**4.15b-CF₃** as a yellow/orange powder (40 mg, 86%).



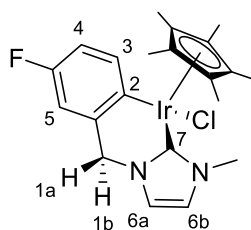
para-**4.15b-CF₃**. ¹H NMR (400 MHz, CDCl₃): δ 1.59 (s, 15H, C₅Me₅), 3.97 (s, 3H, Me), 4.80 (d, *J* = 14.3 Hz, 1H, H^{1b}), 4.97 (d, *J* = 14.3 Hz, 1H, H^{1a}), 6.95 (d, *J* = 1.8 Hz, 1H, H^{6b}), 7.03 (d, *J* = 1.8 Hz, 1H, H^{6a}), 7.16 (br s, 1H, H⁵), 7.21 (br d, *J* = 8.0 Hz, 1H, H⁴), 7.86 (br d, *J* = 7.8 Hz, 1H, H³), ¹³C{¹H} NMR (125 MHz, CDCl₃): δ 9.6 (C₅Me₅), 37.4 (Me), 56.1 (C¹), 97.4 (d, ¹*J*_{C-Rh} = 5.0 Hz, C₅Me₅), 120.6 (q, ³*J*_{C-F} = 3.0 Hz, C⁵), 121.5 (q, ³*J*_{C-F} = 3.0 Hz, C⁴), 122.4 (C^{6a}), 122.8 (C^{6b}), 124.4 (q, ²*J*_{C-F} = 31.1 Hz, C-CF₃), 125.1 (q, ¹*J*_{C-F} = 271.0 Hz, CF₃), 139.5, 141.3 (q, ⁴*J*_{C-F} = 2.0 Hz, C³), 169.0 (d, ¹*J*_{C-Rh} = 32.1 Hz, C²), 174.3 (d, ¹*J*_{C-Rh} = 56.2 Hz, C⁷), ¹⁹F{¹H} NMR (376MHz, CDCl₃): δ -61.5 (CF₃). ESIMS: *m/z* 477 [M-Cl]⁺. HRMS (ESI): Calcd for C₂₂H₂₅N₂F₃¹⁰³Rh [M-Cl]⁺ 477.1025, found 477.10250.

4.15a-F

Following the general procedure, a mixture of **4.13a-F** (30.0 mg, 0.051 mmol), NaOAc (16.5 mg, 0.201 mmol), dry DCM (2.4 mL) and dry MeOH (0.6 mL) was stirred at rt for 2 h. Precipitation from DCM/hexane yielded **4.15a-F** (*ortho:para* ratio 10:1) as a yellow powder (27 mg, 96%).



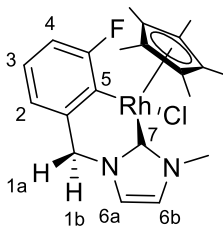
ortho-**4.15a-F**. ^1H NMR (400 MHz, CDCl_3): δ 1.73 (s, 15H, C_5Me_5), 3.89 (s, 3H, *Me*), 4.71 (dd, $J = 13.9, 1.3$ Hz, 1H, H^{1b}), 4.88 (d, $J = 13.9$ Hz, 1H, H^{1a}), 6.76 (m, 3H, H^2, H^3, H^4), 6.90 (d, $J = 1.9$ Hz, 1H, H^{6b}), 6.94 (d, $J = 2.0$ Hz, 1H, H^{6a}), $^{13}\text{C}\{^1\text{H}\}$ NMR (101 MHz, CDCl_3): δ 9.4 (C_5Me_5), 37.0 (*Me*), 57.0 (C^1), 90.04 (C_5Me_5), 114.2 (d, $^2J_{\text{C-F}} = 31.0$ Hz, C^4), 120.3 (C^{6a}), 120.6 (d, $^4J_{\text{C-F}} = 1.6$ Hz, C^2), 121.6 (C^{6b}), 123.8 (d, $^3J_{\text{C-F}} = 8.7$ Hz, C^3), 128.0 (d, $^2J_{\text{C-F}} = 38.9$ Hz, C^5), 141.0 (d, $^3J_{\text{C-F}} = 14.3$ Hz, C), 156.4 (C^7), 167.2 (d, $^1J_{\text{C-F}} = 232.9$ Hz, C-F), $^{19}\text{F}\{^1\text{H}\}$ NMR (376MHz, CDCl_3): δ -87.8 (*F*). ESIMS: m/z 517 $[\text{M-Cl}]^+$. HRMS (ESI): Calcd for $\text{C}_{21}\text{H}_{25}\text{N}_2\text{F}^{193}\text{Ir} [\text{M-Cl}]^+$ 517.1631, found 517.1631.



para-**4.15a-F**. ^1H NMR (400 MHz, CDCl_3): δ 1.66 (s, 15H, C_5Me_5), 3.91 (s, 3H, *Me*), 4.6 (d, $J = 14.1$ Hz, 1H, H^{1a}), 4.81 (d, $J = 13.9$ Hz, 1H, H^{1b}), 6.71-6.74 (m, 2H, H^4, H^5), 6.89 (d, $J = 1.9$ Hz, 1H, H^{6b}), 6.93 (d, $J = 1.9$ Hz, 1H, H^{6a}), 7.51 (dd, $J = 8.3, 7.0$ Hz, 1H, H^3), $^{19}\text{F}\{^1\text{H}\}$ NMR (376MHz, CDCl_3): δ -125.3 (*F*). ESIMS: m/z 427 $[\text{M-Cl}]^+$. HRMS (ESI): ESIMS: m/z 517 $[\text{M-Cl}]^+$. HRMS (ESI): Calcd for $\text{C}_{21}\text{H}_{25}\text{N}_2\text{F}^{193}\text{Ir} [\text{M-Cl}]^+$ 517.1631, found 517.1631.

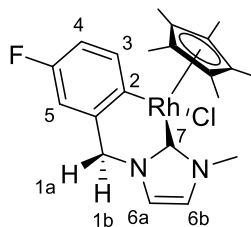
4.15b-F

Following the general procedure, a mixture of **4.13b-F** (25.5 mg, 0.051 mmol), NaOAc (16.7 mg, 0.204 mmol), dry DCM (2.4 mL) and dry MeOH (0.6 mL) was stirred at rt for 2 h. Precipitation from DCM/hexane yielded regioisomers **4.15b-F** (*ortho:para* ratio 10:1) as a yellow powder (22.5 mg, 96%).



ortho-**4.15b-F**. ^1H NMR (400 MHz, CDCl_3): δ 1.66 (s, 15H, C_5Me_5), 3.99 (s, 3H, *Me*), 4.71 (dd, $J = 14.2, 1.0$ Hz, 1H, H^{1a}), 4.97 (d, $J = 14.2$ Hz, 1H, H^{1b}), 6.76 (m, 2 H, H^2, H^4), 6.82 (m, 1H, H^3), 6.97 (d, $J = 1.9$ Hz, 1H, H^{6b}), 7.02 (d, $J = 1.9$ Hz, 1H, H^{6a}), $^{13}\text{C}\{^1\text{H}\}$ NMR (101 MHz, CDCl_3): δ 9.7 (C_5Me_5), 37.8 (*Me*), 56.4 (C^1), 97.5 (d, $^1J_{\text{C-F}}$

$Rh = 5.6$ Hz, C_5Me_5), 114.4 (d, $^2J_{C-F} = 31.0$ Hz, C^4), 120.9 (C^{6a}), 121.3 (C^2), 122.6 (C^{6b}), 124.1 (d, $^3J_{C-F} = 8.7$ Hz, C^3), 141.60 (d, $^3J_{C-F} = 15.1$ Hz, C), 142.8 (m, C^5), 166.9 (d, $^1J_{C-F} = 232.1$ Hz, $C-F$), 174.2 (d, $^1J_{C-Rh} = 54.8$ Hz, C^7), $^{19}F\{^1H\}$ NMR (376 MHz, $CDCl_3$): δ -84.7 (F). m/z 427 $[M-Cl]^+$. HRMS (ESI): Calcd for $C_{21}H_{25}N_2F^{103}Rh [M-Cl]^+$ 427.1057, found 427.1049.



para-4.15b-F. 1H NMR (400 MHz, $CDCl_3$): δ 1.73 (s, 15H, C_5Me_5), 3.99 (s, 3H, Me), 4.68 (d, $J = 14.2, 1.0$ Hz, 1H, H^{1a}), 4.92 (d, $J = 14.2$ Hz, 1H, H^{1b}), 6.73 (dd, $J = 10.0, 3.0$ Hz, 1H, H^5), 6.76 (td, $J = 9.0, 2.8$ Hz, 1H, H^4), 6.97 (d, $J = 1.9$ Hz, 1H, H^{6b}), 7.02 (d, $J = 1.9$ Hz, 1H, H^{6a}), 7.61 (dd, $J = 8.3, 7.0$ Hz, 1H, H^3), $^{19}F\{^1H\}$ NMR (376 MHz, $CDCl_3$): δ -125.0 (F). ESIMS: m/z 427 $[M-Cl]^+$. RMS (ESI): Calcd for $C_{21}H_{25}N_2F^{103}Rh [M-Cl]^+$ 427.1057, found 427.1049.

6.4h General procedure for deuterium incorporation experiments with 4.13a/b-R

An NMR tube was charged with **4.13a/b-R** (1 eq., 5 mg) and CD_3OD (0.5 mL). The 1H NMR spectrum was recorded and then NaOAc (4 eq.) was added. The reactions were allowed to sit at rt overnight. The percentage of deuteration was monitored and determined by 1H NMR spectroscopy by comparing the relative integrations for H^3 and H^5 for the *para*-isomers in the 1H NMR spectra. The deuterium incorporation was additionally confirmed by 2H NMR spectroscopy.

6.5 Bibliography

1. R. G. Ball, W. A. G. Graham, D. M. Heinekey, J. K. Hoyano, A. D. McMaster, B. M. Mattson and S. T. Michel, *Inorg. Chem.*, 1990, **29**, 2023-2025.
2. T. Leermann, F. R. Leroux and F. Colobert, *Org. Lett.*, 2011, **13**, 4479-4481.
3. C. Liu, N. Han, X. Song and J. Qiu, *Eur. J. Org. Chem.*, 2010, **2010**, 5548-5551.
4. Z. Liu, A. Habtemariam, A. M. Pizarro, G. J. Clarkson and P. J. Sadler, *Organometallics*, 2011, **30**, 4702-4710.
5. B. Yang and Z.-X. Wang, *Org. Lett.*, 2017, **19**, 6220-6223.
6. M. L. N. Rao and R. J. Dhanorkar, *Tetrahedron*, 2015, **71**, 338-349.
7. J.-P. Djukic, W. Iali, M. Pfeffer and X.-F. Le Goff, *Chem. Eur. J.*, 2012, **18**, 6063-6078.
8. Y. Boutadla, O. Al-Duaij, D. L. Davies, G. A. Griffith and K. Singh, *Organometallics*, 2009, **28**, 433-440.
9. A. J. Millett, A. Habtemariam, I. Romero-Canelón, G. J. Clarkson and P. J. Sadler, *Organometallics*, 2015, **34**, 2683-2694.
10. M. Brasse, J. Cámpora, J. A. Ellman and R. G. Bergman, *J. Am. Chem. Soc.*, 2013, **135**, 6427-6430.
11. L. Li, W. W. Brennessel and W. D. Jones, *Organometallics*, 2009, **28**, 3492-3500.
12. M. Bielawski, M. Zhu and B. Olofsson, *Adv. Synth. Catal.*, 2007, **349**, 2610-2618.
13. M. Zhu, N. Jalalian and B. Olofsson, *Synlett*, 2008, **2008**, 592-596.
14. L. Zhu, L. Cheng, Y. Zhang, R. Xie and J. You, *J. Org. Chem.*, 2007, **72**, 2737-2743.
15. X. Wang, M. Wang and J. Xie, *Synth. Commun.*, 2017, **47**, 1797-1803.
16. H.-C. Ma and X.-Z. Jiang, *J. Org. Chem.*, 2007, **72**, 8943-8946.
17. T. Lv, Z. Wang, J. You, J. Lan and G. Gao, *J. Org. Chem.*, 2013, **78**, 5723-5730.
18. O. Santoro, A. Collado, A. M. Z. Slawin, S. P. Nolan and C. S. J. Cazin, *Chem. Commun.*, 2013, **49**, 10483-10485.

Appendix

Jaffè analysis

Jaffè analysis is a modification of Hammett equation that allows a correlation of the substituent effects that influence more than one reactive sites at the same time to be plotted.^{41, 43} In Jaffé's equation (3.1 and 3.3) the Hammett equation is divided by one of the two σ values. Depending on which σ is in the denominator the slope of the plot gives one ρ value whilst the y-intercept provides another ρ value (3.2 and 3.4). For LFER to be proven both plots should give the same ρ_m and ρ_p values.

Jaffé equation:

When:

$$\frac{\log\left(\frac{k_x}{k_H}\right)}{\sigma_m} = \frac{\rho_p\sigma_p}{\sigma_m} + \rho_m \quad (3.1)$$

then

$$y = \rho_p X + \rho_m \quad (3.2)$$

When:

$$\frac{\log\left(\frac{k_x}{k_H}\right)}{\sigma_p} = \frac{\rho_m\sigma_m}{\sigma_p} + \rho_p \quad (3.3)$$

then

$$y = \rho_m X + \rho_p \quad (3.4)$$

Table S1: Observed and predicted cyclometallation selectivity of **L3.12-R₁,R₂** with Ir and Rh.

Entry	R ₁	R ₂	Ir, R ₁ *:R ₂ *		Rh, R ₁ *:R ₂ *	
			Observed	Predicted ^a	Observed	Predicted
1	OMe	H	1:1.3	1:1.3 (5.3:4.1)	-	1:1.5(1.7:1.1)
2	Me	CF ₃	1:15	1:17 (5.3×3.2)	-	1:36(1.7×3.8×5.5)
3	F	Me	5.3:1	5.3:1(1.7×3.1)	-	1:9(1.7×5.5)
4	F	OMe	4.1:1	4.0:1(1.3×3.1)	-	1:8.5(1.3×5.5)
5	F	H	3.1:1	3.1:1(5.3:1.7)	5.5:1	-
6	Me	H	1:1.7	1:1.7 (5.3:3.1)	1:1.7	-
7	Me	OMe	1:1.2	1:1.3 (5.3:4.1)	1:1.1	-
8	Cl	F	2.1:1	-	1.9:1	-
9	F	CF ₃	1:3.2	1 : 2.8(15:5.3)	1:3.8	-

Numbers in parentheses correspond to ratios used to calculate predicted ratios

Table S2: Relative rates of cyclometallation of **L3.12-R₁,R₂** with Ir and Rh and their Jaffé modifications.

	R	σ _m	σ _p	σ _p /σ _m	σ _m /σ _p	k _R /k _H	log(k _R /k _H)	log(k _R /k _H)/σ _m	log(k _R /k _H)/σ _p
Ir	Me	-0.7	-0.17	2.43	0.41	0.91	-0.04	0.59	0.24
	H	0	0	-	-	1	0	-	-
	OMe	0.12	-0.27	-2.25	-0.44	0.34	-0.47	-3.90	1.74
	F	0.34	0.06	0.18	5.67	0.31	-0.51	-1.50	-8.48
	Cl	0.37	0.23	0.62	1.61	0.59	-0.23	-0.62	-1.0
Rh	Me	-0.7	-0.17	2.43	0.41	0.83	-0.08	1.16	0.48
	H	0	0	-	-	1	0	-	-
	OMe	0.12	-0.27	-2.25	-0.44	0.43	-0.46	-3.05	1.36
	F	0.34	0.06	0.18	5.67	0.56	-0.25	-0.74	-4.20
	Cl	0.37	0.23	0.62	1.61	1.06	0	0.12	0.18

Table S3: Relative equilibrium constants of cyclometallation of **L3.12-R₁,R₂** with Ir and Rh used for producing plots in **Figure 3.7**.

Group		Me	H	OMe	F	Cl
	σ_m	-0.07	0	0.12	0.34	0.37
Ir	K_R/K_H	0.59	1	1.1	6.6	13.9
	$\log(K_R/K_H)$	-0.23	0	0.04	0.82	1.14
Rh	K_R/K_H	0.59	1	0.84	5.9	11.8
	$\log(K_R/K_H)$	-0.23	0	-0.08	0.77	1.07

Table S4: Computed free energies (kcal mol⁻¹) for reaction profiles for formation of**D-F.**

R ₁	R ₂	D	TS_{D-E}	E	I_{E-F}	F
H	H	-29.6	-21.3	-32.3	-24.5	-49.0
OMe	Me	-29.0	-20.7	-30.9	-23.3	-47.4
Me	OMe	-29.0	-21.0	-31.4	-23.9	-47.7
OMe	H	-29.1	-21.0	-31.4	-23.6	-47.8
H	OMe	-29.1	-21.2	-31.7	-24.4	-48.7
OMe	F	-29.8	-21.5	-31.8	-23.9	-48.9
F	OMe	-29.8	-21.1	-32.7	-25.2	-50.7
Me	H	-28.9	-21.1	-31.5	-24.0	-48.2
H	Me	-28.9	-20.9	-31.7	-24.1	-48.4
Me	F	-30.5	-21.7	-32.1	-24.4	-49.1
F	Me	-30.5	-20.8	-32.4	-25.0	-50.6
Me	CF ₃	-30.6	-22.6	-33.4	-24.9	-50.8
CF ₃	Me	-30.6	-22.2	-34.3	-26.7	-53.3
H	F	-29.9	-21.8	-32.7	-24.7	-49.9
F	H	-29.9	-21.1	-32.6	-25.2	-51.1
F	Cl	-31.6	-22.1	-33.9	-25.8	-52.5
Cl	F	-31.6	-22.3	-34.1	-26.3	-53.1
F	CF ₃	-32.1	-22.6	-34.6	-26.1	-53.7
CF ₃	F	-32.1	-23.0	-35.2	-27.2	-54.7
NO ₂	NMe ₂	-30.6	-22.4	-35.6	-28.4	-55.1
NMe ₂	NO ₂	-30.6	-22.7	-33.0	-24.2	-49.3

Table S5: Computationally calculated favoured regioisomers for cyclometallation of diaryl **L3.12-R₁,R₂** with Ir and the experimentally observed selectivity continuation of **Table 3.14**.

	R₁,R₂	TS_{D-E}	F	Kin.^a	Thermod.^b
1	OMe,H	H≈OMe^a	H	-	H
2	Me,OMe	Me	Me≈OMe^a	-	OMe
3	F,Me	Me	F	-	F
4	Me,CF₃	Me	CF ₃	-	CF ₃

^ain bold marginally favoured isomer, values are regarded as almost equal if the difference between them is less than 0.3 kcal mol⁻¹ the substituent in bold is the marginally favoured isomer,

Table S6: Relative rates of R₁ vs. R₂ intramolecular competition for cyclometallation of **4.10a/b-R₁,R₂** at rt in DCM:MeOH.

Group		H	OMe	F	CF₃
	σ_m	0	0.12	0.34	0.43
Ir	<i>k_R/k_H</i>	1	0.71	0.54	0.59
	log(<i>k_R/k_H</i>)	0	-0.15	-0.27	-0.23
Rh	<i>k_R/k_H</i>	1	0.71	0.51	0.61
	log(<i>k_R/k_H</i>)	0	-0.15	-0.29	-0.22

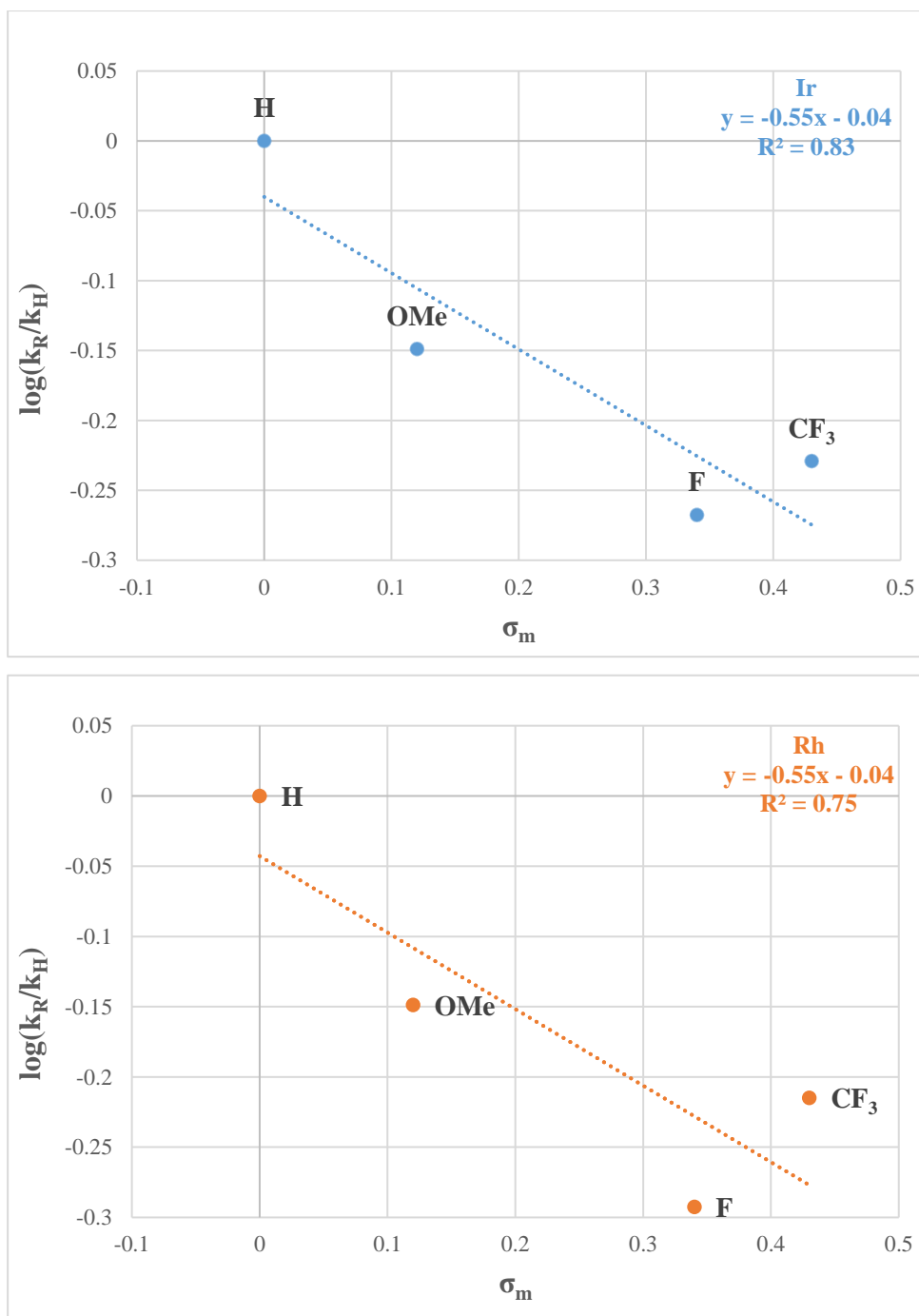


Figure S1: Hammett plot for intramolecular competitions of R₁ vs. R₂ for cyclometallation of Ir (top) and Rh (bottom) complexes **4.10a/b-R₁,R₂**, $\log(k_R/k_H)$ against σ_m in CDCl₃.

Table S7: Relative rates of cyclometallation of **4.10a/b-R₁,R₂** with Ir and Rh and their Jaffé modifications in CDCl₃.

	R	σ_m	σ_p	σ_p/σ_m	σ_m/σ_p	k_R/k_H	$\log(k_R/k_H)$	$\log(k_R/k_H)/\sigma_m$	$\log(k_R/k_H)/\sigma_p$
Ir	H	0	0	-	-	1	0	-	-
	OMe	0.12	-0.27	-2.25	-0.44	0.71	-0.15	-1.25	0.56
	F	0.34	0.06	0.18	5.67	0.55	-0.26	-0.77	-4.33
	CF ₃	0.43	0.54	1.23	0.80	0.79	-0.10	-0.23	0.19-
Rh	H	0	0	-	-	1	0	-	-
	OMe	0.12	-0.27	-2.25	-0.44	0.71	-0.15	-1.25	0.56
	F	0.34	0.06	0.18	5.67	0.51	-0.29	-0.85	-4.83
	CF ₃	0.43	0.54	1.23	0.80	0.79	-0.10	-0.23	-0.19

Table S8: Relative rates of cyclometallation of **4.10a/b-R₁,R₂** with Ir and Rh and their Jaffé modifications in DCM:MeOH.

	R	σ_m	σ_p	σ_p/σ_m	σ_m/σ_p	k_R/k_H	$\log(k_R/k_H)$	$\log(k_R/k_H)/\sigma_m$	$\log(k_R/k_H)/\sigma_p$
Ir	H	0	0	-	-	1	0	-	-
	OMe	0.12	-0.27	-2.25	-0.44	0.71	-0.15	-1.25	0.56
	F	0.34	0.06	0.18	5.67	0.54	-0.27	-0.79	-4.46
	CF ₃	0.43	0.54	1.23	0.80	0.59	-0.23	-0.53	-0.42
Rh	H	0	0	-	-	1	0	-	-
	OMe	0.12	-0.27	-2.25	-0.44	0.71	-0.15	-1.25	0.56
	F	0.34	0.06	0.18	5.67	0.51	-0.29	-0.86	-4.87
	CF ₃	0.43	0.54	1.23	0.80	0.61	-0.22	-0.50	-0.40

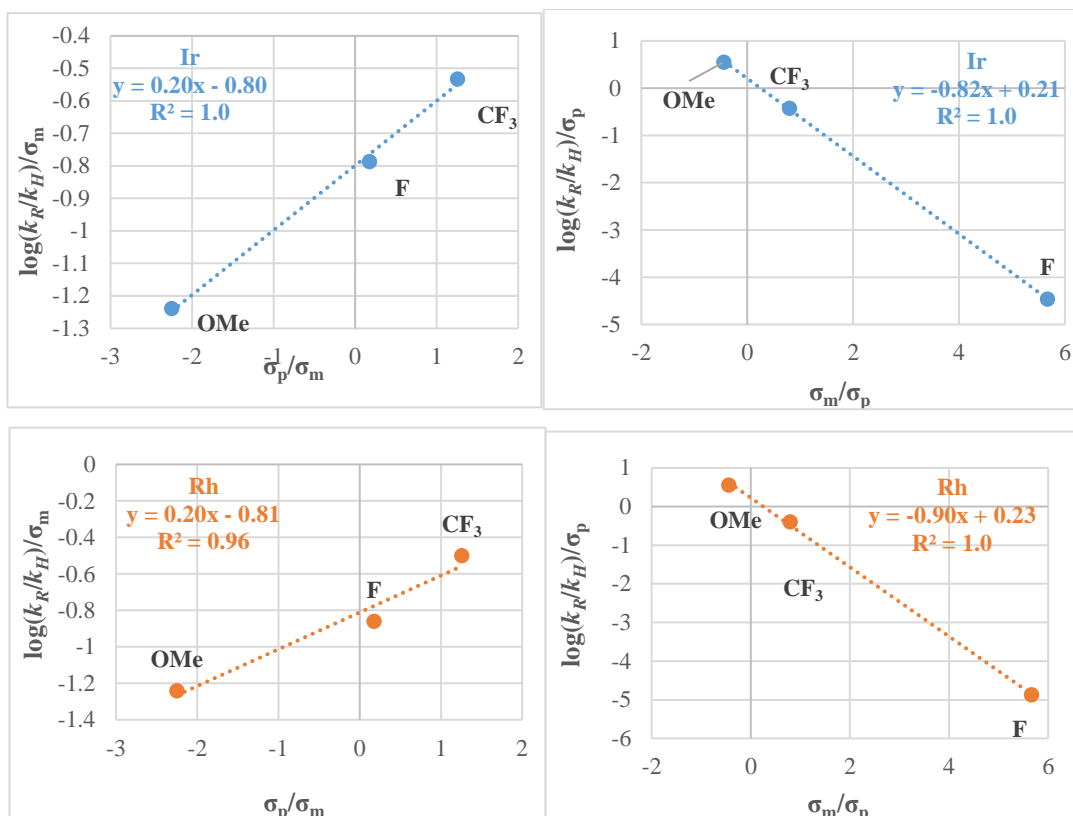


Figure S2: Jaffè plots for intramolecular competitions of R₁ vs. R₂ for cyclometallation of Ir (top) and Rh (bottom) complexes **4.10a/b-R₁,R₂** in DCM:MeOH.

Table S9: Average ρ_m and ρ_p values from Jaffè plots for cyclometallation of **4.10a/b-R₁,R₂** in DCM:MeOH.^a

M	ρ_{m1}	ρ_m	$\rho_{m(\text{average})}$	ρ_{p1}	ρ_{p2}	$\rho_{p(\text{average})}$
Ir	-0.80	-0.82	-0.80	0.20	0.21	0.20
Rh	-0.81	-0.90	-0.90	0.20	0.23	0.20

^a For plots $\log(k_R/k_H)/\sigma_m$ vs. σ_p/σ_m $y = \rho_p x + \rho_m$, for plots $\log(k_R/k_H)/\sigma_p$ vs. σ_m/σ_p $y = \rho_m x + \rho_p$.

Crystallography data for Chapter 2

Table S10: Crystal data and structure refinement for Chapter 2.

	2.6a-F	2.6a-CF₃
Identification code	17104	17091
Empirical formula	C ₂₁ H ₂₂ Cl F Ir N	C ₂₂ H ₂₂ Cl F ₃ Ir N
Formula weight	535.05	585.06
Temperature	150(2) K	150(2) K
Wavelength	0.71073 Å	0.71073 Å
Crystal system	Monoclinic	Monoclinic
Space group	P2(1)/n	P2(1)/c
Unit cell dimensions	a = 7.477(3) Å b = 14.699(5) Å c = 17.404(6) Å α = 90° β = 101.337(6)° γ = 90°	a = 15.581(8) Å b = 7.767(4) Å c = 16.411(8) Å α = 90° β = 92.502(8)° γ = 90°
Volume	1875.5(11) Å ³	1984.3(17) Å ³
Z	4	4
Density (calculated)	1.895 Mg/m ³	1.958 Mg/m ³
Absorption coefficient	7.274 mm ⁻¹	6.898 mm ⁻¹
F(000)	1032	1128
Crystal size	0.43 x 0.11 x 0.07 mm ³	0.32 x 0.21 x 0.03 mm ³
Theta range for data collection	1.83 to 27.00°.	1.31 to 26.00°.
Index ranges	-9 ≤ h ≤ 9, -18 ≤ k ≤ 18, -22 ≤ l ≤ 22	-19 ≤ h ≤ 19, -9 ≤ k ≤ 9, -20 ≤ l ≤ 19
Reflections collected	15318	14362
Independent reflections	4089 [R(int) = 0.0629]	3910 [R(int) = 0.1116]
Completeness to theta = 26.00°	99.7 %	99.9 %
Absorption correction	Empirical	Empirical
Max. and min. transmission	0.831 and 0.365	0.831 and 0.478
Refinement method	Full-matrix least-squares on F ²	Full-matrix least-squares on F ²
Data / restraints / parameters	4089 / 0 / 231	3910 / 15 / 258
Goodness-of-fit on F ²	1.002	1.037
Final R indices [I > 2σ(I)]	R1 = 0.0380, wR2 = 0.0781	R1 = 0.0488, wR2 = 0.0963
R indices (all data)	R1 = 0.0510, wR2 = 0.0818	R1 = 0.0686, wR2 = 0.1022
Largest diff. peak and hole	1.788 and -2.246 e.Å ⁻³	1.812 and -1.030 e.Å ⁻³

Crystallography data for Chapter 3

Table S11: Crystal data and structure refinement for Chapter 3.

	3.12a-F*,OMe	3.12a-F*,H	3.12a-OMe*,OMe
Identification code	16142	17025	17101
Empirical formula	C27 H29 Cl3 F Ir N2 O	C25 H25 Cl F Ir N2	C27 H30 Cl Ir N2 O2
Formula weight	715.07	600.12	642.18
Temperature	150(2) K	150(2) K	150(2) K
Wavelength	0.71073 Å	0.71073 Å	0.71073 Å
Crystal system	Monoclinic	Monoclinic	Triclinic
Space group	P2(1)/c	P2(1)/c	P-1
Unit cell dimensions	a = 10.562(2) Å b = 15.753(3) Å c = 15.635(3) Å α = 90° β = 94.273(4)° γ = 90°	a = 8.448(12) Å b = 15.56(2) Å c = 16.38(2) Å α = 90° β = 94.78(3)° γ = 90°	a = 8.576(4) Å b = 10.495(5) Å c = 13.601(7) Å α = 96.543(8)° β = 90.794(9)° γ = 95.896(9)°
Volume	2594.3(10) Å ³	2145(5) Å ³	1209.5(10) Å ³
Z	4	4	2
Density (calculated)	1.831 Mg/m ³	1.858 Mg/m ³	1.763 Mg/m ³
Absorption coefficient	5.487 mm ⁻¹	6.372 mm ⁻¹	5.657 mm ⁻¹
F(000)	1400	1168	632
Crystal size	0.24 x 0.17 x 0.13 mm ³	0.17 x 0.09 x 0.06 mm ³	0.13 x 0.10 x 0.06 mm ³
Theta range for data collection	1.84 to 27.00°.	1.81 to 26.00°.	1.51 to 26.00°.
Index ranges	-13<=h<=13, - 20<=k<=20, -19<=l<=19	-10<=h<=10, - 19<=k<=19, - 20<=l<=20	-10<=h<=10, - 12<=k<=12, - 16<=l<=16
Reflections collected	21256	16624	9512
Independent reflections	5660 [R(int) = 0.0491]	4222 [R(int) = 0.1750]	4685 [R(int) = 0.0676]
Completeness to theta = 26.00°	99.8 %	100.0 %	98.7 %
Absorption correction	Empirical	Empirical	Empirical
Max. and min. transmission	0.831 and 0.634	0.831 and 0.389	0.837 and 0.561
Refinement method	Full-matrix least-squares on F ²	Full-matrix least-squares on F ²	Full-matrix least-squares on F ²
Data / restraints / parameters	5660 / 0 / 322	4222 / 0 / 276	4685 / 0 / 305
Goodness-of-fit on F ²	0.963	0.972	0.941
Final R indices [I>2σ(I)]	R1 = 0.0287, wR2 = 0.0565	R1 = 0.0595, wR2 = 0.1087	R1 = 0.0406, wR2 = 0.0725
R indices (all data)	R1 = 0.0393, wR2 = 0.0586	R1 = 0.0834, wR2 = 0.1189	R1 = 0.0511, wR2 = 0.0770
Largest diff. peak and hole	1.513 and -0.864 e.Å ⁻³	3.058 and -3.915 e.Å ⁻³	2.346 and -1.762 e.Å ⁻³

Crystallography data for Chapter 4

Table S12: Crystal data and structure refinement for Chapter 4 non-cyclometallated complexes **4.10a-R₁,R₂**

	4.10a-OMe,CF₃	4.10a-CF₃,F
Identification code	18002	18028
Empirical formula	C ₂₉ H ₃₂ Cl ₂ F ₃ Ir N ₂ O	C ₂₈ H ₂₉ Cl ₂ F ₄ Ir N ₂
Formula weight	744.67	732.63
Temperature	150(2) K	150(2) K
Wavelength	0.71073 Å	0.71073 Å
Crystal system	Monoclinic	Monoclinic
Space group	P2(1)/m	P2(1)/m
Unit cell dimensions	a = 7.1408(13) Å b = 24.104(4) Å c = 8.1199(15) Å α = 90° β = 102.462(3)° γ = 90°	a = 7.1332(18) Å b = 23.606(6) Å c = 8.125(2) Å α = 90° β = 103.232(4)° γ = 90°
Volume	1364.7(4) Å ³	1331.8(6) Å ³
Z	2	2
Density (calculated)	1.812 Mg/m ³	1.827 Mg/m ³
Absorption coefficient	5.135 mm ⁻¹	5.262 mm ⁻¹
F(000)	732	716
Crystal size	0.38 x 0.22 x 0.06 mm ³	0.48 x 0.25 x 0.05 mm ³
Theta range for data collection	1.69 to 26.00°	1.73 to 26.00°
Index ranges	-8 ≤ h ≤ 8, -29 ≤ k ≤ 29, -9 ≤ l ≤ 10	-8 ≤ h ≤ 8, -29 ≤ k ≤ 29, -10 ≤ l ≤ 10
Reflections collected	10639	10312
Independent reflections	2739 [R(int) = 0.0705]	2672 [R(int) = 0.0867]
Completeness to theta = 26.00°	100.0 %	99.9 %
Absorption correction	Empirical	Empirical
Max. and min. transmission	0.831 and 0.475	0.831 and 0.405
Refinement method	Full-matrix least-squares on F ²	Full-matrix least-squares on F ²
Data / restraints / parameters	2739 / 70 / 209	2672 / 0 / 199
Goodness-of-fit on F ²	1.057	1.093
Final R indices [I > 2σ(I)]	R1 = 0.0321, wR2 = 0.0753	R1 = 0.0435, wR2 = 0.0944
R indices (all data)	R1 = 0.0360, wR2 = 0.0767	R1 = 0.0481, wR2 = 0.0968
Largest diff. peak and hole	1.503 and -0.719 e.Å ⁻³	2.627 and -1.588 e.Å ⁻³

Table S13: Crystal data and structure refinement for Chapter 4 non-cyclometallated complexes **4.10b-OMe,H** and **4.13a-OMe**.

	4.10b-OMe,H	4.13a-OMe
Identification code	18007	18022
Empirical formula	C ₂₈ H ₃₃ Cl ₂ N ₂ O Rh	C ₂₂ H ₂₉ Cl ₂ Ir N ₂ O
Formula weight	587.37	600.57
Temperature	150(2) K	150(2) K
Wavelength	0.71073 Å	0.71073 Å
Crystal system	Monoclinic	Monoclinic
Space group	P2(1)/n	Pc
Unit cell dimensions	a = 7.102(3) Å b = 46.164(16) Å c = 8.161(3) Å α = 90° β = 103.515(7)° γ = 90°	a = 11.369(6) Å b = 8.613(5) Å c = 12.615(7) Å α = 90° β = 115.248(8)° γ = 90°
Volume	2601.3(16) Å ³	1117.2(11) Å ³
Z	4	2
Density (calculated)	1.500 Mg/m ³	1.785 Mg/m ³
Absorption coefficient	0.886 mm ⁻¹	6.229 mm ⁻¹
F(000)	1208	588
Crystal size	0.32 x 0.15 x 0.11 mm ³	0.47 x 0.17 x 0.05 mm ³
Theta range for data collection	1.76 to 26.00°.	1.98 to 27.00°.
Index ranges	-8<=h<=8, -56<=k<=56, -10<=l<=10	-14<=h<=14, -10<=k<=11, -15<=l<=15
Reflections collected	20284	8857
Independent reflections	5093 [R(int) = 0.1368]	4624 [R(int) = 0.0576]
Completeness to theta = 26.00°	99.9 %	99.2 %
Absorption correction	Empirical	Empirical
Max. and min. transmission	0.831 and 0.471	0.843 and 0.436
Refinement method	Full-matrix least-squares on F ²	Full-matrix least-squares on F ²
Data / restraints / parameters	5093 / 36 / 313	4624 / 2 / 260
Goodness-of-fit on F ²	1.047	1.027
Final R indices [I>2σ(I)]	R1 = 0.0666, wR2 = 0.1311	R1 = 0.0384, wR2 = 0.0873
R indices (all data)	R1 = 0.1123, wR2 = 0.1487	R1 = 0.0408, wR2 = 0.0883
Largest diff. peak and hole	1.202 and -0.904 e.Å ⁻³	2.720 and -1.874 e.Å ⁻³

Table S14: Crystal data and structure refinement for Chapter 4 cyclometallated Ir complexes.

	4.12a-OMe*,H	4.12a-OMe*,CF₃
Identification code	17141	18012
Empirical formula	C ₂₈ H ₃₂ Cl Ir N ₂ O	C ₃₀ H ₃₃ Cl ₃ F ₃ Ir N ₂ O
Formula weight	640.21	793.13
Temperature	150(2) K	150(2) K
Wavelength	0.71073 Å	0.71073 Å
Crystal system	Monoclinic	Monoclinic
Space group	P2(1)/n	P2(1)/c
Unit cell dimensions	a = 13.602(2) Å b = 9.1969(16) Å c = 20.039(4) Å α = 90° β = 98.174(3)° γ = 90°	a = 10.861(2) Å b = 11.519(3) Å c = 24.587(6) Å α = 90° β = 101.199(4) γ = 90°
Volume	2481.3(8) Å ³	3017.2(12) Å ³
Z	4	4
Density (calculated)	1.714 Mg/m ³	1.746 Mg/m ³
Absorption coefficient	5.512 mm ⁻¹	4.736 mm ⁻¹
F(000)	1264	1560
Crystal size	0.22 x 0.18 x 0.03 mm ³	0.27 x 0.17 x 0.06 mm ³
Theta range for data collection	1.70 to 26.00°	1.69 to 26.00°
Index ranges	-16 ≤ h ≤ 16, -11 ≤ k ≤ 11, -24 ≤ l ≤ 24	-13 ≤ h ≤ 13, -14 ≤ k ≤ 14, -29 ≤ l ≤ 30
Reflections collected	18883	22899
Independent reflections	4871 [R(int) = 0.1324]	5939 [R(int) = 0.0714]
Completeness to theta = 26.00°	99.9 %	99.9 %
Absorption correction	Empirical	Empirical
Max. and min. transmission	0.850 and 0.369	0.831 and 0.542
Refinement method	Full-matrix least-squares on F ²	Full-matrix least-squares on F ²
Data / restraints / parameters	4871 / 0 / 304	5939 / 6 / 367
Goodness-of-fit on F ²	0.954	0.968
Final R indices [I > 2σ(I)]	R1 = 0.0592, wR2 = 0.1276	R1 = 0.0394, wR2 = 0.0763
R indices (all data)	R1 = 0.0820, wR2 = 0.1362	R1 = 0.0558, wR2 = 0.0806
Largest diff. peak and hole	5.221 and -3.890 e.Å ⁻³	1.423 and -0.988 e.Å ⁻³

Table S15: Crystal data and structure refinement for Chapter 4 cyclometallated Rh complexes.

	4.12b-OMe,CF₃*	4.12b-OMe,F*	4.12b-OMe*,H
Identification code	18038	18047	18021
Empirical formula	C ₂₉ H ₃₃ Cl F ₃ N ₂ O ₂ Rh	C _{32.50} H _{41.50} Cl F N ₂ O Rh	C ₂₉ H ₃₄ Cl ₃ N ₂ O Rh
Formula weight	636.93	633.54	635.84
Temperature	150(2) K	150(2) K	150(2) K
Wavelength	0.71073 Å	0.71073 Å	0.71073 Å
Crystal system	Monoclinic	Monoclinic	Monoclinic
Space group	Pc	Pc	P2(1)/c
Unit cell dimensions	a = 13.218(9) Å b = 13.401(9) Å c = 8.540(6) Å α = 90° β = 99.628(13)° γ = 90°	a = 12.942(5) Å b = 13.357(5) Å c = 8.527(3) Å α = 90° β = 98.725(7)° γ = 90°	a = 10.8200(18) Å b = 11.414(2) Å c = 23.570(4) Å α = 90° β = 101.313(4)° γ = 90°
Volume	1491.5(17) Å ³	1457.0(9) Å ³	2854.3(8) Å ³
Z	2	2	4
Density (calculated)	1.418 Mg/m ³	1.444 Mg/m ³	1.480 Mg/m ³
Absorption coefficient	0.708 mm ⁻¹	0.713 mm ⁻¹	0.904 mm ⁻¹
F(000)	652	659	1304
Crystal size	0.29 x 0.13 x 0.04 mm ³	0.45 x 0.14 x 0.12 mm ³	0.28 x 0.23 x 0.11 mm ³
Theta range for data collection	1.52 to 26.00°.	1.52 to 26.00°.	1.76 to 26.00°.
Index ranges	-16 ≤ h ≤ 16, 16 ≤ k ≤ 16, 10 ≤ l ≤ 10	-15 ≤ h ≤ 15, 16 ≤ k ≤ 16, 10 ≤ l ≤ 10	-13 ≤ h ≤ 13, 14 ≤ k ≤ 14, -29 ≤ l ≤ 29
Reflections collected	11388	11246	21824
Independent reflections	5708 [R(int) = 0.1061]	5548 [R(int) = 0.1028]	5614 [R(int) = 0.0806]
Completeness to theta = 26.00°	99.8 %	99.7 %	100.0 %
Absorption correction	Empirical	Empirical	Empirical
Max. and min. transmission	0.837 and 0.541	0.831 and 0.419	0.843 and 0.670
Refinement method	Full-matrix least-squares on F ²	Full-matrix least-squares on F ²	Full-matrix least-squares on F ²
Data / restraints / parameters	5708 / 50 / 357	5548 / 20 / 313	5614 / 0 / 331
Goodness-of-fit on F ²	0.958	0.919	0.961
Final R indices [I > 2σ(I)]	R1 = 0.0709, wR2 = 0.1497	R1 = 0.0641, wR2 = 0.1253	R1 = 0.0474, wR2 = 0.0929
R indices (all data)	R1 = 0.1005, wR2 = 0.1611	R1 = 0.0876, wR2 = 0.1357	R1 = 0.0662, wR2 = 0.0987
Largest diff. peak and hole	1.077 and -0.767 e.Å ⁻³	0.865 and -1.447 e.Å ⁻³	1.009 and -0.553 e.Å ⁻³